Miscellaneous Paper GL-98-1
July 1998

US Army Corps
of Engineers
Waterways Experiment
Station

First U.S.-Japan Workshop on Advanced Research on Earthquake Engineering for Dams, 12-14 November 1996

by Mary E. Hynes, Robert Hall, Julia C. Baker, WES
Yoshikazu Yamaguchi,
Public Works Research Institute of Japan

Prepared for U.S.-Japan Cooperative Program in Natural Resources

The contents of this report are not to be used for advertising, publication, or promotional purposes. Citation of trade names does not constitute an official endorsement or approval of the use of such commercial products.

The findings of this report are not to be construed as an official Department of the Army position, unless so designated by other authorized documents.

PRINTED ON RECYCLED PAPER

Miscellaneous Paper GL-98-1
July 1998

First U.S.-Japan Workshop on Advanced Research on Earthquake Engineering for Dams, 12-14 November 1996

by Mary E. Hynes, Robert Hall, Julia C. Baker

U.S. Army Corps of Engineers
Waterways Experiment Station
3909 Halls Ferry Road
Vicksburg, MS 39180-6199

Yoshikazu Yamaguchi

Public Works Research Institute of Japan
1, Asahi, Tsukuba-shi, Ibaraki-ken 305

Final report

Prepared for U.S.-Japan Cooperative Program in Natural Resources (UJNR), Panel on Wind and Seismic Effects, Task Committee D

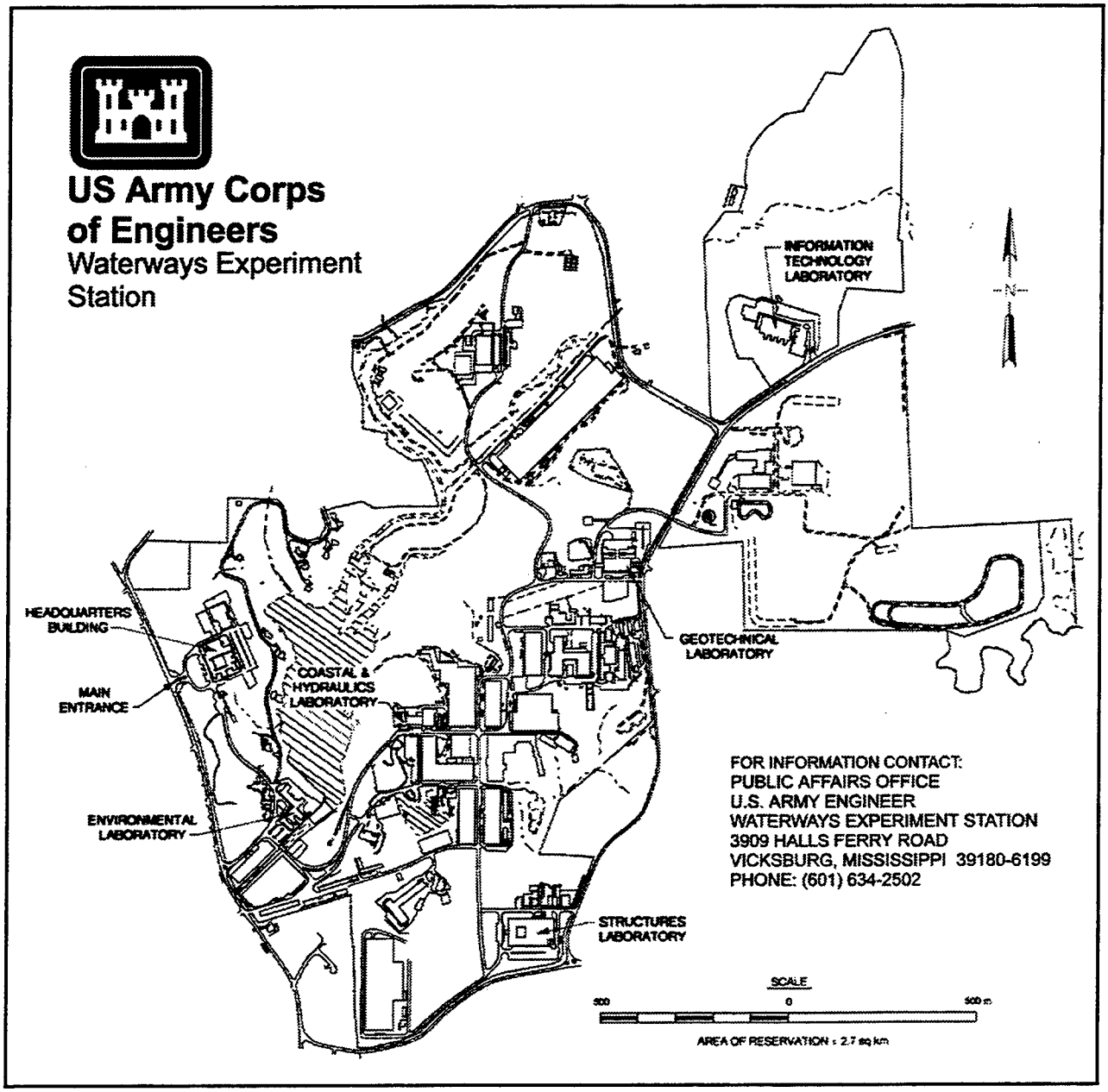

Waterways Experiment Station Cataloging-in-Publication Data

U.S.-Japan Workshop on Advanced Research on Earthquake Engineering for Dams (1st : 1996 : Vicksburg, Miss.)

First U.S.-Japan Workshop on Advanced Research on Earthquake Engineering for Dams, 12-14 November 1996 / by Mary E. Hynes ... [et al.] ; prepared for U.S.-Japan Cooperative Program in Natural Resources (UJNR), Panel on Wind and Seismic Effects, Task Committee D.

388 p. : ill. ; 28 cm. -- (Miscellaneous paper ; GL-98-1)

Includes bibliographic references.

1. Earthquake engineering -- Research -- Congresses. 2. Roller compacted concrete. 3. Concrete dams. 4. Earth dams. I. Hynes, Mary Ellen. II. United States. Army. Corps of Engineer. III. U.S. Army Engineer Waterways Experiment Station. IV. Geotechnical Laboratory (U.S. Army Engineer Waterways Experiment Station) V. United States-Japan Cooperative Program in Natural Resources. Panel on Wind and Seismic Effects. Task Committee D. VI. Title. VII. Title: U.S.-Japan Workshop on Advanced Research on Earthquake Engineering for Dams, 12-14 November 1996. VIII. Series: Miscellaneous paper (U.S. Army Engineer Waterways Experiment Station) ; GL-98-1.

TA7 W34m no.GL-98-1

Contents

Concrete Dams and Outlet Works

Preface

This report summarizes a workshop conducted by the U.S. Army Engineer Waterways Experiment Station (WES) and the Public Works Research Institute of Japan (PWRI) under the auspices of Task Committee D, "Earthquake Engineering for Dams," of the UJNR Panel on Wind and Seismic Effects, in Vicksburg, MS, 12-14 November 1996.

Dr. Mary Ellen Hynes, Earthquake Engineering and Geosciences Division (EEGD), Geotechnical Laboratory (GL), Dr. Robert Hall, Structures Laboratory, and Dr. Yoshikazu Yamaguchi, PWRI, coordinated and conducted the workshop. Mrs. Wipawi Vanadit-Ellis was indispensable during the planning and conduct of the workshop. Mrs. Julia C. Baker ably assisted in the completion of these proceedings by consolidating and organizing the presentation material.

Overall direction at WES for this report was provided by Dr. Lillian D. Wakeley, Acting Chief, EEGD, and Dr. William F. Marcuson III, Director, GL.

At the time of publication of this report, Director of WES was Dr. Robert W. Whalin. Commander was COL Robin R. Cababa, EN.

Workshop Participants

Dr. Robert Whalin
Dr. William Roper
Dr. A. G. Franklin
Dr. Richard Olsen
Dr. Scott Steedman
Mr. Lucian Guthrie
Dr. Robert Hall
Dr. Joseph Koester
Mr. John Nickell
Mr. Francke Walberg
Mr. Vlad Perlea
Dr. Ellis Krinitzsky
Dr. Mary E. Hynes
Ms. Wipawi Vanadit-Ellis
Ms. Wanda Cameron
Mr. Donald Yule
Mr. Richard Ledbetter
Mr. Kenneth Klaus
Mr. Robert Fleming
Mr. Sam Stacy
Dr. John Peters
Mr. Richard Dove
Dr. Robert Ebeling
Dr. Luis De Bejar
Dr. Ashok Chugh
Mr. Dave Hinchliff
Mr. Hitoshi Yoshida
Mr. Tadahiko Sakamoto
Dr. Yoshikazu Yamaguchi
Dr. Choshiro Tamura
Dr. Yoshio Ohne
Mr. Tadahiko Fujisawa
Mr. Atsushi Suzuki
Mr. Tomoya Iwashita
Mr. Nobuyuki Shirakawa
Mr. Isao Nagayama
Mr. Takashi Sasaki

Agenda

First U.S.-Japan Workshop on Advanced Research on Earthquake Engineering for Dams, Task Committee on Dams, U.S.-Japan Panel on Wind and Seismic Effects

12-14 November 1996--Workshop
U.S. Army Engineer Waterways Experiment Station (WES), Vicksburg, MS
POC: Mary E. Hynes, WES

15 November 1996--Field Trip to USAE Dam Projects in northwestern Mississippi
U.S. Army Engineer District, Vicksburg (LMK)
POC: Wayne Forrest (LMK)

11 November 1996

1400-1600	Information Distribution, Harrah's Hotel Lobby Wipawi Vanadit-Ellis and Wanda Cameron, WES
1800-2000	Reception, home of Mary E. Hynes, WES

12 November 1996

0800-0830	Convene Workshop. Introductions. William Roper and Hitoshi Yoshida U.S.-side and Japan-side Chairmen of the Task Committee on Dams
0830-0900	Opening Addresses Robert Whalin and Tadahiko Sakamoto Director, WES, and Director General, PWRI
0900-0915	Relate Workshop Logistics Mary E. Hynes and Yoshikazu Yamaguchi U.S.-side and Japan-side Workshop Organizers

Keynote Lectures
Chair: Gus Franklin, WES
Time Keeper: Joseph Koester, WES

0915-1015 Introduction: Hitoshi Yoshida
Keynote Lecture, Professor Choshiro Tamura
Professor of Nippon University
Honorable Professor, University of Tokyo, Japan

1015-1030 Tea and Coffee Break

1030-1130 Introduction: William Roper
Keynote Lecture, Dr. Ellis Krinitzsky
WES, United States

1130-1230 Introduction: Hitoshi Yoshida
Keynote Lecture, Professor Yoshio Ohne
Professor of Aichi Institute of Technology, Japan

1230-1245 Three-screen Briefing

1245-1300 Tour of Geotechnical Laboratory

1300-1400 Lunch

Overview Presentations
Chair: Frank McLean, USBR
Time Keeper: Donald Yule

1400-1445 Present Condition of Multi-Purpose Dam Projects and Related Technology Development in Japan, Tadahiko Fujisawa, PWRI

1445-1530 U.S. Army Corps of Engineers Civil Works Earthquake Engineering Research Program, Mary E. Hynes and Robert Hall, WES

1530-1545 Tea and Coffee Break

1545-1630 Characteristics of Hyogoken Nanbu Earthquake Motions, Atushi Susuki, Japan Institute for Construction Engineering (JICE)

1630-1715 Effects on Dams, Norihisa Mtsumoto, Akira Nakamura, Takashi Sasaki, and Tomoya Iwashita, PWRI

Embankment Dams and Site Characterization
Chair: Gus Franklin, WES
Time Keeper: Wanda Cameron, WES

1715-1800 Geophysical Methods for Site Characterization and Measurement of In Situ Properties, Robert F. Ballard, Jr., WES

1800-1815 Announcements and Recess

1815 Adjourn Day 1

1815-2000 Traditional "Thanksgiving" Dinner, Home of Robert Hall, WES

13 November, 1996

0800-0815 Announcements

Embankment Dams and Site Characterization I (continued)
Chair: Mary E. Hynes, WES
Time Keeper: Wanda Cameron

0815-0900 Becker Penetration Testing of Gravelly Soils, Joseph P. Koester, WES

0900-0945 Safety Estimation of Rockfill Dams During Major Earthquakes, Tadahiko Sakamoto, Tadahiko Fujisawa, Akira Nakamura, Hitoshi Yoshida, Tomoya Iwashita, PWRI

0945-1030 Newmark Sliding Block Analysis, Joseph P. Koester, WES

1030-1045 Tea and Coffee Break

1045-1145 Behavior of Liquefying Soils, Richard Ledbetter, WES

1145-1300 Lunch

1300-1400 Tour of WES Centrifuge Facility

Embankment Dams and Site Characterization (continued)
Chair: Hitoshi Yoshida, PWRI
Time Keeper: Tomoya Iwashita, PWRI

1400-1445 Evaluation of Shear Strength of Rockfill Materials Considering the Effect of Confining Pressure, Hitoshi Yoshida, Mitsuo Toyoda, Yoshikazu Yamaguchi, PWRI

1445-1530	The Influence of Confining Stress on Liquefaction Resistance, Richard Olsen, WES
1530-1545	Tea and Coffee Break
1545-1630	Dynamic Response Analysis of Rockfill Dams Considering Frequency Dependent Characteristics of Radiation Damping Ration, Hitoshi Yoshida, Tomoya Iwashita, PWRI
1630-1715	Design Requirements for Computer Program to Analyze Large Seismically Induced Deformations, John F. Peters, WES
1715-1730	Announcements and Recess
1730	Adjourn Day 2

<u>14 November 1996</u>

0800-0815	Announcements
	Embankment Dams and Site Characterization (continued) Chair: Hitoshi Yoshida, PWRI Time Keeper: Yoshikazu Yamaguchi, PWRI
0815-0900	Dynamic Analysis of the Tokuyama Dam (Rockfill Dam), Mituaki Mizuno, Kazuo Harita, Hisashi Tachibana, Yoshiro Iida, Nobuyuki Shirakawa, Water Resources Development Public Corporation (WARDEC)
	Concrete Dams and Outlet Works Chair: Lucian Guthrie, Corps of Engineers Civil Works Time Keeper: Richard Dove, WES
0900-0945	Evaluation of Safety of Concrete Gravity Dams During the Hyogoken-Nambu Earthquake, Tadahiko Sakamoto, Tadahiko Fujisawa, Isao Nagayama, Takashi Sasaki, PWRI
0945-1030	Large Scale Vibration Experiments, Robert Hall, WES
1030-1045	Tea and Coffee Break
1045-1130	Effects of Vertical Seismic Motion on Structural Stability of Concrete Gravity Dams, Isao Nagayama and Takashi Sasaki, PWRI
1130-1215	Subbottom Absorption Coefficients for Seismic Analysis of Concrete Dams, Luis Armando De Béjar, WES

1215-1315	Lunch
1315-1400	Tour of Structures Laboratory
	Concrete Dams and Outlet Works (continued) Chair: Isao Nagayama, PWRI Time Keeper: Takashi Sasaki, PWRI
1400-1445	Numerical Model Development for Seismic Analysis of Concrete Dams, Luis Armando de Béjar, WES
1445-1530	Time-Domain, Nonlinear Dynamic Analysis of Concrete Dams, Tommy Bevins, Robert Ebeling, WES
1530-1545	Tea and Coffee Break
1545-1630	Seismic Behavior of Ground and Main Structure of Nagaragawa Estuary Barrage, Katusya Taguchi, Toshiki Kawakami, Yokito Sugimura, Ken-ichi Fujita, Nobuyuki Shirakawa, WARDEC
1630-1715	Preliminary Results of Initial Intake Tower Substructure Experimentation, Richard C. Dove, WES
1715-1800	Workshop Closure. Announcement and Adoption of Resolutions. Tadahiko Sakamoto, Director General, PWRI William Roper and Hitoshi Yoshida U.S.- and Japan-side Chairmen of the Task Committee on Dams
1800	Adjourn Day 3
1830-2030	Celebration Dinner, Ameristar Casino

15 November 1996

0700-2100	Field trip to U.S. Army Corps of Engineers dam projects in northwestern Mississippi, courtesy of the Vicksburg District. POC: Wayne Forrest, CELMK

16 November 1996

After-action meeting to plan next workshop

Resolutions

RESOLUTIONS OF THE FIRST U.S.-JAPAN WORKSHOP
ON ADVANCED RESEARCH ON
EARTHQUAKE ENGINEERING FOR DAMS

U.S. Army Engineer Waterways Experiment Station
Vicksburg, MS, USA
November 12-14, 1996

The First U.S.-Japan Workshop on Advanced Research on Earthquake Engineering for Dams was held under the sponsorship of the U.S. Army Engineer Waterways Experiment Station and the Public Works Research Institute of Japan under the auspices of Task Committee D, "Earthquake Engineering for Dams," the UJNR Panel on Wind and Seismic Effects at the U.S. Army Engineer Waterways Experiment Station, Vicksburg, November 12-14, 1996.

The workshop provided a valuable forum to exchange technical information of earthquake engineering for dams in both countries. The workshop was attended by 11 Japanese participants, 26 U.S. participants, and one visitor from the U.K.

The following resolutions were adopted by the workshop participants:

1. The workshop identified, without priority order, the following topics relevant to dam earthquake engineering for the further cooperative research program:

   a. Methods of analysis for seismic design of dams, including outlet works;

   b. Dynamic characteristics of dam construction materials and site conditions;

   c. Analysis of observed behavior of dams and outlet works during an earthquake.

2. The workshop recognizes the importance of continued exchange of research personnel, technical information, research data, and use of available research facilities in both countries.

3. In view of the importance of cooperative research programs on earthquake engineering for dams, it is recommended to hold the second Workshop in about two years in Japan. The location and time of the workshop will be determined through correspondence between the chairs of Task Committee D of the UJNR Panel on Wind and Seismic Effects.

Summary

SUMMARY OF THE FIRST U.S.-JAPAN WORKSHOP
ON ADVANCED RESEARCH ON
EARTHQUAKE ENGINEERING FOR DAMS

The First U.S.-Japan Workshop on Advanced Research on Earthquake Engineering for Dams was held under the sponsorship of the U.S. Army Engineer Waterways Experiment Station and the Public Works Research Institute of Japan (PWRI) under the auspices of Task Committee D, "Earthquake Engineering for Dams," of the UJNR Panel on Wind and Seismic Effects, in Vicksburg, Mississippi, 12-14 November 1996. The workshop provided a valuable forum to exchange technical information on earthquake engineering for dams in both countries. The workshop was attended by 11 Japanese participants, 26 U.S. participants, and 1 visitor from the U.K. Four agencies and two universities were represented in the Japanese delegation; PWRI, Japan Institute for Construction Engineering, Water Resources Development Public Corporation, Nippon University and Aichi Institute of Technology, all of Japan. The U.S. participants were drawn from the U.S. Army Corps of Engineers (Headquarters USACE, Waterways Experiment Station (WES), Vicksburg District, Kansas City District, and Sacramento District), and the U.S. Bureau of Reclamation. Dr. Scott Steedman, visiting WES from the U.K., attended a portion of the program.

Dr. William Roper (HQUSACE) and Mr. Hitoshi Yoshida (PWRI), the U.S.-side and Japan-side chairs of Task Committee D, convened the workshop and introduced the participants. Dr. Robert Whalin, Director of WES, and Mr. Tadahiko Sakamoto, Director General (recently retired) of PWRI, encouraged a high level of communication and excellence, motivating all the workshop participants. Dr. M.E. Hynes, WES, and Dr. Yoshikazu Yamaguchi, PWRI, were the U.S-side and Japan-side organizers of the workshop. We were fortunate to have three distinguished keynote speakers. The keynote address by Professor Choshiro Tamura, Nippon University, provided new insights to ground motions observed in Japan. Professor Yoshio Ohne, Aichi Institute of Technology, related the results of a number of large-scale shaking table experiments on earthfill and rockfill embankments, which provided new insights on mechanisms of failure for these structures. Dr. Ellis Krinitzsky gave a thought provoking talk on deterministic and probabilistic methods for selecting design level earthquake ground motions.

In addition to the 3 keynote talks, 21 technical papers were presented. The topics provided a background understanding of the types of field conditions and

design problems that engineers face in the U.S. and Japan, and a wide range of approaches for solving these problems. The types of dams discussed included earthfill, rockfill, concrete and roller-compacted concrete structures. The technical presentations triggered lively discussions on material properties and methods of analysis. In the U.S., dam engineers are primarily dealing with the seismic performance of existing dams, most of which were built when earthquake engineering was in its infancy and seismic hazards were neither recognized nor understood. Consequently, U.S. dam engineers deal with large levels of ground motions, potential liquefaction, and large deformations in embankment dams, and potential cracking and damage to concrete dams and outlet works. In Japan, the seismic hazard appears to result in levels of ground motions for design that are less than in the U.S.; the dams are well built, primarily on rock foundations; and liquefaction and deformation for embankment dams and cracking of concrete dams are not issues. The seismic design focus in Japan appears to be primarily on new dams. The presentations by the Japanese delegates also provided a wealth of empirical data, observations of response and performance of their dams during large earthquakes, and insightful analyses of measured response compared with computed response.

In addition to the technical program, the participants enjoyed Vicksburg hospitality--two informal golf tournaments, shopping, banquets, and a tour of the Vicksburg National Military Park. Following the workshop, the Vicksburg District arranged a field trip to visit Sardis and Enid Dams, located in northwestern Mississippi. Sardis Dam, a hydraulic fill dam, was recently remediated to improve its performance during a potential repeat of the 1811-1812 earthquake events. Both Sardis and Enid Dams have potentially liquefiable fine-grained materials in their foundation deposits. Sardis Dam was remediated with an innovative approach, namely nailing the dam in place with 2-ft square, reinforced concrete piles. The seismic performance of Enid Dam, a well-compacted rolled-fill embankment dam, is still under study. The field trip itinerary traversed most of the Mississippi Delta, and provided the participants an opportunity to view numerous catfish farms and cotton fields en route. Dr. Yamaguchi communicated that the Japanese delegation returned safely to Japan and truly enjoyed a successful workshop and the after-hours activities.

DAMS AND EARTHQUAKE MOTION

by
Choshiro TAMURA*

1. Introduction

The Hyogo-ken Nanbu Earthquake of 1995 damaged almost all structures in the epicentral region and in surrounding regions shaken by violent seismic vibrations. In Japan, when it was recognized that dams suffered no genuine damage, the statement that there was deformation was made frequently. Many dams with height of 15m or over are constructed in the vicinity of the epicenter, including some located close to faults, but it has been concluded that the only effects of the earthquake on these dams was deformation.

It appears that in the world many large dams have been subjected to strong earthquake motion in the past about 30 years. Principal reasons for this which can be cited include world wide development accompanied by the construction of many dams and the high frequency of earthquake activity. But it is also possible to conclude that except in a few exceptional cases, recently constructed dams have been almost proved free of damage serious enough to compromise dam body stability, even when located close to the epicenter of an earthquake. With the powerful support of science and technology, we have gained an clear understanding of the actual behavior of dams during earthquakes, but it is still important to study issues that bear on the earthquake resistant strength of dams in order to establish rational earthquake resistant design methods. This report is focussed primarily on earthquake motion that acts upon dams.

2. The Hyogo-ken Nanbu Earthquake

The first thing to consider is the effect of the interval between earthquakes. The Hyogo-ken Nanbu Earthquake of 1995 occurred in the Kansai Region, an area of Japan where there has been little earthquake activity in this 100~150 years, and in part of the concerned region where there has not been an earthquake for 1,100 or more years. Not only that, it was caused by a fault with an activity level of B (average displacement speed of between 0.1 m $\leqq$ $\sim$<1.0 m every 1,000 years) which, according to a study, was active about 2,000 years ago. This was a phenomena which was, under present conditions, very difficult to predict. Although it is assumed that an existing state of earthquake activity is not likely to continue unchanged, on the other hand it is usually not clear when activity will resume.

This earthquake was to some degree forecast by seismologists, and the region was included in those where observations were to be upgraded. Although we say "foreseen," under present circumstances, "foreseen" means within a range of hundreds of years to this type of faults, so dam designers have to consider ways to prepare to deal with the occurrence of earthquakes of this scale.

Figure 1 shows the location of active faults close to Kobe. The earthquake fault in this case was the Nojima Fault in the northern part of Awaji Island. The fault line of this fault slipped slightly to the east at its northern end, and beyond this point, faults in the Rokko Fault system were active. Although many faults run parallel, not one earthquake

*Prof.of Nihon University,
Prof.Emeritus of University of Tokyo,
Tokyo,Japan

had occurred in recent years. In Japan, it is estimated that an active fault with an activity level of B will be active at intervals of several thousand years. This is an extremely long interval
not only in comparison with the length of human life, but quite long when compared with the lifetime of a dam. When an earthquake does not occur in a region for a long time, we are usually prone to be unprepared.

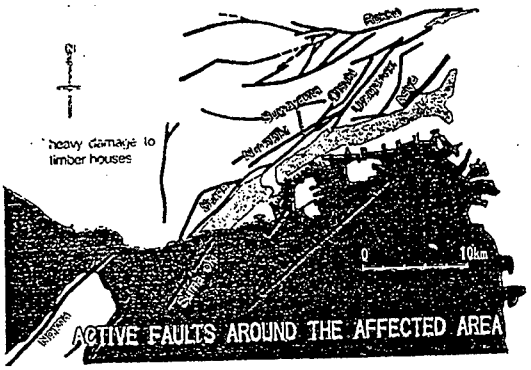

Fig. 1 Heavily suffered area and active faults (by. courtesy of J. S. C. E.)

The next topic is the earthquake motion. The strength of earthquake motion is usually evaluated as so-called seismic intensity. A belt-shaped zone where the seismic intensity ranged from VI to VII (JMA) extended across Kobe and surrounding cities. Accelerations higher than 600 gal were concentrated in this region. A study of the relationship between this zone and the location of faults indicates that earthquake motion was not necessarily strong near these faults. A number of research projects have been carried out in order to find out why strong earthquake motion occurred in this zone which extends almost parallel to the faults but is not necessarily close to the faults. One theory suggests that because the slope of a mainly granite mountain range (Rokko Mountains) which runs parallel to the ocean near the seashore is inclined steeply towards the ocean and is covered with a thick stratum of diluvium under a surface stratum of alluvial deposits, interference was generated during the earthquake motion propagation process, amplifying the earthquake motion. Another theory suggests that because the ground in this zone is terrace soil, although the ground shook violently, unable to attenuate the motion, it was amplified. The third one is the concept that there is a new fault directly under the extremely high seismic intensity VII parts of the disaster area. The author supposes that this reflects the dynamic properties of the surface stratum of the ground.

3. Overview of Dam Behavior During the Hyogo-ken Nanbu Earthquake

This section provides an overview of the behavior of dams during the Hyogo-ken Nanbu Earthquake.

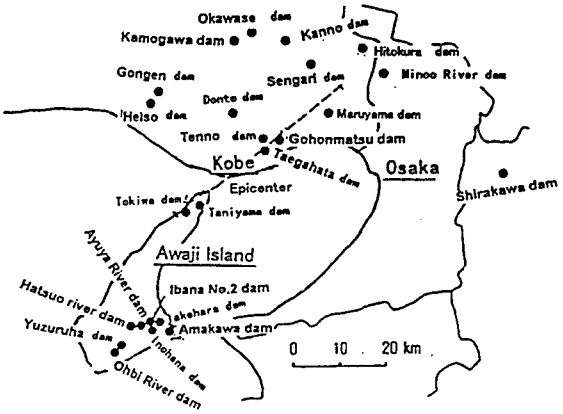

Fig. 2 Dam site in Epicentral Area and at the adjacent Area

Figure 2, which has been refered to a report by the Committee on Earthquake Resistance of Dams, Ministry of construction, Japan, shows the faults and the locations of dam near the faults (● symbol), and reveals that many dams are constructed extremely close to the faults. The earthquake caused deformation in three of them. The earthquake motion was recorded at the Hitokura Dam (concrete gravity dam, height of 75.0 m, 1983) and the Minoo River Dam (rockfill dam, height of 47.0 m, 1982) which are approximately 10 km east of the eastern end of the hypocentral fault.

Fig. 3 Acceleration Recorded at Hitokura Dam, Hyogoken-Nanbu Earthquake of Jan. 17. 1995

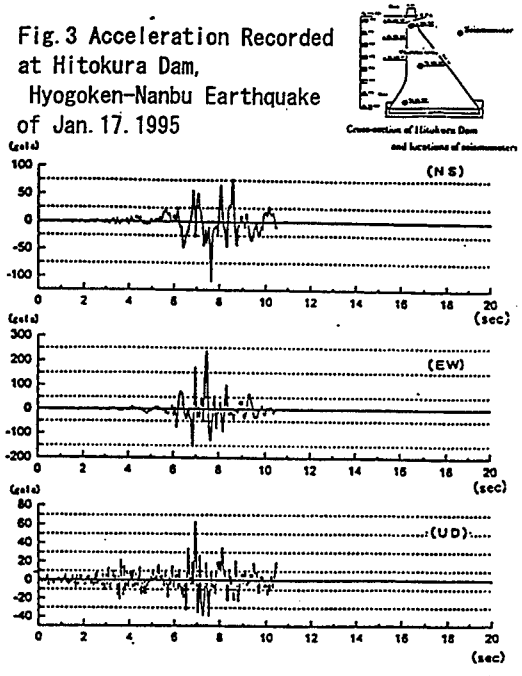

Fig. 4 Acceleration Recorded at Minoo River Dam, Hyogoken-Nanbu Earthquake ofJan. 17, 1995

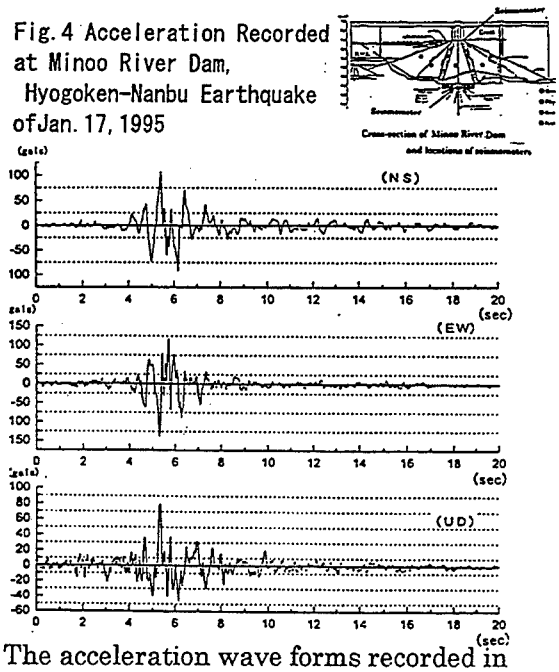

The acceleration wave forms recorded in the bottom galleries of these two dams have a maximum value in the upstream-downstream direction of 183 gal and 128 gal respectively.

These acceleration values are high values considering at the bed rock. But as will be explained below, when corresponding to the earthquake magnitude, this value is not a particularly high value compared with those obtained in the case of past earthquakes. It is estimated that the earthquake motion in the rock at dam sites near the faults had a maximum acceleration of about 200 gal.

At the Tokiwa Dam (earth dam,height: 33.5 m, completed in 1974) about 700 m from the fault, lateral cracks with a length of approximately 5 m and a width ranging from 2 to 3 mm were formed in the dam crest paving on the left and right bank wings of the dam. At the Taniyama Dam (earth dam, height: 28.2 m, completed in 1974) about 2 km from the fault, lateral cracks with a length of approximately 5 m and a width ranging from 2 to 3 mm were formed on the crest paving of the dam. At the Yuduruha Dam (concrete gravity dam, height: 42 m, completed in 1974) 25 km from the fault, the damage was limited to the separation of part of the finishing mortar on the downstream side. At the Hitokura Dam, small collapses occurred at two locations on the lake shore side.

4. Earthquake Motion Near the Epicenter

The Koyna Earthquake (magnitude 7.0), which occurred about 200 km south south-east of Bombay in India in 1967, damaged the Koyna Dam, a concrete

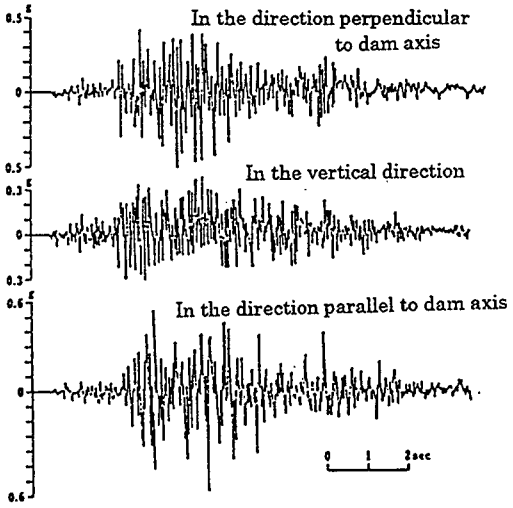

Fig. 5 Acceleration records observed at Koyna Dam (Earthquake of Dec. 11, 1967)

gravity dam with reservoir capacity of 2.8 billion tons, a height of 103 m, and a dam crest length of 853 m located a few kilometers from the epicenter. Water leaked through horizontal cracks in the upstream-downstream direction of the dam body. The design seismic coefficent of this dam is 0.05. A seismometer installed in the dam recorded this earthquake motion.The seismometer was installed in the observation gallery at 10 m high from the bed rock of the block with a height of 31m on the left bank side. The maximum acceleration was 664 gal in the dam axis direction, 511 gal in the direction at right angles to the dam axis, and 862 gal in the vertical direction, and when the block is handled as a two-dimensional structure and the acceleration measured accounting for its dynamic properties is converted to the acceleration of the bed rock location, the acceleration was about 320 gal at right angles to the dam axis. These facts indicate that the dam was subjected to earthquake motion with an fairly extremely high acceleration.

Dams in the epicentral region were damaged during the San Fernando Earthquake (1971, magnitude: 6.6). With a hypocenter depth of 14 km, this earthquake severely damaged nearby bridges, dams, underground water tanks,electric equipments, reinforced concrete hospital buildings, and other structures. A seismometer installed in the top of the ridge on the left bank of the Pacoima Dam standing in the center of the epicentral region recorded a maximum acceleration of 1,250 gal in the horizontal direction. The concrete foundation on which this seismometer was installed was cracked, and a nearby escarpment collapsed. It is assumed that these conditions and the topography influenced the acceleration. The after shocks were recorded and the earthquake motions at the valley bottom and the ridge were compared. The results show that while it was, of course, not an earthquake as strong as this one, in some cases the acceleration at the ridge was amplified from 4 to 5 times of those at the valley bottom depending on the frequency. Other dams around the epicentral region include the severely damaged San Fernando Lower Dam, the San Fernando Upper Dam which was also damaged seriously, and the Bypass Dam which was completely undamaged. Seismographs were installed in the crest and left bank at the San Fernando Lower Dam, but the former was sunk and the latter overshot its scale. According to Dr.

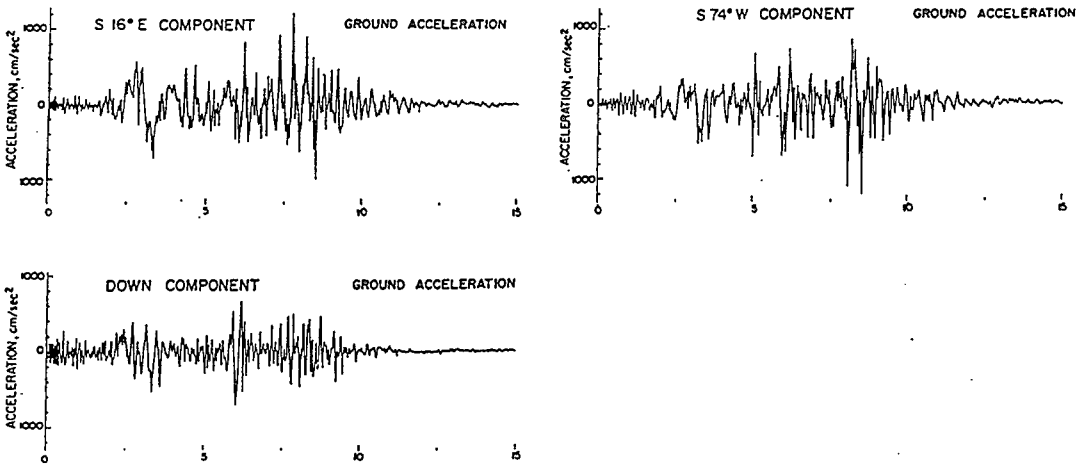

Fig.6 Acceleration records at the Pacoima Dam, San Fernando Earthquake of Feb,9,1971

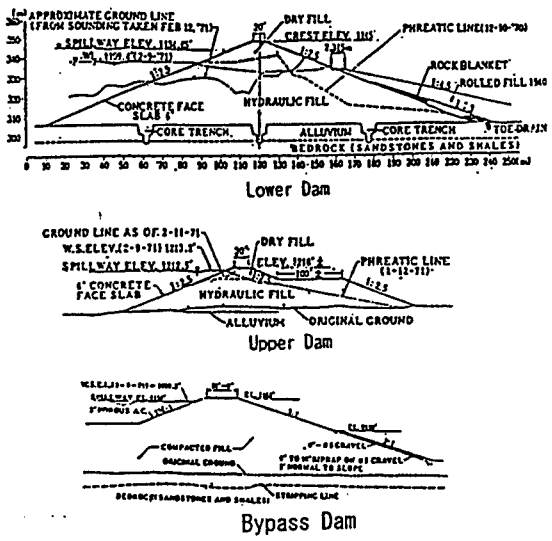

Fig. 7 Cross-section of San Fernando-Lower and -Upper Dams and of Bypass Dam

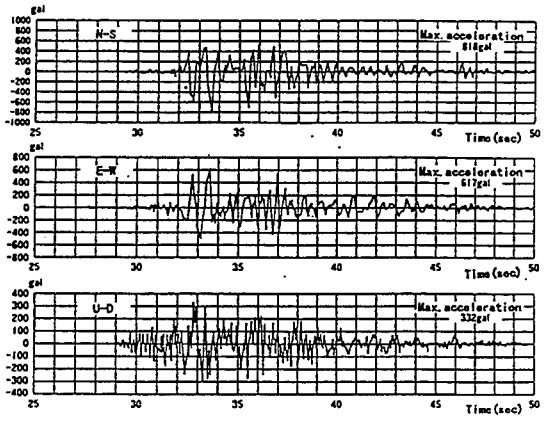

Fig. 8 Acceleration record on the soil ground at Kobe Marine Observatory

Housner, it is assumed that it might have been earthquake motion with a maximum acceleration between 350 and 400 gal.

Returning to the Hyogo-ken Nanbu Earthquake, the highest acceleration recorded on the ground level at the Kobe Marine Observatory was 818 gal. The wave forms reveals that high acceleration earthquake motion continued for several seconds then abruptly ended. The response spectrum curve shown in Figure 10 demonstrates that the response velocity of a structure with natural period of 0.5 seconds and damping coefficient of 5%, is about

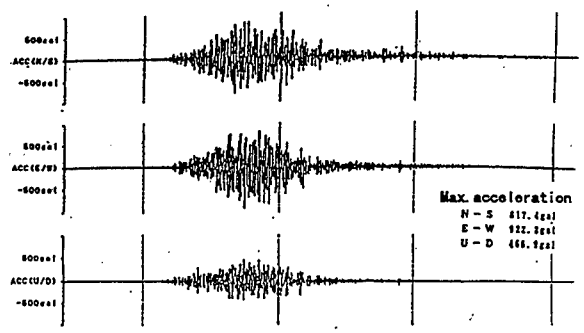

Fig. 9 Acceleration record at Kushiro Meteorological Observatory, 1993 Kushiro-oki Earthquake Jan. 15, 1993

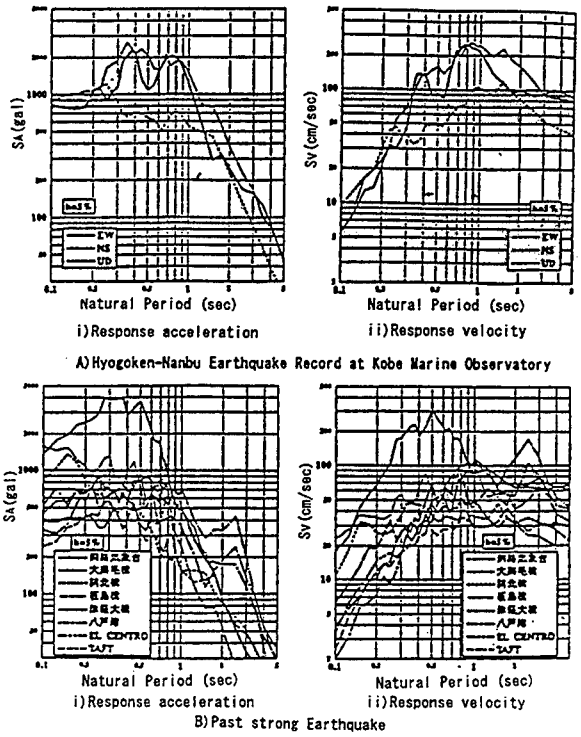

Fig. 10 Response spectrum of strong earthquake motion

90 cm/second to the south-east component acceleration wave form recorded at the KobeMarine Observatory.

Like the spectrum of the Kushiro-Oki Earthquake of 1993, it is extremely large. The earthquakes shown here are well-known powerful earthquakes, but it is correct to say that the Hyogo-ken Nanbu Earthquake was particularly powerful at ground level.

The hypocentral depth of the Kushiro-Oki Earthquake of 1993 (magnitude 7.8) was particularly deep at 107 km. During

this earthquake, a maximum acceleration of 922 gal was recorded on the ground level at the Kushiro Local Meteorological Observatory. But no records were obtained from the bed rock. Serious damage was also caused by the Northridge Earthquake in California, a magnitude 6.8 earthquake which occurred exactly one year before the Hyogo-ken Nanbu Earthquake. The response spectrum of the wave form recorded in the ground at Sylmer near the epicentral region is very similar to the spectrum of the Kobe Marine Observatory records mentioned above.

Figure 12 shows the relationship of the maximum acceleration with the distance from the center of the epicentral region during the Miyagi-ken Oki Earthquake of 1978. The axis of abscissa represents the distance and the axis of ordinates represents the maximum acceleration.

In this figure, a straight line is drawn with M (magnitude) as the parameter, but this requires a little explanation. This is a regression line which indicates the relationship between the epicentral distances or the distances from the center of the epicentral area and the maximum accelerations at the rock ground using the magnitude as the parameter. The acceletion wave forms were recorded at the Sannokai Dam in Iwate Prefecture in the Tohoku Region since 1963 and at an underground power plant in Tochigi Prefecture in the Kanto Region since the same year. Needless to say, it is an empirical formula represented as shown below.

$$\mathrm{Log}(\alpha/1000)=((\Delta+50)/100)(-4.93+0.89M-0.043M^2)$$

Where: α: maximum acceleration (gal).
Δ: Distance (km)
M: Magnitude (M_S)

The symbol ○ in the figure represents the ordinary ground soil, while the symbol x represents the maximum accelerations recorded either in the base of the dam or in the bed rock of the dam

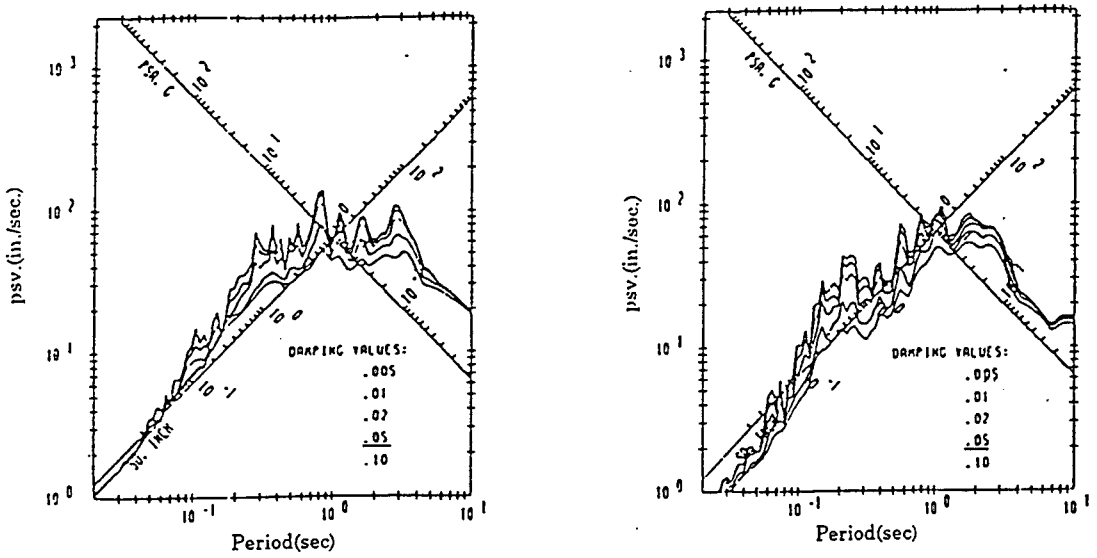

Response spectra of NS direction

Response spectra of EW direction

Fig. 11 Response spectra of the 1994 Northridge earthquake motions at the Sylmar Converter Station

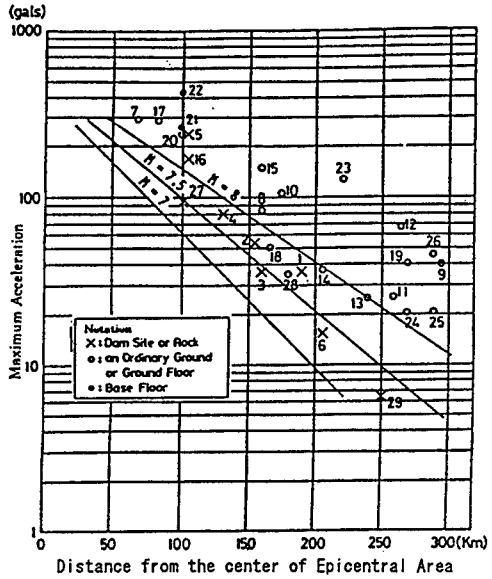

Fig. 12 Max. Acceleration and Distance from Epicentral Area, Miyagi-Ken Oki Earthquake, June 12, 1978 (M=7.4)

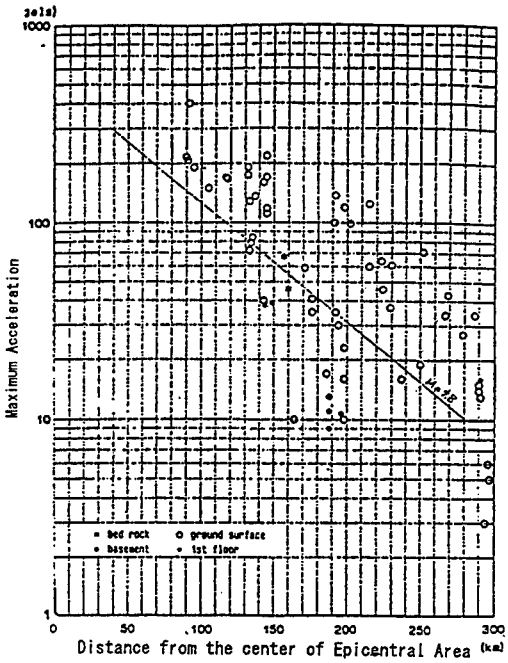

Fig. 13 Max. Acceleration and Distance from the center of Epicentral Area, Hokkaido Nansei-oki Earthquake July. 12, 1933

site. Among many maximum acceleration values, the values for dam sites are aligned at the bottom of this group and the magnitude of the earthquake was 7.4; these two facts indicate that it conforms closely to the regression line.

It is noteworthy that among the group of maximum accelerations, the maximum accelerations obtained in rock or foundations at dam sites are aligned at the bottom. But while these is one large value numbered as 5 in the Figure, this is a large spike value in the wave form at Tarumizu Dam. Generally, the acceleration of earthquake motion varies substantially between ordinary soil ground and rock ground, and according to circumstances, this gap varies considerably by 4 or 5 times.

Figure 13 shows the case of the Hokkaido Nansei-Oki Earthquake of 1993 (magnitude: 7.8). The symbol * indicates the value in rock in the Seikan Tunnel(under sea tunnel). It conforms extremely closely to the values observed from the straight line referred to above. While there is a group of low values between 160~200 km in distance, separated from the straight line, these were all obtained at a measurement point near the City of Sapporo in Hokkaido, and it is assumed that ground conditions at that point differ widely from those at other observation locations.

Figure 14 shows the case of the Nihonkai Chubu Earthquake of 1983 (M=7.7), clearly revealing similar characteristics.

Figure 15 shows values obtained during a 1978 Izu Oshima-kinkai Earthquake (magnitude: 7.0), with the symbol x in the figure representing values obtained in rock. This case clearly does not conform to the epicentral distance - maximum acceleration relationship cited above. It is evident that greater distance sharply increases the attenuation of the maximum acceleration, but the reasons for this are not well understood. This trend is conspicuous in the case of a magnitude 6 earthquake which occurred in Yamanashi Prefecture. It is assumed that this is a result of regional characteristics.

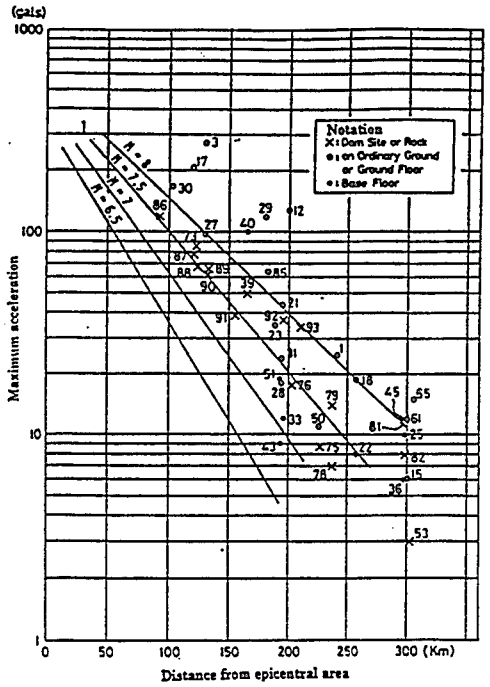

Fig. 14 Max. Acceleration and distance from center of epicentral area, Nihonkai-Chubu Earthquake, May. 26, 1983

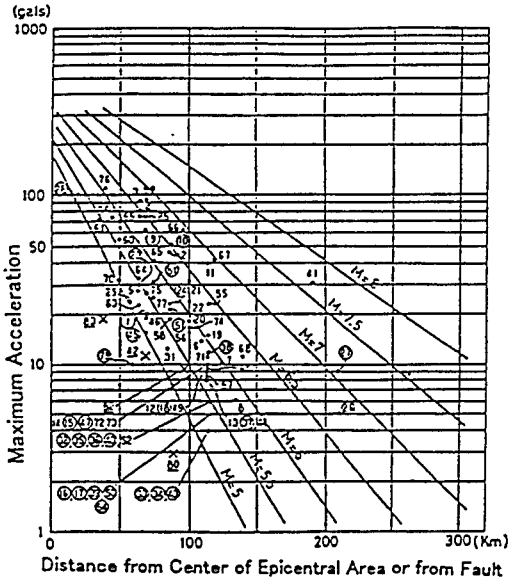

Fig. 15 Maximum Acceleration and Distance from the center of Epicentral Area or from Fault of Izu-Oshima Kinkai Earthquake, Jan. 14, 1978 (M=7.0)

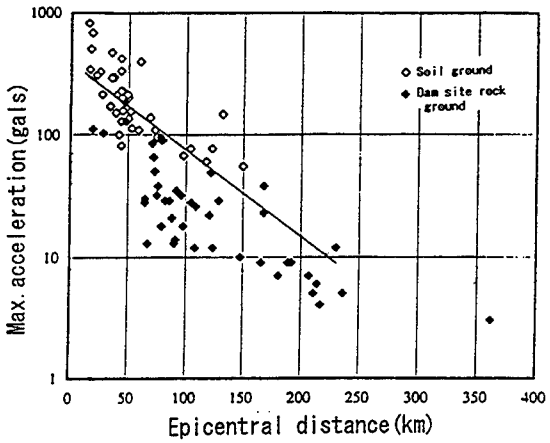

Fig 16 Max. accleration and epicentral distance, Hyogoken-Nanbu Earthquake of Jan. 17, 1995

What about the Hyogo-ken Nanbu Earthquake? Figure 16 was prepared by the Public Works Research Institute of the Ministry of Construction, Japan. The maximum accelerations are the higher of the values in two horizontal directions, and the epicenter is assumed to be in the northern part of Awaji Island. The ◆ symbols represent dam sites while the ◇ represent ordinary soil ground. The figure clearly shows the characteristics described above.

Near the active faults it is possible that the characteristics vary according to the place where the distance was measured from. Figure 17 is a case where the distance was measured from the hypocenter fault instead of the location of the epicenter. It only shows the maximum acceleration obtained at dam sites. This figure allows us to conclude that while this earthquake generated extremely powerful earthquake motion in the ordinary soil ground, judging from the maximum acceleration at the rock, it was not a particularly powerful earthquake. The maximum acceleration - distance relationship described above appears to apply in this case. In the bed rock, the earthquake motion was very low in comparison with that in ordinary soil ground.

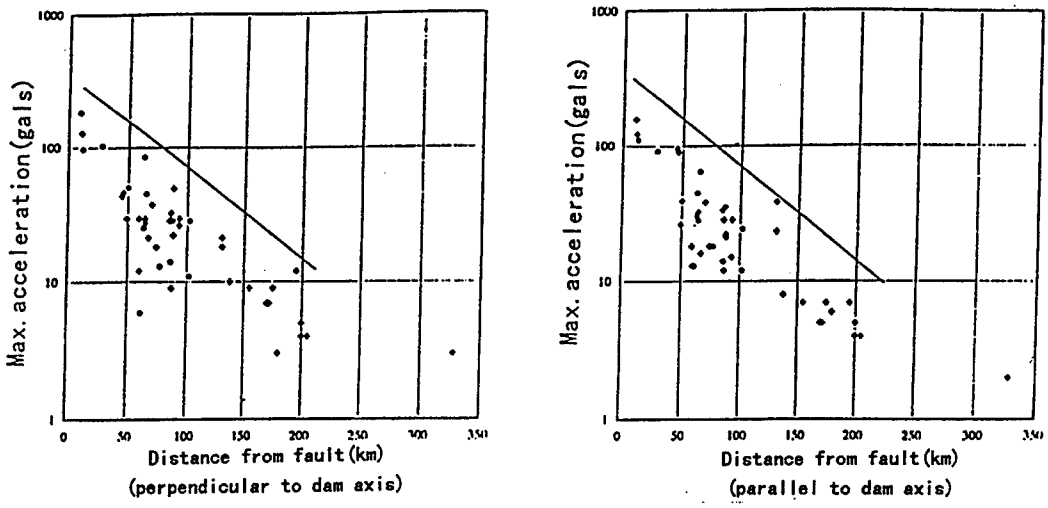

Fig. 17 Maximum acceleration and distance from fault, Hyogoken-Nanbu Earthquake of Jan. 17, 1995

Judging from this, one reason the dams were spared damage seems to be the fact that the earthquake motion in the rock at the dam sites was ordinary strength earthquake motion for rock.

This shows that the concept that dam foundations must be hard rock was a suitable conclusion from the point of view of the earthquake resistance of dams.

5.Behavior of Dams Near the Epicenter

This section describes the behavior of dams subjected to violent earthquake motion close to the active faults.

5.1 Koyna Earthquake

The Koyna Dam referred to in the previous chapter of this report is a concrete gravity dam with a dam height of 103 m,853m in length, a reservoir capacity of 2.8 billion tons, and its reservoir was almost full at the time of the earthquake. The wall tiles of the crane tower at the crest of the dam were knocked down during the earthquake, the remaining wall tiles were lowered. An analysis carried out by Dr. Okamoto indicates that the acceleration at the crest exceeded 0.7 G. This dam features a cross section shape which differs from the triangular shape usually adopted for dams of this kind. For reasons which are explained below,

the gradient of the downstream side changes abruptly at about 2/3 of the height of the dam body so that the top part is almost vertical (1:0.153) and the lower part has a normal gradient of 1:0.725. The earthquake cracked the point at which the dam shape changed. At this point in the vertical crane shaft, water leaked out, primarily on the upstream side, and the point where the shape changed was broken. Other damage occurred in the overflow part of the dam, specifically horizontal cracking at the point where the pier of the spillway was attached, but the dam body itself was completely undamaged. Concrete at the support of the RC control bridge on the spillway was crushed. Concrete along the vertical joints on the upstream side of the dam body monoliths crushed, and RC gate panels assembled vertically at the emergency drainage gate were crushed at the contact surfaces, indicating that the earthquake motion acting on the dam was extremely powerful and the monoliths relatively moved each other.

Vibration model test was carried out for 2 sections: the overflow section and the non-overflow section. The test of the model of the non-overflow section revealed that at the fundamental vibration , the part above the point where the cross section abruptly changed

shook as if there were hinges at the change point, which generated considerable strain at that point (Photograph 1).

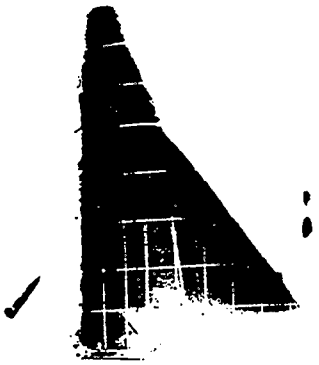

Photo-1 Fundamental vibration mode of non-overflow section

Photograph 2 shows the vibration condition of the model of the overflow section of the dam. It shows that the displacement gradually increases from the foundation of the dam towards its crest and unlike the non-overflow sections, there were no locations where high stress was generated. As stated above, the dam body itself was completely undamaged. Dr.A.K.Chopra, a professor of the University of California has analyzed this dam. The figure shows the distribution of its critical stresses.Becausethe unit of stress

Phpto-2 Fundamental vibration mode of overflow section

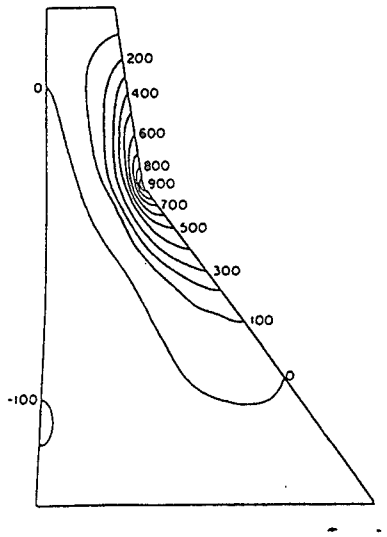

Fig. 18 Critical Stresses in Non-Overflow Monoliths of Koyna Dam Due to Transverse Component of Koyna Earthquake

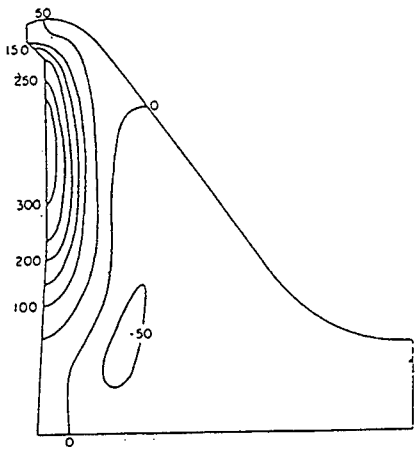

Fig. 19 Critical Stresses in Overflow Monoliths of Koyna Dam due to Koyna Earthquake.

used is psi. 1,000 corresponds to approximately 75 kgf/cm2. When the earthquake motion moved horizontally, tensile stress of about 900 psi was generated. It also shows that in the overflow part, the shaking was more

severe closer to the front, but that the entire dam moved, generating a maximum tensile stress of 400 psi. When vertical motion was applied, tensile stress of about 1,000 psi was generated in the non-overflow part. The compressive strength of the concrete was shown to be more than 300 kgf/cm2 then it is not possible to expect a tensile strength of 75 kgf/cm2, which is probably excessive. It reveals that at the fundamental vibration mode of the overflow part shown in Photograph 2, the entire model vibrates without any strain concentration which means that severe strain was not generated. If it is assumed that there is a tensile stress of 300 psi for example, it is 22 kgf/cm2, and judging from the calculation results, this is within the dynamic tensile strength. The secondary natural vibration mode of the non-overflow part is similar. Judging from these research results, no matter how they are interpreted, it is possible to assume that large strain was generated in the part corresponding to the neck where the cross section shape changed.

At Roorkee University, an experiment was performed involving the dynamic failure of models with a height of about 1.5 m made of plaster and sand, but almost all the models were cracked at the point of abrupt change in the cross section.

The lesson learned from this is that if the non-overflow part of the dam had been designed with a normal triangular shape, it might not have been damaged. The design methods we now employ are suitable for standard cross section shapes, and in cases where a cross section shape which is not standard is to be used, it is essential to carry out a dynamical study of the design.

5.2 San Fernando Earthquake

The following discussion of the behavior of dams in the epicentral region of the San Fernando Earthquake will begin with fill dams. The San Fernando Lower Dam, San Fernando Upper Dam, and the Bypass Dam, three dams located at almost the same location adjoining the epicentral region, were all subjected to severe earthquake motion. Photograph 4 shows the damage to the lower dam. This dam has a height of 43 m and is constructed on fluvial deposit ground with a thickness of about 10 m. Work began on this dam in 1912, the hydraulic fill construction method was used to bring it up to 29 m by 1915, then the normal construction method was executed to

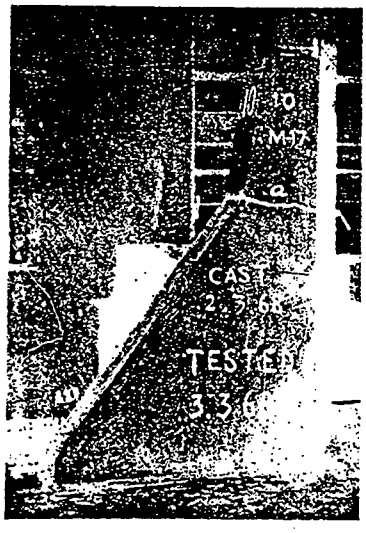

Photo-3 Model non-overflow section cracked by dynamic failure test

Photo-4 San Fernando Lower Dam suffered in San Fernando Earthquake of Feb. 9, 1971

raise its height to 43 m by 1930. The riprap is concrete plates. At the time of the earthquake ,the water level was controled to be slightly lower. During the earthquake, the entire upstream side including the crest slid down to the upstream side. Because the edge of the collapsed downstream side was about 1.4 m above the water level, this must be described as a stroke of good fortune. From the point of view of permeability, the hydraulic fill method of constructing an earth dam is certainly superior, but it is unsatisfactory from the point of view of earthquake resistance strength. A study of its earthquake resistant properties was carried out, and it was reinforced by the addition of gravel to its downstream slope and the compaction of this gravel with rollers about 1940.

The San Fernando Upper Dam is an 18 m high dam completed in 1921. Like the lower dam, the hydraulic fill method was used to construct the first 13 m, then an embankment was constructed above this level. And as at the lower dam, the ground was fluvial deposit ground. The earthquake caused 0.9 m of subsidence at its crest and the top was displaced about 1.5 m on the down stream side. After repairs, it was used with its water level lowered.

The Bypass Dam, a uniform earth dam with a dam height of 27 m, was completed in 1970, or about 1 year prior to the earthquake. Built on rock (sandstone and shale), it was constructed using the most up-to-date compaction method. While the earthquake caused its crest to subside 12 cm, it was completely free of damage and fully operational.

As stated above, violent earthquake motion at the Pacoima Dam during the San Fernando Earthquake cracked the foundation rock around the left bank, which was repaired using concrete grout. It was damaged again in 1994 by the Northridge Earthquake (magnitude 6.8). This time, the saddle of the arch was cracked and the sides and foundation on both banks were cracked. It appears that at the time of the earthquake, the reservoir was nearly empty, with its water level about 60m below the maximum level. Severe land slides occurred in the region surrounding the dam.

5.3 Tangshan Earthquake

The Dou He dam located only about 20 km from the epicenter of the 1976 Tangshan Earthquake (magnitude 7.8) in China was subjected to violent earthquake motion of seismic intensity IX (JMA: V to VI), followed by the vibration of the severest after shock (magnitude: 7.1), suffering serious damage as a result. A dam with a length of 6,115 m and a height of 22 m built by placing sandy clay on alluvial ground and compacting it manually, it was completed in 1956. The major cracking the earthquake caused in the top part of the dam body were longitudinal cracks with a width ranging from 1 m to 1.5 m, one on the upstream side and two on the downstream side, and more than 90 lateral cracks. The dam bulged near the foot of the downstream slope, and jets of water and sand boiling were seen at 60

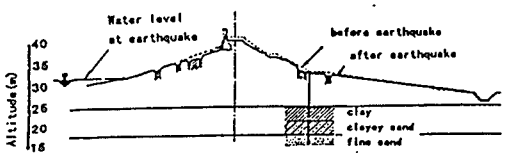

Fig. 20 Damage to Dou He dam, Tangshan Earthquake, July. 28, 1976

locations near the bottoms of slopes on the downstream sides. Analysis results suggest the major cause of the damage was the liquefaction of the ground and the dam body. No earthquake resistant design was performed for this dam.

These findings appear to suggest that the design, including the execution, and ground conditions are important factors in determining the earthquake resistant performance of a fill dam.

5.4 1984 Nagano-ken Seibu Earthquake

Next, let us look at the behavior of dams in and around the epicentral region of the Nagano-ken Seibu Earthquake of 1984 (magnitude 6.8).

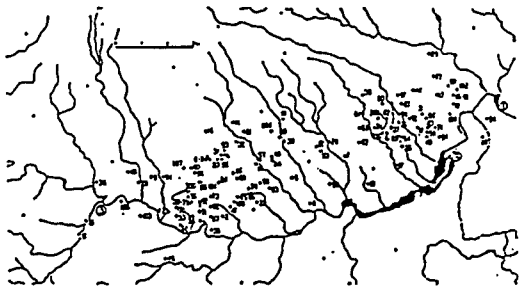

Fig. 21 Locations of after shock of Naganoken-seibu Earthquake , sep. 14, 1984

Figure 21 shows the distribution of the epicenters and the after shocks with the locations numbered in the order of their occurrence. The number 1 represents the main shock and the subsequent numbers show the after shocks. ④ in the figure is the location of Makio Dam (rockfill dam), while other dams are gravity dams. The earthquake occurred a giant collapse with a scale of 30 million m3 on Ontakesan, taking 29 lives. It has been confirmed that lumber was bounced around and rocks buried partially in the ground jumped on the slopes of mountains near the center of the epicenter region. A hydroelectric power tunnel was slightly damaged. The accelerations obtained by differentiating velocity records of after shock ranged from a few hundred gal to more than 1,000 gal, confirming that the earthquake generated powerful earthquake motion. A seismometer was

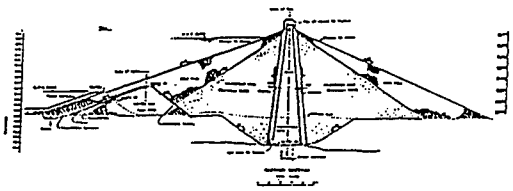

Fig. 22 Standard cross-section of Makio Dam

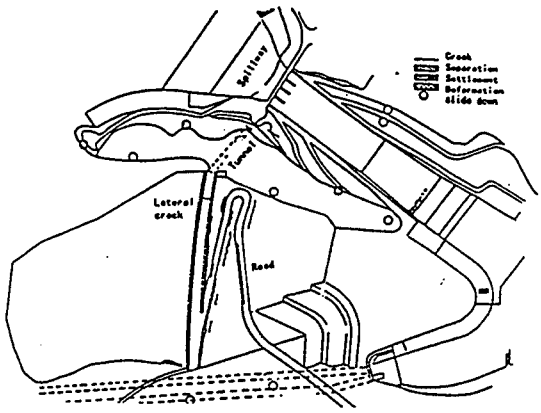

Fig. 23 State of Makio Dam after Earthquake of sep. 14, 1984

installed in the Makio Dam but, as a result of a power failure, it failed to function during the earthquake. The Makio Dam (height: 104.8 m,-1961) is a rockfill dam. On the shoulder of the downstream side of the dam crest, the slope subsided between 30 and 40 cm. A slight unevenness appeared on part of the asphalt paving, but the results of a later test hole excavation and inspection revealed the crack was only about 1 m in depth, so that it did not reach the core. A small collapse was found on the slope adjacent to a road on the downstream side. The road side along the right bank of the reservoir collapsed slightly, and minor land slides occurred at the right bank downstream side.

5.5 Philipine Luzon Earthquake

A earthquake in 1990 in Luzon, Philippines,was a very large earthquake with a magnitude of 7.8. Two rockfill dams called the Ambuklao Dam and Binga Dam stand near the Digdig Fault, which was the active fault that caused this earthquake. The foundations of both dams are bed rock. The Ambuklao Dam is at only about 20 km, the closest to the fault. Mountain slopes surrounding this dam suffered large scale rock falls, a fault slip of 3 to 5 m was observed at a part of the Digdig Fault close to the dam, and slopes on both sides of a river

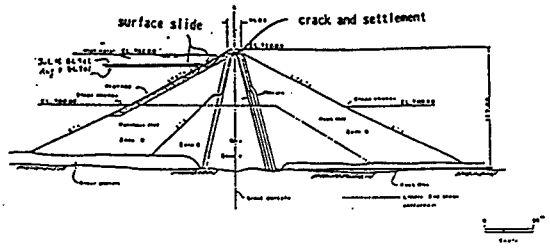

Fig. 24 Standard cross-section of Ambuklao Dam and condition after Earthquake of July. 16, 1990

flowing along the fault and slopes within a distance of 13 km from this river suffered severe slope collapses. From these observations, it is assumed that the earthquake motion was quite severe. Because the author did not check himself, this section refers to a report prepared by Dr.T. Ohmachi,Professor,Tokyo Institute of Technology. Figure 24 shows a section of the Ambuklao Dam. It indicates the water level at the time of the earthquake, revealing that the slippage of the slope surface which is observed often, occurred slightly above the surface of the water. This type of slippage generally occurs only in riprap portions. Deformation at the crest included subsidence of 70cm at the maximum at parts adjacent to the spillway. Figure 25 is a section of Binga Dam. As the figure indicates, this dam suffered only slight deformation.

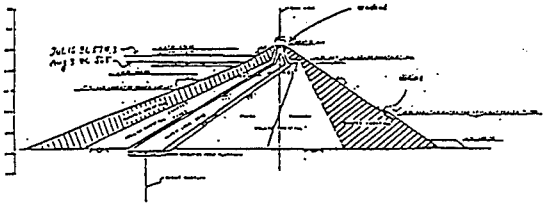

Fig. 25 Typical cross-section of Binga Dam

5.6 Michoacan Earthquake(Mexico)

Next, let us look at the behavior of dams in the epicenter region of the 1985 Michoacan Earthquake in Mexico. In Figure 26, the land area shaped like a cocoon is the epicentral region. The magnitude was 8.1. It was a type of earthquake called a multiple shock earthquake: it began with a strong shock at 1A followed by the failure of a fault at a speed of about 3 km/sec. and ended with another strong shock at 1B. Because it is likely that two magnitude 7.7 earthquakes struck the epicentral region and its surroundings within 30 seconds, the situation differs from a

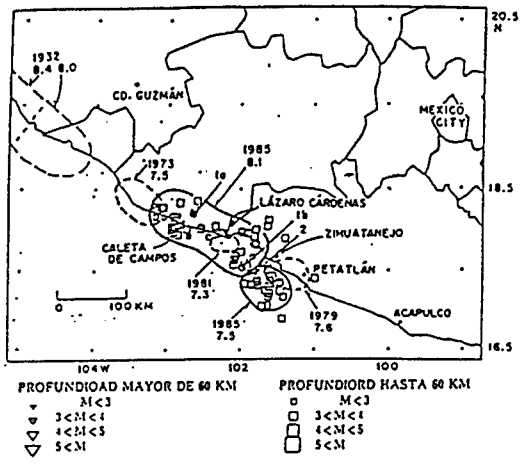

Fig. 26 Distribution of aftershock of Michoacan Earthuake, sep. 19, 1985

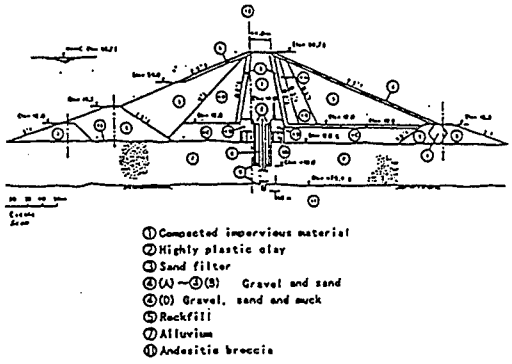

Fig. 27 Cross-section of La Villita Dam

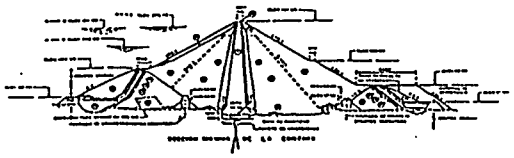

Fig. 28 Cross-section of El Infiernillo Dam

single 8.1 magnitude earthquake case. Even close to the epicenter, the maximum acceleration of the earthquake motion tended to become saturated without rising, and its value was generally about 150 gal. Another earthquake with a magnitude of 7.5 occurred about one day later. Two recently completed rockfill dams stand within the hypocenter region of the earthquake. These are the La Villita Dam (height 64 m, 1965) and slightly to its north, the El Infiernillo Dam (height 138 m, 1988). The former is constructed on a well-compacted thick gravel stratum (70 m thick), while the latter stands on rock. At the La Villita Dam, the crest subsided about 40 cm and longitudinal cracks appeared on the upstream and downstream slope shoulders. A later inspection showed that the cracks did not reach the core. At the El Infiernillo Dam, work on raising the dam was in progress when the earthquake occurred, so the damage is not obvious, but it is reported that the crest subsided about 20 cm, and longitudinal cracking formed on the upstream and downstream slope shoulders. In both cases, the damage can be defined as minor deformation.

5.7 Loma Prieta Earthquake

The Loma Prieta Earthquake of 1989, was caused by action of the San Andreas Fault over a distance between 40 km and 45 km, and many fill dams are constructed close to this active section of the fault. A maximum acceleration of 0.64 G was recorded in the ground at Corralitos, which is extremely close to the epicenter. The dam closest to the fault is the Austrian dam. A fill dam with a height of 56 m, a crest length of 213 m,it was completed in 1950 only about 1 km from the fault. A reinforced concrete spillway connected to the dam on the right bank suffered many lateral cracks and other severe damage. Small cracks were also formed in the dam axis direction on the upstream slope. The area was suffering from a drought at the time so fortunately the water level was extremely low.

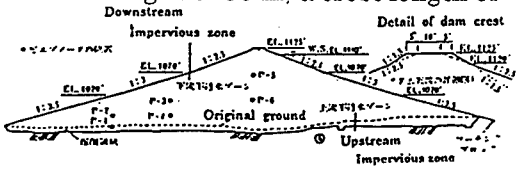

Fig. 29 Cross-section of Austrian Dam

The Lexington Dam also stands close to the San Andreas Fault. Completed in 1953, its dam height is 62 m and its crest length is 247 m. The gradient of its upstream slope is extremely gentle at 1(vertical) : 5.5(horizontal). Because of drought conditions at the time of the earthquake, its water level was very low. Small cracks parallel to the dam axis formed in the middle of the upstream slope, and lateral cracking occurred on the side of the dam at both banks, primarily on the right bank.

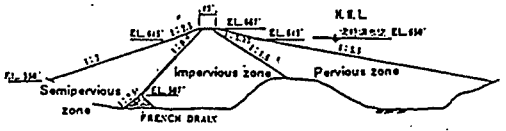

Fig. 30 Cross-section of Lexington Dam

Figure.31 is an acceleration record taken at the Lexington Dam. The wave form at the bottom was recorded at the left bank abutment, but it is almost identical to the wave form recorded at the crest of the dam. In both cases, the maximum acceleration is 0.45 G; presumably because there is no vibration component which would permit the amplification of the dam body vibration. More study of this issue is necessary.

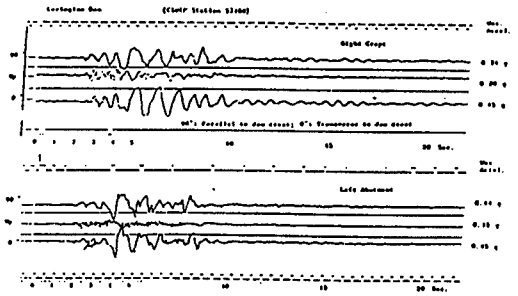

Fig. 31 Accelerogram recorded at Lexington Dam, Loma Prieta Earthquake of Oct. 17, 1989

The Coyote Dam is built across the Calaveras Fault, an active fault parallel to and between 20 km and 25 km to the east of the San Andreas Fault. A rolled earth and rockfill dam completed in 1936, its dam height is 43 m, its crest is 296 m in length, and its gross reservoir capacity is 29.2 x 10^6 m^3. Because it spans a fault, it was designed and executed with great care. At a point about 10 km downstream from the Coyote Dam, the Leroy Anderson Dam (dam height of 73 m, crest length of 422 m) was completed in 1950. A rolled earth and rockfill dam, its gross reservoir capacity is 113 x 10^6 m^3. In addition to supplying water to local water supply systems and functioning as a flood control dam, it serves as a backup dam in the event of the earthquake failure of the Coyote Dam. To permit it to fill this role, its reservoir capacity is continuously controlled so that it can store the water held back by the Coyote Dam.

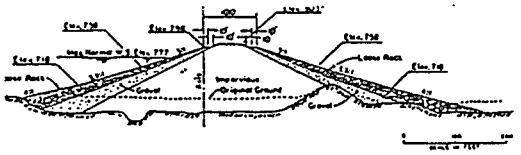

Fig. 32 Maximum section of Coyote Dam

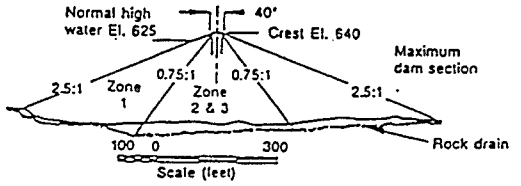

Fig. 33 Maximum section of Leroy Anderson dam

6. The Earthquake Resistant Performance of Dams

This report has examined dam behavior and the intensity of earthquake motion in the epicentral region. As an overall judgement, except for a few exceptional cases, past earthquakes have shown that as one would expect, recently designed and constructed dams display quite good earthquake resistant performance. It is very difficult to quantitatively demonstrate the reasons for this. Regarding rockfill dams,the three-dimensional behavior of dams, the dynamic failure properties from vibration model experiments, and the retaining conditions for shear strength of coarse materials have been analysed and synthesized and the level of earthquake resistance of the dam has been discussed recently. The Committee on Evaluation of Earthquake Resistance of Dams, Ministry of Construction, Japan, has carried out a response analysis based on seismic records from the Hitokura Dam and Minoo River Dam during the Hyogoken Nanbu Earthquake. The rerults demonstrate that gravity dams and rockfill dams display extremely good earthquake resistant propertis.

Further study must be carried out to learn more about the earthquake resistance of dams and to find ways to improve it. This section concludes with

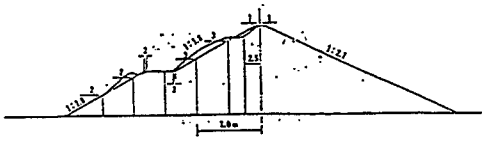

After Vibration failure test on embankment model with large size berm (no impounding)

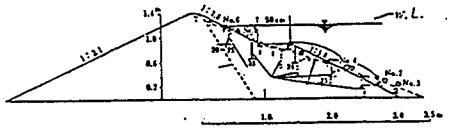

After Vibration failure test on embankment model with large size berm (impounding)

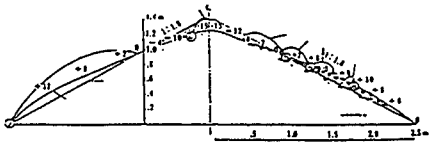

After Vibration failure test on embankment model without berm

Fig. 34 Vibration failure test on embankment model dam model

an outline of 1 or 2 of the results of such work.The first is the effect of berms on the earthquake resistance of fill dams. A model of a dam body with a relatively wide berm constructed in about the middle of the dam height was vibrated until it failed in order to study its failure mechanism. The results indicate that only the slope above the berm failed, while the entire slope did not fail by sliding down. The same failure state was observed in the case of a model dam with a full reservoir. When the slope was straight with no berm, the slope failed entirely in the length of the slope. This suggests that the construction of a relatively large berm reduces the extent of damage to a dam.

Because the vibration frequency during this test was far smaller than the natural frequency of the model, the analysis was performed treating the seismic force statically. When the horizontal vibration is increased in steps from 0 to 0.2g, 0.3 g, and 0.4g, the stress

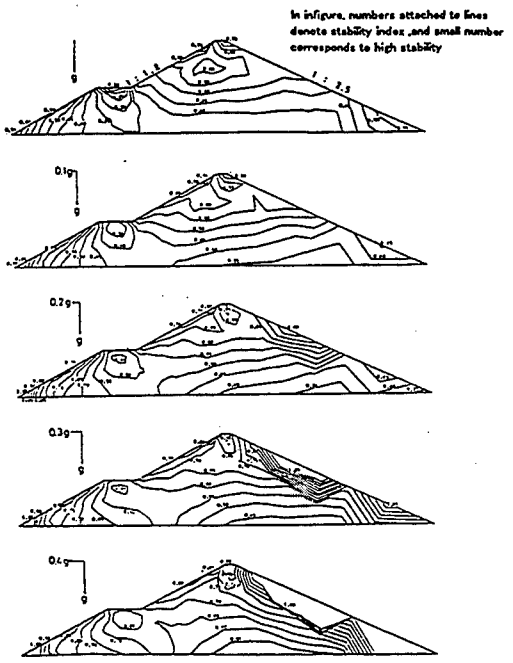

Fig. 35 Numerical analysis on stabliity of embankment model dam with large-size berm

state summarized, and based on this, the conditions for slip stability obtained, a elliptical shaped region with high slip stability appears under the berm(Fig.35).

Another example are vibration failure tests performed using two-dimensional models of a fill dam made of sand. For reasons related to the similarity law, this type of test is done with an analytical model, not a physical model. The black line shown in the photograph is formed by white sand placed in the sand so that the deformation of the model can be observed. As the amplitude of harmonic excitation vibration is gradually increased, the process of failure is revealed. It has demonstrated that the sliding of the slope does not occur uniformly along the

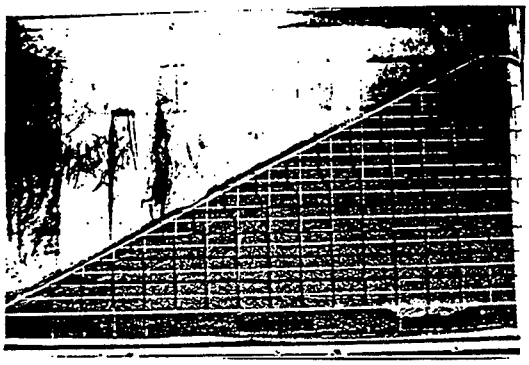

Photo. 5 One step of process forming slip line during vibration failure test on embankment model made with sand. (by courtesy of Dr. J. Dong)

slip line; the failure progresses from the bottom of the slip line each time the vibration is repeated, ultimately forming a slip line so that the entire slope slides down. Research of this kind will likely clarify just what parts of dam bodies should be strengthened.

If a dam is appropriately designed and constructed carefully on a good foundation using high quality materials, it will definitely display fine earthquake resistant performance. It is both fundamental and important to further clarify the reasons for this good

earthquake resistance, and studies to achieve this must continue.

7. Conclusions

In this report, the earthquake motion on the rock ground especially at dam sites , which is one of the basic conditions for earthquake resistant design of dams, has been discussed and dynamic behavior of dams located in the epicentral regions of severe earthquakes or in the adjacent area, has also been discussed in relation with the earthquake motion.

It has been shown that the acceleration of the earthquake motion at the bed rock is lower than that of earthquake motion at the ordinal(soil) ground, with the maximum acceleration equal to a small fraction of that of the ordinal ground. More studies must be carried out, but it seems to be possible to expect its size, including that in the epicentral region.

From overview on the actual behavior of the dams during earthquakes, it has been noted that almost all dams constructed lately have practically high earthquake resistance to severe shocks.

The study on the reasons and the factors of the high resistance must be continued in conjunction with the analysis of real response of existing dam to the earthquake motion.

Deterministic versus Probabilistic Seismic Hazard Analysis for Engineering

by

Ellis L. Krinitzsky*

ABSTRACT

Both the deterministic and probabilistic methods of seismic hazard analysis serve necessary purposes. Probability is needed to obtain operating basis earthquakes, to perform risk analyses, to prioritize projects, and for assigning recurrence estimates to deterministic earthquakes. The probability for these purposes is used as a relativistic measure.

The problem with seismic probability is that it relies on the Gutenberg-Richter b-line, which has severe shortcomings. There are corrections that can be applied, which attempt to remedy the problems. Data are introduced for paleoseismic events, characteristic earthquakes, and slip-rate, or judgments are introduced from logic trees, multiple expert opinions, and de-aggregation of E values. Unfortunately, none are equal to the task. The probabilistic seismic hazard analyses remain fundamentally limited in their dependability. However, the deterministic method can provide evaluations that are at a practical level for engineering. Engineering design must be done deterministically if one is to have seismic safety coupled with good engineering judgement.

The design for critical structures, those for which failure is intolerable, such as dams, nuclear power plants, hazardous waste repositories, etc., must be based on maximum credible earthquakes, obtained by deterministic procedures, in order to assure their seismic safety.

KEYWORDS: Earthquakes, Evaluations Hazards, Probability, Seismicity, Structures,

1 INTRODUCTION

The deterministic and the probabilistic methods of seismic hazard analysis (DSHA and PSHA) are compared in this paper for their suitability in engineering. Of the two, the deterministic method is judged to be the better because the probabilistic method is flawed. Should there be a critical structure, one for which the consequences of failure are intolerable, the deterministic method is the one to use to make the structure seismically safe.

Let's begin with two examples, one for eastern United States, the other for western United States. The difference between them is that earthquakes are less frequent in the east and the fault sources are rarely determinable on the ground surface. In the west, the earthquakes are more frequent and fault sources can be more readily identified. These circumstances call for differences in the way sites are evaluated. A representative site is evaluated in each region both deterministically and probabilistically. Problems encountered in probabilistic analyses are examined in concept and in practice.

2 SEISMIC SOURCE AREAS IN THE UNITED STATES

Figure 1 shows how the major seismic source areas are distributed in the United States.

*Geotechnical Laboratory
United States Army Engineer Waterways Experiment Station
Vicksburg, MS 39180

West of the Rocky Mountain Front, individual fault sources should be located and evaluated. Seismic zones can be added if desired. These are sources for shallow, crustal earthquakes with focal depths ≤ 20 km. In the Pacific Northwest, and along the Pacific Coast of Alaska, deep subduction zone earthquakes, with focal depths > 20 km, must also be evaluated.

East of the Rocky Mountain Front seismic sources are shown as zones. The zones have floating earthquakes. A maximum earthquake is postulated to occur anywhere in a zone.

Seismic zones are determined by patterns of observed earthquakes and the floating earthquakes are determined from the sizes of observed earthquakes. Seismic zones need not coincide with or be related to tectonic or physiographic provinces as the provinces are the results of past tectonism and the zones are from the tectonism of the present.

Within the zones are seismic hotspots. A hotspot requires locally large historic earthquakes, frequent to continuous microearthquakes, and a well-defined area in which these events occur. Hotspots are at New Madrid, MO; Charleston, SC; Giles County, VA; Cape Ann, MA; and the St. Lawrence valley.

Maximum credible earthquakes (MCEs) are shown for the zones and hotspots as modified Mercalli intensities. Magnitude scales can be used but intensity is better because nearly all of the historic record in eastern United States is in intensity, not magnitude.

3 EASTERN UNITED STATES: GATHRIGHT DAM, VIRGINIA

The location of Gathright dam in western Virginia is shown in Figure 2. Also shown are instrumentally located earthquakes, 1933 to 1985, from Bollinger and others (1987). To these was added the Giles County earthquake of 1897, MM = VIII. About a dozen felt earthquakes occurred of which the MM VIII was the largest. Note that in the environs of Gathright dam there has been no seismic activity. The nearest concentration of activity is the hotspot where the Giles County earthquakes occurred. Historic earthquakes during the period of 1774 to 1977 show a close correspondence of source areas (see Krinitzsky and Dunbar, 1990).

Figure 3, from Krinitzsky and Dunbar (1990), shows the seismic zoning and the floating earthquakes that were assigned. The potential for the Giles County hotspot was raised one intensity unit to a MM=IX. The Giles County hotspot is 65 km from Gathright dam and is the principal source for earthquakes that might affect the dam. Microearthquake monitoring at the reservoir recorded no earthquakes at all. The earthquake potential from other sources were judged to be too small and too diffused to be of concern.

3.1 Deterministic Seismic Hazard Analysis (DSHA)

The Giles County hotspot was assigned a maximum credible earthquake of MMI_o= IX, equivalent to M_s = 7.0.

Microearthquakes recorded for the Giles County hotspot indicate a fault or fault zone as shown in Figures 4 and 5 from Bollinger (see Krinitzsky and Dunbar, 1990). Figure 4 shows a plan view on the ground surface and a vertical section looking along the fault. The fault is steep to vertical, suggesting it is strike-slip, and it extends to 20 km in the subsurface, meaning it has the potential for a stress drop sufficient to generate a strong earthquake. Figure 5 shows the area of current activity along this fault. Two interpretations are possible: that of a small area of 200 km^2 and a larger area of 300 km^2. Seismic moments for these areas provide the following values:

Small area: $M_s = 6.3$
Large area: $M_s = 6.8$

The $M_s = 6.8$ is essentially the same as the $M_s = 7.0$ assigned to the hotspot.

The MMI_o = IX was attenuated to the Gathright damsite. The resulting I_s was MM VII.

The MCE of MMI_o = VII was assigned peak horizontal motions for the far field and hard site at a mean + S.D. The motions were

Acceleration: 190 cm/sec^2
Velocity: 14 cm/sec
Duration: 11 sec $\geq$ 0.05g

Time histories and response spectra were assigned to fit these parameters.

3.2 Probabilistic Seismic Hazard Analysis (PSHA)

Figure 6 shows a probabilistic b-value, or b-line, that was developed for this region by Bollinger (see Krinitzsky and Dunbar, 1990). The b-line was developed from seismic data from an area of 100,000 km^2. A 1,000-year event has a magnitude value of $M_s = 7.0$, suggesting that the MCE of M_s 6.8 and 7.0 has a 1,000-year recurrence. But is this interpretation logical? There are several questions that we should ask.

Why was 100,000 km^2 taken as the area? It is a practice first used by Otto Nuttli in the 1970s. This practice is necessary in eastern United States in order to gather enough data to construct a b-line. If Giles County alone were used, the slope of the b-line would have been determined by earthquakes mostly of magnitude about 2. The projection is to earthquake sizes that have energy levels billions or more times greater. The earthquake of MM VIII cannot improve the projection because its recurrence is unknown. That earthquake would simply have been laid on the projection from the magnitude 2 earthquakes. The resulting recurrence for the large earthquake then is obtained by circular reasoning.

But let's assume the b-line for the 100,000 km^2 is reliable. (I will show later that it is not.) Its meaning is that whatever earthquake is taken for a specified level of recurrence, that earthquake can occur anywhere within the 100,000 km^2 area.

Next, let's ask why 1,000-years was selected? There is nothing in the probability calculation that tells you where the recurrence level of the maximum credible earthquake should be. There is no answer. Any rate of recurrence can be taken.

The projection of the b-line sometimes is used to lay out a series of earthquake magnitudes and to show their corresponding recurrences. The probabilist then may say the 5,000-year recurrence is so infrequent, and is so unlikely to occur during the lifetime of a structure, that the magnitude for 1,000 years is the better one to select for design. This is a guessing game using faulty information. We should ask how reliable is the b-line projection itself? It is not reliable. We will have more to say about this later.

4 WESTERN UNITED STATES: RIRIE DAMS, IDAHO

Ririe Dam is located in southeast Idaho, in the Rocky Mountains adjacent to the Snake River Plain (see Figure 7). Ririe Dam is located adjacent to Swan Valley and Star Valley which, together, is known as Grand Valley. Structurally, it is a graben , a fault block down-dropped by major active faults. It is an area where major earthquakes occur as shown in Figure 8. The seismic history in this region is one of the shortest in the contiguous United States, only about 100 years. All faults in this region should be considered active and capable of generating earthquakes. The major faults shown in Figure 7 are capable of great earthquakes.

4.1 Deterministic Seismic Hazard Analysis (DSHA)

Evidence on earthquake hazards and earthquake sources was gathered for the region. Studies were made of the geomorphology, historic earthquakes, patterns of microseismicity, hot springs, volcanism, Bouguer gravity anomalies, magnetometer patterns, and seismic profiles obtained for oil exploration in the region (see Krinitzsky and Dunbar, 1991). Extreme youthfulness of faults was observed through field reconnoitering which was done throughout the region.

Adjacent to Ririe Dam were linear interruptions in the drainage on the surface of plateau areas. Figure 9 shows that these are evidences of fault movement. The faults are blanketed by a cover of loess. The linearity was determined to be from volcanic dikes. Displacements along these dikes was caused by fault activation. Figure 10, from Slemmons and Ramelli in Krinitzsky and Dunbar (1991), shows that these features determine a potential for an earthquake close to the dam. This was a local earthquake, with no attenuation to the dam. A maximum credible earthquake of MM IX, equivalent to M_s = 6.5, was assigned based on fault lengths and the fault-size-to-magnitude relationships of Bonilla (1983).

Within a few kilometers of Ririe Dam is the major graben which formed the Grand and Swan Valleys (Figure 7). Young fault scarps were found that were 20 meters high and tens of km in length. Figure 11 shows a scarp near Heise (Figure 7). The whitish areas are young travertine deposits produced by hot springs that opened during faulting and have since gone dormant. Heise is itself the site of active hot springs. The faults in Swan Valley extend into the Snake River Plain to beyond Rexburg (Figure 7). Figure 12 shows a 20-meter scarp of the fault south of Rexburg. Note that water flowing over the edge of the scarp has hardly begun to erode the face of the scarp. The extreme size and youthfulness of these features indicate a potential for very large earthquakes.

Two representative earthquake sources were selected for the major faults. One was at Heise in the closest proximity to the dam. The other was in Star Valley. These represented extremes of near field and far field motions. Lengths and displacements of the faults were used to estimate MCEs of MMI_o = X and an equivalent M_s = 8.3. Motions were attenuated from these sources to the damsite to establish parameters for free field motions for rock at the dam. Other distances, such as an intermediate distance with its appropriate parameters for the site, can be added for the M_s = 8.3 earthquake if desired.

Table 1. Maximum Credit Earthquakes at Ririe Dam, Idaho, with Peak Horizontal Ground Motions (Mean + S.D.) for a Hard Site

Earthquake Source	Magnitude	Intensity	Acceleration	Velocity	Duration
	M_s	I_s	cm/sec^2	cm/sec	sec ≥ 0.05 g
(1) Local (Near Field)	6.5	IX	1,200	68	22
(2) Grand-Swan Valley 4 and 10 km (Near Field)	8.3	X	1,200	120	33
(3) Grand-Swan Valley 80 km (Far Field)	8.3	VIII	280	25	65

Analogous time histories and response spectra were obtained to fit the above parameters.

The three representative earthquake sources noted above had attenuation distances on parameters for peak horizontal motions (mean + S.D.) on a hard site, as shown in Table 1.

4.2 Probabilistic Seismic Hazard Analysis (PSHA)

Figure 13 shows a probabilistic b-line projection developed by Piety and others (1985) for magnitude M_L to 7.5. The projection was extended to ~ 8.5. The b-line was developed from seismic data from an area of 55,000 km^2.

It is the size of the designated source area that controls the recurrence characteristics of the b-line. Yet, even for a large region, the control for the b-line projection will be from the very small earthquakes as they are the only ones for which recurrence rates can be observed. The larger and more important historic earthquakes are added to the projection of the b-line with no knowledge of the real rate of their recurrence. Inclusion of the larger earthquakes on the projection is, as we noted before, purely by circular reasoning.

Recurrence levels taken on the b-line for 55,000 km^2 have to apply uniformly over the entire area. Therefore, earthquakes of selected magnitudes cannot be applied to specific faults as there are too many such faults. On this basis, Hofmann (1996) demonstrated that Gutenberg-Richter b-values cannot be applied to individual faults. For engineering, the need is to focus on small source areas. Such areas cannot be evaluated probabilistically because there will be still less seismic data in a range to form a convincing b-line.

As we saw at Gathright Dam, the b-line projection does not offer any clue as to what the maximum credible earthquake should be. If one is to learn what the probability level should be for a seismic design in engineering, one must first, do a deterministic analysis and obtain a maximum credible earthquake. Then and only then, can one have an earthquake for which to assign a probability.

One can obtain a design earthquake directly from probability by picking it out from the b-line for an arbitrarily selected recurrence rate. The problem is there is no reality check. An earthquake from probability alone may be too small, in which case the structure is underdesigned, or the earthquake may be too large, and the structure is overdesigned. There is no way to know.

Probabilists can avoid the above dilemma and yet control the design process by assigning a probabilistic earthquake. They obtain a deterministic earthquake and apply to it a recurrence from the b-line only to show that the recurrence is low. Therefore, they reason, it is overly conservative to design for the maximum credible earthquake. They then justify a lesser earthquake based on a greater probability. An earthquake lower than the maximum credible earthquake might be reasonable if the probabilistic recurrence value had temporal significance. It has no such significance. There is absolutely nothing in the b-line that can tell you whether an earthquake of any size will or will not happen during the lifetime of a structure.

Finally, there is a question concerning both the Gathright and Ririe regions that has not been asked: Are those b-lines reliable? Are any b-lines reliable enough to base engineering decisions? There are cogent reasons for believing they are not. We will examine this issue later.

5 COMPARISON OF DETERMINISTIC AND PROBABILISTIC SEISMIC HAZARD ANALYSES

5.1 Procedure for a Deterministic Analysis

To perform a deterministic seismic hazard analysis (DSHA) for an important engineering project, one generally does the following:

Step 1: Establish the location and characteristics of all significant potential earthquake sources that

might affect the site. For each source assign maximum credible earthquakes (MCEs).

Step 2: Select appropriate attenuation relationships to estimate the site ground motion parameters as a function of earthquake magnitude, source to site distance and various site conditions.

Step 3: Select analogous accelerograms and/or response spectra to represent earthquake excitations at the site.

The objective is to design against any reasonable eventuality regardless of time as there is no way to know whether an earthquake, whose recurrence is in any number of years, may not happen during the design lifetime. Uncertainties in the occurrences of earthquakes are covered at a practical level for engineering by taking an 84 percentile (mean + S.D.) of the range in the variables affecting a site.

Competent persons doing a DSHA will have considered all reasonable interpretations, models and values. They will have selected what they judged to be the best. When completed, the work is peer reviewed. The reviewers may or may not agree. The project engineer decides what to accept. He knows the reasons for his decisions and he takes the responsibility for them.

5.2 Procedure for a Probabilistic Analysis

A probabilistic seismic hazard analysis (PSHA) incorporates the element of time in the assessment of the earthquake threat at a site. The objective of a PSHA is to compute for a given exposure time the probability of exceedance corresponding to various levels of a ground motion parameter. Typically the ground motion parameter is either peak horizontal ground acceleration (PGA) or response spectra ordinates. The probability is claimed to be a measure for uncertainty.

The general procedure is as follows:

Step 1: Same as for a deterministic evaluation.

Step 2: Same as for a deterministic evaluation.

Step 3: For each source, the frequency of earthquake occurrence is estimated from earthquake information. The Gutenberg-Richter magnitude and recurrence relation is most commonly used. The b-line obtained from this relation describes the relative rate of occurrence of earthquakes of different magnitudes. In simple or basic PSHA, an exponential-magnitude distribution with an annual probability of exceedance is developed as shown in Figure 14. Motions from the earthquake sources are combined to provide a probability level for a site.

The probability is commonly constructed from data for low magnitude earthquakes and projected to indicate the occurrences of large earthquakes for which no recurrence data exists. It is the large earthquakes that are of engineering significance and the question of applicability and reliability in the projection is crucial.

6 ADVANTAGES AND DISADVANTAGES IN THE PROBABILISTIC METHOD

6.1 Problems in the Simple or Basic Probabilistic Analysis

Each earthquake source in Figure 14 has a distinct effect on the site and should be represented by an appropriate time history which is what is done in the deterministic method. In the probabilistic method, the earthquakes from all of the sources are smeared together to generate the combined probability density function. The resulting values do not represent the real earthquakes that may emanate from the sources as shown by the dashed arrows in Figure 14.

The problems which arise in the appropriateness and applicability of the b-line projection can be seen in Figure 15. What is shown is that the b-line must be generated from small earthquakes and, in effect, is meaningful only for those small earthquakes ($M \leq 5.5$). But those are earthquakes too small to be meaningful for engineering. They are the only ones abundant enough to establish the changes in recurrence. One can do this only if there is a large area and it is seismically active, in this case all of southern California. Any very small part of this area, such as would be crucial for an engineering site, will present problems because there will be insufficient data.

Note that the observed recurrence of small earthquakes is projected to predict large earthquakes for which there are no data. Large experienced earthquakes are added to the projection. It must be kept in mind that they in no way serve to confirm the projection as there is nothing known for the recurrence of those earthquakes. The earthquakes were added simply where their magnitudes fitted the projection. Their place in the projection is obtained by this circular reasoning. Krinitzsky (1993a, 1993b) showed there are dozens of reasons why the projection is not continuous or straight and there is no way to predict what it should be. However, assuming the b-line is correct, any value taken from it would represent an occurrence from anywhere over the entire region. Hofmann (1996) demonstrated that recurrence values obtained this way cannot be applied to individual faults.

So far, we assumed that calculating a b-value results in a single line. Actually, the b-line changes with the influx of new data every time there is a substantial earthquake. Figure 16 illustrates what happens. At Fukui, Japan, the b-line for 1976-1985 bears no resemblance to the effect in 1948-1949 of earthquakes the greatest of which was $M = 7.1$. Note how one b-line would have been totally unpredictive for the other. The situation is reflected in Figure 17 for the new Madrid region. Note that the major historic earthquakes bear no relation to the b-line. Figure 18 shows what happens when the four-month period of 1811 to 1812 is separated and plotted independently. The b-line is not a line at all. It is rather an earthquake-recurrence trend in a nebulous zone. Table 2 from Johnston and Nava (1984) shows another inexactness in b-lines. For a ten-year period, 1974 to 1984, ten different b-lines were created by different seismologists using essentially the same data from the New Madrid region. Note that the resulting recurrences for $M = 6.3$ and $M = 8.8$ vary by a full order of magnitude or 1,000 percent. The discrepancies result when small changes are made in handling the tiny earthquakes and those become magnified in the logorithmic projections.

In short, probabilistic projections are doubtful everywhere and are particularly insufficient when assigned to the relatively small areas which determine the site-specific evaluations for engineering. Yet, the smaller areas can be interpreted easily by the deterministic method using geological and seismological evaluations to get maximum credible earthquakes. We saw how this was done at the Gathright and Ririe damsites. Maximum credible earthquakes obtained deterministically were essential for the evaluations.

What has been described so far for probability is for simple or basic probability. There are methods that are intended to correct some of the deficiencies in probabilistic analyses. These will be examined.

Table 2. Earthquake Recurrences from B-Values in the New Madrid Seismic Source Area. Johnston and Nava (1984).

Authors		Recurrence (Years)	
		M = 6.3	M = 8.8
Nuttli	(1974)	47	773
		58	1,117
Stauder and Others	(1976)	30	224
Nuttli and Herrmann	(1978)	42	810
		37	721
Nuttli	(1979)	21	240
Howell	(1980)	69	1,100
Johnston	(1981)	118	1,687
Perry	(1981)	127	1,741
		176	2,573
Nuttli	(1981)	78	1,050
Stauder	(1982)	Not applicable to large events	
Johnston and Nava	(1984)	70	550
		140	1,100

6.2 Methods for Correcting Probabilistic Analyses

First, let us summarized the pros and cons for simple or basic probability.

a. Simple or basic probability

(1) General: Uses small earthquakes to generate a b-line which projects to large earthquakes.

(2) Advantage: Relatively easy to do, though subject to confused results.

(3) Disadvantage:

(a) Small changes in the data for small earthquakes make huge changes in the large earthquakes. Also, the data set changes, with a large overall effect on the b-value, each time there is a moderate to strong earthquake. A calculated b-line is seldom replicated by different investigators.

(b) Calculation is for an inclusive region. b-Values do not apply to individual faults or smaller areas within the region.

(c) By combining different sources within a region, earthquakes are smeared together. Individual characteristics for earthquake sources are lost.

(d) Mechanics of faulting change with the earthquake magnitude level and the change affects the recurrence rate (Krinitzsky, 1993b). Therefore, the b-line is never a straight-line projection. Small earthquakes do not predict the time and size for large earthquakes.

Following are pros and cons for the principal corrective measures that are introduced into probabilistic evaluations.

b. Paleoseismic data

(1) General: Paleoseismicity uses geologic methods to determine dates and magnitudes of ancient earthquakes. These are applied for adjustments to b-line projections. The field work generally involves

(a) Fault trenching to obtain individual displacements with datable material.

(b) Dating of abrupt displacements of coastal marshes.

(c) Fault movement of soil liquefaction that disturbs archaeological remains.

(2) Advantage:

(a) May provide evidence for previously unknown earthquakes affecting an engineering site.

(b) Can establish if a fault is capable of generating earthquakes or is dead.

(3) Disadvantage:

(a) Recovered data is fragmentary.

(b) Earthquake magnitude estimates are inexact.

(c) Earthquake recurrence patterns are not uniform through space and not uniform through time.

(4) Comment:

(1) Paleoseismicity is not sufficient to make PSHA reliable.

(2) Paleoseismicity can have non-probabilistic uses for assessing seismic hazards to engineering.

c. Characteristic earthquakes:

(1) General: PSHA recognizes that faults do not have orderly occurrences of earthquakes through all magnitudes. Some magnitudes occur more often than others or characteristically. Determining these in the geologic past history may improve prediction.

(2) Advantage: Adds to knowledge of earthquake occurrences.

(3) Disadvantage:

(a) Information on characteristic earthquakes is obtained from paleoseismicity and is both fragmentary and inexact.

(b) Characteristic earthquakes, like all other earthquakes, do not occur uniformly through space nor uniformly through time, therefore a characteristic earthquake may no longer be occurring.

d. Logic trees:

(1) General: For an example of this procedure, see Figure 19 from Power (1994). An investigator lists all the alternative models that may be considered at each step in a PSHA. The investigator gives a weighting to each model based on his opinion of its relative merit. A peak value on a bell curve is taken as the best judgement and that value is brought to the next stage where the process is continued. The objective is to evaluate uncertainty in each of the models and make the best choice.

(2) Advantage: The logic tree shows the alternative models that were considered and the relation of the decision levels to the choices.

(3) Disadvantage:

(a) The method may invite incorporation of unnecessary and improper models in order to create a bell curve for the comparisons.

(b) Weighting is by the opinion of the preparer. This is egocentric. It is not replicable.

(c) The b-values are introduced with all the shortcomings of the basic probability calculation that make them useless for selecting design earthquakes.

(d) Decisions at each step involve comparisons of different models. This comparison creates a problem affecting the value of the interpretation. It is necessary to make such comparisons using equivalent data (see Krinitzsky, 1995). The models that are used cannot be regarded as a uniform data set. Please refer to Figure 20. There are three routes (models): one serves Town A, another is the shortest route, another serves Town B. When these routes are averaged into a single route, which is analogous to picking the crest of a bell curve, the averaged route serves neither town and neither is it the shortest. The resulting route has lost all the pertinent criteria. The problem is that different models cannot the combined without loss of meaning.

(4) Comment: Logic trees do not enhance the seismic probability calculation and can be a source of error.

e. Slip rate of faults

(1) General: Rate of fault slippage is roughly predictive of size of earthquake. Earthquake magnitude from slip rate, if valid, may improve the Gutenberg-Richter b-line projection.

(2) Advantage: None

(3) Disadvantage:

(a) Measurements generally are limited to strike-slip faults. Thrust faults and normal faults ordinarily do not have cumulative slip.

(b) Creep is not accounted for and may cause values to be misleading.

(c) Periods with inactivity usually cannot be identified.

(d) Estimations of earthquake magnitude and recurrence from fault data are inexact and speculative.

f. Statistical averaging of multiple expert opinions:

(1) General: The method solicits independent opinions from a large number of experts. The experts each give their opinions for boundaries of seismic zones, floating earthquakes in the zones, attenuation of ground motions, etc. The opinions are self-weighted by the experts. The opinions of the experts are compared with each other and a revision and iteration follows. The individual opinion values are calculated into Gutenberg-Richter b-values using every permutation and combination of every opinion. Thousands of b-lines are calculated for each site. The b-lines are then combined by a Monte Carlo process into a single, median line. The spread in b-lines provides the ranges for standard deviations. For details on this method see Bernreuter el al. (1987), Bernreuter et al. (1989), Budnitz et al. (1997).

(2) Advantage: None

(3) Disadvantage:

(a) The method aims to get a broad range of views. The Lawrence Livermore National Laboratory (LLNL) used 19 experts in their study. The Electric Power Research Institute (EPRI) used 50. The experts, engaged in such large numbers, cannot be expected to be

equally conversant with the issues that are involved. Many of them clearly did not understand what they were doing. Examples of underlying inexpertise can be seen in Figure 21, from Bernreuter et al (1989). The experts were attempting to create boundaries for zones of equal seismic hazard without a clear understanding of what criteria should determine the zones. However, the experts were allowed to compare their results, to self-weigh them, and to present new boundaries. These steps were intended to bring the interpretations together. Those results are shown in Figure 22. Instead of coming together, the boundaries are farther apart. Expert 5 has a New Madrid seismic source extending in a broad, continuous zone from Canada all the way to Lands End, Louisiana. The prospect of designing for a New Madrid earthquake in southern Louisiana is hardly justifiable. Yet, Expert 6B went one better: he has a New Madrid level of hazard everywhere east of the Rocky Mountains. Meanwhile, try to find the Giles County seismic source that we identified and used for the design of Gathright Dam. It disappeared. Locations of seismic hotspots in central and eastern United States are shown in the lower right corner of Figure 21. Note that the hotspots were either lost in Figures 21 and 22 or were moved over large areas the boundaries of which appear to be arbitrary.

(b) As we noted at Gathright and Ririe Dams, the b-value depends on the nature and extent of the area from which it is derived. Each of the seismic zones in Figures 21 and 22 contributes to a distinct b-value. Those zones are of fundamental importance to the investigation. They are the basis on which the entire evaluation depends. And how good are those zones? What are the ideas behind them? What is their logic? Why weren't they replicable? A fallacy in the process is every expert contribution was accepted at face value. Another fallacy was to allow self weighting by the experts using the percentage degree of confidence that each had of his own judgements. What these experts produced was clearly questionable. If this procedure were followed again, could we expect the same results? It was done again, by EPRI. Figure 23 compares EPRI's results at a site with that of LLNL and they hardly resemble each other.

(c) Budnitz et al. (1997) tried to refine the method, but still by combining the opinions of multiple experts. Possibly, they might screen out some of the extreme differences in Figures 21 and 22. It remains to be seen if a room full of experts can be depended on to consistently come up with better than a camel. But that doesn't matter because Budnitz et al still did not repair any of the other shortcomings that are inherent in the method.

(aa) The b-line is not a dependable projection. Yet, the seismic probabilists use it as if it is valid and exact.

(ab) To get a b-line for design the method requires an averaging of different models. We showed (Figure 20) that different models cannot be averaged meaningfully. Autocorrelation of a variable requires a homogeneous data set. Different models are not a homogeneous data set.

(ac) The b-line smears different earthquakes together and does not furnish properly analogous motions for testing a site.

(ad) The b-line projection cannot indicate a design level. The design value has to be obtained arbitrarily by selecting a recurrence in years. An arbitrary selection is made from an inaccurate line.

g. Double and triple integration for de-aggregation of E-values:

(1) General: Double or triple integration is used to get earthquake probability within a specified area and/or for a specified range of earthquake magnitudes along with peak ground motion values and attenuated E values. E represents exceedance. The objective is to extract more specific information from the probability calculation. Figure 24 shows the form in which the information is presented.

(2) Advantage:

(a) If used to compare the probability calculation for different subareas, it can flag where erratic values may be entering.

(b) It decouples the attenuated values that compose the exceedance.

(3) Disadvantage:

(a) The method exacerbates all the problems in the probability calculation by slicing the results into units that are mostly unjustifiable. Probability has a rough validity for large regions if they have plentiful data for seismic events of all magnitudes. The de-aggregation method, when it works at all, would work for an area, if it contained a single pronounced source such as Charleston, SC or Giles County, VA. However, for such a case, the de-aggregation is not needed because the source is so readily apparent. In more complicated areas the data become questionable for the small segments that are cut apart. For an area with multiple fault sources, the method is plainly misleading. The probability method cannot tell which fault or which part of a fault will be activated. Additionally, slicing up of the area and its faults will produce values that are still further removed from reality because of fragmentation of the sources.

(b) The tails of the exceedance values commonly have no data to support them. Thus, the exceedance relationship is usually imaginary.

6.3 Where Seismic Probability is Appropriate

Despite the above problems, probabilistic values are needed for the following uses in engineering.

a. The operating basis earthquake (OBE), which is a probability concept defined as an earthquake likely to occur during the lifetime of a structure. (For Corps of Engineers dams, the OBE return period is 144 years).

b. Risk analysis where relative comparisons are made to determine

(1) Cost benefits.

(2) Site selection.

(3) The relative merits of different types of construction.

(4) Prioritizing projects to obtain efficiencies in planning.

(5) Estimating a recurrence time for DSHA as needed to relate maximum credible earthquakes to maximum floods, etc.

3 The function of seismic probability in risk analysis is illustrated in Figure 25. Note that the probability serves for direct comparisons of alternatives by which an owner can make cost-risk decisions. The probability is used only in a relativistic sense and only for decisions that are non-critical. Because of the uncertainties in probabilistic values, risk analysis should never be used for design decisions affecting critical structures.

7 SUMMARY AND CONCLUSIONS

7.1 A deterministic study is essential in order to have the data to make sense of a probabilistic analysis.

7.2 The Gutenberg-Richter b-line, on which nearly all probabilistic projections are based, is uncertain. There are corrections that are applied, which attempt to give substance to the b-line. Data are introduced for paleoseismic events, characteristic earthquakes, and slip-rate, or judgements are introduced from logic trees, multiple expert opinions, and de-aggregation of E values. All of them are unequal to the task. The probabilistic seismic hazard analyses remains a fundamentally flawed procedure.

7.3 Engineering design must be done deterministically if one is to have seismic safety coupled with good engineering judgement. However, there is a need for probability.

7.4 Probability is needed to obtain operating basis earthquakes, to perform risk analyses, to prioritize projects, and for assigning recurrence estimates to deterministic earthquakes. The probability for these purposes is non-critical.

7.5 The design for critical structures, those for which failure is intolerable, such as dams, nuclear power plants, hazardous waste repositories, etc., must be based on maximum credible earthquakes, obtained by deterministic procedures, in order to assure their seismic safety.

9 ACKNOWLEDGMENTS

I am especially grateful to Howard A. Spellman and Robert A. Larson who, with the Ethics and Professional Practice Committee and the Committee on Seismic Safety, both in the Association of Engineering Geologists, created the debate on which this paper is based. My colleague Mary Ellen Hynes helped me considerably with comments and in correcting the manuscript. I should mention also that I am deeply indebted to C. Allin Cornell. In about 1976, I hired him to work on the Richard B. Russell Dam project on the Savannah River. It was then that he explained seismic probability to me. The subject, the way it was so quickly and so broadly embraced, and the general lack of intelligent evaluation that went with its acceptance, has fascinated me ever since.

The views in this paper may or may not be in accord with those of the Corps of Engineers.

10 REFERENCES

1 Bernreuter, D. L., Savy, J. B. and Mensing, R. W., 1987. Seismic Hazard Characterization of the Eastern United States: Comparative Evaluation of the LLNL and EPRI Studies. NUREG/CR4885, UCID20696, Lawrence Livermore National Laboratory, U.S. Nuclear Regulatory Commission, Washington, DC, 259 pp.

2 Bernreuter, D. L., Savy, J. B., Mensing, R. W. and Chen, J. C., 1989. Seismic Hazard Characterization of 69 Nuclear Plant Sites East of the Rocky Mountains. NUREG/CR5250, UCID21517, Lawrence Livermore National Laboratory, U.S. Nuclear Regulatory Commission, Washington, DC, Vols. 1-8.

3 Bollinger, G. A., Ehlers, E. G., and Moses, M. J., 1987. Intraplate seismicity in eastern United States, NUREG/CR-4974, U.S. Nuclear Regulatory Commission, Washington, DC.

4 Bonilla, M., 1983. Evaluation of potential surface faulting and other tectonic information, U.S. Geological Survey, Open File Report 82-732, Reston, VA, 88 pp.

5 Budnitz, R. J., Apostolakis, G., Boore, D. M., Cluff, L. S., Coppersmith, K. J., Cornell, C. A., and Morris, P. A., 1997. Recommendations for probabilistic seismic hazard analysis: Guidance on uncertainty and use of experts, Vols 1 and 2, NUREG/CR-6372, UCRL-ID-122160, Lawrence Livermore National Laboratory, Livermore, CA.

6 Hofmann, R. B., 1996. Individual faults can't produce a Gutenberg-Richter earthquake recurrence, Eng. Geol., 43 (1): 5-10.

7 Johnston, A. C., and Nava, S. J., 1984. Recurrence rates and probability estimates for the New Madrid seismic zone, Pro. Symp. New Madrid Seismic Source, U.S. Geological Survey, Open File Report 84-770, Reston, VA, 279-329.

8 Krinitzsky, E. L. and Dunbar, J. B., 1990. Geological-seismological evaluation of earthquake hazards for appurtenant structures at Gathright Dam, Virginia, TR GL-90-10, Waterways Experiment Station, Corps of Engineers, Vicksburg, MS.

9 Krinitzsky, E. L. and Dunbar, J. B., 1991. Geological and seismological evaluation of earthquake hazards at Ririe Dam, Idaho, TR-GL-91-11, Waterways Experiment Station, Corps of Engineers, Vicksburg, MS.

10 Krinitzsky, E. L., 1993a. Earthquake probability in engineering - Part 1: The use and misuse of expert opinion. Eng. Geol., 33(4): 257-288.

11 Krinitzsky, E. L., 1993b. Earthquake probability in engineering - Part 2: Earthquake recurrence and limitations of Gutenberg-Richter b-values for the engineering of critical structures. Eng. Geol., 36(1): 1-52.

12 Krinitzsky, E. L., Gould, J. P. and Edinger, P. H., 1993. Fundamentals of Earthquake Resistant Construction. Wiley, New York, N.Y.

13 Krinitzsky, E. L., 1995. Problems with logic trees in earthquake hazard evaluation, Eng. Geol., 39(1): 1-3.

14 Piety, L. A., Wood, C. K., Gilbert, J. D., Sullivan, J. T., and Anders, M. H., 1985. Seismotectonic study for Palisades Dam and Reservoir, Palisades Project, Seismotectonic draft report 85-3, Bureau of Reclamation, Denver, CO, and Boise, ID.

15 Power, M. S., 1994. Utilization of new developments in ground motion estimation in engineering design practice: Examples for development of site-specific ground motions. Proc. Seminar New Developments in Earthquake Ground Motion Estimation and Implications for Engineering Design Practice, Applied Technology Council, ATC-35-1, San Francisco, CA, 15-1 to 15-35.

16 Watanable, K., 1989. On the duration time of aftershock activity, Bulletin Disaster Prevention Research Institute, Kyoto University, 39: 1 and 2 (339), 1-22.

11 LIST OF TABLES

12 LIST OF FIGURES

Figure 4. Definition of the Giles County, Virginia, seismic source from microearthquakes. From Bollinger in Krintzsky and Dunbar (1990).

Figure 5. Small area, 200 km^2, and large area, 300 km^2, interpreted from microearthquakes as the fault zone in the Giles County, Virginia, seismic source. From Bollinger in Krinitzsky and Dunbar (1990).

Figure 6. Gutenberg-Richter b-line based on 100,000 km^2 in the region of Gathright Dam, Virginia. From Bollinger in Krinitzsky and Dunbar (1990).

Figure 7. Major structural features in the region of Ririe Dam, Idaho. From Krinitzsky and Dunbar (1991).

Figure 8. Historic seismicity in the region of Ririe Dam, Idaho. From Krinitzsky and Dunbar (1991).

Figure 9. A close-up view of a linear feature near Ririe Dam. The surface is a loess-covered basaltic plateau. Note how drainage has been interrupted. From Krinitzsky and Dunbar (1991).

Figure 10. Occurrence of lineaments in relation to Ririe Dam. From Slemmons and Ramelli in Krinitzsky and Dunbar (1991).

Figure 11. Scarp of the fault bordering Swan Valley near Heise, Idaho. Travertine from recently active hot springs is seen on the fault. From Krinitzsky and Dunbar (1991).

Figure 12. A view of the Rexburg fault south of Rexburg, Idaho. Note that interrupted drainage has barely eroded the face of the scarp. From Krinitzsky and Dunbar (1991).

Figure 13. Gutenberg-Richter b-line based on 55,000 km^2 in the region of Ririe Dam, Idaho. Adapted from Piety and others (1985) who created it for nearly Palisades Dam (see Figure 7) and terminated it at M = 7.5.

Figure 14. Generalized procedure for obtaining the probabilistic seismic hazard for a region as peak ground acceleration with annual probability of exceedance. Arrows from sources to the site also show how deterministic assessments would be applied. Deterministic evaluation would provide individual time histories for maximum credible earthquakes that represent earthquake potentials at the sources. The probability combines the earthquakes from these sources and predicts that the combination changes its size in an orderly progression through time.

Figure 15. Probabilistic recurrence rates for earthquakes in Southern California from projections of the Gutenberg-Richter b-line. Recurrence was observed only in small earthquakes. The rest is projection and assumption. Application is collectively for the region and not for any specific site.

Figure 16. Variance in b-lines for earthquakes at Fukui, Japan. From Watanabe (1989).

Figure 17. Probabilistic recurrence rates for earthquakes in the New Madrid region. Recurrence for the historic earthquakes is unknown.

Figure 18. Separated b-lines for New Madrid: 16 December 1811 to 15 March 1812 and 1820 to 1986. A b-line is not a single or exact entity but a broad and uncertain zone. Adapted from Mitchell in Krintzsky (1993b).

Figure 19. Logic tree to evaluate uncertainty for a probabilistic seismic hazard analysis. From Power (1994).

Figure 20. Why different models cannot be averaged: There are three routes, each of which serves a purpose. Route 1 serves Town A, Route 2 is shortest, Route 3 serves Town B. When they are averaged, they produce a route that has no purpose. Their criteria are lost and the result is without useful meaning.

Figure 21. Seismic source zones for eastern United States by eleven experts. From Bernreuter et al. (1989). The location map in the lower right corner was added to show seismic hotspots.

Figure 22. Six alternative seismic source zones for eastern United States by five experts. From Bernreuter et al. (1989).

Figure 23. Ranges of calculated acceleration-through-time curves generated by the Lawrence Livermore National Laboratory and the Electric Power Research Institute for the Vogtle Nuclear Power Plant Site, Georgia. From Bernreuter et al. (1987).

Figure 24. De-aggregations of the probabilistic seismic hazard expressed in distance, magnitude, and peak ground acceleration for southern New England. The steps in the depth blocks are for magnitudes 5.0 to 5.5, 5.5 to 6.0, 6.0 to 6.5, and > 6.5. Adapted from a presentation by Gabriel Toro to the Interagency Committee on Dams at Emmitsburg, MD (1997).

Figure 25. Example of a logic tree or decision tree for evaluating risk.

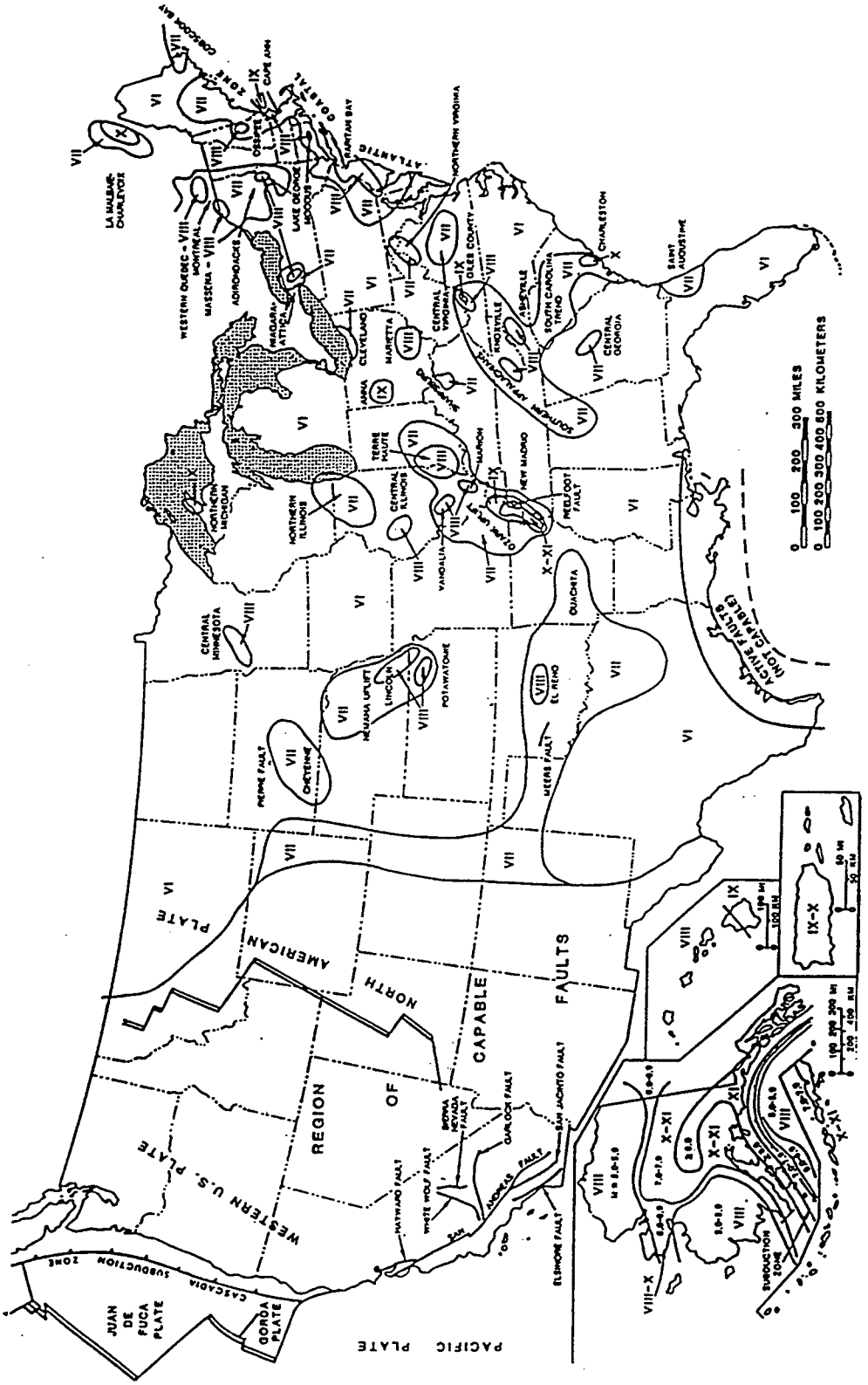

Figure 1. Distribution of seismic source areas in the United States. From Krinitzsky, Gould and Edinger (1993).

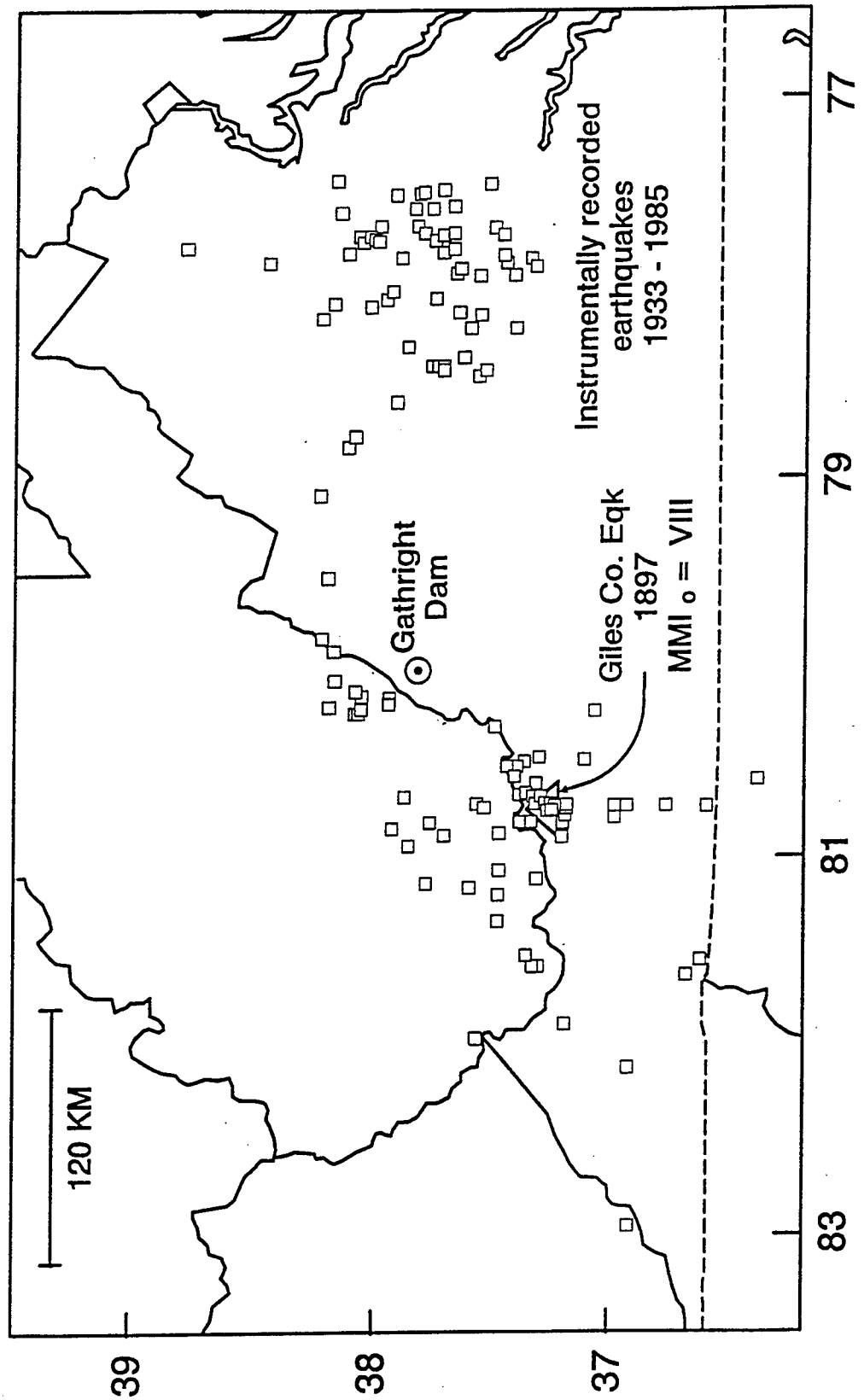

Figure 2. Instrumentally located earthquakes in the region of Gathright Dam, Virginia. From Bollinger and others (1987). The Giles County earthquake of 1897, MM = VIII, was added.

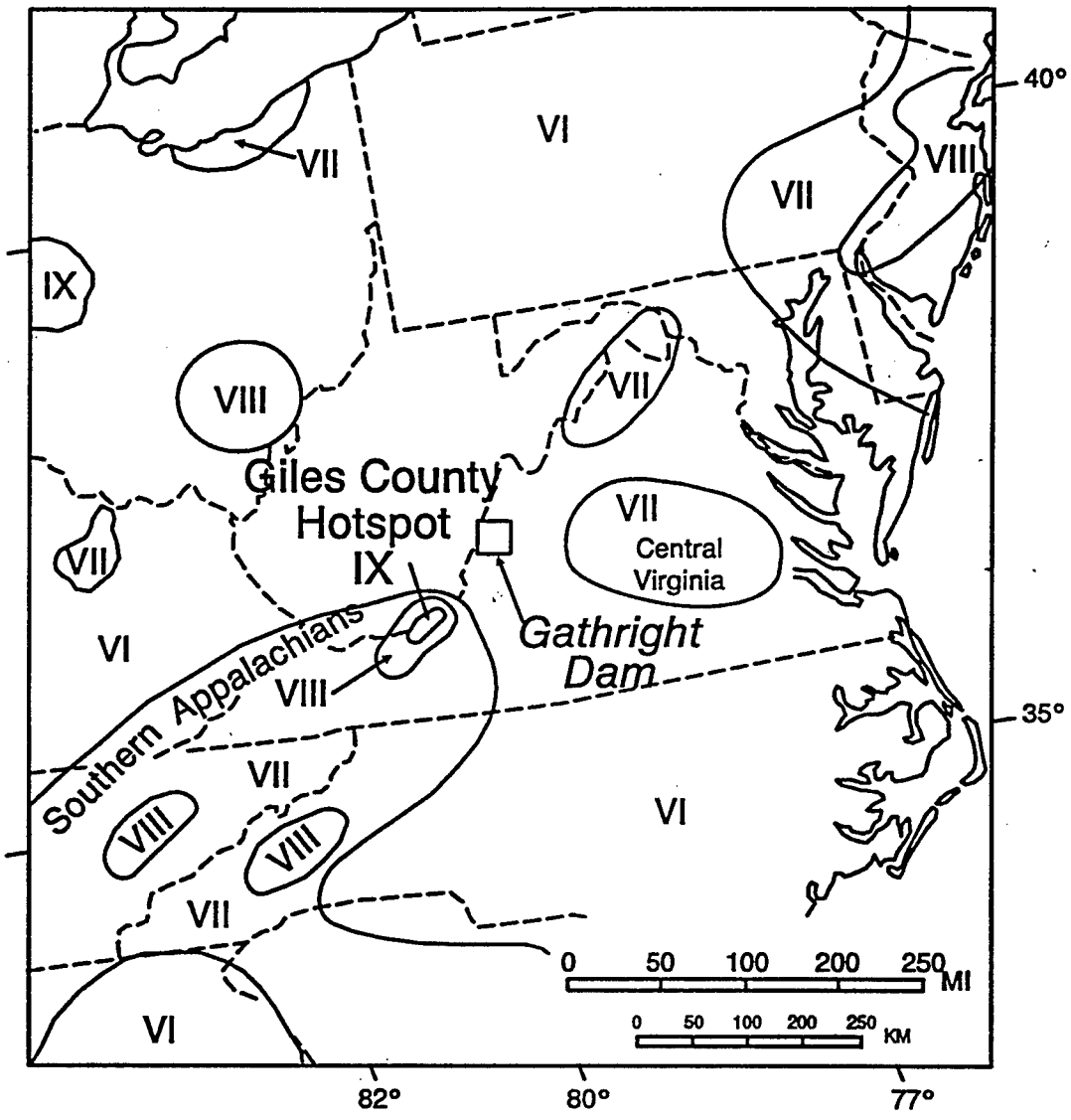

Figure 3. Seismic zones in the region of Gathright Dam, Virginia. From Krinitzsky and Dunbar (1990).

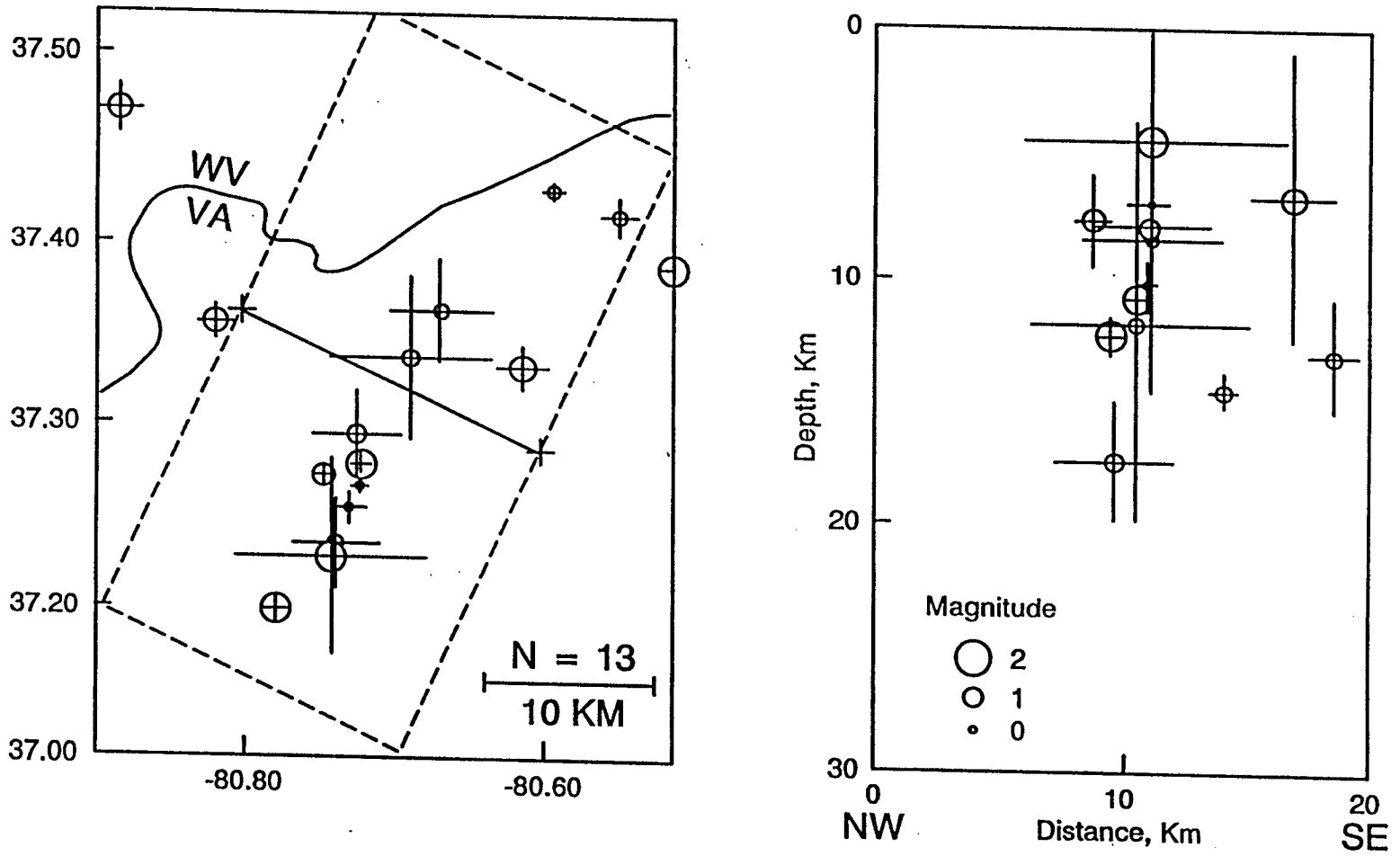

Figure 4. Definition of the Giles County, Virginia, seismic source from microearthquakes. From Bollinger in Krintzsky and Dunbar (1990).

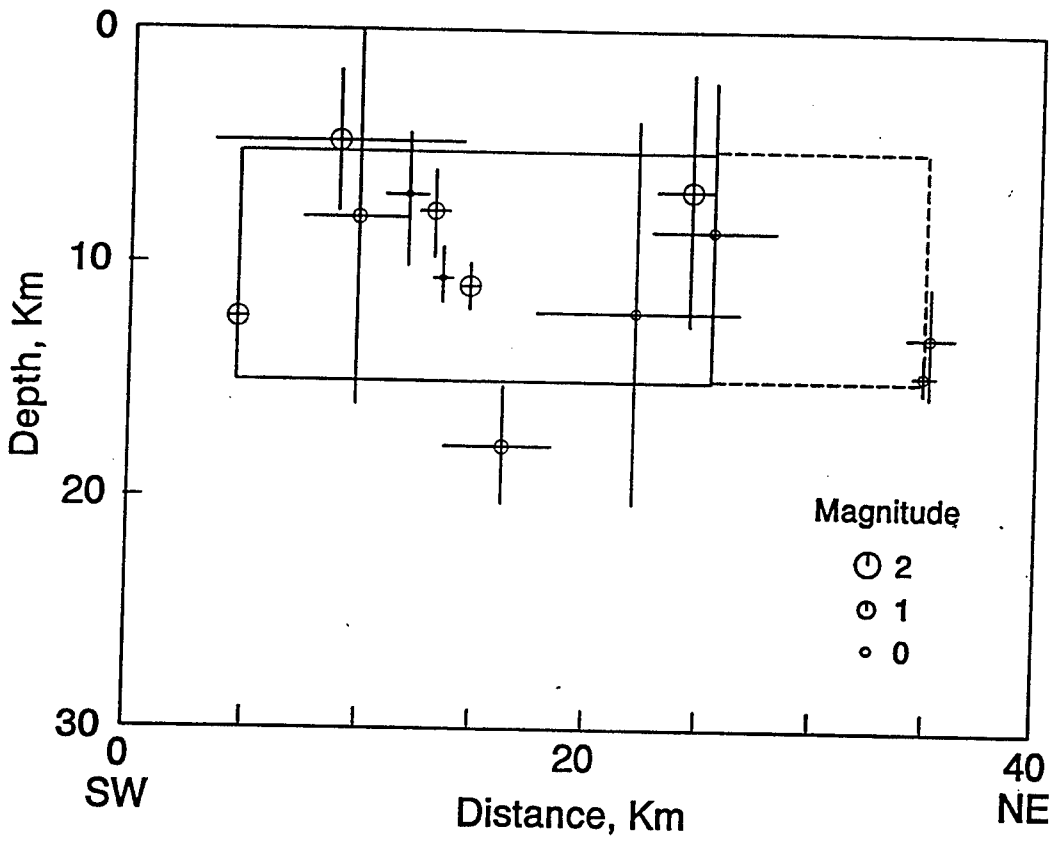

Figure 5. Small area, 200 km^2, and large area, 300 km^2, interpreted from microearthquakes as the fault zone in the Giles County, Virginia, seismic source. From Bollinger in Krinitzsky and Dunbar (1990).

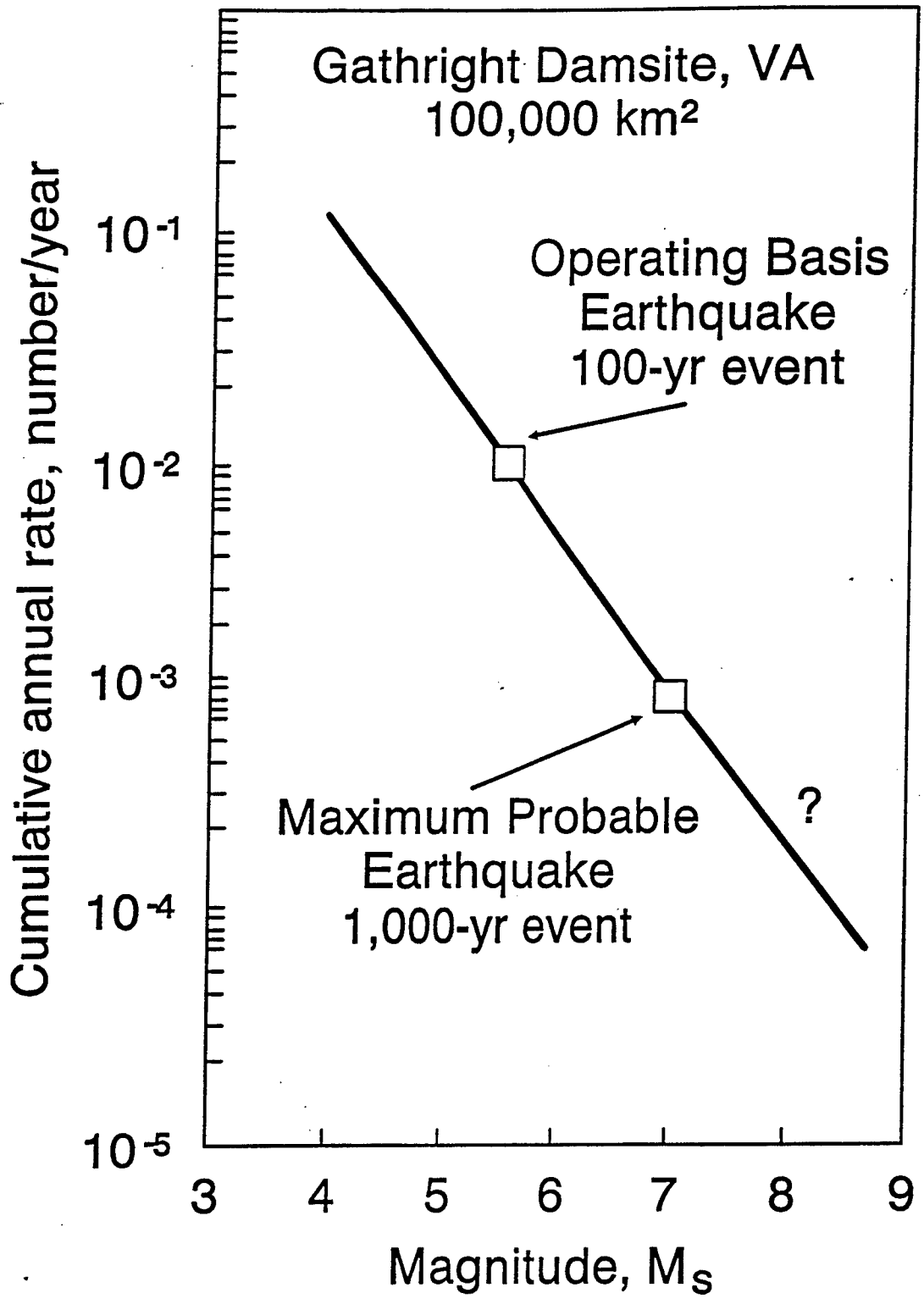

Figure 6. Gutenberg-Richter b-line based on 100,000 km² in the region of Gathright Dam, Virginia. From Bollinger in Krinitzsky and Dunbar (1990).

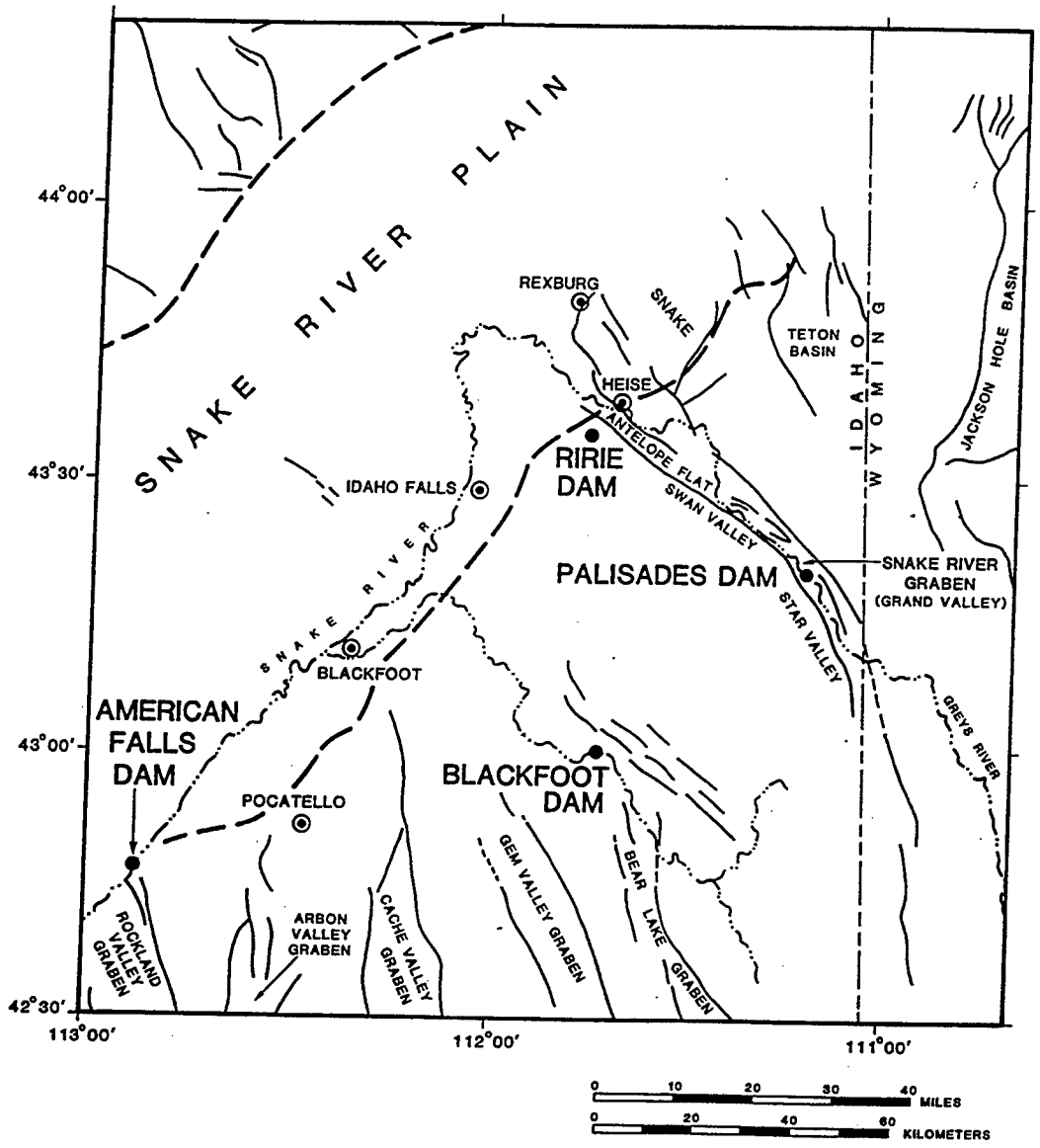

Figure 7. Major structural features in the region of Ririe Dam, Idaho. From Krinitzsky and Dunbar (1991).

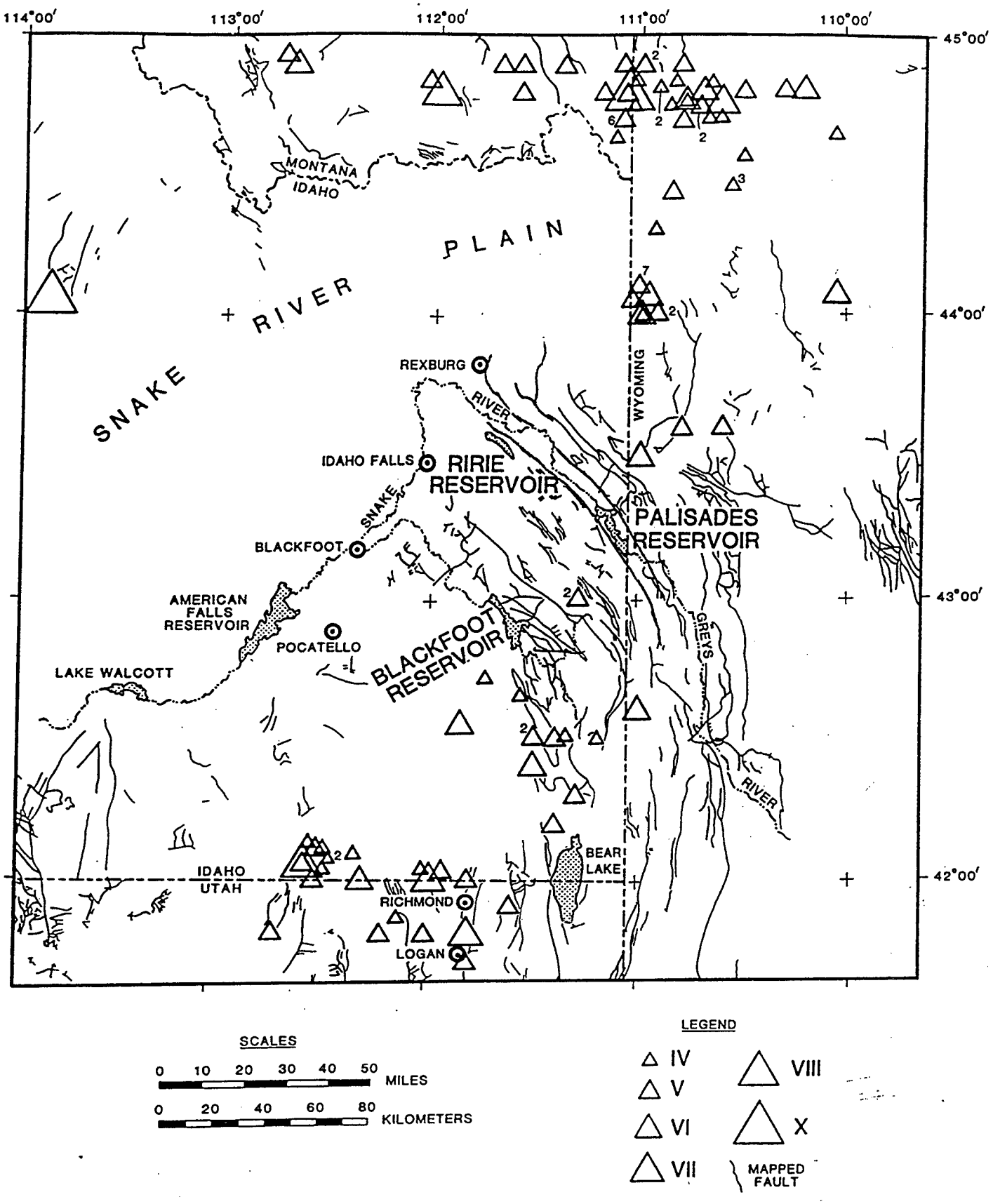

Figure 8. Historic seismicity in the region of Ririe Dam, Idaho. From Krinitzsky and Dunbar (1991).

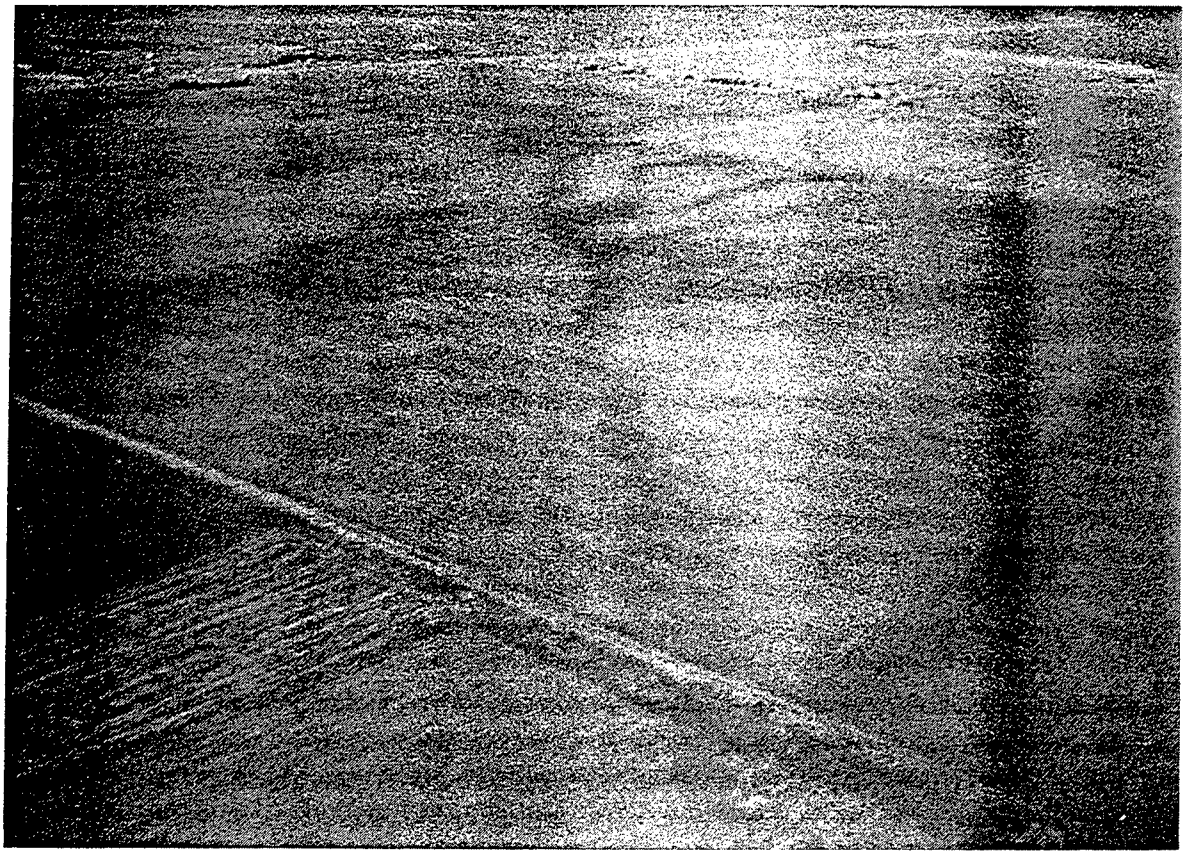

Figure 9. A close-up view of a linear feature near Ririe Dam. The surface is a loess-covered basaltic plateau. Note how drainage has been interrupted. From Krinitzsky and Dunbar (1991).

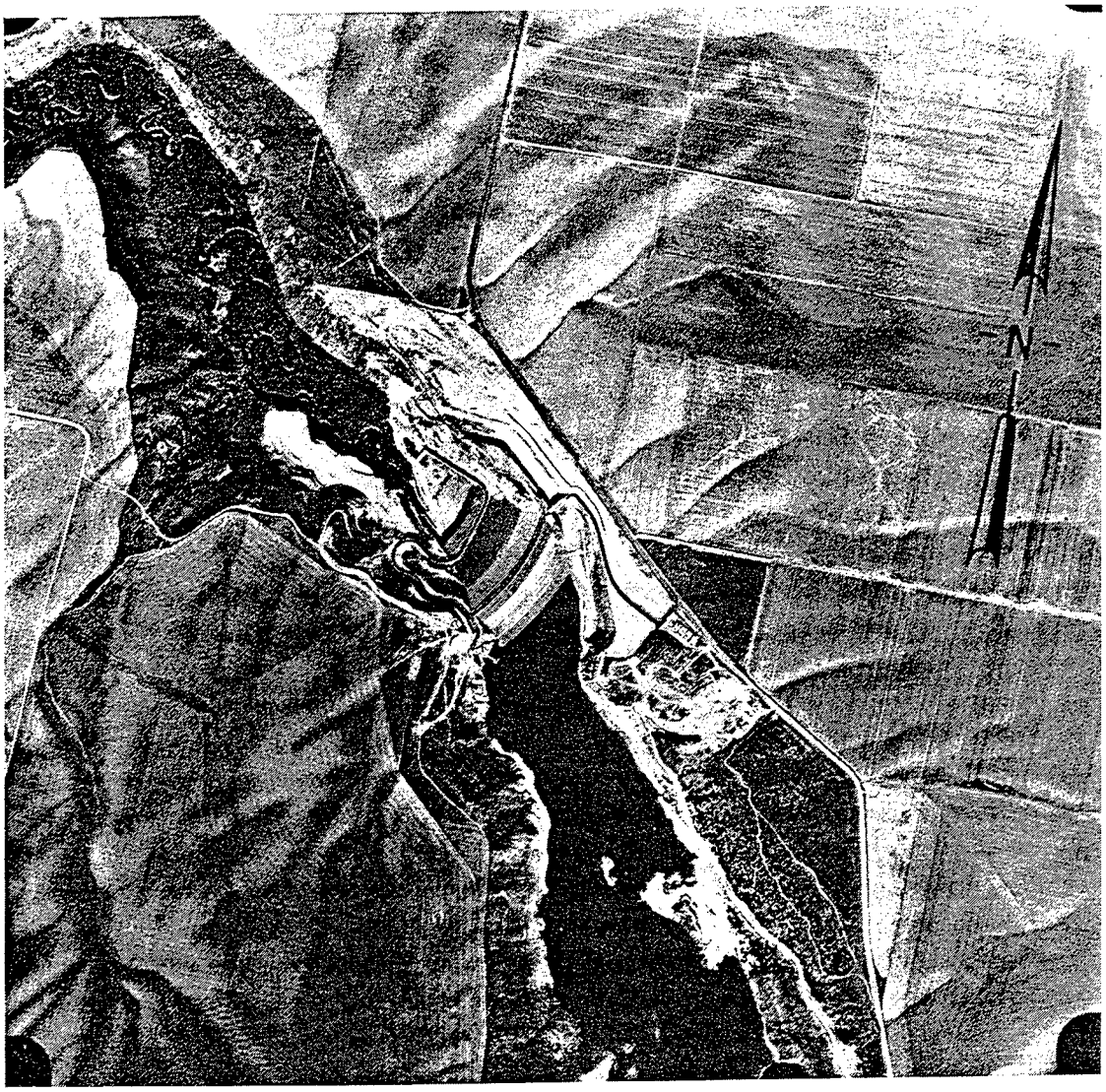

Figure 10. Occurrence of lineaments in relation to Ririe Dam. From Slemmons and Ramelli in Krinitzsky and Dunbar (1991).

Figure 11. Scarp of the fault bordering Swan Valley near Heise, Idaho. Travertine from recently active hot springs is seen on the fault. From Krinitzsky and Dunbar (1991).

Figure 12. A view of the Rexburg fault south of Rexburg, Idaho. Note that interrupted drainage has barely eroded the face of the scarp. From Krinitzsky and Dunbar (1991).

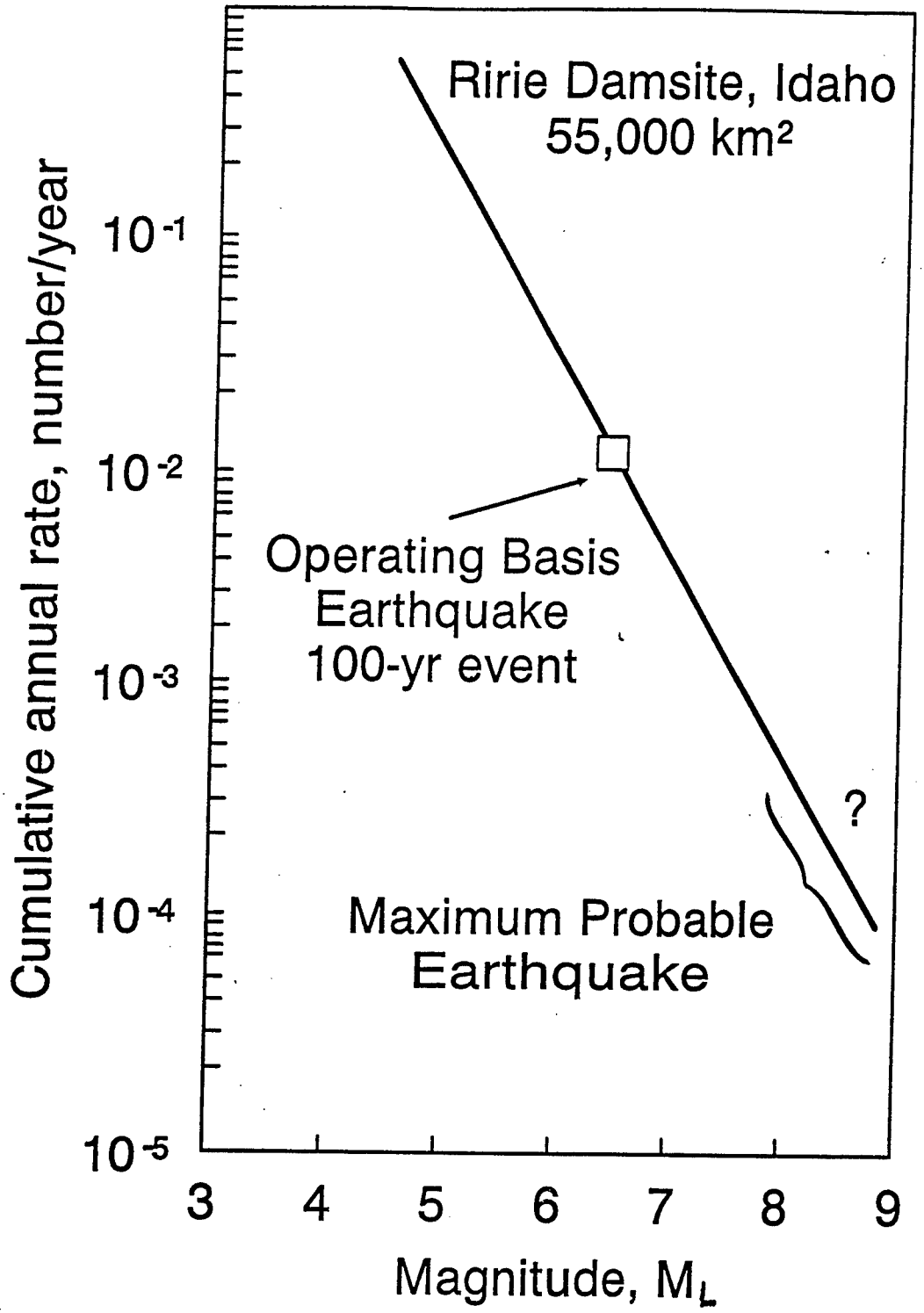

Figure 13. Gutenberg-Richter b-line based on 55,000 km² in the region of Ririe Dam, Idaho. Adapted from Piety and others (1985) who created it for nearly Palisades Dam (see Figure 7) and terminated it at M = 7.5.

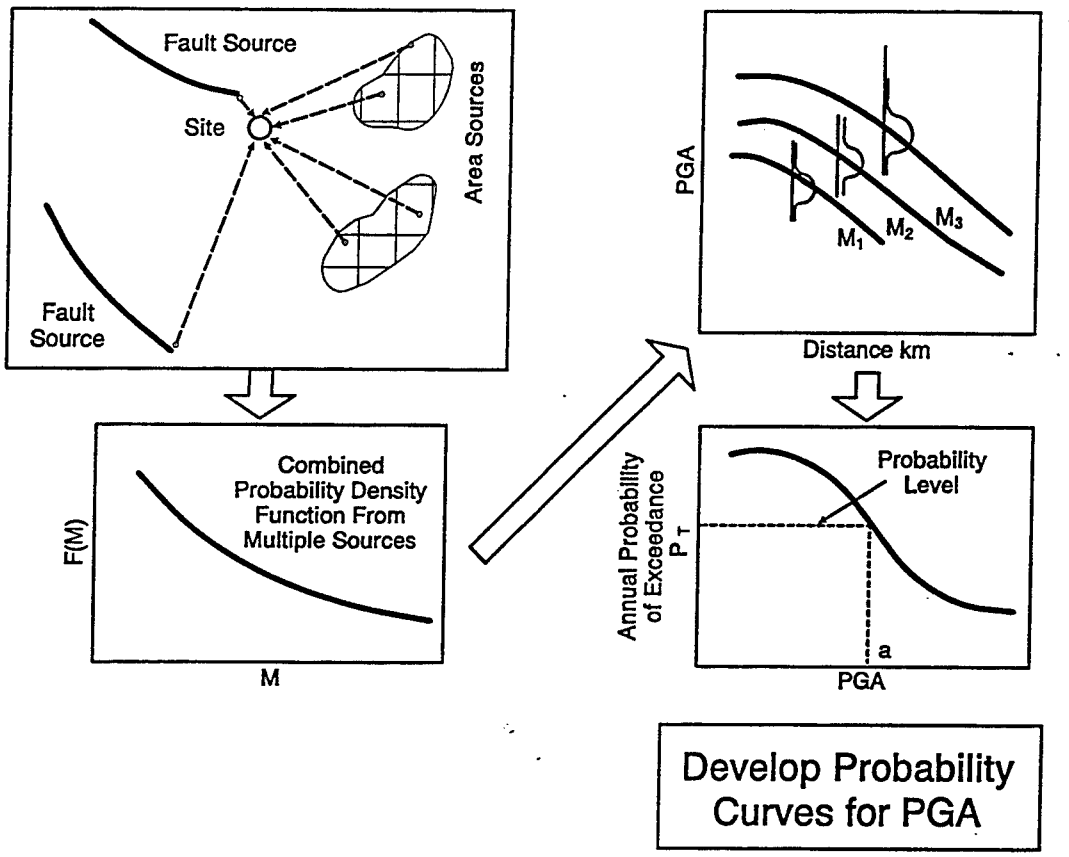

Figure 14. Generalized procedure for obtaining the probabilistic seismic hazard for a region as peak ground acceleration with annual probability of exceedance. Arrows from sources to the site also show how deterministic assessments would be applied. Deterministic evaluation would provide individual time histories for maximum credible earthquakes that represent earthquake potentials at the sources. The probability combines the earthquakes from these sources and predicts that the combination changes its size in an orderly progression through time.

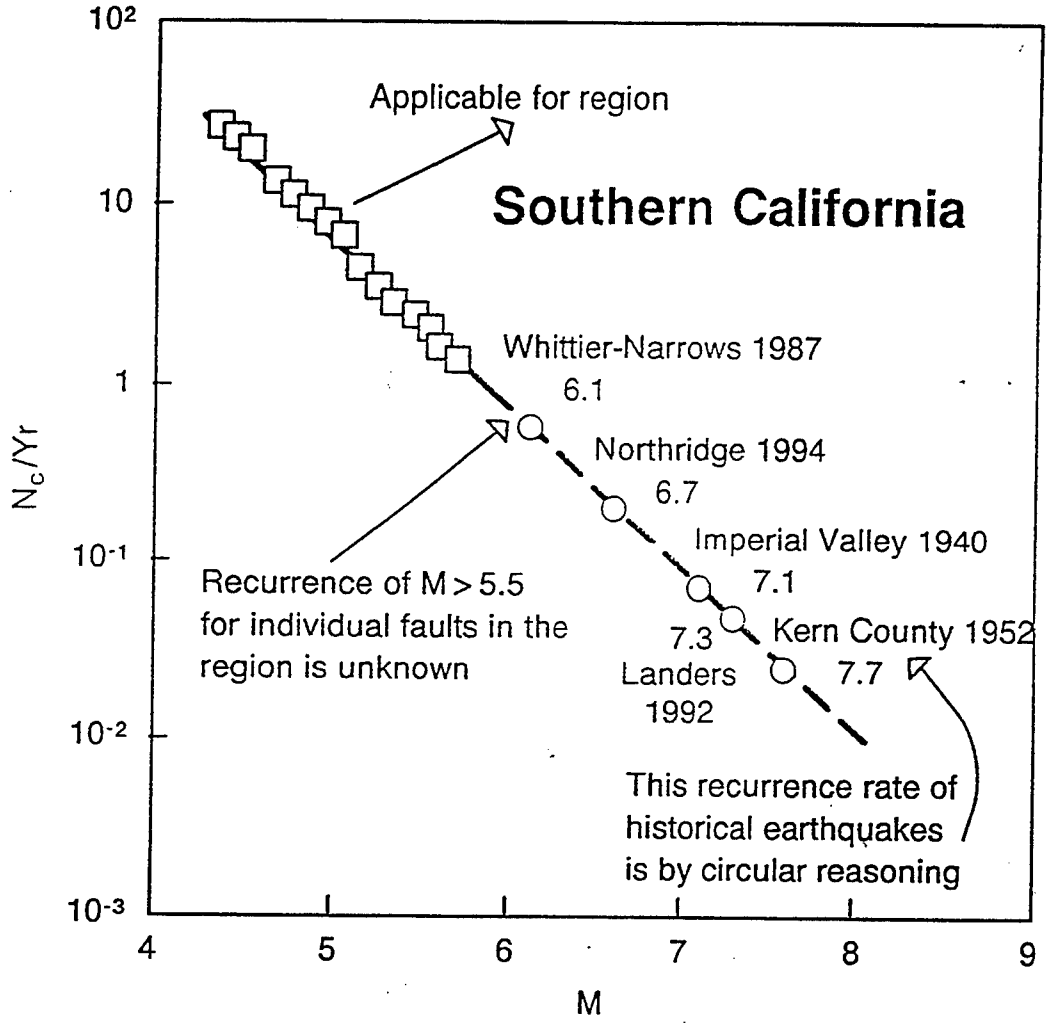

Figure 15. Probabilistic recurrence rates for earthquakes in Southern California from projections of the Gutenberg-Richter b-line. Recurrence was observed only in small earthquakes. The rest is projection and assumption. Application is collectively for the region and not for any specific site.

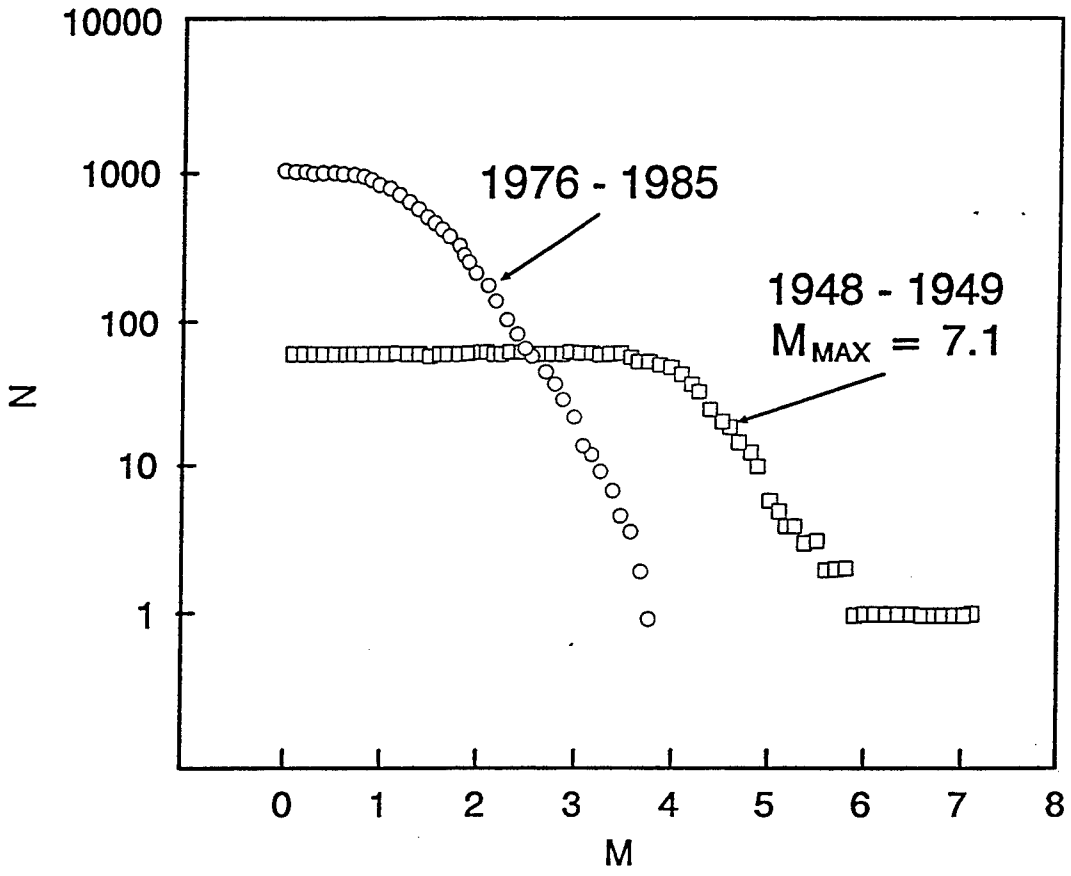

Figure 16. Variance in b-lines for earthquakes at Fukui, Japan. From Watanabe (1989).

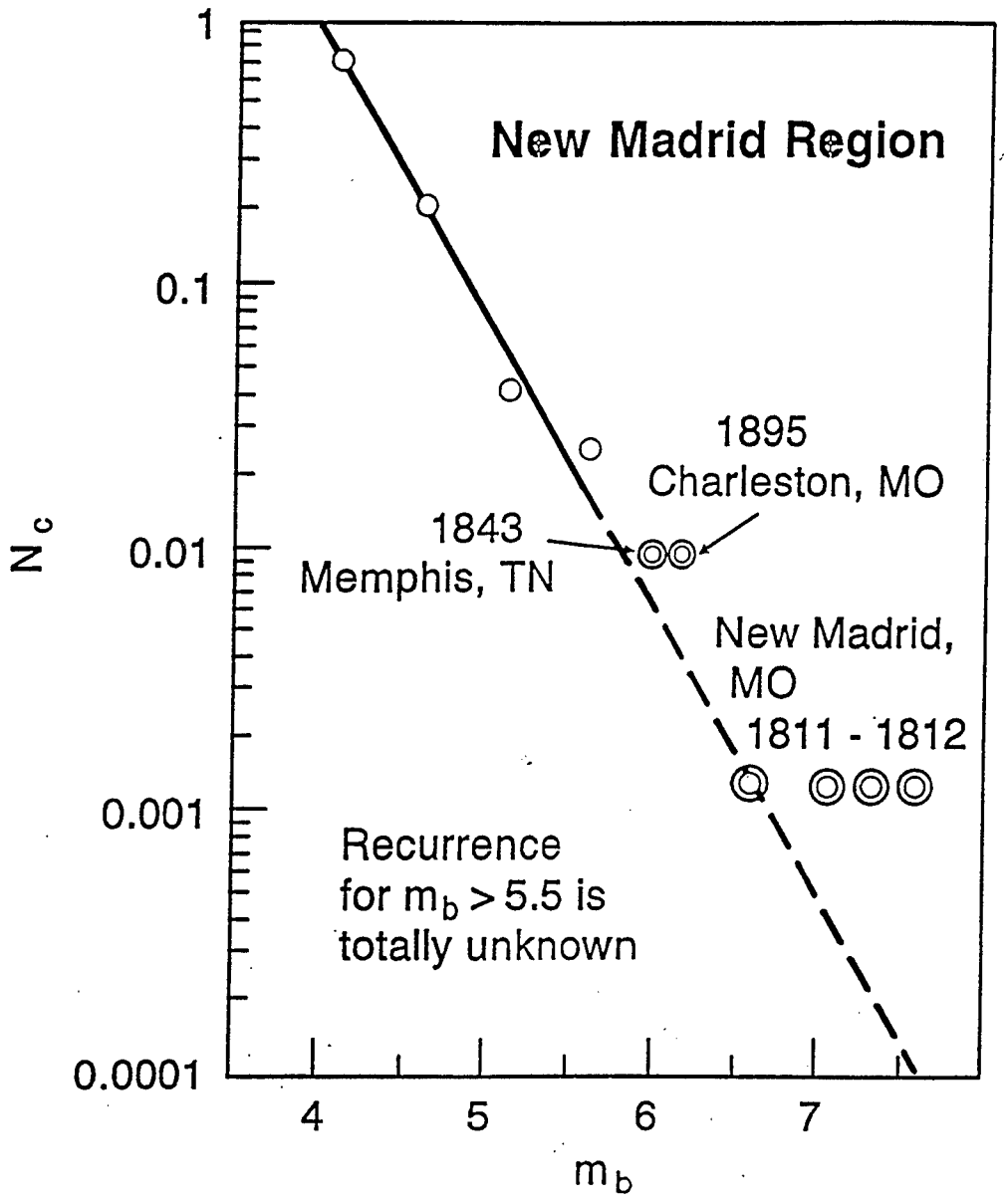

Figure 17. Probabilistic recurrence rates for earthquakes in the New Madrid region. Recurrence for the historic earthquakes is unknown.

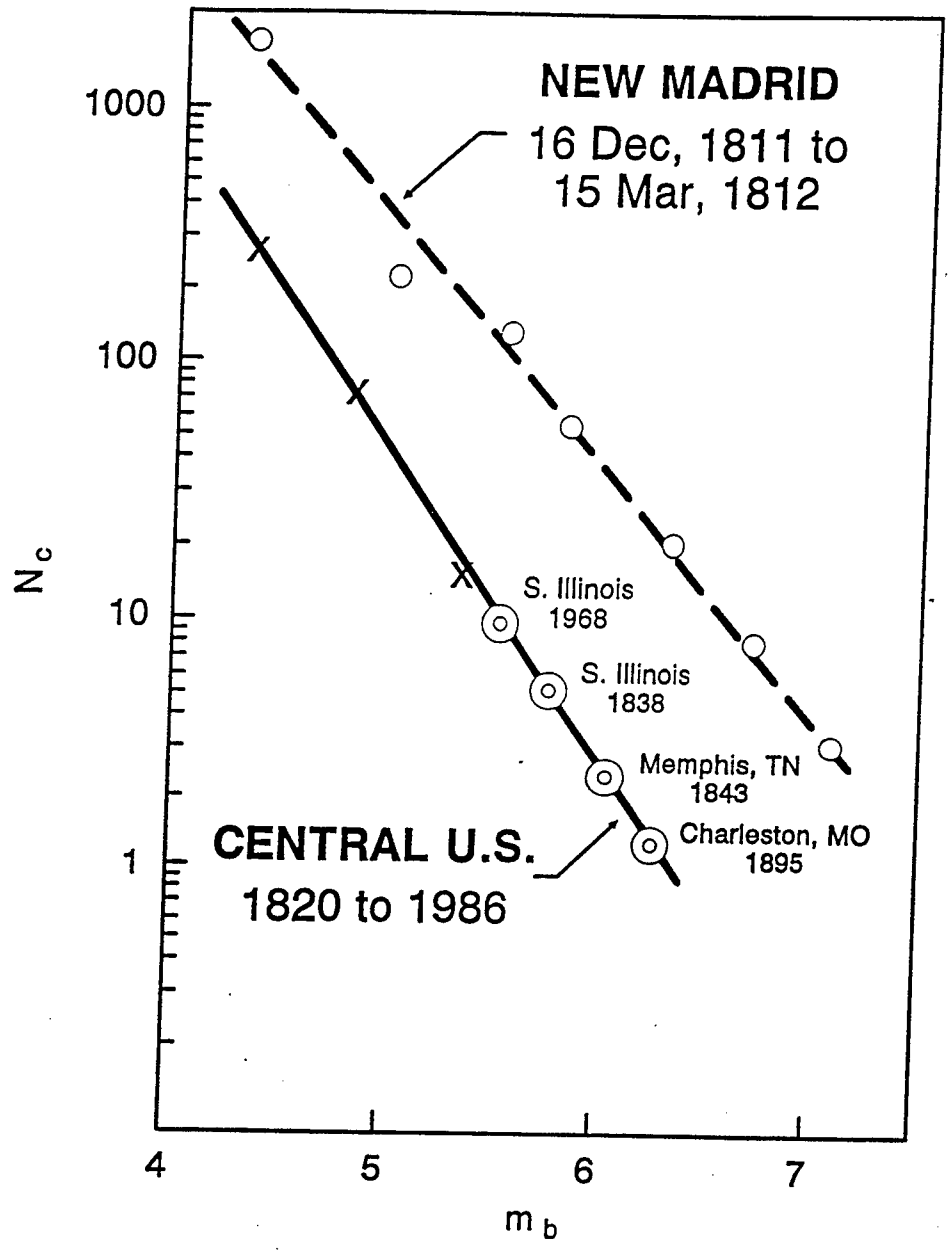

Figure 18. Separated b-lines for New Madrid: 16 December 1811 to 15 March 1812 and 1820 to 1986. A b-line is not a single or exact entity but a broad and uncertain zone. Adapted from Mitchell in Krintzsky (1993b).

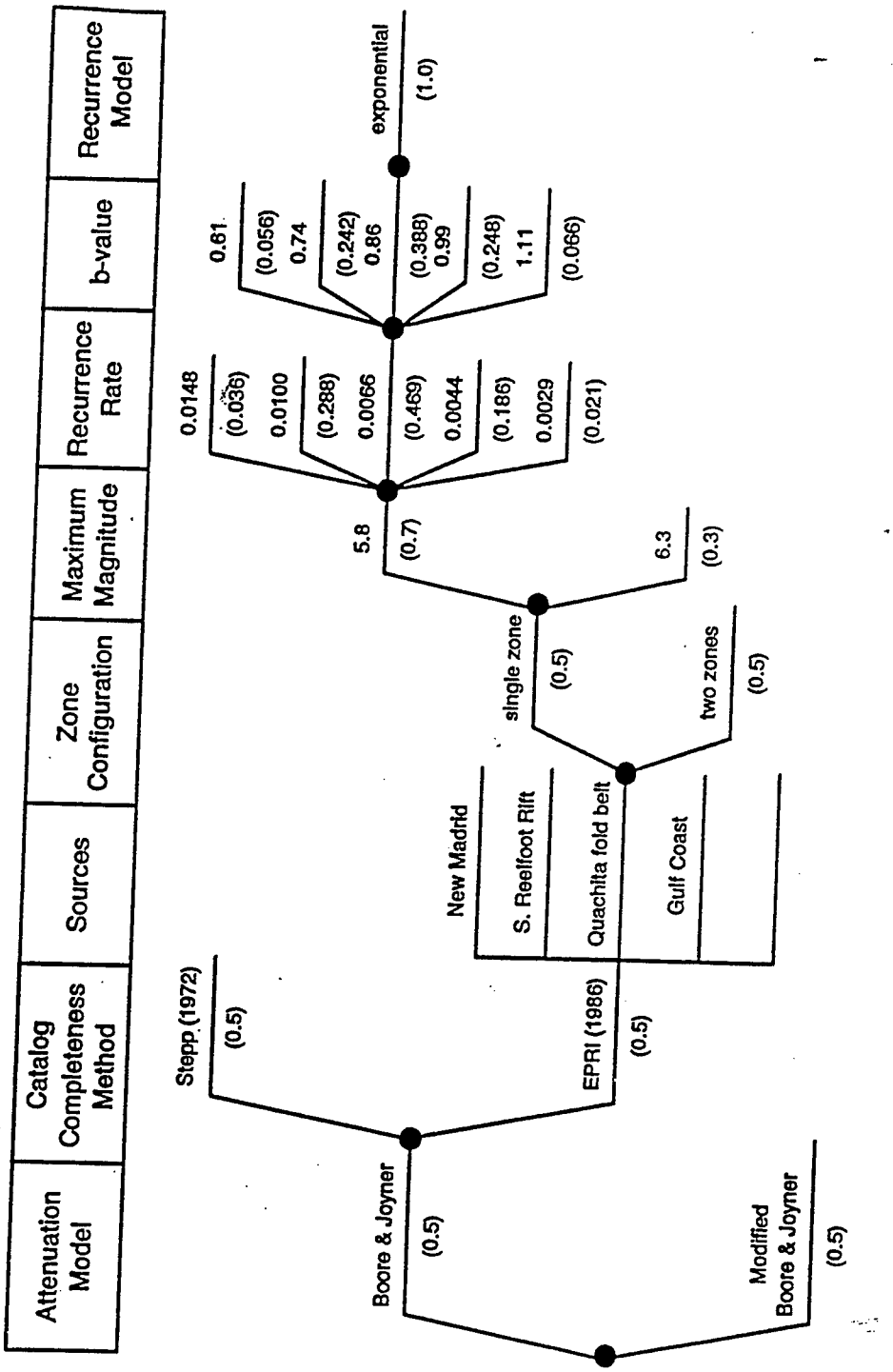

Figure 19. Logic tree to evaluate uncertainty for a probabilistic seismic hazard analysis. From Power (1994).

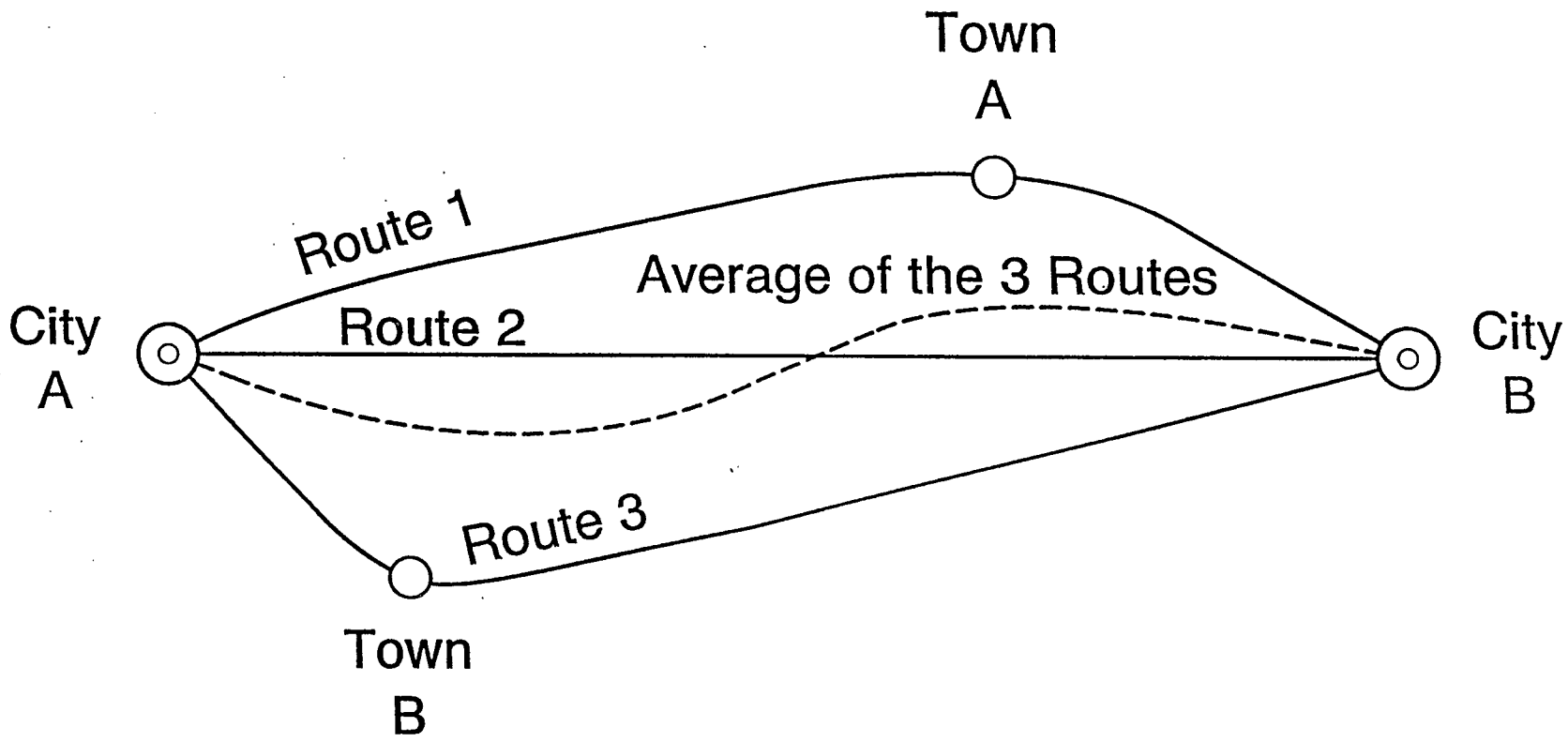

Figure 20. Why different models cannot be averaged: There are three routes, each of which serves a purpose. Route 1 serves Town A, Route 2 is shortest, Route 3 serves Town B. When they are averaged, they produce a route that has no purpose. Their criteria are lost and the result is without useful meaning.

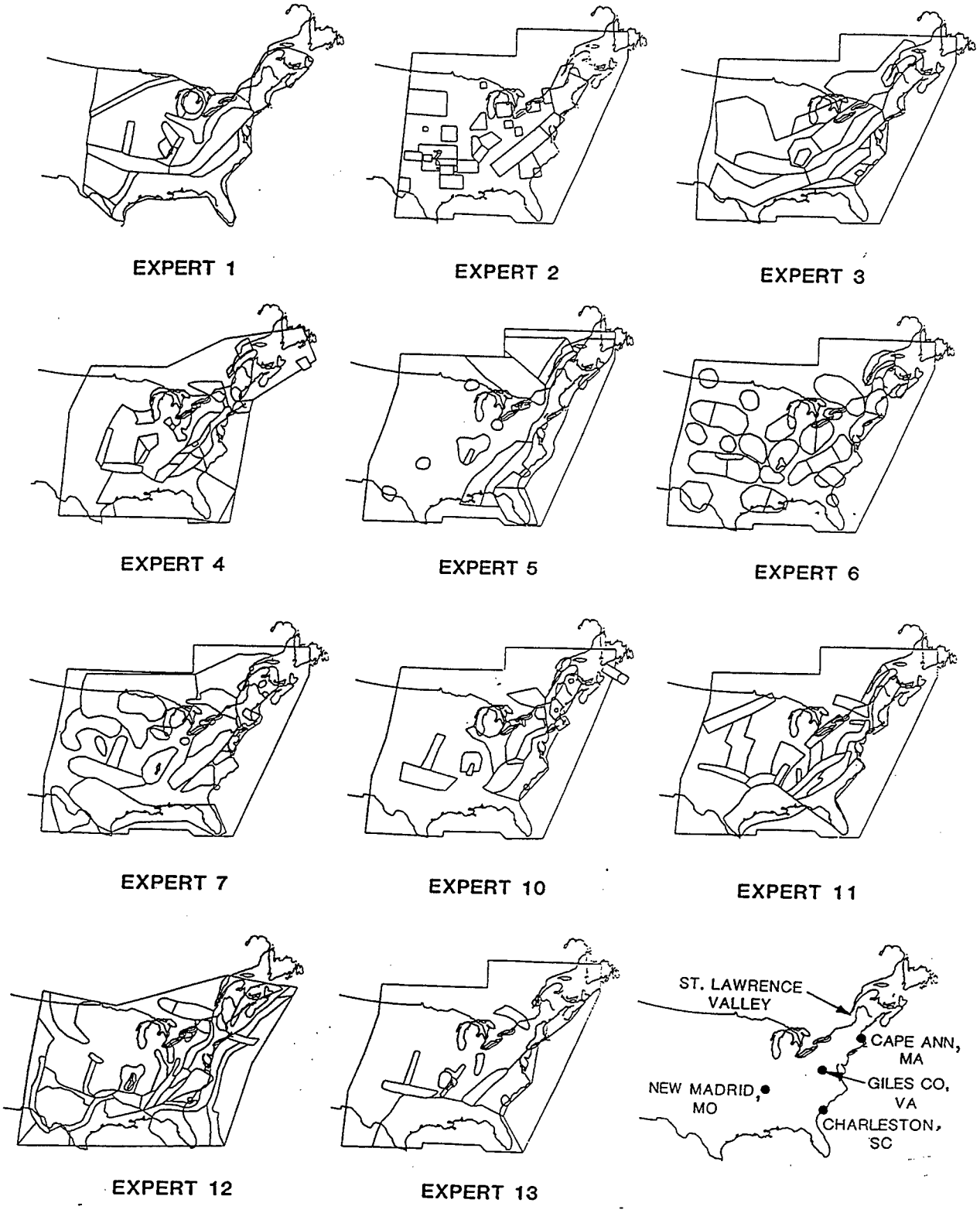

Figure 21. Seismic source zones for eastern United States by eleven experts. From Bernreuter et al. (1989). The location map in the lower right corner was added to show seismic hotspots.

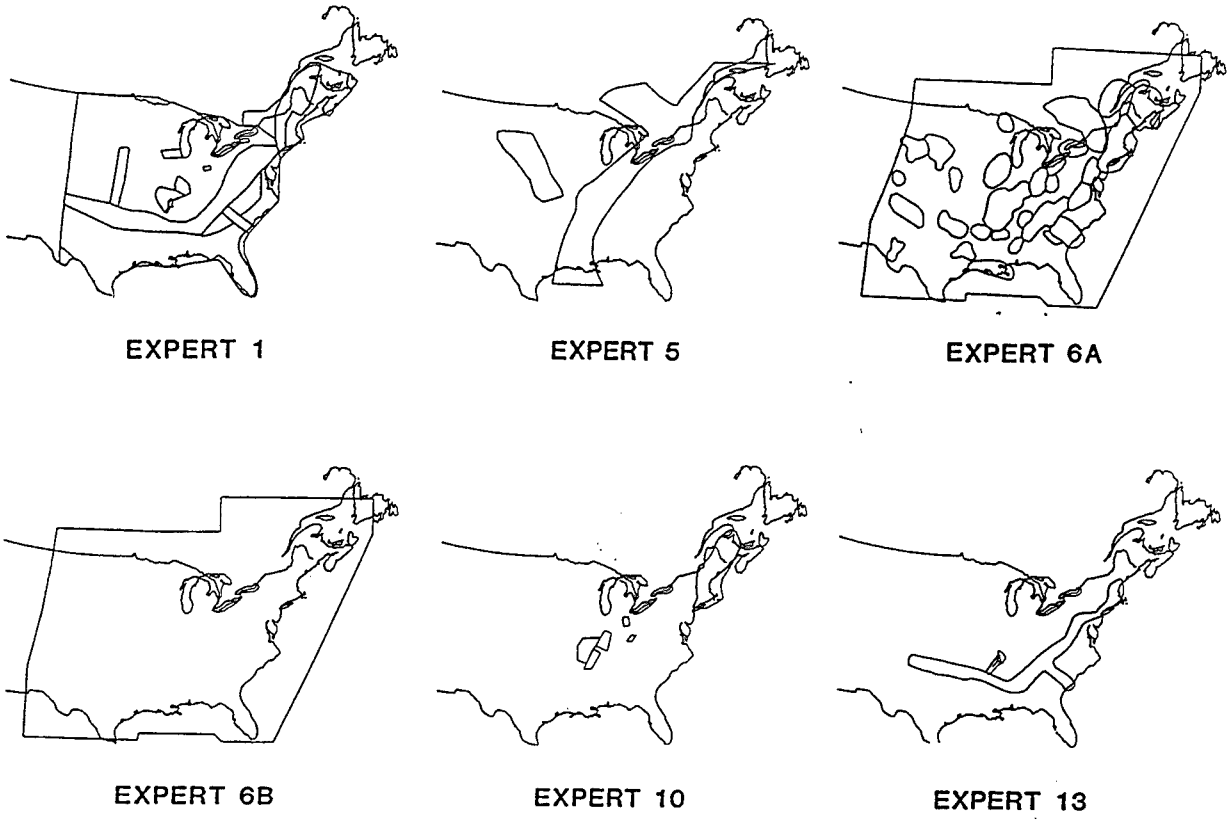

Figure 22. Six alternative seismic source zones for eastern United States by five experts. From Bernreuter et al. (1989).

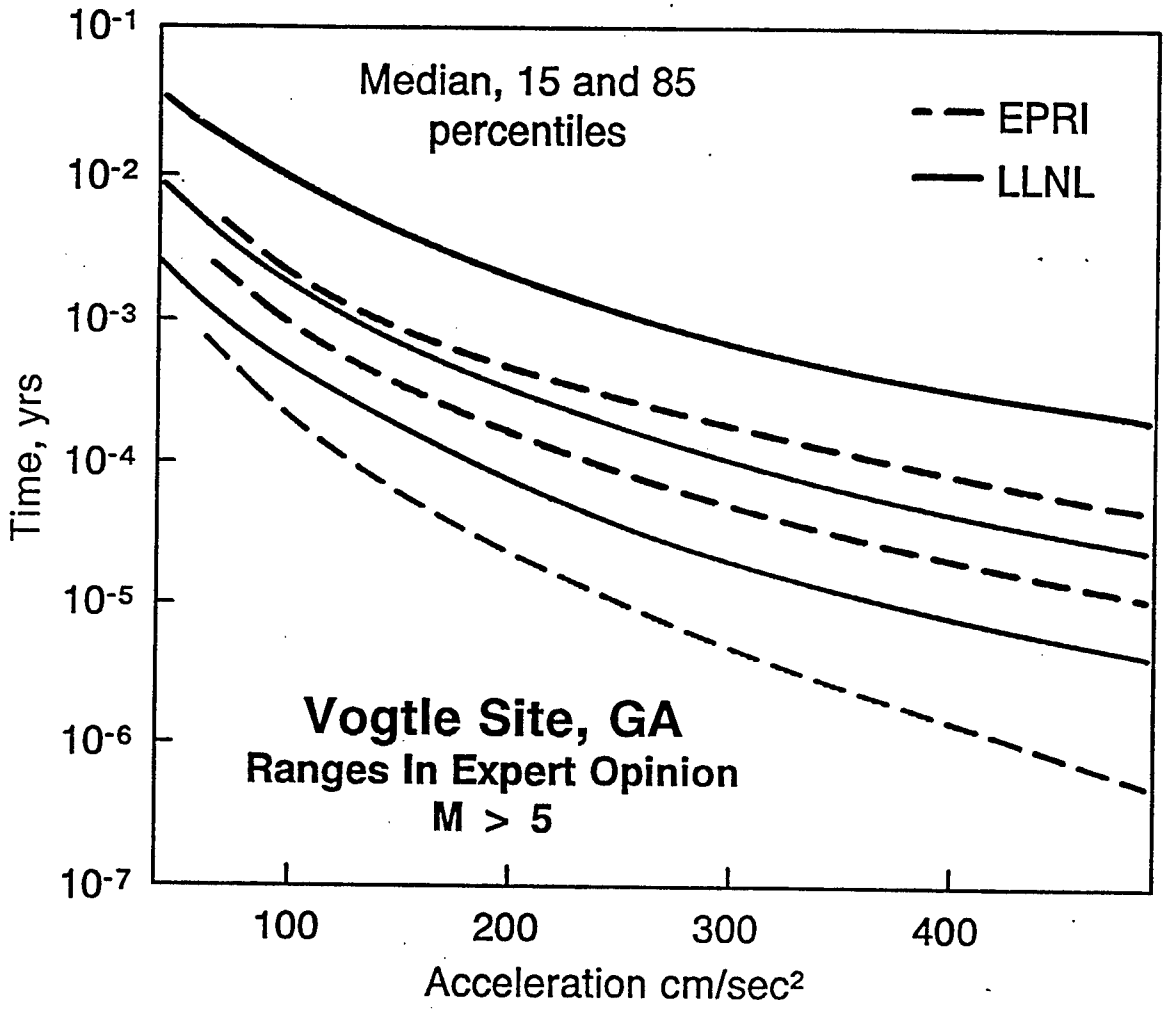

Figure 23. Ranges of calculated acceleration-through-time curves generated by the Lawrence Livermore National Laboratory and the Electric Power Research Institute for the Vogtle Nuclear Power Plant Site, Georgia. From Bernreuter et al. (1987).

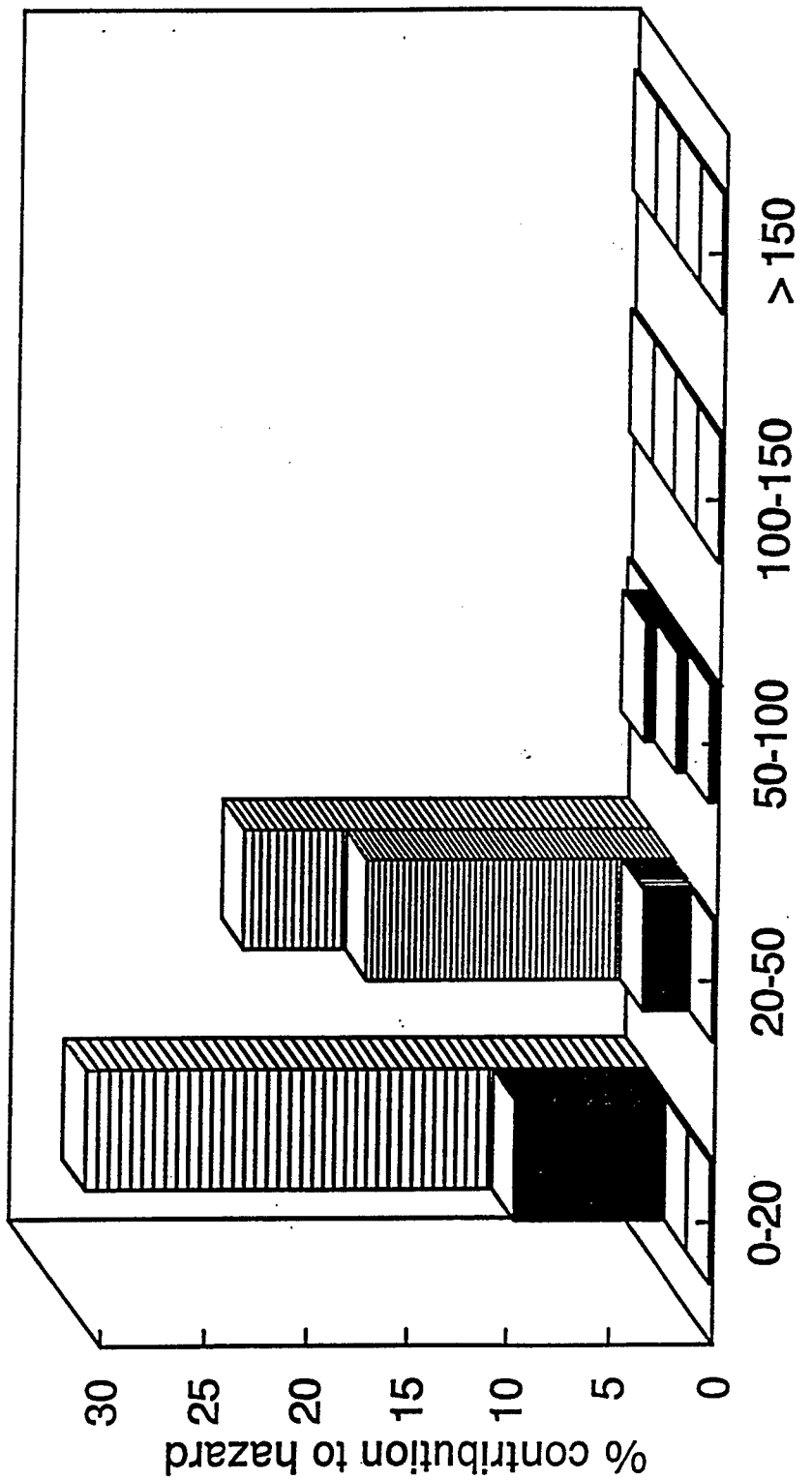

Figure 24. De-aggregations of the probabilistic seismic hazard expressed in distance, magnitude, and peak ground acceleration for southern New England. The steps in the depth blocks are for magnitudes 5.0 to 5.5, 5.5 to 6.0, 6.0 to 6.5, and > 6.5. Adapted from a presentation by Gabriel Toro to the Interagency Committee on Dams at Emmitsburg, MD (1997).

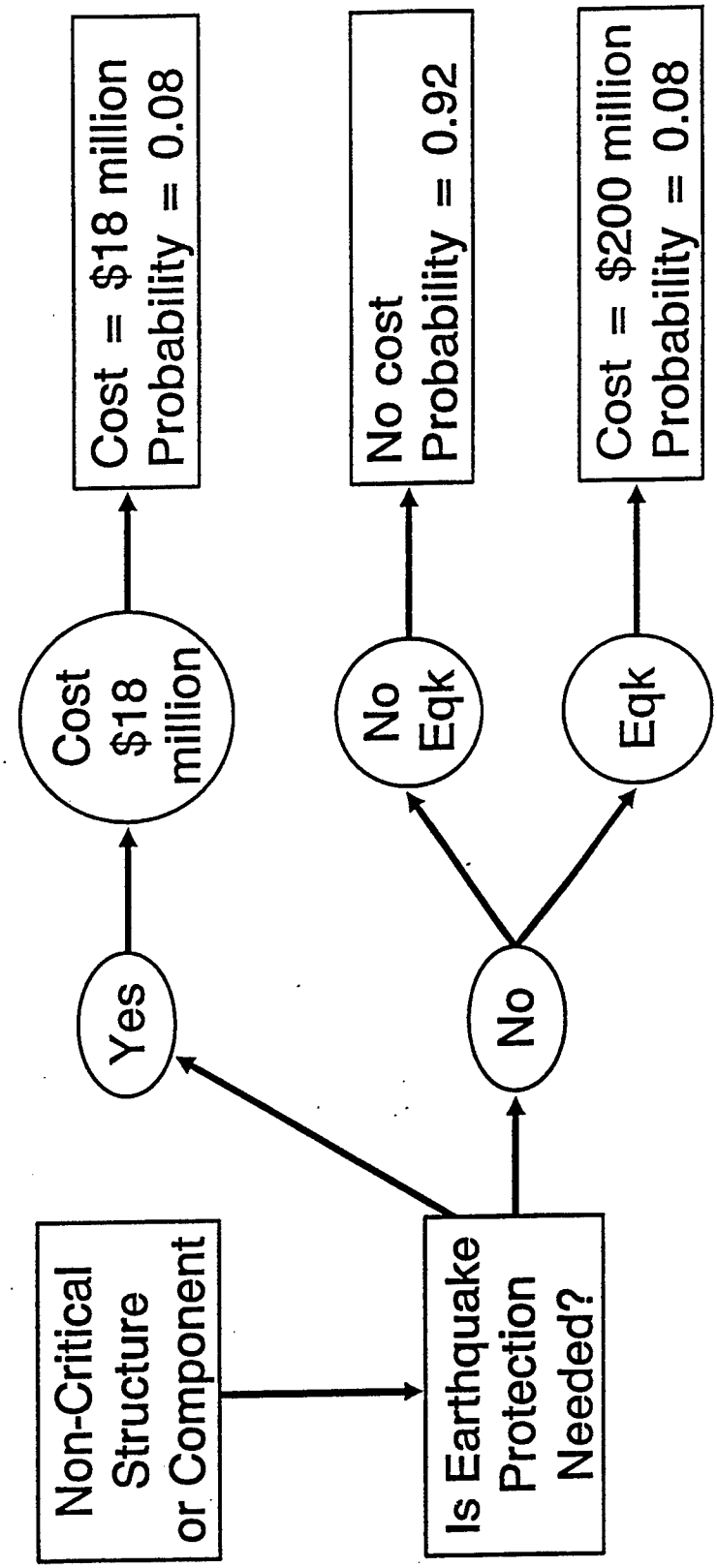

Figure 25. Example of a logic tree or decision tree for evaluating risk.

EVALUATION OF SEISMIC SLOPE STABILITY OF EARTH AND ROCKFILL DAMS

OHNE, Yoshio, Professor, Dept. of Civil Eng., Aichi Institute of Technology, Japan

ABSTRACT

In this paper, some discussions are made on the applicability of the seismic coefficient method (SCM) for use in the earthquake resistant design through laboratory tests on dynamic properties of actual fill materials, large-scale shaking table tests on model earth and rockfill dams and F.E. nonlinear dynamic response analysis of embankments. A practically useful method of evaluating seismic stability of earth and rockfill dams is then proposed by introducing seismic shear strain developed during earthquake as a criterion. Discussions are summarized as follows: 1) for shallow surface sliding in rockfill dams SCM can be applied effectively with a little modification on the frequency dependent parameters, and 2) for interior sliding failures occurring in both earth and rockfill dams safety evaluation in terms of seismic shear strain and associated rigidity reduction of fill materials is considered to be quite reasonable in place of the current SCM design method.

1. INTRODUCTION

The F.E. dynamic response analysis has recently been considered as a practically useful and precise measure to investigate seismic behavior of earth and rockfill dams, nevertheless the seismic coefficient method (SCM) is still widely used in the design stage to evaluate their seismic resistance against slope failure. It has not been reported so far that large earth and rockfill dams have experienced serious damages including sliding failures to cause severe economic and social losses, though they have often been attacked by strong earthquakes of the maximum acceleration far beyond the design value adopted. In the Naganoken-Seibu earthquake in 1984 (Japan, M=6.8), for instance, the epicenter was several hundred meters far from Makio dam, a centrally located core type rockfill dam of 105m in height, and the maximum acceleration at the crest of the dam was estimated to be almost the same as the acceleration of gravity (g) (Ohne,1985).

In the Morgan Hill earthquake in 1984 (USA, M=6.2), the maximum acceleration observed at the left side abutment foundation of Coyote damsite was as large as 1.29 times of g (Shakal, et.al., 1984). Serious damages, however, were not reported in these cases except for small open cracks on the crest and/or shallow surface slip of rockfill slopes even through the embankments were under such strong excitation of more than several times as large as the design value of acceleration. This is to be said due to an essential shortcomings of SCM in which dynamic forces developed in an embankment during earthquake are treated statically by introducing the equivalent seismic inertia forces.

Is this paper, the applicability of SCM for use in the design is discussed through angle of repose tests on rock materials, large-scale shaking table tests on model earth and rockfill dams and F.E. dynamic response analysis of embankments. A practically useful method of evaluating seismic stability of earth and rockfill dams is then proposed by introducing seismic shear strain as a criterion.

2. FAILURE MECHANISM OF EARTH AND ROCKFILL DAMS DURING EARTHQUAKE

According to the investigation reports on earthquake damages of actual embankment

dams and also to the experimental studies through large-scale shaking table tests on the dynamic response of earth and rockfill dams (Ohne, 1983), embankment failures caused by strong excitation are classified into several patterns in their mechanism, as shown in Fig.1.

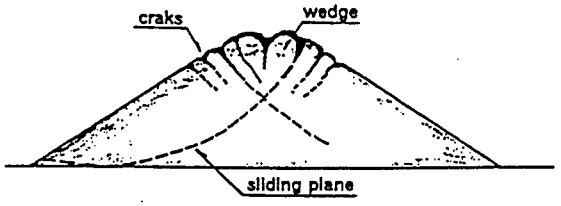

(a) Homogeneous Earthfill Dam

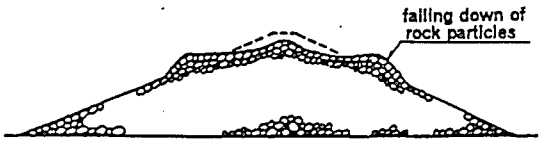

(b) Homogeneous Rockfill Dam

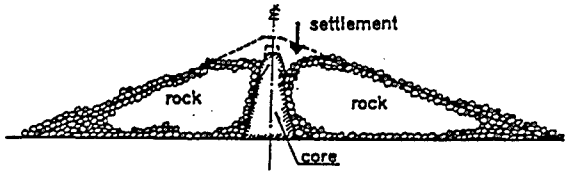

(c) Centrally Located Core Type Rockfill Dam

Fig.1 Failure Mechanism of Embankment Dams during Earthquake

Summarizing of the mechanism on embankment failures due to earthquake excitation, the focus of discussion to the earthquake resistant design of earth and rockfill dams should be placed in this paper on the two main subjects listed below.

(1) falling down of rock particles and/or shallow surface sliding failure in rockfill slopes

(2) deep circular sliding failure in homogeneous earthfill dams, and also in rockfill dams having a soft clayey core in the interior

3. SURFACE SLIP IN ROCKFILL SLOPES

By applying SCM to the evaluation of shallow surface sliding in rockfill slopes, the dynamic angle of repose ϕ_d of rockfill materials under the excitation of the base acceleration α_B can be expressed in the following form (Ohne, 1987)

$$\phi_d = \phi_1 - \tan^{-1}\left(\frac{\alpha_B}{980\lambda}\right) \qquad (1)$$

in which ϕ_1 is the static angle of repose of the same rock materials, and λ stands for a correction factor for SCM-calculation, which depends on material properties of rock particles, shape and size, and also on the magnitude and frequency of the excitation; λ =1 corresponds to so-called SCM.

The relationship between the value of ϕ_1 and the mean particle size D_{50} of six uniformly distributed gravels tested in the laboratory is plotted by open circles in Fig.2, together with the additional test results, shown by solid circles, obtained in the field. It is seen in the figure that the ϕ_1 -value increases with the increase in the value of D_{50} and it approaches to a constant value of 66° to 68° ,which is considered to be a representative value of ϕ_1 of rock materials usually used in rockfill dams.

A representative result of dynamic angle of repose tests is shown in Fig.3 for the gravel of D=30～40mm (D_{50}=35mm), in which the measured values of ϕ_d are plotted against the table acceleration α_B for various frequencies of excitation f . As the test result showed ϕ_1=54° for this material, reference curves of $\phi_d \sim \alpha_B$ of SCM-calculation are drawn by solid lines in the figure by use of Eq.(1) for various values of λ . It is seen that two parameters λ and f contribute to $\phi_d \sim \alpha_B$ relation in a similar manner, showing the increase of λ with the decrease in f ; i,e., λ =1 (true SCM-relation) corresponds to f≒10Hz and λ ≒1.5 to f≒4Hz.

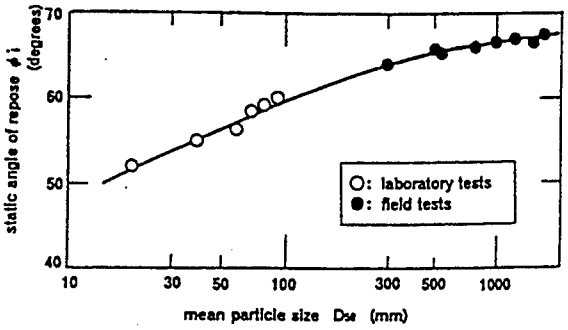

Fig.2 $\phi_i \sim D_{50}$ Relationship

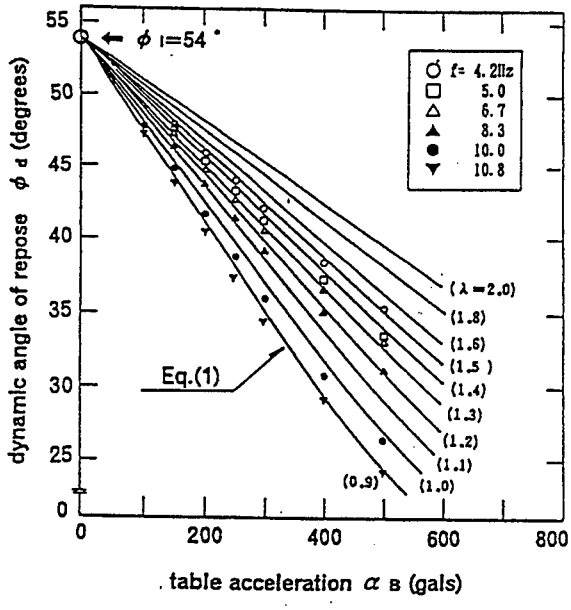

Fig.3 Dynamic Angle of Repose ϕ_d (D_{50}=35mm)

Fig.4 shows the relationship between λ and the frequency (f) for six uniformly distributed gravels having different particle sizes. It is recognized that the value of λ shows somewhat large scatter in the range of $f \leqq 8$Hz but approaches to a certain constant value of $\lambda \fallingdotseq 0.8$ at $f \fallingdotseq$ 11Hz, and that this scatter is not influenced by the particle size.

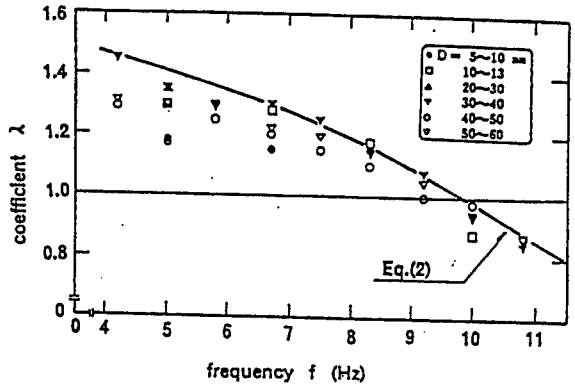

Fig.4 $\lambda \sim f$ Relationship

As the predominant frequency of excitation of hazardous big earthquakes is supposed to be lower than 1～ 2Hz, SCM tends to underestimate a factor of safety in the evaluation of seismic stability against shallow surface sliding of rockfill dams, leading to an uneconomical design, and Eq.(1) then should be modified for use in the actual design corresponding to the frequency of earthquake excitation. A regression curve of the test results, covering upper bound values for a safe side design, is drawn in Fig.4 by a thick solid line, giving

$$\lambda = -0.00488\,f^2 - 0.0163\,f + 1.64 \qquad (2)$$

By denoting the value of ϕ_d modified by Eq.(2) as ϕ_d', a stable angle of rockfill slope during earthquake ϕ_{ds} (the design value of ϕ_d) is expressed with a factor of safety Fs as follows.

$$\tan\phi_{ds} = \tan\phi_d'/Fs \qquad (3)$$

4. EVALUATION OF SEISMIC SAFETY IN TERMS OF SHEAR STRAIN

4.1 Shaking Table Tests on Model Fills

Fig.5 shows a representative result of shaking table tests on a homogeneous model earth-fill, in which the measured value of the average shear strain γ is plotted against the average response acceleration α_m for each of three sections divided in the crest, the middle and the bottom parts of the fill, being denoted below by CREST, MIDDLE and BASE, respectively: γ is defined here as the value of the maximum relative displacement, mean of two absolute peak values in a cycle (Δd/2), divided by the distance between two points i and j and α_m the mean value of response acceleration observed at the same points. It is seen in CREST that all of the data indicated by open circles for various frequencies and amplitudes of the table acceleration exhibit a certain trend to form a relation curve of $\gamma \sim \alpha_m$. Similar relationships of $\gamma \sim \alpha_m$ are demonstrated in other sections of the fill by connecting solid circle data points obtained at the same test conditions of excitation,

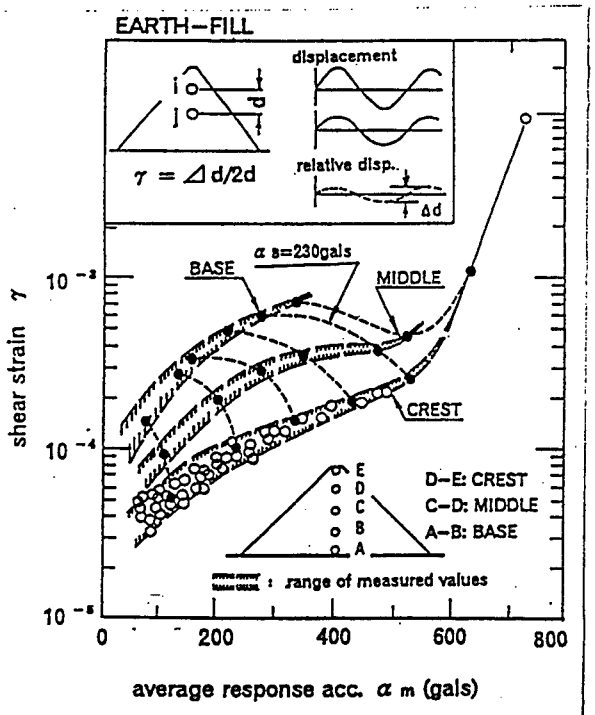

Fig.5 Relationship between Shear Strain and Response Accelaration(Earth-fill)

showing a sharp increase in γ in CREST at a certain value of α_m. This sharp increase in γ is supposed to be a threshold of embankment failure because a deep sliding failure was observed in the test at around α_s=250gals, which is only 20gals larger than the limiting value of α_s of 230gals.

Similar tendency as mentioned above was recognized in the test series of homogeneous rock-fills, where the value of γ increases with the increase in α_m and shows a sharp change at a certain value of α_m: e.g., shallow surface sliding was observed in a test at around α_s =210gals which is only 10gals larger than the threshold value.

It is of great importance in the earthquake resistant design of earth and rockfill dams to discuss with what way, with what parameter and how exactly a sign of embankment failure can be estimated. As noted above , the shear strain γ developed in the embankment during oscillation showed a sharp increase just before the occurrence of sliding failures in both earth and rockfill slopes, so that γ becomes to be one of influential factors closely related to the embankment failure. It is then natural to consider that the shear strain just at the corner point of its sharp increase can be an important parameter in the earthquake resistant design for use in the prediction of a threshold of embankment failure.

In the following discussions, the value of γ and the corresponding response acceleration at the corner point are represented by the yield shear strain γ_y and the yield response acceleration α_{my}, respectively.

4.2 Evaluation of Embankment Failure in Terms of Shear Strain

As the shear strain developed in the embankment during oscillation is considered to have a close relation to the dynamic deformation characteristics of fill materials, modulus of rigidity (G) and damping factor (h), the results of shaking table tests shown in Fig.5 are re-examined by contrasting with those from cyclic triaxial tests on the materials of model fills. The relationship

between the ratio of the modulus of rigidity G/G_0 and the shear strain γ obtained in the cyclic triaxial tests on earth-fill materials is presented in Fig.6, in which three relation curves indicated by CREST, MIDDLE and BASE are the ones calculated by using the following equation of Hardin-Drnevich model with material parameters estimated at the same locations in the fill for the corresponding confining pressures σ'.

$$G/G_0 = \frac{1}{1+\gamma/\gamma_r}$$
$$h/h_0 = \frac{\gamma/\gamma_r}{1+\gamma/\gamma_r} \qquad (4)$$

Eartf-fill: $G_0 = 510\sigma'^{0.47}$
$\gamma_r = 4.8\times10^{-3}\sigma'^{0.75}$
Rock-fill: $G_0 = 1010\sigma'^{0.58}$
$\gamma_r = 7.0\times10^{-4}\sigma'^{0.38}$

As can be seen in the shaking table tests on the earth-fill, as drawn again in Fig.7, the values of shear strain developed at CREST,MIDDLE and BASE when CREST reaches to the yield state are $\gamma=\gamma_y$ (C)$=2.5\times10^{-4}$, $\gamma=3.9\times10^{-4}$ and $\gamma=6.2\times10^{-4}$, respectively, as indicated by solid circles. By applying this yield strain γ_y(C)$=2.5\times10^{-4}$ to the $G/G_0\sim\gamma$ relation in Fig.6, the corresponding value of the ratio G/G_0 is obtained as 0.56; i.e., the yield state comes out at CREST when the rigidity of the material reduces to 56 percent of G_0 (G at small strain of $\gamma=10^{-6}$). Supposing that yielding starts at the same condition of $G/G_0=0.56$ even in MIDDLE and BASE, the yield strains at these locations are taken from Fig.6 as γ_y(M)$=4.4\times10^{-4}$ and γ_y(B)$=7.2\times10^{-4}$,respectively. These values of yield strain are plotted again in Fig.7 as level reference lines, indicating that shear strains developed at MIDDLE and BASE are smaller than their respective yield strains when CREST is in the yield state. A factor of safety (Fs) can then be defined in terms of shear strain for every locations in the fill by the ratio of the shear strain at yield γ_y to that at current state γ. By using the deta mentioned above, the values of Fs are

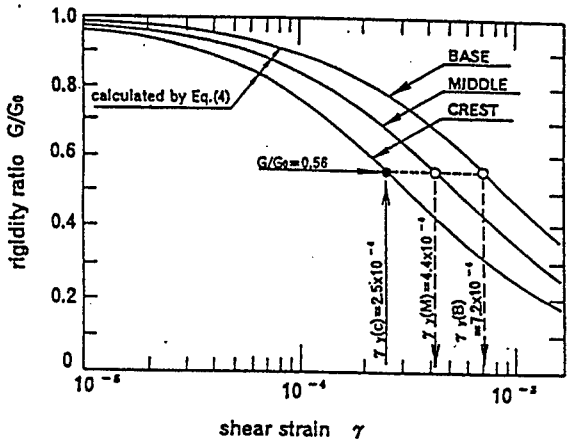

Fig.6 $G/G_0\sim\gamma$ Relationship(Earth-fill)

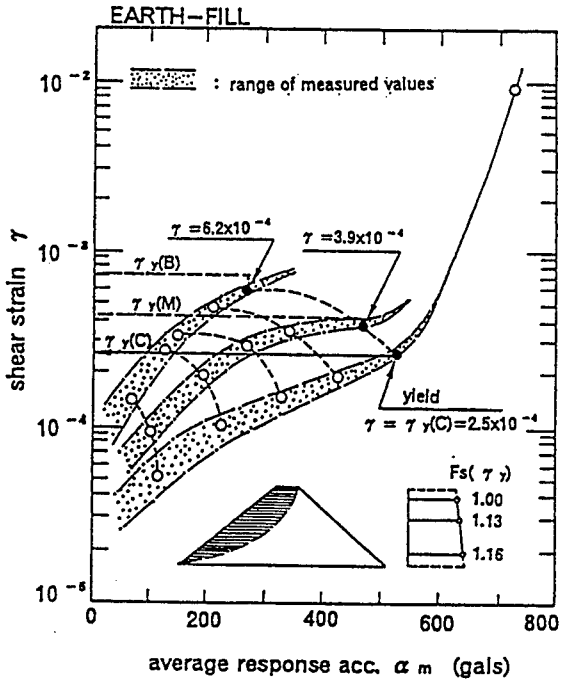

Fig.7 Safety Evaluation in terms of Shear Strain (Earth-fill)

calculated at MIDDLE and BASE as Fs(M)=1.13 and Fs(B)=1.16, respectively, for the critical state of CREST, Fs(C)=1, and the distribution of Fs is drawn along the center line of the fill, as shown in Fig. 7. it is inferred from Fig. 7 that an overall deep sliding failure is probable for earthfill fams because the distribution of Fs is rather uniform, showing equal chance to fail from the top to the

bottom of the embankment.

Similar discussions are given for rockfill dams by comparing the results of shaking table test on a model rock-fill, Fig. 8 and those from cyclic triaxial tests on the same fill material, Fig.9.

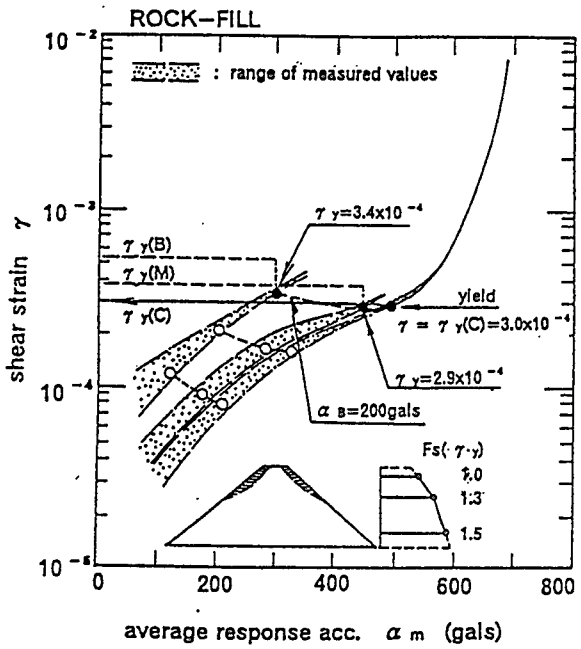

Fig.8 Safety Evaluation in terms of Shear Strain (Rock-fill)

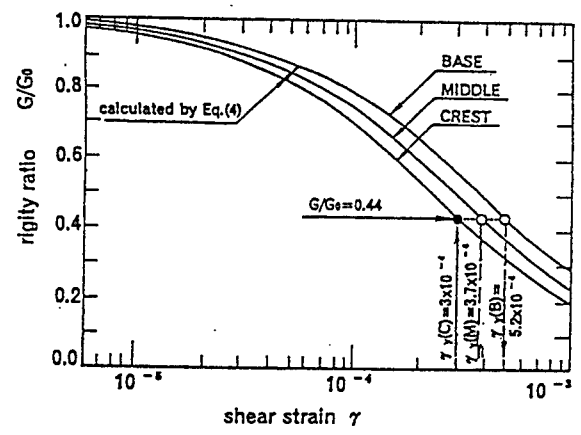

Fig.9 G/Go～γ Relationship(Rock-fill)

In place of the above-mentioned procedure of safety evaluction, where the rate of rigidity reduction at the yield state is assumed to be the same at every locations in the fill , another way of safety evaluation is presented in the following. Taking notice of the value of G/Go which corresponds to the shear strain developed at the time CREST reaches to the yield state, it is recognized in Fig. 10 for a rock-fill that G/Go =0.44 for $\gamma=\gamma_y(C)=3.0\times10^{-4}$ at CREST, G/Go=0.51 for $\gamma=2.9\times10^{-4}$ at MIDDLE, and G/Go=0.55 for $\gamma=3.4\times10^{-4}$ at BASE, respectively: i.e., rigidity reduction is getting higher from the base to the top of the fill. The factor of safety in terms of shear strain is evaluated again in another from for MIDDLE and BASE, taking G/Go=0.44 at CREST as a critical value of G/Go, as Fs(M)=0.51/0.44=1.16 and Fs(B)=0.55/0.44=1.25. similar trend as noticed before is confirmed in this safety evaluation, showing higher possibility to slope failure in CREST, though the variation in Fs with the depth becomes a little smaller as compared with the result presented before. In case of the eath-fill, the rigidity ratio G/Go results in 0.56 at CREST, 0.59 at MIDDLE and 0.60 at BASE, respectively, when yielding occurs at CREST, and a nearly uniform distribution of Fs is recognized as noted before, showing Fs(M)=1.05 and Fs(B)=1.07 against Fs(C)=1.

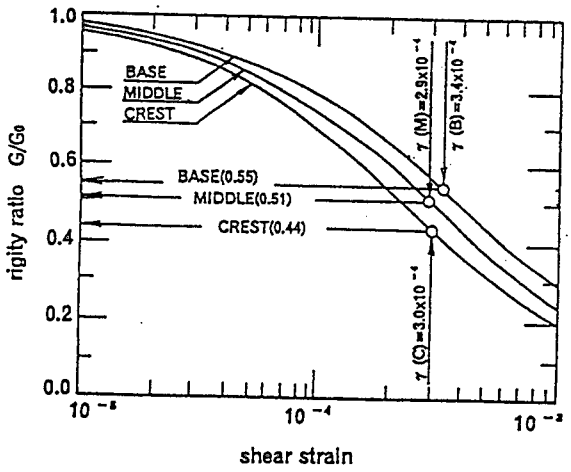

Fig.10 Another Evaluation of Seismic Safety by G/Go (Rock-fill)

4.3 F.E. Evaluation of Yield Starain

In order to examine the validity of the procedure of evaluating embankment failure during earthquake in terms of shear strain,presented in

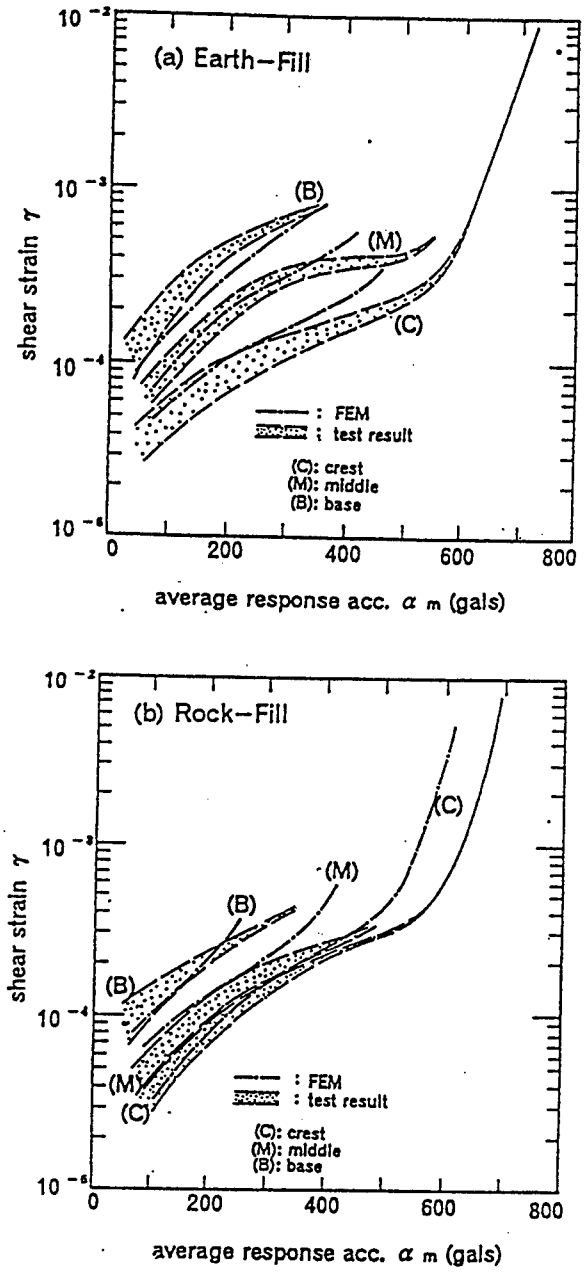

Fig.11 F.E. Computations for Model Earth– and Rock–Fills

the above from experimental investigations,and also to know the feasibility of these discussions for future application to the seismic resistant design of earth and rockfill dams, F.E. dynamic response analysis are carried out on the model fills by taking their nonlinear material properties into account. An equivalent linear QUAD4-type procedure of numerical analysis is used here by representing material nonlinearity of the modulus of rigidity G and the damping factor h by the Hardin-Drnevich model presented in Eq.(4).

The computed relationships of $\gamma \sim \alpha_m$ are compared with the measure ones for the earth- and rock-fills in the shaking table tests,as shown in Figs.11(a) and (b).It is clearly seen in these figures that the computed values of seismic shear strain have a similar trend as noticed before for the test results, showing a sharp increase at a certain level of response acceleration, and that the computed value of the yield strain are comparable to the measured ones in both cases. Somewhat large differences are considered inevitable, however, between the computed and measured values of response acceleration, because material properties, G and h, used in the F.E. response analysis were determined from cyclic triaxial tests on the fill materials having reduced-scale particle sizes, and under relatively high confining pressures as compared to those encountered in model fills of 2m in height.

Although further discussions are necessarily required for the determination of appropriate material parameters for use in the analysis, it is suggested from the above computations that seismic stability of earth and rockfill dams can well be evaluated through a F.E. dynamic response analysis by defining the yield shear strain at the point of sharp increase in γ as described in the shaking table tests.

5.CONCLUSIONS

Concluding remarks drawn from the present study are summarized as follows.

(1) Failure mechanism of embankment dams during earthquake can be classified into two main categories; one is falling down of rock particles and a shallow surface sliding in rockfill slopes, and the other a circular sliding failure passing through the interior of the fill in both earth and.,rockfill dams.

(2) For the former type of failure, safety evaluation on the basis of dynamic frictional properties of fill materials is considered reasonable, and it is confirmed from dynamic angle of repose tests that the current seismic

coefficient method can be applied effectively with a little modification on the frequency dependent parameters.

(3) In shaking table tests on model earth-and rock-fills, the seismic shear strain developed during oscillation shows a sharp increase just before the occurrence of sliding failures at a certain level of response acceleration and the yield shear strain can then be defined for this state as a threshold value of embankment failure.

(4) By taking this yield shear strain as a criterion, safety evaluation of embankment dams is satisfactorily done in terms of seismic shear strain developed in the fill, in which the increase in shear strain is associated with the reduction in rigidity of fill materials to introduce a factor of safety(Fs).

(5) The values of Fs thus determined in earth-fills are uniformly distributed with depth, suggesting that somewhat deep sliding failure is probable. In contrast, comparatively shallow sliding failure may be anticipated in rock-fills because of a sharp increase in Fs with depth.

(6) Similar trend as noticed in the shaking table tests, a sharp increase in shear strain just before the embankment failure, is recognized qualitatively in F.E. nonlinear dynamic response analysis, which proves feasibility of F.E. evaluation of seismic safety of earth and rockfill dams.

Hydraulic fracturing in earth and rockfill dams is another significant issue incidentally to be discussed in the earthquake resistant design. Influential factors associated with the hydraulic fracturing are, for instance, arching action and differential settlement in sort clayey cores and irregular abutment configuration to cause opening of cracks and uneven stress transmission in the core. Some fundamental investigations are now undertaken (Murase,et.al..1995) to propose an appropriate design method by putting together with the above discussions.

REFERENCES

1) Ohne,Y.:"Seismic behaviors of Makio Dam,"A Report of Specialty Session of Naganoken-seibu Earthquake, the 20th JSSMFE Annual Meeting, pp.47-54,1985.(in Japanese)

2) Shakal,A.F.,Sherburne,R.W. and Parke,D.L.: "CDMG Strong-motion records from the Morgan Hill, California earthquake of 24 April 1984," California Department of Conservation Division of Mines and Geology, OSMS Report, 84-7,1984.

3) Ohne,Y., Tatebe,H., Narita,K. and Okumura,T.: "Fundamental study on earthquake resistant design of fill-type dams," Proc.of JSCE, No.339, pp.127-136,1983.(in Japanese)

4) Ohne,Y., Tatebe,H., Narita,K. and Okumura,T.: "Discussions on seismic stability of slopes for rockfill dams," Proc. of International Symposium on Earthquakes and Dams,pp.407-417,1987.

5) Murase,Y. ,Okumura,T. ,Narita,K. and Ohne,Y.: "Study on hydraulic fracturing of core-type rockfill dams," the MWA International Conference on Dam Engineering,pp.363-371,1995.

PRESENT CONDITION OF MULTI-PURPOSE DAM PROJECTS AND RELATED TECHNOLOGY DEVELOPMENT IN JAPAN

by

Tadahiko FUJISAWA[1)]

ABSTRACT

In recent years, various methods on overall river development were introduced to respond to the extensive use of water in the urban area and to diversify the needs in the river basin community. The Ministry of Construction, the Japanese Government, constructed and are constructing many dams for flood control, development of water resources, power generation, etc. which contribute to the economic growth. For better understanding of the characteristics of dam construction in Japan, social and natural conditions surrounding the dam construction were explained. Besides, history of dam technology related to dam construction projects in Japan was summarized, and the rationalized construction methods for concrete dams, such as the RCD method, the PCD method and the ELCM, were described.

Keywords: multi-purpose dam, comprehensive river development project, RCD method, PCD method, ELCM

1. PROMOTION OF DAM CONSTRUCTION PROJECTS IN JAPAN

1.1 Characteristics of the Japanese dam projects

Approximately 75% of the total area of 380,000 km^2 in Japan,, is mountainous with a series of high ridges, and the slopes are very steep. Hence, the rivers in Japan are in general steep and short, and their drainage area is small (Figure 1). The precipitation characteristics in Japan are represented by three events; snow, the rainy season and typhoons. Typhoons, especially, bring 1/4 to 1/3 of the annual precipitation in Japan, which is large enough to be comparable to the world record according to the maximum past precipitation data.

There are the following properties in the runoff of Japanese rivers under these topographic and precipitation features. Floods arrive fast. Peak discharge of flood water is large. Flow is unstable. Amount of transported sediment is large. The hydrograph of the flood in the Japanese rivers exhibits extreme sharpness and changes drastically in a short time compared with the rivers in foreign countries (Figure 2). This type of flood can be controlled effectively by dams.

Another important feature of Japanese dams is in the seismic design. The region surrounding the Pacific Ocean, including Japan, is located in the most active seismic area in the world where large earthquakes frequently occur. Because there is a high probability of a large earthquake occurring in Japan, considerable emphasis is put on the seismic design of dams. In case of embankment dams, for example, the horizontal design seismic coefficient is 0.15-0.20 in the strong earthquake region, 0.12-0.18 in the medium region and 0.10-0.15 in the small region respectively.

1.2 Authorities of dam projects

The history of the Japanese dams started when the oldest dam that still exists was constructed at the Sayama Pond in about 200 A.D., and is more than 1700 years old. Paddy fields in Japan have been developed since the fourth century. Since they have relied on rivers for irrigation, the

1) Director of Dam Department, Public Works Research Institute, Ministry of Construction, Tsukuba Science City, 305, JAPAN

facilities to develop water resources like dams are necessary in most of the rivers.

Dam projects in Japan aim at ensuring irrigation water, hydro-electric power generation, ensuring water for drinking and industry use, and flood control. They are also classified into single-purpose dams and multi-purpose dams that have some of purposes mentioned above.

There are various purposes in dam projects. Single-purpose dams include flood-control dams, irrigation dams, dams exclusively for drinking water, dams to secure water for industrial use and electricity-generation dams. Authority of each type of dam is shown in Table 1. Nowadays it has become more general to build the multi-purpose dams. There are two types of the flood control dams. One is managed by the Ministry of Construction and the other by the prefectural government. These dams are under the control of the Ministry of Construction. The dams for irrigation are constructed either by the Ministry of Agriculture, Forestry and Fishery, by prefectural governments or by land improvement districts. These are under the control of the Ministry of Agriculture, Forestry and Fishery. Some of the dams for drinking water are undertaken by local governments and some by the Board of Water. These are controlled by the Ministry of Health and Welfare. Some of the dams exclusively for industrial use are constructed by local governments and some by the Industrial Water Bureau. These are controlled by the Ministry of International Trade and Industry. The dams for power generation are constructed by local government industry boards, power generation companies, Electric Power Development Corporation or private companies. These are under the control of the Agency of Natural Resources and Energy. The projects of the multi-purpose dams including flood control are managed either by the Ministry of Construction or prefectural governments which administer rivers. The multi-purpose dams for various water uses are realized by making adjustments among the beneficiaries. The Water Resources Development Public Corporation is the main management authority of the dam projects whose main purpose is the development of water resources in wide areas that belongs to the specified river system inside the seven river systems nationwide.

In any dam project, examination of water rights by the administrator of the river is mandatory. The Ministry of Construction and the governor of the prefecture are in that position for the first class rivers and for the second class rivers, respectively.

1.3 Transition of the number of completed dams categorized according to purposes

The dam projects in Japan are carried out, aiming at flood control, development of water resources and power generation. The dams for irrigation have been built for a long time to produce a small reservoir, but the number of these have tended to decrease after World War II because of the decrease in farmers and in farmland due to housing lot use.

Many dams for power generation were constructed from the post war rehabilitation to around 1965, which were the early days of the rapid growth period, and were the driving force for industrial development. However, as the number of the potential dam sites suitable for large electric output decreases, steam-power stations and nuclear power stations have become more dominant in terms of electric output. In these days, the number of dams exclusively for power generation is decreasing rapidly, though a few dams for pumped storage power stations are constructed to cope with the peak demand of electricity.

Backward displacement of levees becomes difficult in downstream areas in Japan where industrial activity is high and there is a high concentration of population. Hence, as river improvement becomes formidable, the flood control by dams becomes more important.

The first modern dam in Japan was constructed for drinking water. Since the great economic growth period that started around

1965, the demand of water for drinking and industry increased with economic growth and improvement of living standards, resulting in the driving force for dam construction. Since then, the multi-purpose dams have been built in order to secure water resources and to control floods.

Making effective use of good dam sites and adjusting the number of users to prevent conflicts for the dam sites, construction of the multi-purpose dams is the mainstream these days. Their major purpose is flood control, and they also aim at maintaining the normal function of river flow, development of water resources and power generation, etc. They are managed by a river administrator controlled by the Ministry of Construction.

1.4 Transition of storage capacity ratio of dams categorized according to purpose

As shown in Figure 3, the change of the number of the completed dams categorized according to purpose truly reflects the change of the capacity for each purpose of the dam construction in Japan.

2. TRANSITION OF DAM CONSTRUCTION PROJECTS AUTHORIZED BY THE MINISTRY OF CONSTRUCTION

Comprehensive river development projects under the jurisdiction of the Ministry of Construction have, since the first such project was carried out, successfully made a great contribution to Japan's social economy.

Figure 4 illustrates a history of these projects: specifically changes in the number of completed dams, the number of dams under construction, and the cost of the projects.

By 1995, 364 comprehensive river development projects were completed, and 327 dams were constructed. In 1996, a budget of 468.2 billion yen is appropriated for dam construction projects related to Ministry of Construction.

As a result of comprehensive river development projects, approximately 3.6 billion cubic meters of water were subject to flood control, cities were supplied with 13.0 billion cubic meters of water per year, and 2.7 billion cubic meters were supplied annually for agricultural purposes by 1995.

The locations of dams constructed as part of comprehensive river development projects in 1995 are shown in Figure 5.

3. VARIOUS DAM PROJECT MEASURES

In order to respond to extensive use of water in the metropolitan area and to diversify the needs in the river basin community in recent years, we have developed various methodologies besides the conventional methods on the overall river development, have combined them with each other, and have executed projects.

For necessary natural ecosystem preservation, ecological environment creation projects around a dam, installation of fish ladders (dam torrent fish ladder installation projects), etc. are being carried out.

For necessary countermeasures against reservoir sedimentation, the projects including expansion of restoration projects from disaster, sand storage dams, removal of deposited sand, preservation and maintenance of sparse woods and creation of recreational area in dams and reservoirs are being carried out.

For necessary preservation of water quality in the reservoir, we execute the tasks such as preservation and maintenance of sparse woods, improvement of water quality in reservoirs, creation of recreational area around dams and in reservoirs.

To respond to the request of securing recreational function, creation of recreational area around dams and in reservoirs, civic designed dam projects, multi-purpose dams for recreational use, lake parks, lake resorts, improvement of the environment around a dam, etc. are being undertaken.

For the request of suitable energy use included in dam reservoirs, the projects including heat pump projects and power generation projects for the dam management are being carried out.

There are the dams being prepared for water shortage, which enable water supply for severer droughts than planned one, leading to an increase in stability of water use.

We are developing various methods to exploit the new water resources in the area where the conventional dams do not provide inexpensive water of good quality. There are, for example, the project promoting extensive use of water such as the effective use of treated sewerage, flow regulating river system to control flow condition by a number of rivers and multi-purpose headraces, underground dams using gravel layers as reservoirs, etc.

Small scaled community dams for flood control and irrigation are constructed in small villages especially lying in mountainous areas.

Underground seepage dam projects are planned, in which floods are controlled by letting it permeate underground.

There are regional regulating dams which control the increased runoff due to the wide area development projects. They are paid by the developers.

Among remarkable features of 3 of these projects will be introduced.

(1) Channel for adjusting of the flows of rivers

A river flow adjustment channel is a multi-purpose water channel constructed to organically link a number of rivers and adjust their flows as a way to prevent flooding, drain the areas behind levees, purify water, and provide sufficient river flow level maintenance water, and at the same time, to develop new water resources. Projects of this kind permit a stable supply from newly developed water resources by integrating the flows of rivers with differing flows. As indicate in Figure 6, the two rivers, river A and river B, share their surplus water, with river A sharing its water when river B can not, and river B sharing its water when river A can not.

(2) Advanced water utilization project

The spread of sewage facilities in Japan has been accompanied by the continuous expansion of water purification activities.

In the urban areas where there is a great demand for water, it is important that this processed sewage should be effectively used as water resource. Aggressive efforts must be made to study the re-use of sewage water.

The characteristic fluctuations of flow volume in Japanese rivers mean that there is a shortage of river water only during a specific period of the year. It would be more economical to use re-processed water drawn from the sewage system only when the river water supply is low than it would be to continuously process it as is done in the case of waste water re-use system

As shown in Figure 7, such projects achieve the following goals:

[1] Supply water maintaining normal river flow to prevent water supply shortages.

[2] At river water purification treatment plants, receive water already treated at sewage plants, carry out advanced processing of this water, then recirculate it upstream.

[3] Return the processed sewage water from step [2] to the river to replace the water supplied to maintain the river flow volume.

(3) Reservoir for drought

The modern society with its high living standards and sophisticated economic activities suffers more damages by frequent water shortages. Hence, in addition to normal water storage capacity, the dams are planned and constructed, which have the capacity large enough to supply the minimum water for household and urban activities to maintain daily life even in the case of water shortage severer than expected. These are called "reservoir for drought" (Figure 8). When extraordinary water shortage worse than expected one happens, the water supply from the conventional dams does

not make up for the entire shortage. Then, the minimum amount of water may be secured both by restricting the amount of intake and by receiving some water from the dam preparing for water shortage. Operating method of dams for drought is explained in Figure 9. The plan and construction of the dams preparing for water shortage are promoted around large cities in the Tokyo Metropolitan area where large damage is expected in case of water shortage.

4. HISTORY OF DAM TECHNOLOGY IN JAPAN

4.1 Progress of dam technology

It is said that the dam technology in Japan started when the rice crops were introduced, and that the technology took root at the end of the fourth century. Among those that were constructed at that time and still exist, the Sayama Pond and the Man-nou Pond are famous. These dams are still in use by continuously rebuilding, heightening and reinforcing the older structures. Dams of this kind reportedly amount to 200,000 nationwide. Due to the establishment of the industrial base and population concentration in large cities associated with the development of the modern industrialization in the Meiji era, new water demand was created and the social request to the dams became much stronger. Those days were the dawn of concrete dams as the technology on dams was imported from the West and a new material, concrete, was used for dams. The first concrete dam in Japan was the Nunobiki Dam in Kobe, made of rubble concrete to secure running water. As for the design of dams, Dr. Nagaho Mononobe published "Characteristics of Gravity Dams for Reservoir and Reasonable Design Methods" in 1925, opening a door to designing the gravity dam. He wrote "Determination of the cross section of the gravity dam considering the hydrodynamic pressure due to seismic excitation" in 1934, and established the seismic design method for gravity dams. Since then, the study on the dam design has continued. The Ministry of Construction published "Manual for River Works in Japan (draft)" in 1958 and "Standard for Dam Structure and Its Details" in 1968. Thus, the first technical standard was established. On the other hand, the new technology on dam construction was frequently tried in those years, resulting in the completion of the Yahagi Dam in 1970, a first parabolic flat arch dam. In 1974, the Committee for Rational Construction of Dams was set up at the Ministry of Construction. Later, many rational construction technologies including the RCD method were born from this committee. It is noteworthy that in the dam planning, the specific discharge diagram by the dam locations in Japan was completed in 1975 by analyzing the nationwide flood data.

The Ministry of Construction, which is in charge of the river administration, put Structure Regulation for River Control Facilities, etc., in effect in 1976 in accordance with River Law. This is an event worthy to remember because it is the first regulation on the safety of dams.

The dam technologies such as the rationalized construction method had become commonly chosen at a site in the 1980's. In 1981, Technical Standard on the RCD method (draft) was enacted and revised in 1989. The Shimaji-Gawa Dam was completed by the RCD method for the first time. In 1985, the Nagayo Dam became the first dam completed by the concrete pump construction method, while the Okawa dam, the first concrete dam of a mat type, was completed in 1987. Then, construction of the Nunome Dam was started by the Extended Layer Construction Method for the first time in 1988.

On the other hand, dam construction by artificially blocking the river flow that has the deepest relation with human life, alters natural rivers into artificial lakes and has a great impact on the natural environment such as the ecosystem. These environmental problems become recognized important by nation. Under these circumstances Technical Standard Details

of Environment Assessment for Projects Administered by the Ministry of Construction -Dam Project Version- (draft) was enacted in 1978. In 1982, the aeration circulation experiment was started at the Midorikawa Dam and the Murokawa Dam for a measure to prevent eutrophication. History of dam technology in Japan is summarized in Table 2.

4.2 Transition of rationalization of concrete dam construction

A sharp hike in personnel expenses during the high growth period from early in the 1960's in Japan made rockfill dams a more attractive choice because of the cheaper construction cost. This was achieved by the progress in the construction method using large construction machines. However, because the rockfill dams have big restrictions such as that a spillway may not be placed on the dam body and that any overflow is not allowed, the technology development toward reduction of construction cost of concrete dams by the construction method using large construction machines was sought.

"Research Committee on Rationalized Construction of Concrete Dams" was organized in 1974, and started to seriously study the rationalized construction methods for concrete dams. Various construction methods born from this research clearly characterize the present dam technologies in Japan.

Through the work of this committee, rationalized technology has been developed and spectacular progress has been achieved. For example, rational execution integrated with the dam concrete work, the RCD (Roller Compacted Concrete for Dams) Construction Method, the PCD (Pumped Concrete Dam) Construction Method , and the ELCM (Expansion Layer Construction Method) have been introduced. The Belt Conveyor Construction Method and others focussed on the issue of concrete transportation, have also been developed.

During the past two decades, about 10 dams under the jurisdiction of the Ministry of Construction have been completed every year. Because of geological conditions at the dam sites, the proportion of these that are fill dams has been on the rise. In the first half of the 1970s, embankment dams accounted for about 8.9% of all constructed dams. This rose to 20.8% in the latter half of the decade, and to 26.8% in the early 1980s. But in the last half of the 1980s this figure fell abruptly to 11.4%. This change was a result of a new awareness of the benefits of concrete dams accompanying rapid progress in the rationalization of concrete dam construction through the introduction of RCD and other construction methods.

Each year, the Ministry of Construction begins construction of about 10 dams. Many of these are concrete gravity dams, and almost all of this type are constructed using the RCD method and other rationalized construction methods. The RCD method has already matured to become a firmly established construction method.

The PCD method, the Belt Conveyor Method, and others have entered a maturation stage. In other words, they are leaving the stage where data obtained through past trial execution is slowly but steadily gathered and analyzed, and moving to the next step: implementing innovations that will expand their application range.

(1) The RCD method

The RCD method is implemented as follows. After the RCD concrete is brought in by dump trucks, etc. a bulldozer spreads and levels it. Next, it is compacted with a vibration roller (Figure 10). The followings are the basic concepts behind this method.

(a) The concrete for the dam is basically placed without contraction joints. The horizontal section of the dam body is divided into 3 or 4 blocks, and concrete is placed without a lift-difference.

(b) The concrete is transported using a high volume transport system consisting of standard equipment. This approach takes account of the

characteristics of dam sites. The machinery used includes a fixed cable crane, incline, dump truck, etc., but it is standard procedure to use dump trucks to carry it on top of the dam body.

(c) The concrete that is poured is lean super-stiff consistency concrete. After spreading of concrete by a bulldozer, it is compacted with a vibration roller. At that time it is spreaded to a thin layer, and about three layers is considered to be one lift.

(d) No longitudinal joints are formed parallel to the dam axis (layer pouring). Transverse joints are made with a vibrating joint cutter after the concrete is spreaded.

(2) The ELCM

A placing method that does not form longitudinal joints is called the ELCM. With the ELCM, 2 blocks or more in the dam axial direction, are poured simultaneously, and raised without lift-difference. This method was developed in order to achieve rationalization by permitting wide construction sites and simplifying the running of highly versatile machinery. In this regard, it is similar to the RCD method, and many features of its use are common to the RCD method. But while the RCD method involves the compacting of lean super-stiff consistency concrete with a vibration roller, when the ELCM is adopted, conventional concrete is compacted with an immersion vibrator. Construction procedure of the ELCM is illustrated in Figure 11.

(3) The PCD method

The pumping method is one of concrete transportation methods. The pump method is successfully used at relatively small-scale projects: buildings, roads, revetments, bridges, electric power stations, and erosion control structures. It is employed to carry a wide range of concrete material: light weight, low slump, lean mix, rich mix concrete, etc. At the Nagayo Dam (Nagasaki Prefecture) completed in 1982, the PCD method was employed. The pump transport system transported about 21,000 cubic meters of concrete (maximum aggregate size: 60mm, slump: 8 to 12 centimeters) from the concrete mixing plant to the placing site on the top of the dam body. Thanks to the development of a new pressurized pump, the PCD method was adopted to pour the concrete for the emergency spillway of Saguri-Gawa Dam, rockfill dam with central core (Ministry of Construction), completed in 1992. Here, the system was used to pour concrete with a maximum aggregate size of 80mm. The PCD method has also been used to place concrete for the energy dissipator and the auxiliary dam at the site of Miyagase Dam (Ministry of Construction) under construction. The procedure of the PCD method shown in Figure 12.

Table 1 Authority of each type of dams in Japan

(a) Single-purpose dams

Purpose	Authority
flood control	the Ministry of Construction
	prefectural government
irrigation	the Ministry of Agriculture, Forestry and Fishery
	prefectural government
	land improvement districts
drinking water	local governments
	bureau of water works
industrial water	local governments
	bureau of industrial water
	specific companies
power generation	department of industry in local governments
	companies(nine power generation companies and Electric Power Development Corporation,etc.)

(b) Multi-purpose dams

Type of Dam	Authorities
multi-purpose dams including flood control in the first class rivers	the Ministry of Construction
multi-purpose dams including flood control in the second class rivers	prefectural government
Development of water resources in wide areas around a specified river within the seven river systems is a main purpose	Water Resources Development Public Corporation
Development of water resources	joint organization of the above mentioned authorities

Table 2 History of Dam Technology in Japan

Year	Event
BC36	Construction of Sayama Pond
701 to 704	Construction of Manno Pond
1900	Completion of the Nunobiki-Gohonmatsu Dam: Japan's first concrete gravity dam
1925	Publication by Dr. Monobe Nagaho of Characteristics of Gravity Dams Used for Reservoirs and A Rational Design Method for Such Dams
1934	Publication by Dr. Monobe Nagaho of Method of Determining the Section of a Gravity Dam Taking Account of Dynamic Water Pressure During an Earthquake (Earthquake Resistant Design Method)
1958	Enactment of the Manual for River Works in Japan
1968	Enactment of Standards and Details of Dam Structure
1970	Completion of the Yahagi Dam: the first Parabolic Flat Arch Dam
1974	Establishment of the Ministry of Construction's Research Committee on Rationalized Construction of Concrete Dams
1975	Preparation of specific discharge diagrams for districts where dams are located throughout Japan
1976	Enforcement of the Cabinet Order Concerning Structural Standards for River Administration Facilities Etc.
1981	Enactment of the Technical Guidelines for RCD Method
1982	Completion of the Shimajigawa Dam: the first dam constructed using the RCD method Commencement of aeration circulation tests at the Midorigawa Dam and Murou Dam to develop eutrophication counter-measures
1985	Completion of the Nagayo Dam: the first constructed using the concrete pump method
1987	Completion of the Okawa Dam: the first mat type concrete dam
1988	Commencement of work on the Nunome Dam: the first to be constructed using the expansion layer method

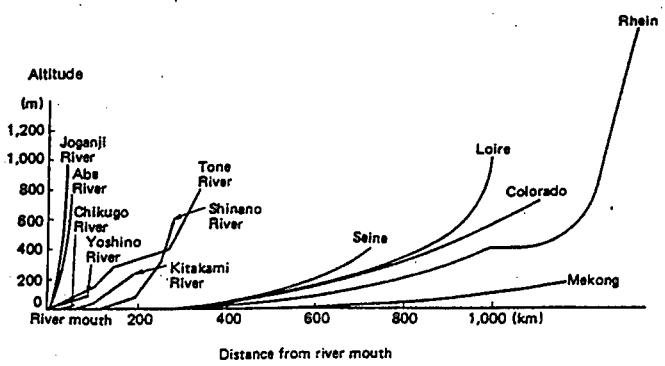

Figure 1 Comparison of main rivers in the world

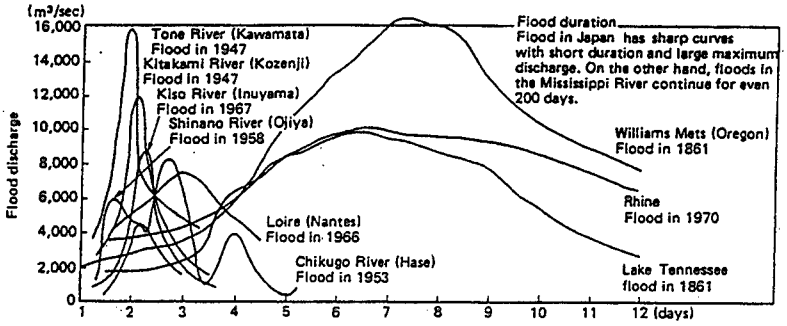

Figure 2 Comparison of flood hydrographs between Japan and the other countries

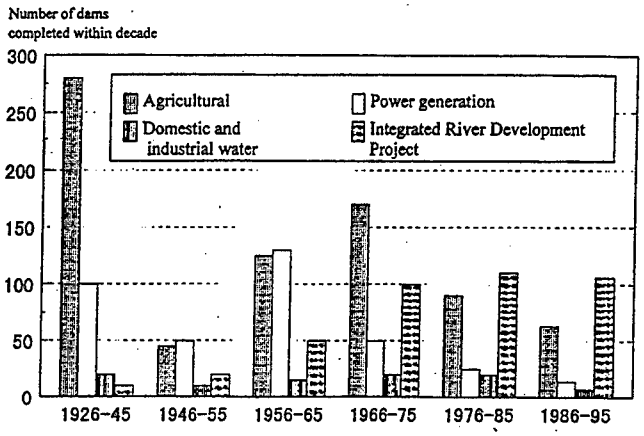

(a) Progress in the number of completed dams by purpose

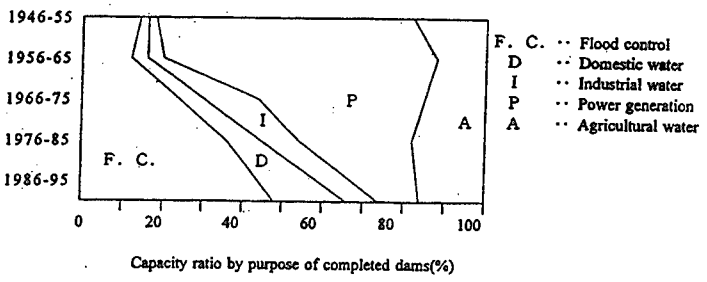

(b) Number of dams completed within decade

Figure 3 The change of the number of the completed dams categorized according to purpose

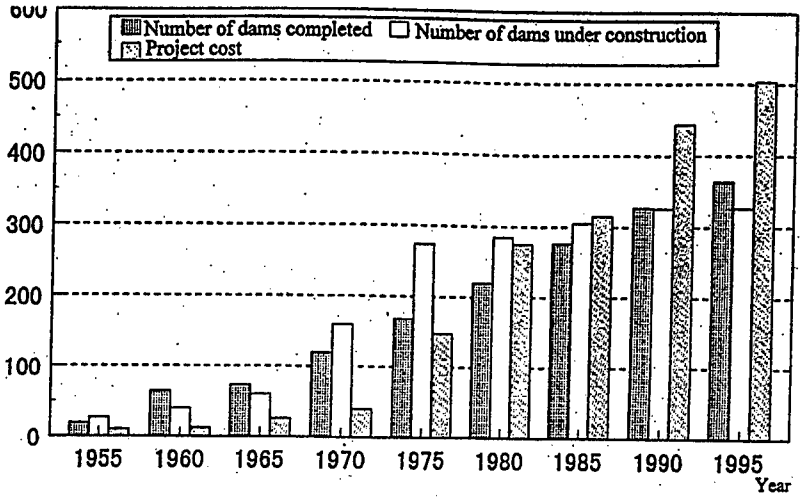

Figure 4 Transition of dam construction project in Japan

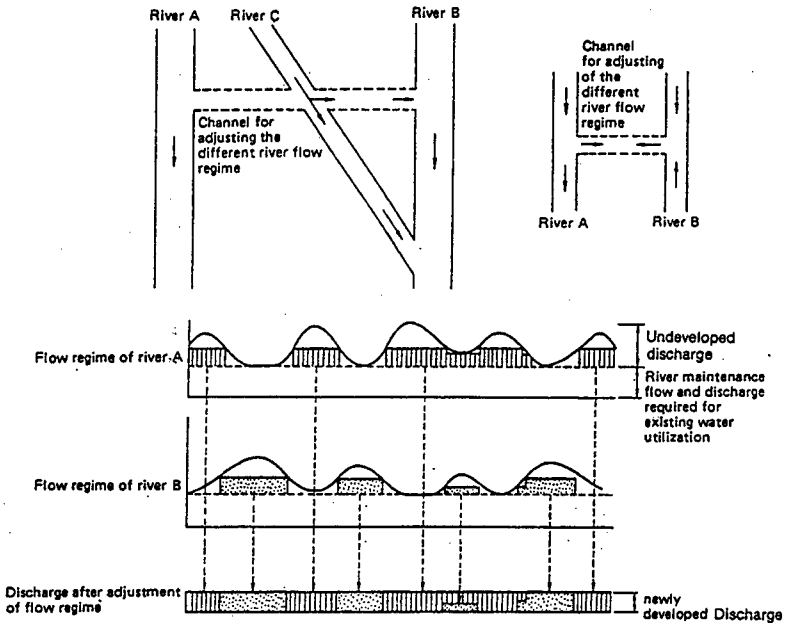

Figure 6 Channel for adjusting the different river flow regime

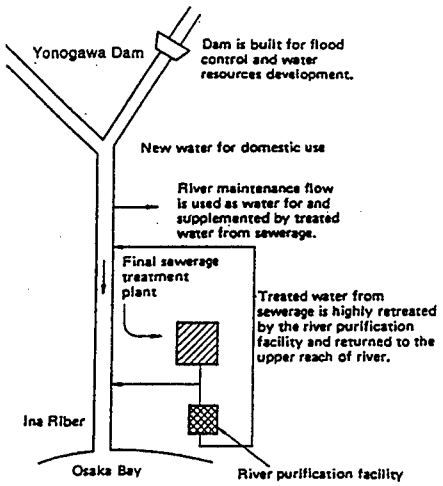

Figure 7 Ina River integrated development project

	Number of Dams		
	Completed	Under Construction	Total
Ministry of Construction	82	102	184
Water Resources Development Public Corporation	20	18	38
Subsidized	262	207	469
Total	364	327	691

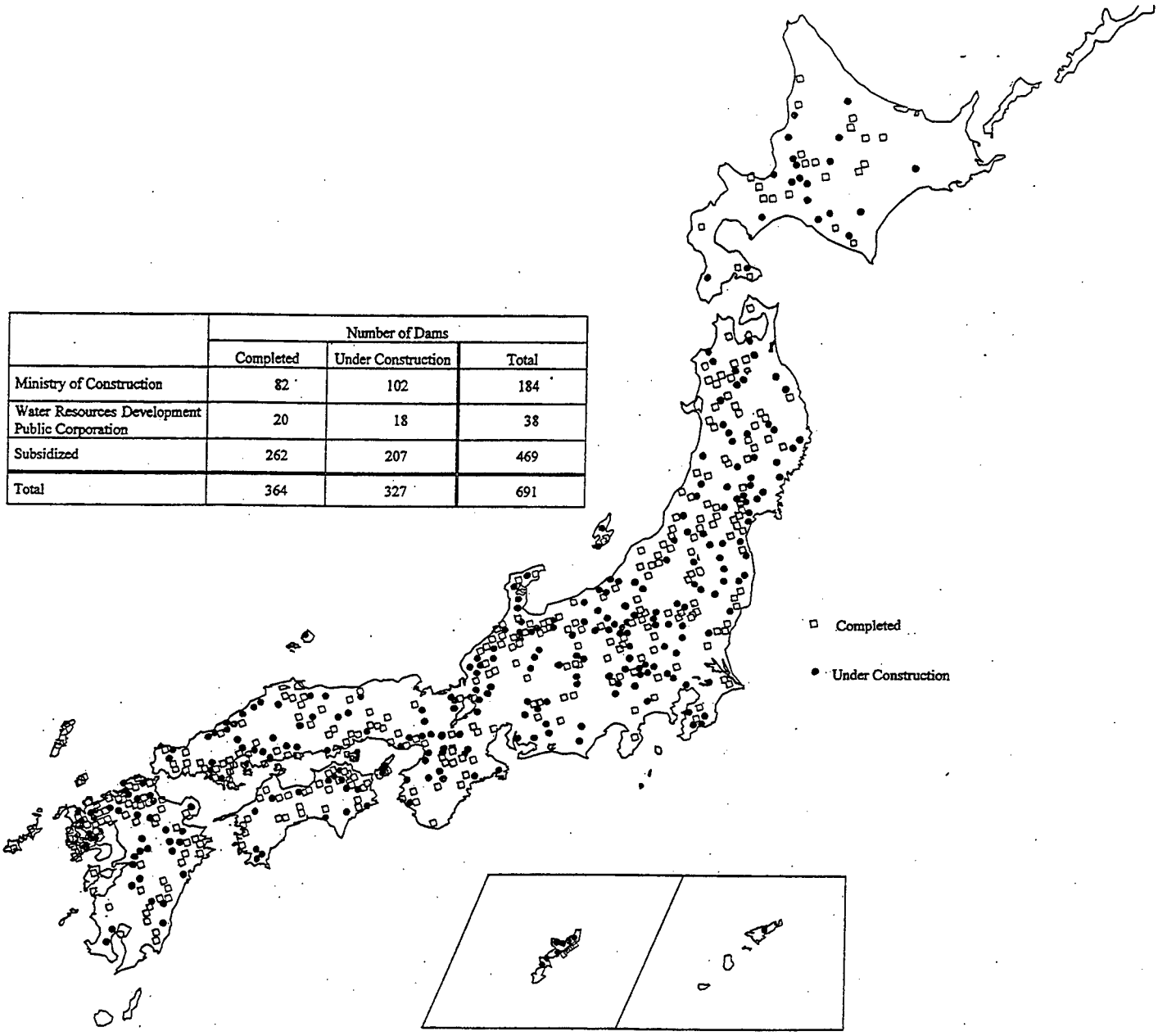

Figure 5 Location map of dams in Japan

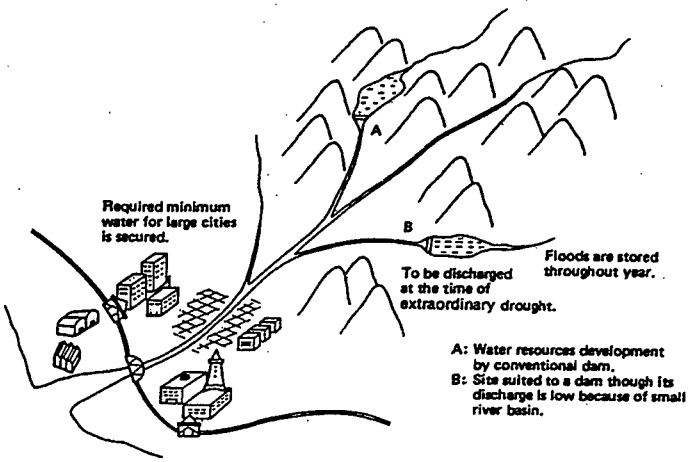

Figure 8 Conceptual diagram of dams for drought

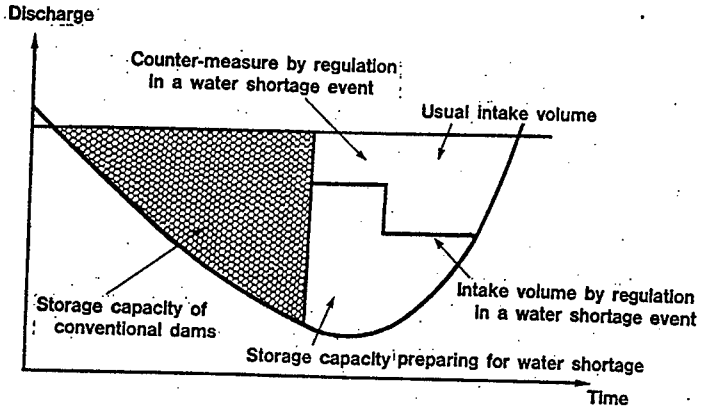

Figure 9 Operation of a dam preparing for water shortage

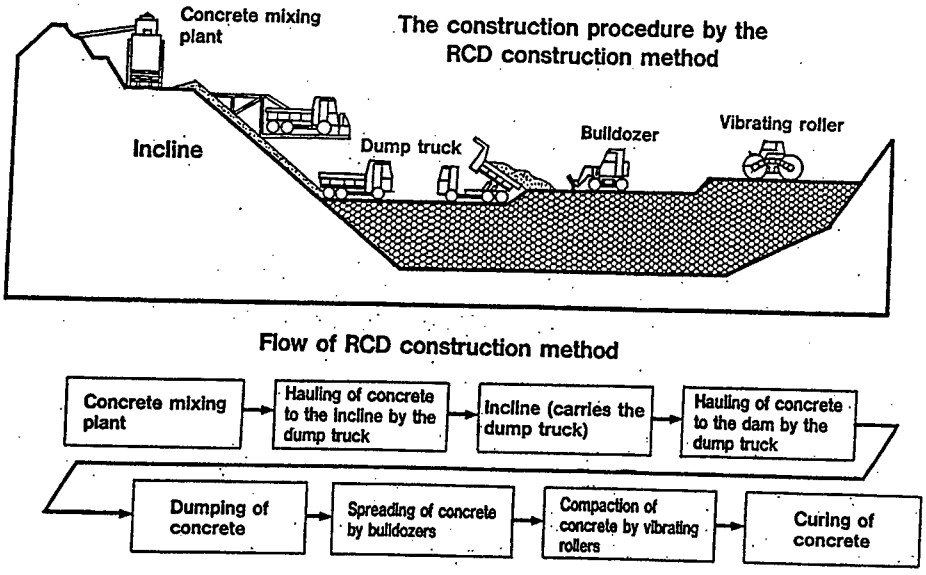

Figure 10 Procedure of the RCD method

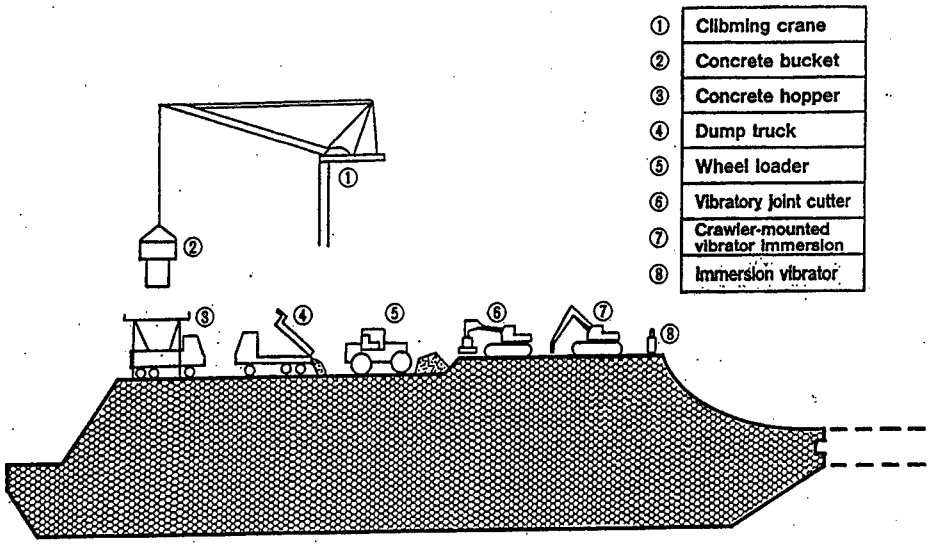

Figure 11 Procedure of the ELCM

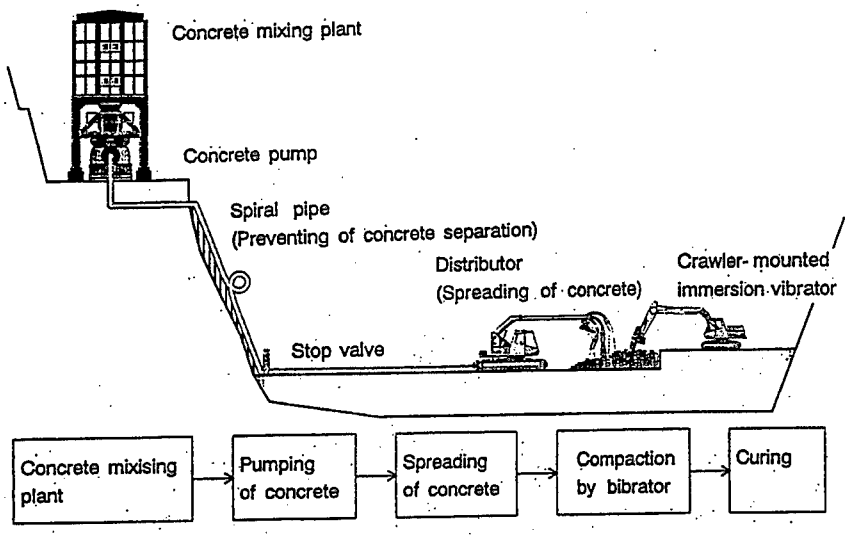

Figure 12 Procedure of the PCD method

U.S. Army Corps of Engineers (USACE)
Civil Works Earthquake Engineering Research Program (EQEN)

by

*Dr. M. E. Hynes and **Dr. R. L. Hall

1 PURPOSE

The Earthquake Engineering Research Program (EQEN) focuses on the seismic safety of reservoir dams--the Corps' most critical structures from a potential loss of life perspective. Expensive remediation actions are planned for many Corps dams. These actions are necessarily conservative to overcome shortcomings in the current state of the art in earthquake engineering. The EQEN was proposed as a multi-year R&D effort focused on eliminating inadequacies in present seismic safety evaluation knowledge. Budget restructuring has extended the time length and cost of the program. There is no other national program at this time to develop seismic safety evaluation criteria for our critical Civil Works structures. This program offers the potential for vast cost savings in seismic remediation efforts by performing focused research to ensure that safe dams are not remediated, and dams that are unsafe are remediated as quickly and efficiently as possible.

2 MOTIVATION

Civil Works research in earthquake engineering has led to the ability of the Corps to remediate seismically unsafe dams instead of direct dam replacement. Research activities associated with recently completed remediation at Sardis Dam in Mississippi, for example, resulted in economic savings of more than $200 million for replacement of a main portion of the dam and averted more than $600 million in losses in the event of dam failure. At Mormon Island Auxiliary Dam, part of the Folsom Dam Project, California, remediation saved more than $10 million for replacement of a portion to $600 million for replacement of the entire dam and potentially averted more than $60 billion in losses if the dam failed.

At least 39 U.S. States have significant seismic hazard posing a life-safety risk. Consequently, most of our existing dam projects are subject to some degree of seismic hazard and were designed and built at a time when this hazard was not well understood. The Corps has identified at least 200 reservoir dams and 73 intake towers as potentially subject to significant levels of earthquake shaking. With the large levels of uncertainty inherent in present seismic safety evaluation procedures and the consequent need for conservatism, several of these dams and all of the intake towers would be found in need of remediation.

In order to assess the seismic safety of our Corps reservoir dams, we need to be able to reliably predict the ground motions for design, and the amount of damage these ground motions will cause to our projects. Although there have been advancements over the last three decades, the present state-of-the-art in earthquake engineering falls far short of our needs. Consequently, every time the Corps faces a serious seismic safety evaluation, the study turns into a research project that takes a long time and requires experimentation in the laboratory, in the field and on the computer.

Even once a logical line of reasoning has been developed to solve the problem, the solution involves a great deal of uncertainty, and may be tentative because of new knowledge provided when earthquakes occur, or because a major state-of-the-art advance may necessitate revisions. To compensate for these shortcomings, we attempt to make design decisions that we hope are sufficiently conservative. The problem is compounded by the fact that most Corps dams were built at a time when earthquake engineering was in its infancy. The problem becomes even more difficult to solve if remediation is required. Examples of these problems were encountered in the seismic safety evaluations for Barkley Dam, Folsom Dam, Sardis Dam, Success Dam, Seven Oaks Dam, and Olmsted Locks and Dams.

*Earthquake Engineering & Seismology Branch,
Geotechnical Laboratory,
**Structural Analysis Group,
Structures Laboratory,
USAE Waterways Experiment Station,
Vicksburg, MS 39180

The EQEN Program was thus developed to provide a focused research program to improve our ability to assess the seismic safety of our unique Corps Civil Works projects. The cost of partial failure of even one facility will be much greater than the cost of the proposed program. Conversely, if even one Corps dam did not need remediation as a result of improved criteria, the cost savings would exceed the program outlay.

3 RESEARCH STRATEGY

The EQEN cooperates with and draws from the basic and applied research elements provided by other Corps R&D efforts, other federal agencies, and academic and professional experts, and extends and integrates these elements with in house work to address Corps seismic safety issues. EQEN is formulated to contain a balance of short-term work units design to address immediate questions related to currently used methods of analysis, and longer-term efforts to provide better methods with stronger theoretical foundations and greater validation. The program was developed by a combination of input from field offices, OCE Technical Monitors and earthquake engineering researchers.

The program content was formulated through discussions of problems encountered in seismic safety evaluations of Corps projects and an examination of shortcomings in each step of the evaluation process. The program thus forms a matrix with the steps in the solution process applied to the reservoir dam structures of concern. The structures of concern in reservoir dam safety are embankment dams, concrete dams and outlet works. The steps in the solution process are a) defining the earthquake ground motions, b) determining the site characteristics, c) assessing the damage these motions will cause to the site, and d) designing appropriate remediation if needed. Through these efforts, the EQEN Program was established as a multi-year effort.

As a result of this program, we want to have better estimates of the earthquake ground motions to use in design and we want to be able to predict more accurately and quantitatively the amount of deformation and damage these ground motions will cause to our facilities. If remediation is found necessary, we want to have effective, efficient options to select from and practical tools to design and implement a remedial action.

The elements required to do this are developed from the solution process: 1) evaluation of the seismic hazard, 2) site characterization and conceptualization, 3) modeling the material behavior and computing the expected damage. The development of effective, economical remedial measures puts even greater demands on steps 2 and 3, since the materials are now complex composites, possibly requiring a three dimensional analysis to evaluate. It is the underlying plan of this research program to provide practical products from each work unit that work together to achieve the advancement in the state-of-the-art we seek.

4 GEOTECHNICAL WORK UNITS

The geotechnical work units address the steps involved in solving a seismic problem for embankment dams: earthquake ground motions, site characterization, liquefaction-deformation-damage assessment, and remedial measures.

Earthquake Ground Motions. Knowledge of the behavior of ground motions advances with each new earthquake and breakthroughs in basic research by seismologists. The ground motion work units will maintain cognizance of these advances and translate the aspects important for engineering analysis into usable tools to provide ground motion input for analysis in the form needed as computational ability advances. These work units are thus closely coordinated with the development of structural and geotechnical numerical models.

Site Characterization. Present methods of site characterization rely mainly on individual borings to provide key information about stratigraphy, velocities and penetration resistance. The work units in this area propose to 1) develop improved geophysical techniques to link together borehole information, and to directly measure soil parameters needed for analysis, and 2) resolve the present controversy regarding interpretation of Becker Hammer measurements widely used in liquefaction evaluation of gravelly soils, and

possibly develop a new in situ testing tool that is more amenable to direct analysis, so that the translation of field information to inputs needed in numerical analysis is as seamless as possible.

Liquefaction-Deformation-Damage. The present procedures for assessing liquefaction potential and post earthquake stability rely almost exclusively on empirical correlations between penetration resistance and cyclic and residual strength. These procedures do not provide a basis for quantitatively predicting deformations and assessing damage. Advances have been made in developing more fundamental constitutive models and numerical dynamic analysis codes that can solve large-deformation problems. To advance beyond present procedures it is proposed to perform a combination of physical and numerical modeling research to:

4.1 Critically examine the shortcomings of existing Seed procedures through two focused series of centrifuge experiments which will provide direct observation of underlying mechanisms of behavior of liquefying materials and the deformations that result. These tests will provide quantitative measurement of residual strength and poorly understood "correction factors" such as K_{sigma} and K_{alpha}; simplified guidance for controlling foundation features necessary to experience large deformations; an improved method of interpreting more traditional laboratory test results; measurement of the actual damage that deformations cause to internal structures such as filter and core zones; and a full-scale performance data base against which various numerical models can be tested.

4.2 Critically examine the present state of development of fundamental constitutive models and large deformation numerical dynamic analysis codes to provide guidance for choosing among them in the short term, and to select the most promising for development, verification and simplification for practical use in the long term. To resolve remediation problems, this effort must work towards a three-dimensional analysis capability.

Remediation. Efforts to advance remediation guidelines have been slowed by the cost of full scale field testing and the difficulty in generalizing results since remedial actions are very site specific. The centrifuge gives us the opportunity to perform these full scale tests on a wide variety of remediation geometries to test our ability to compute their effectiveness. It is proposed to perform such a series of centrifuge tests, and later in the program, to design a test to examine the actual state-of-stress and density field that exists in remediated soils, since this stress history plays a major role in the future cyclic behavior of the soil. These efforts, combined with lessons learned from actual remediated sites should provide a basis for improved guidance so that we only remediate as much as is actually needed.

5 STRUCTURES WORK UNITS

The structures work units are designed to develop the necessary analytical tools and corresponding guidance to predict the dynamic response of concrete dams and outlet works from elastic behavior to the development of failure mechanisms. The understanding of the dynamics of the structural response will allow the determination of the ultimate capacity of these critical structures. The work units necessary to develop these products is divided into the areas of concrete dams, outlet works, and earthquake analysis tools.

Concrete Dams. These work units will focus on determining dynamic ultimate capacity of conventionally placed and roller-compacted concrete dams. These work units will address the nonlinear behavior and failure mechanisms of the different types of dams as well as include component tests, scale model tests, and tests of existing structures.

Outlet Works. These work units focus on determining the ultimate capacity of intake towers and the ductility of other than lightly reinforced concrete members. One major work unit will determine the ductility of lightly reinforced structures. The other work units will focus on other aspects of nonlinear behavior and failure mechanisms of these reinforced concrete structures.

Computational Tools. These work units develop

numerical tools to support the dams and outlet works areas. These work units will produce time-domain numerical analysis tools compatible with the nonlinear materials models, and postprocessing tools to aid in the interpretation and understanding of output from time-history and response spectrum analyses. Other work units will support the appurtenant structures to the outlet works and dams. These work units will address dynamic earth pressures on walls and the dynamic response of piles.

6 SUMMARY OF PROGRAM STRUCTURE

Through this combination of work units we will develop improved methods to predict appropriate ground motions for input to analyses, investigate our sites more economically and more thoroughly, improve our analytical ability to predict the amount of damage that the design level earthquakes cause to out critical Civil Works structures, and provide better guidance as to how to remediate them if needed.

7 IMPLEMENTATION

The R&D results from EQEN form the basis for input to Corps guidance documents (ETL, EC, EM), and are put into practice in ongoing seismic safety evaluation projects as results on improved procedures become available. In addition to technical reports and professional papers, the R&D results in improved software, data bases and user manuals made available to all Corps District offices in some cases directly and in other cases through special projects such as CASE and CAGE. The R&D results form input to workshops, seminars, conference presentations and training courses such as PROSPECT courses. For example, more than 100 copies of the Corps shear wave velocity data base have been distributed to Corps offices, universities, and private industry. This data base provides key input properties for preliminary screening analysis of site response to earthquake ground motions.

8 ACCOMPLISHMENTS TO DATE

8.1 Developed guidelines for assigning ground motions for engineering analysis of near-field sites, including vertical motions.

8.2 Completed conceptual design of comprehensive ground motion analysis system and user interface module. Acquired USGS three-dimensional, elastic, finite difference, full waveform, wave propagation code and have developed software for graphical portrayal of results. Completed accelerogram and response-spectrum data base modules and accelerogram processing tools.

8.3 Incorporated seismic velocity data base from the U.S. Bureau of Reclamation (USBR) in the Corps data base, and added additional data from Corps and USBR projects.

8.4 Held workshop to clarify requirements for integration of acoustic impedance and seismic crosshole tomography techniques and to select test sites for establishing correlations of these geophysical measurements to liquefaction potential. Published workshop proceedings, and conducted first series of field measurements at Success Dam.

8.5 Completed energy and friction correction study for Becker Penetration measurements performed at Success Dam, CA.

8.6 Completed design of centrifuge experiments to determine overburden corrections for liquefaction susceptibility analyses. Acquired materials and instrumentation necessary to conduct these experiments. Completed development of simplified shear stress-strain curve from laboratory measurements. Conducted initial centrifuge experiments to determine overburden corrections for liquefaction susceptibility analyses. Convened an international panel of experts on liquefaction and centrifuge modeling to review findings and guide next series of experiments.

8.7 Completed critical review of existing two- and three-dimensional constitutive models for liquefying soil materials. Critically reviewed validation efforts for these models as well. Selected the best features of these existing models and developed effective stress constitutive equations. Surveyed pre- and post-processing tools and made recommendations. Selected the nonproprietary code STUBBS, developed by Dr. Peters at WES, for modification . Added wave

propagation and solution to the equations of motion to the program.

8.8 Completed comparison of Newmark-sliding-block analysis results with collection of field case histories, to develop guidance for calibration of analysis results with actual field performance and limits of applicability for a range of field conditions.

8.9 Completed critical evaluation of existing nonlinear constitutive models that include crack initiation and propagation for conventionally placed concrete materials. Selected the best features of the existing models and formulated improved model for incorporation in numerical code.

8.10 Completed field sampling and laboratory measurement of roller-compacted concrete properties. Began constitutive model development for this material.

8.11 Completed and reported survey of existing intake towers including key features of their design and past performance during earthquakes. Designed and conducted initial scale model experiments of intake towers and key components of intake towers. Designed and conducted experiments on scaled models of key components of other outlet work structures.

8.12 Evaluated current methods for determining ductility of outlet works structures and surveyed remediation techniques in use for other types of structures.

8.13 In the development of moment/shears/thrust software tools, completed program to screen min/max data from finite element response spectrum analyses. Completed interface to graphically portray these results with existing plotting package. Completed beta version of the code and drafted a user manual. Developed demonstration problem to fully proof and verify moment/shear/thrust program results.

8.14 In the development of post-processors for finite element time history analyses, developed a modal stress calculation procedure, encoded it, and prepared user manual. Developed interface to existing graphics software, and documented software for evaluation of the amplitude, duration and number of occurrences of dynamic stresses that exceed a damaging threshold level.

8.15 Critically surveyed existing two-dimensional codes that can be modified for seismic analysis of complex structure-reservoir-foundation systems, including joint opening. Selected and modified this code and inserted nonlinear constitutive model.

8.16 Conducted acoustic impedance measurements at seven concrete dams and prepared report.

9 PLANNED ACTIVITIES FOR 1997

The Earthquake Engineering Research Program addresses both the geotechnical and structural aspects of water resource facilities. The program features coordination with and participation by other federal and state agencies and academic and professional experts in a multi-discipline/multi-agency approach. The 1997 activities include:

9.1 Geotechnical

9.1.1 Development of criteria for selecting design earthquake ground motions and characterizing earthquake input required for analysis of their impact on the design of new and remediation of existing water resource facilities. This activity involves a continuing effort to incorporate the latest advances in seismology and geology in procedures for assessing appropriate ground motions for engineering analyses and construction of a comprehensive ground motion analysis system to prepare the ground motion input for engineering analyses. Efforts will focus on construction of modules for criteria implementation and processing tools, and advancement of a three-dimensional basin response code for site specific accelerogram development.

9.1.2 Development of cost-effective, reliable methods to determine site characteristics relevant to seismic performance, to map in three dimensions the extent of potentially liquefiable materials subject to ground failure, and to

determine the adequacy of remedial actions such as ground improvement construction. This effort focuses on geophysical and penetration testing techniques. The geophysical activities include completing the integration of seismic impedance and crosshole tomography capabilities and performing the second in a series of field tests with the next generation equipment for three-dimensional liquefaction mapping. The seismic velocity data base will be analyzed and a report of correlations prepared. Also, the seismic velocity data base will be continuously updated with new data, as available. In the penetration testing effort for liquefaction evaluation, activities include conducting field tests at a gravelly site to correct inadequacies in existing Standard Penetration and Becker Penetration Test correlations and energy and friction corrections for interpretation of test measurements for gravels and to report the findings for sands.

9.1.3 Development of reliable, nonlinear analysis methods to predict the capacity of and extent of damage to earth structures subjected to seismic stresses and large, earthquake-induced deformations. This effort involves a combination of physical testing to establish actual seismic material behavior and development of constitutive models for representation of this behavior in numerical dynamic codes. A series of centrifuge tests will be performed to correct inadequacies in currently used initial static shear stress adjustments to cyclic strength of soils. The centrifuge and laboratory test results will be used to develop a reliable, practical, nonlinear analysis technique for soil materials to predict liquefaction, ground failure, large earthquake-induced deformations, and to design effective, least cost remedial construction, if necessary.

9.2 STRUCTURAL

9.2.1 Development of reliable, nonlinear methods of analysis to predict the extent of damage and ultimate capacity of conventionally placed and roller-compacted concrete gravity dams and arch dams subjected to strong earthquake ground motions, and least cost remedial measures to strengthen these dams if necessary. Complete development of a nonlinear material model for predicting nonlinear structural response caused by cracking and large displacements in conventionally-placed and roller compacted concrete materials. Begin insertion of this material model into the numerical dynamic code. Develop the structure-reservoir-foundation interaction features of the numerical code to account for hydrodynamic effects of the reservoir, uplift pressures beneath the dam, and interaction of the concrete dam with the surrounding rock foundation. Begin testing and verification of the revised code.

9.2.2 Development of reliable, nonlinear methods of analysis to predict the capacity of and extent of damage to reservoir intake-outlet structures subjected to strong earthquake ground motions, and least cost remedial measures to strengthen these structures, if necessary. Report the results of physical tests of key components typical of Corps-designed intake towers. Design and perform physical tests to investigate reinforcing details typical of Corps-designed intake towers. Design and perform physical tests on key components of other reinforced concrete outlet works and pile substructures to develop ductility criteria for design. Report criteria developed from physical model testing.

9.2.3 Development of specialized computer tools for seismic analysis of concrete dams and outlet works to include a) conversion of results from typical response spectrum (modal) methods of analysis into moments, shears and thrusts needed for design of concrete structures, and b) pre- and post-processing design aids for handling the large quantities of input and output data from finite element time history analyses. Complete verification of modal stress calculation procedure against example problems and prepare user manual.

10. CONCLUSION

The focus of this research program on seismic adequacy of embankment and concrete dams and intake-outlet structures establishes the basis for Corps seismic design criteria, and results in the development of reliable, specialized design and analysis tools to predict the potential for earthquake-induced damage to these facilities. These unique advanced techniques are essential to

development of innovative design, evaluation and remediation methods, to assure the earthquake safety of dams, the Corps most critical water resource structures. The program products include software and manuals for their use, and advanced technical procedures that will allow us to more clearly distinguish between safe and unsafe dams, and to remediate unsafe dams as quickly and efficiently as possible. This is the only significant federally funded R&D focused on seismic safety of dams. Past R&D investment on this topic has already resulted in construction savings well in excess of the total cost of this program. The cost of partial failure of even one dam would be much greater than the cost of this program. Conversely, if even one Corps dam did not need remediation as a result of improved criteria, the cost savings would exceed the program outlay.

Characteristics of Hyogoken Nanbu Earthquake Motions

by

Atushi Suzuki[1)]

ABSTRACT

The Hyogoken Nanbu Earthquake of January 17, 1995 inflicted severe damage in the Hanshin and Awaji areas such as has not been seen in Japan in recent years. The safety inspections of the dams conducted in the area by site offices and dam experts immediately after the earthquake showed that there was no damage affecting the safety of the dams, although slight damage was observed in several dams. The survey also showed that the peak accelerations at dam sites were much smaller than those at soil sites.

The Ministry of Construction organized the Committee on Evaluation of Earthquake Resistance of Dams after the earthquake.

After the overall assessment of the acceleration records, the Committee estimated that the maximum horizontal acceleration induced by the earthquake was about 220 gal at rock sites where dams might be built in Japan.

Key Words : characteristics of earthquake motions
earthquake source fault
Hyogoken Nanbu Earthquake
maximum horizontal acceleration

1. INTRODUCTION

In the early morning of January 17, 1995, Hyogoken Nanbu Earthquake whose epicenter was in the northern Awaji Island, inflicted severe damage in the Hanshin and Awaji areas. In some parts of the areas, a seismic intensity of 7 was recorded by the Japan Meteorological Agency. A lot of buildings collapsed during the earthquake or were consumed in the fire which followed it. The Hanshin expressway, the Shinkansen line, utility lines such as gas and water, and many other public facilities were also destroyed.

In view of the extensive damage caused by the earthquake, the Ministry of Construction organized the Committee on Evaluation of Earthquake Resistance of Dams to examine the safety of dams designed with the present design criteria for dams in Japan.

This paper presents mainly the characteristics of the acceleration records obtained during the earthquake, which is a part of the Committee Report.

2 OVERVIEW OF HYOGOKEN NANBU EARTHQUAKE

(1) Main Facts of Earthquake

Table1 gives the main facts of the Hyogoken Nanbu Earthquake as announced by the Meteorological Agency.

(2) Seismic Intensities in Different Areas

Fig. 1 shows the seismic intensities recorded in different parts of Japan when the Hyogoken Nanbu Earthquake occurred. As a result of subsequent field surveys by the Meteorological Agency, it was disclosed that the earthquake had registered a seismic intensity of VII on the Japanese scale in the areas of Kobe City and

[1)] Chief Research Engineer, River and Water Resources Division, Japan Institute of Construction Engineering, 2-8-10 Toranomon, Minato-ku, Tokyo, 105 Japan

Nishinomiya City.

(3) Peak Acceleration Observed at Different Dam Sites

Figures 2 and 3 show the peak accelerations observed in the bedrocks of different dam sites (dam foundations or dam bottom gallery) when the Hyogoken Nanbu Earthquake occurred.

(4) Acceleration Waveforms Observed at Dam Sites

As typical acceleration waveforms observed at different dam sites during the Hyogoken Nanbu Earthquake, the acceleration waveforms observed at the Hitokura Dam site (bottom gallery of a concrete gravity type dam) are shown in Fig. 4 and those observed at the Minoogawa Dam site (bottom gallery of rock-fill dam) in Fig. 5.

3. POST-EARTHQUAKE SPECIAL SAFETY INSPECTION OF DAMS

(1) Overview of special safety inspection

Immediately after the earthquake, the special safety inspections of dams were carried out by the site offices within the river reaches administered under the River Act. The special safety inspections consisted of primary and secondary inspections; the former consisted of visual inspections immediately after the earthquake, and the latter consisted of detailed visual inspections and safety check using the data measured by installed instruments. Special safety inspections were conducted at a total of 251 dams. The locations of the inspected dams are shown in Figure 6.

(2) Results of special safety inspection

The special safety inspections of dams were completed by January 21. The results confirmed that no dams had received severe damage that required emergency protective countermeasures, while some dams had slight damage such as minor cracks in the pavement at their crest. The amount of drainage water also increased slightly after the earthquake at 8 dams, but the amount of water was small enough and has decreased or stabilized.

4. CHARACTERISTICS OF EARTHQUAKE MOTIONS

(1) Earthquake motions at dam sites and soil sites

a) Attenuation of Peak Acceleration

The horizontal peak accelerations observed during the earthquake are shown in Figure 7, and the vertical peak accelerations are shown in Figure 8. The figures consist of the accelerations observed at the dam sites and at soil sites. The accelerations at the dam sites include the values obtained at the gallery under embankment dams or at the lowest gallery in concrete dams. The maximum acceleration at the dam sites was 183 gal, which was observed at Hitokura dam. The maximum acceleration at soil sites was 818 gal. The figures indicate that the peak accelerations at dam sites are substantially smaller than those at soil sites for the same distance from the epicenter.

b) Acceleration Response Spectrum

Figure 9 shows the response spectrum of the acceleration (damping ratio of 5%) in the stream direction observed at 25 dam foundations during the Hyogoken Nanbu Earthquake. Each spectrum is normalized so that the maximum acceleration is equal to 1. The average value of the response spectra for the natural period ranging from 0.1 to 0.6 seconds is about

2. The response spectra decreases rapidly when the natural period exceeds about 0.6 seconds. The figure shows for reference purpose the normalized response spectrum of the acceleration observed at 4 soil sites.

(2) Relationship between distance from earthquake source fault and peak acceleration of dam site bedrocks

Earthquake motions are produced by a sudden, rapid fault dislocation. Thus the magnitude of the earthquake motions generated near the fault that caused the Hyogoken Nanbu Earthquake was presumably influenced largely by the distance from the earthquake source fault.

The earthquake source fault emerged on Awaji Island as an earthquake fault along the Nojima fault. For the Kobe area, on the other hand, the Earthquake was presumably attributable to the activity of any one of the known Quaternary faults, although no unified opinion has been formed in this regard. It is difficult, therefore, to define the boundary of the earthquake source fault which was brought into activity in the Kobe area during the Earthquake. However, in view of the fact that the epicenters of aftershocks occurring immediately following the main shock were distributed in a long narrow strip from the northeast to the southwest, the earthquake source faults are assumed in this report as the Nojima fault for Awaji Island and as the center line of the aftershock area on the day of the Earthquake occurrence (January 17, 1995) in the case of the Kobe area. As far as Awaji Island is concerned, the length of the earthquake source fault agrees well with the boundary of the aftershock area.

Fig. 10 illustrates the relationship between the peak accelerations (two horizontal components) observed in the dam site bedrocks and the distance from the earthquake source fault. For the purpose of establishing this relationship, the distance from the earthquake source fault is defined for Awaji Island as the shortest distance from the Nojima fault and for the Kobe area as the shortest distance from the line passing the center of the aftershock area on the day of the earthquake occurrence which is assumed as the earthquake source fault. The positional relationship between the dam sites and the earthquake source fault is illustrated in Fig. 11. The peak acceleration of the dam site bedrock tended to reduce with increasing distance from the earthquake source fault.

(3) Peak acceleration near earthquake source fault

Fig. 12 illustrates distance from the earthquake source fault and the horizontal peak accelerations at the dam sites located less than 100 km from the earthquake source fault.

As shown in Fig. 12, acceleration records of the bedrock of eight dam sites located within 50 km of the earthquake source fault are available. Of the observed bedrock accelerations, the maximum value of 183 gal was recorded at a dam site 10 km distant from the earthquake source fault.

With respect to bedrock accelerations in locations other than dam sites in the vicinity of the earthquake source fault, the horizontal peak acceleration of 213 gal was recorded (Izawa and three others (Matsumura Gumi, Ltd. Technological Research Institute: "Observation Records of Bedrock in Hyogoken Nanbu Earthquake" Collection of Research Papers by

Kinki Branch of Architectural Institute of Japan, June 1995). The recorded peak acceleration pertained to an observation station 10 km distant from the earthquake source fault (epicentral distance: 31 km) and the bedrock of this location, where an elastic wave velocity of Vp = 2.67 km/sec was recorded, is considered to be of similar structure and texture of those of the dam sites under consideration. From an overall judgment of the observation results discussed above, the Committee estimated that the maximum horizontal acceleration induced by the earthquake was about 220 gal at rock sites where dams might be built in Japan.

(4) Horizontal and vertical peak accelerations

Fig. 13 shows the relationship between the horizontal and vertical peak earthquake accelerations observed at dam sites in the Hyogoken Nanbu Earthquake. From this figure, it can be seen that the ratios of the vertical peak accelerations to the horizontal peak accelerations range from 30% to 100%, and that the ratios tend to reduce with increasing horizontal peak accelerations.

(5) Earthquake motions of Dam Structure

Fig. 14 illustrates for each structural type of dam the relationship between the peak accelerations of dam foundation (in stream directions and in direction parallel to dam axis) and peak acceleration of dam top. From the figure, it is seen that the response magnification of the dam top (peak acceleration of dam top v peak acceleration of dam foundation) varies 1 to 5 times for both concrete dams and fill dams.

Table 1 Summary of Hyogoken Nanbu Earthquake

Name of earthquake	Hyogoken Nanbu Earthquake of 1995
Place name of epicenter	Awaji Island
Time and date of occurrence	0546 hours 52 seconds, January 17, 1995
Location of epicenter	N34.6 lat., E135.0 long.
Focal depth.	14 km
Magnitude of earthquake	M 7.2

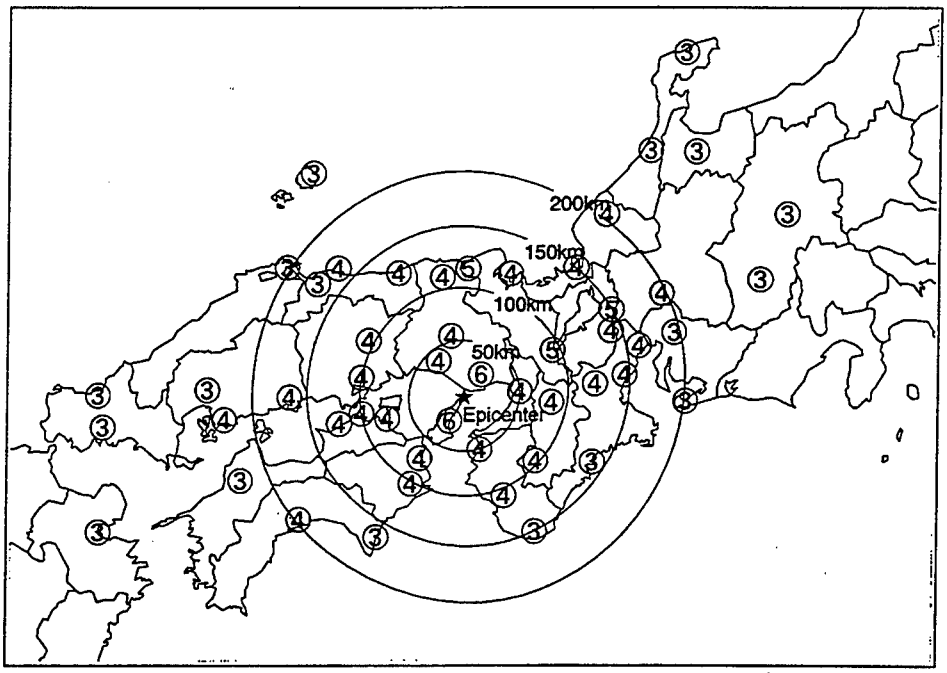

Fig. 1 Seismic intensity distribution of Hyogoken Nanbu Earthquake (Meteorological Agency)

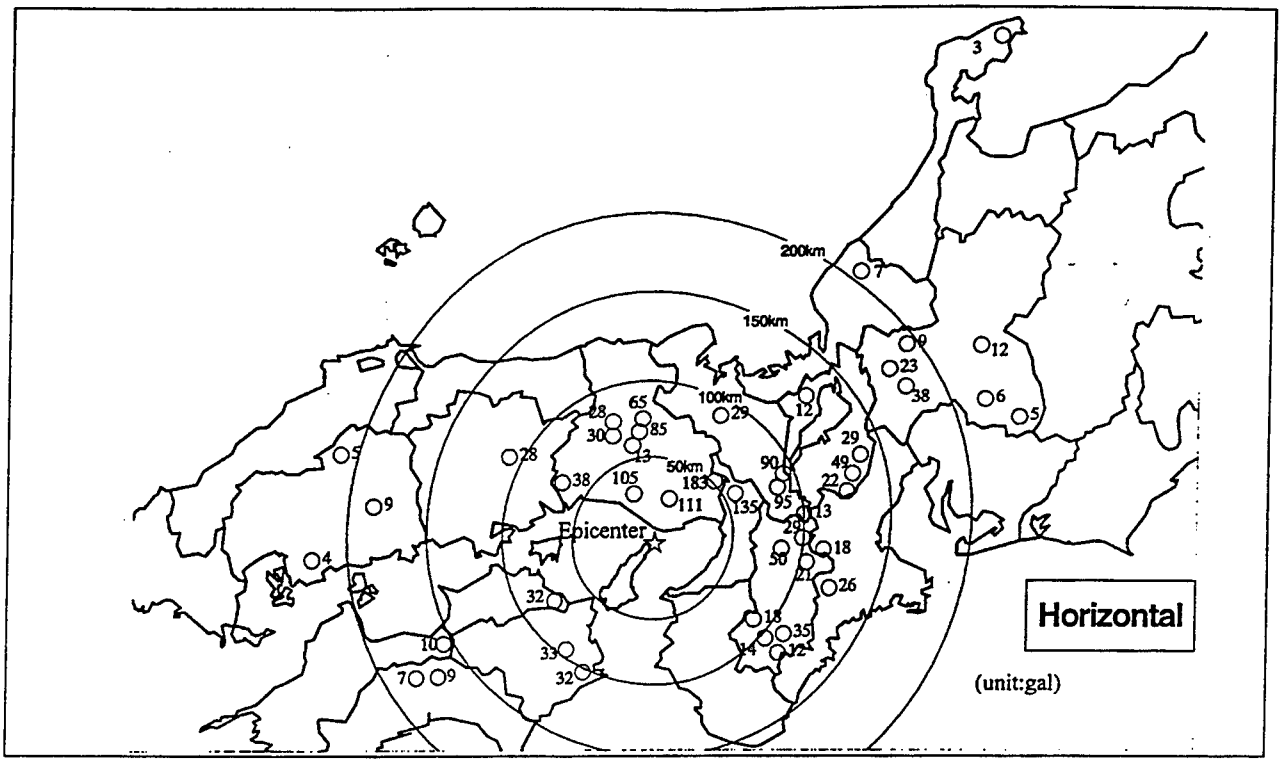

Fig.2 Horizontal peak accelerations observed in dam site bedrocks (in gal)

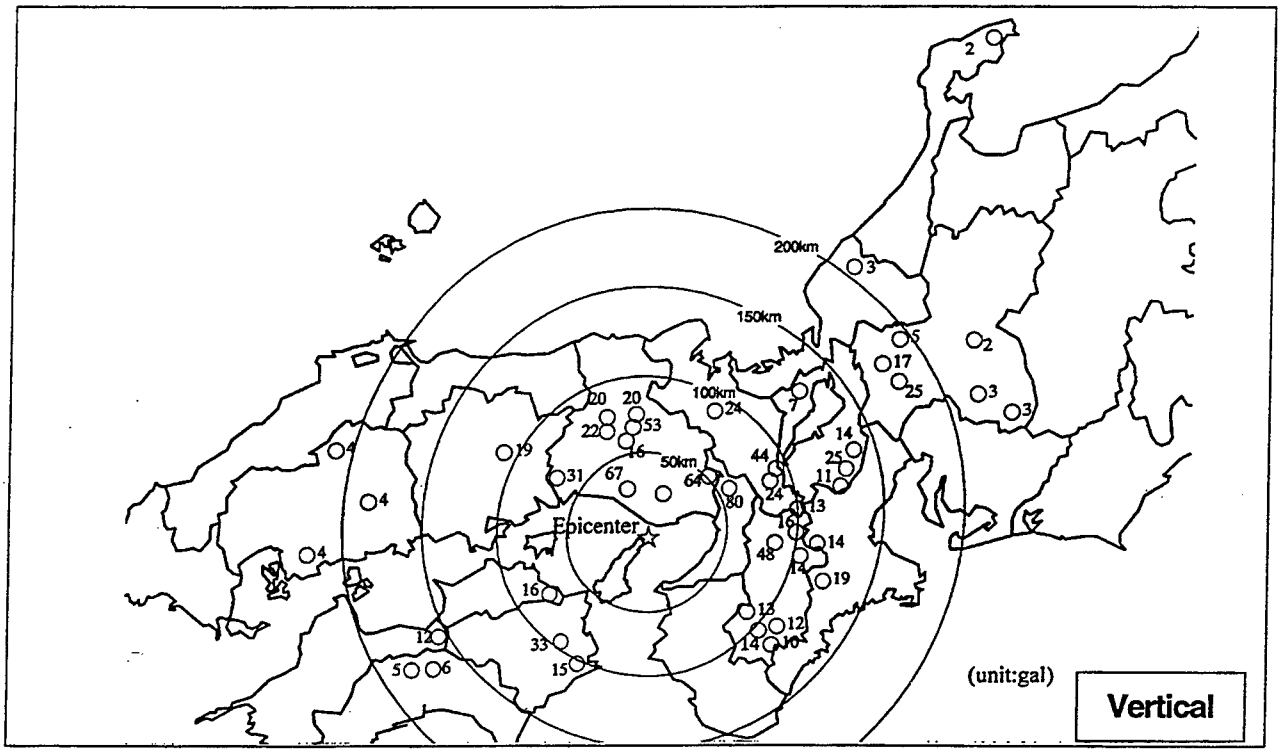

Fig. 3 Vertical peak accelerations observed in dam site bedrocks (in gal)

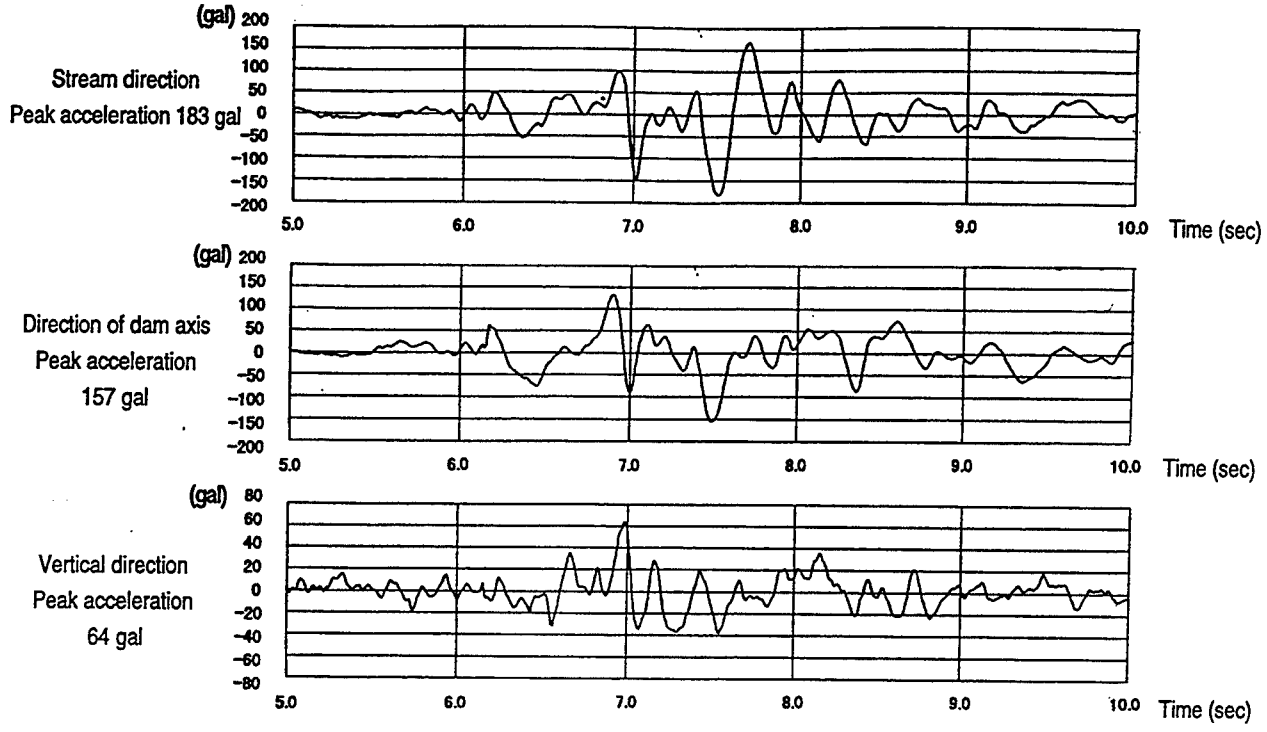

Fig. 4 Acceleration waveforms observed at Hitokura Dam (bottom gallery of concrete gravity dam)

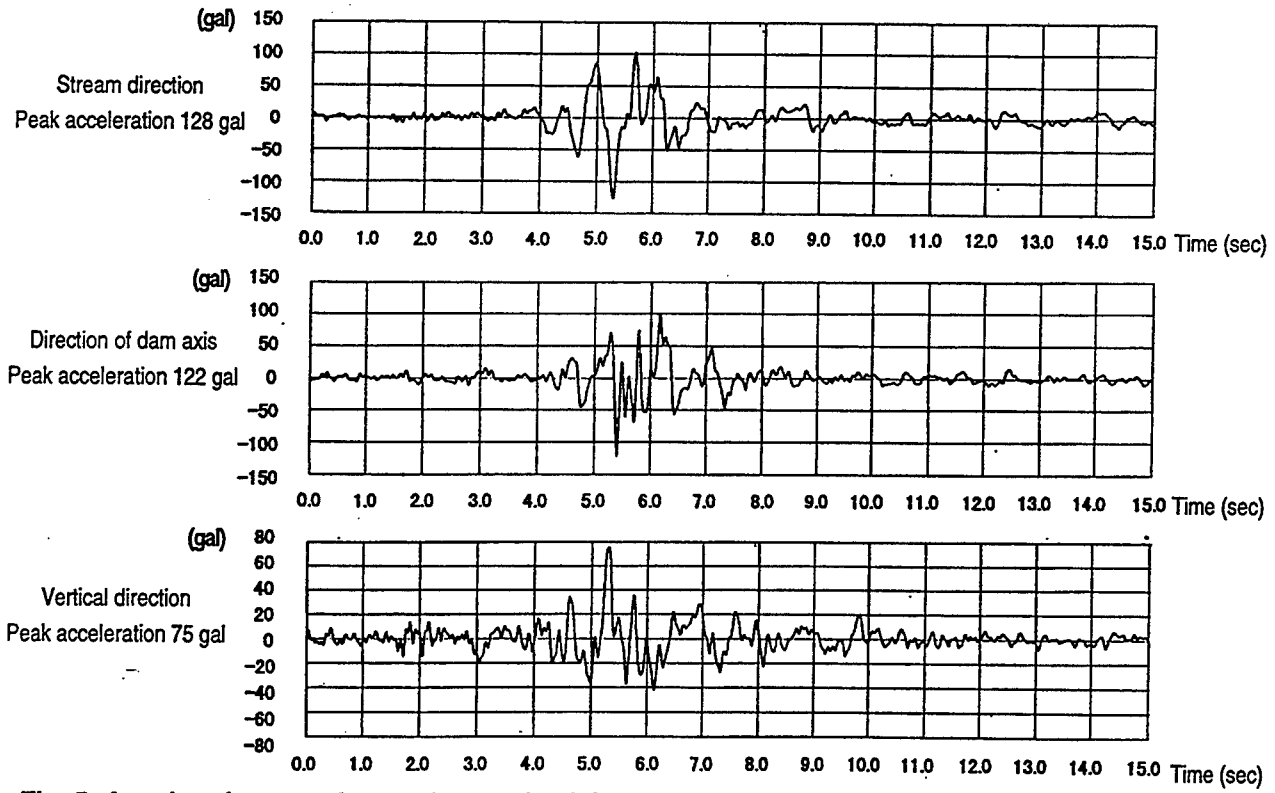

Fig. 5 Acceleration waveforms observed at Minoogawa Dam (bottom gallery of rock-fill dam)

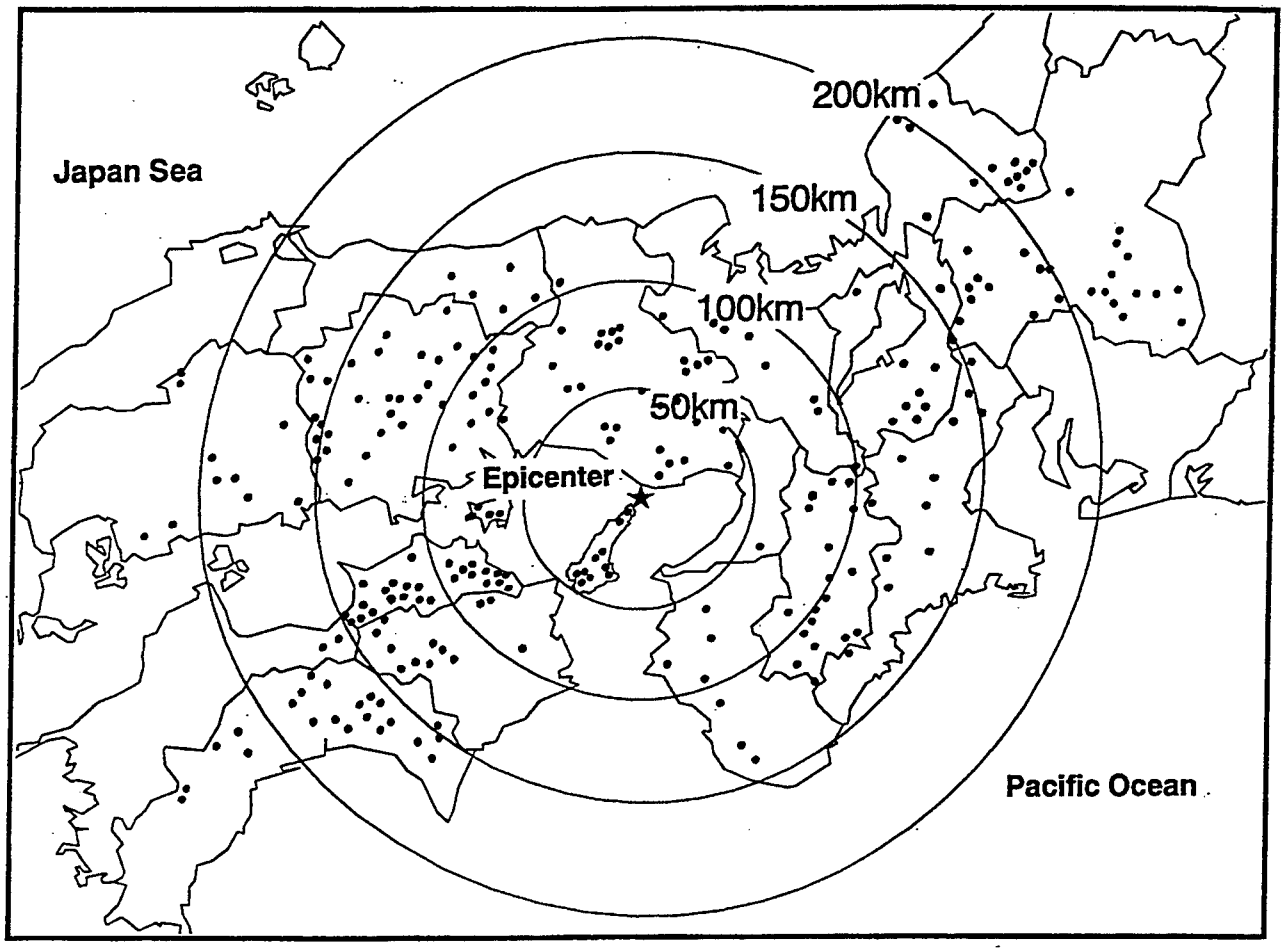

Fig. 6 Location of dams undergoing special inspections

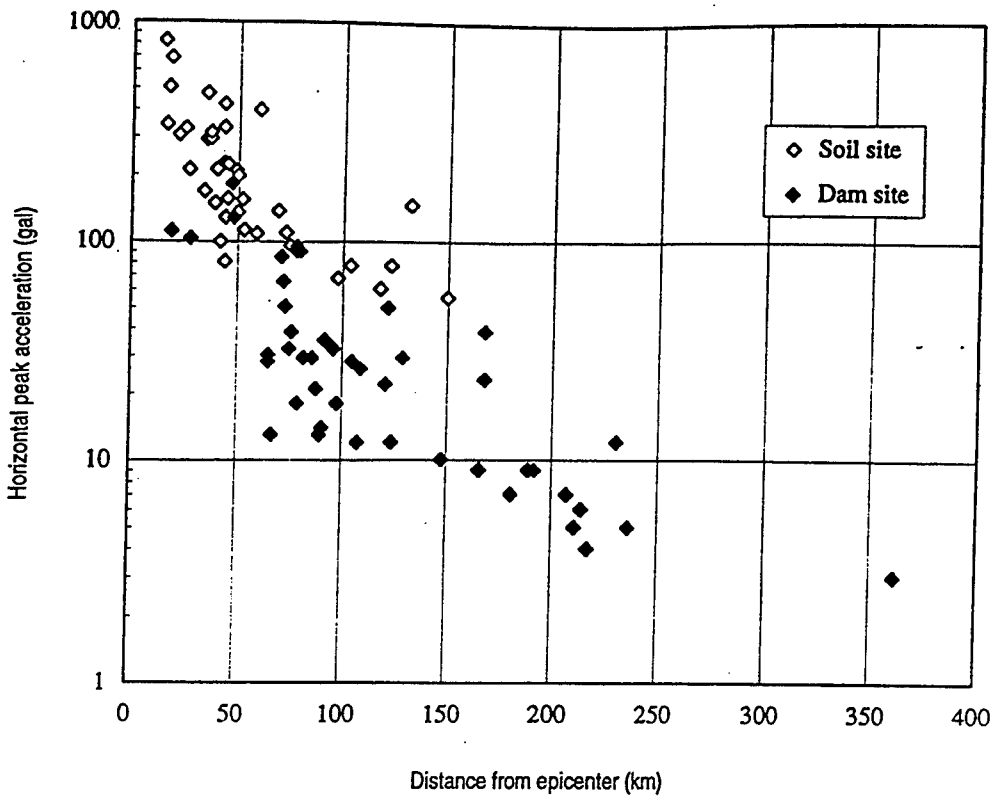

Fig. 7 Attenuation of horizontal peak acceleration with distance from epicenter

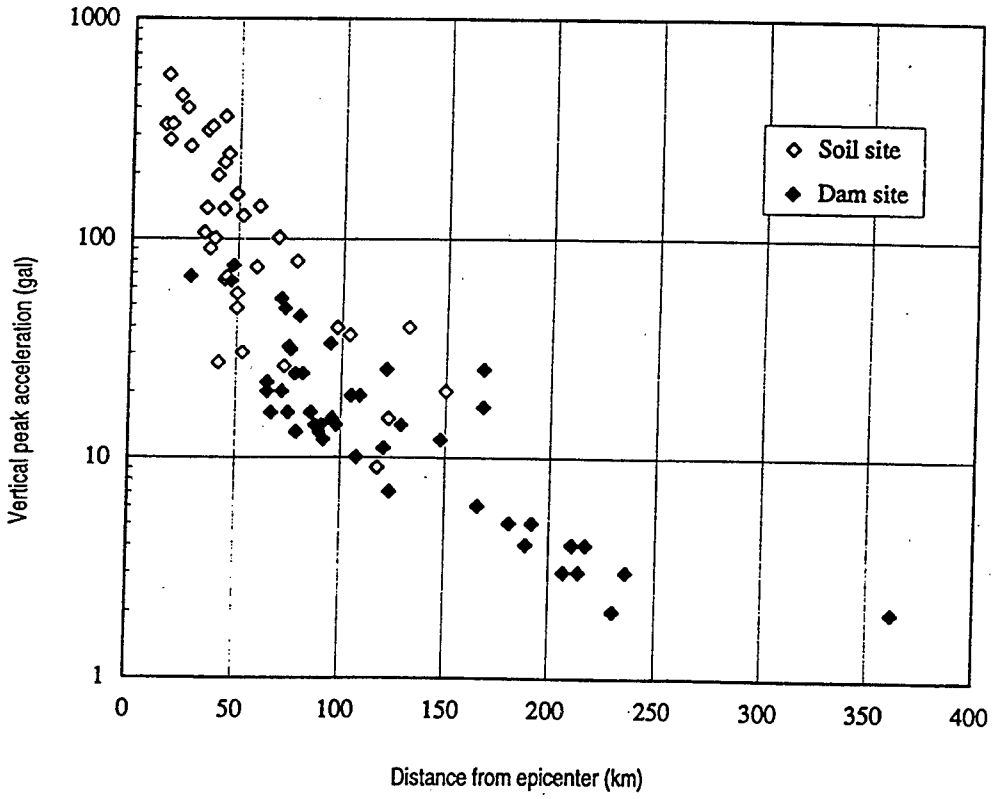

Fig. 8 Attenuation of vertical peak acceleration with distance from epicenter

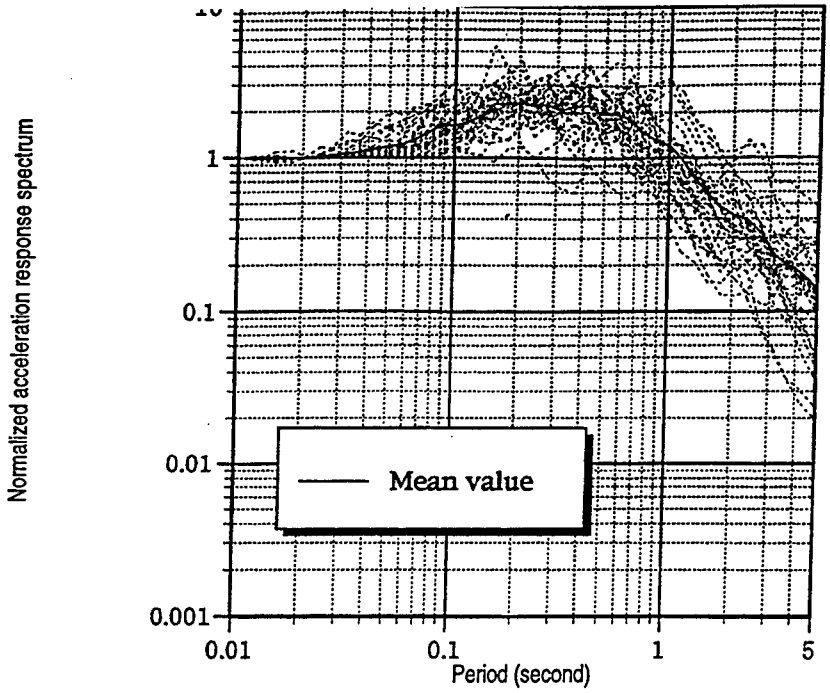

(1) Dam site (stream directions)

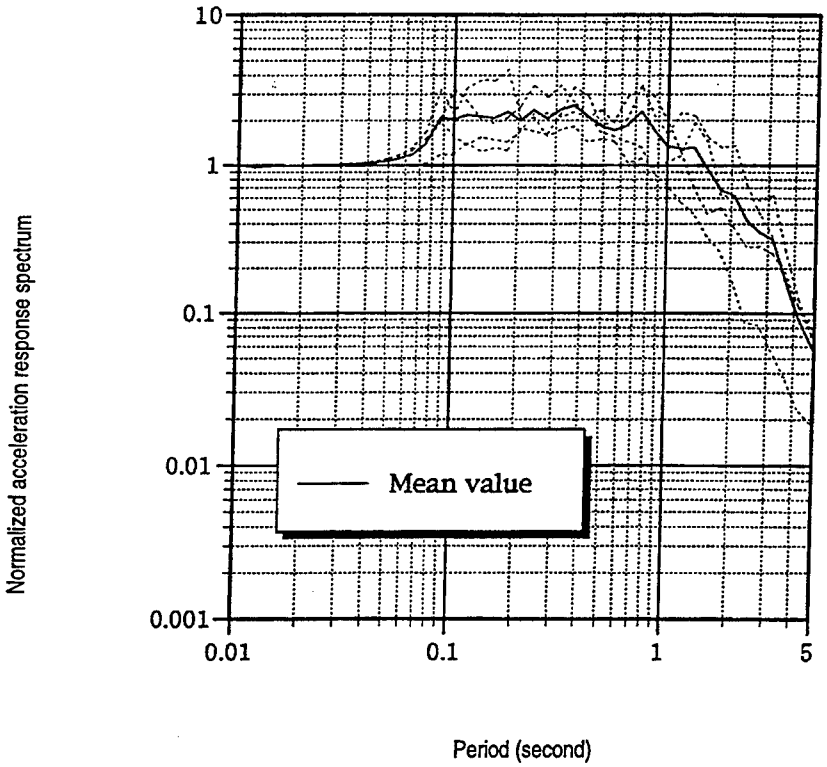

(2) Soil site (horizontal direction)

Fig. 9 Normalized response spectrum of the acceleration (damping ratio h = 5%)

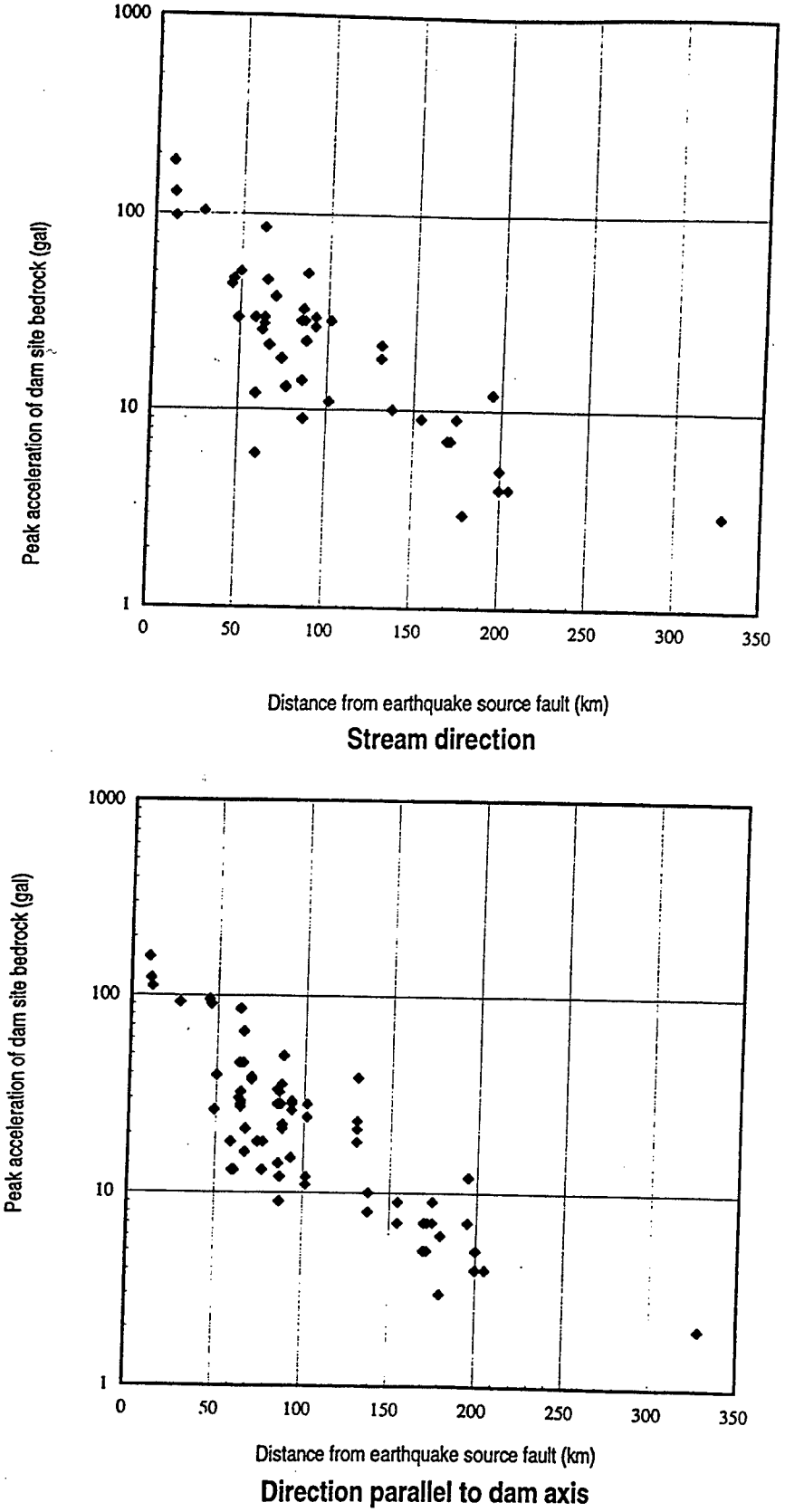

Fig. 10 Horizontal peak acceleration of dam site bedrock and distance from earthquake source fault

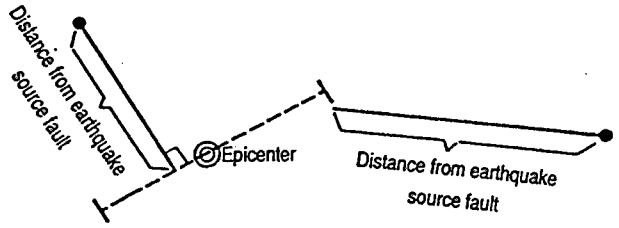

Fig. 11 Locations of dam sites and earthquake source fault

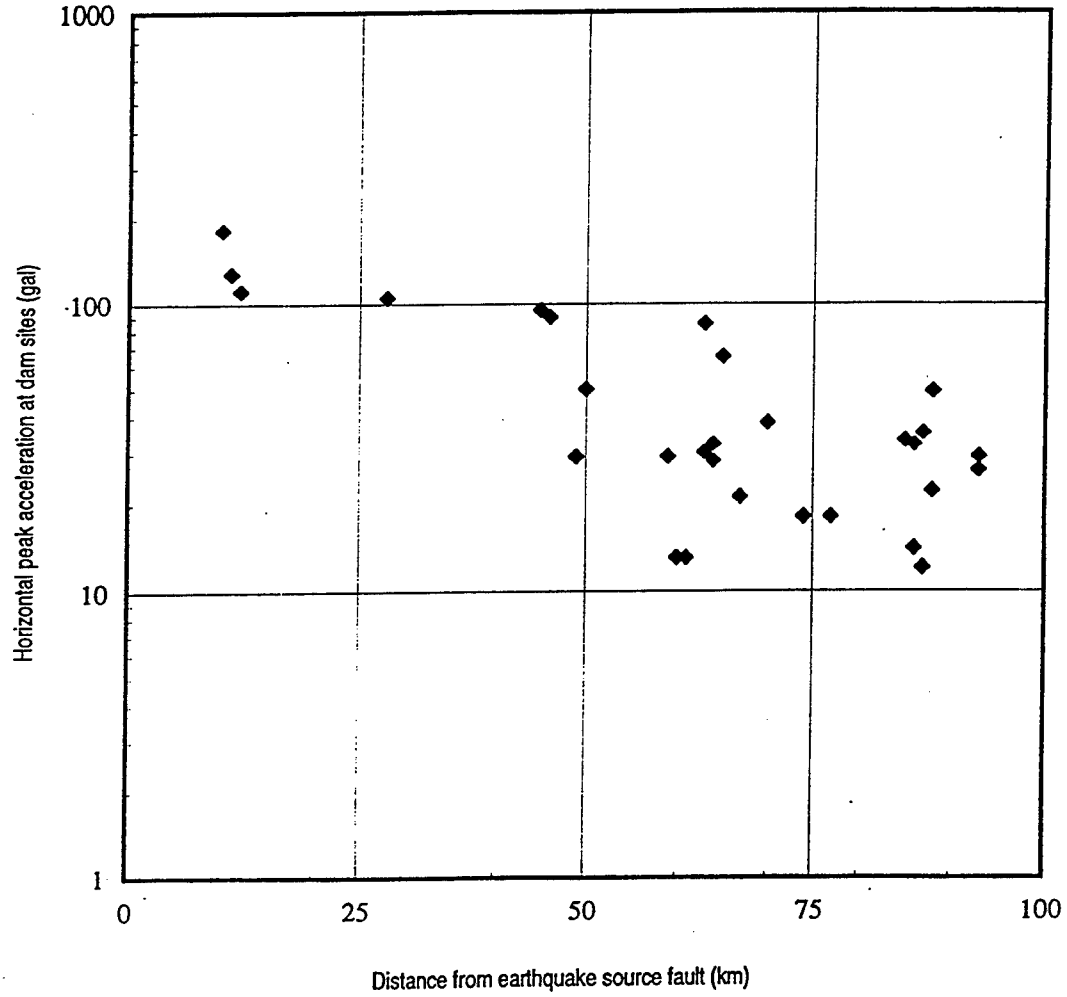

Fig. 12 Attenuation of horizontal peak acceleration with distance from earthquake source fault

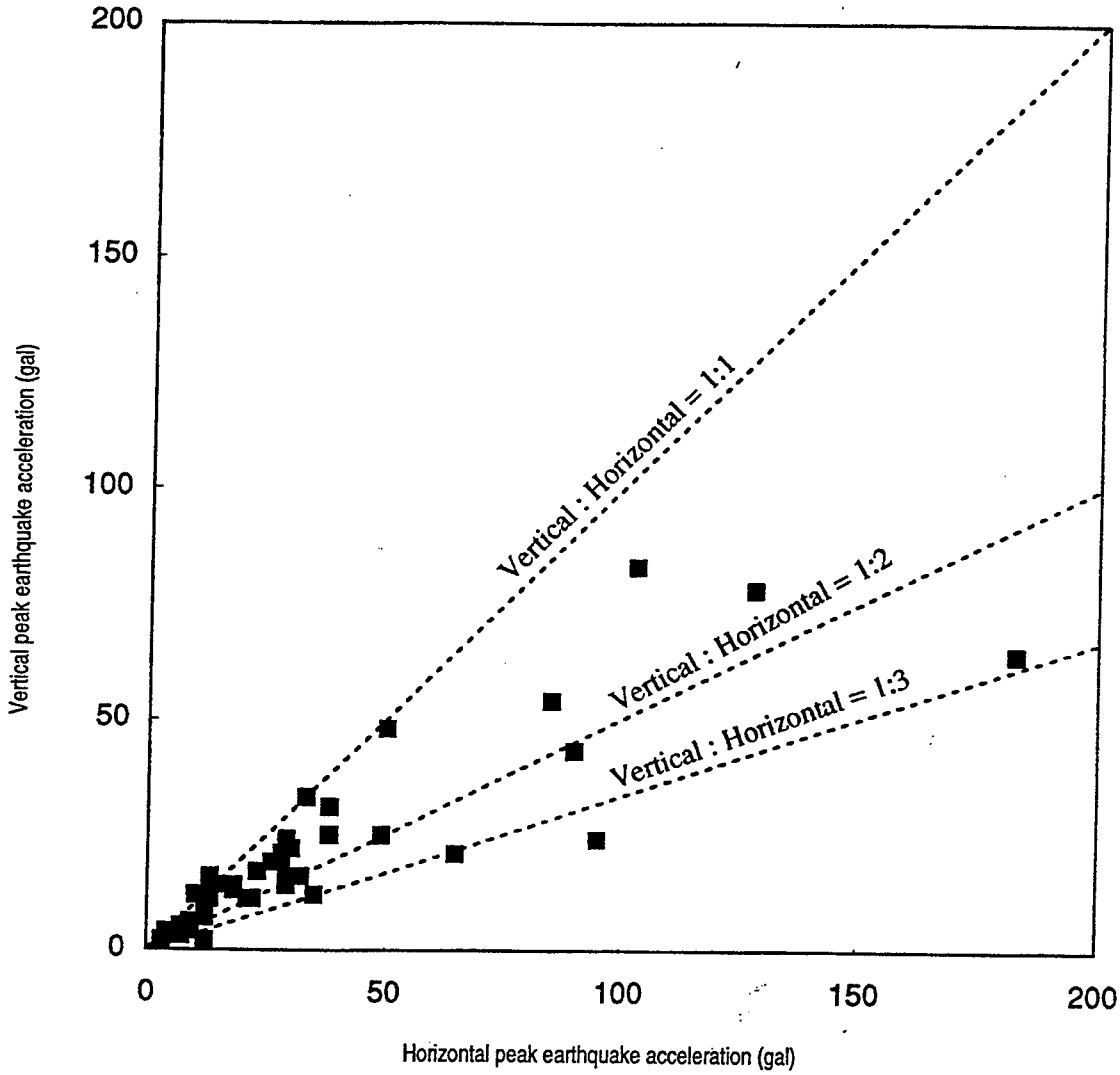

Fig. 13 Horizontal peak acceleration versus vertical peak acceleration

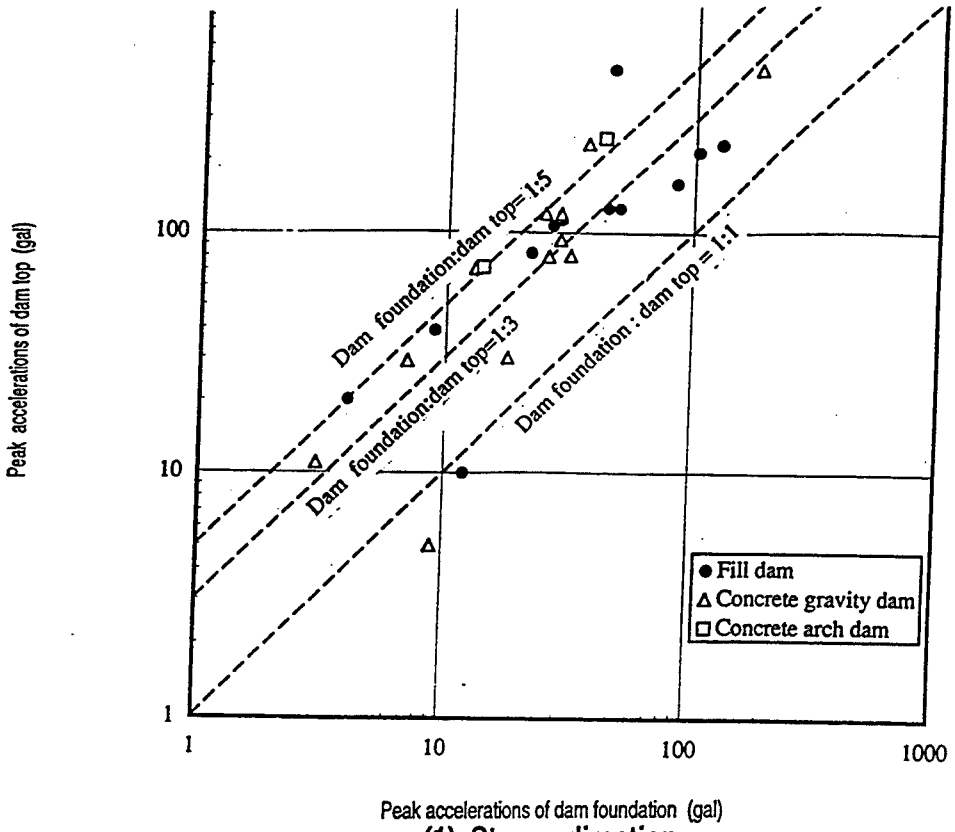

(1) Stream direction

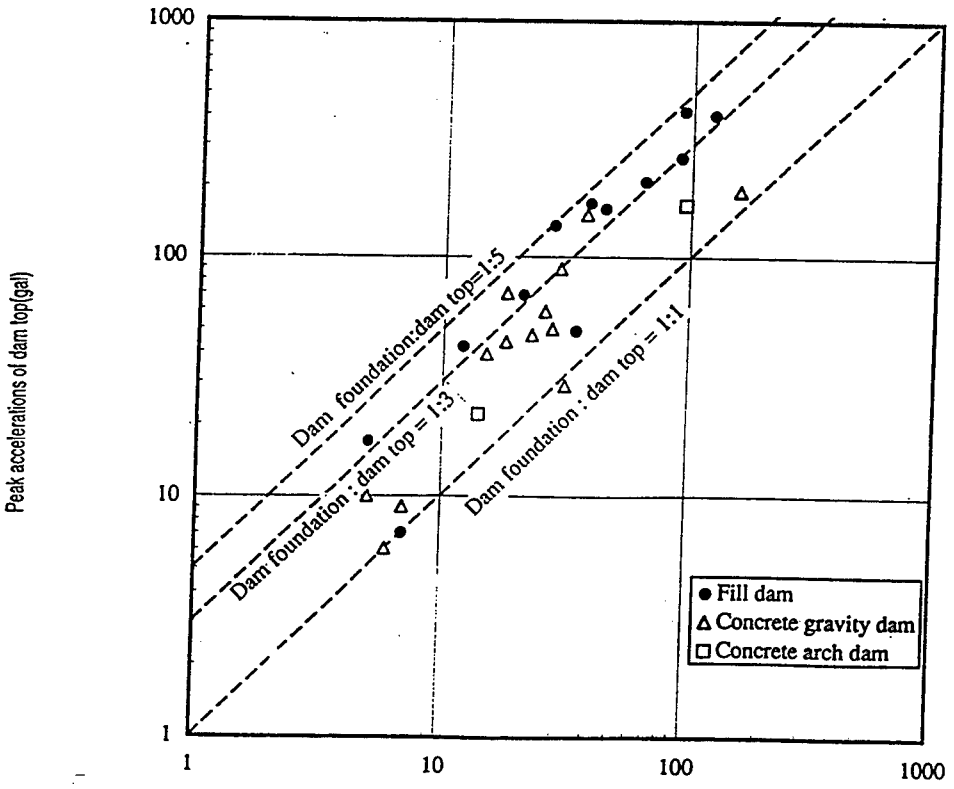

(2) Direction parallel to dam axis

Fig. 14 Peak acceleration of dam foundation and peak acceleration of dam top

Effects on Dams

Norihisa Matsumoto, Akira Nakamura,
Takashi Sasaki, and Tomoya Iwashita

ABSTRACT

Immediately after the earthquake, emergency inspections of dams were carried out in a wide area around the epicenter, and Public Works Research Institute made inspection visits to dam sites to investigate the effects on the dams. Their results are reported in this report. Emergency inspections and investigation by PWRI confirmed that there was no major damage to dams, excluding some slight effects, nor other problems seriously affecting dam safety or requiring immediate protective countermeasures.

Meanwhile many acceleration records were obtained at dam foundations, and they are also showed in this report.

Key words: dam, earthquake, measurement, site investigation (IGC: H4/C7)

This article previously published. Special Issue of Soils and Foundations, 273-281, Jan. 1996, Japanese Geotechnical Society, Sugayama Bldg. 4F, Kanda Awaji-cho 2-23, Chiyoda-ku, Tokyo 101, Japan.

Geophysical Methods for Site Characterization and Measurement of In Situ Properties

by

Robert F. Ballard, Jr.*

ABSTRACT

This paper examines the use of exploratory seismic technology as a tool for measurement of in situ liquefaction potential of saturated, cohesionless soils. Past applications of seismic technology have focused principally on shear velocity as a liquefaction indicator. Inherent in these applications was the assumption of a non-porous, perfectly elastic media; the theory of which provides simple procedures for conversion of combined measurements of distance and travel time to 'shear velocity.' This property, dependent on shear modulus and density of a perfectly elastic solid, is all that can be produced experimentally because of the simplicity of the assumed earth model used as basis for interpretation.

All interpretive geophysical approaches require use of conceptual earth models. For the liquefaction problem, the key to success is choice of a model that incorporates dynamic attributes of fluid-saturated, noncohesive sediments. A Biot model, modified to include fracture porosity and permeability, is proposed as a proper choice. Consequently, assignment of combinations of measured particle motion attributes to earthmodel parameters must be re-evaluated in light of the Biot theory.

A field experiment is proposed with the Biot model and waveform tomography in mind. This experiment embodies concepts relative to current and future data processing capabilities.

KEYWORDS: Liquefaction, Biot, Tomography, Seismic, Soils

1 INTRODUCTION

Engineering geophysics and geology have enhanced geotechnical engineering for at least 2 decades. Seismic stability analyses depend heavily on geophysically determined parameters. This paper will describe a new concept for employing geophysical methods for site characterization and measurement of in situ properties.

2 PROBLEM DEFINED

A safe, cost-effective design of Corps facilities has been severely limited by lack of accurate site condition parameters. A need exists for the development of an in situ technique for more accurately determining site conditions relating to earthquake response. It is a widely known fact that standard penetration tests, which are heavily relied upon, have severe limitations. Geophysical methods offer a cost-effective, viable solution.

*Earthquake Engineering & Geosciences Division
Geotechnical Laboratory,
USAE Waterways Experiment Station,
Vicksburg, MS 39180

3 APPROACH RATIONALE

It is commonly known that broad areal site coverage is more representative of true site conditions than discrete data points obtained through borings or push probes. It is believed that the entire seismic wave train is affected by numerous definable site parameters. It is also known that the relationship between seismic wave train modification and earthquake susceptibility can be established. The acoustic impedance approach to characterize bottom/subbottom materials has been demonstrated successfully at more than 20 sites through the Dredging Research Program. A bore hole imaging and tomographic crosshole system has been developed for location of clandestine tunnels in Korea. It is believed that marriage of the two above systems is feasible, economical, and desirable for development of a new procedure.

4 OBJECTIVE

The objective of the study proposed herein is to develop geophysical procedures to identify and characterize in situ soil materials in terms of their susceptibility to liquefaction when subjected to earthquakes.

5 APPROACH

This proposed study assumes continuation over a period of 6 years. During Year 1, a workshop on the objective of the programs and test sites which might be used for proof of principle testing was conducted. During Year 2, the workshop proceedings were documented, a first series of field tests were completed, and documentation of the state of the art in geophysical/liquefaction potential parameter correlations performed. During Year 3, the present point of the program, it is anticipated to complete seismic impedance/crosshole tomography capability integration and a second series of field tests. Year 4 will consist of documentation of the integrated analyses of field tests, correlation of seismic wave velocities, ratios, and other velocity factors to liquefaction potential indicators. Lastly, correlating seismic wave attenuation and full waveform modification indicators to liquefaction potential. In the course of Year 5, geophysical parameters will be correlated to seismic parameters and liquefaction potential. Field procedures will be improved and "fine-tuned." An engineering technical letter on field procedures will be completed in conjunction with analytical and data processing procedures. During Year 6, the final year of the program, advantages and limitations will be defined and presented in a draft documentation report. Lastly, a final report will be published.

6 RESULTS AND PRODUCTS EXPECTED

Two products (results) are expected to evolve during the course of this study: 1) Development of a seismic method for site characterization using principles of acoustic impedance (energy loss, Q) and seismic signature modifications with emphasis on the shear wave train and 2) correlation between seismically measured parameters (in situ) and earthquake risk analysis procedures.

7 FY95 ACCOMPLISHMENTS

During FY95, four accomplishments can be highlighted: 1) An assessment of Biot theory application to determination of liquefaction potential of sediment was performed; 2) A

study of geophysical parameters to geotechnical parameters to liquefaction potential indicator correlations was initiated; 3) A workshop on liquefaction potential indicators, geophysical parameter correlations, and test site selection was conducted; and 4) Test sites were carefully analyzed and prioritized prior to selection.

7.1 Workshop: Earthquake Engineering Site Characterization.

On 27 -28 June 1995, a workshop was conducted at the United States Army Engineer Waterways Experiment Station, Vicksburg, Mississippi. Workshop topics included: First, Geotechnical Indicators of Liquefaction Potential on In Situ Materials (questions raised were what causes liquefaction and what are the indicators that liquefaction has occurred in the past or may occur in the future?); the key speaker was Dr. Liam Finn, University of British Columbia. The second topic was Geophysical Indicators of Liquefaction Potential (items addressed were geophysical parameter to geotechnical parameter correlations and direct geophysical indicators); key speakers were Professor Kenneth Stokoe, University of Texas; Mr. Phil Sirles, Bureau of Reclamation; and Dr. Richard Rechtien, University of Missouri, Rolla. The third topic was centered on field test sites (the primary question which arose was what are desirable characteristics of test sites for evaluation of geophysical methodology?); the key speaker was Professor Richard Woods, University of Michigan.

7.2 Field Test Site Evaluations

In the course of discussing 10 test sites, objectives for meeting all criteria were established. These objectives were three-fold: 1) To examine potential test sites for relevancy to the development of geophysical techniques; 2) Establish test site criteria; 3) Select and prioritize sites in accordance with the accepted criteria. Figure 1 is a summation of the potential test sites including pros, cons, and subjective priorities.

Site (Owner)	Pro	Con	Priority
Treasure Island (NG)	Well documented EQ emphasis	Man-made, loose sand Bay mud Small, salt-water site	Low
University of Houston (NG)		Clay Too small	Low
Texas A&M (NG)		Doesn't meet requirements	Low
Northwestern (NG)	Loose sands	Not good for long-term study Denser than required	Low
Unity (BR)	Clean sand Documentation Liquefiable	Limited access	High
Conconullay **	Documentation Few fines, clean sand, some gravels	Time factor Complex geology	High POC: Mike Stevens
Bradbury (BR)	Gravelly site SMIP	Partially de-watered	Med/Low
Jackson Lake (BR)		Remediated Limited access	Low
Success (CE) *	Accessible Sands and gravels Documentation Ongoing WES work (possible additional funding)	Borehole placement Affected by four major faults Cemented lenses	High/Med
Wildlife	Liquefiable EQ likely to occur Other tests run there	Boreholes not accessible Difficult access	High/Med

* First choice
** Second choice

Figure 1. Summation of Potential Test Sites

8 FY96 ACCOMPLISHMENTS AND PLANS

During FY96, a combination lecture and workshop was held on the topic of seismic tomography and Biot theory application. Professor Tokuo Yamamoto of the University of Miami was the principal speaker. Also during FY96, a report entitled "In situ Seismic Investigation of Liquefaction Potential of Soils" was completed. Plans for the remainder of FY96 involved 1) Publication of the workshop proceedings; 2) Construction of a test plan and the conduct of initial investigations at Success Dam; and 3) Hire Dr. Barbara Luke (Army Research Office Summer Faculty Program) to plan and assist with the Spectral Analysis of Surface Waves (SASW) portion of the Success Dam investigation.

9 TASK EXECUTION MATRIX

Figure 2 is the task execution matrix which presents 11 tasks identified during the timeframe FY95-FY00. It can be seen that many of these tasks will be conducted concurrently while striving to reach the final product.

10 OVERVIEW OF SEISMIC EARTH MODELS

According to Rechtien (1996), geophysics in general, and seismology in particular, is an interpretive science. In seismology, earth parameters are not measured directly, but are indirectly inferred through comparison of recorded waveform attributes with those derived synthetically through numerical modeling. Consequently, in the application of any seismic method to subsurface exploration, one must have a specific earth model in mind, compatible with a chosen process for numerical synthesis of seismic data. Due to the complexity of numerical modeling, this earth model will necessarily be simplistic; inherently capable, at best, of reproducing gross, dominant attributes of measured seismic waveforms. Realization of correspondence between field measurements and numerical model data will ultimately depend upon: 1) The degree of inclusion of stress-strain subtleties; 2) Significance of these subtleties relative to modification of the seismic waveform; 3) Validity of assumptions of isotropy, homogeneity, and model dimensionality; and 4) Accuracy of numerical simulation of spatial and temporal source characteristics.

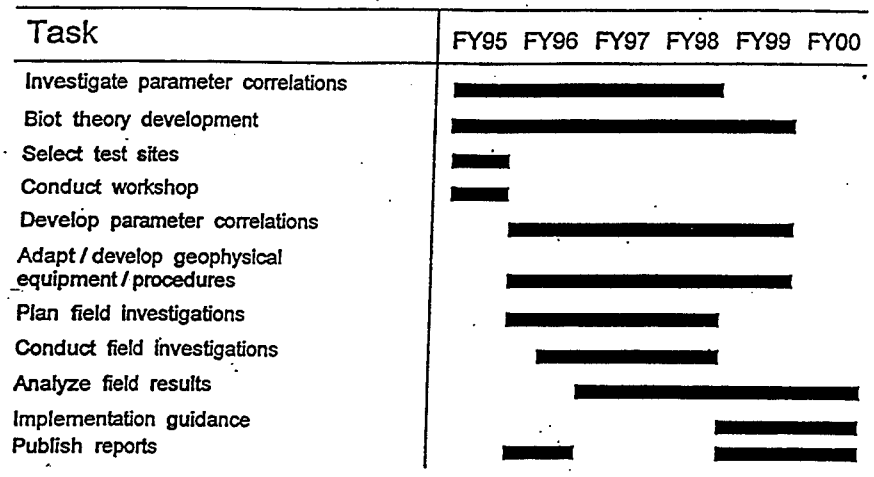

Figure 2. Task Execution Matrix

Following are models suitable for forward wavefield calculations:

10.1 Poroelastic Models

Biot (1962a) presents a unified treatment of the mechanics of deformation and acoustic propagation in porous media. He treats the fluid-solid medium as a complex physical-chemical system with resultant relaxation and viscoelastic properties of a very general nature. For an isotropic, elastic, porous medium, the principal result of this treatment is the field equations describing coupled energy propagation within the porous solid structure and within the fluid. These equations are given by Biot as, (1)

$$2\sum_j \frac{\partial}{\partial x_j}[\mu e_{ij}]+\frac{\partial}{\partial x_i}[\lambda_c\ e-\alpha M\zeta]=\frac{\partial^2}{\partial t^2}[\rho\ u_i+\rho_f\ w_i]$$

and (2)

$$\frac{\partial}{\partial x_i}[\alpha Me-M\zeta]=\frac{\partial^2}{\partial t^2}[\rho_f\ u_i+mw_i]+\frac{\eta}{\kappa}\ \frac{\partial}{\partial t}w_i$$

where,

$$e_{ij}=\frac{\partial}{\partial x_j}u_i\ ;\ e=\sum_i \frac{\partial}{\partial x_i}u_i\ ;\ \zeta=-\sum_i \frac{\partial}{\partial x_i}w_i\ ;$$

$$w_i=\sigma(U_i-u_i)\ ;\ \mu=\mu_r(1+i\delta)$$

u_i is the displacement within the skeletal solid,

U_i is the average fluid displacement,

w_i is the flow of the fluid relative to the frame,

μ_r is the dynamic shear modulus,

ρ_f is the density of the fluid,

λ_c is the adiabatic Lame coefficient,

σ is the porosity,

μ is the complex shear modulus,

δ is the specific loss of the skeletal frame for shear,

η is the kinematic viscosity of the fluid,

m is the virtual mass of the skeletal frame,

ρ is the total mass density,

κ is the hydraulic coefficient of permeability,

α, M are Biot elastic coefficients (Biot(1941))

Equation (1) is the result of the application of the principle of conservation of momentum, while (2) can be interpreted as expressing the dynamics of relative motion of the fluid in a frame of reference moving with the solid. These equations were based on a semiphenomenological formulation of the equations of elasticity for a porous aggregate by Biot (1941; 1956a,b,c; 1962a,b), Frenkel (1944), and Gassmann (1951). The hypothesized form of the microscopic constitutive relationships, which resulted in the equations of motion, was confirmed by Burridge and Keller (1981) in their studies of

the dynamic equations which govern the behavior of the medium on the microscopic scale. Moreover, through experimental observations, Plona (1980) confirmed a fundamental prediction of Biot's model by his observation of a second compressional wave (referred to as the 'slow wave'). Stoll and Bryan (1970) and Stoll (1974) extended Biot's theory to include dissipation due to the frame by incorporating complex moduli.

Successful applications of Biot's theory to various fields, notably to seismic exploration (e.g., Geertsma 1957; Geertsma and Smit 1961; Gardner, Gardner, and Gregory 1974; Domenico 1974; Rosenbaum 1974;) marine acoustics (Stoll 1974, 1977, 1980, 1985; Yamamoto 1983; Badiey and Yamamoto 1985; Turgut and Yamamoto 1988; Yamamoto and Turgut 1988; Yamamoto et al. 1989), and attenuation and dispersion of compressional waves (Dutta and Ode 1979,1983; Stoll and Kan 1981; Ogushwitz 1985; Geli , Bard, and Schmitt 1987; Winkler et al. 1987; Rasolofosaon, 1987; Schmitt, Bouchon, and Bonnet 1988; Yamamoto, Nye, and Kuru 1994, 1995) have demonstrated the utility of the model for a variety of poroelastic problems. The model incorporates eight material parameters (considering η / κ as a single variable), including the liquefaction-sensitive parameters: density, shear modulus, porosity, and permeability. Soil fabric and structure can be included by specification of spatial variation of material coefficients. Thus, the Biot model is a general formulation of small amplitude (linear stress-strain relation) wave propagation in saturated sediment deposits characterized by an elastic, porous frame. In the forward modeling arena (as opposed to interpretational problems of waveform inversion) the system of equations lends itself readily to waveform calculations by means of finite difference (Hassanzadeh 1991; Zhu and McMechan 1991; Dai, Vafidis, and Kanasewich 1995) and finite-element methods (Zienkiewicz and Shiomo 1984).

10.2 Biot-squirt Models

In Biot's model, pore fluid is forced to participate in a solid's oscillatory motion by viscous friction and inertial coupling. A different mechanism of fluid flow during seismic and acoustic wave propagation is associated with the squirting of pore fluid out of thin soft cracks as they are deformed by passing seismic waves. Mavko and Nur (1979) have shown that the squirt-flow mechanism results in much higher and realistic attenuation values in partially saturated rocks than those predicted by Biot's mechanism. Mavko and Nur (1975) have suggested that squirt flow may occur even in fully saturated rocks due to fluid flowing between saturated cracks of different orientation. This mechanism has been shown to be responsible for the measured seismic energy losses and velocity dispersion in sedimentary material for both P- and S-waves (e.g., Murphy, Winkler, and Kleinberg 1986; Wang and Nur 1990) Dvorkin and Nur (1993,) and Dvorkin, Mavko, and Nur (1995) proposed a combined Biot-squirt (BISQ) model where the Biot elastic frame is replaced with a viscoelastic one. They considered a macroscopically homogeneous rock with pore space that has thin compliant (soft) and stiff portions. At high confining pressure, the thin compliant pores close and the observed velocity dispersion is small and can be adequately described by Biot's theory (Mavko and Jizba 1991). However, at small confining pressure the high observed velocity/frequency dispersion and attenuation can be adequately described by the BISQ model.

10.3 Modeling Summary

A BISQ model appears to be appropriate for the description of dynamic response of fully or partially saturated porous media to low amplitude seismic wave energy. This model is reducible, by certain assumptions relative to the independent material parameters listed above, to simpler and standard equations of motion encountered in physics. As for example, assuming the medium to be elastic and non-porous, (2) above vanishes, and (1) assumes the form, (3)

$$2\sum_j \frac{\partial}{\partial x_j}\left[\mu e_{ij}\right]+\frac{\partial}{\partial x_i}\left[\lambda_c e\right]=\frac{\partial^2}{\partial t^2}\left[\rho u_i\right].$$

This equation can be recognized as the isotropic, heterogeneous wave equation for a perfectly elastic solid. Other equations of motion can be similarly produced by appropriate choices of material parameter behavior.

By virtue of the wide application of Biot's theory in the literature and the essential absence of any other widely accepted model, it is concluded that the BISQ model can be considered the starting point for most scientific inquiries of wave motion in porous, partially or fully saturated, earth materials. The equations of motion, (1) and (2), even modified by inclusion of squirt flow, are amenable to numerical solution by Finite difference methods (e.g., Dai, Vafidis, and Kanasewich 1995). Consequently, forward modeling of stress waves in porous media is a matter of application of known and proven numerical methods, and is not a subject requiring extensive research and development.

11 SUMMARY

11.1 Products

In summary, five products can be identified: 1) New geophysical to geotechnical parameter correlations; 2) New or adapted geophysical methods and field procedures; 3) New geophysical data processing procedures; 4) Efficient, cost-effective procedures for assessing in situ liquefaction potential of soils; and 5) Documentation in engineering technical letters, technical reports, and journal articles.

11.2 Tasks to be Accomplished

Four tasks are to be accomplished: 1) Establish theoretical and empirical correlations between geophysical parameters and liquefaction potential indicators; 2) Develops efficient field procedures for measurement of seismic and other geophysical parameters; 3) Develop geophysical data processing interpretation and visualization procedures for 2-D and 3-D data sets; and 4) Use national geotechnical and other well-documented test sites during procedure developments and for validation.

12 ACKNOWLEDGEMENT

The author is indebted to Julia C. Baker for her formatting, editorial, and typing skills which were so capably used in the assembly of this paper.

13 REFERENCES

1 Badiey, M., and Yamamoto, T. (1985). "Inversion of normal incidence seismograms," *Geophysics*, 47, 757-770.

2 Biot, M.A. (1941). "General theory of three-dimensional consolidation," *J. Appl. Phy.* 12, 155-164.

3 ___(1956a). "Theory of propagation of elastic waves in a fluid-saturated porous solid, part 1: Low-frequency range," *J. Acoust. Soc. Am.*, 28, 168-178.

4 ___(1956b). "Theory of propagation of elastic waves in a fluid-saturated porous solid, Part II: Higher frequency range," *J. Acoust. Soc.* Am., 28, 179-191.

5 ___(1956c). "General solutions of the equations of elasticity and consolidation for a porous material," *J. Appl. Mech.*, 78, 91-96.

6 ___(1962a). "Mechanics of deformation and acoustic propagation in porous media," *J. Appl Phy.*, 33, 1482-1498.

7 ___(1962b). "Generalized theory of acoustic propagation in porous dissipative media," *J. Acoust. Soc.* Am., 34, 1254-1264.

8 Burridge, R., and Keller, J.B. (I 98 1). "Poroelasticity equations derived from microstructure," *J. Acoust. Soc.* Am., 70, 1140-1146.

9 Dai, N., Vafidis, A., and Kanasewich, E.R. (1995). "Wave propagation in heterogeneous, porous media: A velocity-stress, finite difference method," *Geophysics*, 60, 327-340.

10 Dvorkin, J., and Nur, A. (1993). "Dynamic poroelasticity: A unified model with the squirt and the Biot mechanism," *Geophysics,* 58, 524-533.

11 Dvorkin, J., Mavko, G., and Nur, A. (1995). "Squirt flow in fully saturated rocks," *Geophysics*, 60, 97-107.

12 Domenico, S.N. (1974). "Effect of water saturation on seismic reflectivity of sand reservoirs encased in shale," *Geophysics,* 39, 759-769.

13 Dutta, N.C., and Ode, H. (1979). "Attenuation and dispersion of compressional waves in fluid-filled porous rocks with partial gas saturation (White model) - Part 1: Biot theory, Part H: Results," *Geophysics,* 44, 1777-1805.

14 Dutta, N.C., and Ode, H. (1983). "Seismic reflection from a gas-water contact," *Geophysics*, 48, 148-162.

15 Frenkel, J. (1944). "On the theory of seismic and seismoelectric phenomena in a moist soil," *J. Phys.*, USSR, 8, 230-241.

16 Gardner, G.H.F., Gardner, L.W., and Gregory, A.R. (1974). "Formation velocity and density: The diagnostic basis for stratigraphic traps," *Geophysics,* 39, 770-780.

17 Gassmann, F. (1951). "Uber die elastizität poröser medien," *Viert. der. Naturf. Gesell. in Zurich*, 96, 1-23.

18 Geertsma, J. (1957). "The effect of fluid pressure decline on volumetric changes of porous rocks," *Trans. AIME,* 210, 331.

19 Geertsma, J., and Smit, D.C. (1961). "Some aspects of elastic wave propagation in fluid-saturated porous solids," *Geophysics,* 26, 169-181.

20 Geli, L., Bard, P.Y., and Schmitt, D.P. (1987). "Seismic wave propagation in a very permeable water-saturated surface layer," *J. Geophys. Res.*, 92, 7931-7944.

21 Hassanzadeh, S. (1991). "Acoustic modeling in fluid-saturated porous media," *Geophysics*, 56, 424-436.

22 Mavko, G., and Nur, A. (1975). "Melt squirt in asthenosphere," *J. Geophys. Res.*, 80, 1444-1448.

23 ___(1979). "Wave attenuation in partially saturated rocks," *Geophysics,* 44, 161-178.

24 Mavko, G., and Jizba, D. (1991). "Estimating grain-scale fluid effects on velocity dispersion in rocks," *Geophysics,* 56, 1940-1949.

25 Murphy, W.F., Winkler, K.W., and Kleinberg, R.L. (1986). "Acoustic relaxation in sedimentary rocks: Dependence on grain contacts and fluid saturation," *Geophysics,* 51, 757-766.

26 Ogushwitz, P.R. (1985). "Applicability of the Biot theory. I. Low-porosity materials," *J. Acoust. Soc.* Am., 77, 429-440.

27 Plona, T.J. (1980). "Observation of a second bulk compressional wave in porous medium at ultrasonic frequencies," *Appl. Phys. Lett.*, 36, 259-261.

28 Rasolofosaon, P.N.L. (1987). "New experimental evidence of the influence of permeability on acoustic wave propagation: Attenuation of ultrasonic guided waves in rock plates," 57th Ann. Inter. Mtg. , *Soc. Expl Geophys. Extended Abstracts,* 670-673.

29 Rechtien, R.D. (1996). "In situ seismic investigation of liquefaction potential of soils," USAE Waterways Experiment Station Contract Report GL 96-1.

30 Rosenbaum, J.H. (1974). "Synthetic microseismograms: Logging in porous formations," *Geophysics,* 39, 14-32.

31 Schmitt, D.P., Bouchon, M., and Bonnet, G. (1988). "Full-wave synthetic logs in radially semi-infinite saturated porous media," *Geophysics*, 53, 807-823.

32 Stoll, R.D. (1974). "Acoustic waves in saturated sediments," *Physics of sound in marine sediments*, L. Hampton Ed., Plenum Press.

33 ___(1977). "Acoustic waves in ocean sediments," *Geophysics,* 42, 715-725.

34 ___(1980). "Theoretical aspects of sound transmission in sediments," *J. Acoust. Soc. Am.*, 68, 1341-1350.

35 ___ (1985). "Marine sediments acoustics," *J. Acoust. Soc. Am.*, 77, 1789-1799.

36 Stoll, R.D., and Bryan, G.M. (1970). "Wave attenuation in saturated sediments," *J. Acoust Soc. Am.*, 47, 1440-1447.

37 Stoll, R.D., and Kan, T.-K. (1981). "Reflection of acoustic waves at a water-sediment interface," *J. Acoust. Soc. Am.*, 70, 149-156.

38 Turgut, A. , and Yamamoto, T. (1988). "Synthetic seismograms for marine sediments and determinations of porosity and permeability," *Geophysics,* 53, 1056-1067.

39 Wang, Z., and Nur, A. (1990). "Dispersion analysis of acoustic velocities in rocks," *J. Acoustic. Soc. Am.*, 87, 2384-2395.

40 Winkler, K.W., Plona, T.J., Froelich, B., and Liu, H.-L. (1987). "Borehole Stoneley waves and permeability: Laboratory results," 57th Ann. Inter. Mtg., Soc. Expl. Geophys., Expanded Abstracts, 12-13.

41 Yamamoto, T. (1983). "Acoustic propagation in the ocean with a poroelastic bottom," *J. Acoust. Soc. Am.*, 73, 1587-1596.

42 Yamamoto, T., and Turgut, A. (1988). "Acoustic wave propagation through porous media with arbitrary pore size distributions," *J. Acoust. Soc, Am.*, 83, 1744-1751.

43 Yamamoto, T., Trevorrow, M., Badiey, M., and Turgut, A. (1989). "Seabed porosity and shear modulus inversion using surface gravity (water) wave-induced seabed motion," *Geophys. J. Int.,* 98, 173-182.

44 Yamamoto, T., Nye, T., and Kuru, M. (1994). "Porosity, permeability, shear strength: Crosswell tomography below an iron foundry," *Geophysics* 59, 1530-1541.

45 Yamamoto, T., Nye, T., and Kuru, M. (1995), "Imaging the permeability structure of a limestone aquifer by crosswell acoustic tomography," *Geophysics,* 60, 1634-1645.

46 Zhu, X., and McMechan, G.A. (1991). "Finite difference modeling of the seismic response of fluid-saturated, porous, elastic media using Biot theory," *Geophysics*, 56, 328-339.

47 Zienkiewicz, O.C., and Shiomo, T. (1984). "Dynamic behavior of saturated porous media: the generalized Biot formulation and its numerical solution," *Int. J. Num. Anal. Meth. in Geomech.,* 8, 71-96.

Becker Penetration Testing of Gravelly Soils

by

Joseph P. Koester*

ABSTRACT

In situ material properties of soils containing gravels and cobbles, including inference of liquefaction resistance and residual strength, are currently estimated by converting Becker Hammer Penetration Test (BPT) blowcounts to equivalent Standard Penetration Test (SPT) blowcounts. BPT/SPT correlations employed to date for Corps projects have considered only combustion conditions within the BPT's diesel pile driver (by means of bounce chamber pressure measurements) in correlations of driving efficiency. BPT efficiency is also strongly influenced by mechanical energy losses, including friction acting along the driven casing. Uncertainties inherent in present BPT/SPT correlations considering only bounce chamber pressure may result in overconservative estimates of cyclic strength (more so with increasing depth). This paper describes the basis, progress, and intentions for an ongoing Civil Works Research and Development project at the US Army Engineer Waterways Experiment Station (WES) to adapt penetration test procedures and results to empirically estimate in situ cyclic and residual strengths of gravelly soils.

* Earthquake Engineering and Geosciences Division
Geotechnical Laboratory, USAE Waterways Experiment Station, Vicksburg, MS 39180

KEYWORDS: Liquefaction, Gravels, Standard Penetration Test, Becker Hammer Penetration Test, Pile Driver Analyzer, In Situ

1 INTRODUCTION

In situ material properties of soils containing gravels and cobbles, including inference of liquefaction resistance and residual strength, are currently estimated by converting Becker Hammer Penetration Test (BPT) blowcounts to equivalent Standard Penetration Test (SPT) blowcounts. BPT/SPT correlations employed to date for Corps projects have considered Becker (diesel) efficiency. Recent studies have concluded from field measurements using Pile Driving Analyzer (PDA) equipment that BPT efficiency is strongly influenced by mechanical energy losses, including friction acting along the driven casing. Uncertainties inherent in present BPT/SPT correlations considering only bounce chamber pressure may result in overconservative estimates of cyclic strength (more so with increasing depth). This study will investigate adaptation of penetration test results to empirically estimate in situ cyclic and residual strengths of gravelly soils.

2 PROBLEM DEFINED

Until relatively recently, coarse-grained soils were considered sufficiently free-draining to preclude development and retention of residual excess pore water pressures during earthquake shaking. The inherently strong frictional nature of granular materials

containing particle sizes larger than sand is the basis for their selection in the construction of earth and rock fill embankments. In addition, the abundance of larger fractions of materials separated during borrow and fill placement makes their use for buttressing impervious compacted zones attractive.

Field observations of soil response during more recent moderate to strong earthquakes have revealed liquefaction and consequent post-earthquake instability in loose to medium dense gravels, both naturally deposited and placed by various artificial processes. Table 1 (Sy, 1996) is a compilation of field occurrence data on liquefaction in gravels during earthquakes worldwide. Most of the observations recorded in the table are from events within the last 20 years; unless the gravels known to have liquefied were at or near the ground surface, there were no investigational tools available prior to the last two decades to confirm or deny the occurrence of liquefaction in gravels in the subsurface.

The Becker Hammer Drill is the tool of choice for in situ investigation of the density and, by inference, strength, of soils containing gravels or cobbles at present. Operation of the Becker Hammer Drill is depicted schematically in Figure 1. Liquefaction resistance and residual strength of gravelly soils are currently estimated by converting Becker Hammer Penetration Test (BPT) blowcounts to equivalent Standard Penetration Test (SPT) blowcounts. BPT/SPT correlations employed to date for Corps of Engineers projects have considered deposit behavior to be largely a function of the operating efficiency of the Becker Hammer drill's double-acting diesel pile driver. Operating efficiency has been judged from measurements of the pressure acting within the bounce chamber of the pile driver apparatus, in the manner described by Harder and Seed (1986) and Harder (1988).

Recent studies have concluded from field measurements using Pile Driving Analyzer (PDA) equipment that BPT efficiency is also strongly influenced by mechanical energy losses, including friction acting along the driven casing (Sy, 1993, Sy and Campanella, 1993 and Sy and Campanella, 1994). Uncertainties inherent in present BPT/SPT correlations considering only bounce chamber pressure may result in overconservative estimates of cyclic strength (more so with increasing depth). Selection of engineering properties inferred from BPT results is also an uncertain science in remediated soils, due to the altered lateral stress conditions in these deposits. Improved correlative techniques are urgently needed to interpret the results of the BPT for a variety of situations where post-earthquake stability is of concern.

3 OBJECTIVES

The objectives of this study are: to develop and validate procedures to properly adapt penetration test results to estimate in situ cyclic and residual strengths of soils empirically, and to evaluate the adaptation of alternate in situ testing technologies for measuring in situ parameters needed for analysis, such as density or void ratio, to characterize dynamic strength.

4 RESEARCH APPROACH

The initial portion of the study, and an ongoing process throughout the course of

the investigations, involves evaluation of prior research by others on penetration testing in coarse-grained soils. One intention of literature review is to determine gradational constraints, e.g., limiting gravel content, on direct comparison of SPT and BPT results at field sites where such comparison is possible. It is imperative to determine whether the use of the two different tests as an index of soil strength results in the same conclusions for each in a given soil type. If suitable field experiment arrangements can be made, direct SPT/BPT comparison tests on deposits of known gradation and density will be attempted.

Adaptation of BPT test results to take advantage of the large data base on SPT correlations is not a straightforward conversion based on only the "footprint", or projected area, of the penetrator. The differences in test procedure are significant, as are the effects of the test environment on penetration resistance. The SPT is, by widely practiced standard procedure, performed in a fluid-filled borehole that has a larger diameter than the penetrator (a split-spoon sampler) above the depth of the test. This has the effect of minimizing borehole friction in strata already traversed, such that the strength being assessed is nearly restricted to the current position of the sampler. On the other hand, the driven casing used in a BPT has typically been lengthened during driving by adding sections of pipe having the same diameter as the leading end, which is itself plugged.

Dr. Alex Sy, Klohn-Crippen Consultants, Ltd., of Vancouver, British Columbia, has extensively studied dynamic energy measurements on the BPT, to the end that he promotes the routine use of the Pile Driving Analyzer (PDA, developed and marketed by Goble, Rausche, Likins and Associates, or GRL) and its associated interpretation software for the assessment of driving efficiency. The PDA was designed to acquire the high speed dynamic stress, strain and acceleration data necessary for the measurement of pile capacity during commercial pile installation. Dr. Sy contends that combustion efficiency as determined by bounce chamber pressure measurements is not as effective in normalizing BPT results obtained using different equipment as is direct measurement of energy transferred from the hammer to the driven casing by means of the PDA.

Dr. Sy has also studied the effects of casing friction on BPT results and their interpretation for liquefaction potential assessment. Current practice, based on bounce chamber pressure correlations, may lead the engineer to severely overestimate in situ cyclic strength when casing friction dominates the penetration resistance of the BPT, according to Dr. Sy. Conversely, when casing friction is very low, as in loose cohesionless soils near the ground surface, he contends that BPT results will be overconservatively interpreted.

PDA measurements, when used to analytically model the soil profile through which a BPT is performed, may be used to estimate the total friction acting along the casing. The computer code CAPWAP, developed by GRL to estimate pile capacity from PDA measurements, has been adapted to permit estimation of the portion of driving resistance due to static shaft friction acting on the Becker Hammer drill casing. The approach is detailed by Sy (1993). This technique requires careful attention to the

selection of soil modeling parameters by experienced personnel and is labor intensive. Dr. Sy recommends running CAPWAP at a few depths along a BPT profile and interpolation of casing friction between the modeled points. CAPWAP friction estimation is imprecise and expensive, and is not widely practiced at present. Typical BPT results are profiled in Figure 2 to illustrate the process described by Sy (1993). Harder (1996) compares and contrasts the two prevalent schools of thought with regard to BPT data interpretation.

Another method proposed for accounting for casing friction involves the lubrication of the casing, by means of injection of a thin-mixed drilling mud into the annular space outside of the drill casing (Wightman, Yan, and Diggle, 1993, and Sy and Lum, 1995). The injection ports for what is now known as the Foundex™ BPT, represented as FBPT in accompanying figures, are located just behind the terminal end of the drill casing to which the plugged crowd-out bit is attached. The terminal section of drill casing is selected to have a slightly larger diameter that the driving casing. Altering the conventional field procedure by the FBPT means is attractive in that friction is directly and drastically reduced, as illustrated by the data plotted in Figure 3, and no complicated computational schemes are required to interpret the test results. It may also be argued that SPT/BPT correlation is improved by lubricating the apparatus during tests. Test result interpretation has proven difficult in a few cases where soil deposits being penetrated are very free draining, and where casing friction is mainly developed at discrete points by large cobbles or boulders.

The most recent studies available, unpublished to date, involve the use of load cells and lifting jacks to measure the force required to pull the drill casing upward a small distance at any point during a BPT. The most convenient opportunity to make pullout force measurements is at the time of each addition of casing sections. Preliminary results of pullout tests on BPT's have revealed close correlation to properly modeled casing friction from CAPWAP analysis. Results from two sites in close proximity to one another, obtained from lubricated and unlubricated BPT's, are shown in Figure 4 to compare measured and modeled friction (Sy, 1996, personal communication). The direct measurement of pullout frictional resistance offers the obvious advantage that complex, expensive modeling needs are drastically reduced or, eventually, eliminated. In addition, users inherently trust direct measurements over "black-box" computer models.

Field experimentation is being planned to include SPT and BPT using dynamic energy input measurements. Field tests will be made to compare modeled and direct measured casing friction to evaluate the theoretical corrections proposed by Sy. Cooperative study with the US Bureau of Reclamation, at a controlled fill test site, is an attractive, cost effective possibility and is being pursued.

The WES Soils Research Facility has developed a large (1.5 m diameter) penetration test chamber that will be used to investigate the influence of several variables on penetration resistance. Boundary effects constrain the use of this chamber to reduced-scale simulation of the BPT, but the device has the potential to provide meaningful data

to relate gradational and frictional effects. A laboratory test program has yet to be fully planned.

5 ACCOMPLISHMENTS

This was a new research start in 1995, augmented with separate reimbursable work for the US Army Engineer District, Sacramento (CESPK) that provided a substantial data base of BPT records obtained along with direct energy measurements at California dams. An extensive program of BPT/PDA exploration were conducted at one earth and rock fill dam; reports on the field work and initial interpretation of results have been prepared for use by CESPK. The collaborative efforts with CESPK during 1995-1996 include crosshole seismic tests, as well as confirmatory SPT's in foundation alluvium at one dam.

A workshop on Becker Hammer procedures and interpretation attended by government and industry users was held in Boulder, Colorado, in June 1995. The BPT has seen widespread use since the workshop, and a network was established to track progress and findings among the participants. Dr. Sy visited WES this summer, and provided valuable current industry data on energy methods and pullout friction measurements. Dr. Sy's data base includes BPT results that have been collected from ongoing field testing at several US and Canadian sites.

6 RESULTS AND PRODUCTS EXPECTED

This research will produce the following products that are of immediate value to users of the Becker Hammer test:

- Quantification of casing friction and equipment variability effects
- Guidelines for performance of BPT's in gravels
- Procedures for evaluating BPT results, with particular application to liquefaction potential evaluation in situ, and ultimately,
- New procedures for measurement of density and void ratio in gravel deposits.

The likely benefits of performing this study include reduced uncertainty, reduced costs of remediation on projects where earthquake-induced strength loss is indicated, and improved techniques for in situ determination of valuable engineering parameters.

7. REFERENCES

Coulter, H.W. and Migliaccio, R.R. 1966. "Effect of the earthquake of March 27, 1964 at Valdez, Alaska, U.S. Geological Survey Professional Paper 542-C.

Harder, L.F. 1988. "Use of penetration tests to determine the liquefaction potential of soils during earthquake shaking," PhD Thesis, University of California, Berkeley, CA.

Harder, L.F. 1996. "Application of the Becker Penetration Test for evaluation of the liquefaction potential of gravelly soils," *Proceedings, National Center for Earthquake Engineering Research (NCEER) Workshop on Evaluation of Liquefaction Resistance,* Salt Lake City, UT, 4-5 January, Draft in process.

Harder, L.F. and Seed, H.B. 1986. "Determination of penetration resistance for coarse-grained soils using the Becker

hammer drill," Report No. UCB/EERC-86/06, University of California, Berkeley, CA.

Ishihara, K. 1985. "Stability of natural slopes during earthquakes," *Proceedings, 11th International Conference on Soil Mechanics and Foundation Engineering,* San Francisco, CA, Vol. 1, 321-376.

Kokusho, T., Tanaka, Y., Kudo, K. And Kawai, T. 1995. "Liquefaction case study of volcanic gravel layer during 1993 Hokkaido-Nansei-Oki earthquake," *Proceedings, 3rd International Conference on Recent Advances in Geotechnical Earthquake Engineering and Soil Dynamics,* St. Louis, MO, 235-242.

Maurenbrecher, P.M., Den Outer, A. And Luger, H.J. 1995. "Review of geotechnical investigations resulting from the Roermond April 13, 1992 earthquake," *Proceedings, 3rd International Conference on Recent Advances in Geotechnical Earthquake Engineering and Soil Dynamics,* St. Louis, MO, 645-652.

Sy, A. 1993. "Energy measurements and correlations of the Standard Penetration Test (SPT) and the Becker Penetration Test (BPT)," PhD Thesis, Department of Civil Engineering, University of British Columbia, Vancouver, BC.

Sy, A., and Campanella, R.G. 1993. "Dynamic performance of the Becker Hammer drill and penetration test," *Canadian Geotechnical Journal*, 30(4): 607-619.

Sy, A., and Campanella, R.G. 1994. "Becker and standard penetration tests (BPT-SPT) correlations with consideration of casing friction," *Canadian Geotechnical Journal*, 31(3): 343-356.

Sy, A., and Lum, K.K.Y., 1995. "Correlations of mud-injection Becker and standard penetration tests," *Proceedings, preprint, 48th Canadian Geotechnical Conference,* Vancouver, B.C., 25-27 September.

Tokimatsu, K. And Yoshimi, Y. 1983. "Empirical correlation of soil liquefaction based on SPT N-value and fines content," *Soils and Foundations*, 23(4): 56-74.

Wang, W.S. 1984. "Earthquake damages to earth dams and levees in relation to soil liquefaction and weakness in soft clays," *Proceedings of the International Conference on Case Histories in Geotechnical Engineering,* St. Louis, MO, Vol. 1, 511-521.

Wightman, A., Yan, L., and Diggle, D.A. 1993. "Improvements to the Becker penetration test for estimation of SPT resistance in gravelly soils," *Proceedings of the 46th Canadian Geotechnical Conference,* Saskatoon, Sask., 27-29 September, pp. 379-388.

Yegian, M.K., Ghahraman, V.G. and Harutiunyan, R.N. 1994. "Liquefaction and embankment failure case histories, 1988 Armenian earthquake," *Journal of Geotechnical Engineering,* ASCE, 120(3): 581-596.

Youd, T.L. , Harp, E.L., Keefer, D.K. and Wilson, R.C. 1985. "The Borah Peak, Idaho earthquake of October 28, 1983 -

liquefaction," *Earthquake Spectra*, EERI,
2(1): 71-89.

TABLE 1. OBSERVED LIQUEFACTION IN GRAVELLY SOILS

YEAR	M	EARTHQUAKE	REFERENCE
1981	7.9	Mino-Owari, Japan	Tokimatsu and Yoshimi (1983)
1943	7.3	Fukui, Japan	Ishihara (1985)
1964	9.2	Valdez, Alaska	Coulter and Migliaccio (1966)
1975	7.3	Haicheng, PRC	Wang (1984)
1976	7.8	Tangshan, PRC	Wang (1984)
1978	7.4	Miyagiken-Oki, Japan	Tokimatsu and Yoshimi (1983)
1983	7.3	Borah Peak, Idaho	Youd, et al. (1985), Harder (1988)
1988	6.8	Armenia	Yegian, et al. (1994)
1992	5.8	Roermond, Netherlands	Maurenbrecher, et al. (1995)
1993	7.8	Hokkaido, Japan	Kokusho, et al. (1995)
1995	6.8	Kobe, Japan	Kokusho (1995)

adapted from Alex Sy, Klohn-Crippen Consultants, Ltd, Richmond, BC, Canada

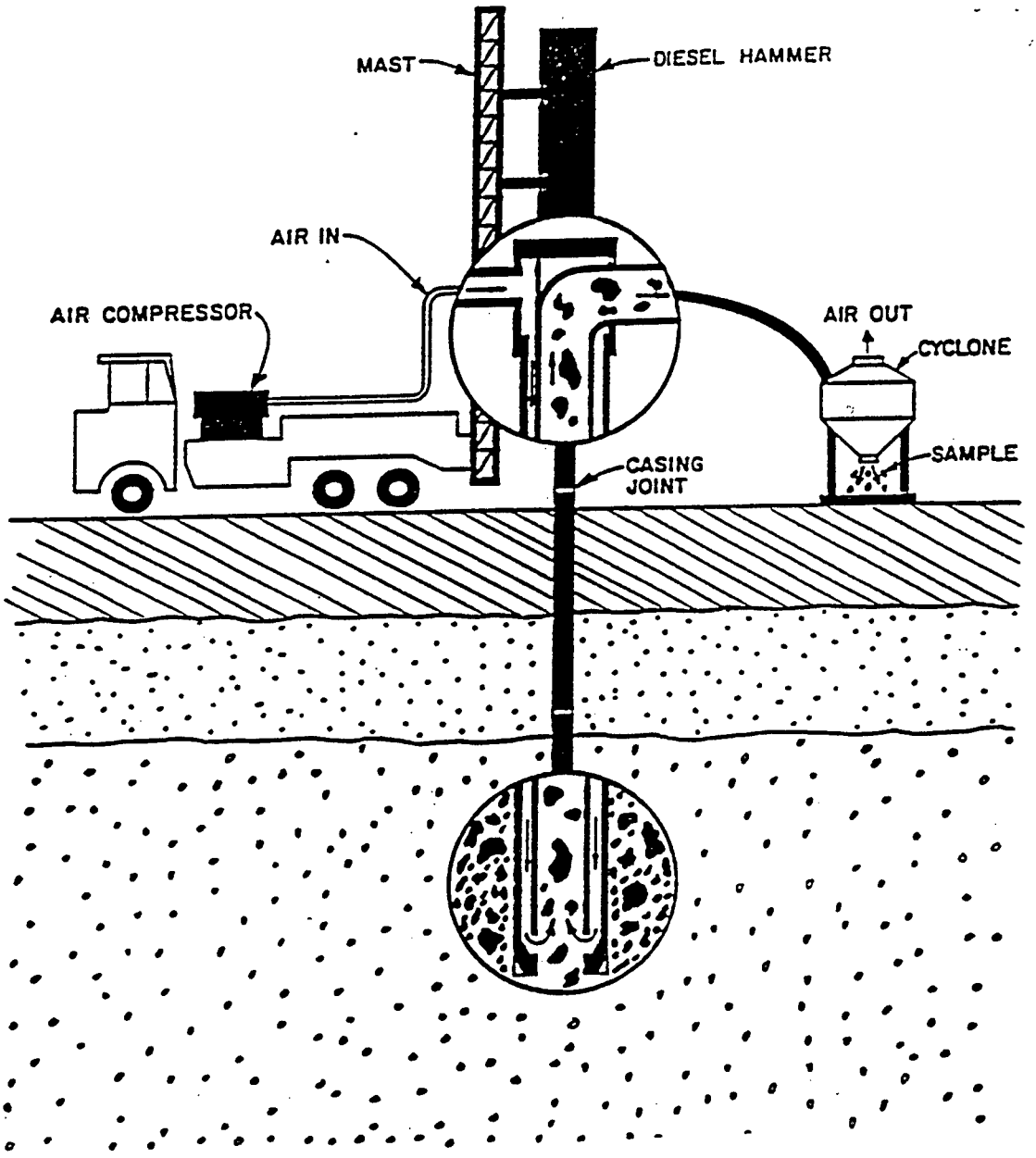

Figure 1. Schematic of Becker Hammer Drill operation
(Harder, 1988)

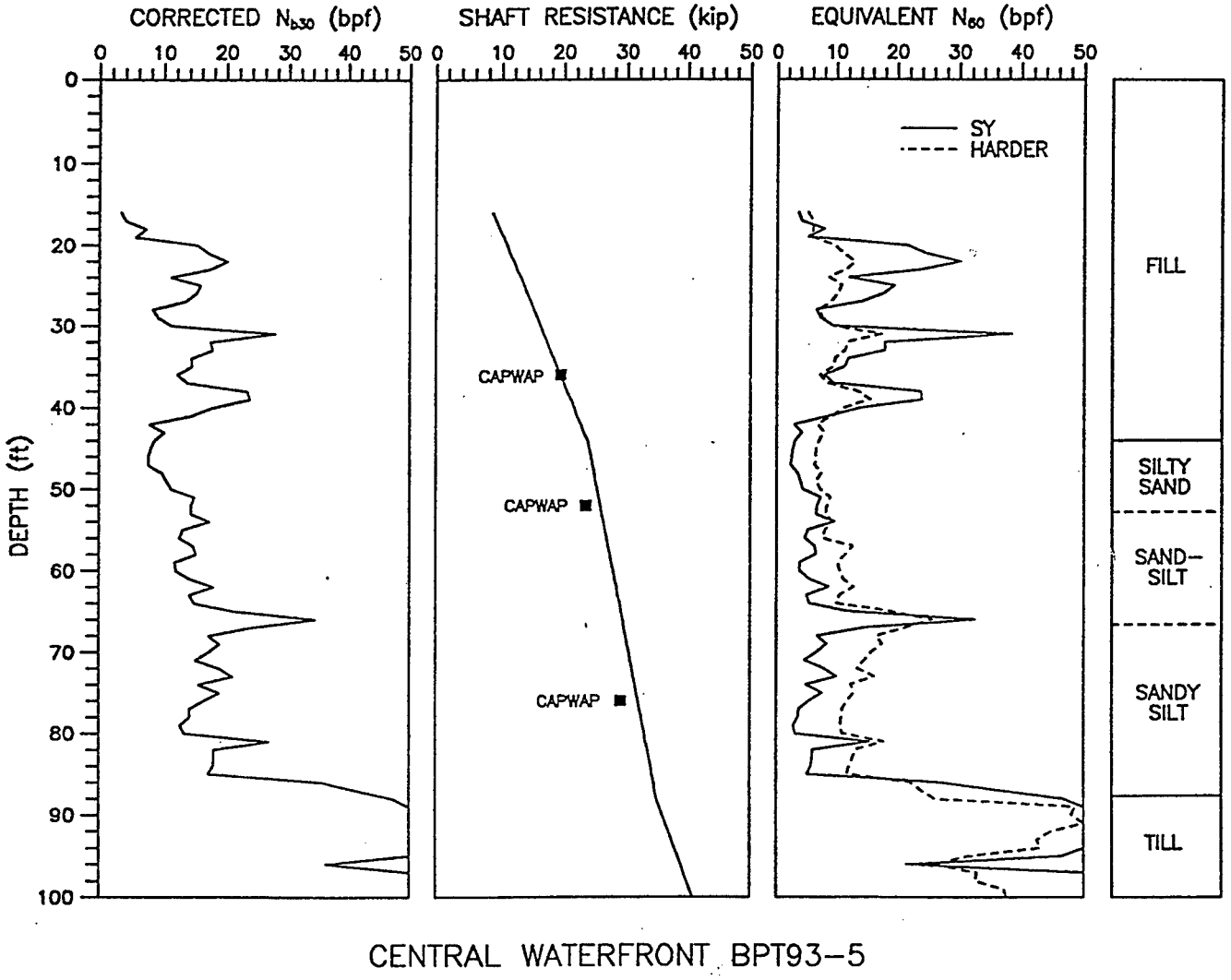

Figure 2. Typical BPT results adjusted for driving energy (N_{b30}) and shaft resistance, as modeled using CAPWAP; comparison of Harder and Sy interpretations (Sy, personal communication, 1996)

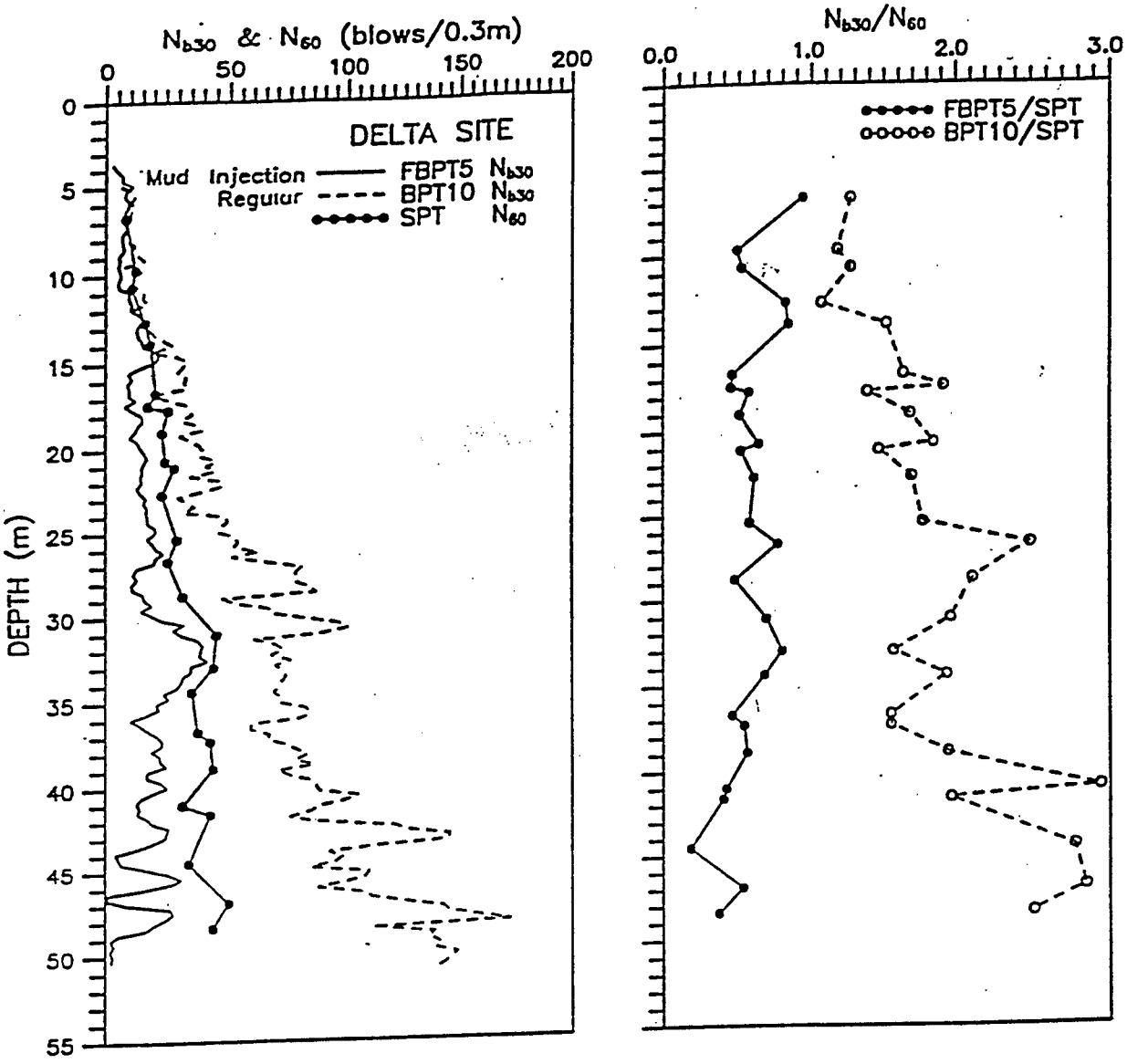

Figure 3. Influence of mud-injection lubrication on BPT results on energy-corrected penetration resistance. Results are compared to SPT results at this sand site. (Harder, 1996, after Sy and Campanella, 1994)

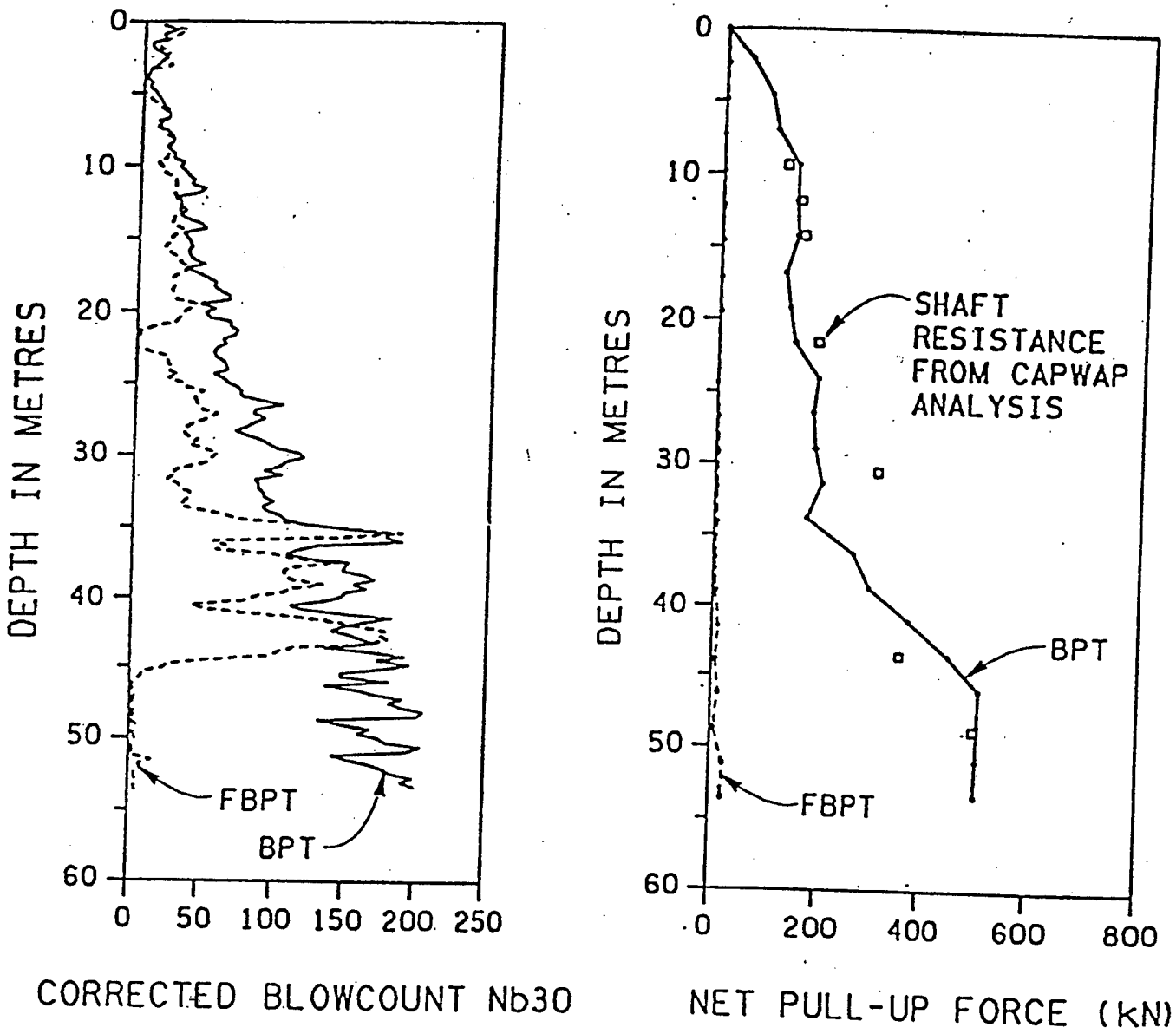

Figure 4. Comparison of measured (from pull-up tests) BPT shaft friction with friction estimated using the CAPWAP computer code. Lubrication effect is also illustrated for this high-friction, sand site (Sy, personal communication, 1996)

Safety Estimation of Rockfill Dams During Major Earthquakes

Tadahiko SAKAMOTO[1], Tadahiko FUJISAWA[2], Akira NAKAMURA[3], Hitoshi YOSHIDA[4] and Tomoya IWASHITA[5]

ABSTRACT

The Hyogoken-Nambu Earthquake (M. 7.2) caused no major damage to dams that affected their safety. Other infrastructures, however, were badly damaged. We therefore evaluated the seismic capacity of rockfill dams designed by the current design method.

We estimated that the maximum horizontal acceleration at dam site rocks near the earthquake source fault was about 220 gal from the attenuation of maximum accelerations observed at dam foundations during the quake. We conducted a dynamic analysis of Minoogawa Dam located near the aftershock distribution zone (earthquake source fault) using the observed acceleration records. We then assessed the accuracy of the dynamic analysis method. Finally, we made dynamic analyses and stability analyses of the rockfill dam models using the current design method. This showed that the dam body of rockfill dams constructed by the current design method would have an enough resistant to sliding even if the input earthquake motion was a little stronger than that which occurred near the source fault of the Hyogoken-Nambu Earthquake.

Key Words : *rockfill dam, seismic design, earthquake motion, dynamic analysis, Hyogoken-Nambu Earthquake*

1. INTRODUCTION

Many infrastructures and buildings were damaged by the Hyogoken-Nambu Earthquake of magnitude 7.2, which occurred on January 17, 1995. In the case of dams, special safety inspections were carried out by site offices within the river reaches administered under the River Act immediately after the earthquake at a total of 251 dams. Later, engineers of the Public Works Research Institute, Ministry of Construction conducted detailed on-site investigations, mainly at the dams which suffered minor damage.

The results confirmed that all the dams generally behaved well and did not require protective countermeasures. However, some slight damage, such as minor cracks in the crest paving, was found at a few dams. The amount of drainage water increased slightly after the earthquake at eight dams, but the total amount was small and either fell or stabilized later (Matsumoto et al., 1996).

In this paper, we reevaluated the seismic capacity of rockfill dams constructed by the current design criteria, in the light of the serious damage of other infrastructures and buildings. We estimated the characteristics and strength of the earthquake

1) Director General, Public Works Research Institute, Ministry of Construction
Tsukuba Science City, 305 Japan
2) Director of Dam Department, ditto
3) Former Head of Fill Dam Division, ditto
4) Head of Fill Dam Division, ditto
5) Research Engineer, Fill Dam Division, ditto

motion near the earthquake source fault from the records of accelerations observed at the foundation of dams. We conducted the dynamic analysis of Minoogawa Dam, with a height of 47 m and located near the earthquake source fault, using the acceleration records observed at the dam to confirm the accuracy of the analysis. We then evaluated the stability for sliding of rockfill dams against input earthquake motions of slightly greater magnitude near this earthquake source fault by dynamic analyses of model dams.

2. EARTHQUAKE MOTIONS AT DAM FOUNDATIONS DURING HYOGOKEN-NAMBU EARTHQUAKE

(1) Peak Acceleration

Figures 1 and 2 show the distributions of the horizontal peak (either of the peak accelerations in the direction of the stream or of the dam axis, whichever is greater) and vertical peak accelerations, respectively, observed at the foundation of dams during the Hyogoken-Nambu Earthquake. These values include the values obtained at the gallery under embankment dams or at the lowest gallery in concrete dams.

The attenuation of the horizontal peak accelerations observed at the dam foundations during the earthquake with epicentral distance is shown in Figure 3, and that of the vertical peak accelerations in Figure 4. These figures also show peak accelerations measured on soil sites (Committee for Investigation on the Damage of Highway Bridges Caused by the Hyogoken-Nambu Earthquake, 1995). The figures indicate that peak accelerations at the dam sites were substantially smaller than those at the soil sites for the same epicentral distance. It can be seen that the earthquake motion at the foundation of a structure constructed on a hard rock site, such as a dam, is considerably smaller than that on a soil site consisting of alluvial or diluvial deposits.

The attenuation of horizontal peak accelerations at dam sites with distance from the earthquake source faults is shown in Figure 5, and that of vertical peak accelerations in Figure 6. Here, the earthquake source faults, which indicate the Nojima Fault on Awaji Island and the center line of distribution of aftershocks occurring on the day of the main shock in Kobe, are shown in Figure 7. The dam's distance from the earthquake source fault indicates the shortest distance from the fault to each dam site. Hitokura Dam, at which a horizontal peak acceleration of 183 gal was recorded during the earthquake, is located about 10 km from the fault. An acceleration record at a rock site besides dam sites was observed at a point 15 m underground which is located 10 km from the fault. The horizontal peak acceleration (component in the EW direction) was 213 gal (Izawa et al., 1995). The elastic wave (P wave) velocity at the point is 2.67 km/s, which is almost equal to those at dam sites. The earthquake motion on a rock site was assessed from the acceleration records shown in Figure 5 and those observed in rock sites close to the earthquake source fault. As a result, it was estimated that the maximum horizontal acceleration in a hard rock site, on which a dam could be constructed, caused by this earthquake was about 220 gal (Committee on Evaluation of Earthquake Resistance of Dams, 1995).

Figure 8 shows the ratio of the vertical peak acceleration to horizontal peak acceleration at dam foundations, which ranges from 1/3 to 1/1. As the peak acceleration rises, the ratio tends to decrease.

(2) Acceleration Response Spectrum

Figure 9 shows the response spectra of the acceleration in the stream direction observed at the foundations of 25 dams during the Hyogoken-Nambu Earthquake at a damping ratio of 10%. The spectra are normalized so that the peak

accelerations are the unit. The average value of the response spectra for a natural period ranging from 0.1 to 0.6 seconds is about 2. The response spectra decrease rapidly at natural periods above 0.6 seconds.

(3) Natural Period of Rockfill Dams

Using the acceleration waves observed at eight rockfill dams, we calculated the ratios of Fourier spectrum at the crest to that at the foundation, which is a frequency response function. We then obtained the fundamental natural period of dam bodies from the predominant frequency of the frequency response function. Figure 10 shows the relationship between fundamental natural period T [sec] and height of dams H [m]. The relationship is nearly linear and within the empirical equation (1) (Okamoto, 1984) , shown in Figure 10, from the earthquake observations and vibration tests.

$$T_{[sec]} = (0.35 \sim 0.65) \times \frac{H_{[m]}}{100} \qquad (1)$$

3. EVALUATION OF SEISMIC CAPACITY OF ROCKFILL DAMS

(1) Seismic Design of Dams in Japan

The structural safety design of dams has been prescribed by the provisions of the "Cabinet Order Concerning Structural Standards for River Administration Facilities, etc." and the "Regulation for Enforcement of Cabinet Order Concerning Structural Standards for River Administration Facilities, etc." These stipulate that the seismic design of dams should be based on the seismic coefficient method.

The concept of seismic design of dams based on the seismic coefficient method was proposed by Dr. Nagaho Mononobe in 1925 in the aftermath of the Great Kanto Earthquake of 1923. Komaki Dam (concrete gravity dam), which was constructed in 1930, was the first dam designed by the seismic coefficient method. The seismic design method was put in a statutory form by the publication of the "Design Criteria for Dams" established by the Japanese National Committee on Large Dams in 1953. Later in 1971, the criteria were partly revised by the publication of the "Design Criteria for Dams (Revised)". In 1976, the Ministry of Construction enacted the "Regulation for Enforcement of Cabinet Order Concerning Structural Standards for River Administration Facilities, etc." as the legally binding design standards for dams. In 1981, the design seismic coefficient was reviewed by the publication of the "Regulation for Enforcement of Cabinet Order Concerning Structural Standards for River Administration Facilities, etc. (Revised)", which has up to the present been in force.

In the "seismic coefficient method," the effect of the inertia force that is produced by the dam body vibration is evaluated as a static horizontal force in proportion to the weight of each section of the dam body. The proportional coefficient is called the design seismic coefficient. The lowest value of the coefficient for rockfill dams is 0.10 to 0.15 in accordance with seismic activity specified in the "Regulation for Enforcement of Cabinet Order Concerning Structural Standards for River Administration Facilities, etc." This stipulates that based on the seismic coefficient method, the safety of a rockfill dam should be secured by ensuring that the safety factor for sliding of the dam body is at least 1.2 without considering the cohesion of rockfill and filter materials.

Rockfill dams designed by the seismic coefficient method have not suffered any damage affecting their structural safety from any earthquakes in the past, including the Hyogoken-Nambu Earthquake. Rockfill dams designed by the seismic coefficient method are thus judged to have a high seismic capacity.

(2) Dynamic Analysis of Minoogawa Dam

Minoogawa Dam is the dam which showed the greatest earthquake acceleration record of all embankment dams during the Hyogoken-Nambu Earthquake. We analyzed the model of the dam using the acceleration records observed at the dam to confirm the accuracy of using dynamic analysis to estimate the seismic capacity of rockfill dams.

a) Profile of Minoogawa Dam

Minoogawa Dam was completed in 1982. It is a 47.0 m-high zoned rockfill dam with a central earth core. The foundation rock of the dam is composed of sandstone and slate of the Tamba group in the Paleozoic or Mesozoic era and is hard, with its P wave velocity, Vp, exceeding 4 km/s approximately. This dam was designed by the seismic coefficient method, and its design seismic coefficient was 0.15. Figure 11 shows its standard cross section.

This dam is located 48 km from the epicenter and 11 km northeast of the east end of the aftershock zone. Seismometers are installed at the foundation (gallery) and the crest, as shown in Figure 11. During the Hyogoken-Nambu Earthquake they recorded acceleration waves with peaks of about 130 gal in the stream and dam axis directions at the foundation, and a peak of about 240 gal in the stream direction and a peak of about 400 gal in the dam axis direction at the crest. The quake caused no major damage. Minor transverse cracks occurred on the crest pavement and the checkpoints on the crest sank only 11 mm at the maximum in comparison with measurements three weeks before the quake.

b) Analysis method and conditions (for details, refer to the paper by Nakamura and Iwashita in 1996)

Dynamic analysis was adopted for the complex response analysis by the equivalent linear method. We set the density of each zone of the dam body based on the results of the control tests conducted during the banking of the dam, as shown in Table 1. The initial shear modulus *Go*, with average effective principal stress were set as shown in Figure 12. The shear strain dependency of the shear modulus ratio *G/Go*, and hysteresis damping ratio h_h were set as shown in Figure 5. Those of the rock materials were obtained from large-scale cyclic triaxial tests. The *Go*, *G/Go* and h_h of filter materials were set the same as those of inner rockfill materials (Rock Ⅱ). We used the test results for the core materials of another rockfill dam as the *Go*, *G/Go* and h_h of the core material. We set the Poisson's ratio using the empirical expression (Sawada et al., 1975) based on measurements of rockfill dams. As the input earthquake waves, we used the acceleration wave, shown in Figure 14, observed at the gallery of Minoogawa Dam during the Hyogoken-Nambu Earthquake.

To take into consideration energy losses because of internal viscous damping, uneven input waves at the dam foundation, dynamic interaction between the dam body, foundation and reservoir and so on, an equivalent damping for these effects must be added to the hysteresis damping ratio h_h of the dam body material. We conducted dynamic analyses for two cases where equivalent damping ratio of 15% and 10% was added to hysteresis damping ratio h_h.

c) Results of dynamic analysis

We compared the analyses and the observation of the time histories (shown in Figure 15) and the Fourier amplitude spectra (shown in Figure 16) of the response acceleration at the crest. In Figure 15, the analysis response wave of the stream direction component agrees well with the observation in the first half of the principal motion (t = 4 to 5.5 sec). The amplitude of the analysis response wave becomes smaller than that of the observation in the second half of the principal motion. The amplitude of the analysis response wave of the vertical direction component is smaller

overall than that of the observation. In Figure 16, the Fourier spectra of the analysis in the stream direction component are almost equal to that of the observation at frequencies up to 1.2 Hz. The spectrum of the analysis is larger than that of the observation at frequencies of 1.2 to 2 Hz and is smaller above 2 Hz. The Fourier spectra of the analysis in the vertical direction component are smaller than that of the observation above 3 Hz, whereas both of the spectra are almost equal up to about 3 Hz. The disagreements between the analysis and observation are largely caused by three-dimensional factors such as input waves of other directions and the topography of the dam site. The observed accelerations in the stream direction are considerably larger in the second half of the principal earthquake motion, which agrees with the time zone when the acceleration in the dam axis direction at the crest exceeded 300 gal. This indicates the great effect of three-dimensional vibration.

The comparison of both the cases of adding a damping ratio of 10 and 15% to the hysteresis damping ratio h_h in Figures 15 and 16 showed that the analysis result in the case of adding 15% agrees better with the observation, accurately reproducing the behavior of the dam during the earthquake.

(3) Seismic Capacity of Rockfill Dams Close to Source Fault of Hyogoken-Nambu Earthquake

a) Input earthquake wave

As noted in section 2, the maximum horizontal peak acceleration at the rock foundation of dams during the Hyogoken-Nambu Earthquake is estimated to have been about 220 gal. Input waves with a horizontal maximum acceleration of 250 gal were, therefore, used in the dynamic analysis to provide an adequate margin of safety. These waves can be considered to be greater than the amplitude of earthquake motions close to the source fault of the Hyogoken-Nambu Earthquake.

We selected as the input earthquake waves four acceleration records (ACC-1 to ACC-4) observed at the dam foundations near the epicenter, changing the level of the accelerations the peaks of which were raised to 250 gal. Our selection took account of the fact that the proportion of rise in the amplitude should be as small as possible and that the selected acceleration waves should have various frequency properties. The vertical acceleration levels were to be changed in the same proportion as their corresponding horizontal ones. Here, we used the input waves without modification of their frequency characteristics and the duration of the observations. Figure 17 shows the acceleration response spectra of the four selected input earthquake waves with a damping ratio of 10%.

b) Modeling and condition of analysis

We prepared dam models to evaluate the seismic capacity of rockfill dams with reference to Shichigashuku Dam (completion in 1991, height of 90 m, design seismic coefficient of 0.15) designed in accordance with the current design method (seismic coefficient method). The finite element mesh of the dam model is shown in Figure 18. The gradient of the upstream slope is 1 : 2.6 and that of the downstream slope is 1 : 2.0. The heights of the dam models to be adopted are 63, 110 and 150 m. The water should be stored up to the water level of 92% as a normal water level.

Direct time integration using the equivalent linear method was used for the dynamic analysis. In the dynamic analysis, the physical properties of the model are assumed to be only rock materials, which account for the greater part of dam bodies. The physical properties of the material for the analysis were set on the basis of the results of the control tests during construction and large-scale triaxial tests for Shichigashuku Dam. We set the wet density at 1880 kg/m^3, saturated density at 2080 kg/m^3 and Poisson's ratio ν at 0.35. The initial shear modulus *Go* (MPa) was set according to the

depth D (m) from the surface of the dam as shown in equation (2) and Figure 19:

$$G_0 = 6.168 \times 10^{-3} \times (2\rho gD/3)^{0.85} \quad (2)$$

where, ρ (kg/m^3) is the density of the dam body, g is the gravity acceleration. Figure 20 shows the curves representing the shear strain dependency of the shear modulus ratio *G/Go* and the hysteresis damping ratio h_h of the rock material. The used damping ratio was obtained by adding 15% to the hysteresis damping ratio of the rock material, based on the comparison study described above for the observed and analytical response of Minoogawa Dam during the Hyogoken-Nambu Earthquake. As the damping matrix for each element, Rayleigh type damping was used considering the dependence on frequency (Iwashita et al., 1995).

Table 2 shows shear strength parameters of the materials for the sliding stability analysis. The shear strength of the rock material was decided from the results of large-scale monotonic loading triaxial tests using the rock materials carried from the quarry sites. We adopted the shear strength τ_f of the coarse grain materials (rock and filter) approximated by the equation (3) as an exponential function. Equation (3) expresses the dependence of internal friction angle ϕ on normal stress σ_n acting on the sliding surface:

$$\tau_f = P_0 \cdot A \times (\sigma n / P_0)^b \quad (3)$$

where, P_0 is 1 MPa. Figure 21 shows the relationship between A and b, which are the parameters of shear strength of rockfill materials filled up in existing and under construction dams. The shear strength parameters input in the stability analyses belong to the shear strength properties of various rockfill materials

We analyzed the stability for sliding of only the upstream slope, because rockfill dams designed by seismic coefficient method usually have greater safety against sliding in the downstream slope than in the upstream slope in reevaluations by modified seismic coefficient method.

c) Peak average acceleration

The seismic inertia force acting on a potential slide mass is expressed by the product of the mass and the acceleration of the slide mass. We evaluated the stability for sliding using "peak average acceleration of slide mass", $a(t)_{max}$. The peak average acceleration of slide mass is the maximum value during the duration in the sliding direction of $a_{ave}(t)$ which is the value of the peak seismic inertia force moment divided by the mass moment of each slide mass by equation (4):

$$a_{ave}(t) = \sum_{i=1}^{N}\left(m_i \times a_{Hi}(t) \times r_{vi}\right) \Big/ \sum_{i=1}^{N}(m_i \times r_{vi}) \quad (4)$$

where, i is the element number, N is the number of elements in the potential slide mass, m_i is the mass of the element i, $a_{Hi}(t)$ is the horizontal response acceleration time series acting on an element i by dynamic analysis and r_{vi} is the vertical height from the center of the slide circle to the center of gravity of element i. In the analyses, the vertical response accelerations $a_{vi}(t)$ were not considered because the effect of $a_{vi}(t)$ on the peak average accelerations of slide mass is about 5% for the these 4 input earthquake motions.

d) Resisting acceleration for sliding

We conducted convergent static stability analyses for the potential circular slide masses as shown in Figure 18. We calculated the accelerations acting on the slide masses (resisting acceleration a_{res}) that would cause the safety factor Fs against sliding to become 1.0 as expressed by equation (5). The resisting acceleration a_{res} is the horizontal acceleration (force) that would cause the potential slide mass to begin to slide.

$$\int_L (\tau_f \times r)dl \Big/ \left(a_{res} \times \sum_{i=1}^{N} m_i \times r_{vi}\right) = Fs = 1.0 \quad (5)$$

Where, τ_f is the shear strength of the dam body materials, r is the radius of the potential slide circle, and L is the length of circular-arc of the slide mass.

e) Evaluation of stability for sliding

Figure 22 show the distribution of peak average accelerations of slide masses with different y/H for three dam-height-models. These figure also show the distribution of resisting accelerations for each potential slide mass a_{res}. Figure 22 show that the peak average accelerations are large values in the upper part of the dam, but the values are within the resisting acceleration in all cases. This indicates that rockfill dams are resistant to sliding. Moreover, the peak average acceleration of slide mass, which represents the maximum value during the duration of an earthquake, does not continue but acts on the dam body only in the peaking instant. Therefore, rockfill dams are actually safer than the results shown in Figure 22.

4. CONCLUSIONS

The Hyogoken-Nambu Earthquake of January 17, 1995, which was an intra-plate earthquake, occurred just below urban areas causing severe damage in Kobe City and on Awaji Island. However, no dam was seriously damaged.

The peak accelerations of earthquake motion observed at rock sites of dams were sufficiently smaller than those on soil sites consisting of alluvial or diluvial deposits. From the attenuation of the peak accelerations observed at dam foundations, we estimated that the maximum horizontal acceleration that would have been caused close to the earthquake source fault was about 220 gal. The construction of dams on hard bed rock sites is considered to be one of the reasons why this earthquake did not inflict major damage on any dam.

We conducted a dynamic FEM analysis of Minoogawa Dam located near the earthquake source fault using the observed acceleration wave. The response acceleration wave of the analysis reproduced the observed wave with good accuracy.

We evaluated the seismic capacity of rockfill dams designed by the current design method based on the seismic coefficient method. We prepared FEM model dams and four input earthquake waves based on the observations and conducted the analysis using them. The analysis results confirmed that the rockfill dams designed by the current design method have sufficient resistance to sliding even against the magnitude of shaking that occurred close to the source fault of the Hyogoken-Nambu Earthquake.

Dams, as large-scale structures, must have sufficient stability even during earthquakes. The seismic design technology for dams and the system for observing earthquakes must be improved.

ACKNOWLEDGMENTS

We would like to extend our deep gratitude to the persons of Osaka and Hyogo Prefectures, Water Resources Development Public Corporation and Kansai Electric Power Corporation for their cooperation in collecting earthquake acceleration records.

REFERENCES

Committee for Investigation on the Damage of Highway Bridges Caused by the Hyogoken-Nambu Earthquake, with T. Iwasaki as the chair (1995): *Report on the Damage of Highway Bridges Caused by the Hyogoken-Nambu Earthquake* (in Japanese)

Committee on Evaluation of Earthquake Resistance

of Dams, with C. Tamura as the chair (1995): *Report of Committee on Evaluation of Earthquake Resistance of Dams* (in Japanese)

Development Division, River Bureau, Ministry of Construction (1991): *Seismic Design Standards for Embankment Dams (Draft)*

Izawa, S. et al. (1995): Measured Earthquake Records in a Rock Site During Hyogoken-Nambu Earthquake, *Architectural Institute of Japan Kinki Chapter Architectural Research Meeting (Structure)* (in Japanese)

Iwashita, T., Yasuda, N., Nakamura, A., Matsumoto, N., Takeda, O. (1995): Dynamic Analysis of Rockfill Dams Considering Frequency Dependent Characteristics of Radiation Damping Ratio, *First International Conference on Geotechnical Engineering*, Vol.1, Balkema, pp. 511-516

Matsumoto, N., Nakamura, A., Sasaki, T., Iwashita, T. (1996): Effects on Dams, *A Special Issue of Soils and Foundations on Geotechnical Aspects of the January 17 1995 Hyogoken-Nambu Earthquake*, JGS, pp.273-281

Nakamura, A. and Iwashita, T. (1996): Behavior and Stability of a Rockfill Dam by Dynamic Analysis During the 1995 Hyogoken-Nambu Earthquake, *Proceedings of Conference on the Great Disaster in Hanshin and Awaji*, JSCE, pp.441-448 (with English summary)

Okamoto, S. (1984): *Introduction to Earthquake Engineering*, pp.474-479, University of Tokyo Press

N Sawada, Y. and Takahashi, T. (1975): Study on the Material Properties and the Earthquake, *Proceedings of the fourth Japan Earthquake Engineering Symposium*, pp.695-702

Table 1 Properties of materials of Minoogawa Dam model

Zoning	Wet Density ρ_t (kg/m^3)	Saturated Density ρ_{sat} (kg/m^3)
Rock I	2120	2320
Rock II	2030	2270
Filter	2230	2350
Core	2180	2180

Table 2 Shear strength parameters for stability analysis of model dams

Zoning	Wet Density (kg/m^3)	Saturated Density (kg/m^3)	Strength Parameter*	
			A (or c)	b (or Φ)
Rock	1880	2080	A=1.128 (c=0)**	b=0.804 (Φ =42°)
Filter	2130	2240	A=0.808 (c=0)	b=0.908 (Φ =36°)
Core	2220	2230	c=98 kPa (c=0)	Φ =35° (Φ =35°)

* $\tau f = Po \cdot A \cdot (\sigma n/Po)^b$ or $\tau f = c + \sigma n \tan \Phi$, where τf is the shear strength, Po is 1 MPa, σn is the normal stress on the sliding plane, c is cohesion, and Φ is internal friction angle.

* * The parenthesized vales are designed shear strength parameters of Shichigasyuku Dam by seismic coefficient method.

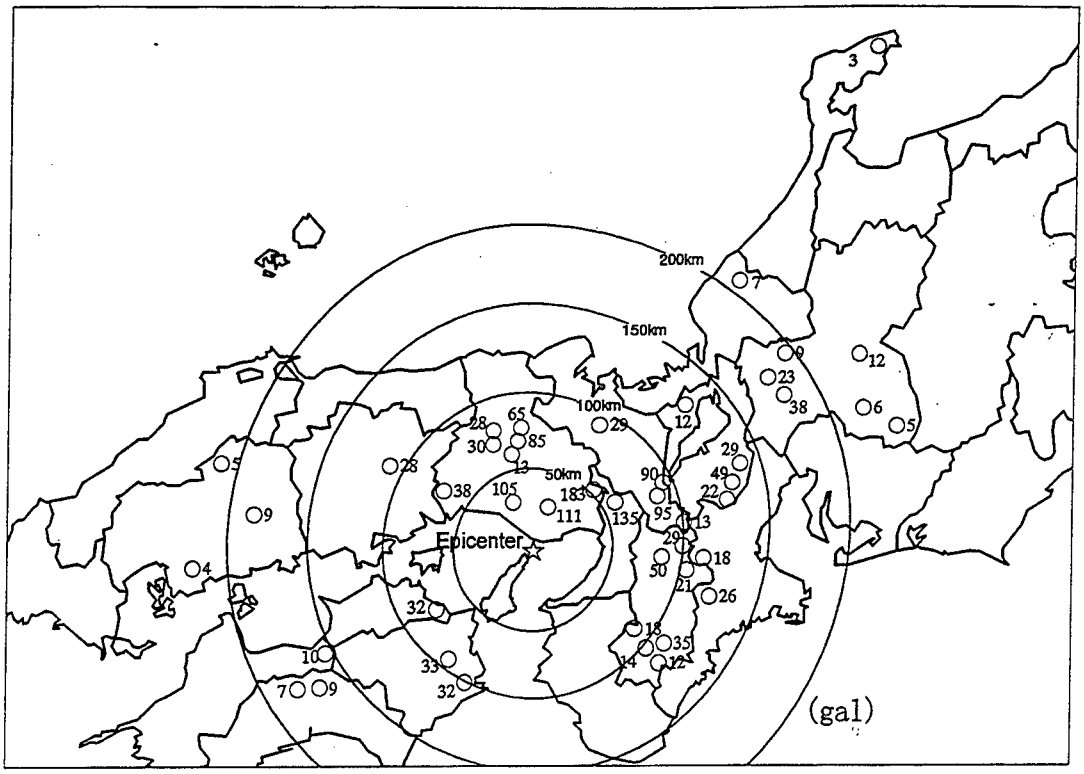

Figure 1 Horizontal peak acceleration at dam foundations

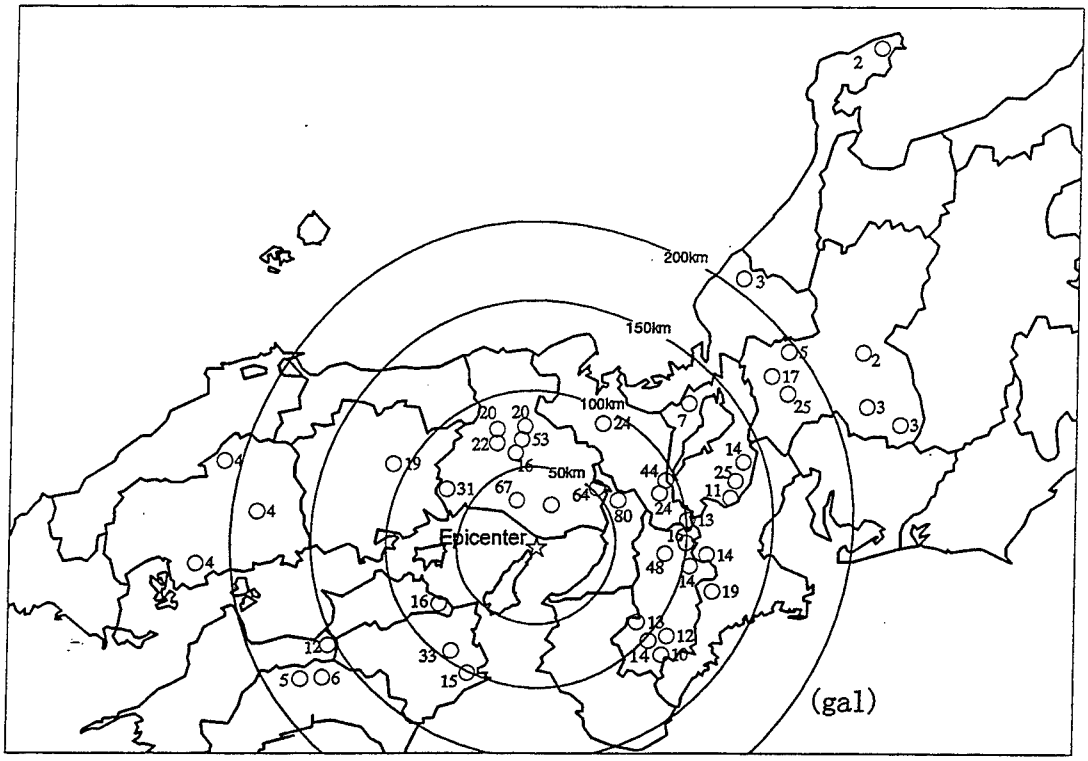

Figure 2 Vertical peak acceleration at dam foundations

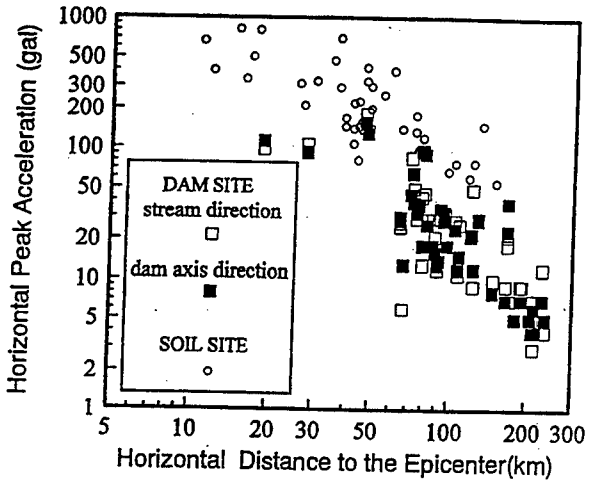

Figure 3 Attenuation of horizontal peak acceleration with epicentral distance

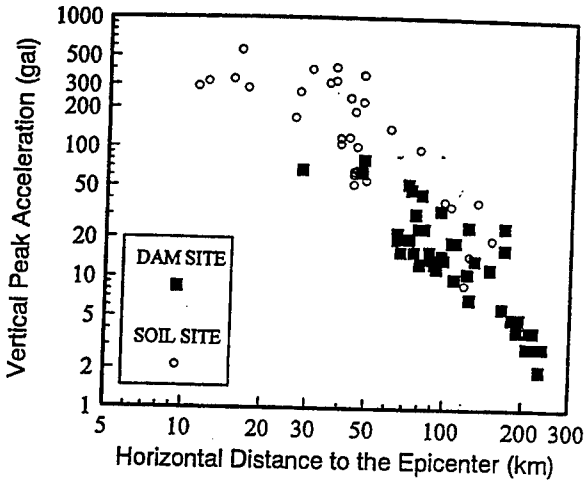

Figure 4 Attenuation of vertical peak acceleration with epicentral distance

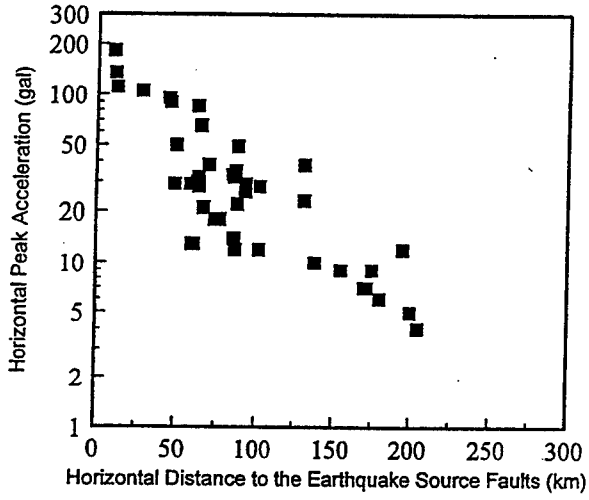

Figure 5 Attenuation of horizontal peak acceleration with distance to the earthquake source fault

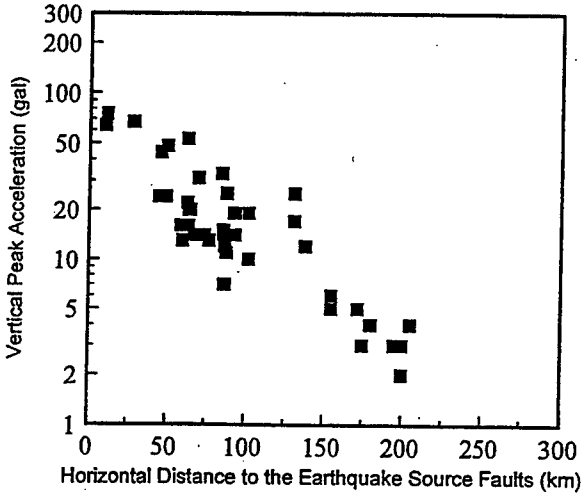

Figure 6 Attenuation of vertical peak acceleration with distance to the earthquake source fault

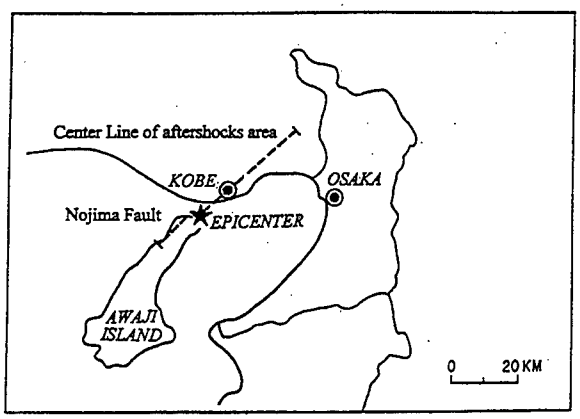

Figure 7 Earthquake source fault

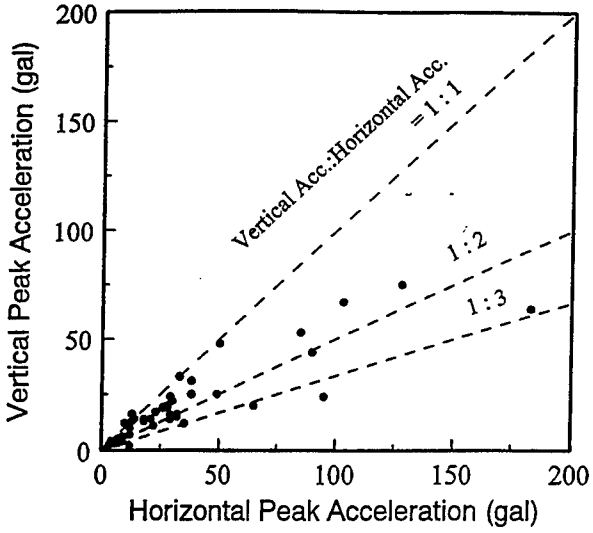

Figure 8 Ratio of vertical peak acceleration to horizontal peak acceleration

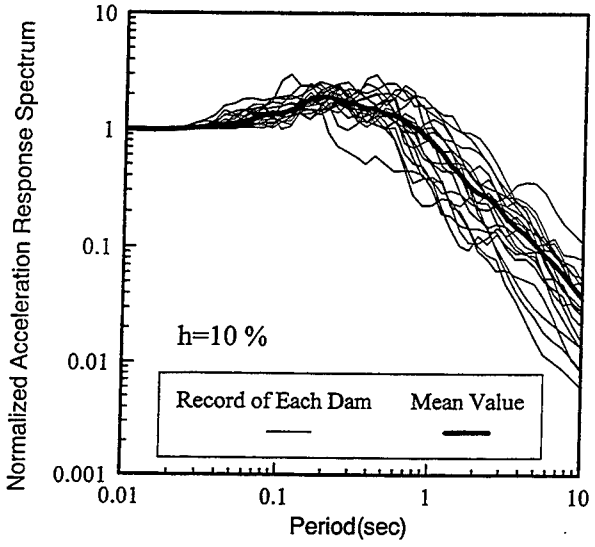

Figure 9 Acceleration response spectra at dam foundations

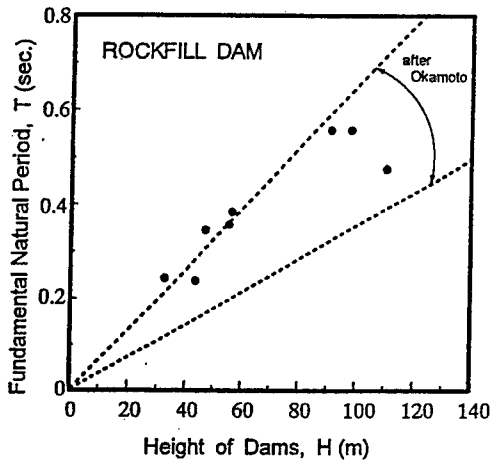

Figure 10 Relationship between natural period and dam height

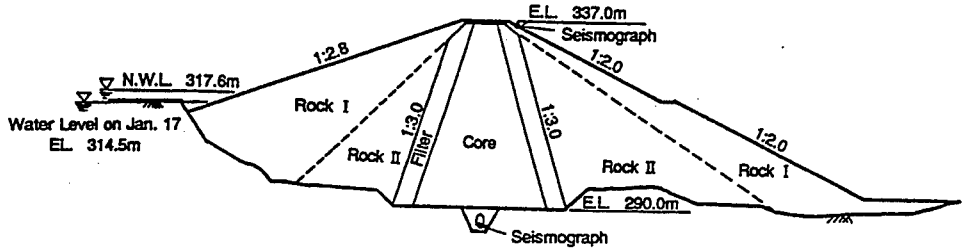

Figure 11 Cross section of Minoogawa Dam

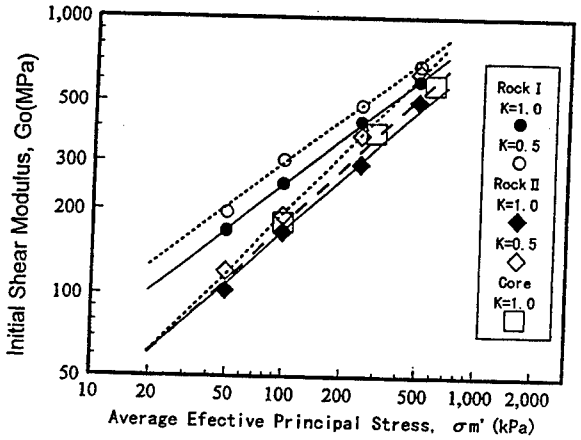

Figure 12 Initial shear modulus with average effective principal stress for Minoogawa Dam model

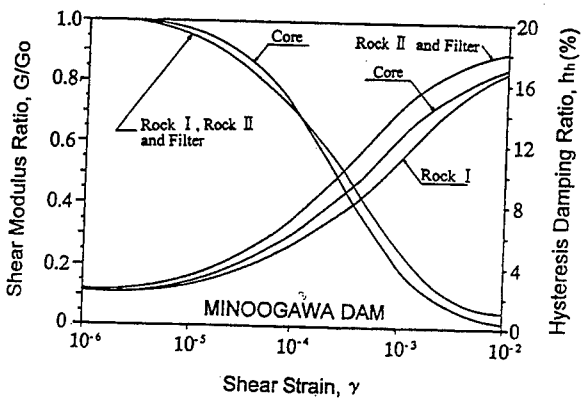

Figure 13 Shear strain dependency of shear modulus ratio and hysteresis damping ratio for Minoogawa Dam model

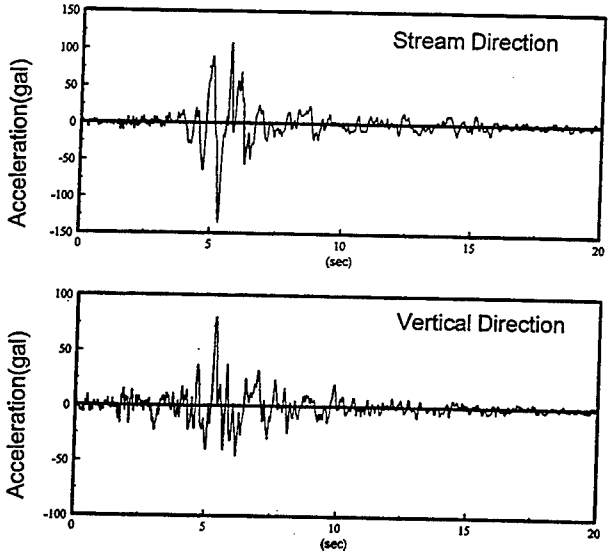

Figure 14 Input acceleration waves observed at gallery of Minoogawa Dam

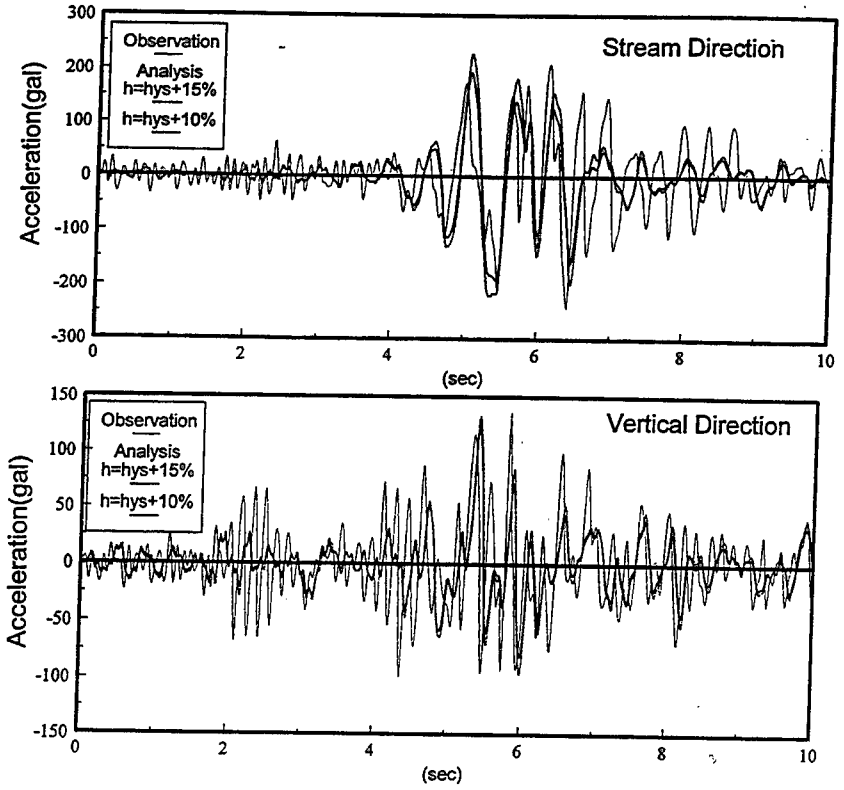

Figure 15 Response acceleration waves at the crest of Minoogawa Dam

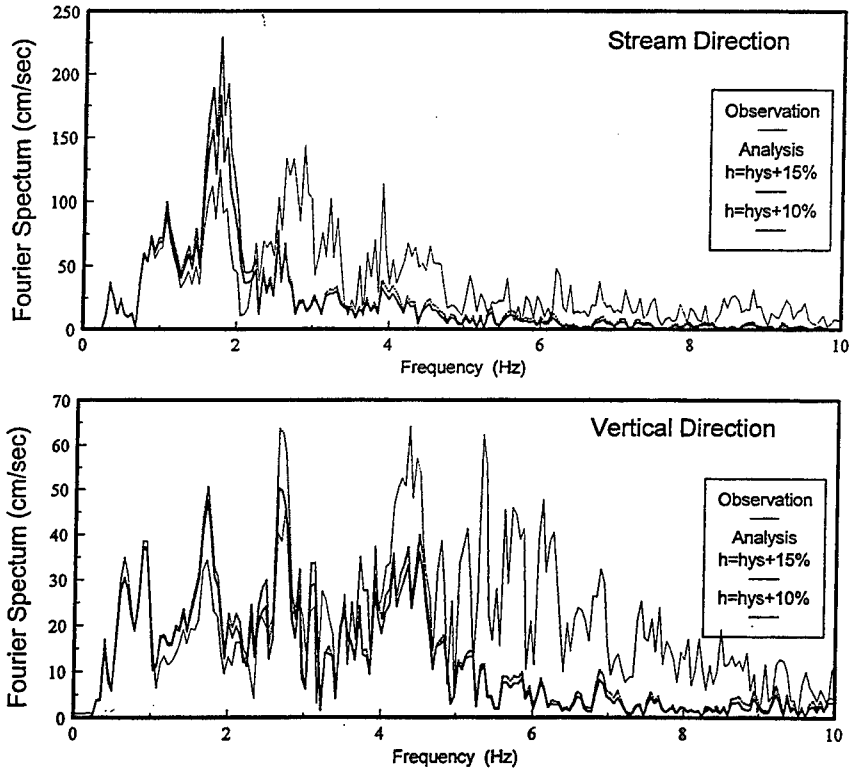

Figure 16 Response Fourier spectra at the crest of Minoogawa Dam

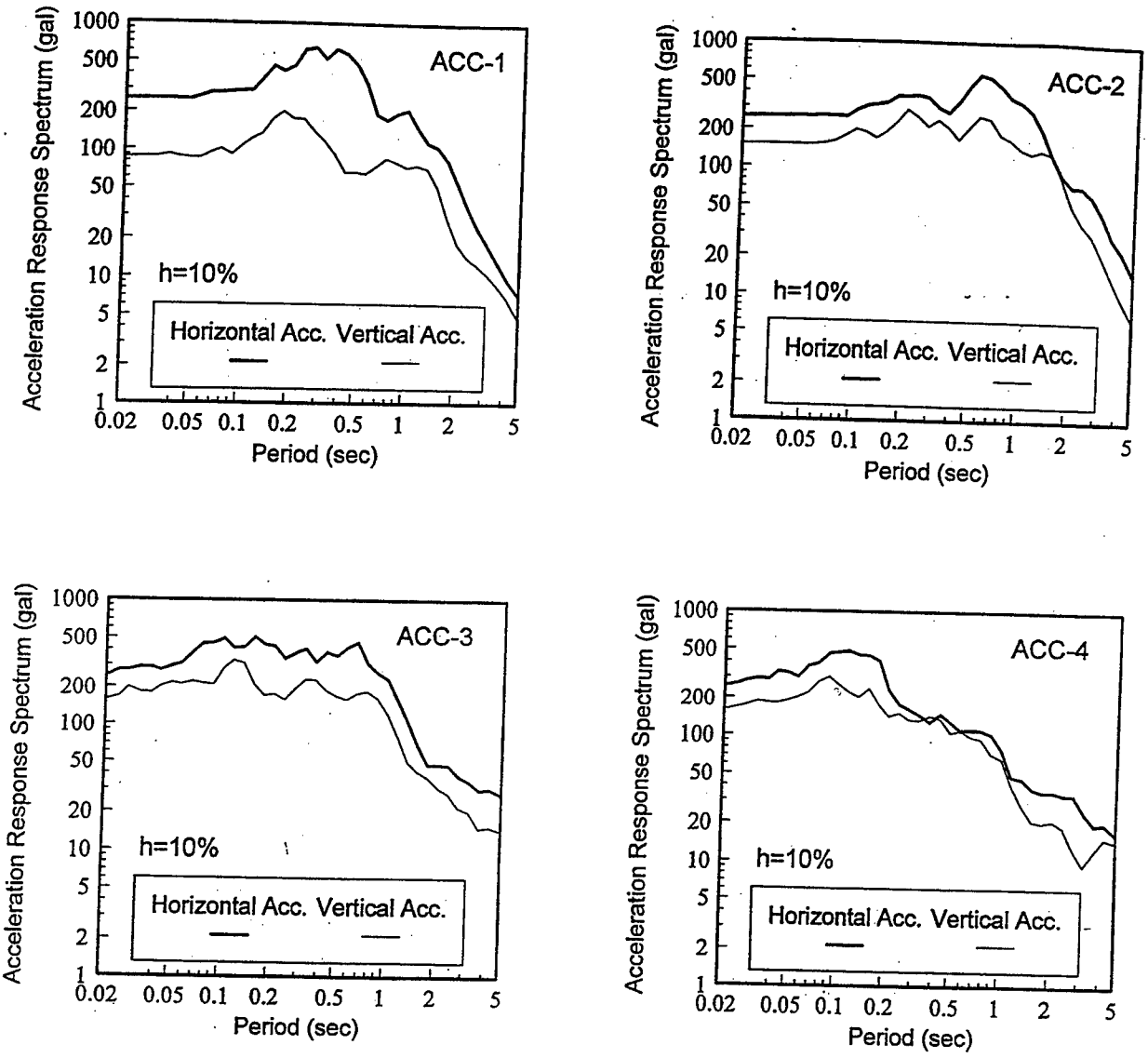

Figure 17 Acceleration response spectra of input acceleration waves for dynamic analysis of model dams

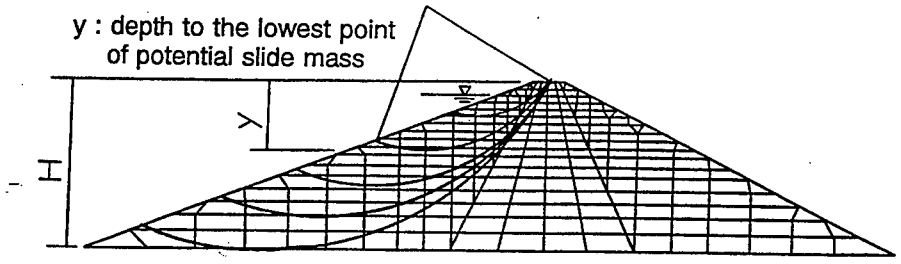

Figure 18 Finite element mesh of model dam and potential slide masses

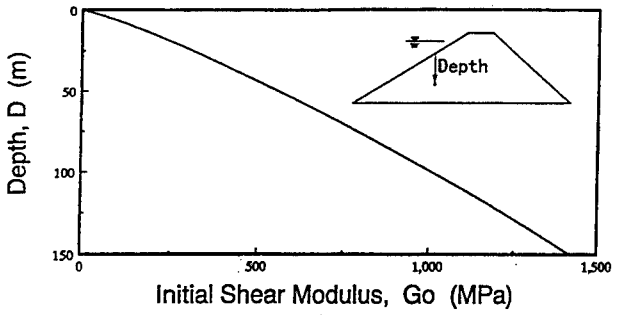

Figure 19 Distribution of initial shear modulus with depth from the slope surface

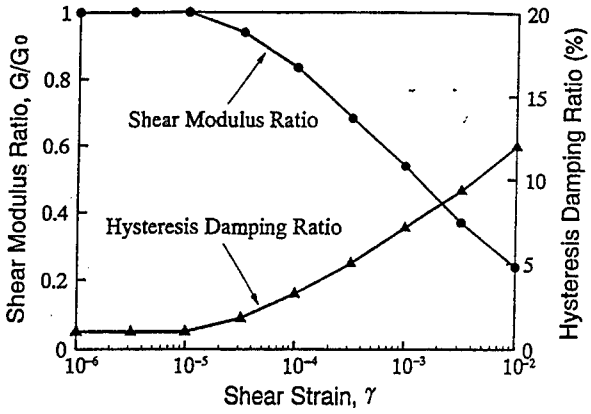

Figure 20 Shear strain dependency of shear modulus ratio and hysteresis damping ratio for model dams

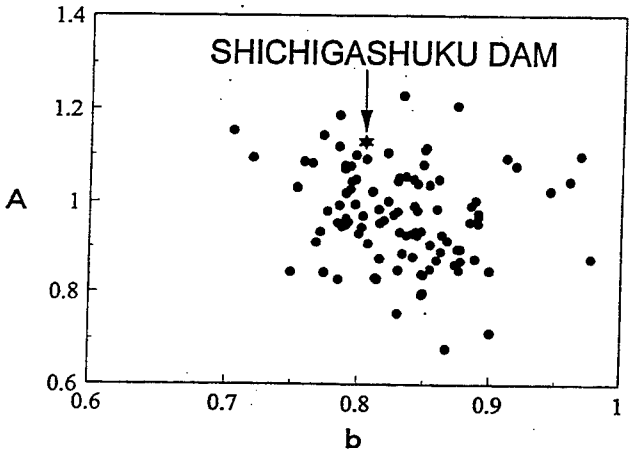

Figure 21 Relationship between A and b of shear strength of rockfill materials

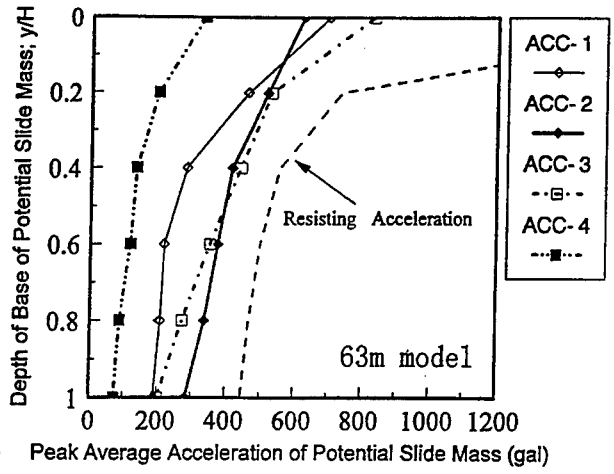

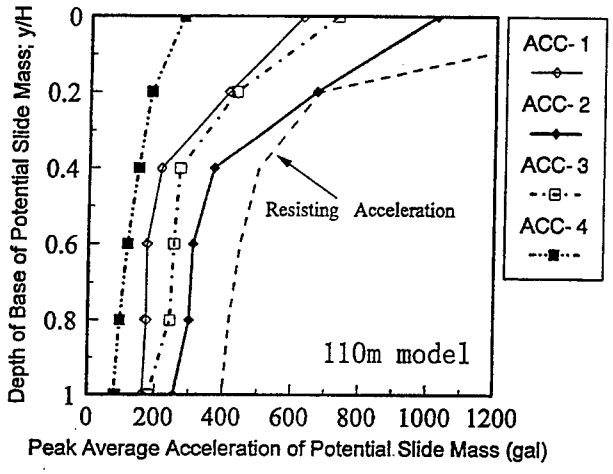

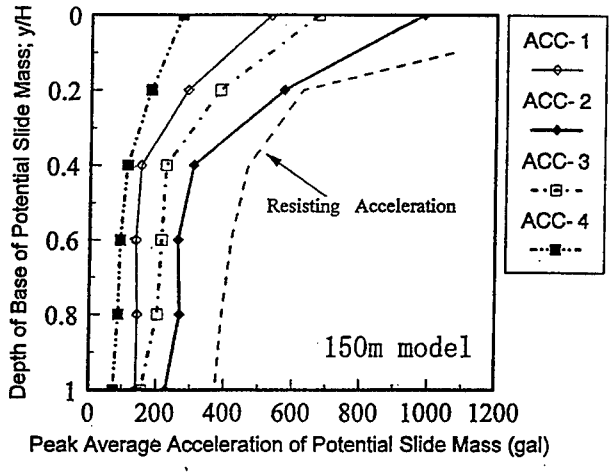

Figure 22 Peak average accelerations and resisting acceleration of potential slide masses for three heights of dam models

Newmark Sliding Block Analysis

by

Joseph P. Koester*

ABSTRACT

This report describes a portion of a study conducted for the author by Dr. Timothy D. Stark and his associates at the University of Illinois. The work was sponsored as part of the Earthquake Engineering Research Program (EQEN) at the US Army Engineer Waterways Experiment Station (WES), specifically Work Unit No. 33019, titled "Seismic Stability and Deformations of Earth Structures and Foundations - Task 1: Calibration of Newmark Analysis with Field Observations." The following objectives were accomplished during the course of the study: (a) compilation of a summary of available data on field occurrences of seismically -induced permanent deformations of 52 earth dams, 22 waste containment facilities, three embankments/roadways, and 13 natural slopes; (b) assessment of the applicability of the Newmark (1960, 1965) sliding block analogy to estimate seismically induced deformations in these types of slopes; © estimation of the magnitude of field displacement required to initiate an undrained post-peak strength loss and determine the resulting shear strength that should be used in a deformation analysis; and (d) development of recommendations for estimating seismically - induced deformations calculated using the Newmark method. Case history data for earth dams are presented in this paper. The eventual final report of the study will detail findings and recommendations from each of the objectives stated above.

KEYWORDS: Permanent Displacements, Slope Stability, Deformations, Newmark Sliding Block, Earth dams, Seismic

1 INTRODUCTION

Early seismic stability evaluations, based primarily on pseudo-static analysis, did not indicate the potential magnitude of seismically-induced permanent deformations. The importance of estimating the magnitude of seismically induced deformations began to be realized during the 1960's and 70's. The amount of freeboard required for an earth dam to ensure reservoir containment during or after earthquake shaking is a function of the magnitude of seismically-induced permanent deformation that may occur. In the 1980's and 90's, most seismic stability design and evaluation involve estimates of seismically - induced permanent deformations to varying degrees of sophistication.

2 PROBLEM DEFINED

The potential magnitudes of seismically-induced downslope permanent deformations in earth embankments where liquefaction is not expected to occur are commonly

* Earthquake Engineering and Geosciences Division
Geotechnical Laboratory, USAE Waterways Experiment Station, Vicksburg, MS 39180

estimated based on a "sliding block" analogy developed by N. M. Newmark (1960, 1965). Permanent deformations so estimated are often critical input to remedial action decisions. Newmark developed the "sliding block" analysis to provide a "quick estimate of the magnitude of the motions to be expected in a sliding wedge of rock or earth in a dam, when it is subjected to the influence of dynamic forces from an earthquake." The calculation is based on the main assumption that the entire sliding mass moves as a single rigid body with resistance mobilized by friction along the sliding surface. In cases where well defined slip planes/zones are likely to develop due to the narrow or limited constraints of the problem soil, rigid-block slope stability analyses may be applicable.

3 OBJECTIVES

The overall purpose of the sponsoring EQEN work unit was to address the urgent need to assess the Newmark "sliding block" analysis technique to determine: whether it adequately models actual performance as it is currently applied; under what conditions it is applicable; and if modifications are needed to calibrate the procedure for varying ground motions and site response characteristics. This paper summarizes progress to date toward accomplishment of these objectives, with focus on earth dams.

4 BACKGROUND ON THE NEWMARK ANALYSIS FOR ESTIMATION OF SLOPE DISPLACEMENTS

The Fifth Rankine Lecture (Newmark, 1965) reported Newmark's definitive work on simplified estimation of the potential magnitude of seismically - induced downslope permanent deformations in earth structures. Several variations of this method have been subsequently published including: Ambraseys (1967); Ambraseys and Sarma (1967); Sarma (1975); Nadim and Whitman (1983); Chang et al. (1984); Constantinou et al. (1984); Constantinou and Gazetas (1984); Hynes-Griffin and Franklin (1984); Dakoulas and Gazetas (1986); Lin and Whitman (1986); Stamatopoulos and Whitman (1987); Ambraseys and Menu (1988); Yan (1991); Yegian et al. (1992); Marcuson et al. (1992); and Gazetas and Uddin (1994).

One of the most commonly used variations of the Newmark method is presented by Makdisi and Seed (1978). This procedure incorporated the dynamic response of an embankment into the Newmark method instead of assuming rigid body behavior below the shear surface. Makdisi and Seed (1978) classified the behavior of dams and embankments during earthquakes in two categories: (1) loose to medium dense sandy embankments, susceptible to rapid increases in pore-water pressure caused by earthquake loading resulting in large movements, and (2) compacted cohesive soils, dry sands, and some dense sands that develop small pore-water pressures and retain most of their static undrained shearing resistance, and thus undergo limited permanent deformation. The Newmark (1965) and Makdisi and Seed (1978) methods are considered applicable only for type (2) embankments, i.e., those that develop negligible pore water pressures during shaking.

The Makdisi and Seed (1978) approach is constrained by the Newmark (1965)

assumptions, namely: (1) no displacement occurs at accelerations below the yield acceleration, (2) deformation occurs plastically along a discrete basal shear surface when the yield acceleration is exceeded, (3) the shear surface is inclined and planar, (4) there is no upslope movement, and (5) the yield acceleration, and thus shear strength, is not displacement or rate dependent and remains constant throughout the analysis. The method involves three main steps: (a) estimate the yield acceleration, which is a function of the geometry of the embankment, the undrained shear strength, and of the location of the sliding mass, (b) estimate the earthquake induced accelerations at the base of the sliding mass, and © for a given potential slide mass, estimate the magnitude of the permanent displacement. Procedural details are not summarized further in this paper, but may be found in Makdisi and Seed (1978) and the previously cited, more recent publications.

5 CASE HISTORIES OF EARTHQUAKE - INDUCED DEFORMATIONS

Roughly 140 published references were located and reviewed for this study to compile a comprehensive summary of earth structures that have experienced earthquake shaking. Thirty-two of these references yielded information on field occurrences of seismically-induced permanent deformations. Fifty-two, twenty-two, three, and thirteen case histories of seismically-induced permanent deformations observed in earth dams, waste containment facilities, embankments and roads, and natural slopes, respectively. This paper will only present the literature review results for earth dams.

It should be noted that case histories involving earthquake-induced liquefaction were not included in the compilation.

Two tables are presented herein to relate results of the extensive literature review just described, with focus on earth dams. Table 1 presents the names of the earth dams studied, the earthquake that they experienced, and the observed permanent deformation or settlements documented in each case. Table 2 gives details, if available, on the structural characteristics of each earth dam, the foundation conditions, and associated references. Various types of movements including settlement, horizontal displacement, differential settlement, and cracking were observed and recorded in the various references studied. It was assumed in this study that reported horizontal displacement corresponds to shear displacement and was comparable to the deformation calculated using the Newmark method.

The majority of observed values of downstream horizontal displacement ranged from less than 0.1 to 0.5 m. Lower Mayurama Dam, as an exception, was reported to have undergone 1.8 m of downstream displacement. Most of the observed values of upstream horizontal displacement ranged from less than 0.1 to 0.15 m. Masiway Dam was the exception here, and was reported to have undergone 1.8 m of upstream horizontal displacement. One possible explanation for the large deformations observed at Lower Mayurama and Masiway Dams may be partial liquefaction, although the authors of the source references in each case did not report any manifestations of liquefaction.

La Villita Dam, located in southwestern Mexico on the Balsas River, provides perhaps the most well-known case history where an earth dam has been subjected to significant earthquake shaking and where instrumental records of ground motion and permanent displacements are available. La Villita is a zoned earth and rock fill embankment (Figure 1) with a clay core and rock fill shells, constructed over an alluvial layer composed of boulders, gravel, sand, and silt. The dam has concrete grouting and a deep cut off wall into the alluvial layer to reduce seepage. The region where this dam is built is associated with the seismically active Pacific subduction zone. The dam is 60 m high and was built during the period 1964-1968. The dam has three accelerographs: one at the right abutment (bedrock), one in the crest, and one at the downstream toe. The dam also has several inclinometers and surface reference points (Figure 2).

The dam experienced six major earthquakes during the period from October 1975 to September 1985, with magnitudes ranging from M_L:4.9 to M_L:8.1 at epicentral distances of 10-121 km. These earthquakes subjected the dam to substantial dynamic loads that contributed to significant measured vertical and horizontal displacements. Vertical settlement and horizontal deformations have been extensively measured during the period 1975-1985. Measurements were recorded on the upstream and downstream shells as well as within the central clay core. According to detailed studies of the deformation history of this dam by Elgamal, et al. (1990) and Succarieh, Elgamal, and Yan (1993), approximately 60% of the vertical settlement and 40% of the horizontal displacements have resulted from earthquake shaking.

Gazetas and Uddin (1994) used the La Villita Dam case history to compute permanent displacement, using a two-dimensional plane-strain finite element model that assumed a pre-existing sliding surface and followed the assumptions inherent to the Newmark analysis. They demonstrated the accuracy of the procedure using the 19 September 1985 (Magnitude 8.1) earthquake. The crest acceleration time history they computed with the assumed sliding mass compared favorably to the observed crest record. In addition, they computed a total permanent displacement of O.32 m, which is in agreement with the observed permanent displacement of 0.25 m. As a result, Gazetas and Uddin (1994) concluded that their procedure provides a reasonable estimate of earthquake-induced sliding deformation. However, they noted that the field deformation can be overestimated when the predominant frequency of a narrow band excitation is close to the fundamental frequency of the dam.

The Newmark method of analysis appears to be suitable for estimation of permanent deformations in earth dams, based on the available case history data. However, the method appears to be most reliable in the range of permanent deformations from about 0.3 m to 1.0 m for maximum accelerations ranging from 0.1 g to 0.5 g, respectively.

6 SHEAR STRENGTH FOR DEFORMATION ANALYSES

Estimates of the dynamic shear strength parameters of the materials along the sliding

surface are required for accurate estimation of the permanent seismic deformations using the Newmark approach. The dynamic shear strengths are used in limit equilibrium analyses to estimate the yield acceleration of the potential sliding surface.

Stark and Contreras (1996a) used field observations at the Fourth Avenue, L Street, and Government Hill landslides that occurred during the 1964 Alaska earthquake to estimate the undrained shear strength of cohesive soil mobilized during these permanent deformations. The mobilized shear strength in these cases, where well-defined clay seams defined the sliding surface, provides an insight to the shear strength that should be used to estimate the yield acceleration. The authors performed regression analysis on back-calculated estimates of mobilized shear strengths during sliding at several sites, and compared these values to peak strengths measured in a program of laboratory undrained shear strength tests. In addition, Stark and Contreras (1996b) describe a program of laboratory undrained residual shear strength tests using a special constant volume ring shear apparatus to determine large-deformation strengths.

Figure 3 depicts comparisons between laboratory undrained shear strengths determined for Bootlegger Cove Clay and back-calculated strengths from 1964 Alaskan earthquake landslide sites. Stark and Contreras (1996a) reported that for displacements associated with the onset of movement, back-calculated strengths agreed well with laboratory undrained peak shear strengths. When the back-calculated strength data from various slide sites were plotted in the manner shown in Figure 4, the data suggest a strength reduction of about 20 percent (from peak undrained values) for movements up to about 0.1 m. The data also indicate a strong sensitivity to deformation amount. When landslide blocks were observed to have moved more than about 1.0 m, back-calculated strengths agreed well with laboratory undrained residual strengths measured in constant volume ring shear tests. The authors contend that these findings should be adapted into practice; they recommend, e.g., the appropriate strength for lateral, earthquake-induced permanent deformation estimation of cohesive soils is 80 percent of the peak undrained shear strength when these deformations are less than 0.1 m, but when analysis indicates larger deformations (up to about 1.0 m), the appropriate strength for analysis is the undrained residual shear strength.

Newmark - type analyses are not recommended for estimation of deformations larger than about 1.0 m, nor are they recommended for evaluation of deformations involving sliding along surfaces through saturated cohesionless soils when high excess pore water pressures (potentially leading to liquefaction) are expected to develop.

7 SUMMARY AND CONCLUSIONS

The main accomplishments of this research were: (a) compilation of a summary of field occurrences of seismically-induced permanent deformations of earth dams and other types of slopes; (b) determination of the applicability of the Newmark (1960, 1965) method to estimate slope displacements during shaking; © estimation of the magnitude of field displacement

required to initiate an undrained post-peak strength loss and the resulting shear strength that should be used in a deformation analysis; and (d) development of recommendations for estimating seismically-induced deformations calculated using the Newmark method. An extensive literature search was conducted to summarize the seismically-induced permanent deformations, if any, observed in during earthquakes. This paper summarized case histories of seismically-induced permanent deformations observed in earth dams, and relates findings that bear on future practice for Newmark - type analyses.

8 BIBLIOGRAPHY

1. Ambraseys, N.N. (1960). "On the behavior of Earth Dams," *Proceedings of the Second World Conference on Earthquake Engineering*, Tokyo and Kyoto, Japan, Vol. 1, pp. 331-356.

2. Ambraseys, N. N. and Sarma, S. K. (1967). "The response of Earth Dams to Strong Earthquakes," *Geotechnique*, vol.17, pp. 181-213.

3. Ambraseys, N. N. and Menu, J.M. (1988). "Earthquake-Induced Ground Displacements," *Earthquake Engineering and Structural Dynamics,* Vol. 16, pp. 985-1006.

4. Anderson, R. (1995). "Forensics on Landfills and Landfill Systems," California Integrated Waste Management Board, Permitting and Enforcement Division, Closure and Remediation Branch. Internal Memorandum.

5. Ashford, S. and Sitar, N. (1994). "Seismic Response of Steep Natural Slopes," Technical Report No. UCB/EERC-94/05, EERC, Berkeley, California.

6. Bonilla, M.G. (1959). "Geologic Observation in the Epicentral Area of the San Francisco Earthquake of March 22, 1957," Special Report 57, California Division of Mines and Geology, pp. 25-37.

7. Buranek, D. and Sangeeta, P. (1991). "Sanitary Landfill Performance during the Loma Prieta Earthquake," *Proceedings of the Second International Conference on Recent Advances in Geotechnical Earthquake Engineering and Soil Dynamics*, St Louis, MO, Paper LP14.

6. Chang, C-J., Chen, W. and Yao, J.T.P. (1984). "Seismic Displacements in Slopes by Limit Analysis," *Journal of Geotechnical Engineering*, ASCE, Vol. 110, No. GT7, pp.860-874.

7. Clough, R.W. and Chopra, A.K. (1966). "Earthquake Stress Analysis in Earth Dams," *Journal of Engineering Mechanics Division*, ASCE, Vol. 92, No. EM2, pp. 197-212.

8. Comision Federal de Electricidad. (1980). *Performance of El Infiernillo and La Villita Dams including the Earthquake of March 14, 1979*, Mexico City, Special publication No. 15.

9. Constantinou, M.C. and Gazetas, G. (1984). "Probabilistic Seismic Sliding Deformations of Earth Dams and Slopes," *Proceedings of the Specialty Conference on Probabilistic Methods and Structural*

Reliability, ASCE, New York, NY, pp.318-321.

10. Constantinou, M.C., Gazetas, G. and Tadjdakhsh (1984). "Stochastic Sliding of Rigid Mass against Asymmetric Coulomb Friction," *Earthquake Engineering and Structural Dynamics*, No. 12, pp.777-793.

11. Dakoulas, P. and Gazetas, G. (1986). "Seismic Shear Strains and Seismic Coefficients in Dams & Embankments," *Soil Dynamics and Earthquake Engineering*, Vol. 5, No. 2, pp.75-83.

12. Earthquake Engineering Research Center. (1994). "Preliminary Report on the Seismological and Engineering Aspects of the January 17, 1994, Northridge Earthquake," Technical Report UCB/EERC-94/01, EERC, Berkeley, California.

13. Earthquake Engineering Research Institute. (1970). "Peru Earthquake of May 31, 1970. Preliminary Report," Earthquake Report Committee 1970, Berkeley, California.

14. Earthquake Engineering Research Institute. (1973). "Reconnaissance Report. Managua, Nicaragua Earthquake of December 23, 1972," EERI, Berkeley, California.

15. Earthquake Engineering Research Institute. (1977). "Reconnaissance Report. Mindanao, Philippines Earthquake August 17, 1976," EERI, Berkeley, California.

16. Earthquake Engineering Research Institute. (1978). "Reconnaissance Report. Miyagi-ken-Oki, Japan Earthquake June 12, 1978," EERI, Berkeley, California.

17. Elgamal, A.W., Scott, R.F., Succarieh, M.F. and Yan L.P. (1990) "La Villita Dam Response During Five Earthquakes Including Permanent Deformation," *Journal of Geotechnical Engineering*, ASCE, Vol. 116, No. GT10, pp.1443-1462.

18. EMCON Associates. (1994). "Sanitary Landfill Performance during the Loma Prieta Earthquake," Prepared for NSF Grant No. BCS-9011102, Project EG1-01.01.

19. Ericksen, G.E., Fernández, J. and Silgado, E. (1954). "The Cusco, Peru, Earthquake of May 21, 1950," *Bulletin of the Seismological Society of America*, Vol. 44, No. 2A, pp. 97-112.

20. Gazetas, G. and Uddin, N. (1994). "Permanent Deformation on Preexisting Sliding Surfaces in Dams," *Journal of Geotechnical Engineering*, ASCE, Vol. 120, No. 11, pp. 2041-2061.

21. Hadley, J.B. (1964). "Landslides and related phenomena accompanying the Hegben Lake Earthquake of August 17, 1959," USGS Professional Paper No. 435, United States Geological Survey, Washington D.C.

22. Hansen,W.R. (1966). "Effects of the Earthquake of March 27, 1964 at Anchorage, Alaska," USGS Professional Paper No. 542-A, United States Geological Survey, Washington D.C.

23. Harder, L.F. Jr. (1991). "Performance of Earth Dams during Loma Prieta Earthquake," *Proceedings 2nd International Conference on Recent Advances in Geotechnical Earthquake Engineering and*

Soil Dynamics, St. Louis, MO, pp. 1673-1690.

24. Hart, E.W., Bryant, W.A., Wills, C.J. and Treiman, J.A. (1990). "The search for Fault Rupture and Significance of Ridgetop fissures, Santa Cruz Mountains, California," *The Loma Prieta (Santa Cruz Mountains) Earthquake of 17 October, 1989*, Special Publication No.104, California Dept. of Conservation, Division of Mines and Geology.

25. Hynes-Griffin, M.E. and Franklin, A.G. (1984). "Rationalizing the Seismic Coefficient Methods," Miscellaneous Paper GL-84-13, U.S. Army Engineer Waterway Experiment Station, Vicksburg, MS.

26. Idriss, I.M., (1985). "Evaluating Seismic Risk in Engineering Practice." *Proc. 11th Int. Conf. on Soil Mech. and Found. Engrg.*, San Francisco, California, Theme paper, Vol. 1, pp. 255-320.

27. Ishihara, K. (1985). "Stability of Natural Deposits During Earthquakes." *Proc. 11th Int. Conf. on Soil Mech. and Found. Engrg.*, San Francisco, California, Theme paper, Vol. 1, pp. 321-376.

28. Kachadorian, R. and Plafker, G. (1967). "Effects of the Earthquake of March 27, 1964 on the Communities of Kodiak and Nearby Islands," USGS Professional Paper No. 542-F, United States Geological Survey, Washington D.C.

29. Koester, J.P. (1995) Personal Communication.

30. Laginha Serafim, L. and Oliveira, C.S. (1987). "Effects Caused by Earthquakes on Dams," *Proceedings of the International Symposium on Earthquakes and Dams*, Beijing, China, Vol. 2, pp. 120-156.

31. Lin, J.S. and Whitman, R.V. (1986). "Earthquake Induced Displacements of Sliding Block," *Journal of Geotechnical Engineering*, ASCE, Vol. 105, No. GT12, pp. 1427-1434.

32. Makdisi, F.I. (1996). Personal communication.

33. Makdisi, F.I. and Seed, H.B. (1978). "A Simplified Procedure for Estimating Earthquake Induced Deformation in Dams and Embankments," *Journal of Geotechnical Engineering*, ASCE, Vol. 104, No.GT7, pp. 849-867.

34. Marcuson, W.F. III, Hynes, M.E. and Franklin, A.G. (1992). "Seismic Stability and Permanent Deformation analyses: the last 25 years," *Stability and Performance of Slopes and Embankments II*, Geotechnical Special Publication No. 31, ASCE, Berkeley, CA, University of California, vol 1, pp. 552-592.

35. Marsal, R.J. (1982). "Monitoring of Embankment Dam Behavior," *Proceedings of the 14th International Congress on Large Dams*, Rio de Janeiro, Brazil, Vol. 1, pp. 1141-1467.

36. Moriwaki, Y. , Idriss, I.M, Moses, T.L. and Ladd, R.S. (1989). "A Re-evaluation of the L Street Slide in Anchorage during the 1964 Alaska Earthquake," *Proceedings of the 12th International Conference on Soil Mechanics and Foundation Engineering*, Rio de Janeiro, Brazil, pp.1583-1586.

37. Murphy, L.M. (ed.) (1973). *San Fernando, California, Earthquake of February 9, 1971*, Geological and Geophysical Studies, U.S. Dept. of Commerce, NOAA, Vol. 3.

38. Murphy, L.M. and Brazee, R.J. (1964). "Seismological Investigations of the Hebgen Lake Earthquake," USGS Professional Paper No. 435, United States Geological Survey, Washington, D.C.

39. Nadim, F. and Whitman, R.V. (1983). "Seismically induced movements of retaining walls," *Journal of Geotechnical Engineering*, ASCE, Vol. 109, No. GT7, pp. 915-931.

40. Newmark, N. (1960). "The Earthquake Resistance of Portage Mountain Dam," Consulting Report submitted to International Power and Engineering Consultants Limited, Vancouver, B.C., Canada, pp. 30.

41. Newmark, N.M. (1965). "Effects of Earthquakes on Dams and Embankments," *Geotechnique*, Vol 15, No. 2, pp. 139-160.

42. Okabe, S. (1929). "General Theory of Earth Pressures." *J. Japan Society of Civil Engineers*. Vol. 12, No. 1.

43. Ohmachi, T. (1987). "Rockfill Sliding Initiated by Ground Shaking," *Proceedings of the International Symposium on Earthquakes and Dams*, Beijing, China, Vol. 1, pp. 379-392.

44. Orr, W.R. and Finch, M.O. (1990). "Solid Waste Landfill Performance During Loma Prieta Earthquake," *Geotechnics of Wastefills--Theory and Practice, ASTM 1070*, Philadelphia:ASTM, pp. 22-30.

45. Sarma, S.K (1975). "Seismic Stability of Earth Dams & Embankments," *Geotechnique*, Vol. 25 No. 4, pp. 743-761.

46. Seed, H.B. and Wilson, S.D. (1967). "The Turnagain Heights landslide, Anchorage, Alaska," *Journal of the Soil Mechanics and Foundation Division*, ASCE, Vol. 93, No. SM4, pp. 325-353.

47. Seed, H.B., Makdisi, F.L. and De Alba, P. (1978). "Performance of Earth Dams during Earthquakes," *Journal of Geotechnical Engineering*, ASCE, Vol. 104, No. GT7, pp. 967-994.

48. Seed, R.B., Dickenson, S.E., Riemer, M.F, Bray, J.D., Sitar, N., Mitchell, J.K., Idriss, I.M., Kayen, R.E., Kropp, A.,Harder, L.F. Jr. and Power, M.S. (1990). "Preliminary Report on the Principal Geotechnical Aspects of the October 17, 1989 Loma Prieta Earthquake," Technical Report No. UCB/EERC-90/05, Earthquake Engineering Research Center, Berkeley, California.

49. Seed, R.B. and Harder, L.F. (1990). "SPT-Based Analysis of Cyclic Pore Pressure Generation and Undrained Residual Strength." *Proc. Memorial H. B. Seed Symposium.* Vol. 2, pp. 351-376.

50. Sherard, J.L., Woodward, R.J., Gizienski, S.F., and Clevenger, W.A. (1963). Earth and Earth-Rock Dams, John Wiley & Sons, Inc., New York, 725 pp.

51. Sitar, N. (1990). "Seismic Response of Steep Slopes in Weakly Cemented Sands and Gravels," *Proceedings H.B. Seed Memorial Symposium*, Vol. 2, pp. 67-82.

52. Skempton, A.W., (1977). "Slope Stability of Cuttings in Brown London Clay." *Proc. 9th Int. Conf. Soil Mech. and Found. Engrg.*, Tokyo, Vol. 3, pp. 261-270.

53. Spittler, T.E., Harp, L.E., Keefer, D.K., Wilson, R.C. and Syndor, R.H. (1990). "Landslide Features and other Coseismic Fissures Triggered by the Loma Prieta Earthquake, Central Santa Cruz Mountains, California," *The Loma Prieta (Santa Cruz Mountains) Earthquake of 17 October, 1989*, Special Publication No.104, California Dept. of Conservation, Division of Mines and Geology, pp. 59-66.

54. Stamatopoulos, C.A. and Whitman, R.V. (1987). "Computation of Earthquake-induced permanent Deformations of Foundation on Liquefaction Susceptible Sand," Research Report No. R8705, Dept. of Civil Engineering, Massachusetts Institute of Technology, Cambridge, Mass.

55. Stark, T.D. and Contreras, I.A. (1996a). "Fourth Avenue Landslide During 1964 Alaskan Earthquake," submitted for review and possible publication in *Journal of the Geotechnical Engineering Division, ASCE*, Vol. 123.

56. Stark, T.D. and Contreras, I.A. (1996b). "Constant Volume Ring Shear Apparatus." ASTM *Geotechnical Testing Journal*, American Society for Testing and Materials, Vol. 19, No. 1, March, 1996, pp. 3-11.

57. Stark, T.D. and Olson, S.M. (1995). "Liquefaction Resistance Using CPT and Field Case Histories." *J. Geotech. Engrg. Div.*, ASCE, Vol. 121, No. 12, pp. 856-869.

58. Succarieh, M.F, Elgamal, A.W. and Yan, L. (1993). "Observed and Predicted earthquake Response of La Villita Dam," *Engineering Geology*, Vol. 34, pp. 11-26.

59. Waller, R.M. (1966). "Effects of the Earthquake of March 27, 1964 in the Homer Area, Alaska," USGS Professional Paper No. 542-D, United States Geological Survey, Washington D.C.

60. Yan, L. (1991). "Seismic Deformation Analysis of Earth Dams: a simplified method," Report No. SML 91-01, Soil Mechanics Laboratory, California Institute of Technology, Pasadena, CA.

61. Yegian, M.K., Ghahraman, V.G., and Gazetas, G. (1992). "Seismological, Geotechnical, and Structural Overview," *The Armenia Earthquake of December 1988*, Northeastern University, Boston, pp. 1-34.

Table 1 Observed Seismic Deformation/Settlement in Earth Dams

EARTH DAM NAME	EARTHQUAKE NAME AND DATE	EQK. MAGNITUDE	EPICENTRAL DISTANCE	GROUND ACCELERATION (recorded/ estimated)	OBSERVED SEISMIC DEFORMATION/ SETTLEMENT
Chabot Dam	San Francisco, CA 04/18/06	M: 8.3	32 km (20 miles)	0.4g (est.)	No deformation observed.
Piedmont Dam	San Francisco, CA 04/18/06	M: 8.3	31 km (19 miles)	0.05g (est.)	Crest cracking; Vertical centerline settlement ~ 0.15 m; Downstream horizontal displacement ~ 0.15 m; Upstream concrete facing settled ~ 0.46 m
San Andreas Dam	San Francisco, CA 04/18/06	M: 8.3	0 km (0 miles)	0.25g- 0.8g(est.)	Longitudinal and transverse cracking in crest caused by settlement; Crest roadway offset 2.1 m by fault motion;
Upper Crystal Springs Dam	San Francisco, CA, 04/18/06	M: 8.3	0 km (0 miles)	0.25g- 0.8g(est.)	Longitudinal and transverse cracking in crest; Dam offset by ~ 2.5 m due to fault rupture.
Lower Mayurama Dam	Kanto, Japan 09/01/23	M: 8.3	140 km (87 miles)	0.12g (est.)	Longitudinal cracking/spreading; Vertical crest settlement = 0.2-0.25 m Downstream berm settlement ~ 1.2 m with 1.8 m of horizontal downstream displacement; Upstream concrete facing blocks settled irregulary ~0.2 m
Ono Dam	Kanto, Japan 09/01/23	M: 8.3	96 km (60 miles)	<0.15g (est.)	Vertical crest settlement = 0.3 m; downstream landslide forming: scarp - 18-20 m long, cracks ~ 10-20 m deep.
Cogoti Dam	Central Chile 04/06/43	M: 8.3	89 km (55 miles)	0.14g (est.)	Vertical crest settlement ~ 0.4 m; Rockslides in downstream slope.
Buena Vista Dam	Kern County, CA 07/21/52	M: 7.7	27 km (17 miles)	0.25g (est.)	Longitudinal cracking; Vertical crest settlement ~ 0.6 - 0.75 m Settlement caused by dissolution of gypsum lenses in foundation material.
Dry Canyon Dam	Kern County, CA 07/21/52	M: 7.7	72 km (45 miles)	0.12g (est.)	Longitudinal cracks in crest with vertical settlement ~ 0.75 m; Horizontal upstream displacement ~ 0.6 - 0.65 m.
South Haiwee Dam	Kern County, CA 07/21/52	M: 7.7	154 km (96 miles)	0.04g (est.)	Longitudinal cracking ~ 1.5 - 2 m deep; Vertical crest settlementrest settlement ~ 25 mm.
Coleman Dam	Fallon, NV 07/06/54	M: 6.6	NA	NA	Reservoir lost due to cracking of earthfill abutments; Freeboard before failure ~ 3 m (?).
Eureka Dam	Eureka, CA 12/21/54	M: 6.6	NA	NA	Crest settlement caused rupture of concrete lining, increased leakage after earthquake.

Table 1 (cont.). Observed Seismic Deformation/Settlement in Earth Dams

EARTH DAM NAME	EARTHQUAKE NAME AND DATE	EQK. MAGNITUDE	EPICENTRAL DISTANCE	GROUND ACCELERATION (recorded/ estimated)	OBSERVED SEISMIC DEFORMATION/ SETTLEMENT
St. Mary's Dam	San Francisco Bay, CA 10/23/55	M: 5.4	NA	0.07g (est.)	Cracks ~ 75 mm wide above concrete core wall; Concrete wall displaced 50 mm downstream.
Hebgen Lake Dam	Hebgen Lake, MT 08/17/59	M: 7.1	~40 km (~ 25 miles)	0.7g (est.)	Cracks in concrete core wall; Settlement of earthfill on both side Vertical crest settlement ~ 1.5 m; Differential settlement ~ 1
Bellavista Dam	Chile 03/28/65	M:7.0	55 km (35 miles)	NA	Reservoir lost due to seismic deformetion; Freeboard before failure ~ 3 m (?).
La Villita Dam	S1, S2 Mexico 10/11/75 11/15/75	M: 4.9 M: 5.9	10 - 52 km (6 - 32 miles)	0.04g - 0.07g bedrock (rec.) 0.21g - 0.35g crest (rec.)	Combined S1 and S2 downstream horizontal displacemen 15 - 20 mm.
El Infiernillo Dam	S3, Mexico 03/14/79	M: 7.6	87 km (54 miles)	0.36g crest (rec.) 0.12g Powerhouse	Longitudinal cracking in crest; Transverse cracking near abut Vertical crest settlement ~ 130 mm; downstream horizon displacement ~ 10 mm
La Villita Dam	S3, Mexico 03/14/79	M: 7.6	108 km (67.5 miles)	0.38g crest (rec.) 0.018g right bank	Downstream horizontal displacement ~ 10 mm; Upstream & downstream slope settlement ~ 45 mm & 35 n Transverse cracking ~ 10 - 15 mm wide.
Long Valley Dam	Mammoth Lakes, CA. 5/25/80	M: 6.3	NA	0.2-0.24g bedrock (rec.) 0.46g crest (rec)	No deformation observed.
Vermillion Dam	Mammoth Lakes, CA. 5/25/80	M: 6.3	20 km (12 miles)	0.24g toe (rec.) crest NA	Crest settlement ~ 50 mm.
La Villita Dam	S4, Mexico 10/25/81	M: 7.4	31 km (19 miles)	0.09g bedrock (rec.) 0.43g crest (rec.)	Downstream horizontal displacement ~ 25 - 30 mm
Anderson Dam	Morgan Hill, CA 04/24/84	M: 6.2	26 km (16 miles)	0.63g crest (rec.) 0.41g D.S. toe	Shallow longitudinal cracking; Cracks overlying contact between shells and core

Table 1 (cont.). Observed Seismic Deformation/Settlement in Earth Dams

EARTH DAM NAME	EARTHQUAKE NAME AND DATE	EQK. MAGNITUDE	EPICENTRAL DISTANCE	GROUND ACCELERATION (recorded/ estimated)	OBSERVED SEISMIC DEFORMATION/ SETTLEMENT
Coyote Lake Dam	Morgan Hill, CA 04/24/84	M: 6.2	NA	1.2g left abutment (rec.)	No deformation observed.
Makio Dam	Western Nagano, Japan 09/18/84	M: 6.8	NA	>0.4g (est.)	Vertical crest settlement ~ 0.5 m.
El Infiernillo Dam	Michoacan, Mexico 09/19/85	M: 8.1	70 km (43 miles)	0.13 bedrock (red.) 0.38g powerhouse	Vertical crest settlement ~ 0.1 - 0.2 m; Downstream horizontal displacement ~ 0.1 m.
La Villita Dam	Michoacan, Mexico 09/19/85	M: 8.1	58 km (36 miles)	0.12g bedrock (rec.) 0.79g crest	Upstream vertical crest settlement ~ 0.2 - 0.3 m; Downstream vertical crest settlement ~ 0.1 - 0.2 m; Upstream horizontal displacement ~ 0.15 m; Downstream horizontal displacement ~ 0.1 m.
La Villita Dam	S6, Mexico 09/21/85	M: 7.5	61 km (38 miles)	0.04g bedrock (rec.) 0.21g crest	Downstream horizontal displacement ~ 0.1 m.
Matahina Dam	Edgecumbe, New Zealand 03/02/87	M: 6.7	23 km (14 miles)	0.33g base (rec.) 0.48g mid-height (rec.) 0.42g crest (rec.)	Vertical crest settlement ~ 0.1 m Downstream horizontal displacement ~ 0.25 m
Anderson Dam	Loma Prieta, CA 10/17/89	M_S: 7.1	~26 km (~ 16 miles)	0.43g crest (rec.) 0.23 DS toe (rec.)	Longitudinal cracking; Vertical settlement of downstream crest edge ~ 4 mm; Vertical settlement of upstream crest edge ~ 10 - 15 mm; Shallow longitudinal cracks overlying contacts between shells and core.
Austrian Dam	Loma Prieta, CA 10/17/89	M_S: 7.1	12 km (7.5 miles)	0.55-0.6g (est.)	Longitudinal cracking; Settlement of downstream crest edge ~ 45 mm; Settlement of upstream crest edge ~ 10 - 15 mm; Shallow longitudinal cracks overlying contacts between shells and core; Downstream horizontal displacement ~ 0.3 - 0.5 m.
Chesbro Dam	Loma Prieta, CA 10/17/89	M_S: 7.1	21 km (13 miles)	0.4-0.45g (est.)	Longitudinal cracking; Minor transverse cracking; Vertical crest Settlement ~ 0.1 - 0.2 m; Upstream horizontal displacement ~ 15 mm.

Table 1 (cont.). Observed Seismic Deformation/Settlement in Earth Dams

EARTH DAM NAME	EARTHQUAKE NAME AND DATE	EQK. MAGNITUDE	EPICENTRAL DISTANCE	GROUND ACCELERATION (recorded/ estimated)	OBSERVED SEISMIC DEFORMATION/ SETTLEMENT
Guadalupe Dam	Loma Prieta, CA 10/17/89	M_S: 7.1	18.5 km (11.5 miles)	0.4-0.5g (est.)	Longitudinal cracking; minor transverse cracking; Vertical crest settlement ~ 0.15 - 0.2 m; Upstream horizontal displacement ~ 15 mm.
Hawkins Dam	Loma Prieta, CA 10/17/89	M_S: 7.1	~51.5 km (~32 miles)	0.2-0.25g (est.)	Minor longitudinal crest cracking; Minor cracking in upstream slope.
Lexington Dam	Loma Prieta, CA 10/17/89	M_S: 7.1	16 km (10 miles)	0.45g R crest (rec.) 0.39g L crest. (rec.)	Transverse cracking ~ 0.9 - 1.5 m deep; Minor longitudinal cracking; Vertical crest settlement ~ 0.25 - 0.3 m; Downstream horizontal displacement ~ 0.08 - 0.09 m.
Mill Creek Dam	Loma Prieta, CA 10/17/89	M_S: 7.1	~29 km (~18 miles)	0.25-0.3g (est.)	Minor crest cracking.
Newell Dam	Loma Prieta, CA 10/17/89	M_S: 7.1	20 km (12.5 miles)	0.4-0.45g (est.)	Longitudinal cracking width ~ 25 mm; Cracking probably due to settelement.
San Luis Dam	Loma Prieta, CA 10/17/89	M_S: 7.1	55 km (34 miles)	0.06 - 0.1g foundation (rec.) 0.14 - 0.25g crest (rec.)	No deformation observed.
San Justo Dam	Loma Prieta, CA 10/17/89	M_S: 7.1	25 km (15 miles)	0.16-0.26g foundation (rec.) 0.39-0.45g crest (rec.)	Longitudinal crest cracking; Vertical crest settlement ~ 30 -35 mm;
Soda Lake Dam	Loma Prieta, CA 10/17/89	M_S: 7.1	~27 km (~17 miles)	0.3-0.35g (est.)	Minor cracking at and below crest.
Vasona Percolation Dam	Loma Prieta, CA 10/17/89	M_S: 7.1	24 km (~15 miles)	0.35-0.4g (est.)	Longitudinal cracking; Vertical crest settlement ~ 45 - 50 mm; Downstream horizontal displacement ~ 25 - 30 mm.
Aya Dam	Philippines 07/16/ 90	M_L: 7.7	6 km (4 miles)	0.5 - 0.6g (est.)	Vertical crest settlement ~ 0.20 m.

Table 1 (cont.). Observed Seismic Deformation/Settlement in Earth Dams

EARTH DAM NAME	EARTHQUAKE NAME AND DATE	EQK. MAGNITUDE	EPICENTRAL DISTANCE	GROUND ACCELERATION (recorded/ estimated)	OBSERVED SEISMIC DEFORMATION/ SETTLEMENT
Canili Dam	Philippines 07/16/ 90	M_L: 7.7	18 kn (11 miles)	0.3 - 0.4g (est.)	Vertical crest settlement ~ 0.15 m.
Diayo Dam	Philippines 07/16/ 90	M_L: 7.7	18 kn (11 miles)	0.3 - 0.4g (est.)	Vertical crest settlement ~ 0.06 m.
Masiway Dam	Philippines 07/16/ 90	M_L: 7.7	3 km (1.9 miles)	0.6 - 0.7g (est.)	Vertical crest settlement ~ 0.9 - 1 m; Upstream horizontal displacement ~ 1. 8 m.
Pantabangan Dam	Philippines 07/16/ 90	M_L: 7.7	6 km (4 miles)	0.5 - 0.6g (est.)	Vertical crest settlement ~ 0.25 m.
Cogswell Dam	Glendale, CA 06/28/91	M: 5.8	4 km (2.5 miles)	0.33g abut. (rec.) 0.44 - 0.58g crest (rec.)	Vertical crest settlement ~ 40 mm; Downstream horizontal displacement ~ 10 - 12 mm.
Cogswell Dam	Northridge, CA 01/17/94	M_w: 6.7	50 km (31 miles)	0.1 - 0.15 g abut. (rec.) 0.3g crest (rec.)	No deformation observed.
Elderberry Dam	Northridge, CA 01/17/94	M_w: 6.7	40 km (25 miles)	0.35g abut. (rec.) 0.25 - 0.45 g crest (rec.)	No deformation observed.
Encino Dam	Northridge, CA 01/17/94	M_w: 6.7	NA	0.23g abut. (rec.)	No deformation observed.
Los Angeles Dam	Northridge, CA 01/17/94	M_w: 6.7	11 km (7 miles)	0.32 - 0.43g abut. (rec.) 0.3g foundation (rec.) 0.56g crest (rec.)	Vertical crest settlement ~ 0.09 - 0.1 m.
Santa Felicia Dam	Northridge, CA 01/17/94	M_w: 6.7	34 km (21 miles)	0.27g downstream (rec.) 0.3g crest (rec.)	Vertical crest settlement ~ 0.01-0.02 m.
Indian Creek Dam	South Lake Tahoe, CA 09/12/94	M:6.3	14 km (9 miles)	0.35g crest (rec.)	NA

Table 2. Background Information on Earth Dams Subjected to Seismic Deformation/Settlement

EARTH DAM NAME	STRUCTURE TYPE	STRUCTURE HEIGHT	FOUNDATION CONDITIONS	STRUCTURE FILL CHARACTERISTICS	REFERENCE NUMBER
Chabot Dam	compacted earthfill	41 m (135 ft)	Gravelly clay and bedrock	Sandy clays and clayey sand with gravel	29, 37, 47
Piedmont Dam	compacted earthfill	15.5 m (51 ft)	Sandy clay and clayey sand (very stiff)	Silty to clayey sand with sandstone fragments	1, 47
San Andreas Dam	compacted earthfill	29 m (95 ft)	Clays mixed with sand and gravel	Sandy clay and clayey sand	1, 47
Upper Crystal Springs Dam	compacted earthfill	23 m (75 ft)	Clays mixed with sand and gravel	Sandy clay and clayey sand	1, 47
Lower Mayurama Dam	compacted earthfill	31 m (101 ft)	Sand and gravel	Shear wave velocity crest: 114 m/s 50 ft below crest: 121 m/s	1, 30, 47
Ono Dam	compacted earthfill	38 m (124 ft)	Gneiss and schist	Shear wave velocity crest: 52 m/s 50 ft below crest: 88 m/s	1, 30, 47
Cogoti Dam	rockfill	84 m (275 ft)	Amorphous sedimentary rock	Dumped rockfill with concrete facing	1, 30, 47
Buena Vista Dam	compacted earthfill	6 m (20 ft)	Alluvium	NA	1, 30, 47
Dry Canyon Dam	semi-hydraulic fill	20 m (66 ft)	Soil	Sand and silty sand	1, 30, 47
South Haiwee Dam	semi-hydraulic fill	25 m (81 ft)	NA	Sand and clayey silt	1, 47
Coleman Dam	concrete earthfill	NA	NA	NA	1, 30
Eureka Dam	exc. between 2 embankments..	NA	Rock	NA	1, 30
St. Mary's Dam	compacted earthfill	17 m (55 ft)	Soil	NA	1, 30
Hebgen Lake Dam	compacted earthfill	26 m (87 ft)	Rock	Slightly cohesive well-graded sand and gravel	1, 21, 30, 38, 47

Table 2 (cont.). Background Information on Earth Dams Subjected to Seismic Deformation/Settlement

EARTH DAM NAME	STRUCTURE TYPE	STRUCTURE HEIGHT	FOUNDATION CONDITIONS	STRUCTURE FILL CHARACTERISTICS	REFERENCE NUMBER
Bellavista Dam	mine tailings dam	20 m (61 ft)	NA	NA	30
La Villita Dam	compacted earthfill /rockfill	61 m (200 ft)	Alluvium	Clay core with rockfill shells	17, 8, 29, 35, 58
El Infiernillo Dam	rockfill	146 m (479 ft)	Gneiss or schist	NA	17, 29, 30, 35
Long Valley Dam	compacted earthfill	55 m (180 ft)	NA.	NA	29
Vermillion	compacted earthfill	50 m (165 ft)	NA	NA	29
Anderson Dam	earth and rockfill	73 m (240 ft)	Alluvium	Clayey sand core, rockfill shells	48
Coyote Lake Dam	rockfill	37 m (121 ft)	NA	NA	43
Makio Dam	rockfill	105 m (346 ft)	NA	NA	43
Matahina Dam	earth and rockfill	85 m (280 ft)	NA	Core: greywacke Shells: ignimbrite	29
Austrian Dam	compacted earthfill	56 m (185 ft)	NA	Clayey, sandy gravel	23, 48
Chesbro Dam	compacted earthfill	24 m (79 ft)	NA	Homogeneous fill	23, 48
Guadalupe Dam	compacted earthfill	43 m (142 ft)	NA	NA	23, 48
Lexington Dam	compacted earthfill	61 m (200 ft)	NA	Sandy clay core, clayey sand and silt shells	23, 48
Hawkins Dam	hydraulic fill	22 m (72 ft	NA	Gravel-sand-clay fill	23
Mill Creek Dam	hydraulic fill	23 m (76 ft)	NA	NA	23
Newell Dam	earth and rockfill	55 m (182 ft)	NA	Clay core and rockfill shells	23, 48

Table 2 (cont.). Background Information on Earth Dams Subjected to Seismic Deformation/Settlement

EARTH DAM NAME	STRUCTURE TYPE	STRUCTURE HEIGHT	FOUNDATION CONDITIONS	STRUCTURE FILL CHARACTERISTICS	REFERENCE NUMBER
San Luis Dam	compacted earthfill	116 m (380 ft)	Alluvium and rock	NA	23, 29
San Justo Dam	compacted earthfill	46 m (150 ft)	NA	NA	29
Soda Lake Dam	compacted earthfill	10.5 m (35 ft)	NA	NA	23
Vasona Percolation Dam	compacted earthfill	10 m (34 ft)	NA	Upstream compacted fine-grained, downstream compacted coarse-grained	23
Aya Dam	compacted earthfill	102 m (335 ft)	NA	NA	29
Canili Dam	compacted earthfill	70 m (230 ft)	NA	NA	29
Diayo Dam	compacted earthfill	60 m (197 ft)	NA	NA	29
Masiway Dam	compacted earthfill	25 m (82 ft)	NA	NA	29
Pantabangan Dam	compacted earthfill	107 m (350 ft)	NA	NA	29
Cogswell Dam	rockfill	81 m (266 ft)	NA	NA	29
Elderberry Dam	compacted earthfill	55 m (180 ft)	NA	NA	29
Encino Dam	compacted earthfill	52 m (170 ft)	NA	NA	29
Los Angeles Dam	compacted earthfill	39 m (130 ft)	NA	NA	29
Santa Felicia Dam	compacted earthfill	64 m (210 ft)	NA	NA	29
Indian Creek Dam	compacted earthfill	21 m (70 ft)	NA	NA	29

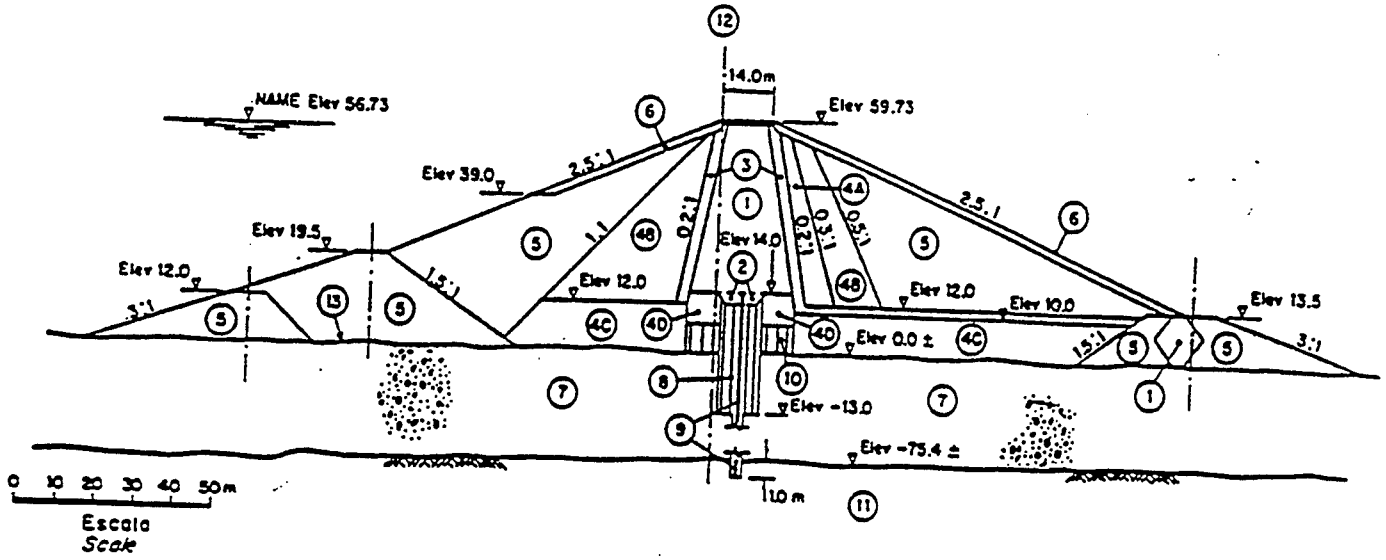

1. Compacted impervious material
2. Highly plastic clay
3. Sand filters
4A. Well graded gravel and sand
4B. Gravel and sand
4C. Dumped gravel and sand
4D. Compacted gravel, sand and muck
5. Rockfill
6. Selected rockfill
7. Alluvium (gravel and sand)
8. Grout curtain
9. ICOS-type concrete cut-off wall
10. Consolidation grouting
11. Andesitic breccia
12. Dam axis
13. Original ground surface

Elev Elevation, in m

NAME Maximum water level

Figure 1 Maximum cross-section through La Villita Dam (from Elgammal et al. 1990)

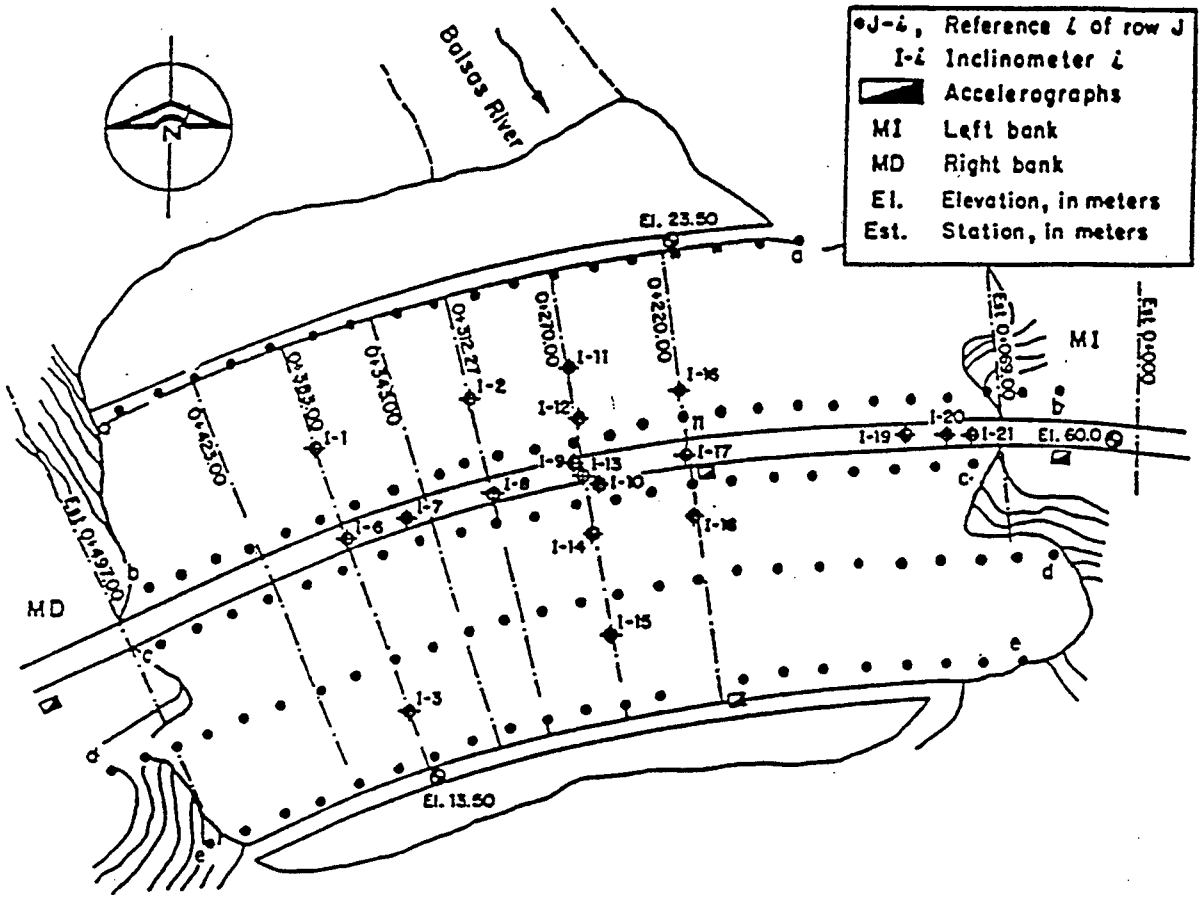

Figure 2. Location of accelerographs, inclinometers, and surface reference points in La Villita Dam (from Elgammal et al. 1990)

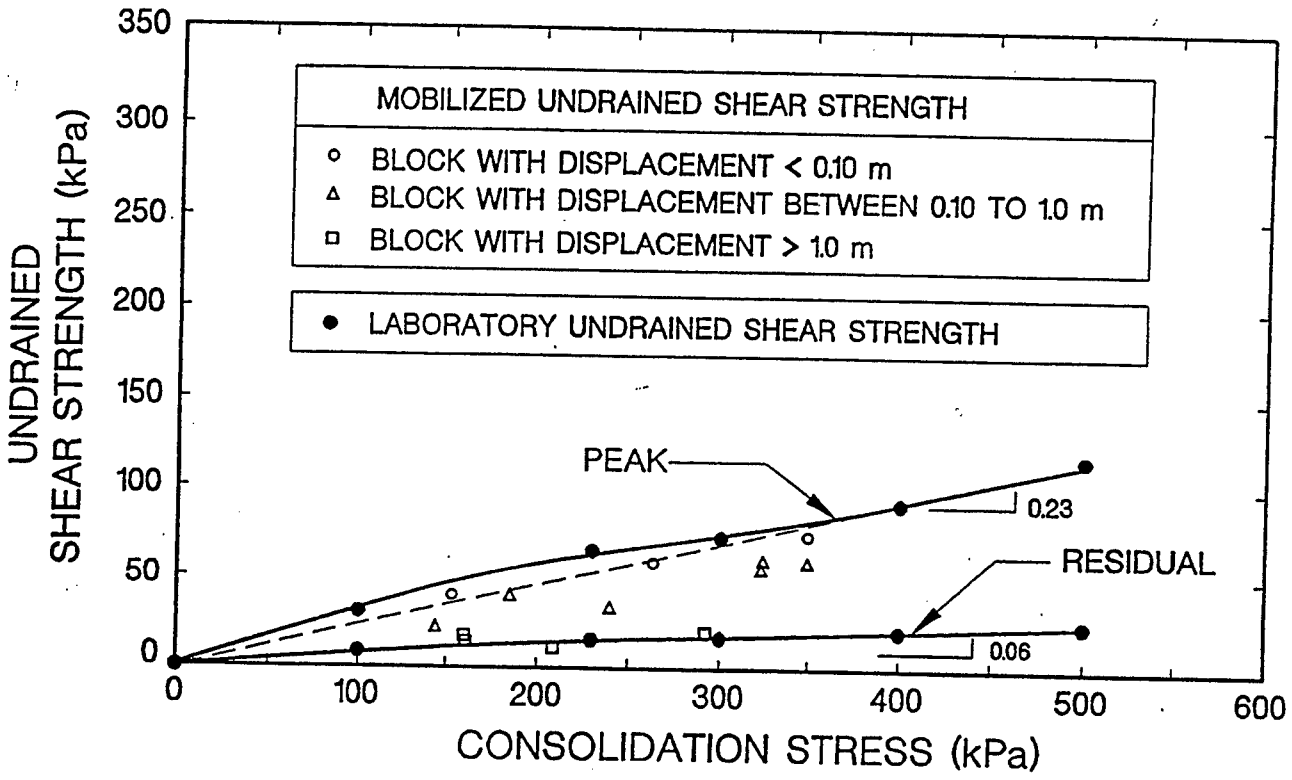

Figure 3. Comparison Between Laboratory and Back-Calculated Undrained Shear Strength for Bootlegger Cove Clay

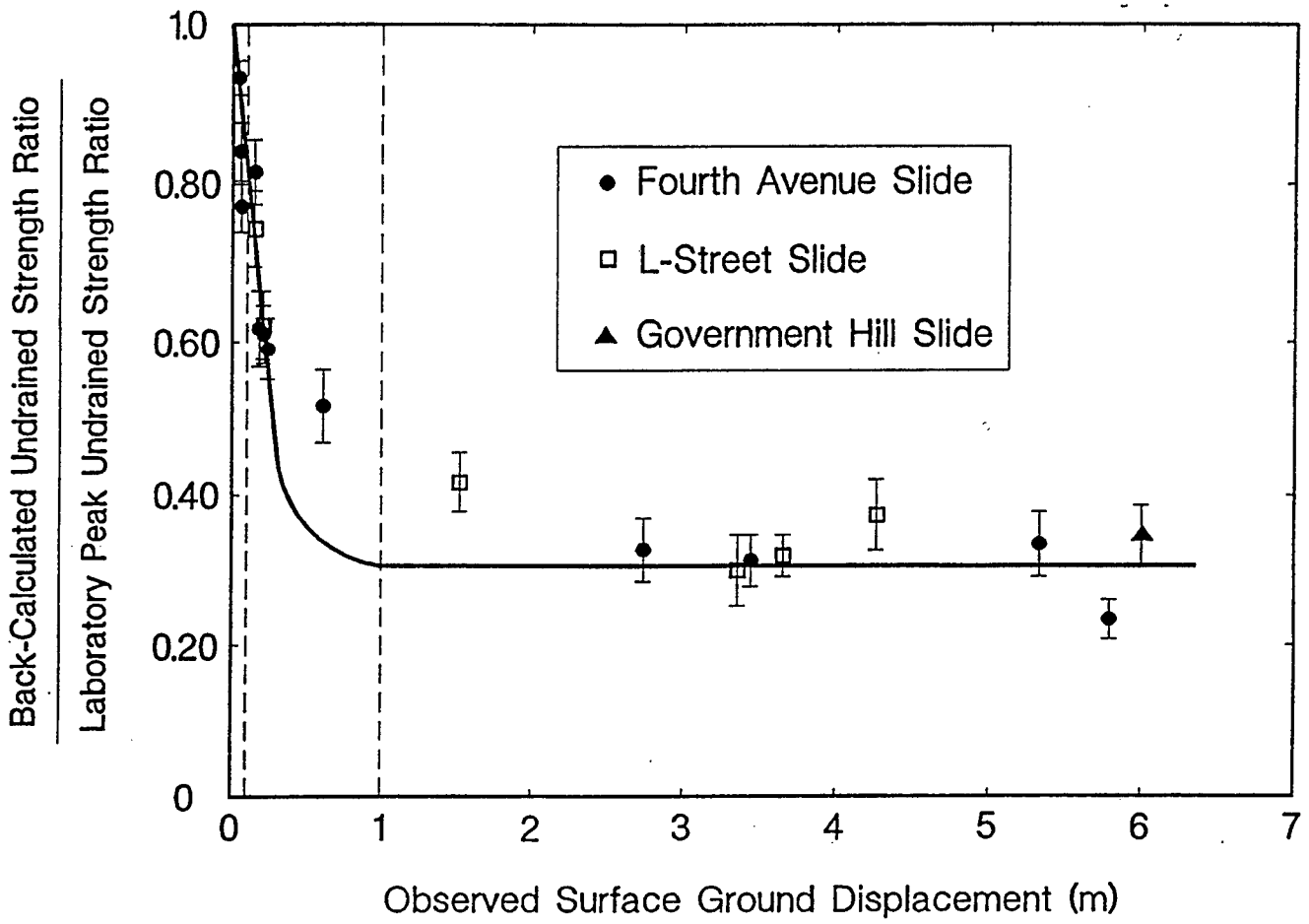

Figure 4. Percentage of undrained strength ratio mobilized with surface ground displacement (from Stark and Contreras 1996a)

BEHAVIOR OF LIQUEFYING SOILS
Research Work Unit

by

Richard H. Ledbetter*

ABSTRACT

Current studies have shown limitations in the state-of-practice involving the in-depth evaluation of liquefaction and for dam seismic remediation design and analysis. The state-of-practice can be forcing us to make possibly unnecessary excessive and costly seismic remediations or unsafe conclusions. We do not have enough information for the sites that form the earthquake response data base and the empirical basis for analysis. Improved definition and physical evidence is needed of the processes and mechanisms involved as a soil progresses to liquefaction and residual strength to allow refined analyses for dam safety and more cost-effective and safe remediation design and analysis. Reliable physical evidence and the reality-checks of analyses must come from field or equivalent-field data of behavior under well known and defined conditions. This paper presents the research plan to use centrifuge testing to get equivalent prototype behavior under dynamic loading. The research is part of the ongoing U.S. Army Engineer Earthquake Engineering Research Program (EQEN) at the U.S. Army Engineer Waterways Experiment Station (WES). The unique WES research centrifuge will be used for tests with dynamic base shaking.

1 INTRODUCTION

This paper will present the brief background and the problem, objective and description of work for the EQEN investigation of the behavior of liquefying soil materials. The state-of-practice assumptions concerning the occurrence and behavior of liquefied soil, residual strength behavior, and dam stability and deformations are not valid as shown by field behavior, numerical analyses and physical model test results. Our objectives are to improve the simplified liquefaction methodology correction factors, define the complete shear stress-strain curve for earthquake loading, define better the behavior of liquefying soil and effects on dam behavior, expand our case history data base with better known conditions and responses, and provide progressive results for immediate use in Corps projects. The approach of this research to investigate the behavior of liquefying soils is to use laboratory testing, analytical procedures and centrifuge dynamic testing.

2 ENGINEERING PROBLEM

2.1 Current state-of-practice

The present state-of-practice for determining the performance of soils that undergo earthquake-induced shear-strain and consequently pore water pressure buildup in saturated soils is to determine if a soil will or will not liquefy. The performance and safety of structures are based on rigid sliding-block/slices limit-equilibrium methods to determine slip-plane stability and deformation

* Earthquake Engineering & Seismology Branch, and Director Centrifuge Research Center, Geotechnical Laboratory,
USAE Waterways Experiment Station,
Vicksburg, MS 39180-6199

using residual strengths in the case of liquefaction.

In-situ methods such as Standard Penetration Test (SPT), Cone Penetration Test and shear wave velocity measurements are used to define the triggering of liquefaction. The potential for liquefaction relies on empirical correlations between the penetration resistance and the performance of soil deposits in past earthquakes (Seed, 1979). The database on triggering liquefaction is based on data from level ground where surface evidence occurred. Soil conditions were shallow at overburden pressures less than about 95.8 kPa (about 4.6m of depth). The data base is normalized to an earthquake of magnitude 7.5. Corrections for other earthquake magnitudes have to be made (Seed & Harder, 1990, NCEER, 1996).

To extend the database to depths representative of foundation soils under dams requires the use of correction factors (Seed & Harder, 1990) for the effects of overburden pressure and initial static shear-stress. Correction for high overburden, $K\sigma$, is based on laboratory test results of the ratio of cyclic-shear-stress, CSS, to cause liquefaction at an overburden effective-stress state, σ'_o, to that at a σ'_o = 95.8 kPa. Correction for initial static shear-stress, $K\alpha$, is based on the ratio of CSS to cause liquefaction with initial static shear-stress applied to that at no initial static shear-stress.

A factor of safety, FSL, against the occurrence of liquefaction, defined as 100 percent pore water pressure, can be calculated as:

$$FSL = f[(N_1)_{60}]Km\ K\sigma\ K\alpha/\tau eq$$

Where $(N_1)_{60}$ is from SPT relations, Km is earthquake magnitude or duration correction factor and τeq is a percentage of peak earthquake induced shear stress.

The FSL can be related to percent excess pore water pressure.

The correction factor $K\sigma$ has a large influence for dam foundations. It reduces the CSS to cause liquefaction to about 45 percent of its in-situ value at pressures about 670 kPa that would exist beneath an embankment dam about 30.5m high. Alternatively, if we were deriving SPT criteria for remedial treatment of this dam to limit the potential level of earthquake generated pore water pressures, the $K\sigma$ factor would cause an increase of more than double in the required penetration values to be measured in the field. Clearly, the correction factor can have a major impact on the potential for triggering liquefaction or the excess residual pore water pressures and on the cost of remediation.

The correction factor $K\alpha$ can also contribute significantly to the reduction of the in-situ strength. However, for relative densities above 45-50 percent, $K\alpha$ can have a positive effect on the in-situ strength. The $K\alpha$ relationships are not well defined.

In application of the state-of-practice, we inherently make the following assumptions: (1) the soil is always undrained, (2) liquefaction occurs instantaneously and the soil shear strength jumps to residual state, (3) residual strength is constant with monotonic loading, (4) liquefaction is independent of soil zone thickness, permeability, or boundary conditions, (5) liquefaction is independent of when the earthquake peak energy arrives, (6) behavior of the liquefied soil and its resultant

effects on a dam are independent of the soil zone thickness, permeability, and boundary conditions, (7) dam stability and deformation are controlled by slip-planes independent of the liquefied soil zone thickness and behavior, and (8) non-liquefied soil at a site is unaffected by the earthquake. Field behavior, numerical analyses, and physical model tests show that these assumptions are invalid.

2.2 Research problem

Current studies for more thorough evaluation of liquefaction and for remediation design and analysis have shown serious limitations in the state-of-practice. The state-of-practice can force us to make costly excessive remediations when possibly no action is required, but it can also lead us to make unsafe conclusions in other cases.

Significant progress is being made in the development of numerical methods for analysis of liquefaction and the consequences. However, the engineering profession will most likely always use empirical correlations (Seed's or others) of in-situ measurements versus potential liquefaction, pore water pressure generation and earthquake response. Every time a site is evaluated for a seismic design or potentially liquefiable soil is improved and a dam remediated, in-situ measurements will be made. A value/range of in-situ measurement to achieve will be specified for a construction/remediation contractor. Some in-situ measure will be used to judge soil conditions/improvement and seismic safety of a dam or site. Therefore, improvement in our current state-of-practice and the empirical correlations between in-situ measures and performance of soil deposits has to be made.

Current studies of the seismically-induced deformation behavior of dams indicate that as soils are progressing toward liquefaction (pore water pressure is increasing and shear strain is occurring) significant deformations of the structure can occur. Failure (damaging levels of deformation) can develop significantly before the complete initial liquefaction stage (100 percent pore water pressure ratio) is reached. Depending on specific conditions involving the location, depth and extent of liquefying soil and the driving forces, a structure may fail at only 50 percent strength reduction. In this case, remediation to assure safe performance is required to prevent serious damage significantly before an initial liquefaction condition and a residual strength stage are arrived at in the soil.

The problems in the current state-of-practice stem mainly from the fact that we do not know for the sites that have liquefied and constitute the empirical basis for analysis: (1) the exact and complete soil conditions and profiles, (2) the real behavior that occurred in the soils during and after the earthquakes or the various influences on the behavior, (3) that the assumed non-liquefied soils (used in comparison to liquefied soils) did not develop pore pressures or strains and change state during the earthquakes, and (4) whether artificial and possibly incorrect conditions in laboratory testing may have led to conclusions not totally applicable to the field behavior.

Improved definition and physical evidence is needed of the processes and mechanisms involved within the continuum as a soil progresses to liquefaction and residual strength. This is needed to allow refined analyses for dam safety and more cost-effective and safe remediation design and analysis. Because we can make various assumptions coupled with

methodologies and numerical analyses that can give solutions or answers to most anything, the reality-check of solutions must come from field or equivalent-field data of behavior under well known and defined conditions.

The earthquake response database needs to be expanded with more complete data to provide: (1) the necessary advance in the state-of-practice, (2) a basis for modification and improvement of current methodology and assumptions, and (3) definition of the physical processes and mechanisms involved in the liquefaction process and resultant effects on dam behavior. This would also provide the fundamentals and basis for development of new methodology and analyses. New methodologies have to be based on correct mechanisms and processes.

Current specific needs for more thorough earthquake engineering analyses can be identified from examination of the last two decades of experience in seismic evaluation of embankment dams and the serious limitations that arise when remediation design is attempted. Studies involving liquefaction, stability, and seismic-induced deformation behavior of dams raise serious questions that impact the safe performance and needs for remediation (e.g., Ledbetter and Finn, 1993, Ledbetter, er. al., 1994, Finn and Ledbetter, 1991, Finn, et. al., 1991 and 1994, Vaid and Chern, 1985, Vaid and Thomas, 1994, Bryne and Harder, 1991). For example, Vaid and Thomas (1994) demonstrated that $K\sigma$ for specific sand types can be substantially less (more than a factor of 2) than suggested by Seed and Harder. Pillai and Byrne (1994) showed for the foundation materials of Duncan Dam, a $K\sigma$ of 0.6 compared with 0.4 from the Seed and Harder relation. This made a difference between recommending remediation and no remediation. Figure 1 presents a summary of $K\sigma$ relations by various researchers. The spread of data is obvious and can influence whether to remediate a dam at costs in the tens of million's of dollars or not remediate.

For the past thirty years, research has primarily concentrated on the triggering of liquefaction of soils both in the laboratory and in field sites. A significant data base has resulted of very important and necessary information concerning the stress-state triggering of liquefaction, cyclic load stress-ratio and the dynamic properties of soils. Newmark, 1965, stressed that what counted was whether the deformations that a dam suffered during an earthquake were tolerable or not. Peck, 1992, stated that of all measures of safety, the most directly applicable results are the anticipated deformations.

Due to the lack of knowledge and experience involving the behavior of liquefiable soils under field conditions, we are forced to make, for the critical safety of dams, simplifying assumptions concerning behavior. We are forced to disregard possible significant controlling influences such as permeability, boundary layers and pore water pressure dissipation and migration.

Some specific needs are: (1) well defined and complete shear stress-strain response curves for earthquake loading including the residual strength portion, (2) strains within a problem soil mass, (3) effects of soil zone thickness, permeability, and boundary conditions, (4) influence of adjacent soil materials and of their permeabilities, (5) dissipation and movement of excess residual pore pressure both during and after an earthquake, (6) redistribution of

stresses as a soil is losing strength, (7) interaction of remediation materials and adjacent soil, (8) dynamic response of remediation materials and of remediated zones, (9) improved Kσ and Kα factors for the field evaluation of remediation achievement and for improved first estimates of liquefaction potential, (10) effects of strong aftershocks and (11) dam internal behavior and failure mechanisms in response to earthquake loading and strength degradation.

3 RESEARCH OBJECTIVES

The objectives of this research are:

a. Define more completely and improve the Kσ and Kα correction factors.

b. Define the complete shear stress-strain curve for earthquake loading and simplified methods for obtaining it.

c. Define the behavior of liquefying soils and affects on dam behavior:

(1) Strain, deformation, softening.

(2) Importance of permeability.

(3) Boundary condition importance and effects.

(4) Layer thickness importance and effects.

(5) Behavior before initial liquefaction occurs.

(6) Post earthquake behavior.

d. Significantly expand and enhance our earthquake case history data base with more completely known and defined conditions and earthquake responses.

e. Provide progressive results for immediate use in Corps projects.

4 DESCRIPTION OF RESEARCH

Accomplish the objectives by conducting investigations employing laboratory testing, analytical procedures, and centrifuge testing. Soil behaves non-linearly and is stress-state dependent. Centrifuge testing is the best, most practical, most economical, and the only method for properly investigating and verifying earthquake induced prototype behavior in soil.

The WES has a large and exceptionally powerful (1,144,000 g-kg) research centrifuge; 6.5m radius, maximum payload of 8000 kg to 143 g decreasing to 2000 kg at 350 g. The uniquely large shaker designed to be capable of exciting dynamic motions up to 200+ g will be used with the equivalent shear beam box in this research.

Centrifuge testing will be used to produce prototype response under laboratory conditions and with measured base shaking input motions and propagation. From the tests, it is planned to: (1) obtain high-quality detail and data for earthquake behavior case histories, (2) investigate the Kσ and Kα correction factors under dynamic loading by shaking of the continuum rather than by laboratory element tests, (3) measure and investigate pore pressure behavior and response under various conditions during and after earthquakes, (4) measure and investigate strain, deformation, and softening behavior during and after earthquakes, (5) measure and investigate the controlling effects of permeability on pore pressure behavior during and after earthquakes, and (6) measure and investigate the effects of boundary conditions on the behavior of liquefying soil.

Each centrifuge test will yield results relevant to several of the objectives in defining the behavior of liquefying soils and effects on dam response.

Laboratory testing will be used to: (1) develop and define the complete shear stress-strain curve for earthquake-induced liquefying soil behavior including the residual portion and the development of simplified methods for obtaining the curve, (2) determine the properties of soils used in the centrifuge dynamic tests for both pre and post test conditions, (3) determine the complete shear stress-strain curve for the soils used in the centrifuge dynamic tests and (4) conduct cyclic tests for the laboratory-based determination of $K\sigma$ and $K\alpha$ for comparison to the centrifuge dynamic test results.

Analytical procedures employing both numerical dynamic-analysis and conventional static-analysis methods will be used for: (1) analysis of the centrifuge results as an equivalent prototype and as a bridge between the results and existing field case history data, (2) identification of anticipated important parameters and sensitivities for consideration in the centrifuge dynamic tests, (3) careful design of centrifuge dynamic tests to maximize the results and to obtain results from each test that are applicable to several of the objectives, (4) analyses of pre, during and post dynamic test conditions, (5) extrapolation and comparison of centrifuge test results to limit the number and extent of needed tests and (6) important assistance in the necessary understanding and definition of the physics of the mechanisms and processes being investigated.

Results from the work of other researchers studying residual strength, causes of liquefaction and flow of liquefied soil will be incorporated and collaboration will be made. However, this study is unique in that it addresses the fundamental effective-stress behavior and mechanisms of soil as it is in the process of liquefying and not just the end point of a liquefied state. The entire process of liquefaction and the controlling conditions are key to eventual accurate predictions of anticipated deformations; how much and where.

4.1 Centrifuge test plans

The first tests and studies will be concerned with evaluating $K\sigma$ in centrifuge tests of the behavior of level ground for comparison with laboratory values. Two soils, Ottawa and Nevada sand, and a mixture with silts will be used for the tests. Both of these soils are well known with extensive laboratory investigations. Another soil or mixture with silt will be used for low permeability and will be placed at a non-liquefiable density to bound/confine liquefiable test soil layers. It will also be used to provide a deep foundation layer beneath the liquefiable soil and a transition from the rigid base through which the input motion propagates to the test layers.

At least three test layer depths and possibly five will be used for each soil at three relative densities and at prototype overburdens of 95.8 to 575 kPa. Figure 2 shows the model test plan cross-section at prototype scale.

Pore pressure and acceleration transducers placed redundantly and about every 1.5 m of prototype depth will be used to measure test behavior. $K\sigma$ can be calculated for each layer in ratio to the top layer at 95.8 kPa. Several dynamic excitations will be used during each test period to determine the effects of dynamic

excitation history and previous liquefaction on soil and Kσ behavior.

Following the Kσ test program, a centrifuge test program will be developed for Kα behavior similar to the Kσ test program. The tests will be conducted with embankment dam loading to induce initial static shear stresses in the foundation layers.

Test programs will also be conducted in similar fashion to get equivalent prototype data addressing the influences of permeability, boundary conditions and layer thickness and liquefiable soil zone thickness on the behavior of liquefying soil. This will yield significant effects on dam response both external and internal; strains, softening, response during and post earthquake, global behavior and failure modes. The detailed design of this program of tests will follow completion of the Kα experiments.

5 ISSUES FOR DEBATE / DISCUSSION

Issues for debate and discussion include the following:

- Construction techniques and effects on Kσ and Kα.
- Density change monitoring.
- In-situ properties and conditions before during and after dynamic excitation.
- Undisturbed sampling for laboratory testing.
- Load tests after liquefaction/high-pore-pressure occurrence to induce failure planes/zones to get data on residual strength.
- Effects of dynamic excitation history and aftershocks on liquefaction and Kσ and Kα.
- Effects of stress history and previous higher stress states on Kσ and Kα by increasing centrifuge acceleration above the test level, allowing equilibrium conditions to occur and then decreasing to the test acceleration and testing.
- Flushing of fluid upward through the test layers to fluidize the soil and erase the existing stress states and histories including the construction history. Allow the soil layers to redeposit and conduct dynamic excitation to determine the effects on Kσ and Kα.

6 CONCLUSIONS

The research described in this paper will provide definition and clarification of the Kσ and Kα correction factors for use in the evaluation of dam remediation and in the initial determination of liquefaction potential. The results of this program will enhance significantly our understanding of dam response and our capability to determine and define liquefaction occurrence, its potential to cause damage, and the need for mitigation. Economic benefits will result in improved analysis, design, and remediation requirements. The threat of liquefaction will be lessened through better understanding of the process and conditions for earthquake induced strength loss and liquefaction. Significant enhancement of the data base of earthquake response will be made which will provide; (1) modification and improvement of current methodology and assumptions, and (2) definition of processes

and mechanisms for development of new analysis methodology.

7 REFERENCES

1 Byrne, P. M. And Harder, L. F. (1991). Terzaghi Dam, Review of Deficiency Investigation, Report No. 3, prepared for B C Hydro, Vancouver, British Columbia.

2 Finn, W. D. Liam and Ledbetter, R. H. (1991). Evaluation of Liquefaction Effects and Remediation Strategies by Deformation Analysis, *Proceedings, International Conference on Geotechnical Engineering for Coastal Development, GEOCOAST 91,* Yokohama, Japan.

3 Finn, W. D. Liam, Ledbetter, R. H., Fleming, R. L., Jr., Templeton, A. E., Forrest, T. W., and Stacy, S. T. (1991). Dam on Liquefiable Foundation: Safety Assessment and Remediation, *17th Congress on Large Dams, International Commission on Large Dams,* Vienna, Austria.

4 Finn, W. D. Liam, Ledbetter, R. H., and Marcuson, W. F., III, (1994). Seismic Deformations in Embankments and Slopes, *Proceedings, Symposium on Developments in Geotechnical Engineering (From Harvard to New Delhi, 1936 - 1994),* Bangkok, Thailand.

5 Ledbetter, R. H. and Finn, W. D. Liam (1993). Development and Evaluation of Remediation Strategies by Deformation Analysis, *Proceedings of the specialty conference Geotechnical Practice in Dam Rehabilitation,* Raleigh, North Carolina, Geotechnical Special Publication No. 35.

6 Ledbetter, R. H., Finn, W. D. Liam, Hynes, M. E., Nickell, J. S., Allen, M. G., and Stevens, M. G. (1994). Seismic Safety Improvement of Mormon Island Auxiliary Dam, *18th Congress on Large Dams, International Commission on Large Dams,* Durban, South Africa.

7 National Center for Earthquake Engineering Research (NCEER), (1996). Workshop on Evaluation of Liquefaction Resistance, Salt Lake City, Utah.

8 Newmark, N. M., (1965). Effects of Earthquakes on Dams and Embankments, *5th Rankine Lecture, Geotechnique,* Vol. 15, No. 2.

9 Olsen, R. S. (1996). The Influence of Confining Stress on Liquefaction Resistance, *Draft WES Report.*

10 Peck, R. B., (1992). Written comments on the review of remediation for Mormon Island Auxiliary Dam.

11 Pillai, V. S. and Byrne, P. M., (1994). Effect of Overburden Pressure on Liquefaction Resistance of Sand, *Canadian Geotechnical Journal,* Vol. 31.

12 Seed, H. B., (1979). Considerations in the Earthquake-Resistant Design of Earth and Rockfill Dams, *19th Rankine Lecture, Geotechnique,* Vol. 29, No. 3.

13 Seed, R. B. and Harder, L. F., (1990). SPT-Based Analysis of Cyclic Pore Pressure Generation and Undrained Residual Strength, *Proceedings of the H. Bolton Seed Memorial Symposium,* University of California, Berkeley, Vol. 2.

14 Vaid, Y. P. and Chern, J. C., (1985). Cyclic and Monotonic Undrained Response of Saturated Sands, *Advances in the Art of Testing*

Soils under Cyclic Conditions, ASCE Convention, Detroit.

15 Vaid, Y. P. and Thomas, J., (1994). Post Liquefaction Behavior of Sand, *Proceedings of the 13th International Conference on Soil Mechanics and Foundation Engineering,* New Delhi, India.

16 Zing, X. and Schofield, A. N., (1996). Design and Performance of an Equivalent-Shear-Beam Container for Earthquake Centrifuge Modelling, *Geotechnique,* Vol. 46, No. 1.

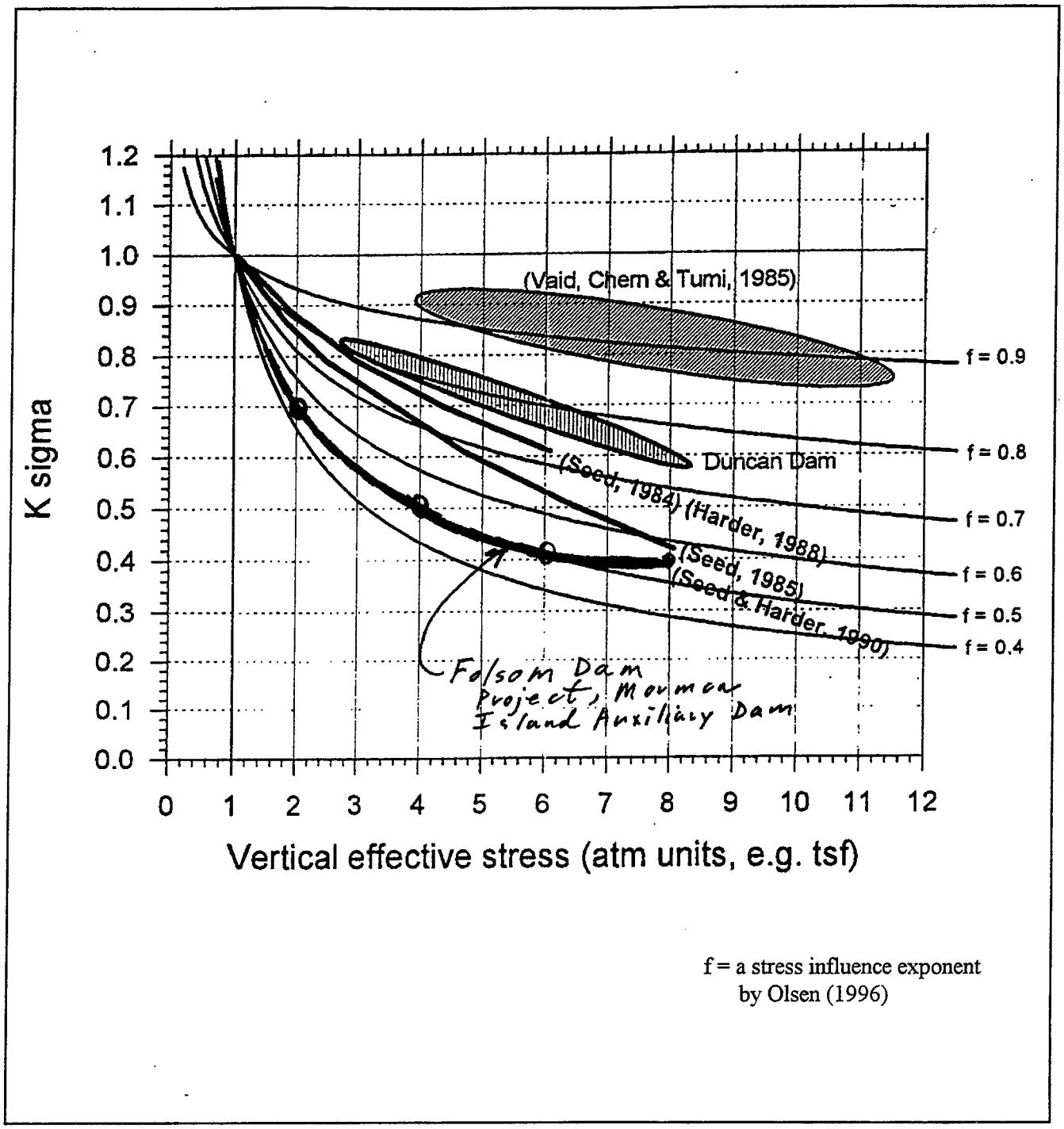

Figure 1. Summary of Kσ relations by various researchers; base figure from Olsen (1996).

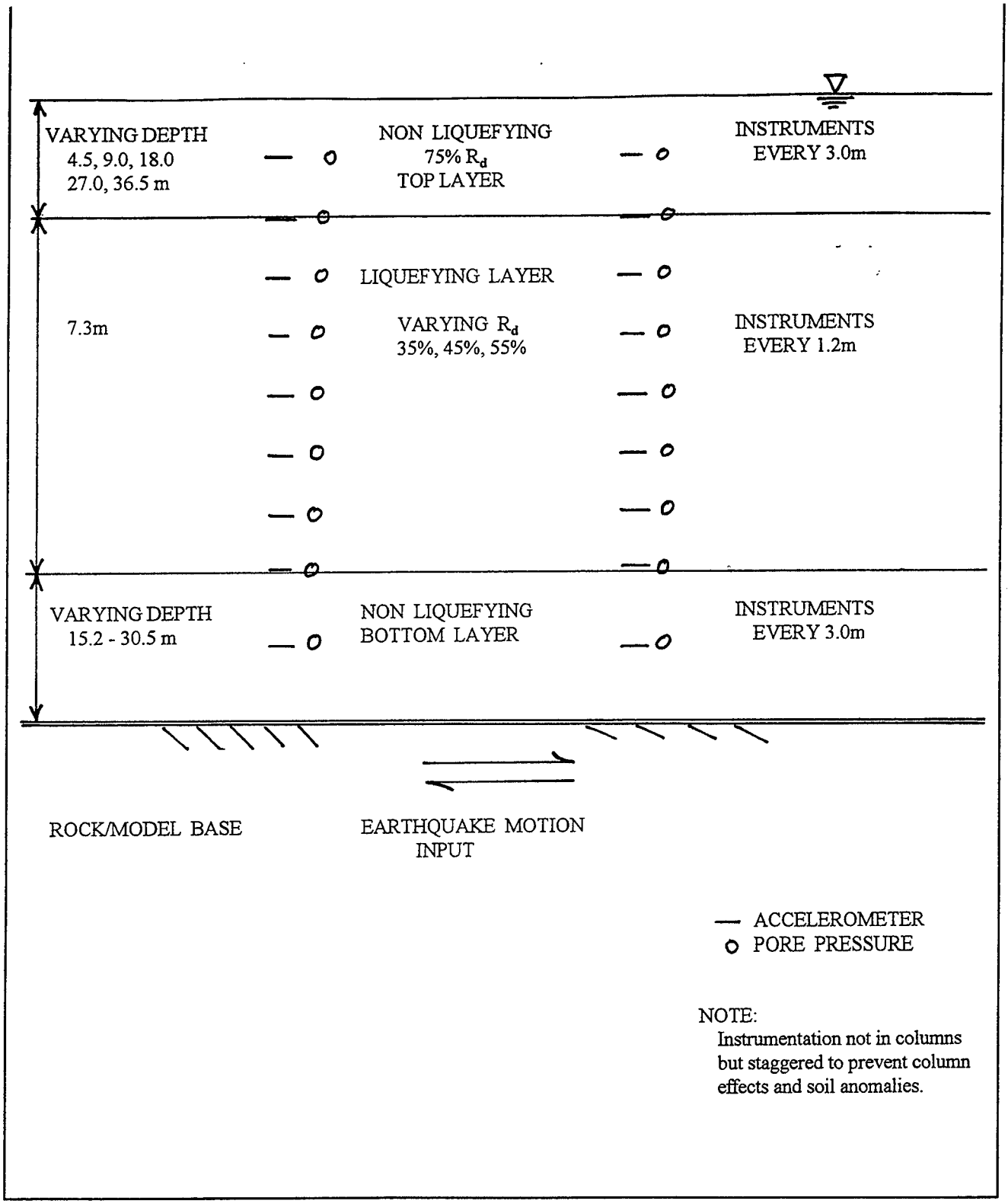

Figure 2. Centrifuge model test plan for Kσ investigations; prototype scale.

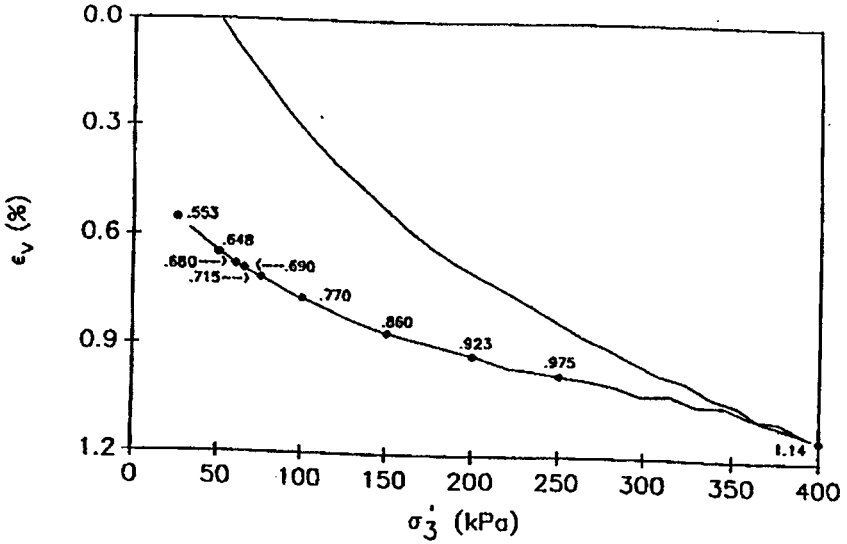

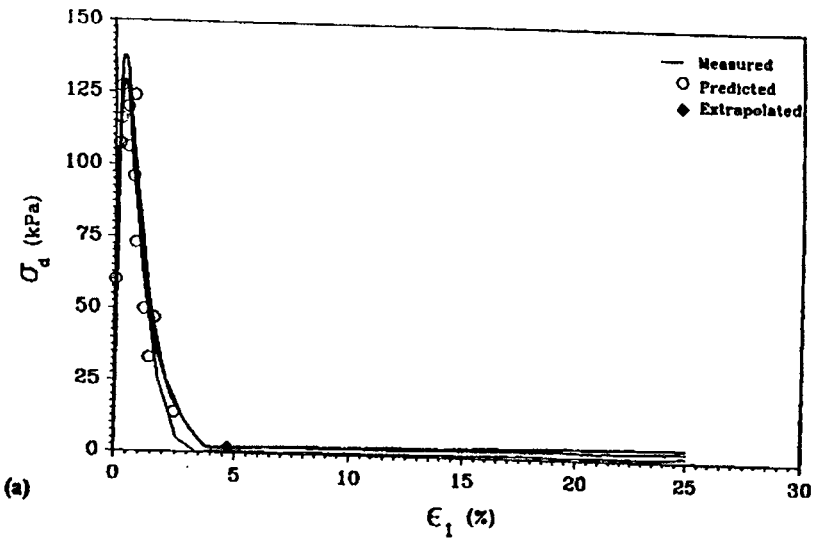

Figure 3. Isotropic consolidation and rebound response, Nevada loose sand.

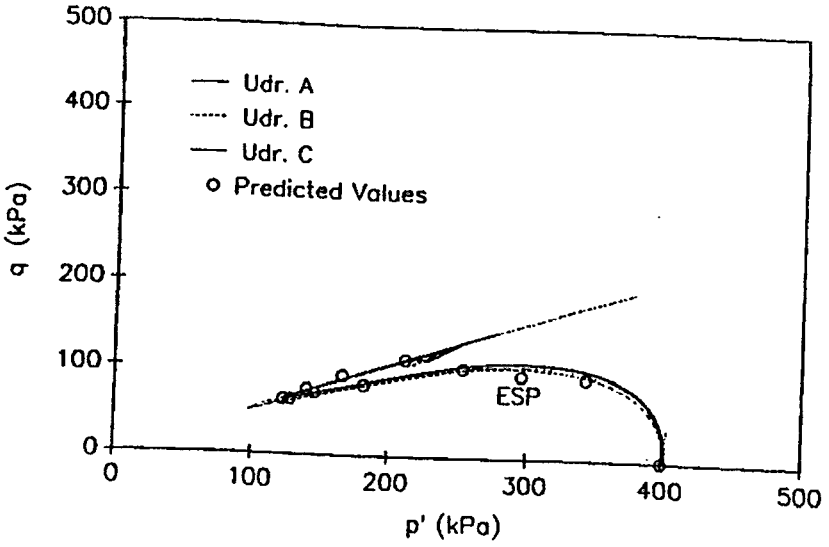

Figure 4. Undrained effective stress paths, Nevada loose sand.

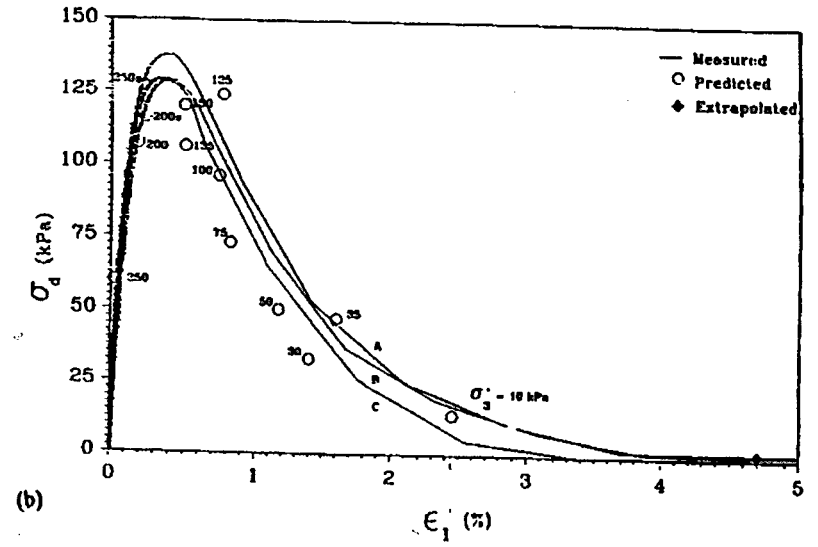

Figure 5. Undrained stress-strain response, Nevada very loose sand σ_{3c} = 400 kPa: (a) ϵ_1 to 25 % and (b) ϵ_1 to 3%.

Evaluation of Shear Strength of Rockfill Materials Considering the Effect of Confining Pressure

by

Hitoshi YOSHIDA[1], Mitsuo TOYODA[2] and Yoshikazu YAMAGUCHI[3]

ABSTRACT

The shear strength of rockfill materials is one of the most important design values in examining the stability of rockfill dams. In Japan, it is generally evaluated using large-scale triaxial compression tests. We conducted systematic experiments to evaluate the shear strength of rockfill materials considering the effect of confining pressure.

Key Words: *Rockfill Dam, Rockfill Material, Triaxial Compression Test, Confining Pressure.*

1. INTRODUCTION

When examining the stability of rockfill dams, the shear strength of rockfill materials, which constitute approximately 80% volume of the dams, is one of the most important design values. In Japan, the sliding surface method is applied for examining the stability of rockfill dams, and seismic forces acting on the potential sliding mass are determined by the static method assuming a seismic coefficient, according to the Cabinet Order Concerning Structural Standards for River Administration Facilities, etc. (Japanese Government, 1976). The seismic coefficient is assumed to be the same from the bottom to the crest. Besides the shear strength of rockfill materials is evaluated mainly by triaxial compression tests using specimens with a diameter of 30 cm and a height of 60 cm. The test results obtained under several lateral pressures are analyzed according to Mohr-Coulomb's failure criterion, then the design shear strength is evaluated using the internal friction angle with fixing the apparent cohesion at zero. It has not been any serious damage that affects to the safety of rockfill dams designed by the pseudo-static method combining the constant seismic coefficient and the design shear strength stated above.

However, judging from the observations of behavior of rockfill dams during earthquakes, the top part of a dam vibrates exceedingly compared to the bottom part. Therefore, it is thought reasonable to take the design seismic coefficient at the larger value for the higher part of a dam. In addition, many results of triaxial compression tests for rock materials recommended that the shear strength should be evaluated as a function of the internal friction angle and confining pressure. In consideration of these conditions, "Seismic Design Standard for Embankment Dams (Draft)" (River Bureau, Ministry of Construction, 1991) was proposed in June 1991, as the new design guideline for rockfill dams in Japan. The design method according to this standard is called as the modified

1) Head, Fill Dam Division, Public Works Research Institute, Tsukuba, Japan
2) Senior Research Engineer, ditto
3) Dr. Eng., Senior Research Engineer, ditto

pseudo-static method. But the conventional design method, that is, the pseudo-static method is still effective.

We conducted systematic experiments to evaluate the shear strength of rockfill materials considering the effect of confining pressure, and our research results played an important role in establishing the new standard. In this paper, this research work will be discussed.

2. PREVIOUS RESEARCH WORKS

Marsal (1965) used large-size specimens with a diameter of 113 cm and a height of 250 cm composed of the coarse grained materials with a maximum grain size of about 200 mm, and performed a series of triaxial compression tests under lateral pressures in the range of σ_3=196 to 2,452 kN/m^2 (2 to 25 kgf/cm^2). These results showed that the principal stress ratio σ_1/σ_3 at failure decreases according to the increase of σ_3, and that grain crushing is becoming higher.

Leps (1970) examined the relation between the shear strength of rockfill specimens and confining pressure based on the published results of large number of triaxial compression tests. He concluded that ϕ_0, which is the friction angle assuming that the cohesion is zero, decreases almost linearly with $\log\sigma_n$ (σ_n = normal stress at failure). He also reported that ϕ_0 is especially large at low confining pressure; this has an important effect on the stability of rockfill dams because low rockfill dams constructed with the relatively steep slopes are stable for a long time.

Banks and MacIver (1971) pointed out from the opposite side that if the relation between shear strength and confining pressure is ignored, then the shear strength may be overestimated at the higher confining pressure.

In the 17th Rankine Lecture, deMello (1977) reported the test results of Marsal and others, and showed that the shear strength of rockfill materials can be approximated quite accurately using the equation $\tau=A\sigma_n^b$ (σ_n= normal stress at failure; A and b are test constants). He also described that the safety factor for deep sliding is smaller than that for shallow sliding when the shear strength is expressed as a function of the confining pressure.

Charles and Watts (1980) investigated the decrease of ϕ_0 as a lateral pressure increases by performing triaxial compression tests using rockfill specimens with a diameter 23 cm and a height of 50 cm, and evaluated the shear strength using the same equation as deMello. He concluded that the safety factor of rockfill dams is proportional to $1/z^{(1-b)}$, where z is the depth of the sliding surface.

Thus these previous studies clearly show that the dependency of internal friction angle on confining pressure is significant when calculating the shear strength of rockfill materials. It is also apparent that this not only affects the design strength, but that it may have a direct influence on stability analysis.

3. CONVENTIONAL METHOD IN JAPAN

The construction of large-scale rockfill dams in Japan such as the Mihoro Dam and the Makio Dam was really started in the 1960's . At the time, there was no large-scale equipment available for testing rockfill materials, nor was there any established testing method. Hence, the design values of shear strength of rockfill materials were determined from the angle of repose, from direct shear tests, or by refering to design cases in other countries.

Recently in Japan, the shear strength of rockfill materials is usually estimated using

large-scale triaxial compression tests performed under several lateral pressures. The design strength is evaluated using a liner approximation of Mohr's envelope.

However, previous studies suggest that there is a problem in a linear approximation for the shear strength from the apparent cohesion and internal friction angle based on the Mohr-Coulomb's failure criterion. For rockfill materials, Mohr's envelope is not straight but curved. This means that when the angle ϕ_0 is determined by the tangent of Mohr's stress circle drawn from the origin, then ϕ_0 decreases as the confining pressure increases.

In particular, when rockfill materials are collected from quarry site by blasting, it appears that this decrease in ϕ_0 is caused by the weakening of the dilatancy effect due to compaction and grain crushing caused by shearing. Since grain crushing is closely related to confining pressure, the shear strength depends on both the confining pressure and grain crushing.

The relation between test and design values of shear strength of rockfill materials in Japan is investigated. As stated earlier, although the apparent cohesion c and internal friction angle ϕ are obtained from a linear approximation of Mohr's envelope, c is not evaluated as the design value and it is restricted to ϕ.

The design value for ϕ is usually determined by subtracting some allowance value from the test value. This allowance value is based on a technical estimate considering the difference in gradation between test and actual materials, scattering of test results and so on. However, the basis of the estimation is not clear. Figure 1 shows the relation between the internal friction angle obtained from the test and that used for actual design for 17 major rockfill dams constructed in Japan. The design internal friction angle has an allowance of 0 to 7 degrees over the test value for all the investigated dam, but 0 to 3 degrees for almost dams.

4. TRIAXIAL COMPRESSION TESTS FOR ROCKFILL MATERIALS

4.1 Testing method

Triaxial compression tests using typical materials were performed to confirm that the shear strength of rockfill materials depends on confining pressure and other parameters.

Specimens with a diameter of 30 cm and a height of 60 cm were used in 22 different test cases, varying rock types, moisture content, coefficient of uniformity and void ratio. A total of 178 specimens were used in this series of tests. The test cases are summarized in Table 1.

Figure 2 shows the triaxial compression test apparatus for rockfill materials. The type of test is a consolidated-drained one in which the strain is controlled. The speed of strain is set at a rate of 0.5% of the specimen height per minute, and the test ends when the principal strain exceeds 15%. The confining pressure of the test is equal to a lateral pressure ranging from 49 to 1,372 kN/m^2 (0.5 to 14 kgf/cm^2; 0.5, 1, 1.5, 2, 4, 6, 8, 10, 14 kgf/cm^2). The air-dried specimens had a moisture content of less than 1%, while the saturated specimens were made by letting water flow in air-dried specimens for 24 hours after passing carbon dioxide through them.

4.2 Test results

Examples of stress-strain curves obtained from triaxial compression tests are shown in Figure 3. The figure compares the principal stress difference versus axial strain curves for varying lateral pressures for both loosely compacted and densely compacted

materials. In the densely compacted materials, a peak occurs in the principal stress difference. However, in the loosely compacted condition, the principal stress difference does not rise as fast as in the densely compacted condition. In this case, a peak is not observed under the higher lateral pressure, and the maximum value occurs at the end of the test when the strain is approximately 15%. Although not illustrated in this paper, stress-strain curves do not often have a peak when a saturated specimen is tested under the higher lateral pressure.

When a peak is observed in the principal stress difference of the stress-strain curve, the shear strength of the rockfill dam is taken as this peak value. If a peak is not observed, then the shear strength is taken as the value at the strain of 15%. This paper described test results focusing on these two values, the peak strength and the 15% strain strength. In triaxial compression tests, 15% strain is the critical value because the axial displacement cannot measured precisely in the strain over 15%, the specimen is shaped like a barrel at this point, and the value is supposed to be close to residual strength. The internal friction angle ϕ_0 discussed later can be determined from Figure 4 using the following equation:

$$\phi_0 = \sin^{-1}((\sigma_{1f} - \sigma_3) / (\sigma_{1f} + \sigma_3)) \qquad (1)$$

In granular materials such as sand and gravel, and rockfill materials, factors such as dilatancy, which is volumetric change caused by shearing, and grain crushing have a considerable effect on the value of ϕ_0. Therefore, the effect of confining pressure on these factors is investigated before discussing the dependency of strength on confining pressure.

First, the effect of dilatancy is examined by measuring the dilatancy ratio $(-d\varepsilon_v / d\varepsilon_a)$, which is obtained by dividing the increase in volumetric strain $d\varepsilon_v$ by the increase in axial strain $d\varepsilon_a$. Figure 5 shows the relation between the dilatancy ratio and ϕ_0 for air-dried specimens at lateral pressures of 98 kN/m² (1 kgf/cm²) and 785 kN/m² (8 kg/cm²). The dilatancy ratio is smaller at the larger lateral pressure. This indicates that the smaller the confining pressure, the larger the influence of dilatancy on ϕ_0.

Next, the relation between grain crushing and internal friction angle ϕ_0 is examined. In Figure 6, grain crushing ratio determined by the Marsal's method is shown on the x-axis and ϕ_0 is on the y-axis. These results are obtained under the saturated condition keeping the initial void ratio constant (e_0=0.35). Because grain crushing ratio is calculated by comparing the gradations before and after triaxial compression tests, this value expresses the grain crushing condition when the axial strain is slightly more than 15%. Here, ϕ_0 decreases as grain crushing increases, even for the same initial void ratio. In addition, grain crushing increases as the lateral pressure increases. Thus, dilatancy and grain crushing are both related to confining pressure.

These observations are then used to examine the dependency of internal friction angle on confining pressure as a function of internal friction angle ϕ_{0p} at the peak strength, and internal friction angle ϕ_{015} at 15% strain for some typical experimental cases.

In the first place, the test results for granite of CM class and uniformity coefficient of 12 are performed using specimens with two initial void ratio; the relation of ϕ_{0p} and ϕ_{015} to σ_n are shown in Figure 7a. In the second place, the relation of ϕ_{0p} and ϕ_{015} to σ_n for both air-dried and saturated specimens are shown in Figure 7b for schalstein, which has a relatively low strength. These tests are also carried out

for andesite which has a high strength, as shown in Figure 7c.

These three figures leads to the following:

1) ϕ_0 is dependent on confining pressure for all experimental cases, as both ϕ_{0p} and ϕ_{015} decrease linearly as the normal stress σ_n increases in the range 78 to 2,942 kN/m² (0.8 to 30 kgf/cm²).

2) The difference between ϕ_{0p} and ϕ_{015} is large when σ_n is small, but it decreases as σ_n increases.

3) From Figure 7a, it is clear that the slope of the linear equation of ϕ_{015} is not much dependent on the void ratio. Although not shown here, the same tendency was confirmed for changing values of uniformity coefficient.

4) Figure 7c shows that the difference between ϕ_{0p} and ϕ_{015} is smaller under saturated conditions than air-dried conditions.

5. EFFECT OF CONFINING PRESSURE

5.1 Evaluation method of shear strength

A rockfill dam is considered stable against sliding failure when its safety factor SF is greater than 1.2. The safety factor is calculated as the ratio of the resisting force and the sliding force of the sliding mass using the slice method which assumes a circular sliding surface. In the method, it is necessary to determine the ratio between the effective normal stress σ_n and shear resistance force τ_f, which act on the bottom of the slice along sliding surface. The effect of confining pressure on the strength of rockfill materials is thus given by the following equations, as a function of shear strength:

$$\tau_f = A\sigma_n^b \qquad (2)$$

$$\tau_f = \sigma_n \tan\phi_0 \qquad (3)$$

where $\tau_f=0$ when $\sigma_n=0$ for non-cohesive materials such as sand and gravel or rockfill materials. A and b are test constants.

However, as ϕ_0 changes little near $\sigma_n=0$, then ϕ_0 in equation (3) will become a function of σ_n as follows:

$$\phi_0 = \phi_{max} - a\log(\sigma_n / \sigma_0) \quad (\sigma_n \rangle \sigma_0)$$

$$\phi_0 = \phi_{max} \qquad (\sigma_n \le \sigma_0) \qquad (4)$$

ϕ_{max} is the maximum internal friction angle for a small confining pressure, and a is a coefficient which indicates the rate that the internal friction angle decreases as the confining pressure increases. Furthermore, the internal friction angle will become a constant ϕ_{max} if the normal stress becomes less than σ_0. ϕ_{max} and σ_0 can be determined experimentally for specific rockfill materials.

In order to obtain σ_0 in equation (4), experiments must be conducted for a very low confining pressure and with great precision. Although our triaxial compression test apparatus can control a minimum lateral pressure σ_3 on the test specimen of only 49 kN/m² (0.5 kgf/cm²), this is still too large to determine the precise value of σ_0 in equation (4). Therefore, the following simplified equation (4) is used:

$$\phi_0 = \phi_{01} - a\log\sigma_n \qquad (5)$$

When kN/m² (kgf/cm²) is used as the unit for the stress in equations (2) and (3), the following relation between A in equation (2) and ϕ_{01} in equation (5) is obtained. This is because when σ_n=98 kN/m² (1.0kgf/cm²), then τ_f has the same value in both equations (2) and (3).

$$A = \tan\phi_{01} \qquad (6)$$

The value of ϕ_{01} in this equation is the value ϕ_0 when σ_n=98 kN/m² (1.0kgf/cm²).

5.2 Shear strength

As noted before, equations (2) and (3) may be used to evaluate shear strength. We compared the shear strength obtained from these equations using the triaxial compression test data for the peak shear strength and the 15% stain strength.

Figure 8 shows an example of Mohr's envelopes for the peak strength and the 15% strain strength approximated by equation (1). Figure 9 shows the relation between A and b for all the experiments performed. For the peak strength, the value b ranges from 0.75 to 0.85, and value A ranges from 2.0 to 1.2. The value A tends to decrease as b increases.

In the case of the 15% strain strength, value b ranges from 0.85 to 0.95, while A ranges from 1.3 to 1.0. Here, A also tends to decrease as b increases, but not as markedly as in the case of the peak strength.

Figure 10 compares the test constants for the peak strength and 15% strain strength for both A and b. At 15% strain strength, the almost constant value of A is less than at the peak strength, while the value of b at 15% strain strength is larger than at the peak strength. This increases in b indicates that Mohr's envelope becomes more linear and less curved.

Figure 11 shows the relation between the value of ϕ_{01} and the value of a obtained from equation (5). ϕ_{01} ranges from 49 to 63 degrees for the peak strength, and from 45 to 53 degrees at 15% strain strength, thus the latter produces a smaller range of angle. The value of a, which is the slope of the linear equation (5), ranges from 8 to 14 for the peak strength, and from 3 to 10 for 15% strain strength. Thus, the value of a is larger for the peak strength. For both peak strength and 15% strain strength, ϕ_{01} tends to increase as a increases.

Besides, the difference in the value τ_f which is given by evaluating the shear strength from equation (2) or equation (5) is 3% for σ_n=294 kN/m^2 (3 kgf/cm^2) and less than 1% for σ_n=981 kN/m^2 (10 kgf/cm^2). Thus the difference is estimated to be small.

6. EFFECTS ON SLIDING FACTOR

The safety factor against sliding failure of the model rockfill dam was examined for the following two cases:

1) the peak shear strengths obtained by equation (2) (called the Ab method) and by equation (3) (called the ϕ_0 method) were compared.

2) the peak strength and 15% strain strength were compared using the Ab method.

In order to simplify the problem, case 1) was calculated using an infinite slope. Figure 12 shows the depth of sliding surface on the x-axis and the safety factor on the y-axis. When the depth of the sliding surface is small, the safety factor is large using both the Ab method and the ϕ_0 method. However, the safety factor decreases as the depth of sliding surface increases. There is little difference in the safety factor between the Ab method and the ϕ_0 method.

In the case 2), the model rockfill dam with a central core show in Figure 13 was used. A circular sliding surface for varying central angles was considered in order to calculate the safety factor using the simplified slice method. The length of the slope was assumed to be 100 m, the dry density of the dam was 2.0 t/m^3, and the constant design seismic coefficient was set at 0.12. The model shows that the depth of the sliding surface increases as the central angle increases. Shear strength constants for densely compacted granite of CM class (e_0=0.29) and loosely compacted one (e_0=0.48) were used for the calculation. Table 2 shows the values for the constants A and b given by equation (2) for shear strength in the four cases A, B, C and D.

In Figure 14, the value and

characteristics of the safety factor against sliding failure depend on whether the peak strength or 15% strain strength is used. When peak strength is used, the safety factor is large in the small depth of sliding surface. However, the safety factor decreases as the depth of the sliding surface increases in cases A and C. These characteristics are not prominent for 15% strain strength. The safety factor remains almost constant regardless of the depth of the sliding surface, and is smaller than that calculated using the value obtained at the peak strength in cases B and D. For example, when the central angle is 40 degrees, the safety factor for 15% strain strength is approximately 30% smaller than that for the peak strength.

7. CONCLUSIONS

We investigated methods of evaluating the shear strength of rockfill materials in the design process, using a curvilinear approximation rather than a linear approximation of Mohr's envelope. Systematic triaxial compression tests were conducted to study the effect of confining pressure on shear strength, and the sliding stability was analyzed using equations for the shear strength and confining pressure. The following results were obtained:

1) The internal friction angle is greatly affected by dilatancy at low lateral pressure, and is closely correlated to grain crushing at high lateral pressure.

2) Both ϕ_{0p} and ϕ_{015} decrease as the normal stress σ_n increases in the range of 78 to 2,942 kN/m^2 (0.8 to 30 kgf/cm^2). There is a linear relation between ϕ_{0p}/ϕ_{015} and σ_n.

3) Equation (3) gives slightly smaller values of shear strength than equation (2).

4) When the shear strength is evaluated using $\tau_f = A\sigma_n^b$ based on a curvilinear approximation, then the value of A for 15% strain strength is smaller than for peak strength, while the value of b is correspondingly larger. The difference between the shear strength values for peak strength and for 15% strain is large when the normal stress is small. This difference decreases as the normal stress increases.

5) When the sliding safety factor using the peak shear strength expressed as $\tau_f = A\sigma_n^b$ and $\tau_f = \sigma_n \tan\phi_0$ is compared using a model calculation assuming both edges of the sliding circle are fixed, then the safety factor is large when the depth of sliding surface is small. The safety factor is small when the depth of sliding surface is large.

In addition, the 15% strain strength gives considerably smaller safety factor of the surface of the dam is than the peak strength. However, the safety factor does not depend on the depth of the sliding surface in the case.

REFERENCES

Bank, D. C. and MacIver, B. N. (1971): Discussion on Review of Shear Strength of Rockfill, J. Soil Mech. Found. Div., ASCE, Vol.97, SM5, pp.791-794.

Charles, J. A. and Watts, K. S. (1980): The Influence of Confining Pressure on the Shear Strength of Compacted Rockfill, Geotechnique, 30-4, pp.353-367, 1980.

de Mello, V. F. B. (1977): Reflections on Design Decisions of Practical Significance to Embankment Dams, Geotechnique, 27-3, pp.279-355.

Japanese Government (1976): Cabinet Order Concerning Structural Standards for River Administration Facilities, etc.

Leps, T. M. (1970): Review of Shearing Strength of Rockfill, J. Soil Mech. Found.

Div., ASCE, Vol.36, SM4, pp.1159-1170,

Marsal, R.J (1965): Discussion, Proc. 6th International Conference on Soil Mechanics and Foundation Engineering, Vol.3, pp.310-316.

River Bureau, Ministry of Construction (1991): Seismic Design Standard for Embankment Dams (Draft).

Table 1 Test conditions.

Case	Material	Moisture condition	Uniformity coefficient Uc	Initial void ratio e_0	Number of specimens
1	Granite CH	Air-dried	12	0.35	9
2	Granite CH	Saturated	12	0.35	9
3	Granite CM	Air-dried	12	0.35	9
4	Granite CM	Air-dried	12	0.29	9
5	Granite CM	Air-dried	12	0.42	9
6	Granite CM	Saturated	12	0.35	9
7	Granite CM	Air-dried	3	0.55	9
8	Granite CM	Air-dried	3	0.48	5
9	Granite CL	Air-dried	12	0.35	9
10	Granite CL	Saturated	12	0.35	9
11	Gabbro	Air-dried	12	0.35	9
12	Gabbro	Saturated	12	0.35	9
13	Schalstein	Air-dried	12	0.35	9
14	Schalstein	Saturated	12	0.35	7
15	Limestone	Air-dried	12	0.30	9
16	Limestone	Saturated	12	0.30	7
17	Basalt	Air-dried	12	0.36	7
18	Andesite	Air-dried	12	0.36	7
19	Andesite	Air-dried	12	0.32	7
20	Andesite	Saturated	12	0.32	7
21	Welded tuff	Air-dried	12	0.33	7
22	Welded tuff	Saturated	12	0.33	7

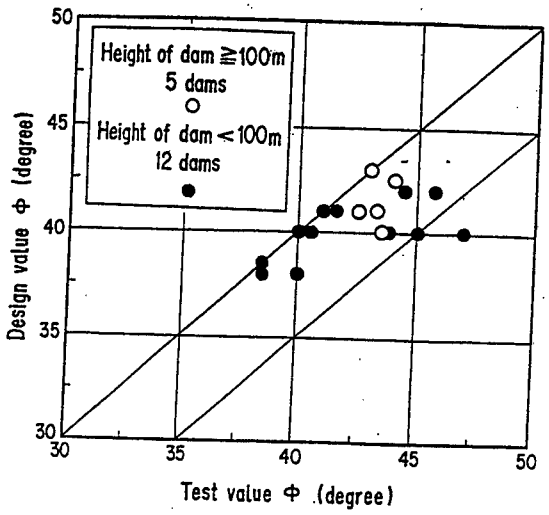

Figure 1 Relation between design and test values of internal friction angle for rockfill materials.

Table 2 Calculating conditions.

Case	Material	Shear strength constants	A	b	Initial void ratio e_0	Remarks
A	Granite CM	Peak	1.762	0.797	0.29	Case 4
B		15% strain	1.148	0.921		
C		Peak	1.425	0.774	0.48	Case 8
D		15% strain	1.047	0.901		

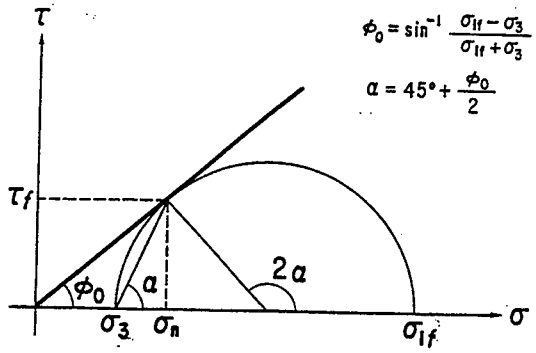

Figure 4 Definition of ϕ_0

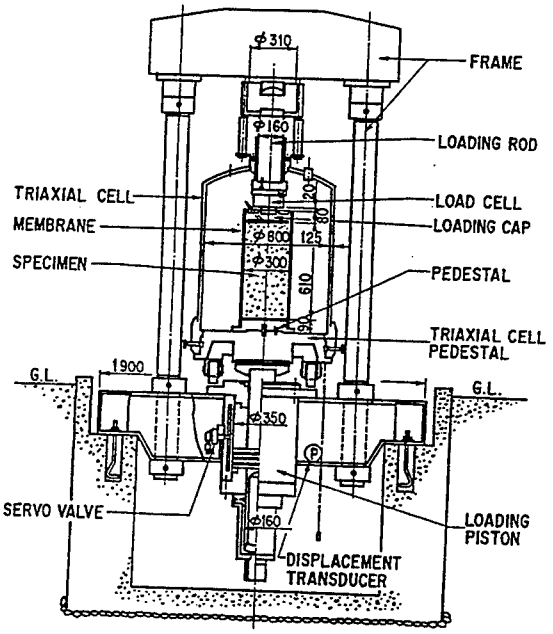

Figure 2 Triaxial compression testing apparatus.

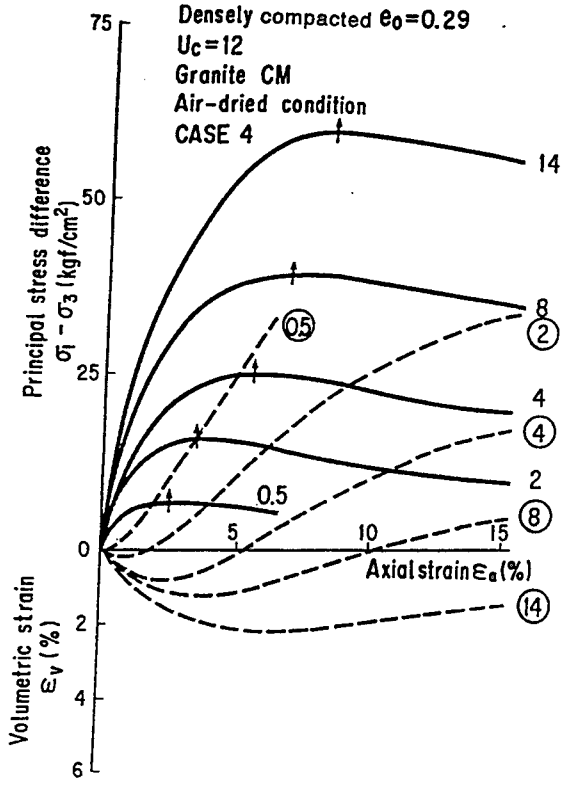

(a) Case 4

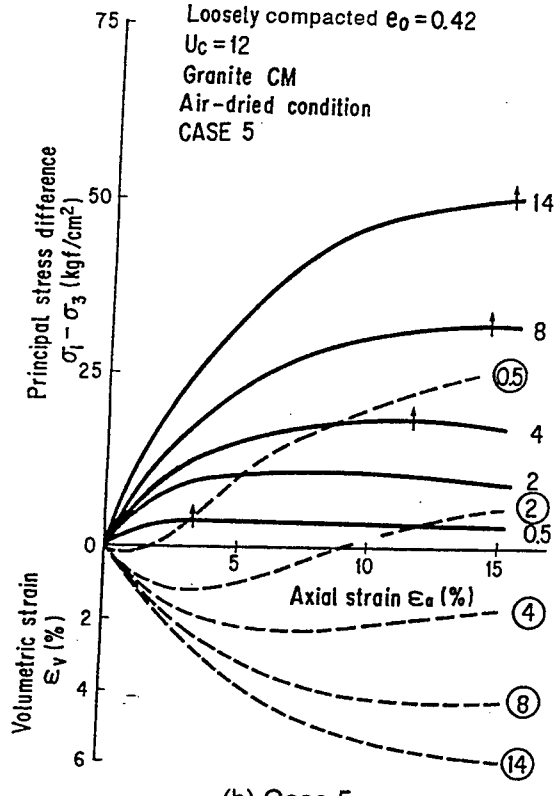

(b) Case 5

Figure 3 Examples of stress-strain curves.

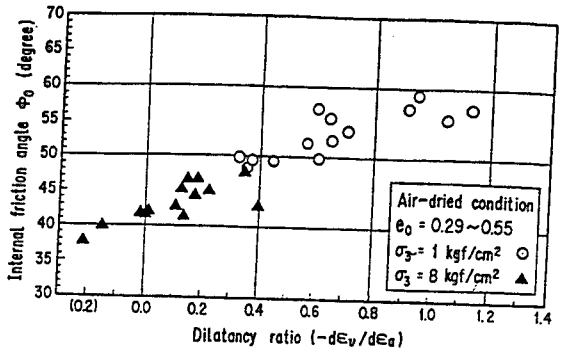

Figure 5 Relation between dilatancy ratio and internal friction angle.

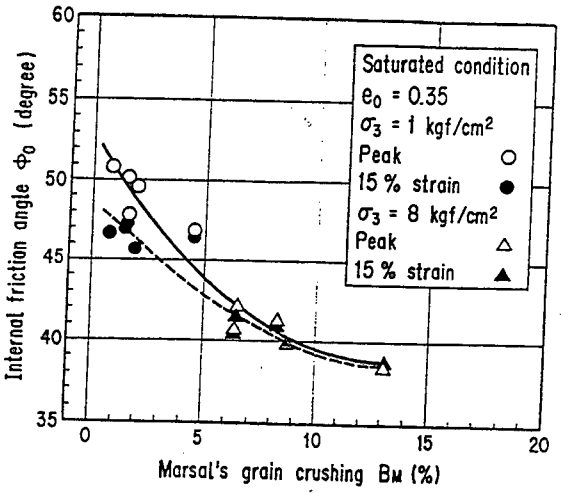

Figure 6 Relation between garain crushing and internal friction angle.

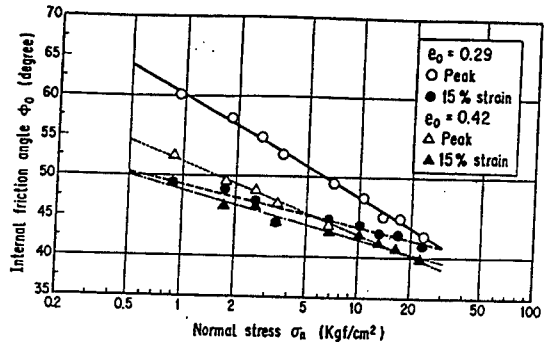

(a) Granite, CM, Air-dried, Uc=12

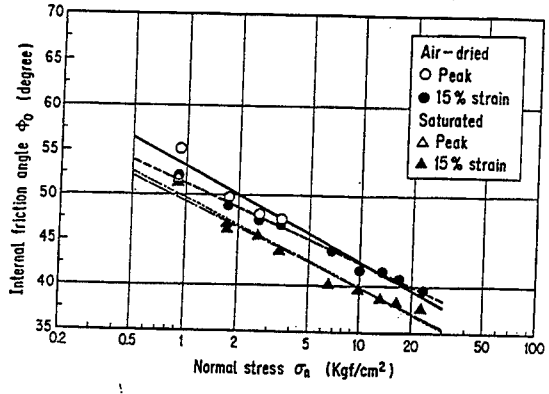

(b) Schalstein, Uc=12, e_0=0.35

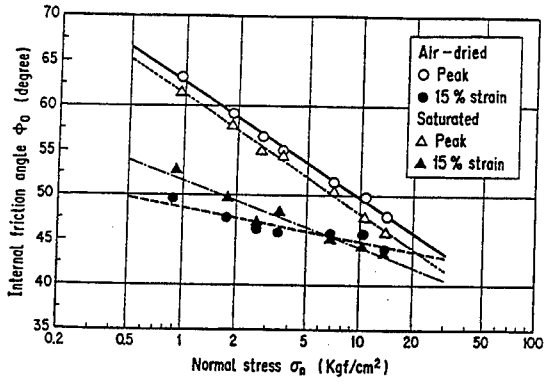

(c) Andesite, Uc=12, e_0=0.32

Figure 7 Relation between internal friction angle and normal stress.

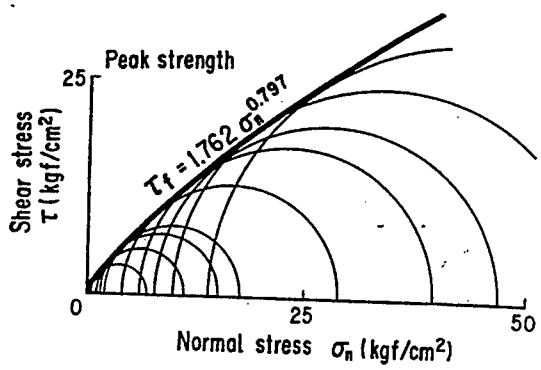

(a) Peak strength

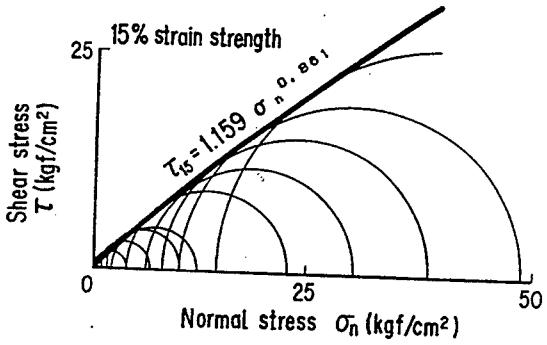

(b) 15% strain strength

Figure 8 Mohr's envelope for Case 4.

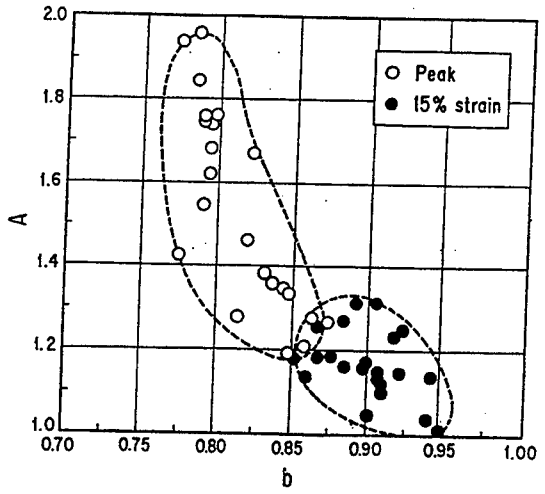

Figure 9 Relation between A and b.

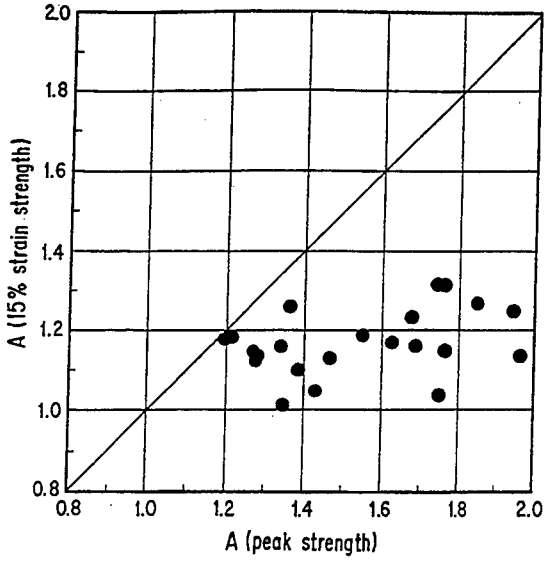

(a) Constant A

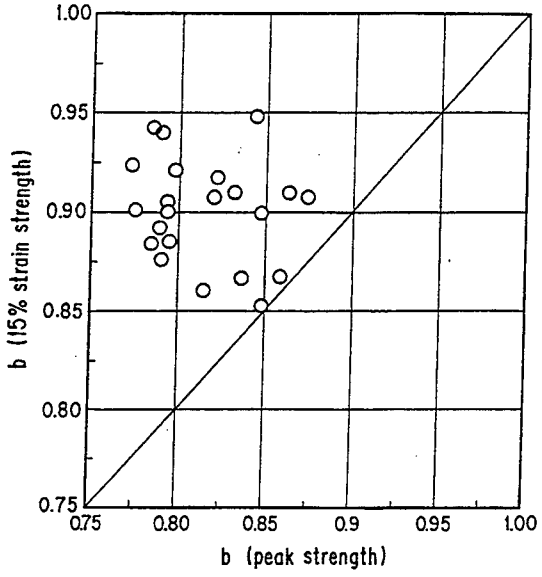

(b) Constant b

Figure 10 Comparison of test constants.

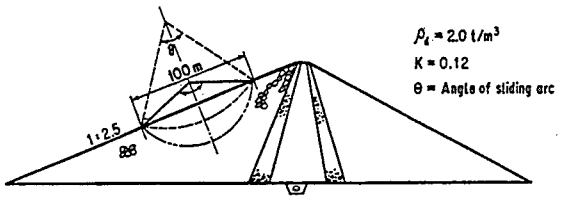

Figure 13 Model dam for stability analysis.

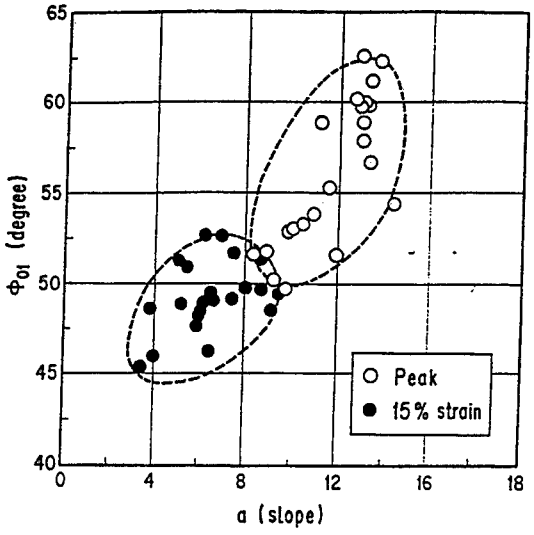

Figure 11 Relation between a and ϕ_{01}.

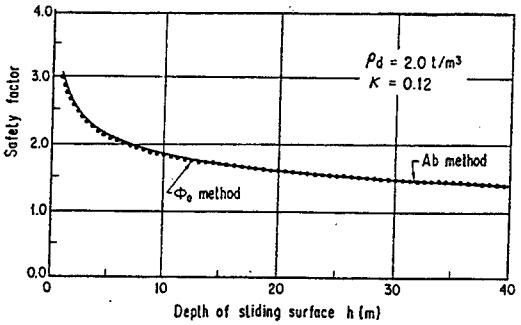

Figure 12 Relation between depth of sliding surface and safety factor.

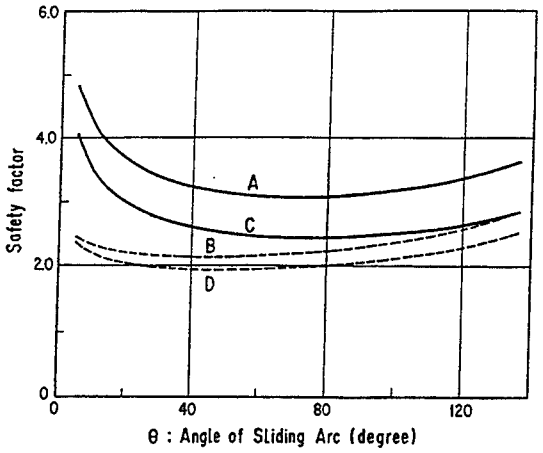

Figure 14 Relation between angle of sliding arc and safety factor.

The Influence of Confining Stress on Liquefaction Resistance

by

Richard S. Olsen*

ABSTRACT

A review of published correlations on confining stress effects on liquefaction resistance was performed and a new approach developed. Historical approaches (laboratory testing and the K_σ chart) were described and evaluated. The laboratory based approach will only reveal information on a single sand type and a single relative density. The K_σ chart approach is well published, there is even a NCEER recommendation. However, published data (from a wide range of soils) indicates a wide range of K_σ relationships. A new technique was developed using the Stress Focus theory which accounts for soil type and relative density.

KEYWORDS: Liquefaction, liquefaction resistance, K sigma, normalization, stress effects, Stress Focus, silts, CRR.

1 INTRODUCTION

Many factors influence liquefaction resistance including the non-linear influence of overburden stress. Liquefaction resistance (sometimes referred to as cyclic strength) is the strength level resisting initiation of liquefaction ground failure (e.g. major strength reduction) and/or sand boil expression on the ground surface. Liquefaction resistance is controlled by three factors; 1) soil type (i.e. material type, gradation, index properties, etc.,), 2) relative consistency (i.e. relative density for sands), and 3) effective confining pressure. For a given soil type and relative consistency, the increase of liquefaction resistance with increased effective stress is known to be less than linear. The issue for project work is to determine or estimate liquefaction resistance knowing that there is a non-linear stress relationship.

The non-linear liquefaction resistance versus vertical effective stress relationship can be estimated with published relationships or determined based on a large number of cyclic laboratory tests. This non-linear relationship is soil type dependent, therefore a relationship determined for one soil type can't be used for other soil types at given site. Also, an established relationship is also only for a given relative density level. Which ever approach is utilized, liquefaction resistance is always represented at the Cyclic Resistance Ratio (CRR) (i.e. ratio of liquefaction resistance divided by the vertical effective stress). The CRR decreases with increasing vertical effective stress.

The in situ CRR is calculated using K_σ parameter (from a K_σ chart) and CRR_1 (equivalent CRR at a vertical effective stress of 1 atm) using Equation 1. The K_α and K_m factors are static shear stress and earthquake influence factors (Seed, et al. 1986).

$$CRR = CRR_1 \, K_\sigma K_\alpha K_m \qquad (1)$$

where

- CRR = CRR for the field in situ overburden stress conditions (earthquake and stress level corrected)
- CRR_1 = Equivalent CRR at $\sigma'_v = 1$ *atm* (normally predicted based on in situ tests)
- K_σ = Confining stress influence factor (one for a vertical effective stress of 1 atm)
- K_α = static shear stress influence factor (one for level ground)
- K_m = earthquake magnitude influence factor (one for a 7.5 magnitude earthquake)

*Earthquake Engineering and Seismology Branch, Geotechnical Laboratory,
USAE Waterways Experiment Station,
Vicksburg, MS 39180

The CRR_1 can be determined from liquefaction resistance determination techniques using the in situ tests such as the Standard Penetration Test (SPT), Cone Penetration Test (CPT), or Shear wave velocity (V_s), or based on laboratory cyclic testing. The state-of-the-art for estimating CRR_1 using the SPT is Seed et al (1986), using the CPT is Stark et al (1995) or Olsen & Koester (1995), or using the V_s is Antrus and Stokoe (1995).

2 USE OF CONVENTIONAL APPROACHES

Historically, researchers have known that the relationship between liquefaction resistance and confining stress level was non-linear. If cyclic laboratory tests performed at a confining stress of 1 atm (i.e. 100 Kpa or 1 tsf) are linearly extrapolated to high confining stresses levels, the calculated liquefaction resistance are too high. Therefore, this ratio of liquefaction resistance to confining stress (known as the Cyclic Resistance Ratio, CRR) decreases with increasing confining stress.

2.1 Laboratory based determination of stress effects on CRR

The most direct means of determining the non-linear CRR versus overburden stress relationship is to perform a large number of laboratory based cyclic liquefaction tests for a given soil type and relative density level. If information on another relative density and/or sand type is required then another series of cyclic tests are required. To establish a relationship requires as a minimum 4 data points (over a sufficient range of overburden stresses).

For each overburden stress level, several tests are required at several induced shear stress levels to determine the CRR which matches the liquefaction failure criterion (i.e. 5% strain at 15 cycles). While the probable induced shear stress for a given overburden stress condition can be estimated prior to testing, several induced shear stress levels are still required to achieve or to interpolated to the failure criterion condition. Inherent testing variability also necessitates many tests (covering a range of induced shear stress levels) so a trend can be established to determine the CRR at the liquefaction failure criterion.

Cyclic laboratory testing is very expense. If each cyclic laboratory test is 15 more expense than static triaxial test, then the cost to establish a liquefaction resistance stress relationship might be 60 times more costly than to establish a static strength relationship. It is therefore typically cost prohibited to do a laboratory test program for given sand type and a single relative density level.

2.2 K_σ chart estimation of stress effects on CRR (historical approach)

The geotechnical earthquake engineering convention for estimating the non-linear CRR versus overburden stress relationship is by means of K_σ chart. The late Professor H.B.Seed developed the K_σ factor to account for stress influence on CRR, because laboratory-based cyclic triaxial tests are very expensive. The K_σ adjustment factor (Equation 2) (verbally dictated as the K sigma factor) is the ratio of liquefaction resistance at a given effective confining stress to liquefaction resistance at 1 atmospheric effective confining stress (approximately 1 tsf).

$$K_\sigma = \frac{CRR}{CRR_1} \qquad (2)$$

where

K_σ = Stress influence factor for liquefaction resistance

CRR = CRR at the in situ vertical effective stress level

CRR_1 = CRR at a $\sigma'_v = 1\ atm$ (normalized CRR)

The earliest published K_σ chart was by Seed (1981) as shown in Figure 1. K_σ charts are always presented in terms of K_σ (on the vertical axis) versus vertical effective stress(on the horizontal axis). The horizontal effective stress axis should be in terms of atmospheric units (i.e. 1 atm = 100 Kpa ≈1 tsf). The K_σ chart was updated by Seed (1984) and Harder (1988) as shown in Figure 2 and again by Seed (Raymond Seed) & Harder (1990) as shown in Figure 3. The NCEER recommended K_σ chart

relationship is also shown in Figure 3. Published CRR based data and K_σ trends (taken from a wide range of soils) indicate a wide range of possible K_σ relationships. The NCEER recommended relationship represents the average for all tested soil types and relative density levels. Medium dense to dense clean sands produce the lowest K_σ factors (for a given confining stress level) while loose silts produce the highest K_σ values (0.8 to 0.9). The NCEER recommended relationship is probably inaccurate for these extremes (i.e. medium dense (to dense) clean sands and loose silts). Selecting the best K_σ relationship is difficult, the NCEER recommended relationship represents an average but the alternative requires selecting a relationship based on soil type and relative density levels.

2.3 Historical research toward establishing the K_σ factor

Almost all publications concerning the "influence of confining stress on liquefaction resistance" have been in terms of the K_σ chart (Vaid, Chern and Tumi 1985, Seed 1981, Seed 1987, Seed and Harder 1990, Pillai and Byrne 1994).

Vaid, Chern and Tumi (1985) presented laboratory results for Ottawa sand (in another format) as shown in Figure 4. Pillai and Byrne (1994) replotted the Vaid, Chern, and Tumi data in the K_σ chart format as shown in Figure 5. Figure 6 shows interpreted data results from the Duncan Dam study together with results from previously described data trends (Vaid, Chern and Tumi (1985)). The results from large diameter cyclic triaxial chamber tests on gravels are shown in Figure 7 (Hynes 1988).

The common discussion in these historic publications is that previous K_σ relationships did not match newly plotted data trends. Vaid & Thomas (1993) stated that the K_σ relationship should be dependent on relative density but they did not develop an approach. It appears that soil type (or sand type) and sand relative density are both required to best estimate the K_σ parameter.

3 STRESS FOCUS APPROACH

All geotechnical properties are non-linearly influenced by confining stress and can be explained with exponential relationships (Olsen, 1994). This paper will show that confining stress influence on liquefaction resistance can also be explained with exponential relationships, specifically by means of the Stress Focus theory. The Stress Focus theory (Olsen 1994, Olsen and Mitchell 1995) will show that this confining stress influence is dependent on soil type and relative consistency (i.e. relative density for sands).

3.1 Background for the stress focus theory

The Stress Focus concept (Olsen, 1994) will be used to develop a new technique for estimating confining stress effects on liquefaction resistance. Dilation and failure envelope curvature will be initially described before Stress Focus theory is introduced. A simple equation based on graphical interpretation of the Stress Focus theory will be shown to determine the in situ liquefaction resistance strength level.

All geotechnical strength properties experience dilation during shear and show failure envelope curvature over a range of confining stresses. Failure envelope curvature is graphically generalized in Figure 8. The friction angle of sands decrease with increased confining stress (due to failure envelope curvature) as shown in Figure 9. Failure envelope curvature therefore reduces the friction angle with increasing confining stress.

The major reason that dense sands have a higher friction angle compared to loose sand is because of dilation. Components of shear strength for granular soils are; dilation, grain rearrangement, crushing, and true friction as shown in Figure 10. Dilation can be defined as the tendency for grain-to-grain reorientation during shear (Mitchell, 1993). As relative density increases (from loose to dense sand) the contribution of dilation starts at zero and increases. It can also be shown that dilation decreases with increasing confining stress as shown in Figure 9 and 11. This observation is based on high pressure static triaxial tests and the Stress

Focus theory. Failure envelope curvature results in a decreased friction angle with increased confining stress.

3.1.1 Cone resistance stress focus

The Stress Focus theory was initially developed using CPT cone resistance data because the trends were so obvious. Stress Focus theory will therefore be introduced in this section based on CPT trends before moving to the discussion of confining stress effects on liquefaction resistance.

CPT cone resistance chamber trends with increasing confining stress point toward the Stress Focus (which is dependent on sand type). Typical CPT cone resistance calibration chamber trends (shown in Figure 12) can be replotted using log scales as shown in Figure 13. The trends in Figure 13 pointed to a Stress Focus. Failure envelope curvature reduces available strength with increased confining stress until the Stress Focus is achieved. All initial relative densities for a particular sand have the same strength at the Stress Focus. At the Stress Focus, all initial relative densities have an available friction angle equal to that of initially loose sand which was consolidated to a high confining stress. An annotated description of the Stress Focus for the CPT cone resistance is shown in Figure 14. For sands, this Stress Focus occurs approximately at a vertical effective stress of 140 atm (140 tsf or 14 MPa, at depth of approximately 1 kilometer) as shown in Figure 14.

The Stress Focus location changes with soil type. As soil type changes from sand to clay, the Stress Focus location changes (Olsen, 1994) as shown in Figure 15 and this line is the Stress Focus boundary.

3.1.2 Cone resistance stress exponent approximation for sand

The CPT stress exponent, c, is very important for normalization of the cone resistance measurement because it defines the slope of the cone resistance trend to the Stress Focus. The CPT normalized cone resistance, q_{cle}, (Olsen, 1988, 1994) is defined as:

$$q_{cle} = \frac{q_c}{\left(\sigma_v'\right)^c} \qquad (3)$$

where

q_c = measured cone resistance (atm units)
q_{cle} = normalized cone resistance (in terms of envelope curvature)
σ_v' = initial vertical effective stress (atm units)
c = CPT stress exponent

The cone resistance stress exponent, c, decreases as the sand relative density increases and can be approximated for sand as shown below using the relative density, D_r (Olsen and Mitchell 1995):

$$c = 1 - \left(D_r - 10\%\right)0.007 \qquad (4)$$

3.1.3 Cone resistance stress exponent for all soil types

A special procedure is required to estimate the CPT cone resistance stress exponent, c, for all soil types and strength levels (Olsen, 1988). Contours of stress exponent, c, on the CPT soil characterization chart are shown in Figure 16 and were established using normalized CPT data from 65 uniform soil layers (Olsen 1994). These stress exponent contours exhibit several predictable trends: 1) high values for loose sands (i.e., low failure envelope behavior), 2) very low values for over consolidated sands, 3) values of approximately 1.0 (and slightly lower) for normally consolidated clays (little if any failure envelope curvature), 4) values slightly below unity (i.e., 0.75 to 0.9) for slightly over consolidated clays, and 5) values as high as 1.2 for unstable silty clay mixtures (collapsible structure). These stress exponent contours are used for normalization of the cone resistance (Equation 1).

3.2 Stress Focus for Liquefaction resistance evaluation

In this section, the normalized liquefaction resistance (CRR_1) will be derived using the Stress Focus theory. The relationship of liquefaction resistance versus vertical effective stress will also be shown based on the Stress Focus theory. Finally, CRR_1 will be related to the K_σ factor (described in a previous section).

The first step is deriving a relationship which exponentially relates liquefaction resistance to vertical effective stress. Normalized liquefaction resistance strength, τ_1, can be graphically depicted in Figure 17, and defined using normalization concepts (Olsen, 1994) as:

$$\tau_1 = \frac{\tau}{\left(\sigma_v'\right)^f} \qquad (5)$$

Where

- τ_1 = Normalized liquefaction resistance strength (atm units)
- τ = Liquefaction resistance strength in the field (atm units)
- σ_v' = Vertical effective stress (atm units)
- f = Liquefaction stress exponent from graphic construction (see Figure 17)

At σ_v'=1 atm the τ_1 is equal to CRR_1 (i.e. τ_1/σ_v') because σ_v'=1.

$$CRR_1 = \tau_1 = \frac{\tau}{(\sigma_v')^f} \qquad (6)$$

The next step is deriving how relative density can be related to the Stress Focus. Figure 18 shows a range of relative densities which can be expressed using Equation 6. An example of a single relative density trend (with increasing confining stress to the Stress Focus) is shown in Figure 19. Each data point represents a cyclic triaxial test at 15 equivalent cycles; which must be determined from a series of cyclic triaxial tests shown in Figure 20. Each point in Figure 20 represents a different cyclic deviator stress level. A curve connecting these data points (in Figure 20) is established and the CRR for 15 cycles is determined and plotted as an individual point on Figure 19. Each relative density trend has a normalized CRR_1 value (as shown in Figure 18) and points to the Stress Focus for that sand type.

The cyclic liquefaction resistance strength (Equation 5 and Figure 18) for each relative density trend can now be express in terms of CRR as shown below:

$$CRR_1 = \frac{\left(\frac{\tau}{\sigma_v'}\right)}{\left(\frac{(\sigma_v')^f}{\sigma_v'}\right)} = CRR\ (\sigma_v')^{(1-f)} \qquad (7)$$

and in a more simplified version;

$$CSR = \frac{CRR_1}{(\sigma_v')^{(1-f)}} \qquad (8)$$

where

- CRR_1 = normalized liquefaction resistance cyclic stress ratio
- CRR = field based liquefaction resistance cyclic stress ratio
- f = liquefaction based stress exponent (see Figure 18)

The next step is relating K_σ (Equation 2) to Equation 8 (CRR_1 in terms of the stress exponent). When CRR_1 from Equation 7 is combined with K_σ from Equation 2 the result is;

$$K_\sigma = \frac{CRR}{CRR_1} = \frac{1}{(\sigma_v')^{(1-f)}} \qquad (9)$$

and the resultant is;

$$K_\sigma = \left(\sigma_v'\right)^{(f-1)} \qquad (10)$$

Equation 10 can be plotted graphically in the K_σ chart format as shown in Figure 21. Past published data trends are also shown in this figure. Silty

materials (Vaid, et al, 1985; Duncan dam) have a high stress exponent (0.8 to 0.9) while sands generally have a stress exponent between 0.6 and 0.75 (Seed, et al, 1984, 1988, 1990 tests on standard sands). Remember, a stress exponent of 1 represents a linear strength gain with increased vertical effective stress; a stress exponent less than one represents a strength gain which is less than linear with increase vertical effective stress.

In 1983, Olsen (1984) generalized the data trends from preliminary version of Figure 2 (Seed, 1983) together with project data at WES into an expression similar to Equation 10. The stress exponent, f, in Equation 10 was reported to range from 0.6 to 0.95 with 0.7 recommended for sands (Olsen, 1984). This range is close to the trends shown in Figure 21 and discussion to follow in the next section.

3.3 CRR data plotted using the Stress Focus Concept

Laboratory based liquefaction resistance data from published resources and WES project files were cataloged and entered into a computerized database. The data from this data base were plotted as trends in Figure 22. Solid lines represent sands (clean and silty sands). There are also two data trends for silts plotted as dashed lines. Many of the sand trends are probably very silty sand; they could not be segregated from clean sand because much of data is poorly documented.

Examination of Figure 22 reveals several key observations concerning relative density and the stress exponent. Sands trends having high relative densities (i.e. high K_2) also have high CRR_1 levels (the equivalent CRR for the trend at σ_v = 1 *atm*), which is predictable. Data trends having high CRR_1 values also have low stress exponents (i.e. f slope trend of 0.6 to 0.8). Remember, a low stress exponent (i.e. 0.6) represents high relative density and a more dilative behavior (Olsen, 1994). Data trends having low CRR_1 levels (i.e. very loose sands) have high stress exponents (an f = 1 represents linear relationship). All of these observations are similar to trends of CPT cone resistance with confining stress described in previous sections of this report and support the liquefaction resistance based Stress Focus concept.

Examination of Figure 22 also reveals observations about data trends to the soil dependent Stress Focus. The liquefaction resistance trends for sand point to a focus in Figure 22. This is the liquefaction resistance Stress Focus for sand. The Sand Stress Focus is located at a vertical effective stress of 120 atm and has a liquefaction resistance level of 30 atm. A few of the sand trends have steep slopes (i.e. Oroville dam), probably indicating over consolidated behavior. The liquefaction Stress Focus for sand occurs at approximately the same overburden stress as the cone resistance Stress Focus for sand in Figure 18.

For silt, the liquefaction resistance data trends point to a silt Stress Focus location also shown in Figure 22. While this silt Stress Focus location was constructed using only two data trends, it's relative location is similar to the cone resistance Stress Focus boundary. The slope of a line connecting the liquefaction based Stress Focus for silt to sand is similar to the CPT cone resistance trends in Figure 15.

The point between the liquefaction resistance Stress Focuses for sand and silt in Figure 22 is assumed to represent dirty sand. The resulting soil type depend liquefaction resistance Stress Focus boundary in Figure 23 represent the "Stress Focus boundary for liquefaction resistance". Also shown is the Stress Focus boundary for static strength from Olsen (1994).

Figure 24 illustrates a means of estimating the confining stress dependent liquefaction resistance. The first step is determining the location of the Stress Focus based on the general soil type. The second step is calculating CRR_1 using either CPT or SPT liquefaction potential techniques. The third step is establishing a line (the trend) between the CRR_1 point and the soil type dependent liquefaction resistance Stress Focus. The next step is calculating the log-log slope of the trend. The final step is determining the in situ liquefaction resistance either graphically (using the data trend and in situ vertical effective stress) or using Equation 8.

6 Conclusions

A review of published correlations on confining stress effects on liquefaction resistance was performed and a new approach developed. In addition, project and published laboratory cyclic triaxial data from publications and WES projects were entered into a computer database. Accounting for the non-linear confining stress effects on liquefaction resistance can be accomplished by three means; laboratory testing, K_σ chart, or Stress Focus approach. The historical approaches (laboratory testing and the K_σ chart) were described and evaluated. A new technique was developed using the Stress Focus theory which accounts for soil type and relative density.

The laboratory testing approach is very expensive and requires a large number of cyclic triaxial tests. This approach only reveals information on a single sand type and a single relative density level. If information on another relative density and/or sand type is required then another series of cyclic tests are required.

The K_σ chart approach is well published, there is even a NCEER recommendation. However, published data (from a wide range of soils) indicates a wide range of K_σ relationships. The NCEER recommendation is the average for all tested soil types and relative densities. Medium dense clean sands and loose silts represent extremes where the NCEER recommended relationship is probably inaccurate. Therefore, the major issue with the K_σ chart approach is determining which of the published relationships to use.

Stress Focus theory, originally developed for the CPT cone resistance, was investigated as a means of explaining the non-linear behavior of confining stress on liquefaction resistance. Cyclic laboratory data was evaluated using Stress Focus theory and shows a unique trend explaining how confining stress influences liquefaction resistance. The "Stress Focus boundary for liquefaction resistance" was established, it describes (based on the soil type) the Stress Focus location on the liquefaction resistance versus vertical effective stress diagram. The in situ cyclic liquefaction resistance ratio (CRR) can be determined using the normalized cyclic liquefaction resistance ratio (CRR_1) and the soil type determined Stress Focus.

7 References

Hynes, M.E. (1988). Pore pressure characterization of gravels under undrained cyclic loading, PhD dissertation, University of California at Berkeley.

Olsen, R.S. (1984) Liquefaction analysis using the Cone Penetrometer Test (CPT), In Proceedings of the Eighth world conference on Earthquake Engineering, July, San Francisco.

Olsen, R.S. (1994). Normalization and Prediction of Geotechnical Properties using the Cone Penetrometer Test (CPT), University of California at Berkeley.

Olsen R.S. and Mitchell J.K. (1995). CPT stress normalization and prediction of soil classification, in proceedings of International Symposium on Cone Penetrometer Testing - CPT'95, Linkoping, Sweden, October.

Pillai, V.S, and Byrne, P.M. (1994). Effect of overburden pressure on Liquefaction resistance of sands", Canadian Geotechnical Journal, Vol. 31, pg 53-60

Phukunhaphan, A., Tsai, C.F., and Thiers, G.R. (1982) Dynamic behavior of tailings material, In the proceedings of dynamic stability of tailing dams, ASCE

Seed, H.B. (1983). Earthquake-Resistance Design of Earth Dams, In Proceedings of a symposium entitled seismic design of embankments and caverns, May, pg 41-64

Seed, H.B. (1983), Personal communications

Seed, R.B. and Harder, L.F. (1990). SPT-based analysis of cyclic pore pressure generation and undrained strength. In Proceedings of the H. B. Seed Memorial Symposium, May 1990, Vol. 2, pg 351-376.

Thomas, J. (1992). Static, cyclic and post liquefaction undrained behavior of Fraser River Sand, Masters Thesis, University of British Columbia, Canada, October

Vaid, Y.P., Chern, J.C., and Tumi, H. (1985) Confining pressure, grain angularity, and liquefaction, Journal of Geotechnical Engineering, ASCE, October, Vol. 111, No. 10, pg 1229-1235

Vaid, Y.P. and Thomas, J. (1994). Post liquefaction behavior of sand, In Proceedings of the 13th International Conference on Soil Mechanics and Foundation Engineering, New Delhi, India

Vaid, Y.P, and Thomas, J. (1995). Liquefaction and post liquefaction behavior of sand, Journal of Geotechnical Engineering, Vol. 121, No. 2, February, pg 163-173

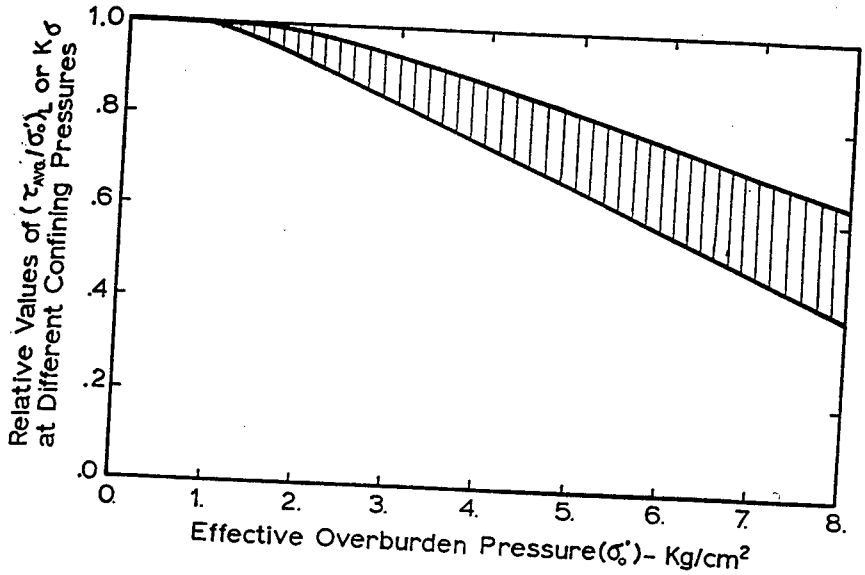

Figure 1 Typical reduction in cyclic stress ratio causing liquefaction with increase in initial confining stress (Seed, 1983)

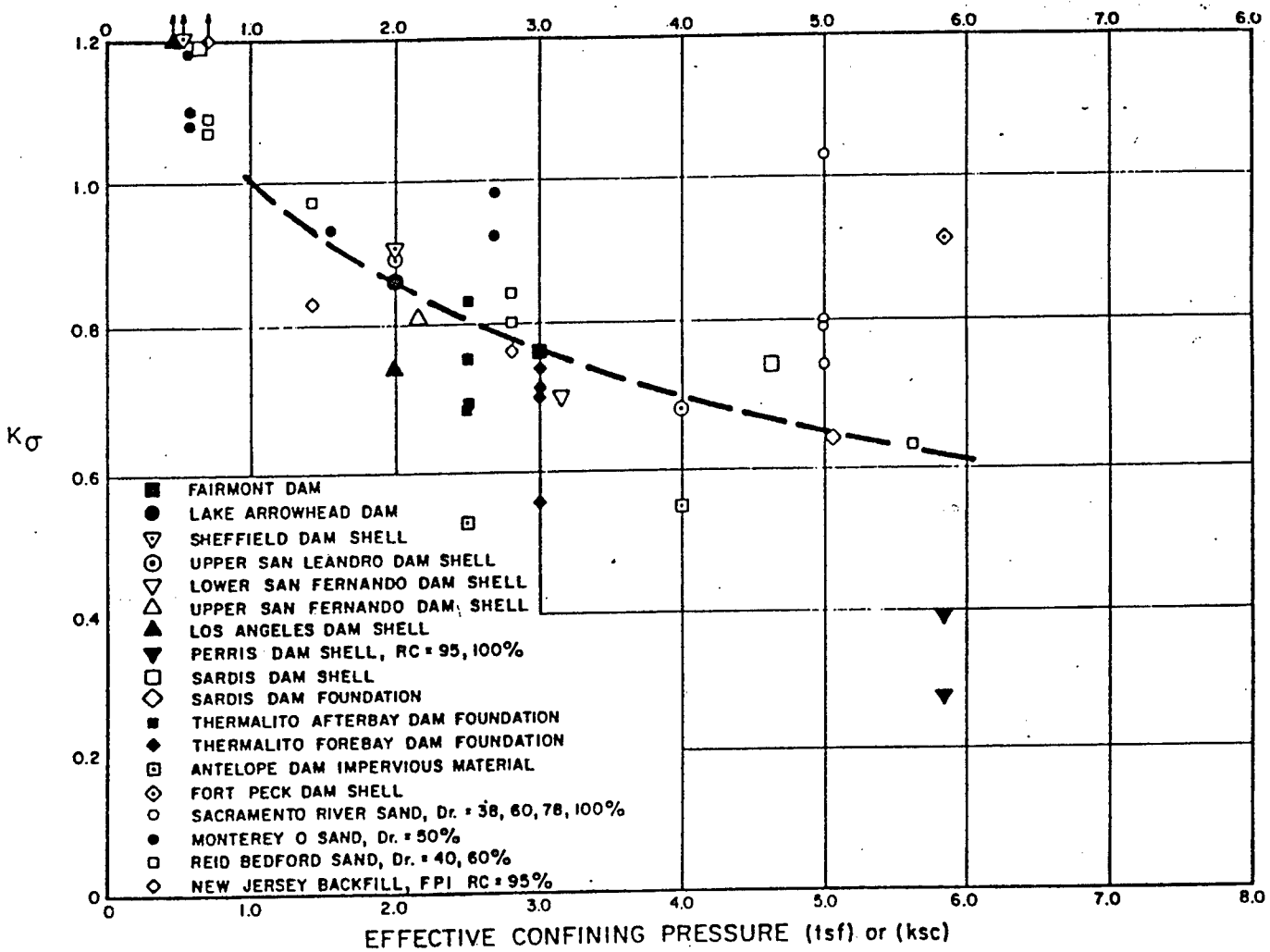

Figure 2 Typical reduction in the cyclic stress ratio required for failure with increased confinement (Harder, 1988)

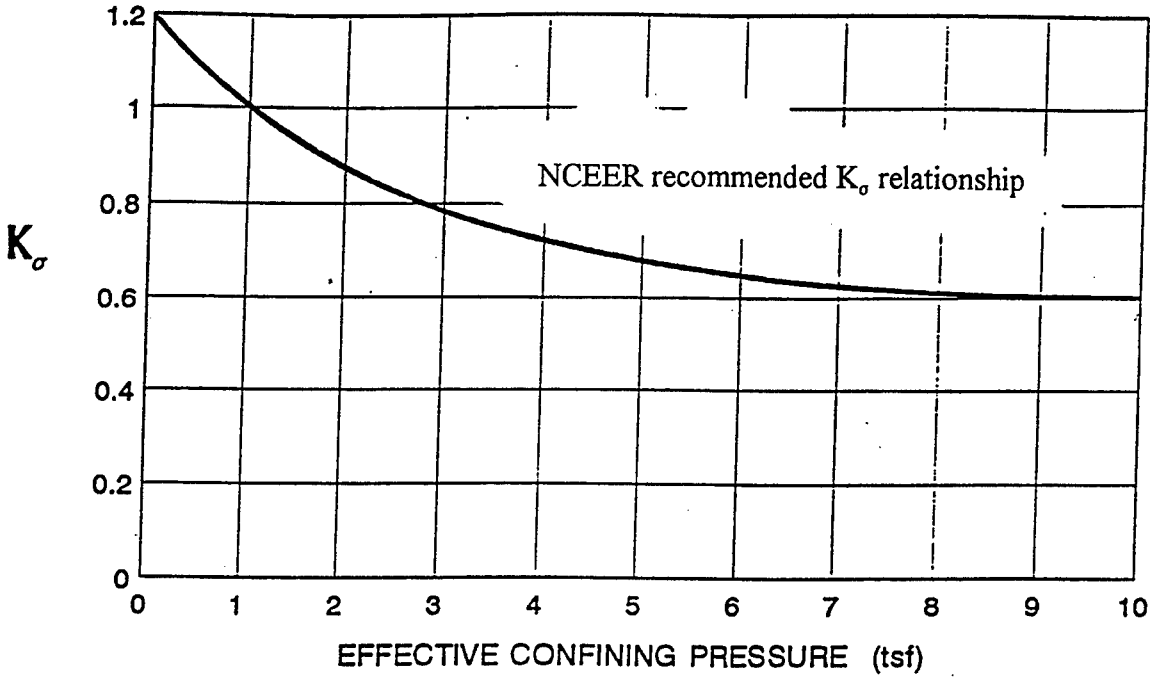

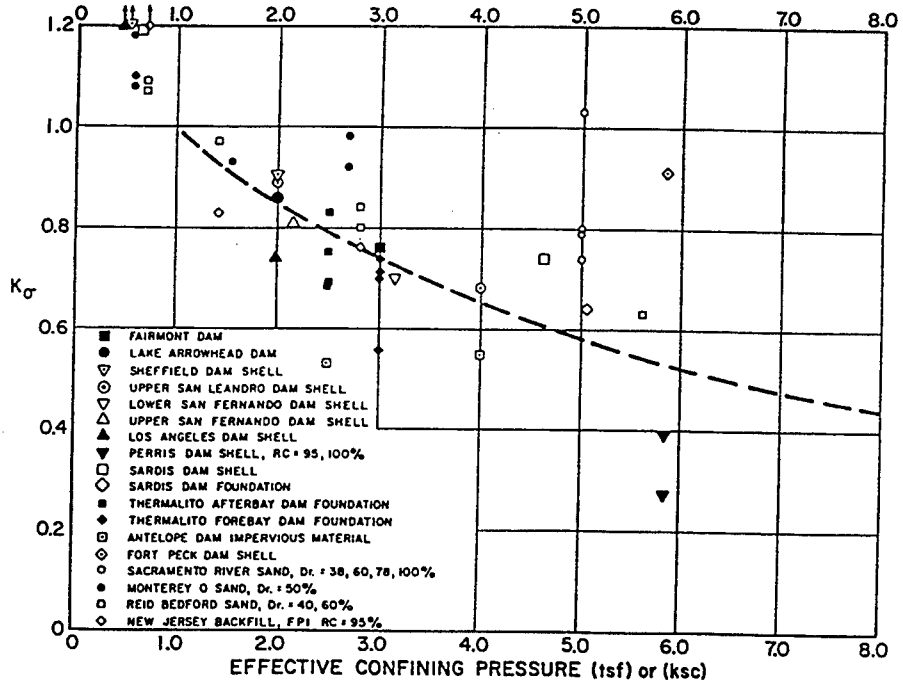

Figure 3 Typical reduction in the cyclic stress ratio required for failure with increased confinement (Seed & Harder, 1990)

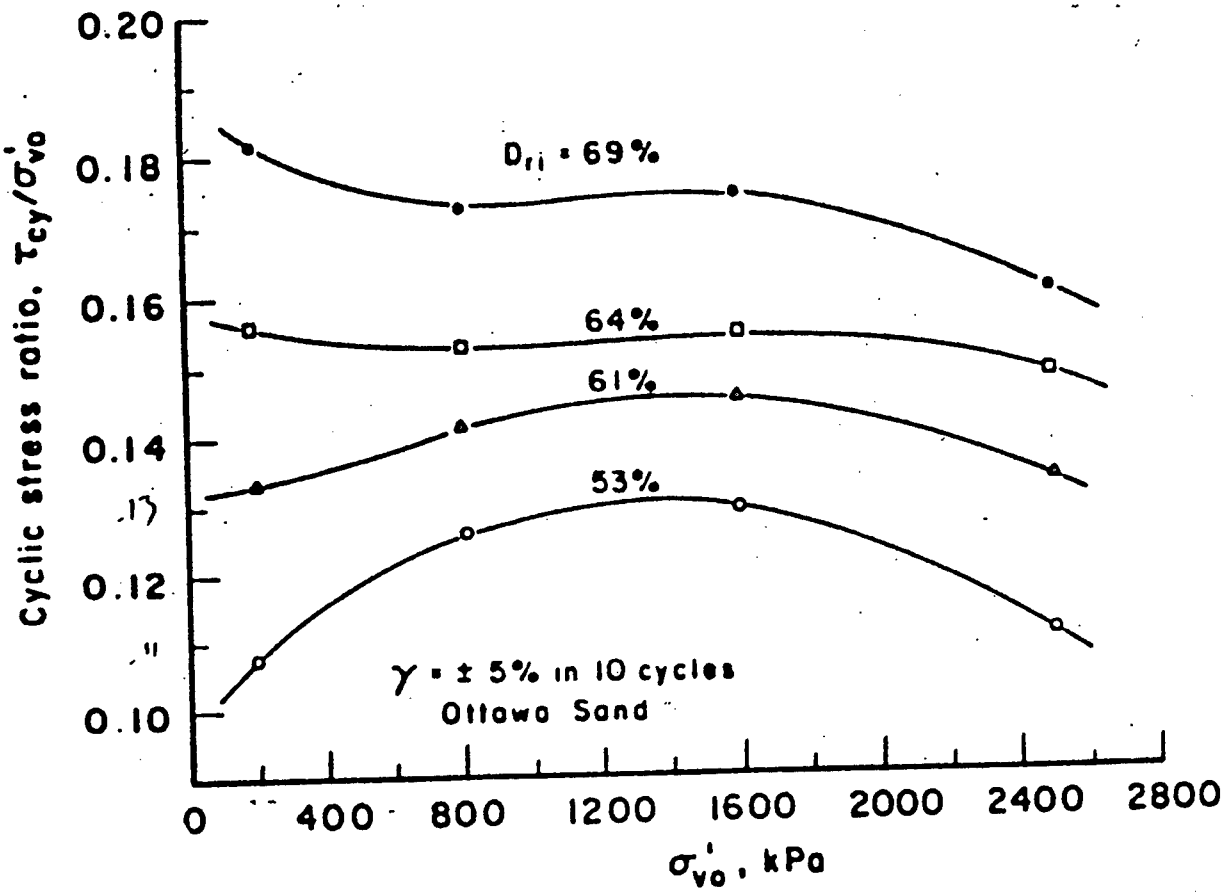

Figure 4 Effect of confining pressure on liquefaction resistance of sands prepared at various initial relative densities (D_r = 43-70% and D_r=53-69%) (Vaid, Chern, & Tumi, 1985)

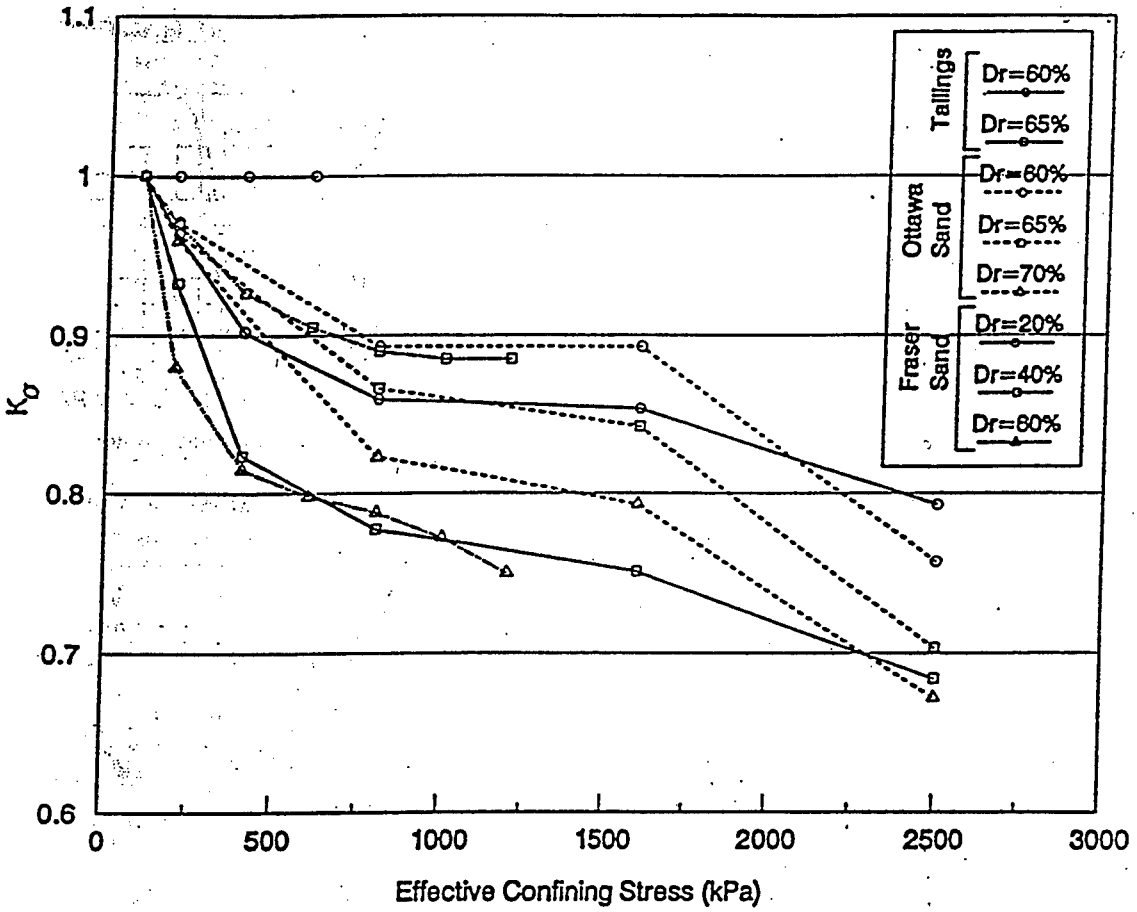

Figure 5 Relationship between effective overburden pressure and K_o (University of British Columbia data) (Pillai & Byrne, 1994)

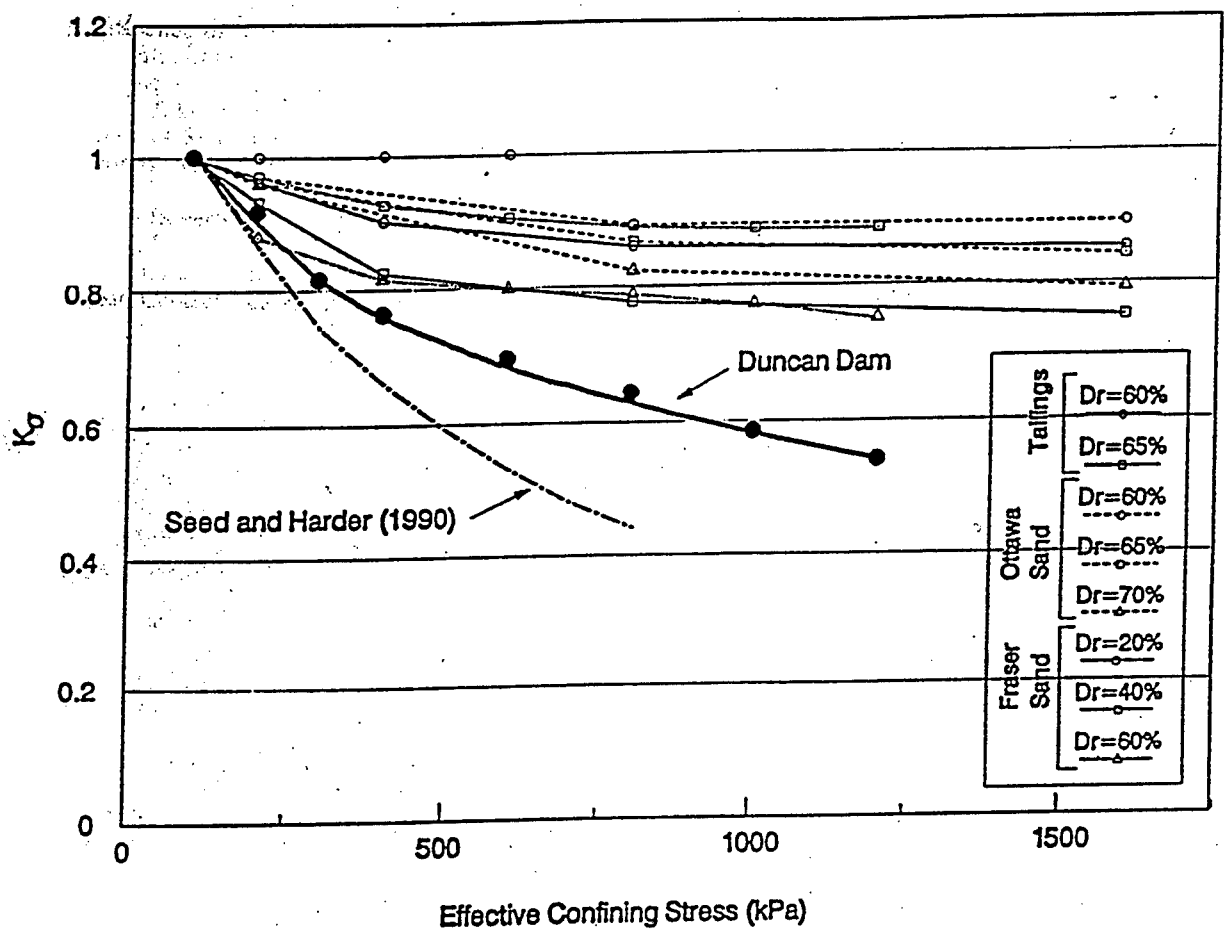

Figure 6 Relationship between effective overburden pressure and K_o for data from three projects (Pillai & Byrne, 1994)

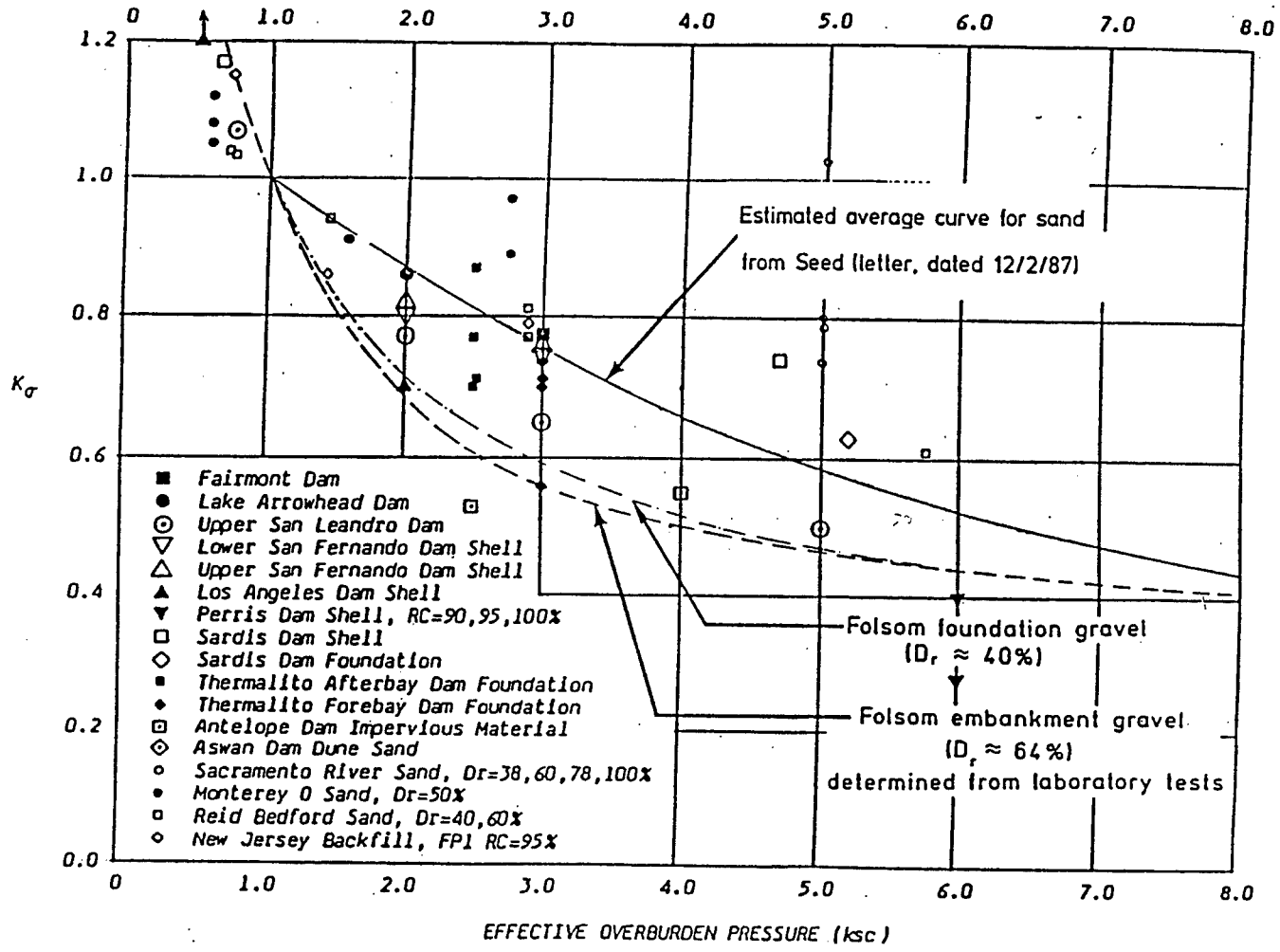

Figure 7 Relationship between overburden stress and K_o for Folsom Dam gravel (Hynes, 1988)

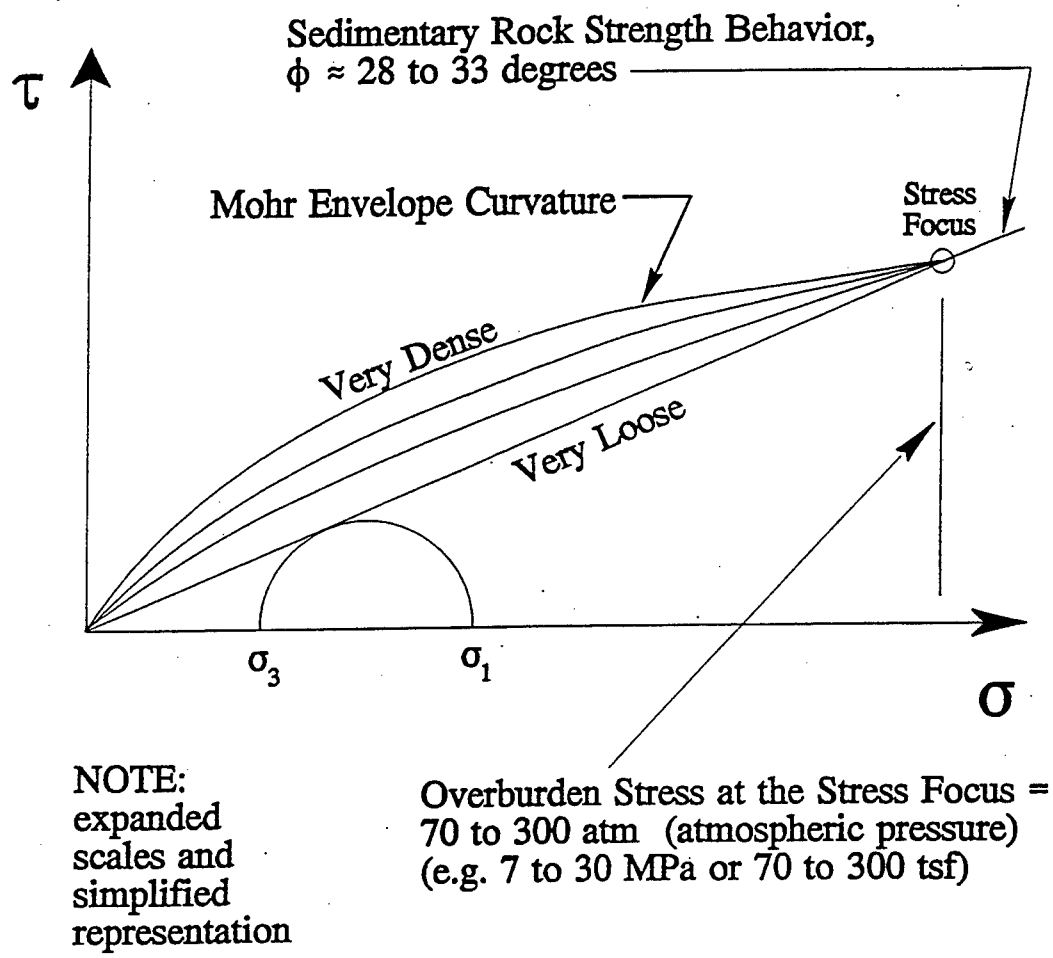

Figure 8 Simplified representation of the Stress Focus using the Mohr envelope curvature (Olsen, 1994)

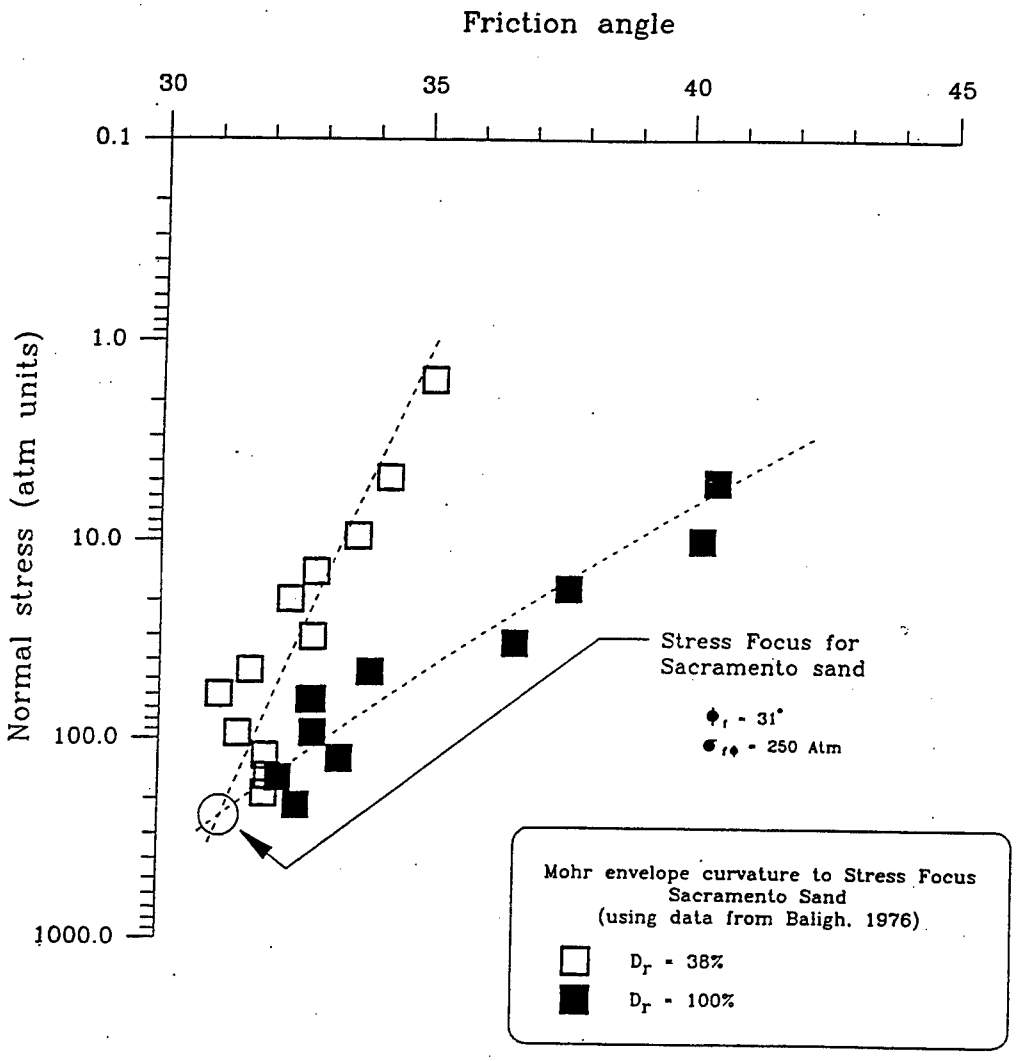

Figure 9 Strength stress focus described for sacromento sand in terms of friction angle and overburden stress (data from Baligh, 1976)(Olsen, 1994)

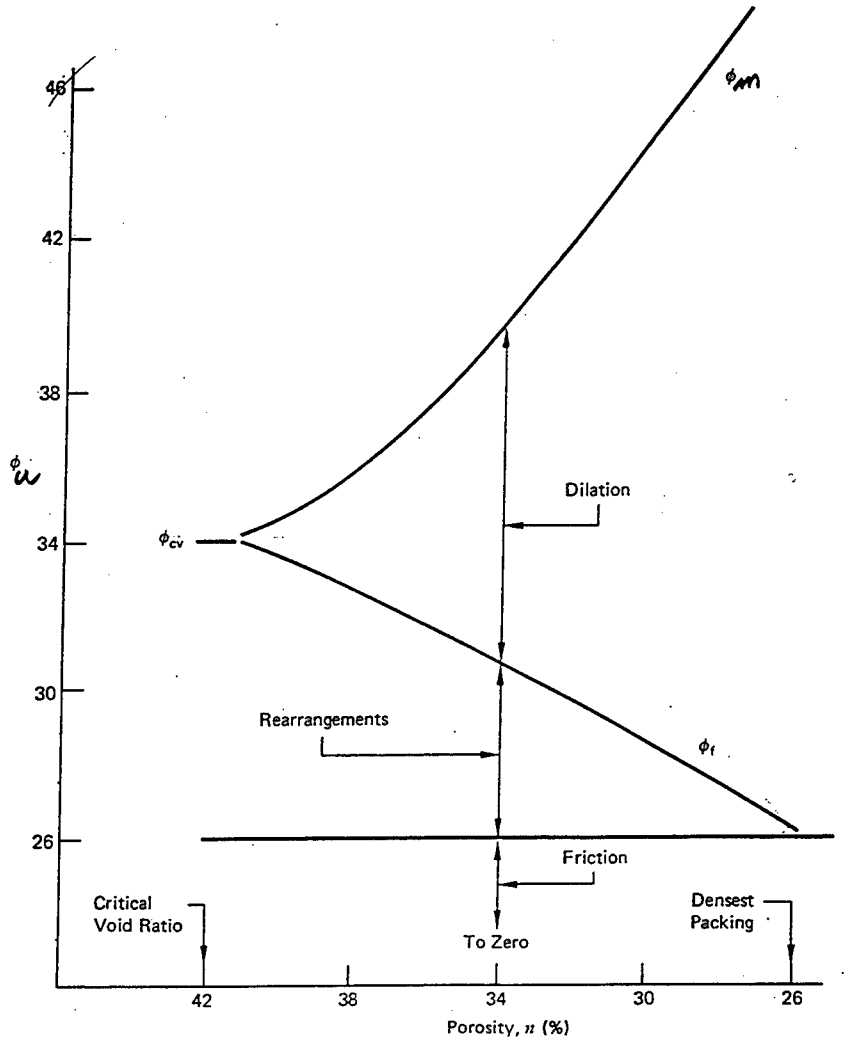

Figure 10 Components of shear strength in granular soils (after Mitchell, 1993, and Rowe, 1962)

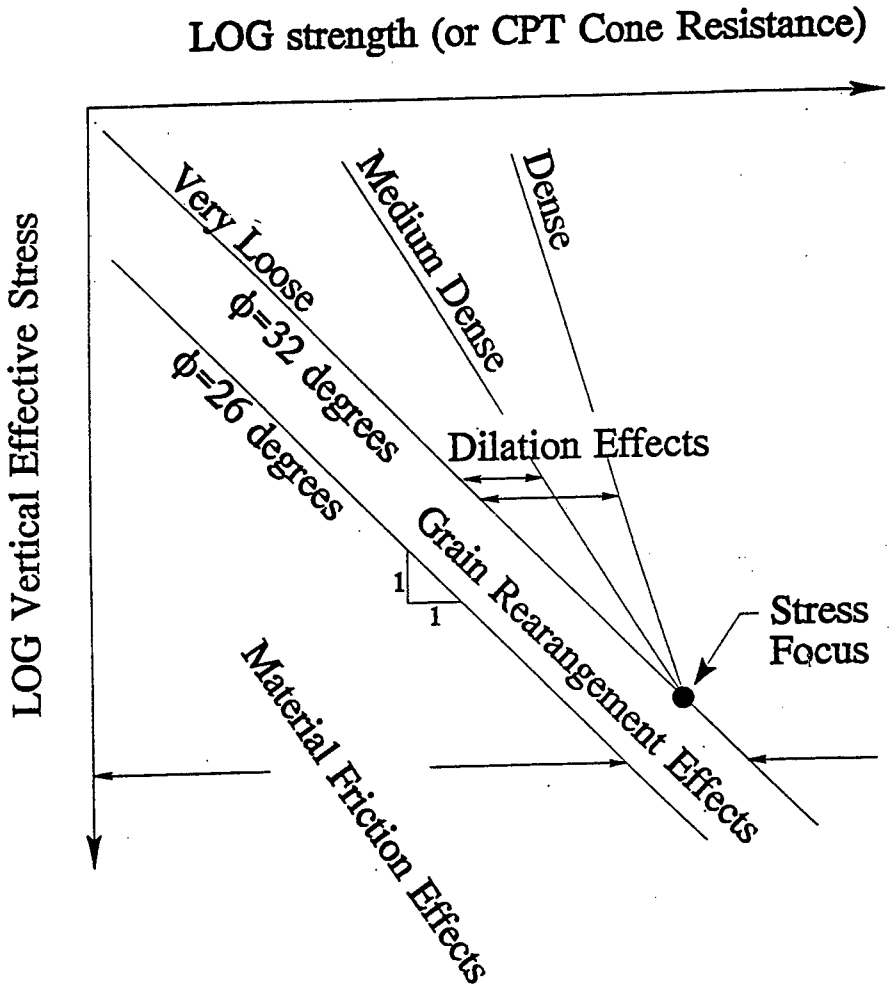

Figure 11 Proposed interaction of friction angle and stress focus concept (Olsen, 1994)

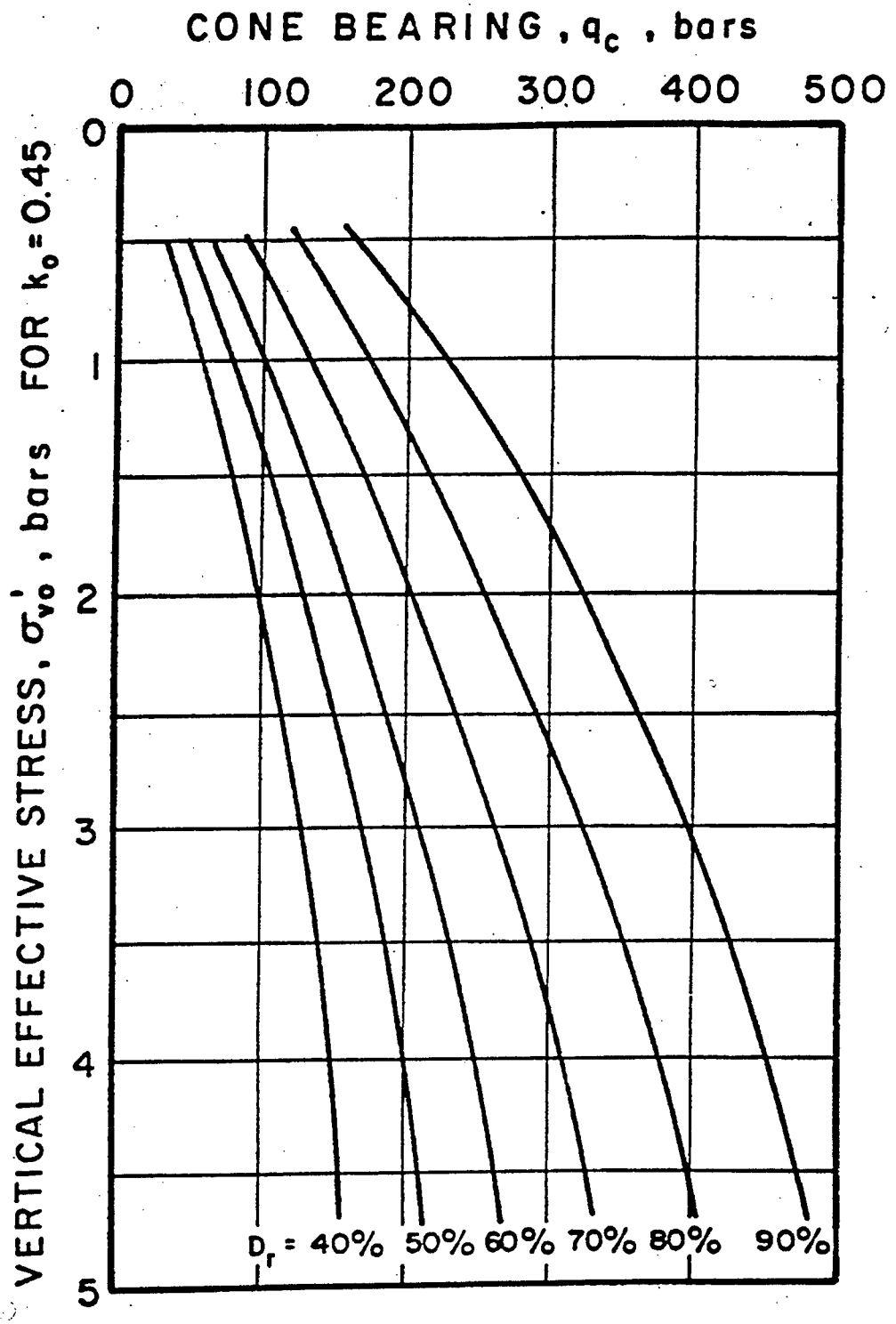

Figure 12 Trends of cone resistance versus vertical effective stress for Ticino sand (Baldi, et. al. 1981)

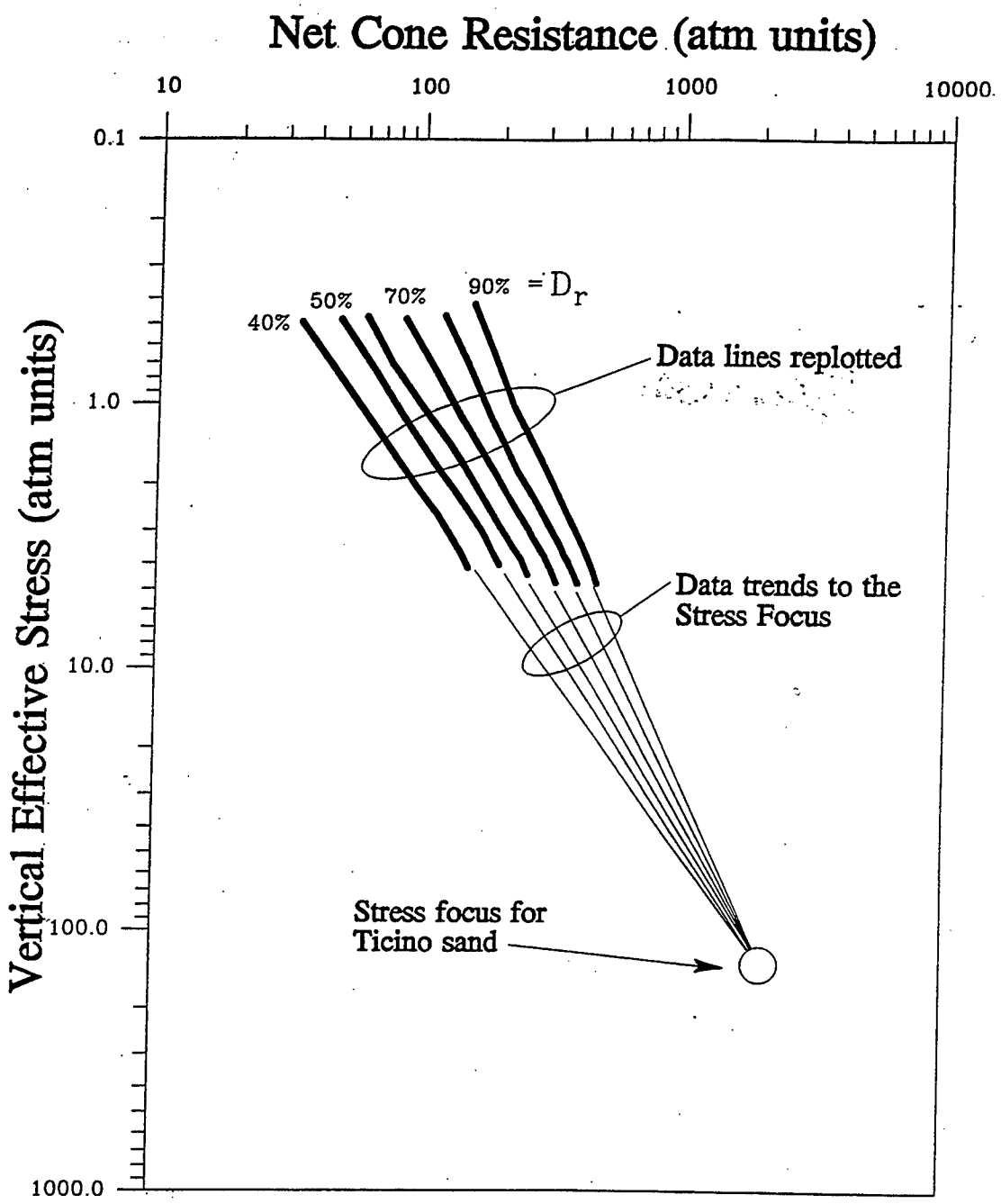

Figure 13 Replotting of Baldi, et. al, 1981 data curves from Figure 12 in terms of $\log_{10}$ net cone resistance versus $\log_{10}$ vertical effective stress (Olsen, 1994)

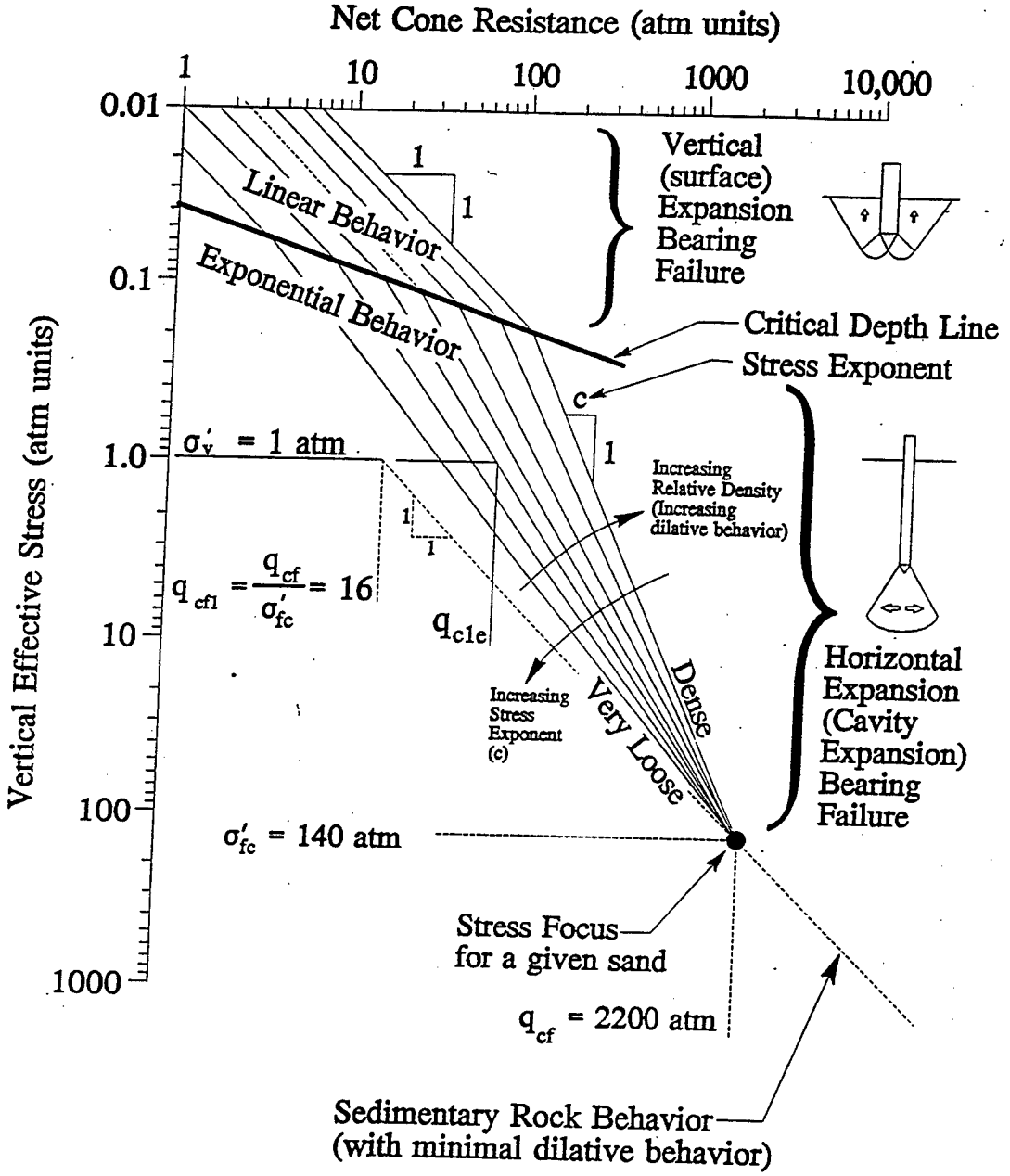

Figure 14 Annotated description of the cone resistance Stress Focus together with bearing stress divided into vertical expression failure and cavity expansion failure (Olsen, 1994)

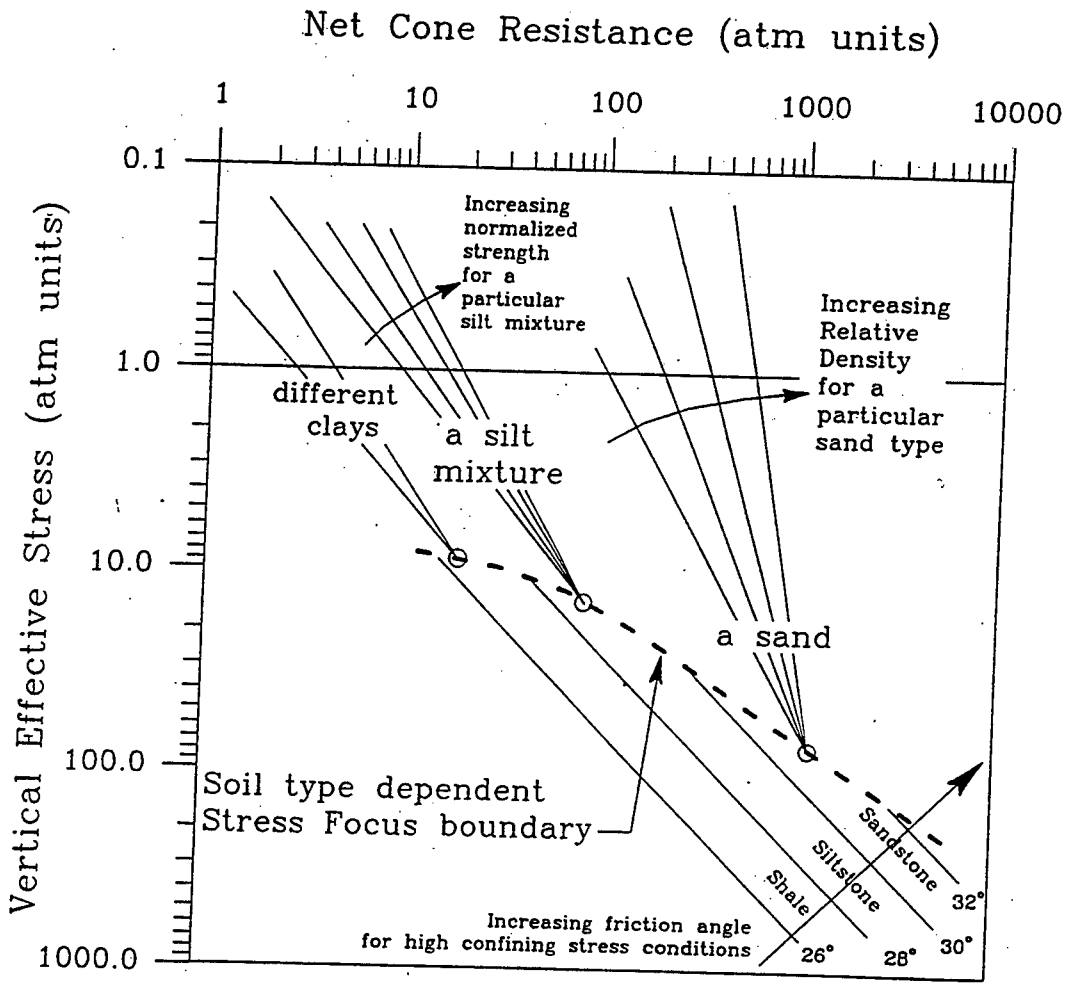

Figure 15 Inferences concerning the soil type dependent Stress Focus (the Stress Focus boundary) (Olsen, 1994)

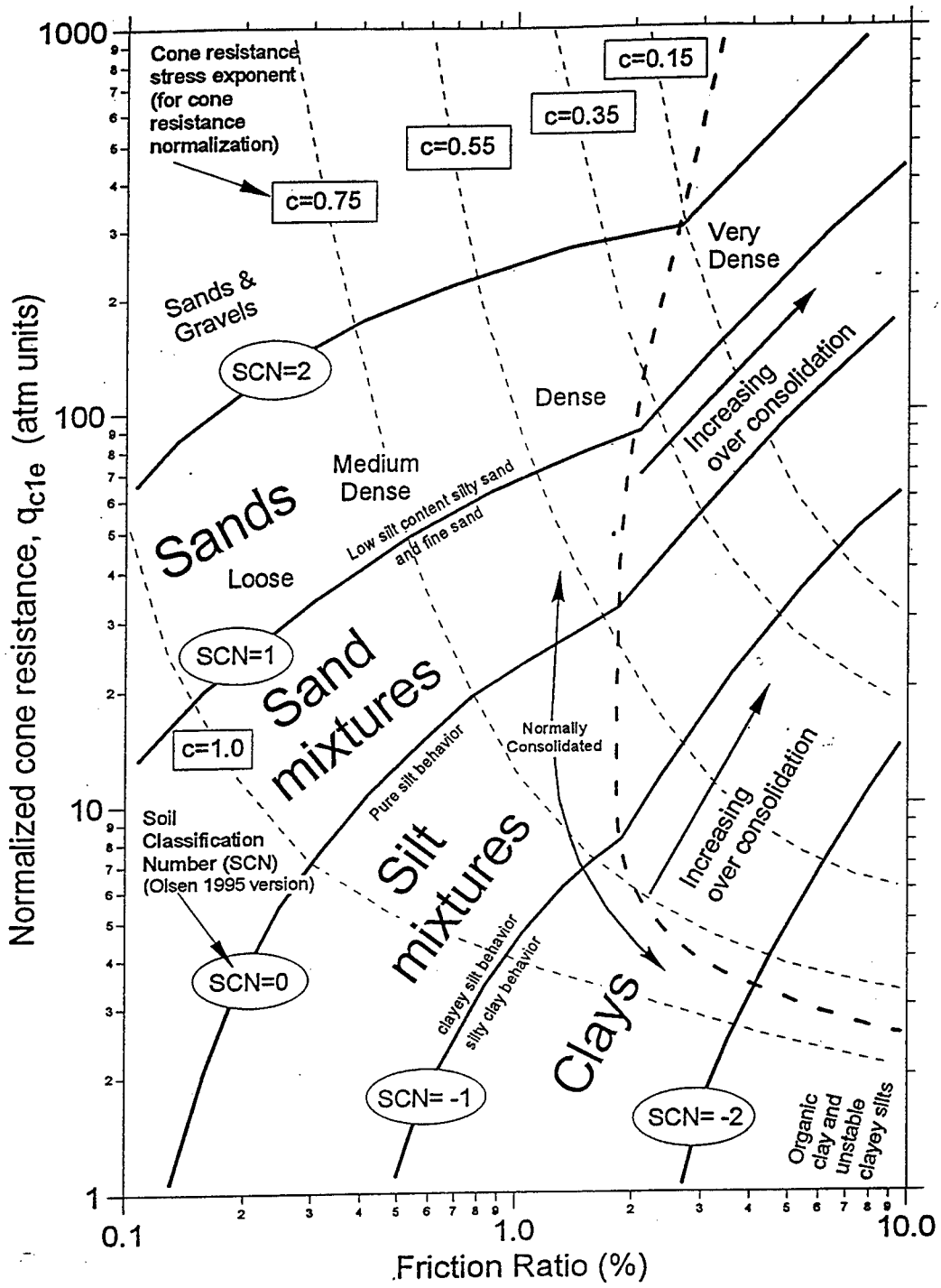

Figure 16 Annotated CPT soil characterization chart having the CPT cone resistance stress exponent, c (Olsen & Mitchell, 1995)

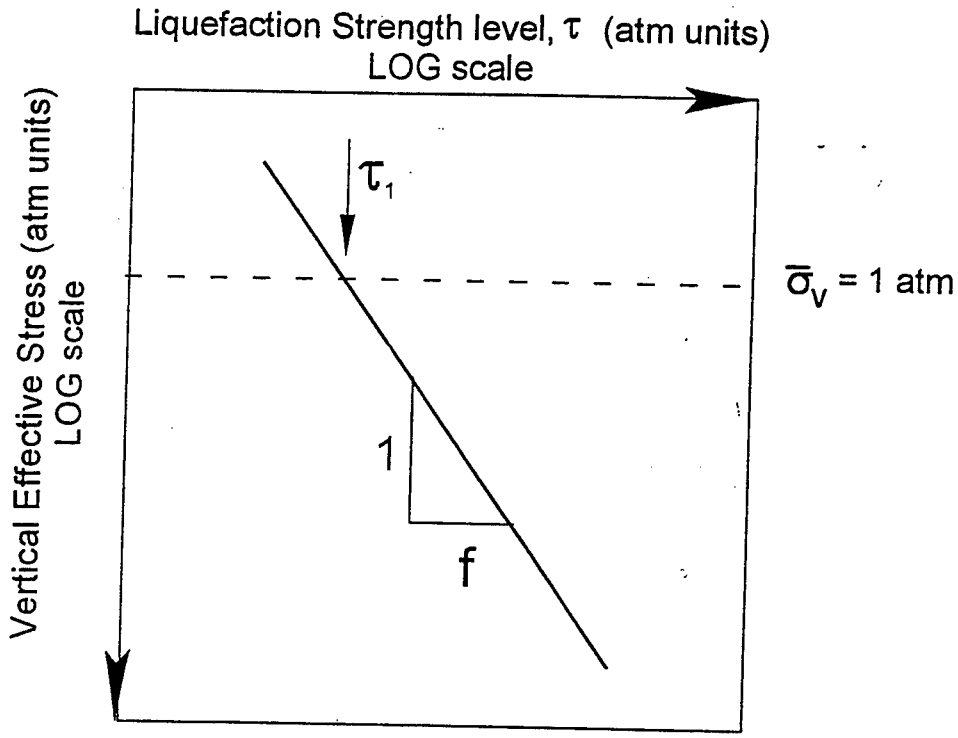

Figure 17 Graphics definition of the normalized liquefaction resistance strength using log-log graphical representation in terms of vertical effective stress

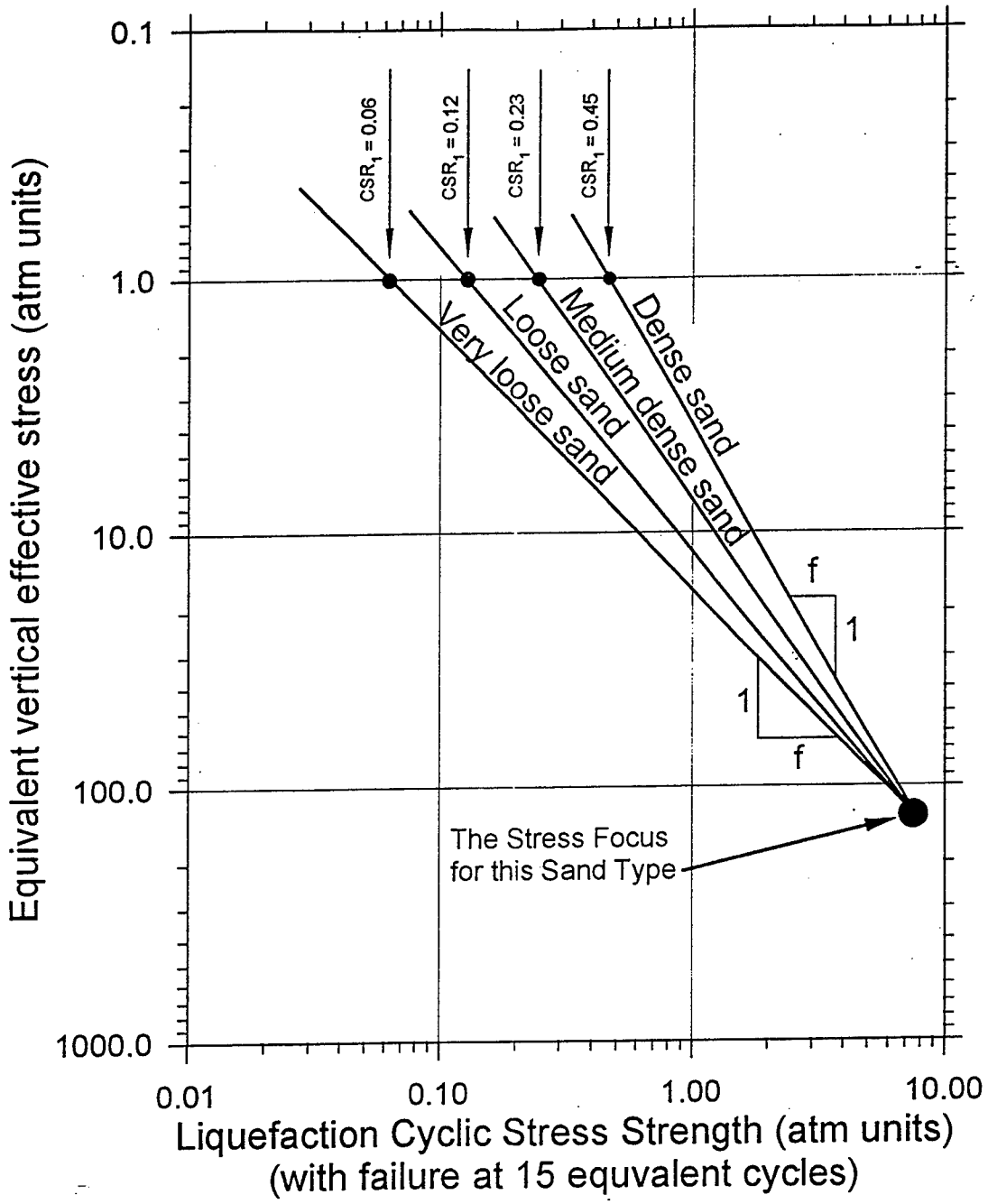

Figure 18 Various relative density trends to the sand dependent stress focus

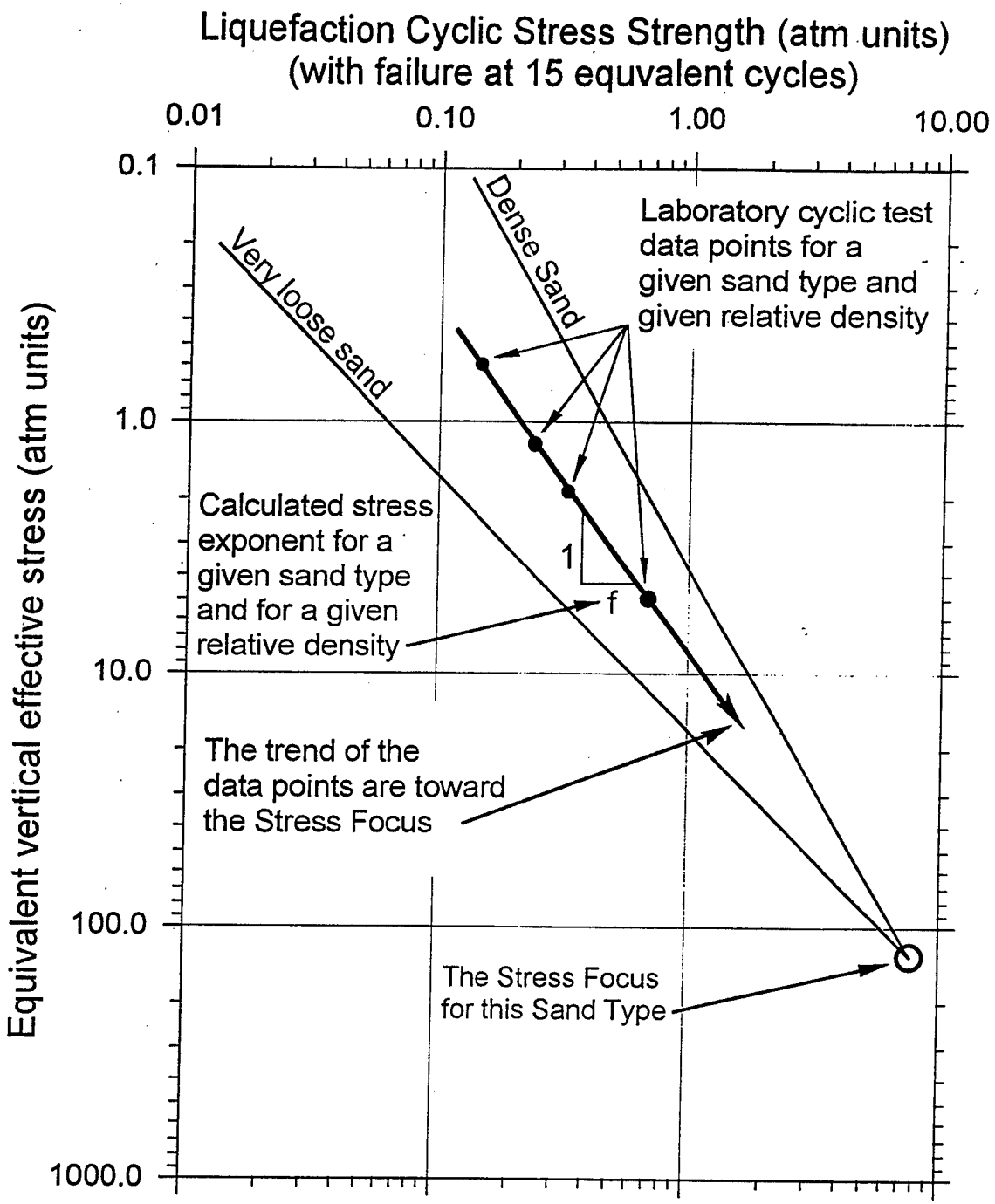

Figure 19 Data points at different confining stress levels for a given sand of constant relative density pointing toward the Stress Focus

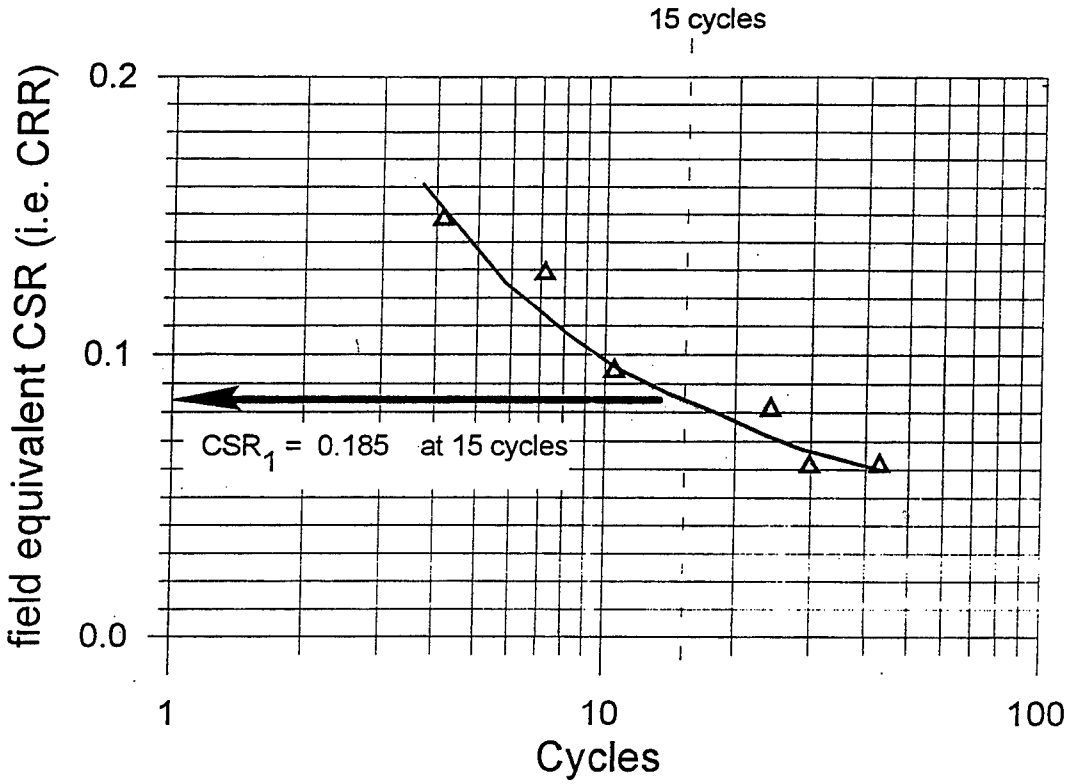

Figure 20 Data points at different triaxial deviator stress levels for a given sand and given confining stress level.

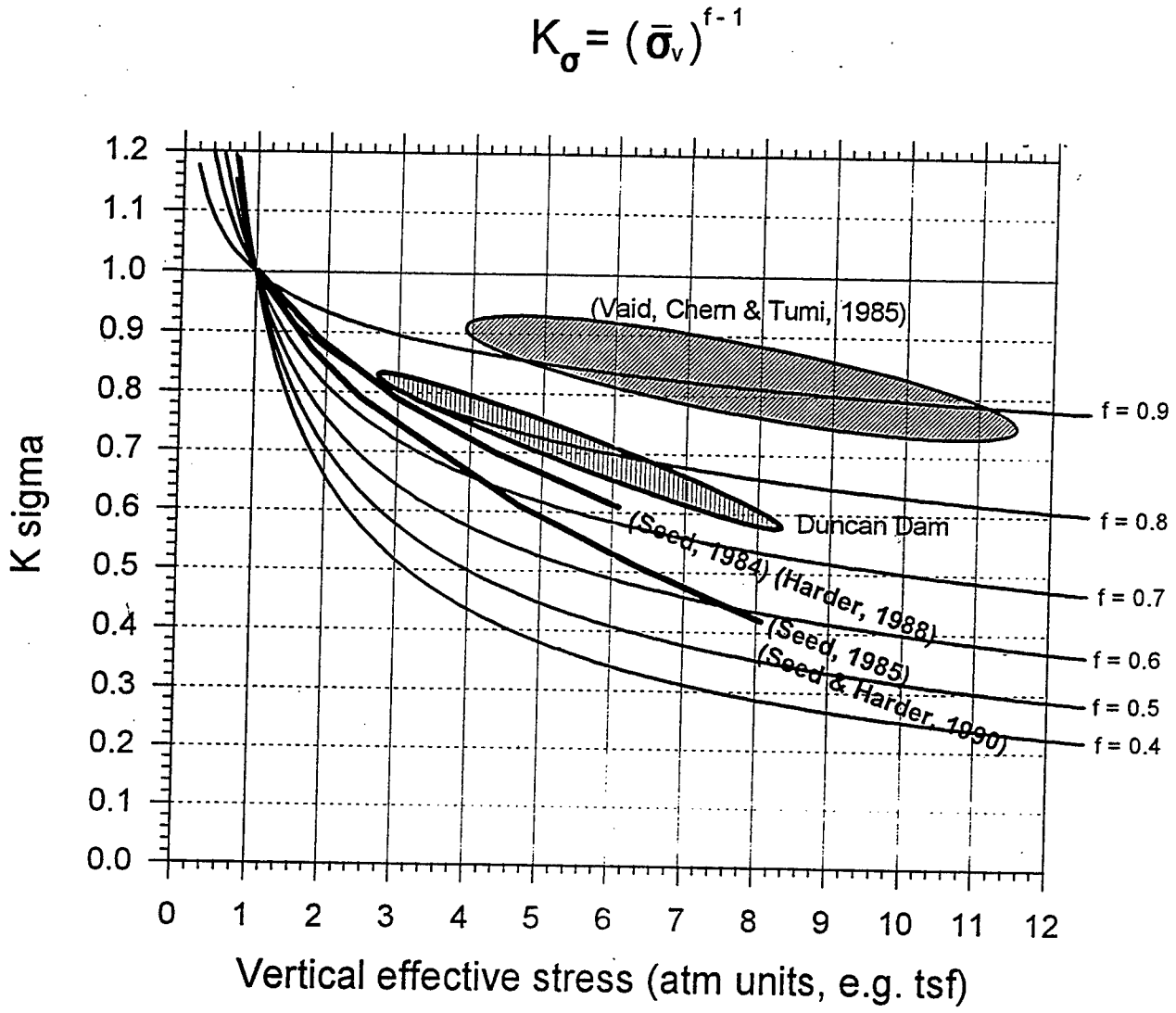

Figure 21 Contours of liquefaction stress exponents on the K_o chart

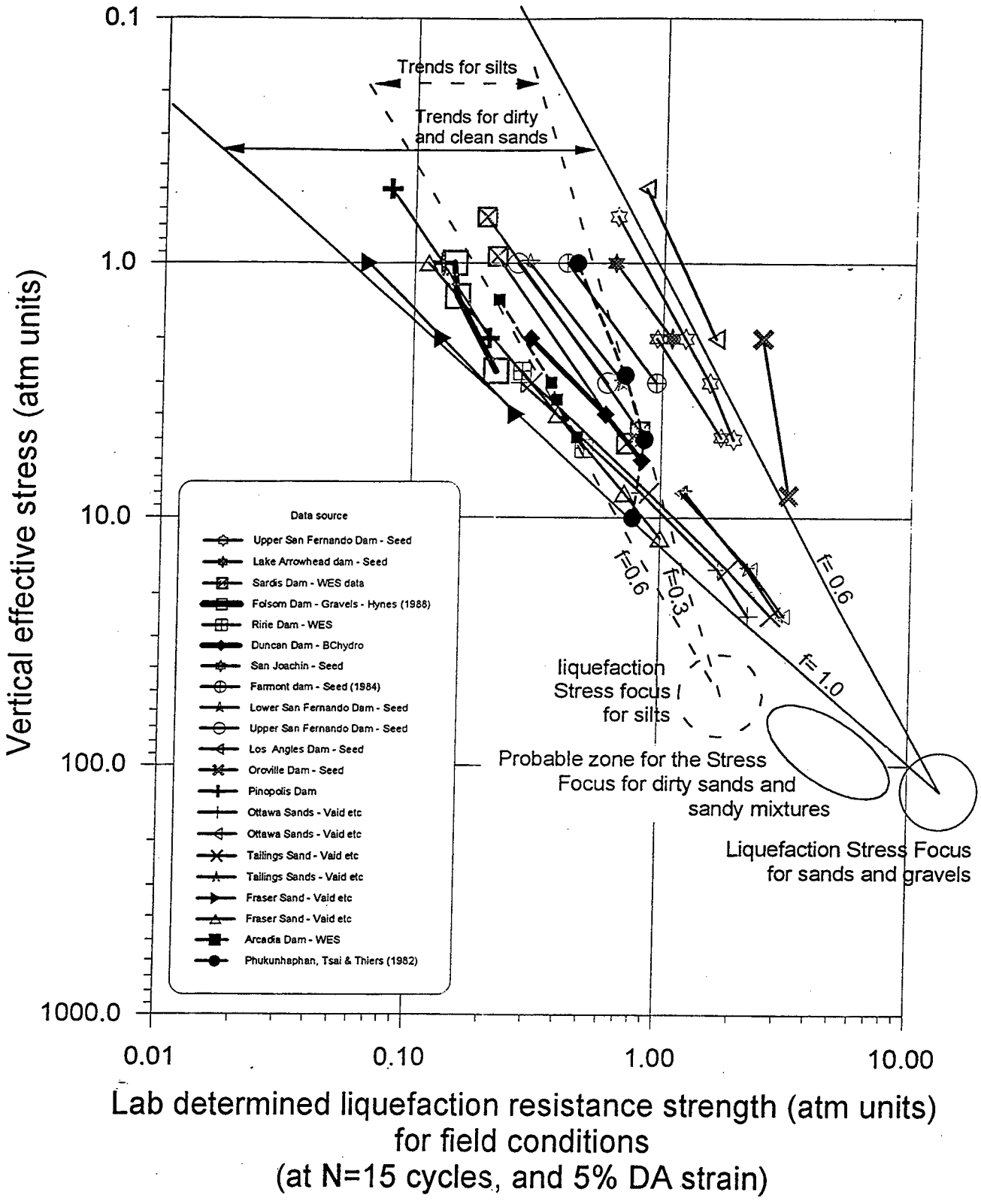

Figure 22 Trends of all the cyclic triaxial liquefaction resistance based strengths on the Stress Focus graphic format (trends to the sand sand silt stress focus locations are also shown)

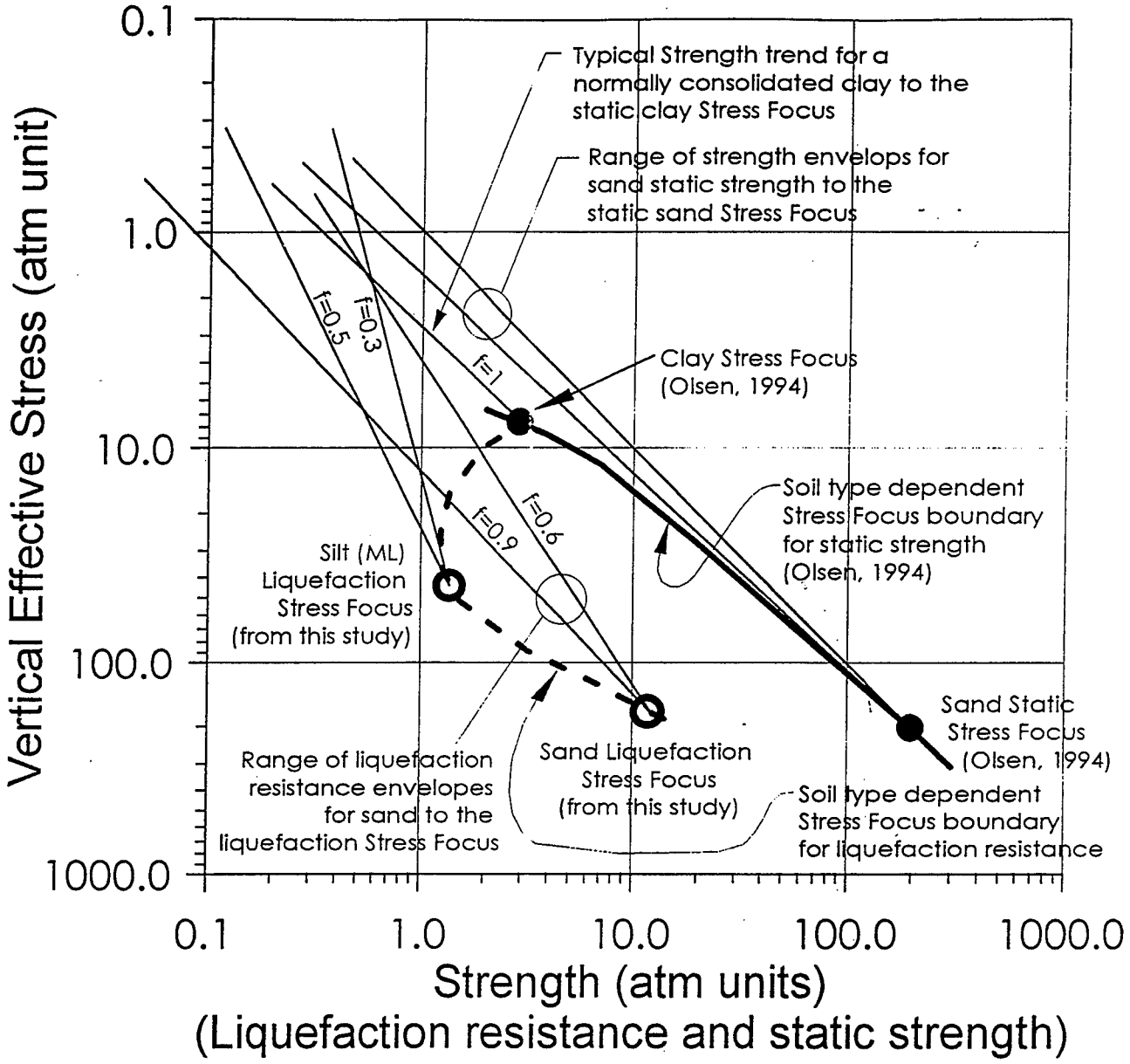

Figure 23 Stress Focus boundaries for liquefaction resistance and static strength (Olsen, 1994)

This example
Given: Silty sand (low silt content) soil type and SPT determined $CSR_1 = 0.29$
Need: the liquefaction resistance at a vertical effective stress of 4 atm
Answer: liquefaction resistance resistance = to 0.7 atm (i.e. CSR= 0.18 or $K_\sigma = 0.6$)

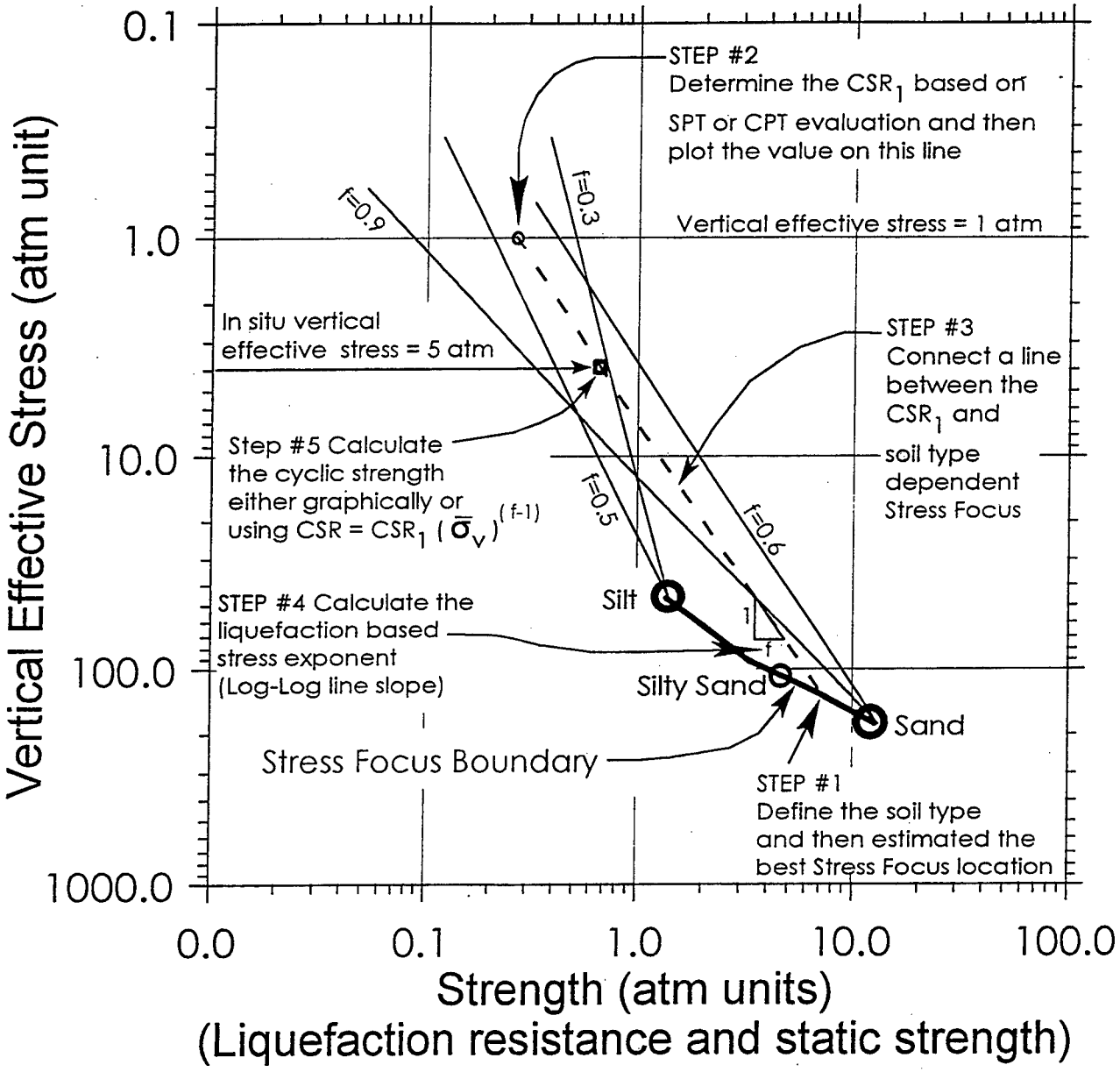

Figure 24 Proceedure for determing in situ liquefaction resistance using Stress Focus concepts together with CPT or SPT predicted CSR_1 and the generalized soil type.

Dynamic Response Analysis of Rockfill Dams Considering Frequency Dependent Characteristics of Radiation Damping Ratio

Hitoshi YOSHIDA[1)]

Tomoya IWASHITA[2)]

ABSTRACT

To ensure accurate dynamic analysis of rockfill dams, it is important to evaluate the damping ratio appropriately. In the present method, the total damping ratio is evaluated from the hysteresis damping of rockfill materials with the addition of a constant radiation damping ratio in FEM analyses with a rigid base. The frequency dependence of the radiation damping ratio is not taken into consideration in dynamic analysis. In this study, the radiation damping ratio was estimated by subtracting the hysteresis damping ratio obtained by laboratory tests of rockfill materials from the total damping ratio calculated by response analysis of observed earthquake motions. Furthermore, the frequency dependence of the radiation damping ratio was evaluated. The frequency dependent characteristics of the damping ratio can be represented by using the parameter α in the Rayleigh damping matrix to be 0.9. The two-dimensional dynamic analysis QUAD-4 for rockfill dam models with a rigid base was computed considering the frequency dependence of the damping ratio. The calculated response results of the analysis agreed closely with the observed maximum acceleration.

Key Words : *rockfill dam, dynamic analysis, radiation damping, frequency dependence, Rayleigh damping*

1. INTRODUCTION

For the dynamic analysis of rockfill dams, we used a simple analytical model with rigid base because the stiffness of the base rock is much greater than that of the dam body. The shear modulus and hysteresis damping ratio obtained by laboratory tests are used as input data to the dynamic analysis. The reliability of the shear modulus was confirmed by comparison with in-situ tests (Iwashita et al., 1995). Since it is difficult to estimate accurately the radiation damping ratio by the dissipation of wave energy into the base rock from the dam body, a constant radiation damping ratio which was independent of frequency was used. The number of rockfill dams constructed at sites with unfavorable geological foundations has increased in recent years. In these cases, the impedance ratio between the dam body and the dam foundation increases as the stiffness of the dam foundation decreases, and also the radiation damping ratio increases. Therefore, it is important in the dynamic analysis of rockfill dams to evaluate the radiation damping ratio quantitatively and to estimate the frequency dependent characteristics of the radiation damping ratio.

In this study, we estimated the radiation damping ratio by subtracting the hysteresis damping ratio of rockfill materials obtained by laboratory tests from the total damping ratio obtained by response analysis of observed earthquake motions at existing dams, and clarified the frequency dependent characteristics

1) Head of Fill Dam Division, Dam Department, Public Works Research Institute, Ministry of Construction, Tsukuba City, 305 Japan

2) Research Engineer, Fill Dam Division, ditto

of the radiation damping ratio. From the results, we computed the two-dimensional dynamic analysis QUAD-4 of rockfill dam models with rigid base considering the frequency dependent characteristics of the radiation damping ratio by adopting the parameter α in the Rayleigh damping matrix. We compared the calculated maximum response acceleration with the observed value.

2. EARTHQUAKE MOTIONS OBSERVED AT DAMS

This study used earthquake motions observed at two existing dams: Miho Dam and Oya Dam. These dams are zoned rockfill dams with a central core and are 95 m and 56.5 m high respectively. Figures 1(a) and (b) show the sections of the dams and the locations of seismographs. For Miho Dam, seismographs have been installed at the crest and downstream toe foundation, and for Oya Dam, seismographs have been installed at the crest and in the limb tunnel on the left abutment. Tables 1 (a) and (b) list the earthquake records used in this study.

We calculated the natural frequencies of the dam bodies from the frequency response functions at the dam crest corresponding to the foundation in the upstream-downstream component. In the response analysis, we need to use rock outcrop earthquake motions. Seismographs, however, have not been installed at rock outcrop sites near the two dams. We considered that the earthquake motions observed at the downstream toe foundation of Miho Dam were nearly equal to those monitored at the rock outcrop site, because the vibration of the dam body had little effect on the motions of the downstream toe foundation during earthquakes. In Oya Dam, we used earthquake motions observed in the limb tunnel on the left abutment in the same manner. We smoothed the frequency response functions using a Parzen window with a band width of 0.6 Hz. Figures 2 (a) and (b) show the typical frequency response functions for each dam.

3. QUANTITATIVE ESTIMATION AND FREQUENCY DEPENDENT CHARACTERISTICS OF RADIATION DAMPING RATIO

We estimated the total damping ratio $h_{t,i}$ of dams for the first to third resonance frequencies from the frequency response functions at the dam crest corresponding to the foundation of observed accelerations by the half power method as expressed by equation (1) and as shown in Figure 3:

$$h_{t,i}(\%) = \frac{\Delta f_i}{2 \cdot f_i} \times 100 \qquad (1)$$

We carried out large-scale cyclic triaxial laboratory tests on specimens 300 mm in diameter and 600 mm high using rockfill materials transported from the quarry site for each dam and obtained the hysteresis damping ratio h_h of the rockfill materials. Figures 4 (a) and (b) show the relationships between the total damping ratio $h_{t,1}$ of the dam body and the shear strain γ_1 for the first natural frequency during each earthquake and also the relationships between the hysteresis damping ratio h_h and shear strain γ obtained from laboratory tests. We calculated the shear strain γ of the dam body from the maximum acceleration a_{max} at the crest (Iwashita et al., 1995):

$$\gamma = \frac{d_{max}}{H} = \frac{a_{max}}{(2\pi f_1)^2 \cdot H} \qquad (2)$$

where H is the height of dam.

As shown in Figures 4 (a) and (b), the total damping ratio $h_{t,i}$ at each strain level from the response analysis of observed earthquake

accelerations consists of both the internal damping ratio, which is almost covered by the hysteresis damping ratio h_h for earth structures, and the radiation damping ratio $h_{r,i}$.

The each vibration mode has different participation in the shear strain. We calculated the shear strain γ_i for the i-th vibration mode from the ratio of the Fourier spectrum amplitude of the shear strain wave at the crest for the i-th natural frequency against the peak amplitude (Sugito et al., 1994), as expressed by equation (3) and as shown in Figure 5:

$$\gamma_i = \gamma \cdot \frac{F_{\gamma,i}}{F_{\gamma max}} \tag{3}$$

where $F\gamma_{,i}$ is the Fourier spectrum amplitude of the shear strain for the i-th natural frequency and $F\gamma_{max}$ is the maximum amplitude of the Fourier spectrum of shear strain.

We estimated the radiation damping ratio $h_{r,i}$ by subtracting the hysteresis damping $h_h(\gamma_i)$ from the total damping ratio $h_{t,i}$, as expressed by equation (4):

$$h_{r,i} = h_{t,i}(\gamma_i) - h_h(\gamma_i) \tag{4}$$

Figures 6 (a) and (b) show the relationships between radiation damping ratio $h_{r,i}$ for each earthquake motion and the first to third natural frequency of the dam body.

Ohmachi (1981) derived the radiation damping ratio $h_{r,i}$, as expressed by equation (5), by modeling a two-dimensional triangle-shaped elastic dam body on a homogeneous semi-infinite elastic base, and by replacing the equation of motion in the i-th vibration mode for a non-damping shear vibration model with that for a damping-free vibration model with a single degree of freedom.

$$h_{r,i} = \frac{1}{zi} \cdot \beta \tag{5}$$

where β is the vibration impedance ratio between the dam body and the foundation, and z_i is the i-th value that gives zero in the Bessel function of the first kind of order zero.

Toki (1981) derived the radiation damping ratio $h_{r,i}$, as expressed by equation (6), by equating the resonance amplitude of the surface displacement for a non-damping layer ground model on the elastic base with that for a complex stiffness surface ground model on a rigid base:

$$h_{r,i} = \frac{2}{(2i-1)\cdot\pi} \cdot \frac{\beta}{\sqrt{1-\beta^2}} . \tag{6}$$

Sato (1983) derived the radiation damping ratio $h_{r,i}$, as expressed by equation (7), by equating the natural circular frequency of a non-damping elastic two-layer ground model with that for a Voigt type viscoelastic surface ground model on a rigid base:

$$h_{r,i} = \frac{1}{(2i-1)\cdot\pi} \cdot \ln\frac{|1+\beta|}{|1-\beta|} . \tag{7}$$

The radiation damping ratios with the parameter γ from equations (5), (6) and (7) are plotted together in Figures 6 (a) and (b). The radiation damping ratios $h_{r,i}$ of the two dams from the response analysis of observed earthquake motions and laboratory tests decrease with higher vibration mode. These results show a similar dependence to the results of simple model analyses obtained by the three researchers Ohmachi, Toki, and Sato.

4. ESTIMATION OF PARAMETER FOR ADJUSTMENT OF FREQUENCY DEPENDENCE OF RAYLEIGH DAMPING

When a dam body is taken to be a homogeneous triangle-shaped shear beam, the radiation damping ratio $h_{r,i}$ and the natural circular frequency ω_i of the i-th vibration mode are expressed by equations (8) and (9) respectively (Ohmachi, 1981 and Matsumura, 1934), and the relationship between the radiation damping ratio $h_{r,i}$ and natural circular frequency ω_i is expressed by equation (10):

$$h_{r,i} = \frac{1}{z_i} \cdot \beta, \qquad \frac{h_{r,i}}{h_{r,1}} = \frac{z_1}{z_i} \tag{8}$$

$$\omega_i = \frac{V_{SD}}{2\pi H} \cdot z_i, \qquad \frac{\omega_i}{\omega_1} = \frac{z_i}{z_1} \tag{9}$$

$$\frac{h_{r,i}}{h_{r,1}} = \frac{\omega_1}{\omega_i} \tag{10}$$

where V_{SD} is the S-wave velocity in the dam body.

Consequently, the total damping ratio for the first vibration mode $h_{t,1}$ is expressed by equation (11) with hysteresis damping ratio $h_{h,i}$ (=$h_{h,1}$=const.) of rockfill materials and the parameter m, which is the ratio of the radiation damping and the hysteresis damping for the first vibration mode $h_{r,1}/h_{h,1}$:

$$\frac{h_{t,i}}{h_{t,1}} = \frac{\left(1 + m \cdot \omega_1/\omega_i\right)}{1+m} . \tag{11}$$

The Rayleigh type damping was considered as damping matrix [C]. The Rayleigh type damping matrix is viscoelastic type and expressed as the complex of mass matrix [M] and stiffness matrix [K] by equation (12):

$$[C]_q = h_{t,q} \cdot \omega_1 \cdot [M]_q + \frac{h_{t,q}}{\omega_1} \cdot [K]_q \tag{12}$$

where q is element number, and $h_{t,q}$, $[C]_q$, $[M]_q$, $[K]_q$ are the total damping ratio, damping matrix, mass matrix and stiffness matrix for element q, respectively. Here, let total damping ratio $h_{t,q}$ be constant in all elements, giving:

$$[C] = h_t \cdot \omega_1 \cdot [M] + \frac{h_t}{\omega_1} \cdot [K] . \tag{13}$$

By the modal analysis method, the equation of motion for the reference coordinate of the i-th vibration mode is expressed by equation (14) using the Rayleigh damping of equation (13):

$$\ddot{X} + 2h_t \frac{1}{2}\left(\frac{\omega_1}{\omega_i} + \frac{\omega_i}{\omega_1}\right)\omega_i \dot{X} + {\omega_i}^2 X = -\varphi_i \ddot{y}_0 \tag{14}$$

where X is relative displacement of system, y_0 is displacement of base, ψ is participation factor. From equation (14), the total damping ratio $h_{t,i}$ is obtained by:

$$h_{t,i} = \frac{h_t}{2} \cdot \left(\frac{\omega_1}{\omega_i} + \frac{\omega_i}{\omega_1}\right) . \tag{15}$$

The total damping ratio $h_{t,i}$ for the i-th vibration mode increases as the natural circular frequency ω_i increases as shown by equation (15). Since $h_{t,1}$ is equal to h_t for the first vibration mode, equation (15) becomes the following:

$$\frac{h_{t,i}}{h_{t,1}} = \frac{1}{2} \cdot \left(\frac{\omega_1}{\omega_i} + \frac{\omega_i}{\omega_1}\right) . \tag{16}$$

Matsumoto et al. (1983) modified the Rayleigh damping matrix [C] as in equation (17) using the parameter α, which is the coefficient of the mass and stiffness matrix terms, to adjust

the dependence of the damping ratio on frequency. The total damping ratio for the i-th vibration mode $h_{t,i}$ is expressed by equation (18) through equation (17):

$$[C]=(1+\alpha)\cdot h_{t,1}\cdot\omega_1\cdot[M]+(1-\alpha)\cdot\frac{h_{t,1}}{\omega_1}\cdot[K] \quad (-1\le\alpha\le 1) \quad (17)$$

$$\frac{h_{t,i}}{h_{t,1}}=\frac{1}{2}\cdot\left\{(1+\alpha)\cdot\frac{\omega_1}{\omega_i}+(1-\alpha)\cdot\frac{\omega_i}{\omega_1}\right\} \quad (18)$$

Matsumoto et al. (1983) used a value of parameter α of 0.4 to 0.6 because the hysteresis damping ratio of rockfill materials is not dependent on the frequency. Figures 7 (a) and (b) compare the frequency dependent characteristics of the total damping ratio $h_{t,i}$ from equation (11) with the parameter m, from equation (18) with the parameter α, and from the response analyses of each observed earthquake motion by the half power method.

We estimated the value m in equation (11) by response analysis of observed earthquake motions and laboratory tests for Miho Dam and Oya Dam as listed in Tables 2 (a) and (b). The values of m range from 1.3 to 3.2 for Miho Dam and from 2.8 to 5.4 for Oya Dam. As shown in Figures 7 (a) and (b), the parameters α=0.7 to 0.9 are suitable for the frequency dependent characteristics of damping ratio, on the basis of the comparison of Rayleigh damping with the parameter α, the damping ratio with the parameter m by shear beam theory, and the damping ratio obtained by response analysis of observed earthquake motions.

5. TWO-DIMENSIONAL DYNAMIC ANALYSIS FOR DAM MODELS

We computed the dynamic analyses for models on the rigid base of Miho Dam and Oya Dam using QUAD-4 (Idriss et al., 1973) with the parameter α in the Rayleigh damping matrix. Figures 8 (a) and (b) show finite element meshes of each dam. We input the shear strain dependent curves of shear modulus and hysteresis damping ratio from laboratory tests as shown in figures 9 (a) and (b). We analyzed four cases for each dam as listed in Table 3. We computed two cases of the parameter α=0.4 and 0.9. The damping ratio $h_{t,i}$ when the value of α is 0.4 is independent of frequency, whereas $h_{t,i}$ when the value of α is 0.9 depends on frequency. We computed two cases using the first mode radiation damping ratios obtained from equation (5) after Ohmachi (1981) and the response analyses of each observed earthquake motion.

Figures 10 (a) and (b) compare the observed and calculated maximum accelerations at the dam crest. The vertical axis of the figures represents the ratio of calculated to observed maximum acceleration. The calculated maximum accelerations in the case of α=0.9 agree with the observed values. As for the radiation damping ratio for the first vibration mode $h_{r,1}$, the calculated results agree more closely with the observed acceleration when $h_{r,1}$ was adopted from the response analysis of observed earthquake motions.

6. CONCLUSIONS

We estimated the radiation damping ratio from the response analysis of observed earthquake motions at existing dams and laboratory tests of rockfill materials. We computed the two-dimensional analysis with the Rayleigh damping for the dam models on a rigid base considering the dependence on frequency characteristics of the radiation damping ratio by using the parameter α.

The main conclusions were as follows:

(1) We proposed a method of estimating the radiation damping ratio from the response

analysis of observed earthquake motions at existing dams and the laboratory tests of rockfill materials.

(2) The radiation damping ratio decreases as the vibration mode becomes higher.

(3) The frequency dependent characteristics of damping ratio, which is the sum of hysteresis damping and radiation damping, in a dam model on a rigid base can be represented by using the parameter α of the Rayleigh damping matrix to be 0.9. The maximum accelerations calculated in two-dimensional analysis with the parameter α of 0.9 agreed with the observed values.

REFERENCES

Idriss,I.M., Lysmer,J., Wang,R., and Seed,H.B.(1973) : "QUAD-4, A Computer Program for Evaluating the Seismic Stability of Soil Structures by Variable Damping Finite Element Procedures", EERC-Report No.73-16, Univ. of California.

Iwashita,T., Yasuda,N., Nakamura,A., and Takeda,O. (1995) : "Dynamic Deformation characteristics of Rockfill Materials from Laboratory Test, In-Situ Test and Earthquake Motion Analysis", *Proceedings of the Third International Conference on Recent Advances in Geotechnical Earthquake Engineering and Soil Dynamics*, Vol. Ⅰ, pp.175-178.

Matsumoto,N. and Kondo,S. (1983) : "Dynamic Analysis and Estimation of Damping of Embankment Dams", *Engineering for Dams*, Vol.1-3, pp.46-53. (In Japanese)

Matsumura,M. (1934) : "Deformation of Embankments During Earthquakes", *Report of Public Works Experiment Station*, Ministry of Interior, Government of Japan, No.28, pp.1-67. (In Japanese)

Ohmachi,T. (1981) : "Calculation of Underground Radiation Damping in the Vibration of Embankment Dams", *Proceedings of the 36th Annual Conference of the Japan Society of Civil Engineering*, 3, pp.570-571. (In Japanese)

Sato,T. (1983) : "Effect of the Underground Radiation Damping on Vibration Mode of Ground", *Proceedings of the 17th JSCE Earthquake Engineering Symposium*, pp.147-150. (In Japanese)

Sugito,M., Goda,H., and Masuda,T. (1994) : "Frequency Dependent Equi-linearized Technique for Seismic Response Analysis of Multi-layered Ground", *Proceedings of JSCE*, No.493/Ⅲ-27, pp.49-58. (In Japanese)

Toki,K. (1981) : "Seismic Analysis of Structures, New System Civil Engineering 11", pp.90-101, Gihodo-Publication. (In Japanese)

Table 1 (a) The earthquake records at Miho Dam

Point of Epicenter	Date	Distance (km)	Depth (km)	Magnitude
①Izu Peninsula Off	Jun. 29, 1980	57	10	6.7
②East Yamanashi Pref.	Apr. 14, 1981	13	40	4.5
③West Kanagawa Pref.	Aug. 8, 1983	12	30	6.0
④East Chiba Pref. Off	Dec. 17, 1987	131	58	6.7
⑤Hakone	Aug. 5, 1990	24	14	5.1
⑥Tokyo Bay	Feb. 2, 1992	73	90	5.7

Table 1 (b) The earthquake records at Oya Dam

Point of Epicenter	Date	Distance (km)	Depth (km)	Magnitude
①Noto Peninsula Off	Feb. 7, 1993	31	25.0	6.6
②Noto Peninsula Off	Feb. 8, 1993	37	25.7	4.9
③Noto Peninsula Off	Feb. 16, 1993	28	24.8	5.0
④Noto Peninsula Off	Feb. 22, 1993	9	26.5	4.8
⑤East Ishikawa Pref.	Dec. 8, 1993	42	21.0	5.0
⑥Noto Peninsula Off	Jun. 7, 1994	40	20.0	4.9

Table 2 (a) Damping ratio for Miho Dam

No.	a_{max} at dam foundation (gal)	a_{max} at dam crest (gal)	$h_{h,1}$ (%)	$h_{t,1}$ (%)	$h_{r,1}$ ($h_{t,1}$-$h_{h,1}$) (%)	m value ($h_{r,1}/h_{h,1}$)
①	30.9	66.4	4.0	16.7	12.7	3.2
②	31.2	87.2	4.5	10.8	6.3	1.4
③	147.7	256.7	7.8	17.7	9.9	1.3
④	11.0	65.6	3.8	13.0	9.2	2.4
⑤	27.8	79.8	4.3	13.2	8.9	2.1
⑥	12.0	31.8	2.9	9.7	6.8	2.3

Table 2 (b) Damping ratio for Oya Dam

No.	a_{max} at dam foundation (gal)	a_{max} at dam crest (gal)	$h_{h,1}$ (%)	$h_{t,1}$ (%)	$h_{r,1}$ ($h_{t,1}$-$h_{h,1}$) (%)	m value ($h_{r,1}/h_{h,1}$)
①	65.8	192.8	5.7	21.7	16.0	2.8
②	6.7	38.0	3.1	11.7	8.6	2.8
③	9.8	29.6	2.2	14.0	11.8	5.4
④	14.4	53.1	2.9	12.7	9.8	3.4
⑤	4.3	14.7	2.5	10.6	8.1	3.2
⑥	5.0	10.4	2.3	10.6	8.3	3.6

$h_{h,1}$:Hysteresis damping ratios are obtained from laboratory tests.

$h_{t,1}$:Total damping ratios are obtained from response analysis of observed earthquake motions by half power method.

Table 3 Calculation cases of dynamic analyses

Case	Parameter α	Radiation damping ratio $h_{r,1}$ (%)	
		Miho Dam	Oya Dam
①	0.4	10.0 ※1	21.0 ※1
②	0.4	※2	※2
③	0.9	10.0 ※1	21.0 ※1
④	0.9	※2	※2

※1:From the equation (5) by triangle-shaped shear beam theory

※2:From response analysis of observed earthquake motions and laboratory tests for each earthquake

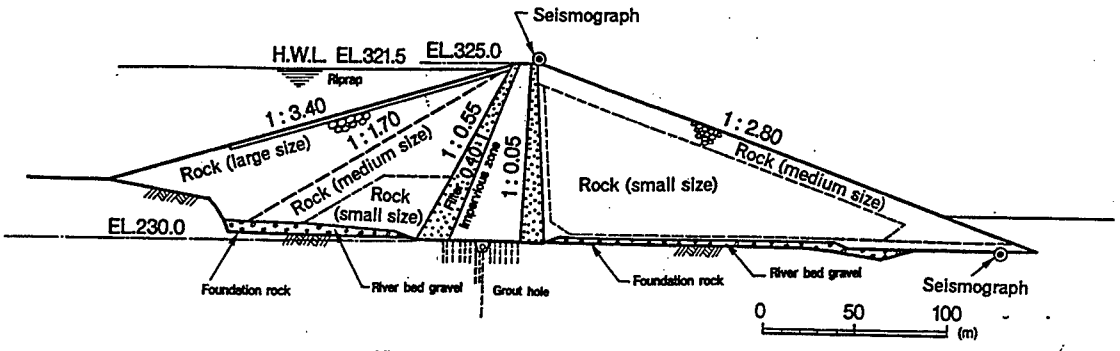

Fig. 1(a) Standard cross section and location of seismographs for Miho Dam

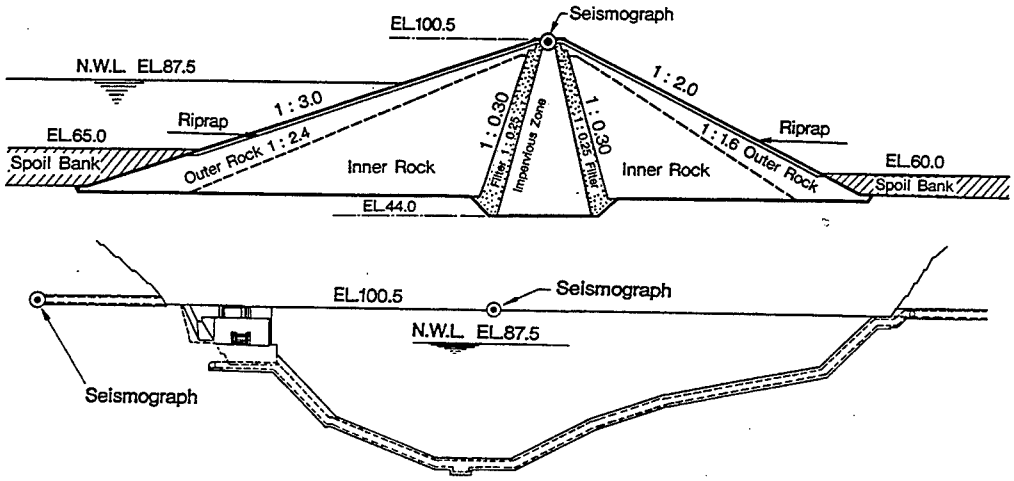

Fig. 1(b) Standard cross section, longitudinal section and location of seismographs for Oya Dam

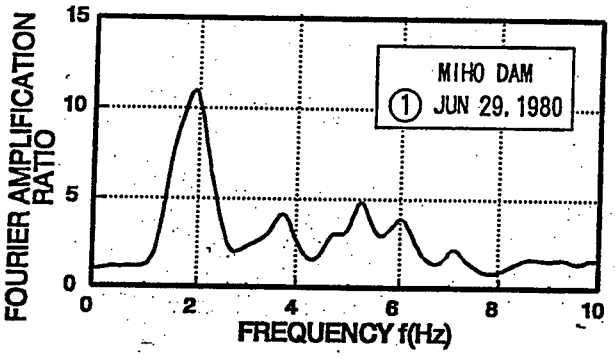

Fig. 2(a) Frequency response function of acceleration observed at Miho Dam

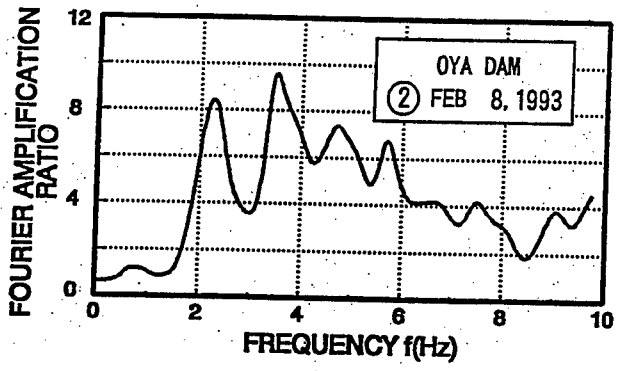

Fig. 2(b) Frequency response function of acceleration observed at Oya Dam

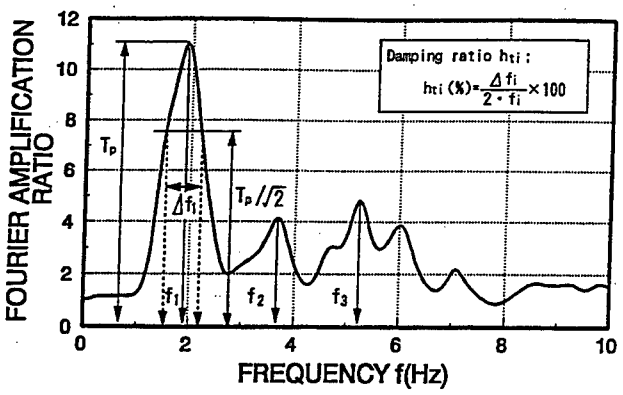

Fig. 3 Calculation of total damping ratio by half power method

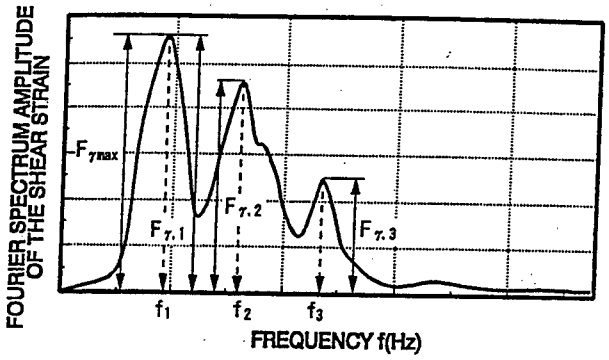

Fig. 5 Schematic Fourier spectrum amplitude of shear strain wave at crest

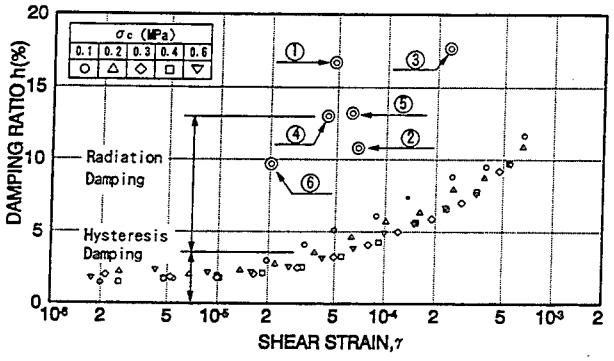

Fig. 4(a) Hysteresis damping ratio h_h obtained from laboratory tests and total damping ratio $h_{t,1}$ of the first vibration mode by observed earthquake analysis versus shear strain γ relationships for Miho Dam

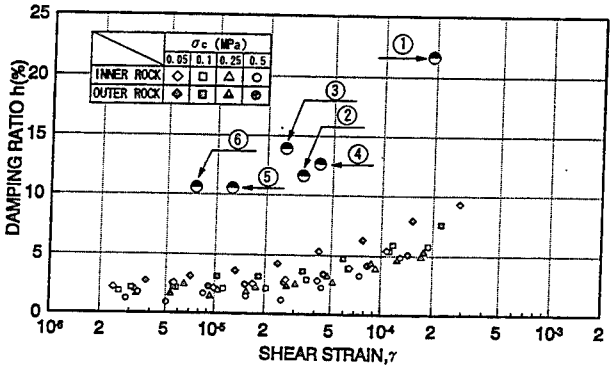

Fig. 4(b) Hysteresis damping ratio h_h obtained from laboratory tests and total damping ratio $h_{t,1}$ of the first vibration mode by observed earthquake analysis versus shear strain γ relationships for Oya Dam

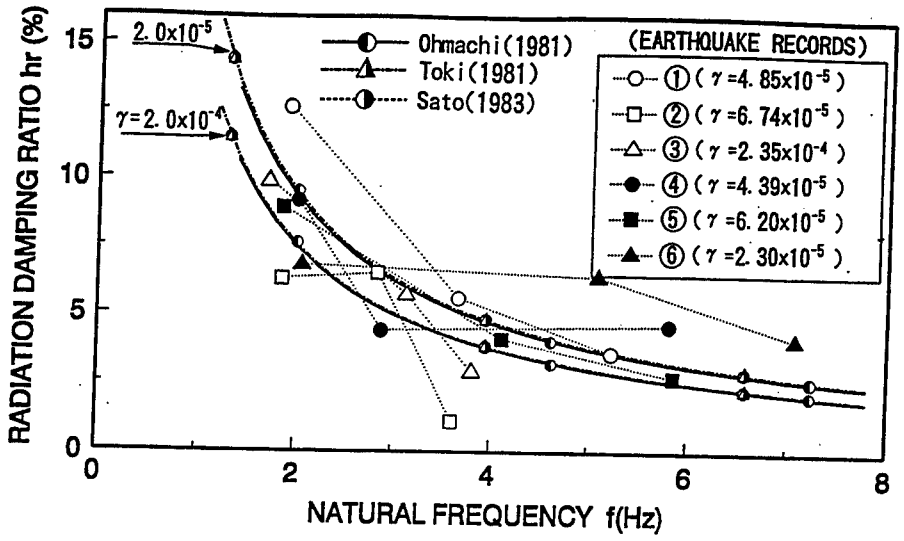

Fig. 6(a) Radiation damping ratio $h_{r,i}$ with natural frequency f_i for Miho Dam

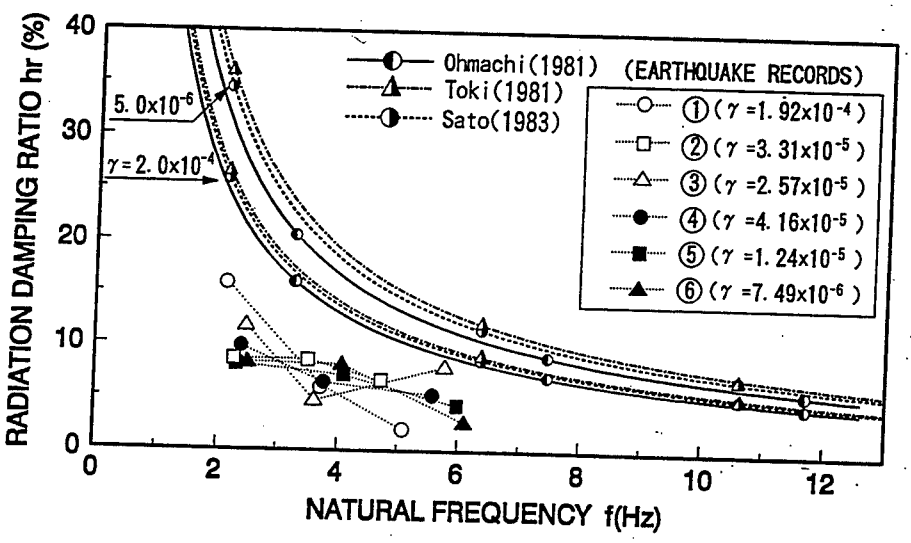

Fig. 6(b) Radiation damping ratio $h_{r,i}$ with natural frequency f_i for Oya Dam

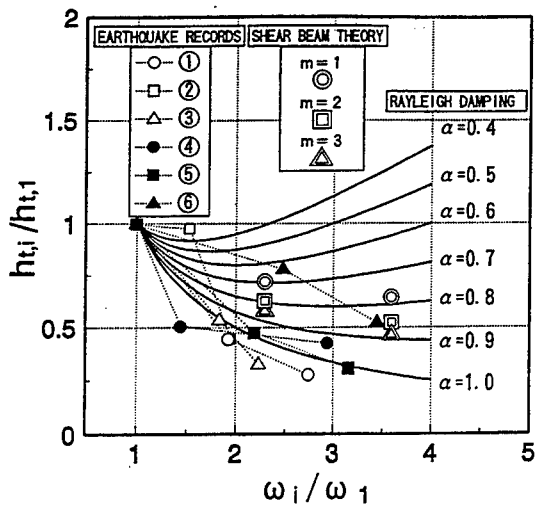

Fig. 7(a) Frequency dependent characteristics of damping ratio from Rayleigh damping with the parameter α, from shear beam theory with the parameter m and from analysis of observed earthquake motions for Miho Dam

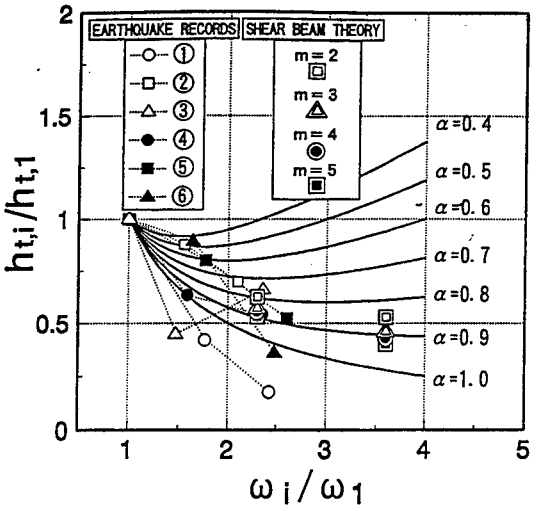

Fig. 7(b) Frequency dependent characteristics of damping ratio from Rayleigh damping with the parameter α, from shear beam theory with the parameter m and from analysis of observed earthquake motions for Oya Dam

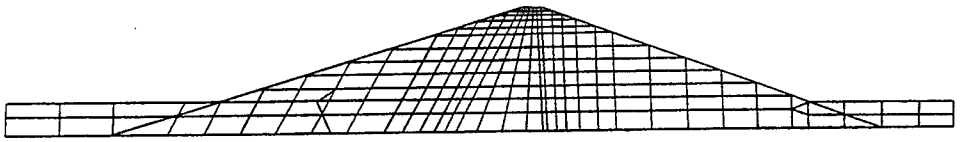

Fig. 8(a) Finite element mesh of Miho Dam

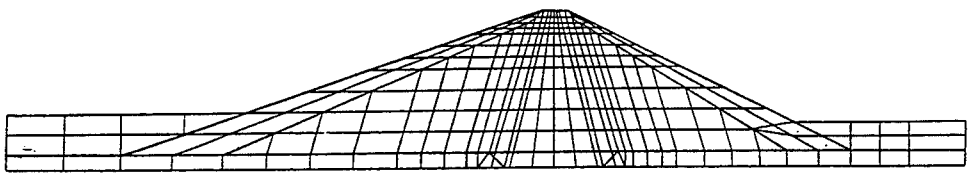

Fig. 8(b) Finite element mesh of Oya Dam

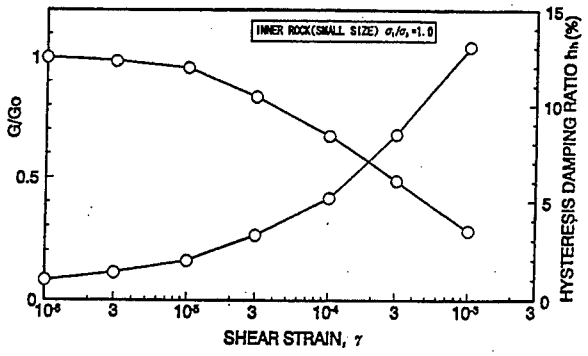

Fig. 9(a) Shear strain dependent curves of shear modulus and hysteresis damping ratio for the dynamic analyses of Miho Dam

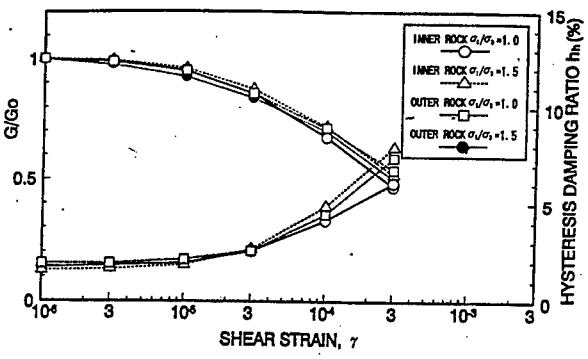

Fig. 9(b) Shear strain dependent curves of shear modulus and hysteresis damping ratio for the dynamic analyses of Oya Dam

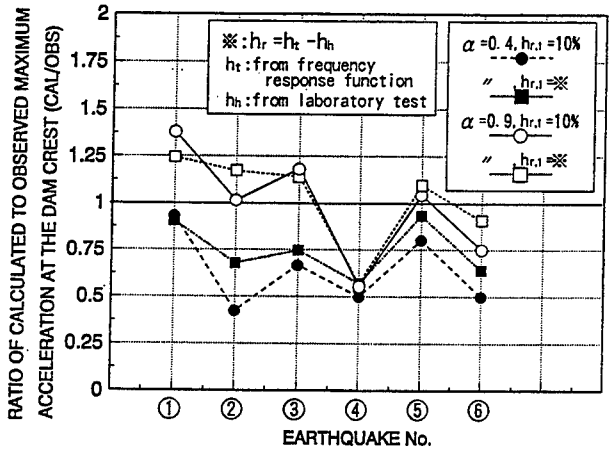

Fig. 10(a) Comparison of observed and calculated maximum acceleration at the dam crest for Miho Dam

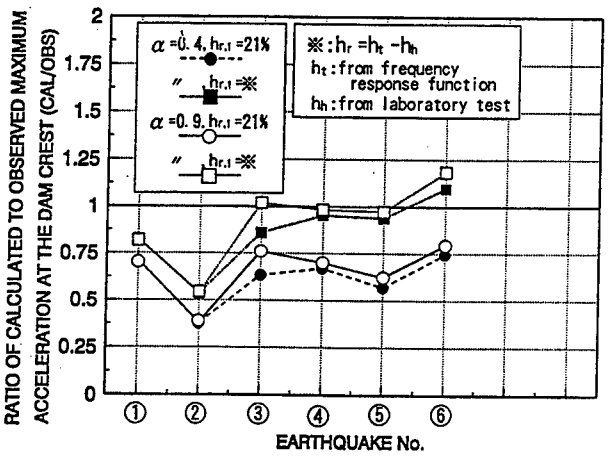

Fig. 10(b) Comparison of observed and calculated maximum acceleration at the dam crest for Oya Dam

Design Requirements for Computer Program to Analyze Large Seismically Induced Deformations

by

John F. Peters *

ABSTRACT

Remediation of embankment dams requires more emphasis on deformations versus factors of safety as computed by limit equilibrium analysis. To be useful, deformation analyses must model mechanical response of the soil, pore pressure development, and mechanisms leading to catastrophic failure. At present, no numerical model is completely satisfactory for such analyses because real technology gaps still exist. These gaps include: constitutive response to discontinuous stress paths, mathematical validity of physically realistic constitutive equations, physics of large deformations, and numerical methods for large deformation problems. Current research is aimed at sufficiently resolving these issues to produce a practical computer code.

KEYWORDS: Constitutive Equations, Large Deformations, Embankment Dams, Seismic Analysis, Soil Mechanics

1 INTRODUCTION

As more attention is paid to safety of existing embankment dams, requirements for their engineering analyses change. The observed performance of these dams demonstrates their adequacy for conditions considered during construction. Under re-analysis, consideration turns to geotechnical and hydrologic details not considered during their construction. In particular, seismic analysis has changed considerably in the past 40 years. Design ground motions have changed owing to expanded data base of earthquake records, improved understanding of earthquake mechanisms, and well instrumented case histories of damaging earthquakes. A analysis methods have improved through better theoretical understanding of the seismic problem, availability of high-speed computers, and empirical data from case histories and model studies. Knowledge of soil behavior has greatly expanded from laboratory investigations and well documented field studies. The net result of our improved understanding is that damaging earthquakes are now considered possible in areas where they were once though rare, the expected ground motions have tended to increase with more damaging frequency characteristics, and geotechnical materials such as gravel, once thought to be ideal foundation materials are now known to be susceptible to liquefaction. As a result of the growth of seismic analysis, geotechnical conditions that were once considered adequate or favorable are now considered to be suspect.

The greatest problem with analysis of existing dams is not the more stringent requirements, but the fact that remediation of an existing structure is fundamentally different from construction of a new one. With new construction a conservative approach to design often does not greatly increase cost especially if it is anticipated prior to construction. With an existing dam, nearly any change in design is costly and potentially disruptive to the impounded reservoir. The analysis philosophy is also different for remediation studies. Design computations are oriented toward insuring suf-

*Soil and Rock Mechanics Branch, Geotechnical Laboratory, USAE Waterways Experiment Station, Vicksburg, MS 39180

ficient factor of safety against expected failure modes. Computations for remediation take on a more predictive flavor because remediation itself entails risk and there must be less reliance on large factors of safety. As a result analyses requirements are more stringent. It is no longer sufficient to determine that conditions are conducive to liquefaction, the ramifications of liquefaction must be determined. Further, if remediation is required, the detailed knowledge of the potential mode of failure is essential for effective and economical redesign.

A requirement of analysis for remediation is the ability to follow deformations beyond what would be traditionally unacceptable. In traditional analyses, a factor of safty of less than one was not acceptable. By this approach, limit equilibrium or static stress analysis assuming small deformations was adequate. However, stress states that are deemed unstable under small strain conditions may be stable when permitted to deform under what is acceptable from a survivability standpoint. More important, to understand potential mechanism, deformations must be permitted to fully develop.

A predictive seismic analysis of an embankment dam involves solution to the equations of motion coupled to equations of fluid flow including movement of the piezeometric surface. Further, many problems involve geometric aspects that dictate fully three dimensional analysis. The general numerical methods for these analyses have been known for over twenty five years but their implementation in real projects required the advent of high performance computing. While the computational task remains daunting, the greatest gap in knowledge is the physics of deformation in granular media. This remains true despite concerted efforts by a large segment of the geotechnical research community.

This paper outlines difficulties in mathematical simulation of soil behavior and how research has been directed to arrive at a practical analysis procedure. Details of finite element formulation, which can be found elsewhere, will not be discussed. Nor is an assessment made of current models. Instead, research issues common to all models are discussed. The discussion begins with a reflection on how a deformation analysis differs fundamentally from a limit equilibrium analysis. Next constitutive equations for soils are briefly discussed followed by observations on essential deficiencies found in all models presently proposed for seismic analyses. Finally problems with large deformations are reviewed including a proposal for a new class of numerical methods that are better suited for simulating the kinematics of large deformations.

2 DEFORMATION ANALYSIS

The goal of deformation analysis is to determine the potential for deleterious deformations due to a seismic event. The deformations may be caused by seismic loading (Newmark displacements), but for embankment dams it is more likely that serious deformation will be related to pore water pressure buildup that results from the loading. From an engineering standpoint, this goal is similar to that of limit analysis.

2.1 Failure Mechanism

Possibly the most important information provided by the deformation analysis is the mechanism. The elements of a failure mechanism include deformations, pore pressure development, and formation of localized zones of shear that lead to catastrophic movement. The limit equilibrium method requires specification of the mechanism for which a factor of safety is assigned. The goal of a limit equilibrium analysis is to find the critical mechanism which, presumably, represents the likely mode of failure. For a relatively simple problem, the critical mechanism amounts to finding the slip surface which has the minimum factor of safety (or, the highest probability of failure). When the mechanism includes factors such as pore pressure development, the critical mechanism is not as clear. The important fact is that the limit equilibrium computation only provides the factor of safety for a specified mechanism. The search for the specific

mechanism is external to the limit analysis.

2.2 Unique Failure Mechanism

A deformation analysis gives the unique deformation for the specified initial conditions, boundary conditions, and property distribution. A factor of safety is not obtained. Therefore, if deformations fall within acceptable limits, there is no direct way of knowing how close one might be to unacceptable movements. Sound practice requires that a limit equilibrium analysis should be performed in conjunction with the deformation analysis to establish a factor of safety. However, because the deformation mechanism may include factors not considered in the limit computations (e.g. the pore pressure development and dissipation rates), the factor of safety may not tell the entire story. A more systematic approach is also needed in which key factors are varied, in light of their probably of occurrence, to determine *reliability.*

2.3 Design/Remediation

An important feature of deformation analysis is the wealth of information that provides insight for creative remediation design. This information includes displacements, stresses, and generation and dissipation of pore pressures. By knowing how and why deformations can develop, more cost-effective designs can be devised. A limit equilibrium analysis can only give an indication of the likelihood that a particular mechanism will be unstable.

2.4 Constitutive Model

Deformation analyses require more details about the soil than limit equilibrium computations. Limit equilibrium computations require only the unit weight and shear strength. For a deformation analysis, the complete constitutive response of the soil is needed. Not only is more analysis of laboratory data involved but the variations on models is much greater because the constitutive model for soil is still an open question. Deformation analysis requires a significantly greater level of expertise than an equilibrium analysis to formulate up the problem, prepare data files, and analyze the results.

2.5 Level of Investigation

An important point in the comparison of the two methods is that each has its purpose and the choice to perform one or the other (or both) should be based on the engineering question to be answered. Quite often there is an inclination to perform an analysis based on the amount of information required from the field. In fact, both require the same level of field investigation. In ranking the importance of information the three most important items needed from a field investigation are: geologic conditions (including groundwater conditions), sequence of loading, and finally properties of the individual materials. If enough information is not available for a deformation analysis, there is probably insufficient information for a limit equilibrium analysis as well. Generally, the answer to critical questions comes down to knowing an important geotechnical detail that is common of all type of analyses. While deformation analyses require much greater effort and expertise that an equilibrium analysis, the quality of both is tied to the quality of the field investigations.

The level of investigation needed for a three dimensional analysis has a similar answer. The need for three dimensional analysis arises from site geometry and load configuration. Often, a simplified three dimensional analysis gives a better picture of behavior than a sophisticated two dimensional analysis because the third dimension carries with it critical modes of deformation. In any case, the site geologic conditions must be known, the loading must be accurately defined and the physical properties must be determined before the question of which analysis method can be addressed.

3 CONSTITUTIVE MODELS

The constitutive model is the distinguishing technical feature of earthquake analysis codes. All codes stem from the same formulation of dynamics which is implemented by one of relatively few choices of numerical methods. Thus the differences in physics captured in the analysis depends on the constitutive relationship that models the soil.

Even a cursory review of literature over the past 25 years reveals a large assortment of constitutive models that can be applied to seismic analysis. However, all theoretically consistent models applicable to soils for the rate of loading considered in seismic analysis fall into the category of rate-independent plasticity with both isotropic and kinematic hardening. Here, theoretically consistent means that the model is formulated to be consistent with thermodynamic principles as opposed to empirical models that are multi-dimensional extensions of simple laboratory experiments. The distinction between the two classes of models is not clear cut because it is possible to contrive an empirical model that does not violate thermodynamic principles. However, for the present discussion, models constructed from a well founded *formalism* will be considered. The key features of models developed from the formalism of the theory of plasticity are as follows:

3.1 Rate Independence

The response of soil depends on the sequence of loading but not on the rate at which the loads are applied. [1] The distinction between rate dependent and rate-independent is important because the loading history of a rate dependent model can be parameterized by time whereas for a rate independent model there is no convenient measure of loading duration. As a result, the classical theory for linear viscoelastic materials is elegantly expressed in terms of irreversible thermodynamics whereas plasticity is expressed through the inelegant vehicle of the yield surface. Further, viscoelasticity theory is relatively unified whereas in the absence of a strict formalism, plasticity theories abound. In an attempt to bring some order to the subject, plasticity will be described in terms of the endochronic theory of Valanis (1971 and 1980). Application of endochronic plasticity, as it applies to the present discussion, can be found in Valanis and Read (1986), Peters (1989), Valanis and Peters (1991), Reddy and Saxena (1992), and Issa et. al. (1995).

The endochronic theory grew out of the questions of why does plasticity lack the elegance of viscoelasticity and can plasticity be given a thermodynamic treatment? An interesting fact emerged. Nowhere in thermodynamic theory is it necessary to drive the evolution equations with time. The laws of thermodynamics are homogeneous in time and they work just as well in incremental form where the actual duration of an event is left unspecified. Because the question of time is left open, one is free to specify any monotonically increasing variable as the intrinsic time for the material in question. In fact, by replacing the time parameter in a classical linear viscoelastic model for incompressible materials with the inelastic strain path length, the classical von Mises theory of plasticity emerges. Thus, the endochronic theory (and similar theories based on the concept of internal variables) contain the seeds from which all models of plasticity can be grown.

3.2 Rate Equations

Rate equation relate internal forces to their thermodynamic conjugate internal variable rates. The rate equations for a rate independent theory of rate independent material are equivalent to flow rules in the theory of plasticity. Because the internal forces in a frictional material are proportional to the mean stress, the flow rule is non-associated (Valanis and Peters, 1991). As Discussed in Section 4, the model is unstable in the sense of Drucker (1951).

[1] Soils do show rate dependent features such as creep but these effects are considered to be secondary effects for the problems considered here.

3.3 Yield Condition

Rate independence implies a yield condition (see Valanis (1980), Valanis and Peters (1992), and Peters and Valanis (1992)). In classical plasticity theories the yield condition takes the form of a yield surface which bounds the stress states for which the material will deform elastically. The endochronic model contains the possibility of a vanishingly small elastic domain so that the yield condition is not expressed as a surface (Valanis, 1980). In this limiting case, the response to a load depends on the direction of the loading increment.

3.4 Kinematic Hardening

Kinematic hardening results from the existence of multiple internal mechanisms in a model. To capture the response to cyclic loading it is necessary to have kinematic hardening. In traditional plasticity, kinematic hardening represents a complication but arises naturally from a theory based on internal variables such as the endochronic plasticity (Valanis and Peters, 1991). In fact, experiments show that the principal plastic mechanism in real soils is kinematic hardening (Alawaji et. al., 1990).

3.5 Isotropic Hardening

Isotropic hardening in soils is an expansion or contraction of the yield surface related to mean effective stress and void ratio. To have a predictive model, the isotropic hardening effect is essential. The mean stress acting as a parameter in the model is central to the question of stability discussed in Section 4.

A plasticity model with these characteristics can, in principle, capture behavior relevant to the seismic problem. At present several kinematic hardening plasticity models are adequate to a limited extent. In particular, hysteretic behavior and pre-liquefaction pore pressure generation are modeled relatively well. However, all of these models fail with respect in two critical aspects of the problem, mathematical well posedness and softness to side loading.

4 STABILITY AND WELL-POSEDNESS

For a model to be well posed a solution must exist, it must be unique, and it must depend continuously on the initial and boundary conditions. It is now well known that for the initial boundary value problem to be well posed, the material model must be positive meaning that the product of stress rate and strain rate must be positive (Valanis, 1985). The approach to defining a well posed wave propagation (initial-boundary value) problem dates from Hadamard (1949) and is closely tied to the shear localization problem as described by Thomas (1961), Hill (1962), Mandel (1964), Rice (1976), and Rudinicki and Rice(1975). The consequence of ill posedness on numerical solutions is not always apparent because a computer program executes a specified set of instruction. Thus, there is always a solution and it is always unique. The numerical symptoms of an ill-posed problem is a solution that grows wildly out of bounds or one that shows extreme sensitivity to mesh design and time step length. Mesh sensitivity means that the solution does not converge (i.e. the solution does not asymptotically approach a unique answer as the mesh is refined or as the time step is made smaller). Thus, nonphysical decisions related to the analysis lead to different answers (e.g. Hsu et. al. 1987). Physically significant results cannot be obtained for ill-posed problems.

The behavior for which the engineer attempts to design against is associated with phenomenon that arise because of non-positive material behavior. Drucker (1951) proposed that the stability of a material could be tied to conditions of well posedness where a stable material is defined as one for which the product of stress and strain increment is always greater than zero. For example, strain softening materials are physically unstable and satisfy Drucker's definition of an unstable material. Mandel (1964) noted that frictional materials inherently demonstrate non-positive behavior and yet are stable in the sense that displacements do not

run away under a sustained load. Thus, the tie between mathematical well-posedness and the physical concept of stability is not clear for frictional materials. The key feature that leads to non-positive behavior in frictional materials is the fact that the mean stress plays a dual role as a *parameter* in frictional models as well as a stress *state variable*. Shear can be induced by changing the *parameter* mean stress. Because the shear strain does no work against the mean stress *state variable*, there is no direct link between cause and effect. One can find stress paths imitating from stable states that can induce positive, negative or zero work increments. Experiments by Lade and his co-workers (Lade et. al. 1988 and Lade et. al. 1993) confirmed Mandel's analysis that sand exhibits non-positive behavior even in stable (pre-failure) conditions. Peters (1991) noted that all of Lade's experiments are predictable using the simplest elastic-plastic models for frictional materials based on a Mohr-Coulomb yield surface and a non-associated flow rule. For example, the tendency for very loose sand to be stable under drained shear but unstable under undrained shear is explained through application of simple model. The unstable phenomenon of shear banding are also tied directly to the non-positive character of friction materials (Mandel (1964), Rice (1976), Rudinicki and Rice (1975), Peters et. al. (1986)).

The question of well-posedness remained an open question for frictional materials because uniqueness proofs tended to offer only sufficient conditions for well-posedness. Thus, frictional models could not be shown to be well posed nor was there clear evidence that they were not. Also, the question of uniqueness was tied to the idea of stability, which Mandel showed to be a vague concept in the case of frictional media. Many attempts were made to devise models with a frictional character yet preserve the conditions of stability (e.g. cap models). Experimental evidence pointed to models that violated conditions of stability (Poorooshasb, 1966 and Tatsuoka and Ishihara, 1974) but never in a way that did not involve defining the yield surface. The experiments of Lade et. al. (1988) were designed to illustrate the point in a direct way by producing stable experimental configurations that violated conditions for stability without reference to a yield surface. The experiments by Lade and his co-workers confirmed that any realistic model for sand must display non-positive behavior. On the mathematical side, a recent analysis by Valanis and Peters (1996) resolved the relationship between stability and well-posedness and showed conclusively that mathematical models for frictional materials, that captured physically relevant non-positive behavior, do not lead to well posed boundary value or initial–boundary value problems. The paper by Mandel (1964) contained all the ingredients to resolve the issue.

So, we are left with a dilemma whereby constitutive models that are experimentally supportable and contain the physical attributes necessary to model real engineering problems, do not lead to mathematically valid models. In extreme cases we cannot even model the laboratory experiments from which the data for model calibration are obtained. The experiments are correct and the mathematics are correct. Our fundamental assumptions about the continuum mechanics formulation of soil mechanics problems must be flawed.

The situation, has not affected engineering analysis greatly because there is still considerable reliance on empirical models to capture features such as pore pressure and failure. Also, many analyses are performed using only one mesh. The real problem comes with the next generation of models that employ sophisticated mesh refinement schemes. The resolution of the problem will come only with the development of so-called non-local continuum models. These models introduce a size effect into the formulation that is missing from traditional continuum formulations. Development of constitutive models constitutes a significant research effort. For while the traditional local continuum mechanics has over 200 years of development, non-local models have been under investigation for only 30 years.

The importance of non-local models to the stability problem about has been appreciated for only 15 years. (For a sampling of efforts to introduce non-local effects into constitutive models see Pietruszczak and Mroz (1981), Bazant and Belytschko (1985), Bazant and Lin (1988), De-Borst et. al. (1993), Valanis and Peters (1992), Valanis et. al. (1993), Valanis and Peters (1996), and Vardoulakis and Aifantis (1991)). A practical non-local plasticity model to suppress spurious mesh sensitivity in mesh refinement schemes is described by Pastor, et. al. (1993).

5 LIMITATIONS OF CONSTITUTIVE EQUATIONS

Another serious problem with developing predictive models is that for many types of loadings the constitutive response is too stiff. Specifically, the constitutive response to a sharp turn or kink in a stress path is typically not modeled well even for models with good comparisons to calibration curves. Such loadings are termed side loadings because they are deviate significantly away from the prevailing stress path. The problem has not been apparent until recently because it does not appear in standard triaxial tests. The difficulty was first observed in model comparisons to cubical triaxial test (e.g. Lewin, 1978) although at the time, it was not recognized as a general limitation of plasticity models as a class. A review of the modeling efforts at the Case Western Conference (Saada and Bianchini, 1989) clearly shows that, in general, kinematic hardening models are too stiff for side loadings. This appears to be a general problem not easily resolved through simple ad hoc modifications to the models. Kinematic hardening models are calibrated from monotonically loaded tests. Side loadings do not bring in new parameters. If the model does not predict the soft response to side loading, it cannot be made to fit without softening its response to other loadings (see Peters, 1989). The significance of the side loading problem to seismic analysis is that stiffness and strength are over-estimated for random motions.

Another difficulty with kinematic hardening models is their inadequacy in modeling complete liquefaction. The models capture the build-up in pore pressures with cyclic loading and the associated reduction in strength. However, the pore pressure buildup and strength loss appear to be subdued by the increased dilative tendency at the reduced mean stress. Complete liquefaction is never reached.

As for local continuum models, kinematic hardening models seem to lack physical details needed to capture important physical effects. The most common approach to enhance the theory is to consider incrementally non-linear plastic rates in which the plastic strain rate depends not only on the stress state but on the stress increment. An early justification for such a model was the yield vertex. The idea of a vertex on the yield surface is motivated by slip plain models where different slip systems are activated by different stress paths (Rice, 1971, and Rudnicki and Rice, 1975). At present, the most notable incrementally non-linear model is the hypoplastic model (Kolymbas and Wu, 1993). Unfortunately, hypoplastic models lack the internal variable formalism that gives plasticity theory some predictive power for cyclic loading. The incrementally non-linear effects are still an open question.

6 REMARK ON CONSTITUTIVE THEORIES

It should be kept in mind that constitutive models are not derived straightforwardly from clearly defined axioms. They are mathematical contrivances, restricted by principles of mechanics and thermodynamics, used to replicate behavior observed in a highly limited selection of experimental results. The McGill conference (Yong and Ko, 1981) was the first widespread attempt to model the circular stress path in a cubical triaxial test. Most predictions for the test were based on isotropic hardening models and results were not good. At about the same time Arthur et. al. (1980) published data on the directional shear cell that showed large plastic strains are generated by principal axes rotation even when

the principal stresses are held constant. At the Case Western conference (Saada and Bianchini, 1989), everyone was familiar with the importance for kinematic hardening to capture the behavior of the circular test path or principal axis rotation and predictions of these test were improved (although as already mentioned nearly all were too stiff). However the torsional shear tests with a discontinuous rotation of principal stress axes, an extreme case of side loading, were modeled poorly. Perhaps the current crop of models would perform better. The point to keep in mind is that even though modelers have tried hard to base models on sound physical principles, it is difficult to see beyond the bounds defined by the current experimental data base. As far as unique stress paths are concerned, or even stress paths expected in field loading situations, this data base is quite small. Moreover, the expectation of extending this data base in the near future is not great considering the severe difficulty in performing experiments with multi axial loading or rotation of stress axes and the general lack of funding for such work. Therefore, it is necessary to assess model performance indirectly based on field data or centrifuge model studies.

7 LARGE DEFORMATION ANALYSIS IN SOILS

Deformations are said to be large when higher order terms in the mathematical description of deformation cannot be disregarded. Accordingly, small-strain approximations become inaccurate when the derivatives of displacement approach 10 percent. These derivatives contribute to both strain and rotation and a small strain approximation may still be inadequate in the presence of large rotations. Relationships that remain valid for arbitrarily large deformations and rotations are well known and can be elegantly cast in the formalism of differential geometry. Unfortunately, considerably more is involved in mathematical simulations of large deformations than mathematical formalism. The problem lies in the greater array of physical phenomenon that appear when deformations become large. At present little is known about the tie between the constitutive relationships and deformation. In fact there is a close interplay among the mathematical formulation, the constitutive relationship, and the numerical method used. Most work in large deformations in geotechnical problems has concentrated on geometric (mathematical) aspects using formulations borrowed from classical investigations of other materials. At present, a cogent physical theory for large deformation of granular material does not exist. Such a theory must account for the details of history-dependent solid behavior ranging from constitutive behavior under small strains to the flow-like behavior of large deformations in a continuous way. The principal issues are outlined in the following subsections.

7.1 Statement of Problem

An initial configuration of the media is described in terms of "material" points located on a spatial grid which is assumed here to be Cartesian. The material points are mathematical constructs, rather than actual soil particles. The motion of these points are assumed to be "affine" such that the topological relationships among the points does not change. Material points that define a square in the undeformed state will enclose an area within which each point can be continuously mapped back to the original square. Thus, the material points that lie on grid lines in the original configuration will form a distorted curvilinear material grid in the deformed media. The key assumption is that a material point's location relative to the material grid does not change during deformation. Therefore, one may wish to describe the kinematics based on an Eulerian description, in which material points are referenced to a stationary spatial grid, or a Lagrangian description, in which material points are referenced to the moving material grid. The Eulerian point of view watches the material go by while the Lagrangian point of view moves with the material. While the two views are related mathematically, the decision to use one over the other is strongly dictated by the constitutive response of the material. Traditionally, fluid

mechanics has favored a Eulerian description because 1) it is not convenient to follow fluid "particles", and, more important, 2) fluids have no memory of previous configurations and a material description is unnecessary. Solid mechanics has favored a Lagrangian description for the opposite reasons of 1) Solid objects are more easily described by a grid attached to the material and 2) elastic materials have perfect memory of previous configurations and it is necessary to keep track of material points.

The difficulty in defining constitutive response under large deformation theory is ensuring that the stress is defined in terms of the proper reference frame. The most straight forward definition of stress is the Cauchy stress. The Cauchy stress is that stress acting on a differential element cut from the body in the current configuration of the body. The Cauchy stress is natural for a spatial grid. However, as the material deforms, the Cauchy stress acting at a particular differential element in the spatial frame describes tractions acting on different material points. Therefore, the history of Cauchy stress at a fixed spatial point has no relationship to a particular material point.

Stress changes as seen from a spatial reference have three causes. First material is moving through the differential element. Second, the material coordinates are changing relative to the spatial frame. Third, the stress changes in response to deformations. A proper stress rate therefore contains two terms in addition to the constitutive response. One is the usual convective term that appears in the material derivative of a scalar quantity and one accounts for the motion of the material grid relative to the spatial grid. Vectors defining a differential element in the initial material grid (which for simplicity is assumed to initially coincide with the spatial grid) are stretched and distorted by deformation into a new configuration. Whatever mechanisms we posit to exist in the material, their change in dimension and orientation follows the change in location of material points to which they are attached. Thus, if the forces developed in these mechanisms are history dependent, the constitutive response must be written in terms of the deformation along these material vectors. The mechanisms will not only move with the differential material element (convect), but their orientations will change as the element deforms; the forces they produce will act in ever changing directions. In fact, if the magnitude of the forces in the mechanisms remain constant, the Cauchy stress will change because of the changing geometry. Note that stresses in a fluid depend only on the current velocity gradient and history information is not needed. Thus, the Cauchy stress defines the stress of a fluid without reference to material points.

The proper definition of stress rate has long been a question of controversy in large deformation theory. Typically, the question is addressed through the principle of objectivity. Most commonly, the Jaumann stress rate is used. The Jaumann adds to the convective term a component composed of the product of current stress and rigid body rotation. The Jaumann stress rate is objective but has been found to give spurious oscillations under simple shear. Valanis (1990) showed that the Jaumann rate is in fact the average of two other rates defined in terms of the covariant and contravariant components projected from the material to the spatial reference frame. Both of these rates are objective and neither give rise to spurious stress oscillations. Objectivity only addresses changes in observational coordinates due to rotation. Components due to distortion are present in the covariant and contravariant rates, but with opposite sign. Deformation is therefore missing in their average. Valanis' main point is that the covariant and contravariant rates relate to changes in the material coordinates and therefore have physical meaning. The Jaumann rate has no such tie to the material system.

Unfortunately, a choice must be made between the two rates because starting from the same form of constitutive relationship, the covariant and contravariant descriptions predict different

constitutive responses, purely from the result of kinematics. There is no mathematical way to resolve the difficulty, for each gives an equally valid view of the material coordinate system. Resolution of the issue must come from the physics. It is necessary to inspect the mechanisms that give rise to change in stress state and relate the dimensional changes of these mechanisms to the relevant components of the material coordinates. At variance to the situation in small strain theory, constitutive relationships cannot be devised without detailed consideration of the deformation mechanism.

It is conceptually simpler to develop the constitutive response completely within the material coordinate system. The stress used is the second Piola-Kirchhoff stress which is the tractions acting in the material frame. The stress now acts within a constant material coordinate system and stress rate does not contain terms for convection, rotation, or deforming reference frame. Constitutive equations in the material system can be written in terms of strain history with a clear physical meaning. The Cauchy stress can be obtained as a transformation of the second Piola-Kirchhoff stress. An interesting feature of the material description is that a plastic material has a fluid-like loss of memory of its initial configuration. This appears to be the case for soils because contacts are completely lost after a few percent strain such that, the initial configuration of the particles has no bearing on the current thermodynamic state. Thus, soil fits the general framework of a plastic fluid which has been described in the formalism of endochronic plasticity by Valanis (1977).

7.2 Numerical Method

Traditional finite element methods can be classified as Lagrangian, Eulerian and mixed (arbitrary Eulerian-Lagrangian or ALE). As might be surmised from the preceding discussion, Lagrangian elements move with the material points whereas Eulerian elements are fixed in space. Accordingly, Lagrangian formulations are used in solid mechanics applications whereas Eulerian formulations are used in fluid mechanics. ALE methods are used for problems that have elements of both.

The difficulty with large deformations is that at small strains soil acts like a solid whereas at large strain it behaves as a plastic fluid. None of the traditional finite element methods work well for such a problem. Lagrangian formulations suffer large numerical errors because of mesh distortion. Eulerian methods require material to be transported which leads to excessive diffusion. Lagrangian methods with remeshing lead to diffusion of the plastic state because of interpolations necessary to describe the state within refined elements.

Particle methods, used originally in astrophysics (Monagahan, 1985), have been recently introduced into solid mechanics by Belytschko et. al. (1994) to avoid difficulties in remeshing during fracture formation. In these methods, the governing equations are mapped to discrete points (particles) based on a "moving" interpolation among particles. The particles are thus not tied to a fixed mesh as are finite element nodes. Particle methods are ideal for problems of changing material topology although boundary condition specification is not as straight forward as for mesh-based methods. Another problem with particle methods is the need to continually update the connectivity among particles. Therefore, under small deformations, the methods require significantly more computational time than finite element methods.

All numerical methods can be viewed as special cases of weighted residual approximations to the governing conditions. Each method results from the particular choices of 1) weighting (or smoothing) function, 2)interpolation, 3) treatment of derivatives within the approximating integral, and 4) spatial or material coordinates. A combination currently under investigation produces a particle approximation that is tied to a structured spatial mesh similar to the particle-mesh method described by Hockney and Eastwood (1988). In this method the par-

ticles act as moving integration points and, under small deformations, give a result similar to a Lagrangian formulation using a quadrilateral element. However, unlike finite element methods, the particles are free to move through the mesh. In effect the particles serve as a vehicle to transport the plastic state. The equations of motion are approximated at the nodes. Boundaries of the media and the properties distribution are defined by distribution of the particles. Boundary conditions can be applied as forces acting on the particles, forces acting on the nodes, or displacements (and/or velocities) applied at the nodes.

8 CONCLUSION

Remediation studies require specific information on failure mechanisms which involve large deformations and pore pressure buildup. Modeling requirements for large seismically induced deformation are more stringent than numerical models based on small deformations. Methods for seismic analysis by time-domain integration are well developed to a mature state. However, to advance the state of the art significantly, several technology gaps must be overcome. Areas specific to deformations of granular media are:

1. Constitutive equations for soils must be improved to obtain a more realistic response to side loading.

2. Large deformation formulations must account for the fluid-like motions of soil.

3. The question of how to formulate a well posed mathematical problem using physically realistic constitutive equations must be resolved.

4. Numerical methods that permit arbitrarily large deformations with changing topology must be developed to the level of maturity of the finite element method.

These issues have not been resolved to date and, in the case of the well-posedness problem, a serious attack on the problem still lies in the future. Progress in the near future will depend on devising plausible engineering approximations based on experience in case histories and model studies. It is important that investments continue to be made in a research program that is balanced among theory, computation, experiments, and case studies.

9 ACKNOWLEDGMENT

The approach to modeling deformations in granular media in this paper was developed under a number of projects at the Waterways Experiment Station of the United States Army Corps of Engineers. Permission is granted by the Chief of Engineers for publication of this paper.

10 REFERENCES

1 Alawaji, H., Alawi, M., Ko, H.-Y., Sture, S., Peters, J. F., Wood, D. M. (1990) Experimental Observations of Anisotropy in Some Stress Controlled Tests on Dry Sand,*Mechanical Engineering Publications* , London, pp. 251–264.

2 Arthur, J. F., Chua, S., Dunstan, T. and Rodriguez del C., J. I. (1980) Principal Stress Rotation: A Missing Parameter, *Journal of the Geotechnical Engineering Division*, American Society of Civil Engineers, Vol. 106, No. GT4, pp. 419–433.

3 Bazant, Z. P. and Belytschko, T. (1985) Wave Propagation in a Strain Softening Bar: Exact Solution, Journal of Engineering Mechanics Division, American Society of Civil Engineers, Vol. 111, pp. 381–389.

4 Bazant, Z. P. and Lin, F-B. (1988) Non-Local Yield Limit Degradation, *International Journal for Numerical Methods in Engineering*, Vol. 26, pp. 1805–1823.

5 Belytschko, T., Liu, Y. Y., and Gu, L. (1994) Element Free Galerkin Methods, *International Journal for Numerical Methods in Engineering*, Vol. 37, pp. 229–256.

6 De Borst, R., Sluys, L. J., Muhlhaus, Pamin, J. (1993) Fundamental Issues in Finite Element Analysis of Localization of Deformation, *Engineering Computations*, Vol. 10, pp. 99–121.

7 Drucker, D. C. (1951) A more Fundamental Approach to Stress-Strain Relations,' *Proceedings, First U. S. National Congress of Applied Mechanics*, American Society of Mechanical Engineers, pp. 487–491.

8 Hadamard, J. (1949) *Lecons sur la Propagation des Ondes et les Equation de l'Hydrodynamique*, Cholsea Publishing Co., N.Y.

9 Hill, R., J. (1962) Acceleration Waves in Solids, *Journal of Mechanics and Physics of Solids*, Vol. 10, pp. 1–16.

10 Hockney, R. W. and Eastwood, J. W. (1988) *Computer Simulation using Particles*, Adam Hilger Publishing.

11 Hsu, T. S., Peters, J. F., and Saxena, S. K. (1987). Importance of Mesh Design for Capturing Strain Localization, *Proceedings of the Second International Conference on Constitutive Relationships*, Tucson, AZ, pp. 857–863.

12 Issa, C. A., Peters, J. F., and Jones, E. W. (1995) Structural Effects of Perlite Compaction on Cryogenic Storage Vessels Subjected to Thermal Cycles and Vibrations, *International Journal for Pressure Vessels and Piping*, Vol. 64, pp. 51–65.

13 Kolymbas, D. and Wu, W. (1993) Introduction to Hypoplasticity, *Proceedings of Modern Approaches to Plasticity*, Elsevier, Amsterdam, pp. 213–223.

14 Lade, P. V., Nelson, R. B., and Ito, Y. M. (1988) Instability of Granular Materials with Non-associated Flow, *Journal of Engineering Mechanics Division*, ASCE, Vol. 114, No. 12, pp. 2173-2191.

15 Lade, P. V., Bopp, P. A., and Peters, J. F. (1993) Instability of Dilating Sand," Mechanics of Materials, Vol. 16 pp. 249–264.

16 Lewin, P. I. (1978) *The Deformation of Soft Clay Under Generalized Stress Conditions*, Ph. D. dissertation, University of London, Kings College.

17 Mandel, J., Conditions de Stabilite et Postulat de Drucker (1964) *Proceedings of IUTAM Symposium on Rheology and Soil Mechanics*, Grenoble, pp. 58–68.

18 Monagahan, J. J. (1985) Particle Methods for Hydrodynamics," *Computer Physics Reports 3*, North-Holland Physics Publishing, pp. 71–124.

19 Pastor, M., Zienkiewicz, O. C., Guang-Dou, Xu, and Peraire, J. (1993) Modeling of Sand Behavior: Cyclic Loading, Anisotropy, and Localization, *Proceedings of Modern Approaches to Plasticity*, Elsevier, Amsterdam, pp. 469–491.

20 Peters, J. F., Lade, P. V., and Bro, A. (1986) Shear Band Formation in Triaxial and Plane Strain Tests, ASTM STP 977, *Advanced Triaxial Testing of Soil and Rock*, pp. 604–627.

21 Peters, J. F. (1989) Internal Variable Model for Frictional Materials, *Constitutive Equations for Granular non-Cohesive Soils*, A. A. Balkema, pp. 551–569.

22 Peters, J. F. (1991) Discussion to 'Instability of Granular Materials with Non-associated Flow', by Lade, P. V., Nelson, R. B., and To, Y. M., ASCE *Journal of Engineering Mechanics*, Vol. 117, No. 4, pp. 934–936.

23 Peters, J. F. and K. C. Valanis (1993) Computational Aspects of Endochronic Plasticity, *Proceedings of Modern Approaches to Plasticity*, Elsevier, Amsterdam, pp. 325–346.

24 Pietruszczak, ST. and Mroz, Z. (1981) Finite Element Analysis of Deformation of Strain-Softening Materials, *International Journal for Numerical Methods in Engineering*, Vol. 17, pp. 327–334.

25 Poorshasb, H. B., Holubec, I., and Sherbourne, A. N. (1966) Yielding and Flow of Sand in Triaxial Compression: Part I, *Canadian Geotechnical Journal*, Vol. 3, pp. 179–190.

26 Reddy, K. R. and Saxena, S. K. (1992) Constitutive Modeling of Cemented Sand, Mechanics of Materials, Vol. 14, pp. 155–178.

27 Rice, J. R. (1971) Inelastic Constitutive Relations for Solids: An Internal Variable Theory and its Applications to Metal Plasticity, *Journal for Mechanics and Physics of Solids*, Vol. 19, pp. 433–455.

28 Rice, J. R. (1976) The Localization of Plastic Deformation, *Proceedings of the 14th IUTAM Congress on Theoretical and Applied Mechanics*, Editor, Koiter, W. T., North-Holland, Amsterdam, pp. 207–220.

29 Rudinicki, J. W. and Rice, J. R. (1975) Conditions for the Localization of Deformation in Pressure-Sensitive Dilatant Materials, *Journal for Mechanics and Physics of Solids*, Vol. 23, pp. 371–394.

30 Saada, A. and Bianchini, G. (1989) *Constitutive Equations for Granular Non-Cohesive Soils*, A. A. Balkema, Rotterdam.

31 Tatsuoka, F. and Ishihara, K. (1974) Yielding of Sand in Triaxial Compression, *Soils and Foundations*, Vol. 14, No. 2, pp. 63–76.

32 Thomas, T. Y. (1961) *Plastic Flow and Fracture of Solids*, Academic Press, N.Y.

33 Valanis, K. C. (1971) A Theory of Viscoplasticity without a Yield Surface, Part I, General Theory, *Archives of Mechanics*, Vol. 23 pp. 517–533.

34 Valanis, K. C. (1977) Proper Tensorial Formulation of the Internal Variable Theory, *Archive of Mechanics*, Vol. 29, pp. 173–185.

35 Valanis, K. C. (1980) Fundamental Consequences of a New Intrinsic Time Measure: Plasticity as a Limit of the Endochronic Theory, *Archives of Mechanics*, Vol. 32, pp. 171–191.

36 Valanis, K. C. (1985) On the Uniqueness of Solutions of the Initial Value Problem in Softening Materials, *Journal of Applied Mechanics*, Vol. 52, pp. 649–653.

37 Valanis, K. C. and Read, H. E. (1986) An Endochronic Plasticity Theory for Concrete, *Mechanics of Materials*, Vol. 5, pp. 227–295.

38 Valanis, K. C. (1990) Back Stress and Jaumann Rates in Finite Plasticity, *International Journal of Plasticity*, Vol. 6 pp. 252–367.

39 Valanis, K. C. and Peters, J. F. (1991) An Endochronic Plasticity Theory with Shear-Volumetric Coupling, *International Journal for Numerical and Analytical Methods in Geomechanics*, Vol. 13, pp. 77–102.

40 Valanis, K. C. and Peters, J. F. (1992) Configurational Plasticity in Granular Media, *Proceedings of Modern Approaches to Plasticity*, Elsevier, Amsterdam, pp. 1–17.

41 Valanis, K. C., Peters, J. F. and Gill, J. (1993) Configurational Entropy, Non-Associativity and Uniqueness in Granular Media, *Acta Mechanica*, Vol. 100, pp. 79–93.

42 Valanis, K. C. and Peters, J. F. (1996) Ill-Posedness of the Initial and Boundary Value Problems in Non-Associative Plasticity, *Acta Mechanica*, Vol. 114, pp. 1–25.

43 Vardoulakis, I., Aifantis, E. S. (1991) A gradient flow theory of plasticity for granular materials, *Acta Mechanica*, Vol. 87, pp. 197–214.

44 Yong, K. and Ko, H-Y (1980) *Limit Equilibrium, Plasticity, and Generalized Stress-Strain in Geotechnical Engineering*, American Society of Civil Engineers, New York.

Dynamic Analysis of the Tokuyama Dam (Rockfill Dam)

by

Mitsuaki Mizuno[1], Kazuo Harita[2], Hisashi Tachibana[3], Yoshiro Iida[4], Nobuyuki Shirakawa[5]

ABSTRACT

Dams designed by the seismic coefficient method did not suffer any damage that would threaten their structural safety by the 1995 Hyogo-ken Nanbu earthquake (17 January 1995; magnitude 7.2), which was one of the most disastrous earthquakes in the Japanese history. However, because other types of civil engineering structures were severely damaged, the earthquake resistance of dams need to be investigated more thoroughly.

Because the area around the site of the Tokuyama Dam experienced the Nobi earthquake (28 October 1891; magnitude 8.0), which was one of the greatest epicenter-on-the-land-type earthquake in the Japanese observational history, the safety of the dam was investigated through dynamic analysis by using different actual earthquake ground motions with various frequency properties. This paper reports the outline of the investigation.

Key words: *Embankment Dam, Seismic Design, Dynamic Analysis*

1. OUTLINE OF THE DAM

1.1 Dam Facility

The Tokuyama Dam, a rockfill dam with central clay core, is now under construction at a site about 70 km north of Nagoya City. The dam will have the greatest reservoir capacity in Japan (approx. 660-million m^3).

Specifications and a typical cross section of the dam are shown in Table 1 and Fig. 1, respectively.

Table 1 Specifications

Location	Fujihashi-mura, Ibi-gun, Gifu-ken
Height	161.0 m
Crest Length	440.0 m
Width	20.0 m
Volume	14,700,000 m3
Crest Elevation	EL. 406.0 m
Foundation Elevation	EL. 245.0 m

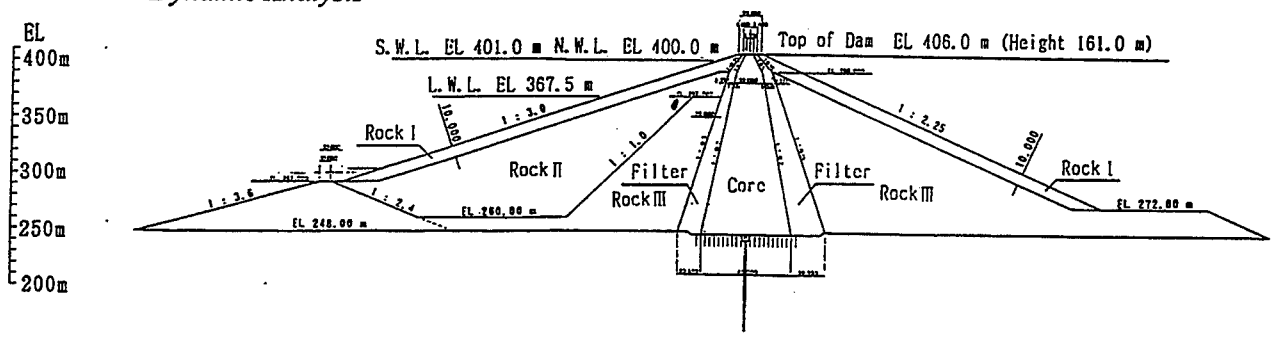

Fig .1 Typical Cross Section

1) Director, First Construction Depertment, Water Resources Development Public Corporation (WARDEC)
2) Chief, Planning and Coordination Office, Planning Depertment ,ditto
3) Project Manager, Tokuyama Dam Construction Office, ditto
4) Head, Fill Dam Division, Research Institute,ditto
5) Senior Research Engineer ,Fill Dam Division, Reserch Institute, ditto, 936 Jinde Urawa-shi, Saitama-ken,338 Japan

1.2 Geology

The geology of the dam site consists of Mesozoic bedrock and overlying Quaternary sediments. The Mesozoic consists of such strata as chert, schalstein, and slate, and the Quaternary consists of terrace, talus, and riverbed deposits.

A geologic cross section of the Tokuyama Dam site is shown in Fig. 2. Beneath the riverbed, a river-gravel bed of about 10m thick, a thick hard chert layer, and hard schalstein are distributed in descending order. Around the dam abutments, weathered rock is distributed near the surface of the right and left banks. The weathered zone is considered to be rather thicker on the right bank than the left bank. While a high permeability with a Lugeon unit of 20 Lu or greater is observed near the surface of both banks, the Lugeon unit decreases down to a value of 2 Lu or less with increasing distance from the surface. Even at a distance from the surface, some local zones have high permeability with Lugeon units exceeding 20 Lu.

Considering the above characteristics of permeability, the foundation excavation line drawn in Fig. 2 has been planned so that suitable rock can be utilized as the foundation. Part of the zones with high permeability is planned to undergo foundation treatment.

There are no Quaternary faults near the dam site (within 300 m from the dam body). All the faults that need to be considered are more than approximately 2 km away from the dam, and their orientations do not pose a threat to the dam site.

1.3 Outline of the Design

1.3.1 Materials

Schalstein and slate are used as rock materials. In view of efficient use and strength properties of the materials, hard schalstein (designed internal friction angle of $\phi = 41$ deg) is laid out to constitute the outer portions of both the upstream and downstream dam sides, and hard slate ($\phi = 41$deg) is laid out to constitute the inner portion of the upstream dam side. Unweathered schalstein and slate ($\phi = 39$ deg) are laid out to constitute the inner portion of the upstream dam side beneath the minimum operating level, and the inner portion of the downstream dam side (Fig. 1).

River gravel with a suitable grain distribution is used as a filter material.

Overlying sediments including residual high-weathered rock, talus deposits and terrace deposits are used as core materials. Also, materials that themselves are not suitable core materials are planned to be used as core materials after proper mixing.

1.3.2 Design

The design of the dam is based on the seismic coefficient method. A design horizontal seismic coefficient of 0.18 is adopted as one of the greatest value ever adopted for a Japanese rockfill dam. This is based on the consideration of earthquake records and the fault distribution; the dam site is located at approximately 11.2 km from the epicenter of the Nobi earthquake, and approximately 6.0 km from the nearest section of the Neo-dani Fault (estimated extension of approximately 40 km), which caused the Nobi earthquake. In Japan, dams designed by the seismic coefficient method have never suffered any earthquake-induced damage that would threaten their structural safety.

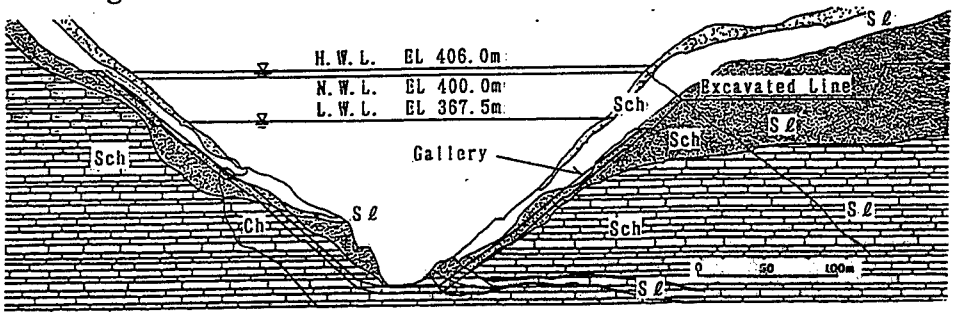

Fig.2 Geologic Cross Section

2. OUTLINE OF THE ANALYSIS

The dam safety during an earthquake event was investigated in a way in which analytical results could be compared with the seismic coefficient method. The maximum average acceleration of the bulk dam material on a rotational slip surface was compared with the limit (or yield) acceleration, which is the minimum acceleration needed for the occurrence of sliding. Response characteristics of the dam were also investigated.

2.1 Analytical Method

As for the basis of the analysis, the equation of seismic force at a given time is written as

$$M\ddot{u} + C\dot{u} + Ku = R$$

where,

M = mass matrix
$\ddot{u}$ = acceleration vector
C = damping matrix
$\dot{u}$ = velocity vector
K = stiffness matrix
u = displacement vector
R = seismic load vector

and the equation is solved by a complex response analysis.

2.2 Analytical Models

A two-dimensional analysis was carried out by using the finite element method in a cross section perpendicular to the dam axis. The models used for the analysis are shown in Fig. 3.

To calculate stress and displacement values accurately, the load of embankment has to be divided into at least 8 to 10 classes (layers). In the present analysis, division was made as many as 18 classes (layers).

As for the boundary condition, the foundation was coupled as a rigid body, and only the dam body was considered for analysis.

2.3 Physical Properties

The densities and shear modulus and others of different dam materials are shown in Tables 2 and 3, respectively. The physical properties were determined mainly by triaxial laboratory tests.

Table 2 Densities

	Rock I	Rock II	Rock III	Filter	Core
ρt	2.20	2.08	2.05	2.05	2.14
ρsat	2.34	2.27	2.21	2.23	2.06

Notes ρt :Wet Density (g/cm3)
ρsat:Saturated Density (g/cm3)

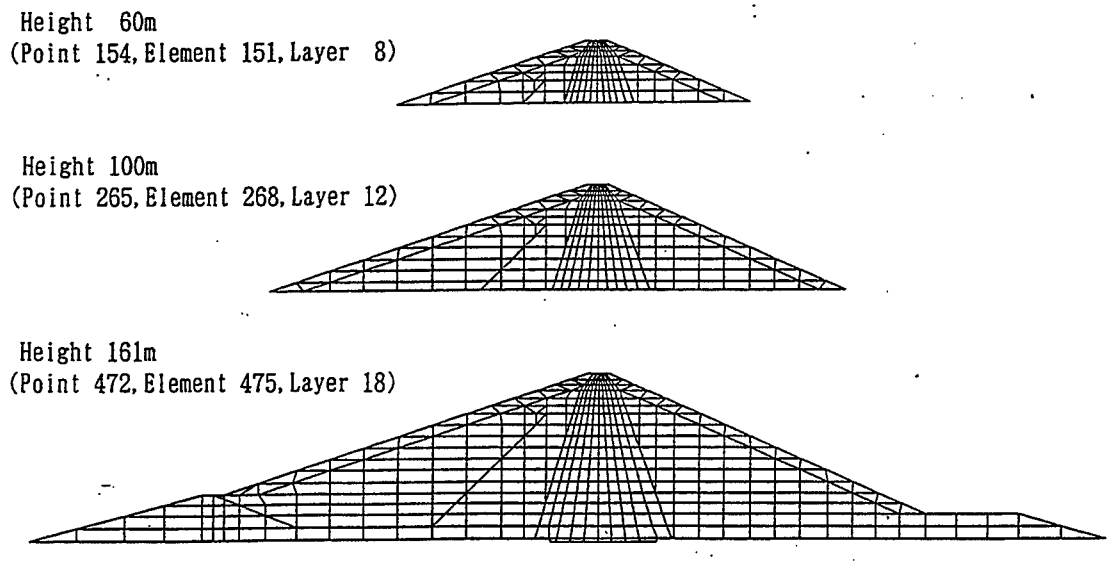

Fig.3 Analytical Models

Table 3 Shear Moduls and Others

	Shear Modulus G (kgf/cm²)	Initial Shear Modulus G_0 (kgf/cm²)	Damping Coefficient h
Rock I	$\frac{1}{1+\gamma/1.91\times10^{-4}} \times G_0$	$2,000\sigma_m^{0.58}$	$\frac{\gamma/1.91\times10^{-4}}{1+\gamma/1.91\times10^{-4}} \times 0.14$
Rock II	$\frac{1}{1+\gamma/2.17\times10^{-4}} \times G_0$	$1,900\sigma_m^{0.58}$	$\frac{\gamma/2.17\times10^{-4}}{1+\gamma/2.17\times10^{-4}} \times 0.13$
Rock III	$\frac{1}{1+\gamma/3.11\times10^{-4}} \times G_0$	$1,700\sigma_m^{0.58}$	$\frac{\gamma/3.11\times10^{-4}}{1+\gamma/3.11\times10^{-4}} \times 0.15$
Filter	$\frac{1}{1+\gamma/2.30\times10^{-4}} \times G_0$	$1,600\sigma_m^{0.63}$	$\frac{\gamma/2.30\times10^{-4}}{1+\gamma/2.30\times10^{-4}} \times 0.13$
Core	$\frac{1}{1+\gamma/2.67\times10^{-4}} \times G_0$	$1,600\sigma_m^{0.60}$	$\frac{\gamma/2.67\times10^{-4}}{1+\gamma/2.67\times10^{-4}} \times 0.17$

Notes γ : Shear Strain σ_m : Mean Principal Stress (kgf/cm²)

Strength constants are shown in Table 4. Because the shear force τ_R, which was used for the investigation of sliding, depends on confining pressure when rockfill and filter materials are concerned, shear force was investigated by using the ϕ_0 method, by which confining pressure can be taken into consideration.

$$\tau_R = \sigma \tan\phi_0$$

$$\phi_0 = \phi_{max} - a \log\left(\frac{\sigma}{\sigma_0}\right) \quad \text{at} \quad \sigma > \sigma_0$$

$$\phi_0 = \phi_{max} \quad \text{at} \quad \sigma \leqq \sigma_0$$

where,

ϕ_0 = internal friction angle (deg) defined in Fig. 4

ϕ_{max} = maximum internal friction angle(deg) when confining pressure is small

α = factor for the decrease in the internal friction angle with increasing confining pressure

σ_0 = stress at which the internal friction angle becomes ϕ_{max} for vertical stress of σ_0 less(kgf/cm²)

σ = vertical stress (kgf/cm²)

For the investigation of the upstream face of the dam, shear strength values that reflect the decrease of strength by water saturation were adopted.

Respecting adhesive core materials, effective stress determined by an undrained test was regarded as drained stress. Thus, the shear strength values obtained by the C ϕ method were adopted, and cohesion, C, was conservatively set to zero.

In addition, a dissipative damping ratio of 0.15 was adopted, based on the results of eismic exploration of the bedrock of the Tokuyama dam and example of analysis of existing dams.

Table 4 Strength Constants

	ϕmax	a	ϕmax	a
Rock I	61.1°	9.75	58.4°	9.75
Rock II	60.3°	9.45	57.6°	9.45
Rock III	55.5°	8.20	52.7°	8.20
Filter	55.5°	8.20	52.7°	8.20
	Dry		Saturated	

Notes Core:Only ϕ=34.5° considered
σ0=0.3kgf/cm²

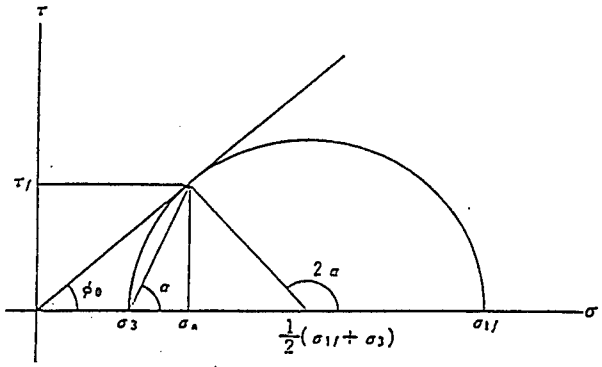

Fig.4 Definition of ϕ_0

2.4 Earthquake Ground Motions

Frequency properties of actual ground motions, which vary in frequency components, have a great influence over the evaluation of seismic force acting on a dam. A response analysis therefore has to be conducted by using various ground motions with different frequency properties.

For the investigation of the average acceleration of bulk dam material, nine accelerograms, which were recorded at the bedrock of existing dams and which have different frequency properties, were selected, based on the following considerations. (1) Two accelerograms were selected from the 1995 Hyogo-ken Nanbu earthquake. One is from the Minoogawa Dam, where a large maximum acceleration was recorded. Pertaining to this dam, the greatest average acceleration of bulk material on a rotational slip surface was observed for a dam height of 150 m in the investigation of earthquake resistance of rockfill dams described in the Report of the Committee on the Evaluation of Earthquake Resistance of Dams[1] (abbreviated to the Committee Report). Another accelerogram is from the Hitokura Dam, where a large maximum acceleration was recorded and the greatest ground motion caused by the earthquake was observed. The dam was located at only 10 km away from the activated fault. (2) In addition, seven out of the eight actual accelerograms presented by the Seismic Design Guideline for Embankment Dams: Draft[2] (abbreviated to the Draft Guideline) were selected. The Nihonkai-chubu earthquake recorded at the Gosho Dam was excluded from the selection because the vertical ground motion was not recorded.

Regarding the maximum acceleration of the horizontal ground motion, 200 Gal was adopted in the present study since 196 Gal was recommended in the Draft Guideline. The Committee Report evaluated the whole available acceleration records of the 1995 Hyogo-ken Nanbu earthquake, and estimated the upper limit for the maximum acceleration of horizontal ground motion in rock suitable for

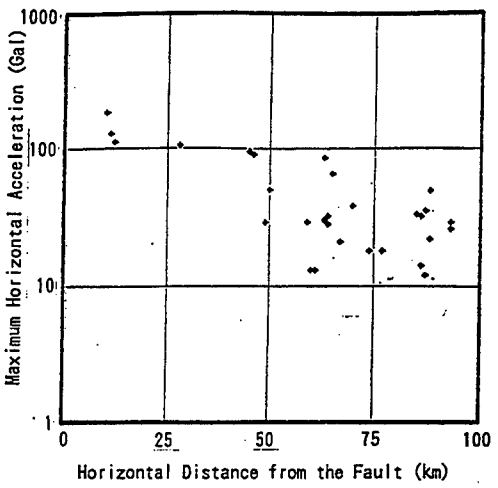

Fig.5 Decrease of Maximam Horizontal Acceleration with Distance from the Fault (Revised The Reference Literature[1])

dam foundation to be 220 Gal (Fig. 5). Based on this limit, the committee used a value of 250 Gal for the maximum horizontal acceleration of input ground motion to investigate the earthquake resistance of dams. Thus, 250 Gal was also used in the present study for the cross section with a height of 161 m. Because of these large values, some of the wave forms had to be amplified with a large factor.

Vertical components were also investigated in the 161-m-high section. The vertical component of each of the nine wave forms was amplified to provide an input ground motion, by using the same amplification factor as the horizontal component.

For the investigation of response characteristics in the 161-m-high section, the accelerograms recorded at the Minoogawa Dam and the Hitokura Dam during the 1995 Hyogo-ken Nanbu earthquake were used while adjusting the maximum acceleration of horizontal motion to 250 Gal. Also used is the accelerogram of the Minase Dam, which exhibited the greatest average acceleration of the bulk material on a rotational slip surface in the 161-m-high section.

And vertical components were also investigated. Properties of earthquake ground motions are summarized in Table 5, and time histories of acceleration are shown in Fig. 6.

Table 5 Properties of Earthquake Groumd Motions

Dam	Earthquake (Epicenter)	Date	Magnitude	Depth (km)	Distance (km)	Maximum Acceleration (Gal)			Ratio	Frequency	Period	
						α_0	α_1	α_2	α_2/α_1	f (Hz)	T (s)	f/f_1
Minoogawa	The 1995 Hyogo-ken Nanbu Earthquake	1995.01.17	7.2	17.9	48.0	127.95	127.95	250.00	1.95	1.69 (0.97)	0.59 (1.03)	1.55 (0.94)
						75.33	75.33	147.19		0.87 (0.78)	1.15 (1.28)	0.8 (0.72)
Hitokura	The 1995 Hyogo-ken Nanbu Earthquake	1995.01.17	7.2	17.9	47.2	182.76	185.42	250.00	1.35	2.05 (2.05)	0.49 (0.49)	1.88 (1.88)
						63.15	63.03	84.99		0.78 (0.78)	1.28 (1.28)	0.72 (0.72)
Minase	The Miyagi-ken Oki Earthquake	1978.06.12	7.4	40	167.0	47.98	46.16	250.00	5.42	0.78 (0.78)	1.28 (1.28)	0.72 (0.72)
						20.61	20.46	110.84		0.95 (0.97)	1.05 (1.03)	0.87 (0.89)
Yokoyama	(The Central of Gifu-ken)	1969.09.09	6.6	0	60.0	14.42	15.03	250.00	16.63	1.07 (1.07)	0.93 (0.93)	0.98 (0.98)
						16.94	14.28	237.56		1.17 (1.17)	0.85 (0.85)	1.07 (1.07)
Tokachi	(The North of the Hidaka Mountains)	1987.01.14	7.0	119	62.0	17.96	16.92	250.00	14.78	1.61 (1.66)	0.62 (0.60)	1.48 (1.52)
						9.63	8.14	118.48		10.1 (2.34)	0.1 (0.43)	9.27 (2.15)
Tase	The Nihon-kai Chubu Earthquake	1983.05.26	7.7	14	264.0	8.72	9.08	250.00	27.53	2.36 (2.44)	0.42 (0.41)	2.17 (2.24)
						5.45	5.24	144.42		1.07 (1.07)	0.93 (0.93)	0.98 (0.98)
Gosho	(North of Iwate-ken)	1987.01.09	6.6	72	67.0	38.06	38.41	250.00	6.51	3.24 (3.22)	0.31 (0.31)	2.97 (2.95)
						19.22	19.59	127.50		3.00 (3.02)	0.33 (0.33)	2.75 (2.77)
Miho	(Central Shore of the Izu Peninsula)	1980.06.29	6.7	10	56.0	21.81	20.72	250.00	12.07	4.15 (4.10)	0.24 (0.24)	3.81 (3.76)
						12.85	12.03	145.17		3.12 (3.12)	0.32 (0.32)	2.86 (2.86)
Miho	(Border of Kanagawa-ken & Yamanashi-ken)	1983.08.08	6.0	22	12.0	149.37	149.14	250.00	1.68	6.59 (6.54)	0.15 (0.15)	6.05 (6.00)
						54.59	52.83	88.56		5.85 (6.34)	0.17 (0.16)	5.37 (5.82)

Notes Earthquake, Magnitude, Depth: After Meteorological Agency
Distance: Quote from the reference literature 1) & 2)
α_0 : Value for all original records α_1 : Value for using Filter for all records α_2 : Value for the limited records used for analysis
Pedominant Frequency f : Smoothing value using Parzen Window (For all records…0.3Hz, For the limited records used for analysis…0.4Hz)
Natural Frequency f_1 : The 1st order Natural Frequency of the analysis model (1.09Hz)
(cf The 2nd order or more Natural Frequency of the analysis model f =1.70Hz, f =1.87Hz, f =1.96Hz, f =2.10Hz, f =2.23Hz)
Upper column: Values for horizontal motions Lower column: Values for vertical motions
Out of parentheses: Values for all records In of parentheses: Values for the limited records for the analysis

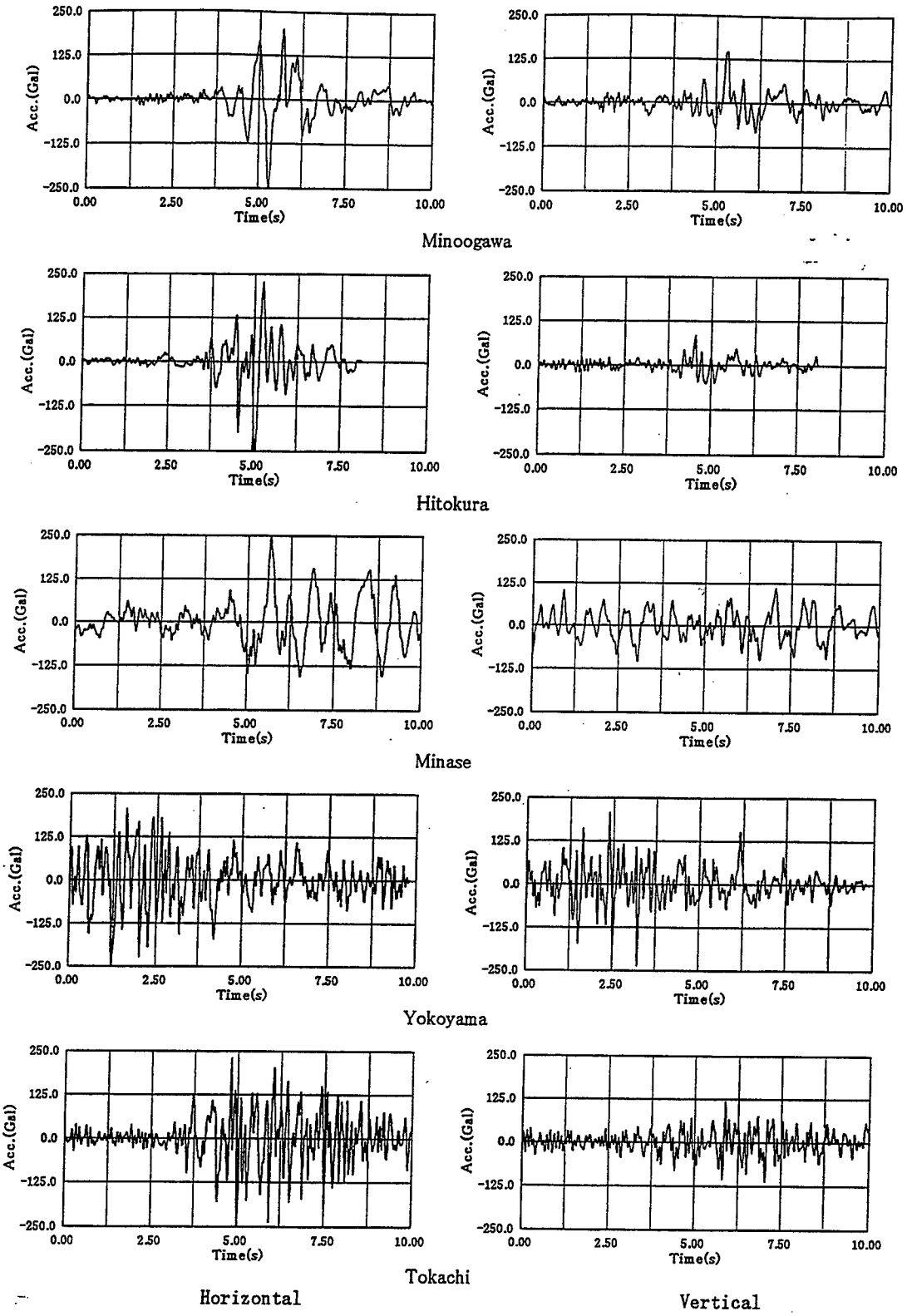

Fig. 6(1) Time Histories of Earthquake Acceleration (Minoogawa, Hitokura, Minase, Yokoyama, tokachi)

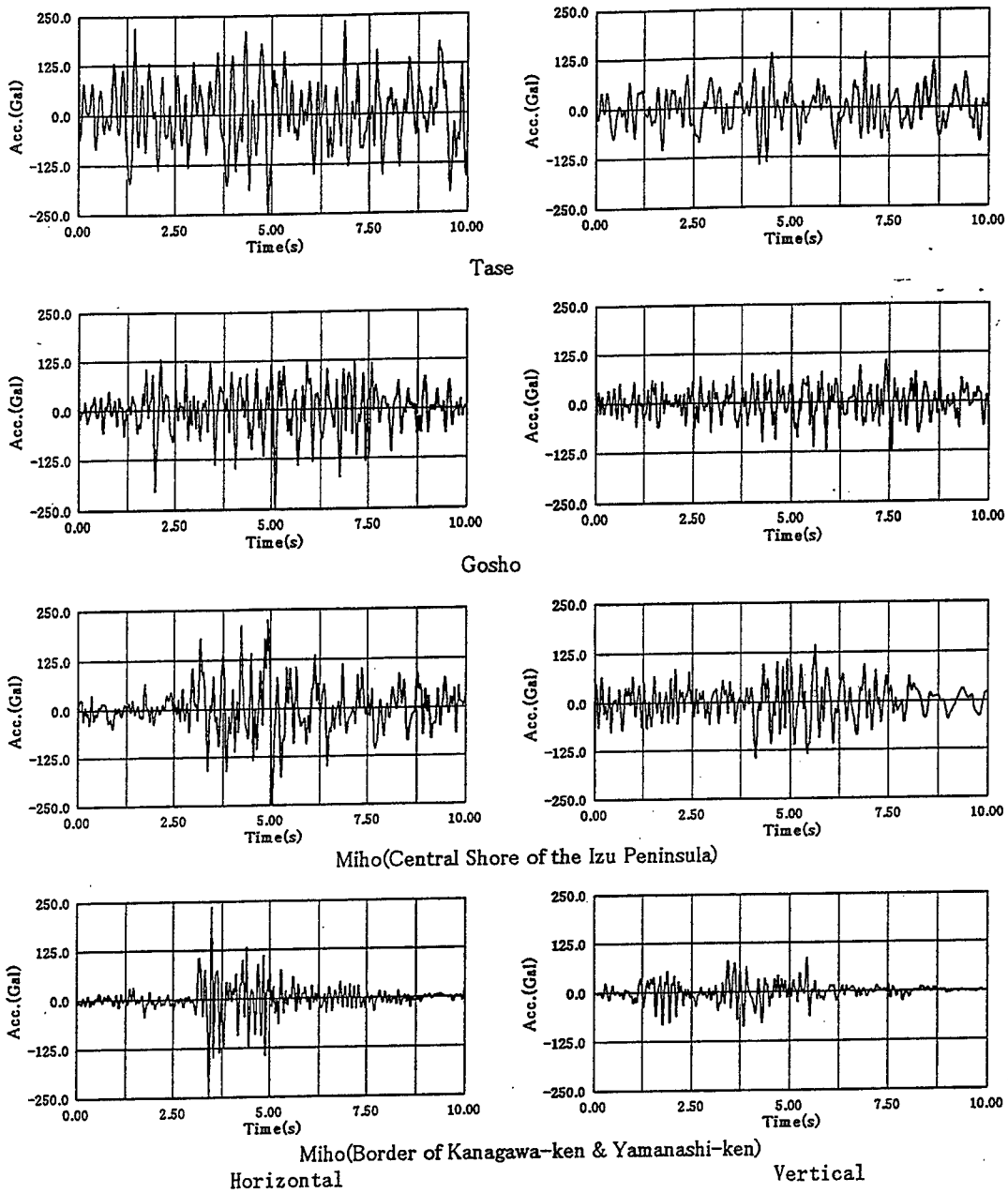

Fig.6(2) Time Histories of Acceleration(Tase,Gosho,Miho)

3. AVERAGE ACCELERATION OF BULK MATERIAL

The maximum average acceleration of the bulk material on a rotational slip surface was determined for each of the above-stated nine wave forms.

The average acceleration, $\bar{a}(t)$, is given by

$$\bar{a}(t)=\frac{\Sigma\{m_i a_{Hi}(t)\}}{\Sigma m_i}$$

where,

m_i = mass of node i within the bulk material on a rotational slip surface

$a_{Hi}(t)$ = time history of the horizontal acceleration response of node i within the bulk material on a rotational slip surface

The rotational slip surfaces investigated are shown as arcs in the cross section of Fig. 7.when the dependence of shear strength on

confining pressure is taken into consideration,a slip surface that provides a minimum safety factor intersects the central part of the top of dam. Thus, slip surfaces that intersect the central part of the top of dam were investigated in this study.Because the downstream face generally has a greater safety margin than the upstream face, the average acceleration of bulk material was calculated for the upstream face in the cross sections with heights of 60 and 100 m.

The maximum average acceleration of bulk material is given by the acceleration related to the maximum seismic force generated in bulk material during an earthquake event (average seismic coefficient) for different non-dimensional heights of y/H (vertical distance between the top of dam and the lowest level of the slip surface/vertical distance between the top of dam and the foundation surface of rockfill).

The maximum average acceleration values of bulk material for the upstream faces of some dams are shown in Fig. 8. There is no difference in the general trend between shallow and deep slip surfaces. Though depending on the input ground motion, responses at levels close to the top of dam decrease with increasing height of dam. For the 60- and 100-m-high sections, the accelerogram of the 1995 Hyogo-ken Nanbu earthquake recorded at the Minoogawa Dam generally provides the greatest average acceleration of bulk material. For the 161-m-high section, on the other hand, the accelerogram of the Miyagi-ken Oki earthquake recorded at the Minase Dam generally provides the greatest average acceleration of bulk material. No difference in the general trend is observed between the cases where only horizontal motion was input and where both horizontal and vertical motions were input.

The magnitudes of limit (or yield) acceleration are also shown in Fig. 8. The maximum average acceleration of bulk material in every case is smaller than the limit (or yield) acceleration.

In the present analysis, the maximum acceleration in a time history was regarded as an average acceleration of bulk material. Because this high level of acceleration is not continuous but momentary, the safety of the actual dam is considered to be higher than the analytical results.

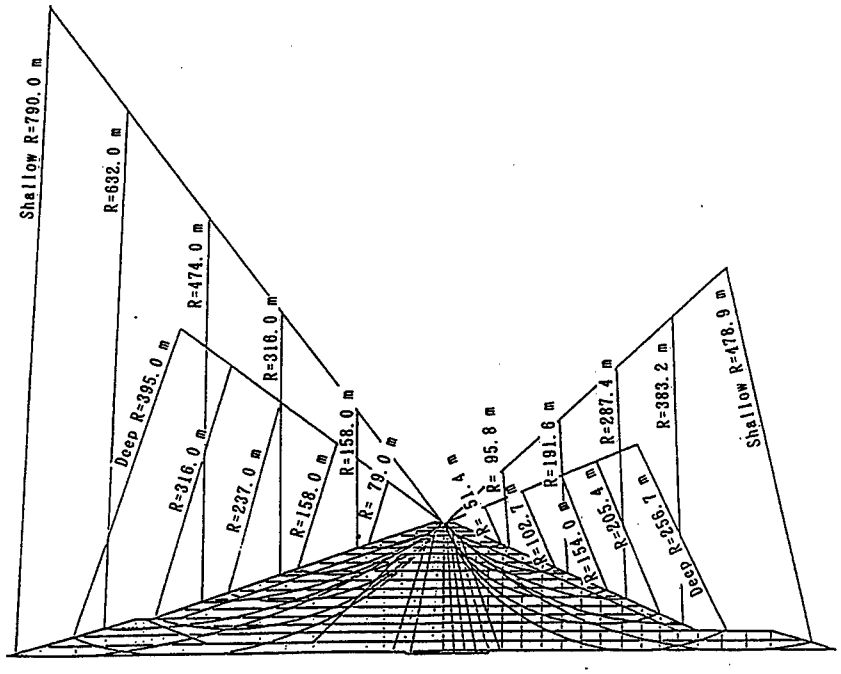

Fig.7 The Rotational Slip Surfaces

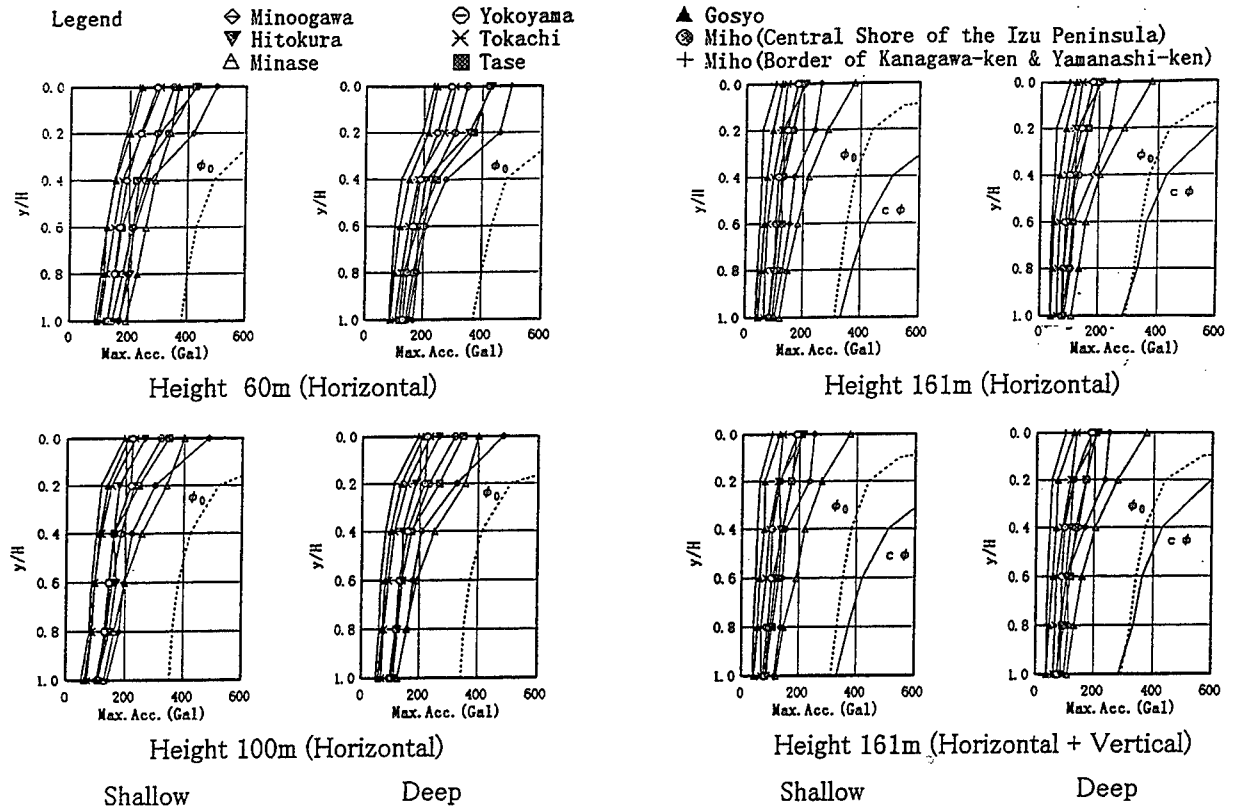

Fig. 8 Maximum Average Acceleration Values of Bluk Material (Upstream Faces)

4. RESPONSE CHARACTERISTICS AND SAFETY FACTORS

In addition to response acceleration and displacement , safety factors were evaluated from the internal stress of the bulk material on a hypothetical rotational slip surface in the 161-m-high section.

Because no difference in the general trend was observed between the cases where only horizontal motion was input and where both horizontal and vertical motions were input, only the results of the latter case is presented here.

4.1 Response Acceleration and Displacement

The focused axes and nodes are shown in Fig. 9. The distributions of maximum acceleration along the focused axes, which are perpendicular to the dam axis, are presented in Fig. 10, maximum response accelerations and displacements are listed in Table 6, and time histories of response acceleration are exemplified in Fig. 11.

At intermediate dam levels, the greatest response acceleration was obtained when the accelerogram of the Minoogawa Dam was used for input, and the greatest response displacement was found when the accelerogram of the Minase Dam was used. In the direction perpendicular to the dam axis, the maximum response acceleration was approximately 340 Gal and the maximum response displacement was approximately 10 cm. At dam top levels, on the other hand, the greatest responses were obtained when the accelerogram of the Minase Dam was used. In the direction perpendicular to the dam axis, the maximum response acceleration is approximately 300 Gal, and the maximum response displacement is approximately 16 cm. In any case, response acceleration was not greatly amplified from the maximum horizontal acceleration input of 250 Gal. Also, response displacement found in the 161-m-high section was small enough. Shear strain at some portions reached the level of 1×10^{-3}, indicating the state of elastoplasticity.

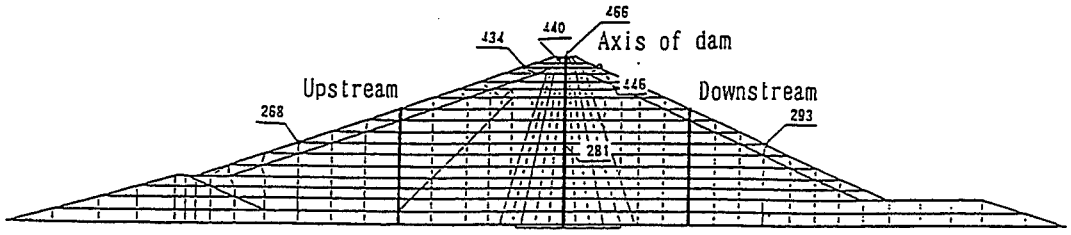

Fig.9 Focused Axes and Nodes

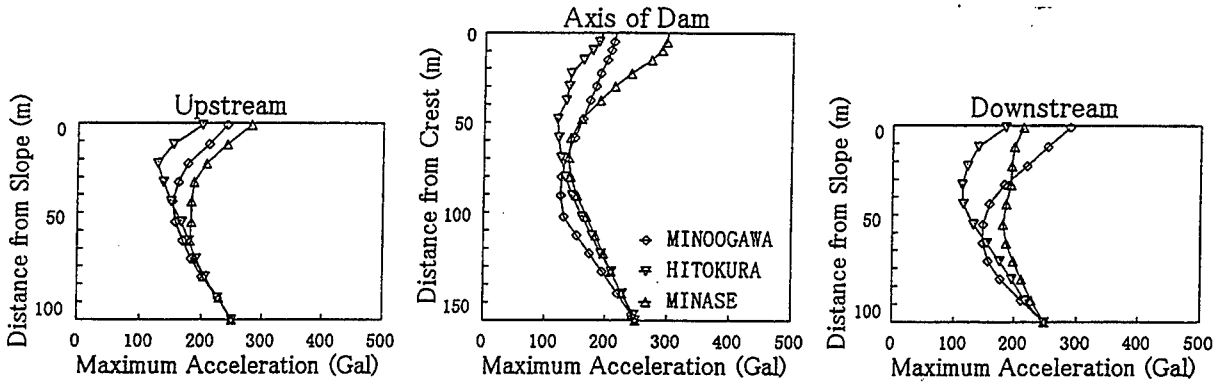

Fig.10 Distributions of Maximum Response Acceleration along the Focused Axes (Perpendicular to Dam Axis)

Table 6 Maximum Response Accelerations and Displacements on the Focused Nodes

		Focused Node								
		268	281	293	434	440	446	466		
Wave	Minoogawa	-337	127	-316	221	206	-200	214	Acceleration	Perpendicular to Dam axis
	Hitokura	206	-133	246	151	176	149	194		
	Minase	294	142	261	283	288	276	299		
	Minoogawa	6.7	-5.8	5.7	-12	-11	-11	-12	Displacement	
	Hitokura	4.0	4.6	3.4	6.6	6.6	6.6	6.8		
	Minase	-9.7	-7.5	-6.0	-16	-16	-16	-17		
	Minoogawa	268	123	174	160	177	193	185	Acceleration	Vertical
	Hitokura	-79	64	66	-66	-83	-83	-86		
	Minase	156	-108	-155	-141	-181	-140	-179		
	Minoogawa	-2.5	-1.9	-1.5	-3.5	-4.0	-3.4	-4.1	Displacement	
	Hitokura	0.8	-0.8	0.4	-1.4	1.4	-1.1	1.4		
	Minase	-2.4	2.6	1.5	4.0	5.1	3.9	5.1		
		Intermediate			Top					

Notes Unit:Acceleration (Gal), Displacement (cm)
Maximum Vertical Acceleration:Minoogawa…147.2Gal, Hitokura…85.0Gal, Minase…110.8Gal
+:Perpendicular to Dam axis…Downstream Side, Vertical…Up Side
-:Perpendicular to Dam axis…Upstream Side, Vertical…Down Side

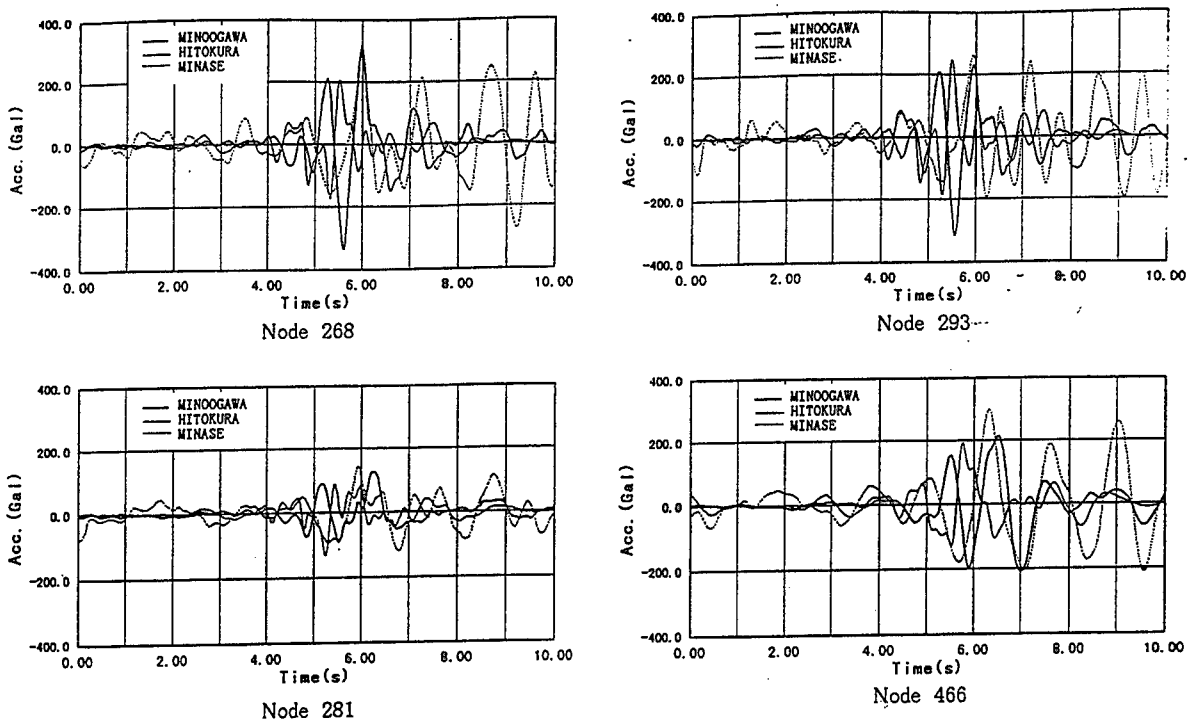

Fig. 11 Examples of Time Histories of Response Acceleration(Focused Nodes 268,281,293,466)

4.2 Safety Factors for Earthquakes

Safety factors were evaluated from the state of stress by superimposing dynamic stress upon static stress.

To compare with the analytical results of average acceleration of bulk material, the arcs shown in Fig. 7 were treated as potential slip surfaces, and local safety factors were averaged along each arc to calculate a safety factor.

Other than the slip surfaces that intersect the top of dam, the arcs shown in Fig. 12 were also investigated; these arcs are considered to provide low safety factors, or high possibility of sliding, in the seismic coefficient method. Arc 7 provides a low safety factor when the shear strength value obtained by the $c\phi$ method (cohesion of c = 0) is used in the seismic coefficient method, and arcs 4 and 8 provide low safety factors when the shear strength values obtained by the ϕ_0 method are used in the modified seismic coefficient method. Additionally, arcs 1 and 2 were selected to investigate surficial sliding on the upstream face, arc 3 was selected to investigate shallow sliding, and arcs 5 and 6 were selected to investigate surficial sliding on the downstream face. The smallest safety factor for each postulated slip surface is listed in Table 7 for different accelerogram.

All the safety factors resulted from the arcs of both Figs.7 and 12 exceed 1.0. Shallow arcs resulted in relatively low safety factors because vertical stress, therefore shear strength, is very small in the region close to the surface. This trend is highlighted on the upstream face, where the decrease of strength by water saturation was taken into consideration.

A safety factor was calculated from

$$F = \frac{\Sigma \tau_{Ri} \ell_i}{\Sigma \tau_i \ell_i}$$

where

τ_{Ri} = shear strength of material at minimal element i on a slip surface(kgf/cm^2)

τ_i = shear stress at minimal element i on a slip surface(kgf/cm^2)

l_i = length of minimal element i on a slip surface(cm)

Some examples of time histories of safety factor of postulated slip surfaces are shown in Fig. 13.

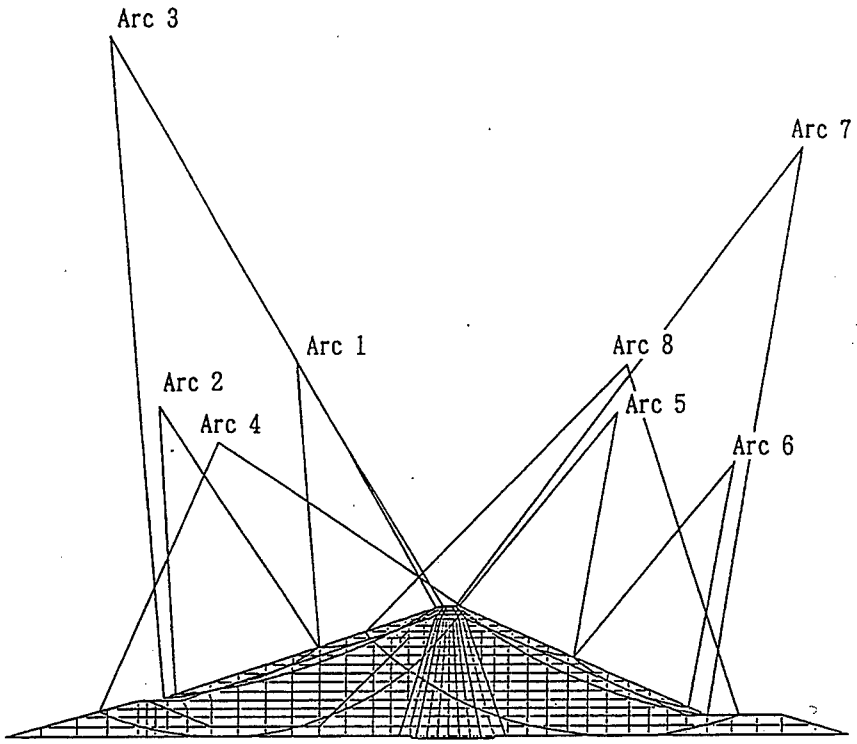

Fig.12 The Rotational Slip Surfaces

Table 7(1) The Smallest Safety Factor for Each Postulated Slip Surfaces (Arcs of Fig.7)

		y/H										
		0.2	0.4	0.6	0.8	1.0	0.2	0.4	0.6	0.8	1.0	
Wave	Minoogawa	1.59	1.43	1.88	2.18	2.14	2.58	1.96	1.96	1.86	2.09	Shallow
	Hitokura	2.37	2.03	2.27	2.51	2.48	2.60	2.05	2.11	2.02	2.12	
	Minase	1.42	1.40	1.60	1.86	1.97	2.46	1.95	2.11	2.07	2.26	
	Minoogawa	1.35	1.80	2.14	2.28	2.12	2.40	2.56	2.26	2.12	2.11	Deep
	Hitokura	2.04	2.48	2.51	2.59	2.42	2.51	2.76	2.50	2.35	2.22	
	Minase	1.23	1.83	1.90	1.99	2.01	2.33	2.57	2.43	2.35	2.29	
		Upstream Side					Downstream Side					

Table 7(2) The Smallest Safety Factor for Each Postulated Slip Surfaces (Arcs of Fig.12)

		Arc							
		1	2	3	4	5	6	7	8
Wave	Minoogawa	1.20	1.56	1.92	2.19	1.93	2.03	2.03	2.18
	Hitokura	1.85	2.10	2.24	2.39	2.00	2.40	2.14	2.17
	Minase	1.12	1.07	1.49	2.08	2.00	2.32	2.24	2.19
		Upstream Side				Downstream Side			

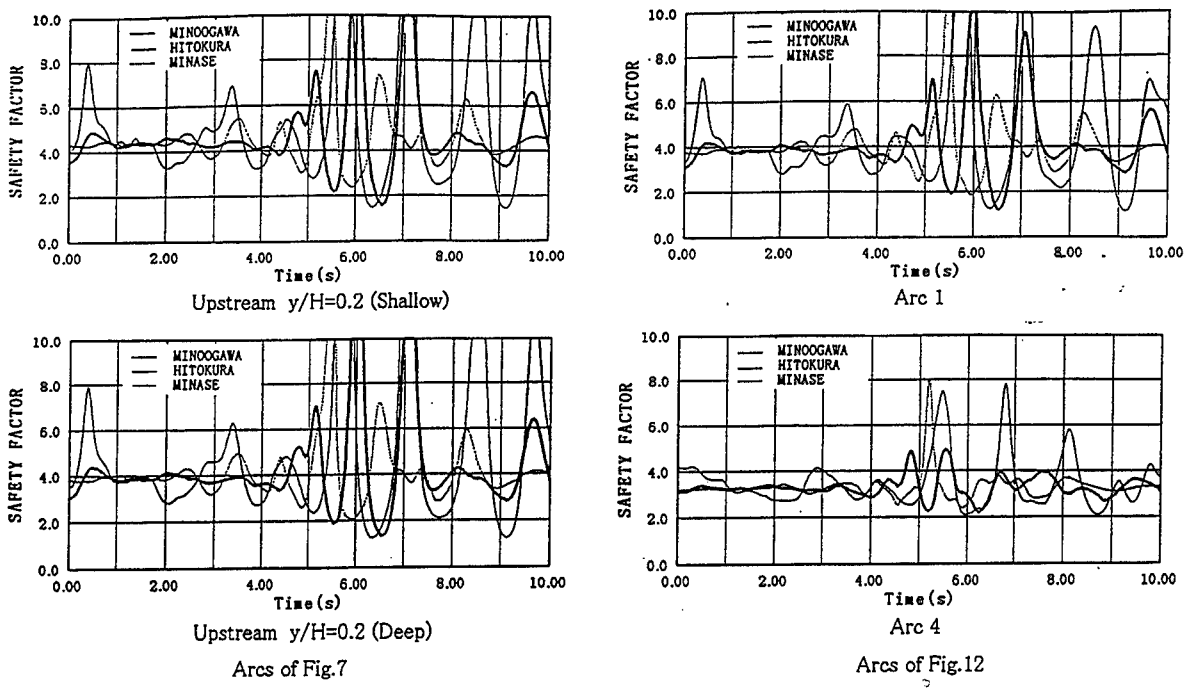

Fig. 13 Examples of Time Histories of Safety Factor(Arcs of Both Figs.7 and 12)

5. SUMMARY

The earthquake resistance of the Tokuyama Dam was studied by comparing the average acceleration of bulk material and limit (or yield) acceleration for sliding, by investigating response characteristics and evaluating safety factors for earthquakes. The maximum average acceleration of the balk material on a rotational slip surface, in any case, was found to be smaller than the limit (or yield) acceleration for the occurrence of sliding. Also, safety factors evaluated from internal stress were small enough.

A design horizontal seismic coefficient of 0.18 was adopted to calculate the stability of the Tokuyama Dam by the seismic coefficient method. Also, sufficient width was secured for the top of dam and the core zone, and core materials of good quality were selected to enhance the earthquake resistance of the dam. Further improvement in such areas as efficient use of materials is now being pursued.

ACKNOWLEDGMENTS

The authors are grateful to Emeritus Professor Shunzo Okamoto of Tokyo University, Professor Masami Fukuoka of Science University of Tokyo, Professor Choshiro Tamura of Nihon University, and Professor Hiroyuki Watanabe of Saitama University for providing valuable advice.

And most of the accelerograms used in this study are maintained by the Public Works Research Institute of the Ministry of Construction. The authors are thankful to Mr. Tadahiko Fujisawa, the Director of the Dam Department of the institute, and the staff of the department for providing valuable data and advice.

REFERENCES

1) The committee on the evaluation of earthquake resistance of dams ; The Report of the Committee on the Evaluation of Earthquake Resistance of Dams,1995

2) River bureau of Ministry of Construction ; The Seismic Design Guideline for Embankment Dams : Draft, 1991

Evaluation of Safety of Concrete Gravity Dams During the Hyogoken-Nambu Earthquake

by

Tadahiko Sakamoto[1], Tadahiko Fujisawa[2],
Isao Nagayama[3], and Takashi Sasaki[4]

ABSTRACT

The Hyogoken-Nambu Earthquake of January 17, 1995 inflicted severe damage on many structures in the Hanshin and Awaji areas such as had not been experienced in Japan in recent decades. However, there was no damage on dams which affected the their safety.

This paper introduces the characteristics of ground acceleration observed at dam sites during the Hyogoken-Nambu Earthquake and discusses the safety of concrete gravity dams in such big earthquakes. The result of the dynamic analysis shows that concrete gravity dams have the high safety against such big earthquakes.

Key Words:
concrete gravity dam, dynamic analysis, earthquake, seismic resistance

1. PREFACE

In the early morning of January 17, 1995, the Hyogoken-Nambu Earthquake inflicted severe damage in the Hanshin and Awaji areas. The epicenter was in the north of the Awaji Island. The seismic intensity of 7 (by the Scale of the Japan Meteorological Agency) was recorded in some parts of the areas. A lot of buildings collapsed during the earthquake or were consumed in the fire which followed it. The Hanshin Expressway, the Shinkansen Line and many other public facilities were severely destroyed. Table 1 shows the outline of the Hyogoken-Nambu Earthquake and Figure 1

Table 1 Outline of the Hyogoken-Nambu Earthquake

Date	Jan 17, 1996 5 : 46 : 52
Epicenter	Latitude 34.6° N
	Longitude 135.0° E
Depth	14km
Magnitude	7.2

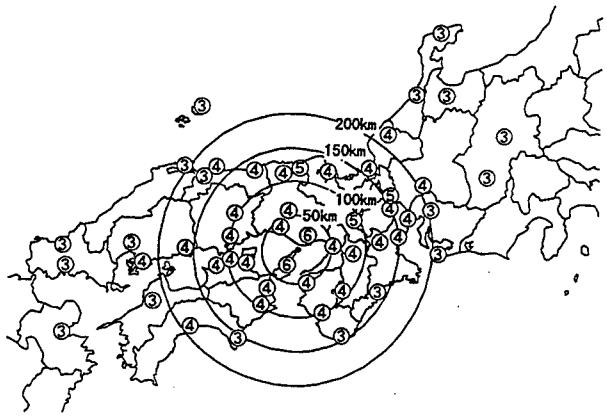

Figure 1 Distribution of the Seismic Intensity

[1] Director General, Public Works Research Institute, Ministry of Construction, Tsukuba Science City, 305 Japan
[2] Director, Dam Department, ditto
[3] Head, Dam Structure Division, Dam Department, ditto
[4] Senior Researcher, Dam Structure Division, Dam Department, ditto

shows the distribution of the seismic intensity.

About 250 dams received the shock of the earthquake within 300 km of its epicenter. The Tokiwa Dam was located in a distance only 800 m from the Nojima earthquake fault. There were also a number of old dams in Kobe City where the earthquake damage was most severe. The Gohonmatsu Dam was the oldest concrete gravity dam (rubble masonry) in Japan built in 1900. The dam safety inspection immediately after earthquake showed that there were no damage on the dams which affected their safety.

This paper introduces the characteristics of ground acceleration observed at dam sites during the Hyogoken–Nambu Earthquake and discusses the safety of concrete gravity dams in such big earthquakes.

2. CHARACTERISTICS OF EARTH-QUAKE MOTION AT DAM SITES

2.1. Maximum Acceleration at Foundation of Dams

(1) Attenuation of Peak Acceleration

About 50 ground acceleration records were obtained at dam sites during the Hyogoken–Nambu Earthquake. All the dams were constructed on the rock foundation. Table 2 shows the peak acceleration recorded at the foundation of dams during the earthquake (including the acceleration obtained at the lowest gallery in the concrete dams or at the gallery beneath the embankment dams). The maximum ground acceleration is 183 gal which was recorded at the lowest gallery of the Hitokura Dam (concrete gravity dam, height = 75 m). The dam was located in a distance of 47 km from the epicenter or only 10 km from the estimated earthquake source fault in the ground. The location of the earthquake source fault in the Kobe area was estimated from the distribution of aftershocks on January 17, while it coincides with the Nojima fault in the Awaji area.

Table 2 Peak Acceleration Recorded at Foundation of Major Dams

Dam Site	Acceleration (gal)	
	Horizontal Direction	Vertical Direction
Hitokura	183	64
Minoo	128	75
Donto	111	—
Gongen	103	67
Kisenyama	90	44
Kurokawa	85	53
Tataragi	65	20
Shirakawa	50	48
Zao	49	25
Yasumuro	38	31
Nishidaira	38	25
Seto	35	12
Masaki	33	33
Senzoku	32	16
Fukui	32	15
Hase	30	22

The attenuation of the horizontal peak acceleration of the foundation of dams is shown in Figure 2, and the attenuation of the vertical peak acceleration in Figure 3. The envelopes of the peak acceleration can be expressed by a straight line in the semi–logarithm plot. They are expressed as follow:

$$\ln Ah = \ln 217 - 0.0170\,L$$
$$\ln Av = \ln 93 - 0.0114\,L$$

where Ah : horizontal peak acceleration (gal)
Av : vertical peak acceleration (gal)
L : distance from the earthquake source fault (km)

From the figure and the above equation, it can be estimated that the maximum of horizontal peak acceleration induced at the rock sites near the earthquake source fault was about 220 gal.

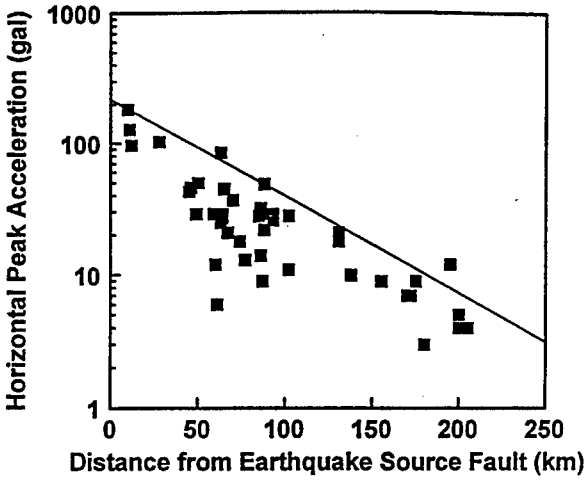

Figure 2 Attenuation of Horizontal Peak Acceleration

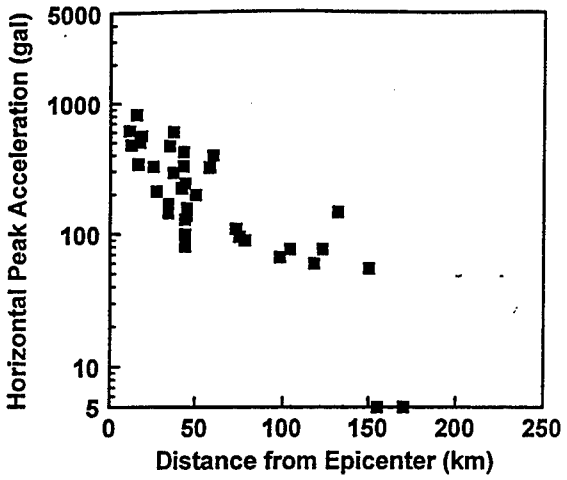

Figure 4 Attenuation of Horizontal Peak Acceleration at Soil Sites

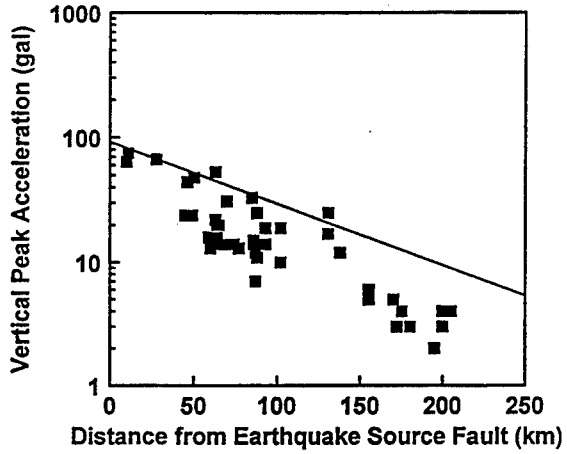

Figure 3 Attenuation of Vertical Peak Acceleration

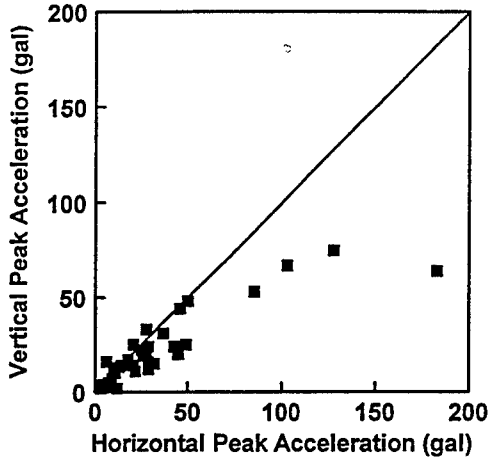

Figure 5 Horizontal Peak acceleration versus Vertical Peak Acceleration

Figures 4 shows the attenuation of the horizontal peak acceleration observed at soil sites. The figure shows that the maximum of horizontal peak acceleration at soil sites was 818 gal. It indicates that the peak acceleration at rock sites is substantially smaller than that at soil sites. It is because the rock sites were much harder than the soil sites, and the acceleration is not enlarged so much at the surface.

(2) Horizontal Peak Acceleration versus Vertical Peak Acceleration

Figure 5 shows the relationship between the horizontal peak acceleration and the vertical peak acceleration observed at dam sites during the Hyogoken–Nambu Earthquake. The ratio of the vertical peak acceleration to the horizontal peak acceleration ranges from 1/3 to 1/1. This ratio tends to decrease as the horizontal peak acceleration increases.

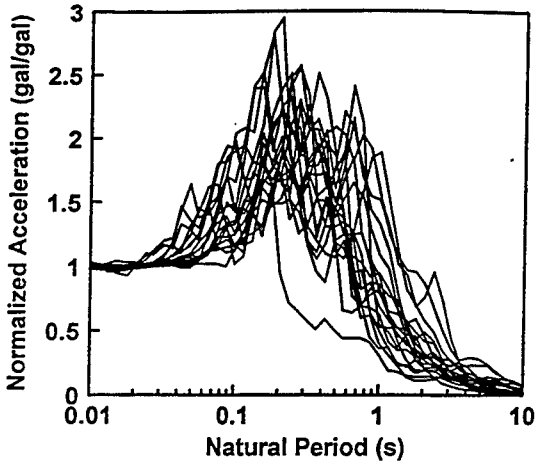

Figure 6 Normalized Response Spectrum of Acceleration (Horizontal Direction)

2.2. Acceleration Response Spectrum

The response spectra of the acceleration in the stream direction (damping ratio of 10%) at 19 dam sites in the Hyogoken–Nambu Earthquake are shown in Figure 6. Each spectrum is normalized so that the maximum ground acceleration is equal to 1. The average value of the normalized response spectra is about 2 for the natural period ranging from 0.1 to 0.6 seconds. The response spectra decrease rapidly when the natural period exceeds about 0.6 seconds.

3. EARTHQUAKE RESISTANCE DESIGN OF DAMS IN JAPAN

3.1. Methodology

The earthquake resistance design of dams is made using the Seismic Coefficient Method under the present design criteria in Japan. The seismic coefficient is as stipulated in Table 3 according to the type of the dam and its location.

The Seismic Coefficient Method cannot represent the actual behavior of dams during earthquakes because the uniform seismic coefficient is assumed in the dam body. However, the dams designed with the Seismic Coefficient Method have not suffered any damage affecting their safety during earthquakes in the past. It is considered that the adequate safety factor compensates for the defect of the assumption of the Seismic Coefficient Method.

Table 3 Seismic Coefficient in Design Criteria

Type of Dams	Regional Seismicity		
	High	Moderate	Low
Concrete			
Gravity	0.12	0.12	0.10
Arch	0.24	0.24	0.20
Embankment			
Zoned	0.15	0.12	0.10
Homogeneous	0.15	0.15	0.12

3.2. Safety Requirements of Concrete Dams

Safety Requirements of Concrete Dams are summarized as follows:

(1) No tensile stress in the vertical direction should exist at the upstream face of the dam.

(2) The safety factor against sliding of the dam should be no smaller than 4.

(3) The stress in the dam should be within the allowable stress of concrete. The allowable compressive stress of concrete should be no larger than one quarter of the compressive strength of the standard specimen of concrete.

4. EVALUATION OF SEISMIC RESISTANCE OF CONCRETE DAMS

4.1. Model Concrete Gravity Dams

The concrete gravity dams used in the analysis have a typical cross section in accordance with the abovementioned design criteria. The downstream slope of the dams is 0.8:1, and the upstream slope is vertical (0.0:1) at the upper part and 0.3:1 at lower part. The height of the dams ranges from 25 m to 150 m.

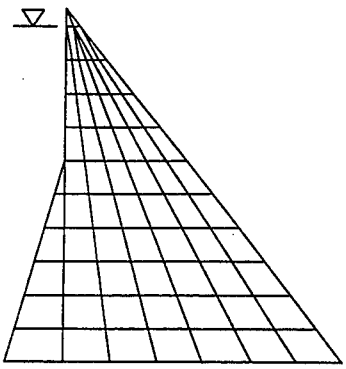

Figure 8 Finite Element Model of Concrete Gravity Dam

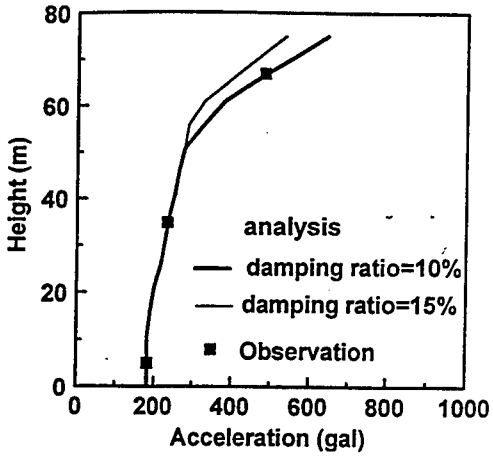

Figure 9 Distribution of Acceleration at the Hitokura Dam

Table 3 Physical Properties of Material

Item	Value
Concrete	
Density	2300 kg/m ^{3}
Elastic Modulus	30 kN/mm ^{2}
Poisson's Ratio	0.2
System	
Damping Ratio	10 %

Figure 8 shows the finite element model of the dams, and Table 4 shows the physical properties of the material.

4.2. Methodology

The response spectrum method with the modal analysis was used in the analysis [5] . The first 6 modes of vibration were considered. The damping ratio was assumed 10 %. This value is based on the results of behavior analysis of the Hitokura Dam (height = 75 m), where the acceleration of the foundation was 183 gal and the acceleration of the top gallery (8 m lower than the crest of the dam) was 482 gal in the Hyogoken–Nambu Earthquake. Figure 9 shows the result of the analysis of the Hitokura Dam.

The effect of reservoir water was accounted for as the added mass matrix in the modal analysis [5] . The added mass matrix is calculated assuming that reservoir water is incompressible.

4.3. Acceleration Records Used in Analysis

Two types of acceleration were used in the analysis. At first, 21 original acceleration records were used and the results of the analysis were examined with regard to the distance from the earthquake source fault. Then, the typical 4 acceleration record which were observed at the dam sites near the earthquake source fault were used. In this case, the horizontal peak acceleration was enlarged as much as 250 gal. The value of 250 gal was determined in consideration of the adequate margin of safety for the estimated maximum acceleration of 220 gal in the Hyogoken–Nambu Earthquake. The analysis includes the effect of the vertical acceleration. The vertical acceleration was enlarged at the same rate as the horizontal acceleration. Figure 10 shows the response spectrum of acceleration records ACC–1 to ACC–4 (damping ratio = 10 %).

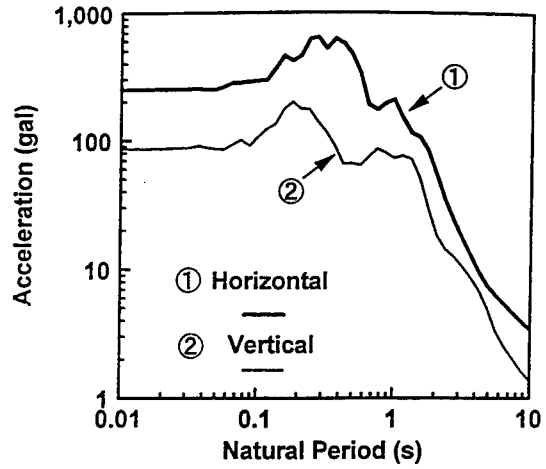

[1] ACC−1

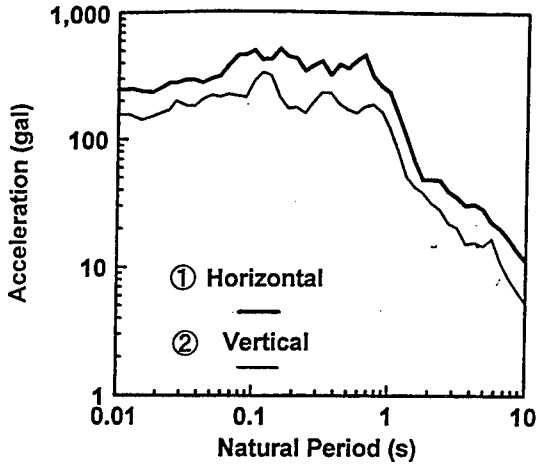

[3] ACC−3

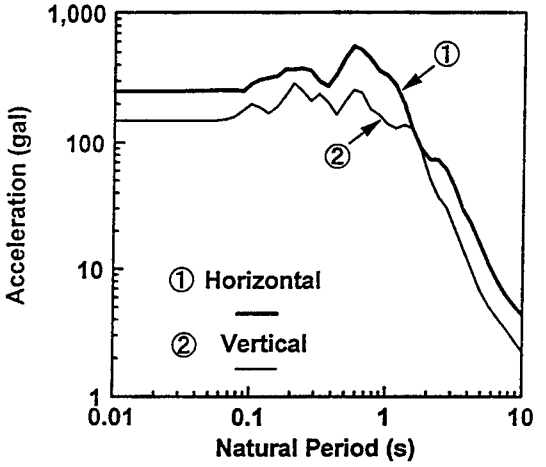

[2] ACC−2

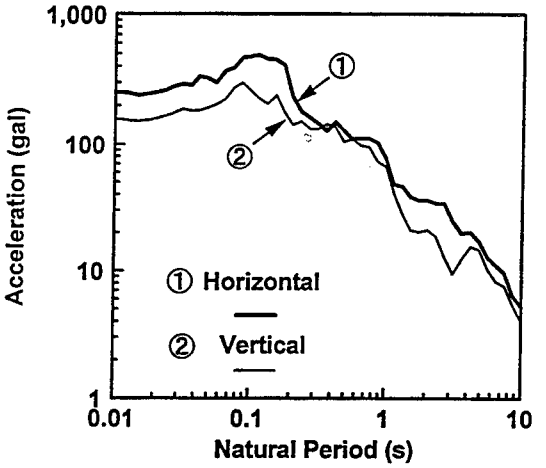

[4] ACC−4

Figure 10 Modified Response Spectra of Four Acceleration Records

4.4. Results of Analysis

(1) Tensile Stress

a) Maximum Tensile Stress versus Distance from Earthquake Source Fault

The maximum tensile stress was induced at the middle portion of the upstream face of the dams in all cases. Figure 11 shows the maximum tensile stress in the dams excluding static stress with regard to the distance from the earthquake source fault. The envelope is almost in a straight line, although the maximum tensile stress has wide range depending on the characteristics of the acceleration records. Figure 12 shows the maximum tensile stress in the dams including static stress with regard to the distance from the earthquake source fault. It can be estimated from the figures that the maximum tensile stress induced in the dams near the earthquake source fault is about 2.2 N/mm^2 in 150m high dams, 1.3 N/mm^2 in 100 m high dams and 0.6 N/mm^2 in 50 m high dams.

b) Maximum Tensile Stress for Ground Acceleration of 250 gal

Figure 13 shows the maximum tensile stress in the dams of the different height induced by the ground acceleration of ACC−1

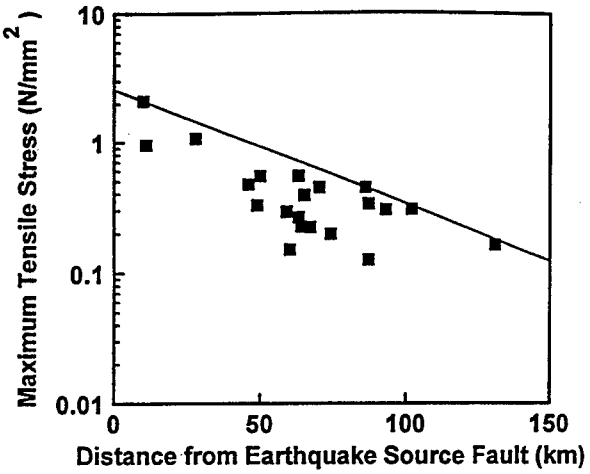

[1] Dam Height = 150 m

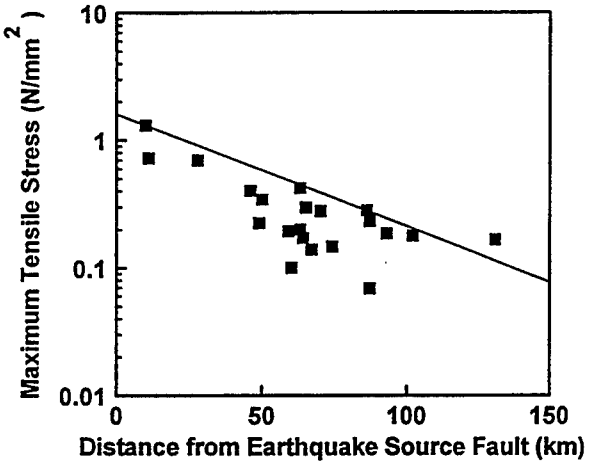

[2] Dam Height = 100 m

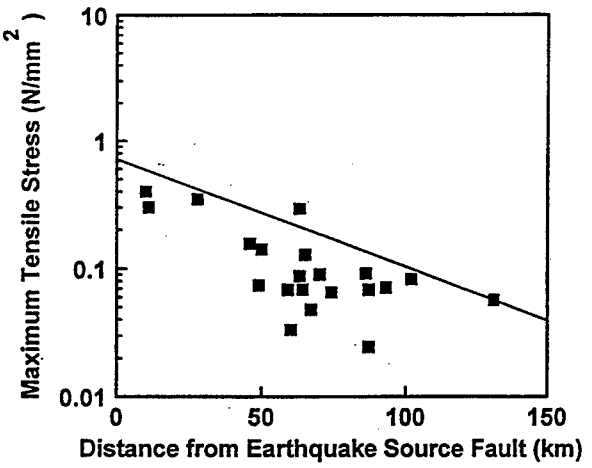

[3] Dam Height = 50 m

Figure 11 Maximum Tensile Stress versus Distance from Earthquake Source Fault (Excluding Static Stress)

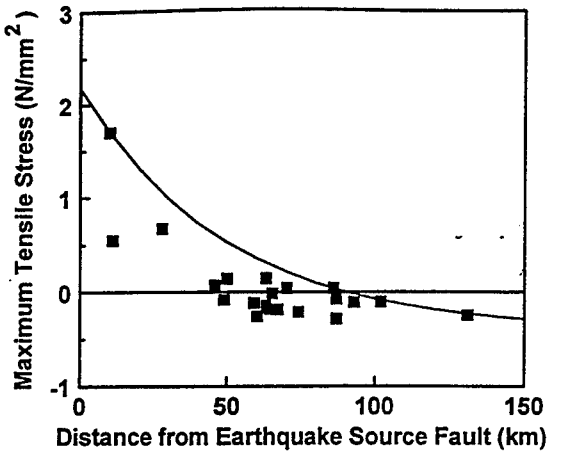

[1] Dam Height = 150 m

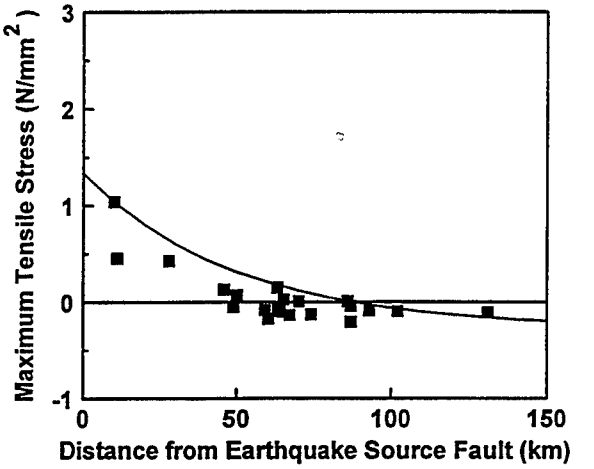

[2] Dam Height = 100 m

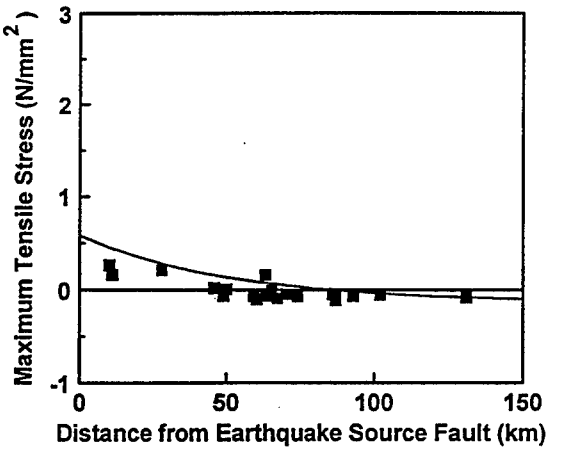

[3] Dam Height = 50 m

Figure 12 Maximum Tensile Stress versus Distance from Earthquake Source Fault (Including Static Stress)

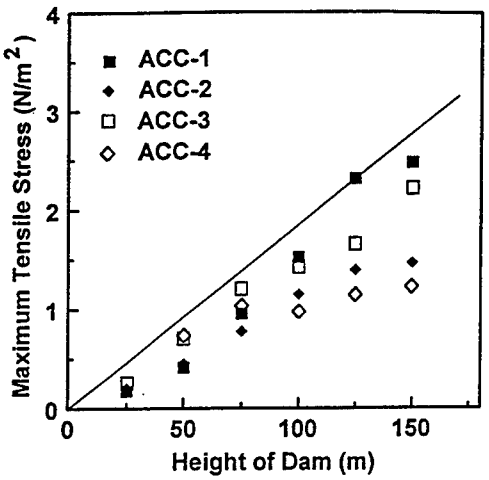

Figure 13 Maximum Tensile Stress versus Height of Dams

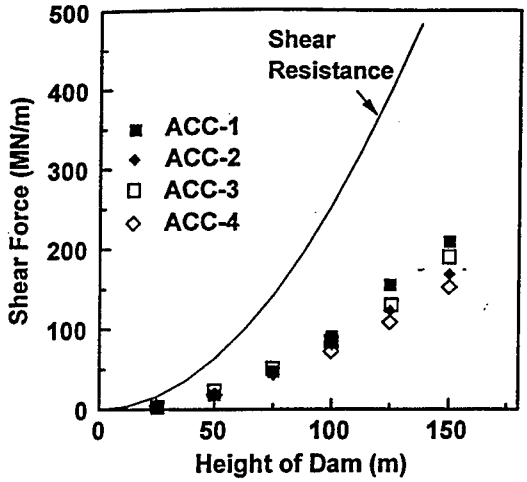

Figure 14 Comparison between Shear Force and Shear Resistance

to ACC−4. The stress includes the static stress in all cases. The acceleration ACC−1 produces the largest stress in higher dams, since the dominant period of the acceleration is close to the natural period of those dams. On the contrary, the acceleration ACC−4 produces the lowest stress in higher dams, since the dominant period of the acceleration is far from the natural period of those dams.

The figure shows that the maximum tensile stress increases in proportion to the height of the dam. The envelope is expressed as:

$$\sigma = 0.0185\,H \quad \text{(at 250 gal)}$$

or

$$\sigma = (0.00848\,\alpha - 0.27)\,H/100$$

where σ : maximum tensile stress (N/mm^2)
α : maximum ground acceleration (gal)
H : height of dam (m)

It can be estimated from the figure or the above equations that the maximum tensile stress by the ground acceleration of 250 gal is about 2.8 N/mm^2 even in 150 m dams. Since the dynamical stress occurs instantaneously, it is considered that dams can withstand such a level of tensile stress.

(2) Shear Resistance

Figure 14 shows the maximum shear force induced by the acceleration ACC−1 to ACC−4 and the shear resistance along the base of dams. Here, the shear strength of the foundation rock was assumed so that the safety factor was 4 in the seismic coefficient method (seismic coefficient = 0.12). The figure shows that the maximum shear force is much smaller than the shear resistance. The dams are therefore safe against shear force induced by the earthquakes.

5. CONCLUSION

The Hyogoken−Nambu Earthquake of January 17, 1995 inflicted severe damage in the Hanshin and Awaji areas such as had never been experienced in Japan in recent decades. However, there was no damage on the dams affecting their safety.

This paper introduces the characteristics of ground acceleration observed at dam sites during the Hyogoken−Nambu Earthquake and discusses the safety of concrete gravity dams in such big earthquakes. The results of the

analysis are as follows:

(1) It is estimated that the maximum peak acceleration at rock sites induced by the Hyogoken–Nambu Earthquake was about 220 gal. The acceleration at rock sites was much smaller than that at soil sites.

(2) It is estimated that the maximum tensile stress in the concrete gravity dams induced by the earthquakes is:

$$\sigma = 0.0185\,H \quad \text{(at 250 gal)}$$

or

$$\sigma = (0.00848\,\alpha - 0.27)\,H/100$$

where σ : maximum tensile stress (N/mm^2)

α : maximum ground acceleration (gal)

H : height of dam (m)

Therefore, the maximum tensile stress in 150 m high concrete gravity dams induced by the ground acceleration of 250 gal is about 2.8 N/mm^2.

(3) The shear force induced at the base of concrete gravity dams by the earthquakes is much lower than the shear resistance.

(4) The concrete gravity dams are safe in such big earthquakes as the Hyogoken–Nambu Earthquake.

REFERENCES

(1) Committee on Evaluation of Earthquake Resistance of Dams: Report of Committee on Evaluation of Earthquake Resistance of Dams, November, 1995

(2) Committee for Investigation on the Damage of Highway Bridges Caused by the Hyogoken–Nambu Earthquake: Report on the Damage of Highway Bridges by the Hyogoken–Nambu Earthquake, December, 1995

(3) Cabinet Order Concerning Structural Standards for River Administration Facilities, 1976

(4) Bylaw Concerning Structural Standards for River Administration Facilities, 1976

(5) I. Nagayama, S. Jikan: Study on Dynamic Behavior of Concrete Dams During Earthquake with Hydrodynamic Interaction, Int. Symp. on Earthquake & Dams, China, 1987

Large Scale Vibration Experiments

by

Robert Hall*

1 BACKGROUND

Vibration experiments on full-scale structures provide valuable data defining the dynamic performance of complex structural systems. Vibration experiments on concrete dams have been used to define the dynamic characteristics of the structure, hydrodynamic loads, effect of the reservoir bottom, and the response of monolith joints.

This paper will summarize three vibration experiments on concrete dams; i.e., the Richard B. Russell Concrete Gravity Dam, the Dongjiang Dam, and the Seven Mile Dam. Analytical and experimental studies were conducted on the R. B. Russell Concrete Gravity Dam (Wright, Chiarito, and Hall 1988). Linear elastic three-dimensional finite analyses of the dam were used to model the structural response both with and without reservoir effects. These analyses were compared with experimental results from prototype vibration experiments before and after reservoir impoundment. Experimental studies were conducted on the Dongjiang Dam in China (Ghanaat et al. 1993). The principal purpose of this research was to develop new testing procedures for exciting the entire dam-water-foundation system with explosives and to obtain data sufficient for the validation of existing analytical procedures. The third study was a series of dynamic experiments on the Seven Mile Dam (Duron 1995). This structural system was studied during the summer and the winter periods to determine the influence of monolith joints on the dynamic response of concrete dams.

2 R. B. RUSSELL

The Richard B. Russell Dam, built by the U.S. Army Corps of Engineers in 1983, is approximately 170 miles from the mouth of the Savannah River between Georgia and South Carolina (Figure 1). The crest of the concrete gravity section of the dam is 1,884 ft long. The dam is composed of 13 non-overflow, 8 intake, and 11 spillway monoliths, the tallest of which is approximately 200 ft high.

Two forced vibration experiments were made on the R. B. Russell Dam before and after impoundment of the reservoir to determine the natural frequencies, mode shapes, modal damping ratios, and relative joint movements (Wright, Chiarito, and Hall 1988). The abutments of the sides of the dam restrain the end monoliths. However, the abutment on the Georgia side was not complete during the first experiment and was approximately 60 ft below the completed crest.

The reservoir impoundment decreased the natural frequencies of the dam. The damping estimates and natural frequencies from the two experiments are shown in Table 1.

---

*Structural Mechanics Division,
Research Analysis Group,
Structures Laboratory,
USAE Waterways Experiment Station,
Vicksburg, MS 39180-6199

The reservoir impoundment resulted in first modes and corresponding natural frequencies being decreased by 10 percent, while the higher modes had smaller decreases. Measurement from both experiments indicated relative motions between monoliths. The dam behaved as a single structure for the lower natural frequencies. However, for the high frequency, the natural frequencies were governed by the dynamic characteristics of independent monoliths. The finite-element analyses correctly predicted the natural frequencies of the lower modes. However, the nonlinear effects of the monolith joints were not modeled. That resulted in the increased errors for the higher mode shapes and corresponding frequencies. Table 3 provides a comparison of the experimental and analytical results.

3 EXPERIMENTAL STUDY OF DONGJIANG DAM

This study was funded by the National Science Foundation under the US-China Protocol on Earthquake Studies described by Clough et al. (1984a, 1984b). The two collaborating organizations were Quest Structures of Emeryville, California, and the Institute of Water Conservancy and Hydroelectric Research (IWHR) of Beijing, China. Dr. Yusof Ghanaat of Quest Structures and Professor Hou-Qun Chen of IWHR were the principal investigators. Professor Clough and Dr. C. G. Shen of IWHR were Project Advisers. The structural response measures were performed by the U.S. Army Engineer Waterways Experiment Station.

The Dongjiang Dam is located on the Leishui River in Hunan Province and is the tallest double curvature concrete dam currently in operation in China (Figure 2). The dam is 157 m (515 ft) high with a 442 m (1,450 ft) crest length. Dongjiang Dam is a single-centered arch dam and has uniformly thick arches with short-radius fillets toward the abutments. The structure was constructed in 29 monoliths separated by vertical contraction joints.

A total of 600 kg of explosives were placed in five holes 800 m downstream from the center of the dam for the first experiment. A total of 600 kg of explosives were place in four of the original five holes for the second dynamic response study.

Acceleration time histories of the ground motions were taken at rock abutments. The structural response acceleration time histories were taken across the crest of the dam and within three lower galleries. Location of the seismographs and accelerometers is shown in Figure 3. Hydrodynamic pressure histories were taken at eleven locations on the upstream face of the dam (Figure 4). The recorded signals for both blasts were similar.

The computer program GDAP was used to calculate the structural response. The measured ground motions from the blast experiment were used as input to GDAP in order to demonstrate the ability to predict dynamic response of the dam. The GDAP program models the entire dam-foundation system and models the reservoir as an incompressible fluid. As seen in Figures 5 and 6, the GDAP program provides an accurate numerical model for predicting the dynamic response of the dam.

The results of these experiments validate that explosive experiments excite the fundamental dynamic characteristics of these complex systems. The use of this explosive technique will provide the ability to study the complex interactions between the reservoir and reservoir bottom and the interaction between the dam, the foundation, and the reservoir. These data will be critical to validate additional analytical tools.

4 SEVEN MILE DAM

The Seven Mile Dam is owned and operated by the British Columbia Hydro and Power Authority and is located about six miles downstream at the confluence of the Pen Oreille and the Columbia Rivers. The dam is concrete gravity structure approximately 1,140 ft long with a maximum height of 263 ft. The dam is comprised of four sections: north gravity, power intake, spillway, and the south gravity section shown in Figure 7.

Both ambient and forced vibration experiments were conducted. The force vibration experiments were conducted with a single shaker producing 18,000 lb of force. Acceleration levels produced by the shaker were about the same as ambient levels resulting from water intake during power generation. Vibration experiments were conducted in the summer and in the winter to determine the influence of monolith joints on the dynamic characteristics of concrete gravity dams. Table 2 lists the frequencies for the first experiments conducted 20-26 February 1995, for both the ambient and the forced vibration experiments. These results demonstrate that ambient vibration experiments can be used to determine the dynamic characteristics of concrete gravity dams. Figure 8 shows the difference in the forced response between August and February experiments. The differences are due to thermal effects and changes in the joint behavior. The primary factor affecting the response of the Seven Mile Dam was joint behavior.

5 CONCLUSIONS

The study on the R. B. Russell Dam demonstrated that finite-element procedures can be used to predict the dynamic response of concrete gravity dams. This provides engineers with validated procedures for predicting the linear elastic response of these critical structures during the dynamic excitation resulting from earthquake ground motions.

The study of the Dongjiang Dam demonstrated that explosives can successfully be used to excite the fundamental frequencies of the entire dam-reservoir-foundation system. This validated procedure can now be used to study the details of the complex interactions taking place between the different components of this complex system.

The study of the Seven Mile Dam demonstrated that the influence of monolith joints needs to be accounted for in the seismic evaluation of concrete gravity dams. Those results indicate that the dynamic response of arch dams may also be influenced by the behavior of monolith joints.

6 ACKNOWLEDGMENT

The investigation described and the resulting data presented herein, unless otherwise noted, were obtained from research conducted under the Earthquake Engineering Research Program of the United States Army Corps of Engineers by the U.S. Army Engineer Waterways Experiment Station. Permission was granted by the Chief of Engineers to publish this information.

7 REFERENCES

1. Duron, Z.H. (1995). "Seven Mile Dam Vibration Testing - Results from the first series of tests performed February 20-27, 1995," British Columbia Hydro and Power Authority, Burnaby, B.C., April 1995.

2. Duron, Z.H. (1995). "Seven Mile Dam Vibration Testing – Results from the second series of tests performed August 14-20, 1995," British Columbia Hydro and Power Authority, Burnaby, B.C., October 1995.

3. Wright, R.S., Chiarito, V.P., and Hall, R.L. (1988). "Summary of the Richard B. Russell Concrete Dam Vibration Study," Technical Report SL-88-10, U.S. Army Engineer Waterways Experiment Station, Vicksburg, MS, February 1988.

4. Ghanaat, Y., Hou-Qun, C., Redpath, B., and Clough, R. (1993). "Experimental Study of Dongjiang Dam for Dam-Water-Foundation Interaction," Quest Structures, Emeryville, CA.

5. Clough, R.W., Chang, K.-T., Chen, H.-Q., Wang, G.-L., and Ghanaat, Y. (1984a). "Dynamic Response Behavior of Xiang Hong Dian Dam," Report No. UCB/EERC-84/02, Earthquake Engineering Research Center, University of California, Berkeley.

6. Clough, R.W., Chang, K.-T., Chen, H.-Q., Stephen, R.M., Ghanaat, Y., and Qi, J.-H. (1984b). "Dynamic Response Behavior of Quan Shui Dam," Report No. UCB/EERC-84-20, Earthquake Engineering Research Center, University of California, Berkeley.

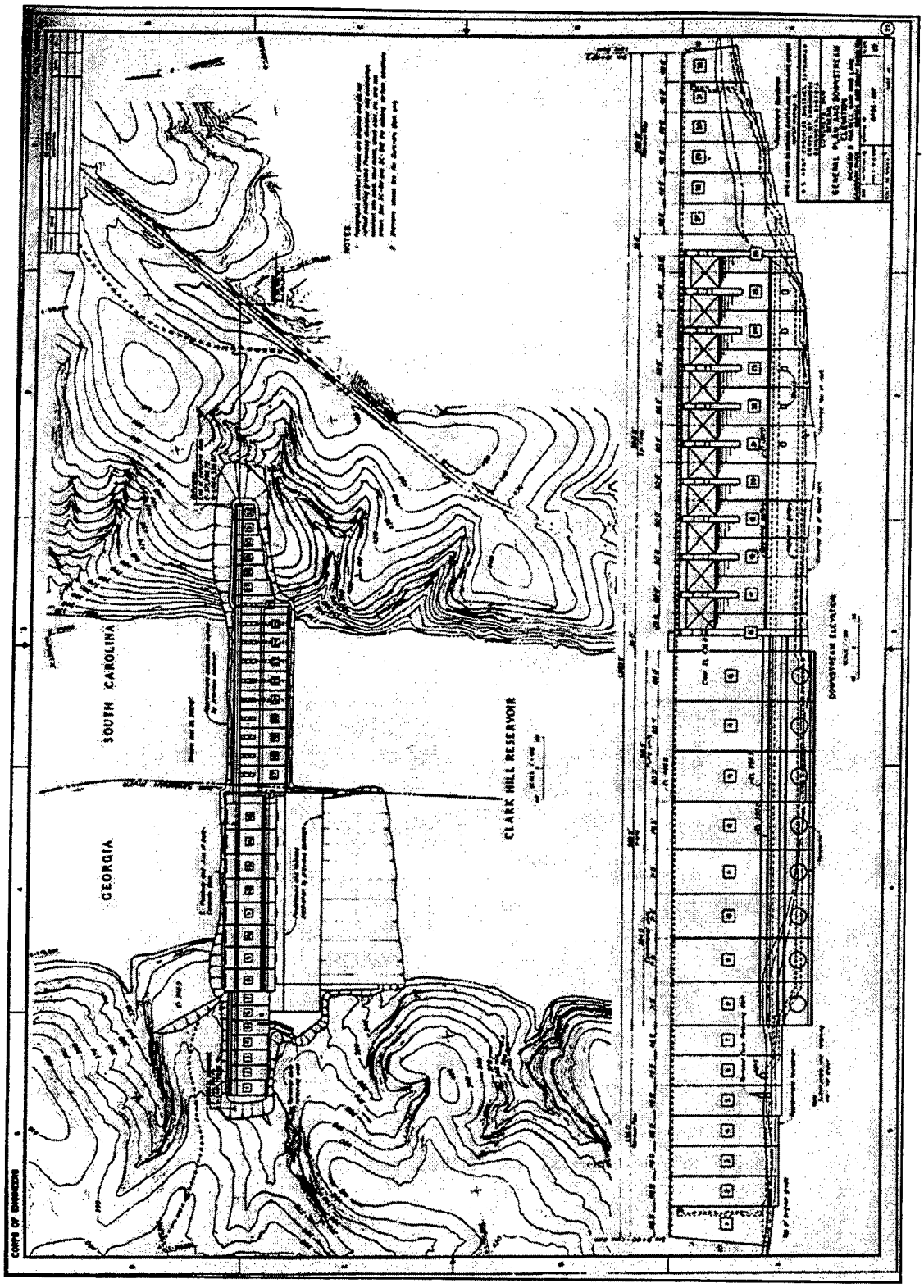

Figure 1. Plan and elevation of the Richard B. Russell Dam

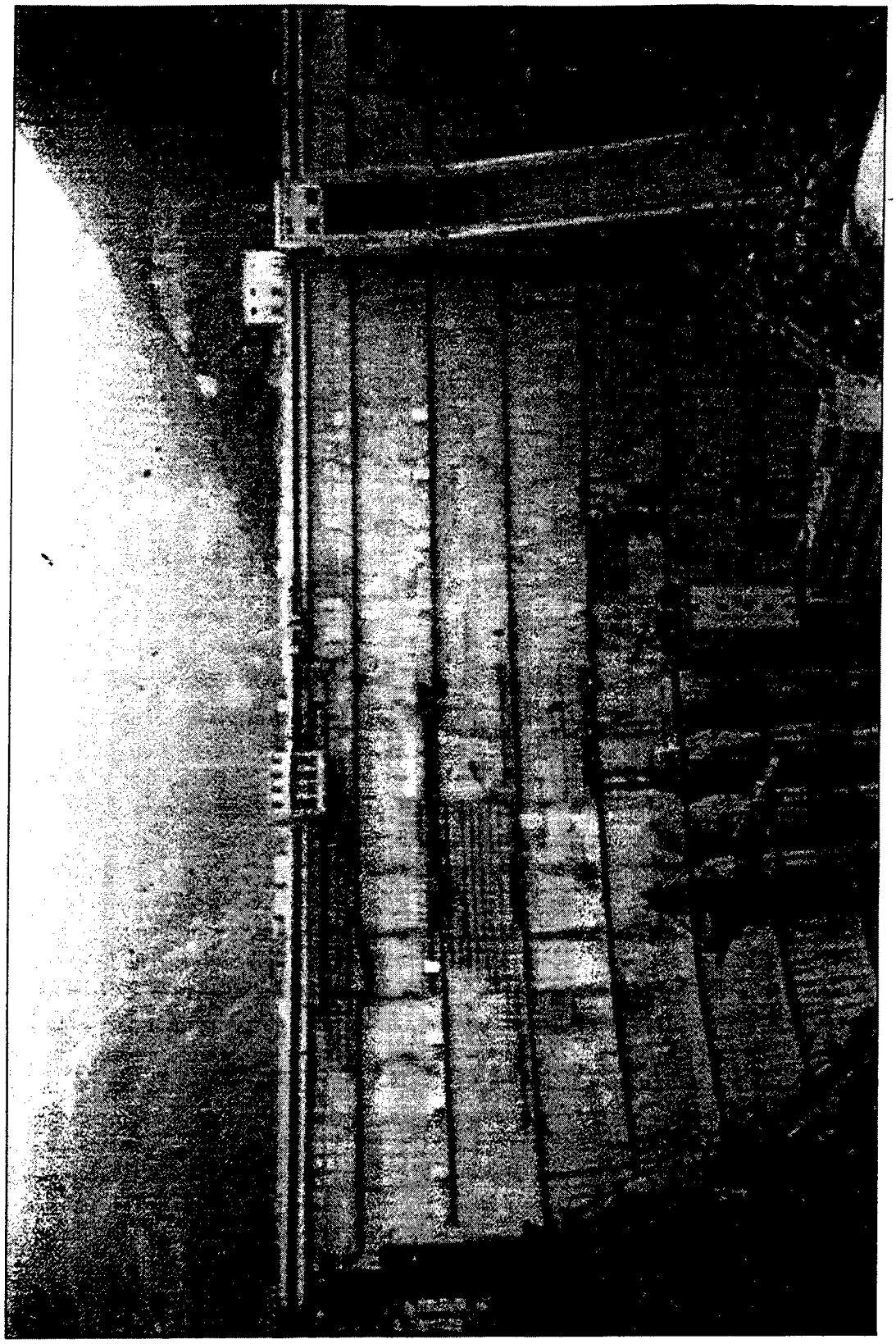

Figure 2. Dongjiang Dam

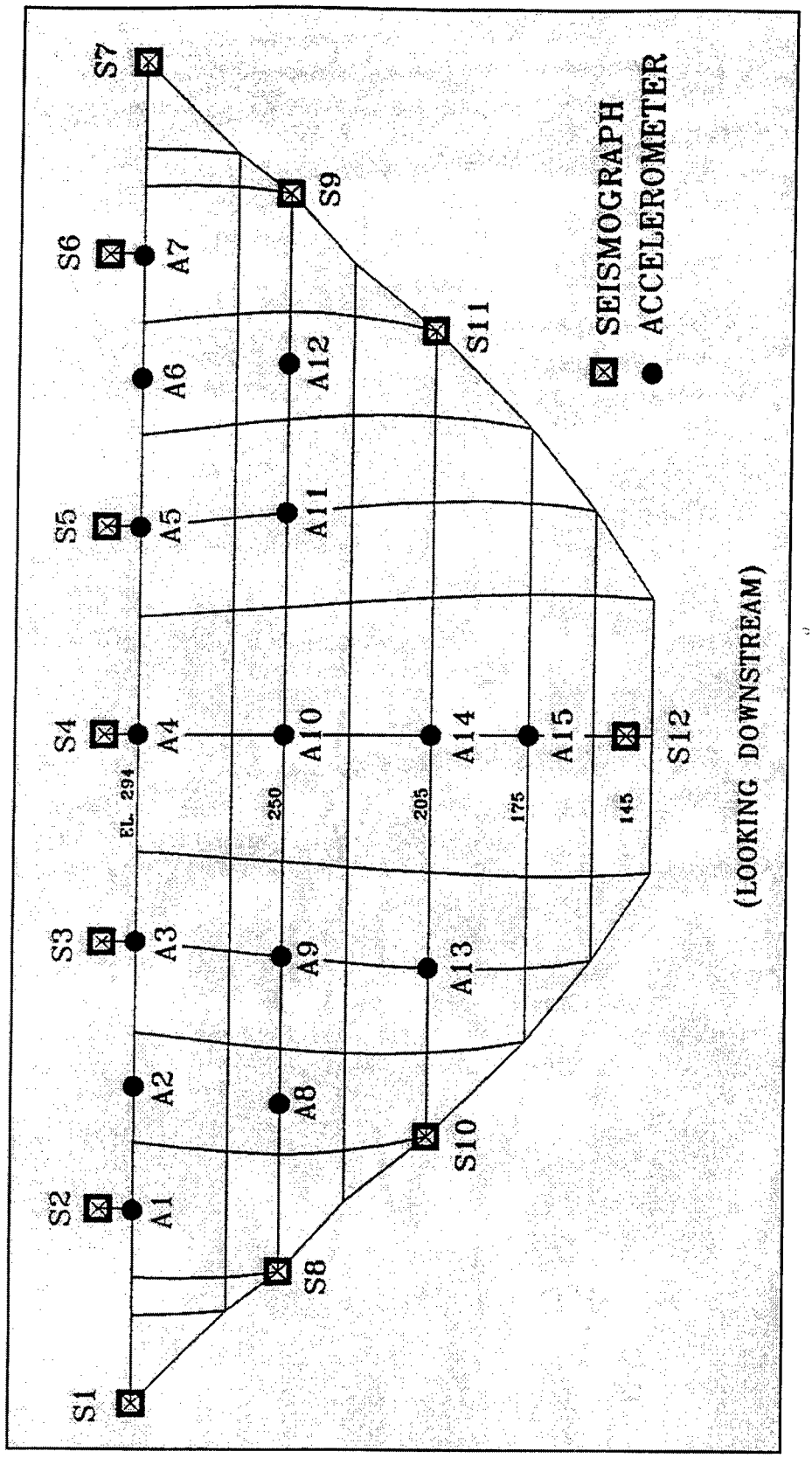

Figure 3. Location of the seismographs and accelerometer

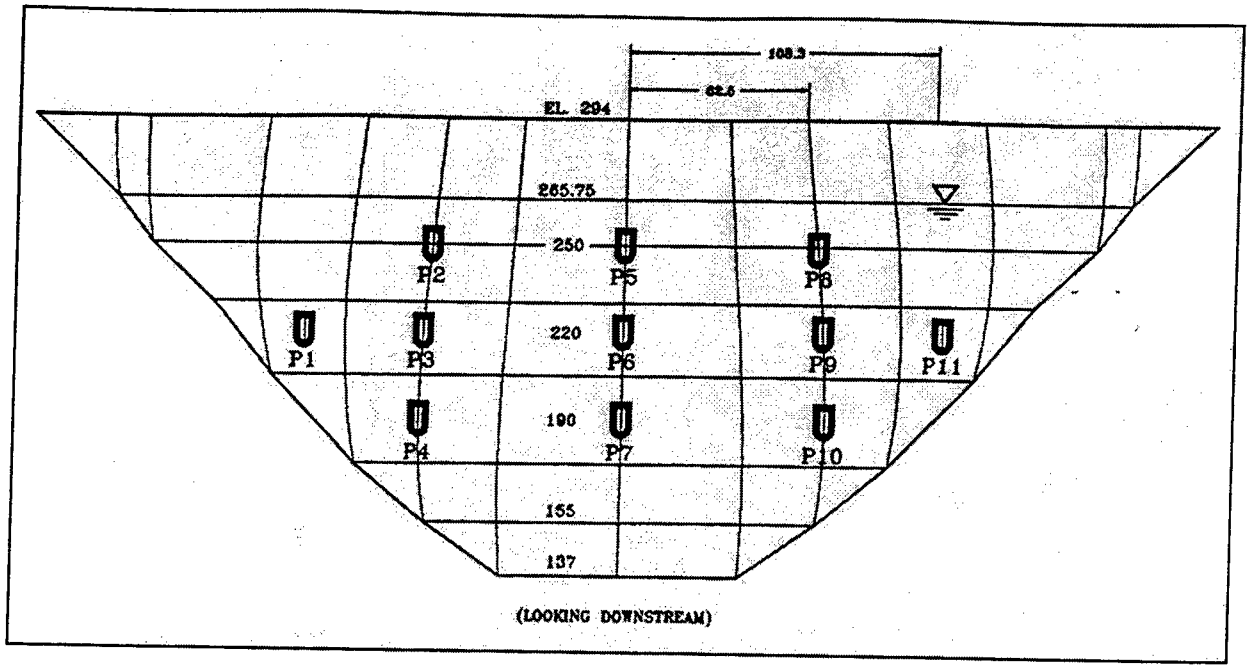

(a) Location of Pressure Sensors on Dam Face

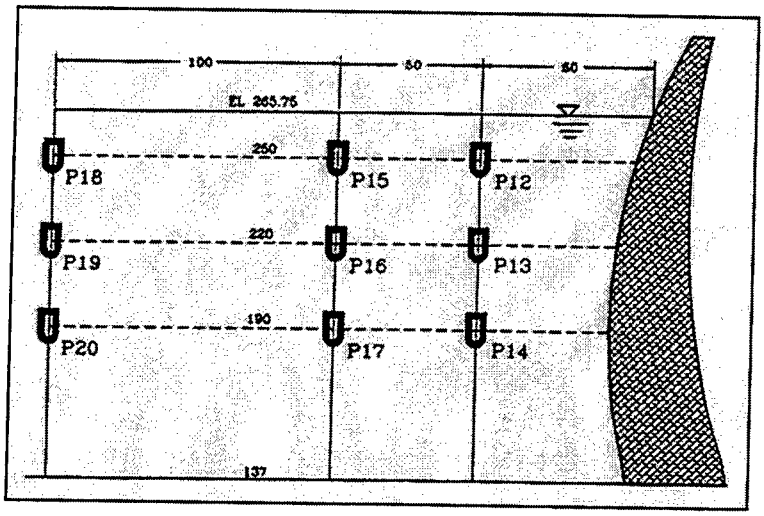

(b) Location of Pressure Sensors Inside Lake

Figure 4. Location of pressure histories on the upstream face of the dam

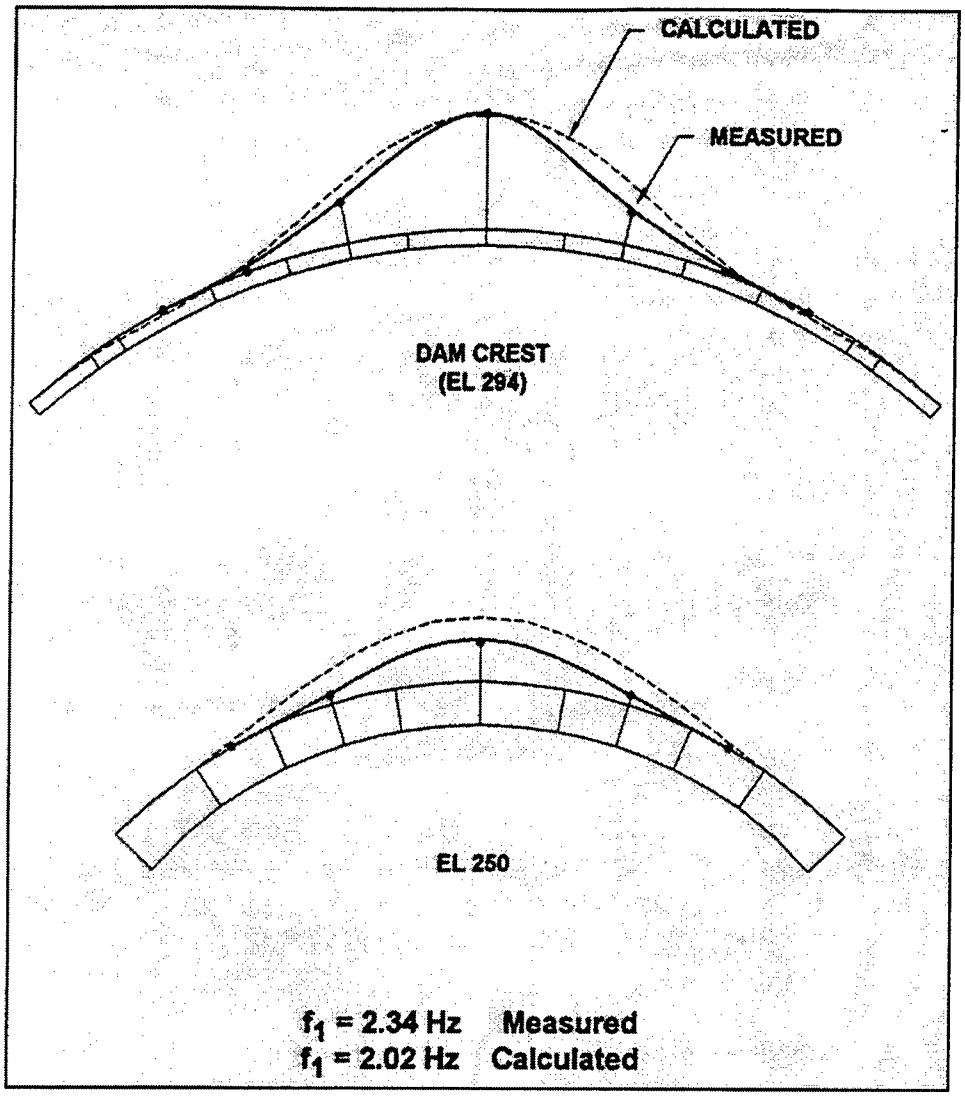

Figure 5. Numerical model for determining the dynamic response of the dam

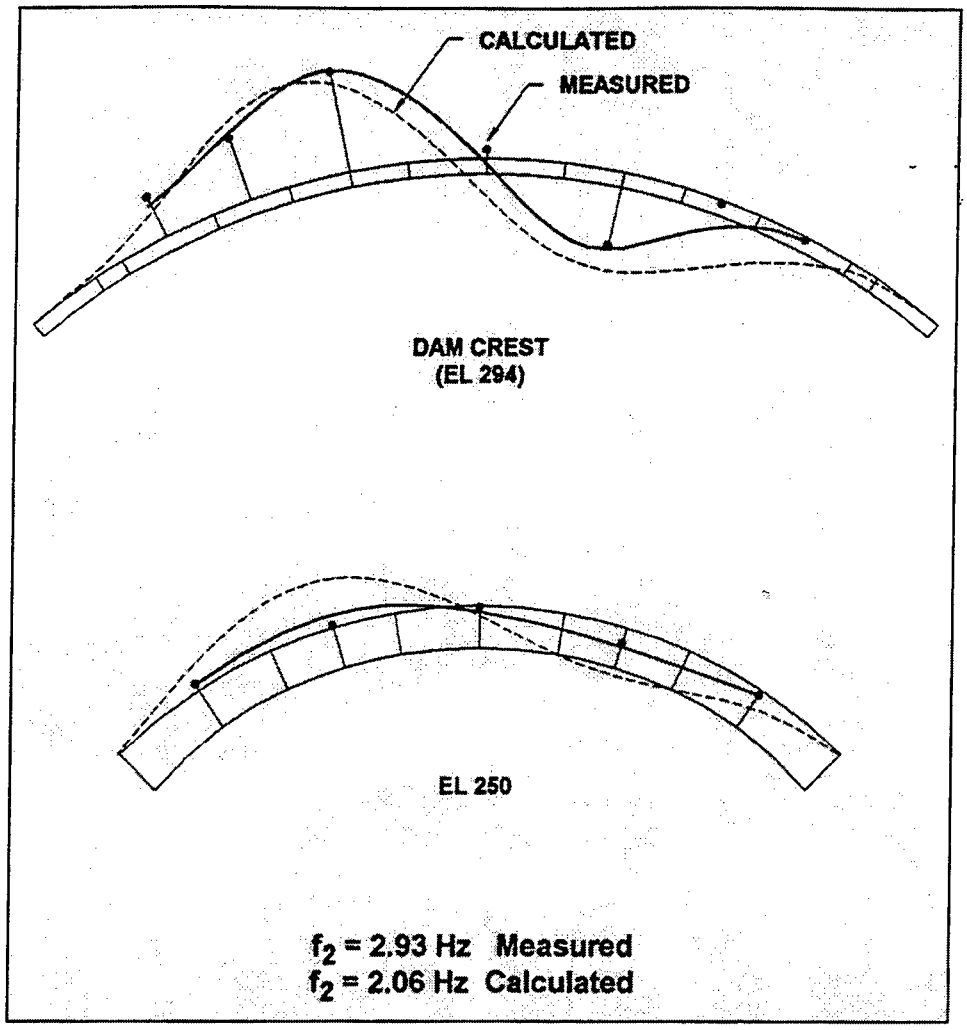

Figure 6. Numerical model for determining the dynamic response of the dam

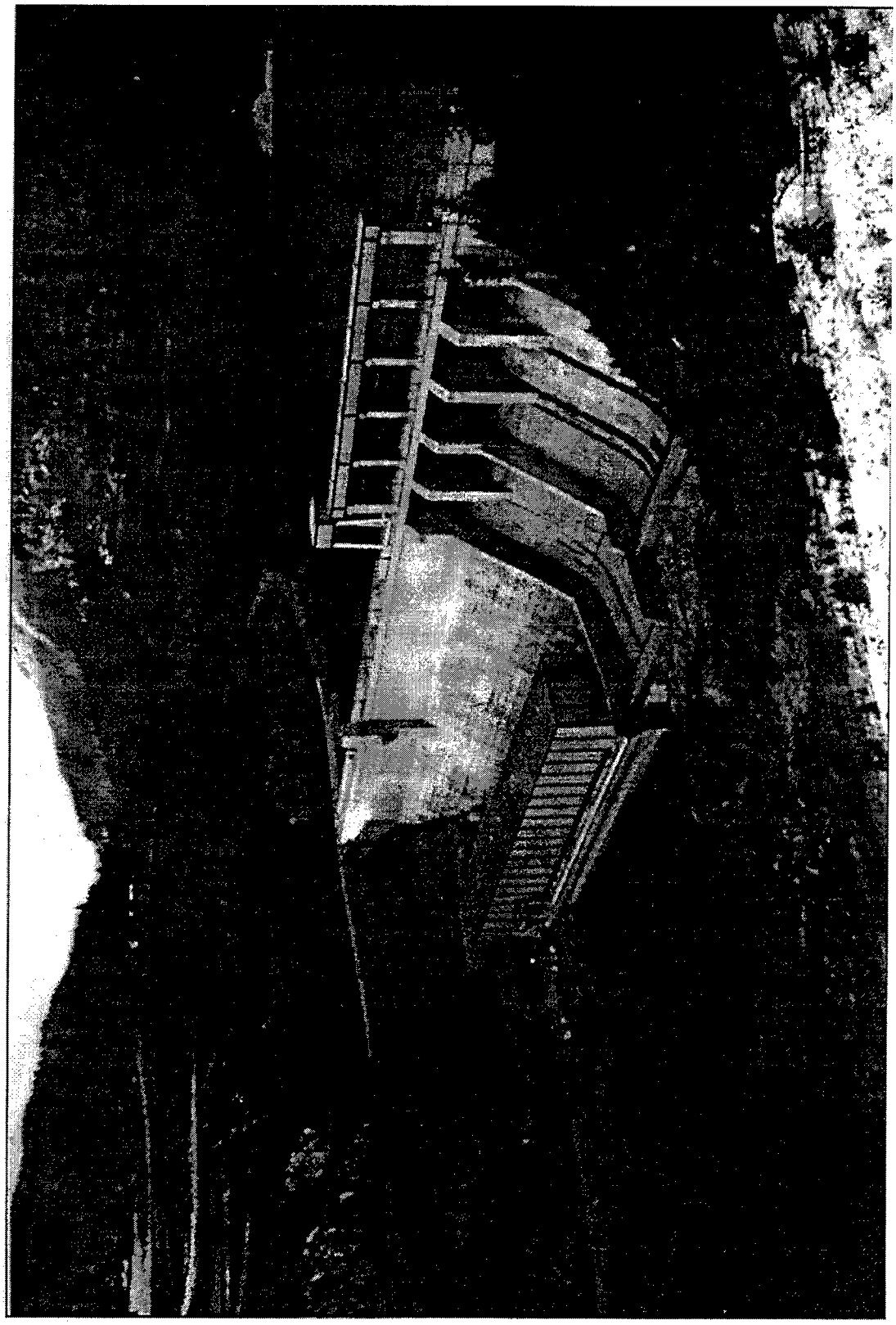

Figure 7. Seven Mile Dam

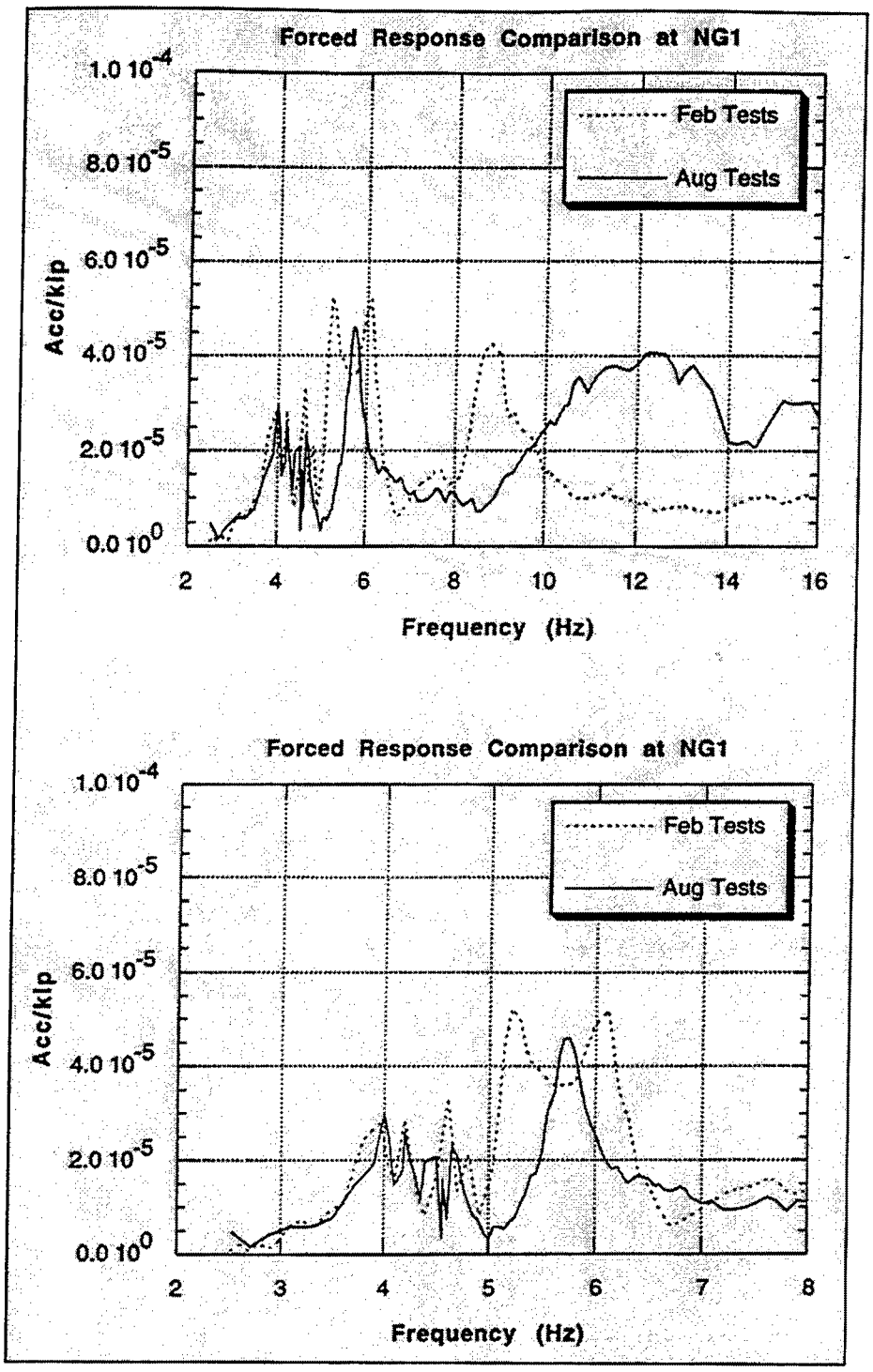

Figure 8. Difference of forced response between August and February (bottom figure is a close-up between 2- and 8-Hz)

Experimental Damping Estimates Before and After Reservoir Impoundment

Crest Mode No.	Damping Before Impoundment percent	Damping After Impoundment percent
1	4.29	4.41
2	2.07	2.76
3	3.11	3.69
4	Not measured	1.52
5	5.16	2.90

Table 1. Damping estimates and natural frequencies from the two experiments

FFT/Amb (Hz)	MEM/Amb (Hz)	Forced Vib (Hz)	Damping (%)
4.	4.	4.	3.7
5.07	5.05	5.1	2.8
6.06	6.06	6.1	3.2
7.45	7.45	7.6	5.4
8.4	--	8.4	--
8.86	8.76	9.	3.8
10.17	10.1	10.6	--
11.32	11.26	11.3	--
12.8	12.9	12.8	2.6
14.1	14.25	14.1	1.7
15.8	16.	--	--

Table 2. Frequencies for the first experiments conducted on 20-26 February for the ambient and forced vibration experiments

Crest Mode Comparisons – Dam Without Reservoir (Experiment versus Analysis)

Crest Mode No.	Prototype Vibration Test Frequency, Hz	Three-Dimensional Finite Element Analyses			
		Fixed Base Frequency, Hz	MAC*	Flexible Base Frequency, Hz	MAC*
1	5.9	7.1	0.73	6.6	0.74
2	6.8	7.9	0.63	7.4	0.63
3	7.6	9.3	0.64	8.7	0.61
4	Not measured	10.4	--	9.6	--
5	8.2	10.7	0.41	10.0	0.13

* Modal Assurance Criterion

Cross-Section Comparisons Without Reservoir (Experiment versus Analysis)

Crest Mode No.	Experimental Frequency, Hz	Finite Element Fixed Base Frequency, Hz	Modal Monolith 7	Assurance Monolith 16	Criterion Monolith 22
1	5.9	7.1	0.73	0.37	0.00
2	6.8	7.9	0.40	0.74	0.00
3	7.6	9.3	0.73	0.94	0.47
4	Not measured	10.4	--	--	--
5	8.2	10.7	0.72	0.79	0.84

Table 3. Comparison of the experimental and analytical results

Effects of Vertical Seismic Motion on Structural Stability of Concrete Gravity Dams

by
Isao NAGAYAMA[1] and Takashi SASAKI[2]

ABSTRACT

In this paper, the effects of vertical seismic motion on the behavior of concrete gravity dams are examined by means of frequency response analysis and response spectrum analysis using measured seismic acceleration records. It is shown that the effect of the vibration mode of the first order is the largest for horizontal seismic motion while the effect of the vibration mode of the third order is the largest for vertical seismic motion, but that the maximum tensile stress developed by vertical seismic motion is much smaller than the maximum tensile stress developed by horizontal seismic motion.

Key Words: *Concrete Gravity Dams, Dynamic Analysis, Vertical Seismic Motion, Dynamic Response*

1. INTRODUCTION

Seismic design of dams in Japan is based on the seismic coefficient method. The earthquake resistance of the dams thus designed is high, and such dams have never been severely damaged by earthquakes. In addition, the report of the Committee on Evaluation of Earthquake Resistance of Dams, formed after the Hyogoken-Nambu Earthquake on January 17, 1995, concluded that dams constructed in accordance with the present design standards have sufficient earthquake resistance to such seismic motion as was induced in the Hyogoken-Nambu Earthquake (Committee on Evaluation of Earthquake Resistance of Dams, 1995).

However, the uniform distribution of acceleration in a dam body which is assumed in the seismic coefficient method differs remarkably from the observation records of actual dams during earthquakes and it is therefore necessary to establish a more reasonable seismic design method to ensure the safety of dams during earthquakes. One of present authors previously proposed a modified seismic coefficient method (Nagayama, 1991) in which the dynamic response characteristics of dams were taken into consideration, but the effects of vertical seismic motion were not taken account of. Many dynamic analyses have been made, taking account not only of horizontal seismic motion but also vertical seismic motion, but almost no analyses have been made in which the effects of vertical seismic motion on the dynamic response of dams were quantitatively studied. This paper describes the results of an examination of the

1) Head of Dam Structure Division, Public Works Research Institute, Ministry of Construction, Tsukuba Science City, 305 JAPAN
2) Senior Research Engineer, Dam Structure Division, ditto

effects of vertical seismic motion on the acceleration and the stress of concrete gravity dams.

2. METHOD OF ANALYSIS

2.1 Vibration Equation

Generally speaking, water in the reservoir is treated as a compressible fluid in the dynamic analysis of dams, but the analysis is sufficiently accurate even if water is assumed to be an incompressible fluid (Nagayama and Jikan, 1987). If water is assumed to be an incompressible fluid, the effects of water can be taken into account in the analysis by an added-mass matrix and the dynamic response characteristics of the dam can be analyzed in detail by means of the modal analysis technique. Thus, in this paper, water is treated as an incompressible fluid. If a structural system that is dynamically linear (concrete gravity dam as shown in Figure 1) is subjected to seismic motion, the relative displacement of the structural system {u(t)} is expressed by the following equation based on the formulation using the finite element method:

$$([M]+[Mw])\{\ddot{u}\}+[C]\{\dot{u}\}+[K]\{u\} = -([M]+[Mw])\{i\}a(t) \quad (1)$$

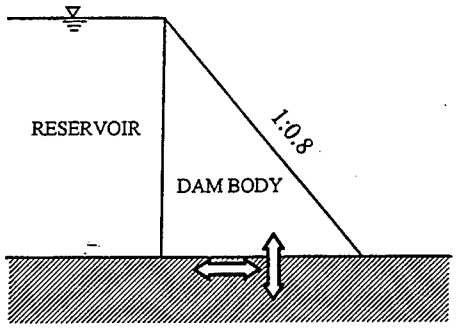

Figure 1 Analytical model of concrete gravity dam

In this equation, [M], [C] and [K] are the mass, damping and stiffness matrices, respectively, while [Mw] is the added-mass matrix that represents the effects of water in the reservoir; a(t) is acceleration at the foundation, and {i} is the directional vector that indicates the direction of inertia force acting on the system due to the acceleration a(t).

2.2 Modal Analysis Technique

According to the modal analysis technique, the relative displacement of the system {u(t)} can be expressed as the superposition of the vibration mode of displacement $\{u_s\}$ as follows:

$$\{u(t)\} = \sum_s \beta_{si}\{u_s\}\phi_s(t) \quad (2)$$

where $\{u_s\}$ is the eigenvector obtained from the following eigenvalue problem:

$$[K]\{u\} = \omega^2[M^*]\{u\} \quad (3)$$

where [M*]=[M]+[Mw].

β_s is expressed by the following equation and is called the s-th modal participation factor:

$$\beta_{si} = \frac{\{u_s\}^T[M^*]\{i\}}{\{u_s\}^T[M^*]\{u_s\}} \quad (4)$$

Then, $\phi_s(t)$ is the solution of the following equation and is called the s-th normal coordinates:

$$M_s\ddot{\phi}_s + C_s\dot{\phi}_s + K_s\phi_s = -M_s a(t) \quad (5)$$

where

$$\left.\begin{aligned} M_s &= \{u_s\}^T[M^*]\{u_s\} \\ C_s &= \{u_s\}^T[C]\{u_s\} = 2h_s\omega_s M_s \\ K_s &= \{u_s\}^T[K]\{u_s\} = \omega_s^2 M_s \end{aligned}\right\} \quad (6)$$

Here, the damping matrix [C] is assumed to be orthogonal. Also, h_s represents the s-th damping ratio, and ω_s is the s-th natural

circular frequency ($\omega_s = 2\pi f_s$:f_s is the s-th natural frequency). On the other hand, stress developed on the system $\{\sigma(t)\}$ can be expressed by

$$\{\sigma(t)\} = \sum_s [S]\beta_{si}\{u_s\}\phi_s(t) \quad (7)$$

In this formula, [S] denotes a matrix representing the relation between displacement and stress. Now, the s-th vibration mode of the stress is defined as

$$\{\sigma_s\} = [S]\{u_s\} \quad , \quad (8)$$

where the stress $\{\sigma(t)\}$ can be expressed as

$$\{\sigma(t)\} = \sum_s \beta_{si}\{\sigma_s\}\phi_s(t) \quad (9)$$

2.3 Frequency Response Function

When the ground acceleration a(t) is given in the harmonic vibration $a_o \exp(j\omega t)$, the solution of Eq. (5) is expressed by

$$\phi_s = R_s(\omega)a_o\exp(j\omega t) \quad (10)$$

where Rs(ω) is called the s-th frequency response function of the normal coordinates ϕ_s, and is given by

$$R_s(\omega) = \frac{-1}{-\omega^2 + 2jh_s\omega_s\omega + \omega_s{}^2} \quad (11)$$

Thus, from Eq. (2) and Eq. (9), the relative displacement $\{u(t)\}$ and stress $\{\sigma(t)\}$ can be expressed as

$$\{u(t)\} = \sum_s \beta_{si}\{u_s\}R_s(\omega)a_o\exp(j\omega t) \quad (12)$$

$$\{\sigma(t)\} = \sum_s \beta_{si}\{\sigma_s\}R_s(\omega)a_o\exp(j\omega t) \quad (13)$$

The relative acceleration $\{\ddot{u}(t)\}$ is obtained by differentiating Eq. (12) by t twice to give

$$\{\ddot{u}(t)\} = -\sum_s \beta_{si}\{u_s\}\omega^2 R_s(\omega)a_o\exp(j\omega t) \quad (14)$$

where

$$\{u(\omega)\} = \sum_s \beta_{si}\{u_s\}R_s(\omega) \quad (15)$$

$$\{\sigma(\omega)\} = \sum_s \beta_{si}\{\sigma_s\}R_s(\omega) \quad (16)$$

$$\{\ddot{u}(\omega)\} = -\sum_s \beta_{si}\{u_s\}\omega^2 R_s(\omega) \quad (17)$$

are the frequency response functions of relative displacement, stress and relative acceleration.

2.4 Response Spectrum Method

In the system of one degree of freedom where $T_s(T_s = 1/f_s)$ is the natural period and h_s is the damping ratio, the maximum response of the relative displacement of the system induced by the acceleration a(t) is expressed by $S_D(T_s, h_s)$, and is called the displacement response spectrum. For structures in general, the maximum responses of the s-th vibration mode of displacement $\{\bar{u}_s\}$ and the s-th vibration mode of stress $\{\bar{\sigma}_s\}$ are given by

$$\{\bar{u}_s\} = \beta_{si}\{u_s\}S_D(T_s, h_s) \quad (18)$$

$$\{\bar{\sigma}_s\} = \beta_{si}\{\sigma_s\}S_D(T_s, h_s) \quad (19)$$

Therefore, the maximum response values of relative displacement $\{\bar{u}\}$ and stress $\{\bar{\sigma}\}$ satisfy

$$\{\bar{u}\} \leqq \sum_s \beta_{si}\{u_s\}S_D(T_s, h_s) \quad (20)$$

$$\{\bar{\sigma}\} \leqq \sum_s \beta_{si}\{\sigma_s\}S_D(T_s, h_s) \quad (21)$$

However, since the times at which the response to each vibration mode gives the maximum value differ from one another, the maximum response value of the structural system will not correspond to the right side of

the above formula, and is generally approximated by the square root of the sum of the square of the maximum response value for each vibration mode:

$$\{\overline{u}\}_e = [\sum_S \beta_{si}^2 \{u_s\}_e^2 S_D(T_s,h_s)^2\ ]^{0.5} \quad (22)$$

$$\{\overline{\sigma}\}_e = [\sum_S \beta_{si}^2 \{\sigma_s\}_e^2 S_D(T_s,h_s)^2\ ]^{0.5} \quad (23)$$

where $\{u_s\}_e$ and $\{\sigma_s\}_e$ are the "e"-th component of $\{u_s\}$ and $\{\sigma_s\}$.

3. FINITE ELEMENT MODEL

The model of the dam body is shown in Figure 2. The effect of water in the reservoir is taken into consideration as an added-mass matrix. The foundation is not taken into consideration and the seismic motion is input from the base of the dam. The modal analysis technique is used for dynamic analysis, and vibration modes of up to the 6th order are considered. The response spectrum method is used in the analyses for the acceleration recorded at dam sites. The physical properties of the model are shown in Table 1. The damping ratio is set to 10% for all vibration modes. The height of the dam ranges from 50 to 150 m. The reservoir level is at the top of the dam body.

4. STUDY IN FREQUENCY DOMAIN

The results of the analysis of a dam with a dam height of 100 meters are shown below. The similarity law can easily be used to obtain the results for dams of different height. Specifically, the natural frequency is inversely proportional to the height of the dam, the acceleration response does not depend on the height of the dam, and the stress response is proportional to the height of the dam.

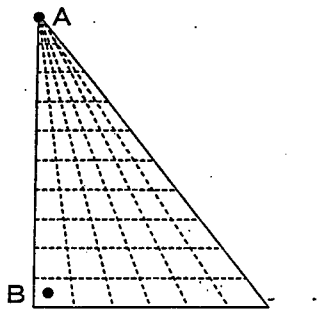

Figure 2 Finite elements of concrete gravity dam

Table 1 Physical properties of materials used in analysis

Dam body (Concrete)	
Elastic modulus (N/mm^2)	3.0×10^4
Poisson's ratio	0.2
Density (kg/m^3)	2300
Foundation	
Elastic modulus (N/mm^2)	∞
Water	
Density (kg/m^3)	1000
System	
Damping ratio (%)	10

4.1 Response of Relative Acceleration at Top of Dam

When a concrete gravity dam is subjected to seismic motion, the maximum acceleration generally develops at the top of the dam (Point A in Figure 2). The frequency response function of the horizontal acceleration at the top of the dam to horizontal and vertical seismic motion was obtained as shown in Figure 3. The figure shows that in terms of the response to horizontal seismic motion, the vibration mode of the second order has the largest effect, followed by the vibration mode of the first order. As for the response to vertical seismic motion, the vibration mode of the third order has the largest effect, followed by the vibration

mode of the sixth order. The largest value of the frequency response function of horizontal acceleration for each vibration mode is shown in Table 2. The table shows that the maximum response value of vibration mode of the third order to vertical seismic motion is about 40% of that of vibration mode of the second order to horizontal seismic motion, and that vertical seismic motion has a smaller effect on the horizontal acceleration at the top of the dam body than horizontal seismic motion.

The frequency response function of vertical acceleration for horizontal and vertical seismic motion at the top of the dam is shown in Figure 4. The figure shows that in terms of the response to horizontal seismic motion, the vibration mode of the second order has the largest effect, followed by the vibration mode of the first order. As for the response to vertical seismic motion, the vibration mode of the third order has the largest effect, followed by the vibration mode of the sixth order. The maximum value of the frequency response function of vertical acceleration to each vibration mode is shown in Table 3. The table shows that the maximum response of the vibration mode of the third order to vertical seismic motion is about 1.2 times that of the vibration mode of the second order to horizontal seismic motion, and that vertical

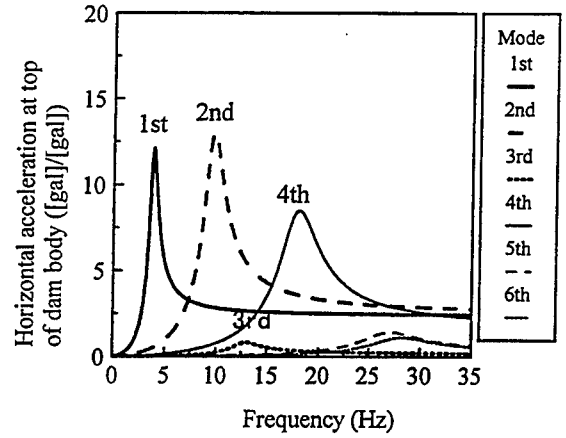

(a) Response to horizontal seismic motion

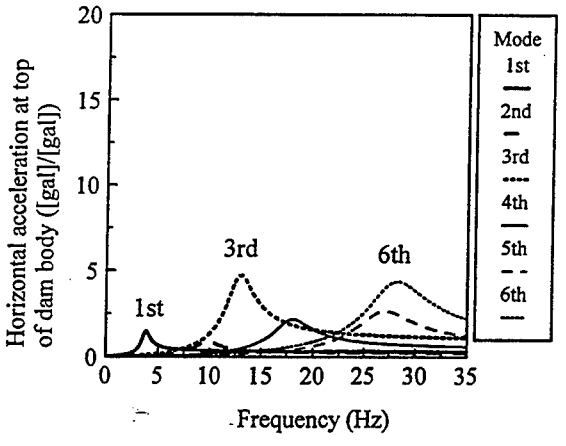

(b) Response to vertical seismic motion

Figure 3 Response of horizontal acceleration at top of dam

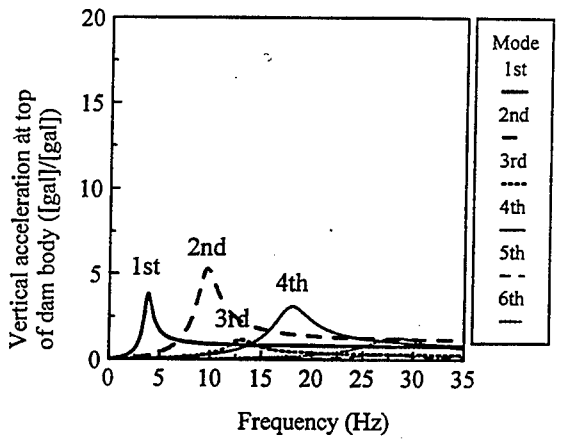

(a) Response to horizontal seismic motion

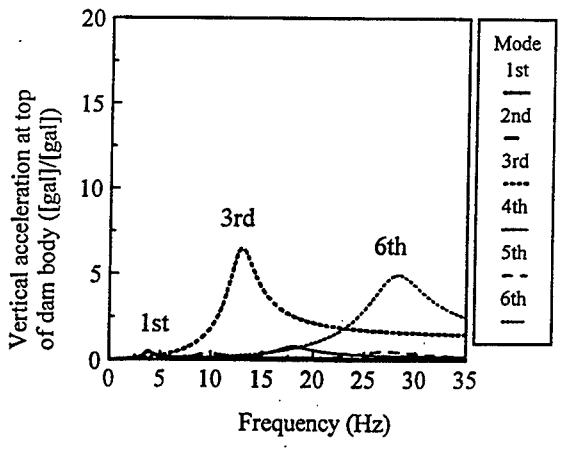

(b) Response to vertical seismic motion

Figure 4 Response of vertical acceleration at top of dam

seismic motion has a slightly larger effect on vertical acceleration at the top of the dam than horizontal seismic motion.

4.2 Response of Vertical Stress at Heel of Dam

When a concrete gravity dam is subjected to seismic motion, the maximum tensile stress generally develops almost vertically at the heel of the dam (Point B in Figure 2). The frequency response function of vertical stress at the heel of the dam for the horizontal and vertical seismic motions was obtained as shown in Figure 5. The figure shows that in terms of the response to horizontal seismic motion, the vibration mode of the first order has the dominant effect, and that the other vibration modes have a very small effect. Regarding the response to vertical seismic motion, the vibration mode of the third order has the largest effect, followed by the vibration mode of the first order.

The maximum value of the frequency response function of vertical stress at the heel of the dam for each vibration mode is shown in Table 4. The table shows that the maximum response of the vibration mode of the third order to vertical seismic motion is about 20% of that of the vibration mode of the first order to horizontal seismic motion, and that the effect of vertical seismic motion on vertical stress at the heel of the dam is much smaller than the effect of horizontal seismic motion.

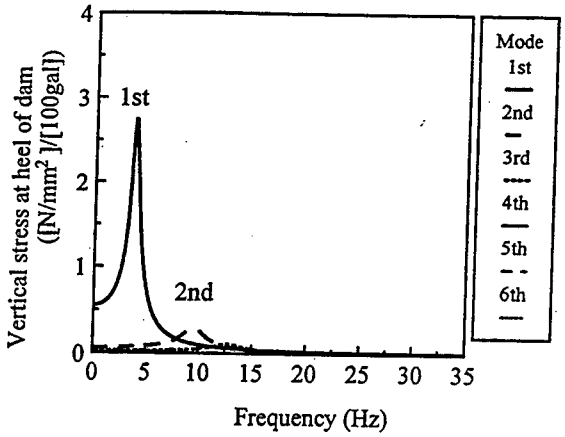

(a) Response to horizontal seismic motion

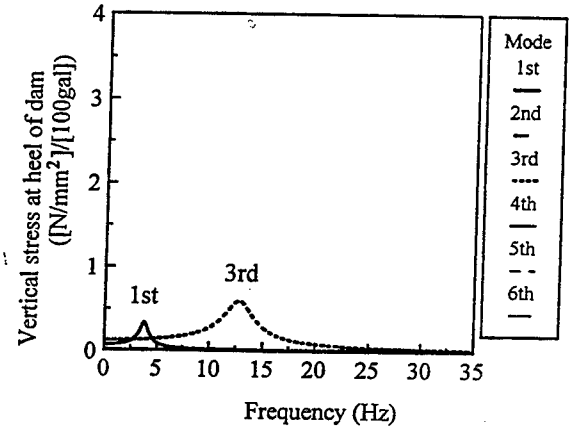

(b) Response to vertical seismic motion

Figure 5 Response of vertical stress at heel of dam

Table 2 Maximum response value of horizontal acceleration at top of dam

Type of seismic motion	Maximum response value for each order ([gal]/[gal])					
	1	2	3	4	5	6
Horizontal seismic motion	12.100	12.899	0.807	8.496	1.420	1.121
Vertical seismic motion	1.466	0.907	4.696	2.169	2.646	4.356

Table 3 Maximum response value of vertical acceleration at top of dam

Type of seismic motion	Maximum response value for each order ([gal]/[gal])					
	1	2	3	4	5	6
Horizontal seismic motion	3.809	5.275	1.114	3.092	0.278	1.275
Vertical seismic motion	0.455	0.371	6.481	0.789	0.519	4.951

Table 4 Maximum response value of vertical stress at heel of dam

Type of seismic motion	Maximum response value for each order ([N/mm^2]/[100gal])					
	1	2	3	4	5	6
Horizontal seismic motion	2.744	0.292	0.102	0.009	0.013	0.011
Vertical seismic motion	0.328	0.021	0.591	0.002	0.025	0.042

4.3 Consideration

From the above results, the response characteristics of concrete gravity dams for horizontal and vertical seismic motion can be summarized as follows:

1) As for the response of relative acceleration at the top of the dam to horizontal seismic motion, the vibration mode of the second order has the largest effect, followed by the vibration mode of the first order. On the other hand, as for the response of relative acceleration to vertical seismic motion, the vibration mode of the third order has the largest effect, followed by the vibration mode of the sixth order.
2) With regard to horizontal acceleration at the top of the dam, vertical seismic motion has a smaller effect than horizontal seismic motion (about 40%). On the other hand, as for vertical acceleration, vertical seismic motion has almost the same effect as horizontal seismic motion (about 1.2 times).

Next, at the heel of the dam where the maximum tensile stress develops:

3) As for the response of vertical stress at the heel of the dam to horizontal seismic motion, the vibration mode of the first order has the largest effect, while the other vibration modes have a small effect. On the other hand, as for the response of vertical stress at the heel of the dam to vertical seismic motion, the vibration mode of the third order has the largest effect, followed by the vibration mode of the first order. The other vibration modes have a small effect.
4) As for the vertical stress at the heel of the dam, vertical seismic motion has much smaller effect than horizontal seismic motion (about 20%).
5) Vertical seismic motion has a smaller effect on stress than on relative acceleration.

Then, the results are analyzed First, the reason why the horizontal seismic motion and vertical seismic motion have different outstanding vibration modes is examined. Figure 6 shows the vibration mode of displacement. The figure indicates that the vibration modes of the first, second and fourth order show flexural vibration in the horizontal direction, while the vibration modes of the third, fifth and sixth order show expanding vibration in the vertical direction in addition to flexural vibration in the horizontal direction (however, this is not so clear for the vibration mode of the fifth order). Therefore, it is considered that the vibration modes showing flexural vibration in the horizontal direction have a large response to horizontal seismic motion, and that the vibration modes showing expanding vibration in the vertical direction have a large response to vertical seismic motion. Since $M_s\beta_{sx}$ and $M_s\beta_{sy}$ (x represents the horizontal direction and y the vertical direction) are directly proportional to the horizontal and vertical momentum of the system, respectively, it is

considered that the main vibration direction of each vibration mode is judged from the relative magnitude of participation factors β_{sx} and β_{sy}. The value of the participation factor for each vibration mode is shown in Table 5 (these values are obtained when the maximum value of component $\{u_s\}$ is equal to 1). The table indicates that the horizontal seismic motion becomes significant for the vibration modes of the first, second and fourth order, while the vertical seismic motion becomes significant for the vibration modes of the third, fifth and sixth order.

Next, the reason why the vertical seismic motion has a smaller effect on stress than on relative acceleration is examined. The frequency response of stress is proportional to the frequency response of relative displacement, not to the frequency response of relative acceleration. This is clearly shown by Eq. (15) and Eq. (16). On the other hand, as indicated by Eq. (15) and Eq. (17), the frequency response of relative displacement is obtained by dividing the frequency response of relative acceleration by the square of the frequency. For this reason, even if the frequency response of relative acceleration is the same, the vibration modes of a higher order (larger natural frequency) have a smaller frequency response of displacement. Vertical seismic motion has a significant effect in the vibration mode of the third order, which is of a higher order than the vibration mode in which the horizontal seismic motion has a significant effect (the vibration mode of the first order). Therefore, vertical seismic motion has a smaller effect on stress.

Table 5 Natural frequency and participation factor

Modes	Natural frequency fs (Hz)	Participation factor	
		β_{sx}	β_{sy}
1	3.805	2.408	0.288
2	9.659	-2.567	0.181
3	12.896	-0.251	1.458
4	17.881	1.691	0.432
5	26.810	-0.283	0.527
6	27.986	-0.254	-0.985

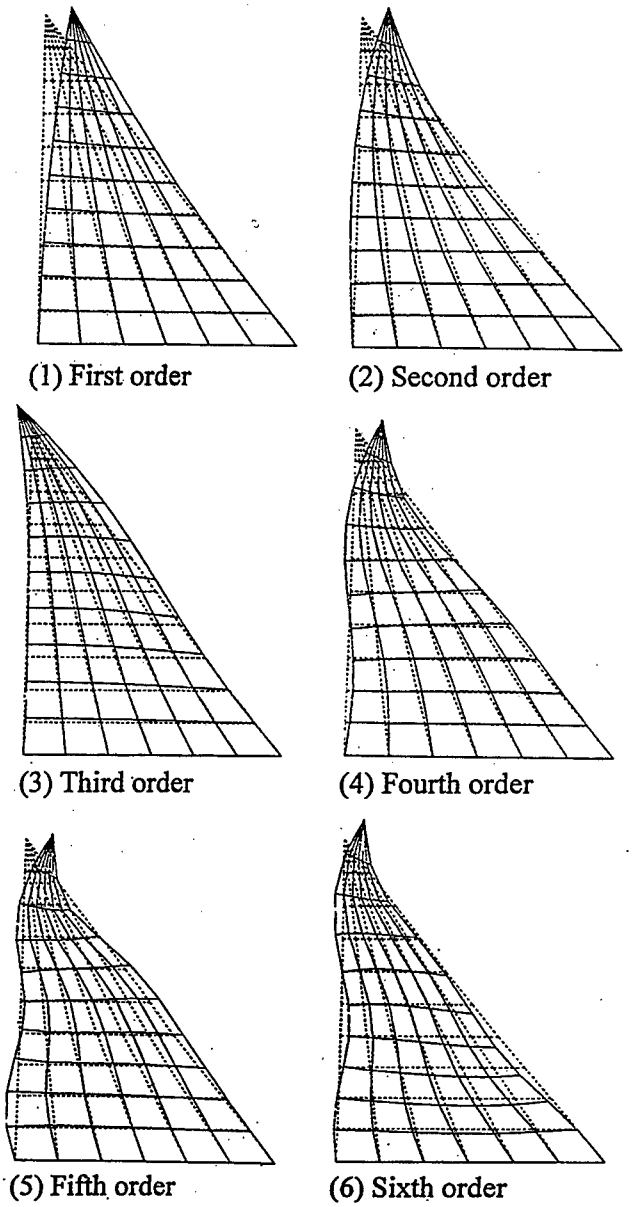

Figure 6 Vibration modes of relative displacement

5. ANALYSIS USING MEASURED SEISMIC ACCELERATION RECORDS

5.1 Response of Stress in Dam

In the preceding section, the response characteristics of concrete gravity dams to harmonic vibration were discussed. In this section, the results of a dynamic analysis using acceleration records obtained at the foundations of 20 dam sites (including those measured in the bottom gallery in the dam body) are outlined. Before making the analysis, the acceleration records were adjusted so that the maximum value was 100 gal for both horizontal and vertical acceleration.

Figure 7 compares the results of the maximum response of vertical stress at the heel of the dam when the horizontal seismic motion and vertical seismic motion are separately applied to the dam shown in Figure 2. The figure shows that the vertical stress at the heel of the dam generated by the vertical seismic motion is about 20% - 40% of the vertical stress generated by the horizontal seismic motion. The vertical stress generated by horizontal seismic motion varies widely, but the vertical stress generated by vertical seismic motion varies little. Thus, the greater the vertical stress generated by horizontal seismic motion is, the smaller the effect of vertical seismic motion becomes. To eliminate the differences in characteristics of input acceleration records between the horizontal and vertical seismic motion, the record of vertical seismic motion was replaced by that of horizontal seismic motion, then a similar analysis was conducted. The results of the analysis are shown in Figure 8. This figure has the same tendency as Figure

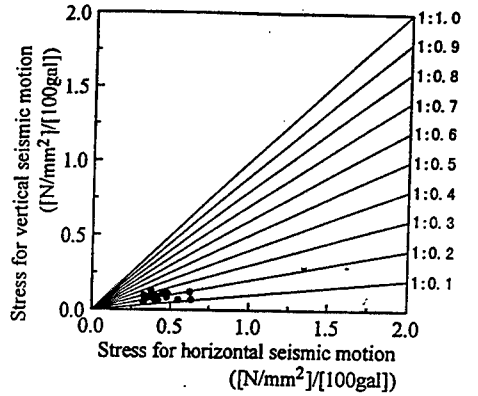

(a) Height of dam: 50 m

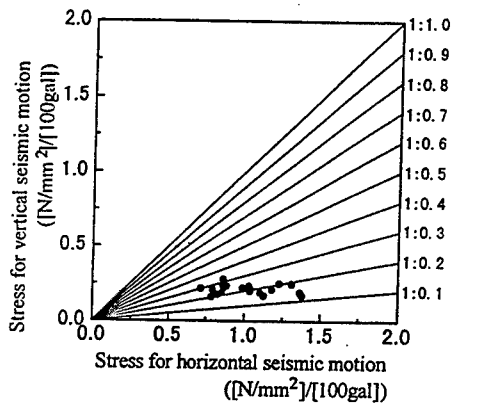

(b) Height of dam: 100 m

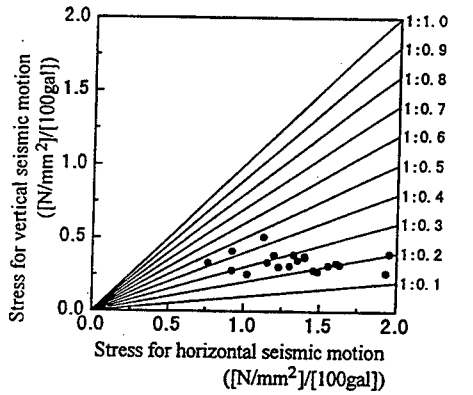

(c) Height of dam: 150 m

Figure 7 Comparison of vertical stress at heel of dam generated by horizontal seismic motion and vertical seismic motion
(Vertical seismic motion: measured vertical acceleration record)

7, and the effects due to the difference in acceleration records between horizontal and vertical seismic motion are considered to be small.

5.2 Consideration

From the above analyses, the response characteristics of concrete gravity dams for the measured seismic acceleration records can be summarized as follows:

1) The magnitude of vertical stress generated at the heel of the dam by horizontal seismic motion largely depends on the input acceleration, but the magnitude of vertical stress generated at the heel of the dam by vertical seismic motion does not depend so much on the input acceleration.
2) When the horizontal seismic motion and vertical seismic motion have the same maximum acceleration, the vertical stress generated at the heel of the dam by vertical seismic motion is about 20%-40% of the vertical stress generated by horizontal seismic motion.

Then, these results are reviewed. First, it is examined that why the vertical stress generated by horizontal seismic motion largely depends on the input acceleration, whereas the vertical stress generated by vertical seismic motion does not. Figure 5 shows that the vibration mode of the first order has a significant effect on horizontal seismic motion, and that the other vibration modes have a small effect. For this reason, the magnitude of vertical stress at the heel of the dam is determined by the amount of components close to the natural frequency of the first order contained in the input acceleration record. On the other hand, the

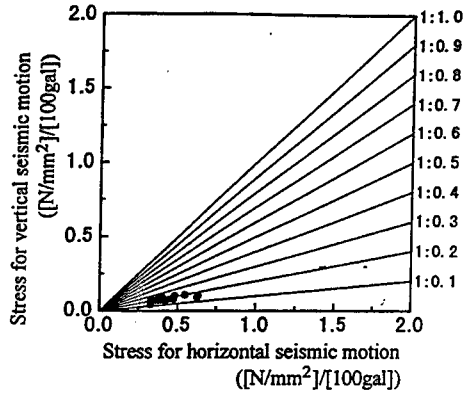

(a) Height of dam: 50 m

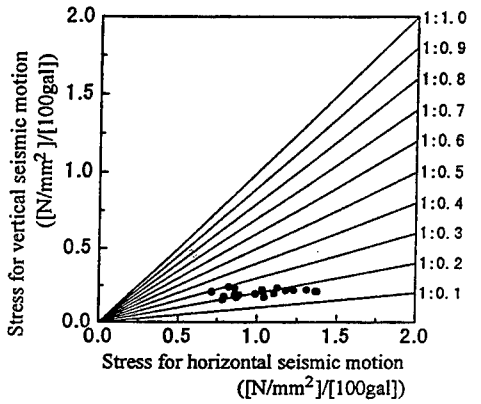

(b) Height of dam: 100 m

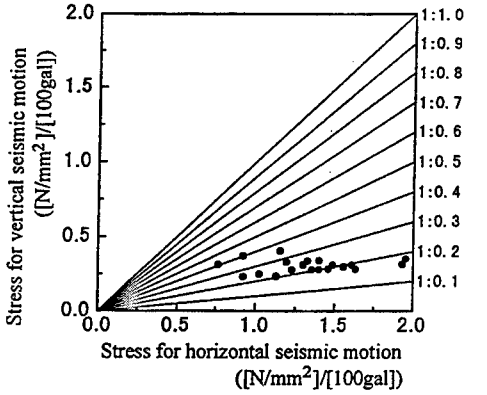

(c) Height of dam: 150 m

Figure 8 Comparison of vertical stress at heel of dam generated by horizontal seismic motion and vertical seismic motion
(Vertical seismic motion: measured horizontal acceleration record)

vibration mode of the first order in addition to the vibration mode of the third order has a large effect on vertical seismic motion. Therefore, the magnitude of vertical stress does not depend much on the frequency component of the input acceleration record.

Figures 9 and 10 show the extent of effects of the vibration mode of the first order and the vibration mode of the third order contained in the response of vertical stress at the heel of the dam. The figures indicate that the magnitude of vertical stress generated by horizontal seismic motion depends on the response of the vibration mode of the first order, while the magnitude of vertical stress generated by vertical seismic motion is affected by the response of the vibration mode of the first order in addition to the response of the vibration mode of the third order.

Secondly, according to the frequency response analysis discussed in the preceding section, the vertical stress at the heel of the dam is greatly affected by the vibration mode of the third order for the vertical seismic motion and by the vibration mode of the first order for the horizontal seismic motion, and the ratio of the effect of vertical seismic motion to the effect of horizontal seismic motion is about 20%. On the other hand, in the analysis using measured acceleration records described in this section, the ratio increased to 20%-40%, larger than the above value. The reason is considered to be as follows. The magnitude of the vertical stress at the heel of the dam generated by vertical seismic motion does not depend on the frequency component of the input acceleration, while the magnitude of the vertical stress generated by horizontal seismic motion depends on how much component near the natural frequency of the first order is contained in the

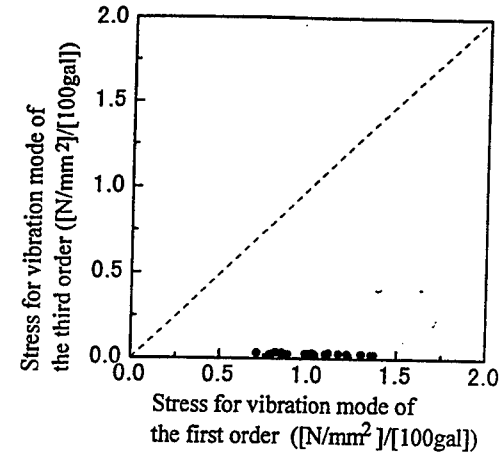

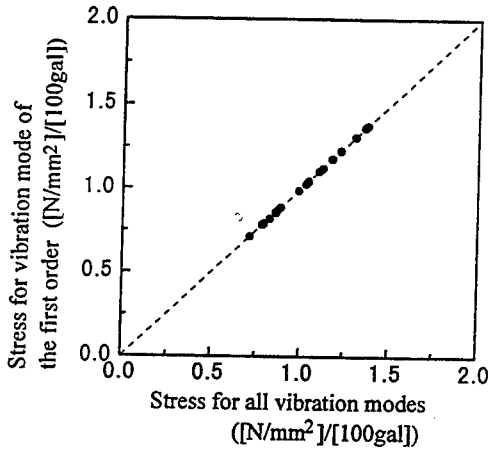

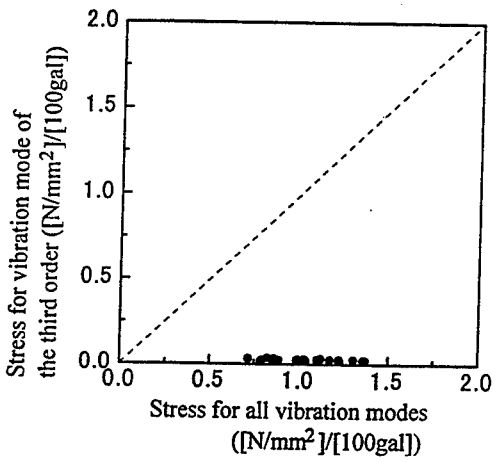

Figure 9 Comparison between response for vibration mode of the first order and response for vibration mode of the third order to horizontal seismic motion

input acceleration record. It is therefore considered that if the component near the natural frequency of the first order is not largely contained in the horizontal acceleration record, then the vertical stress becomes smaller, and the ratio of vertical stress generated by vertical seismic motion to vertical stress generated by horizontal seismic motion becomes larger. However, if a large component near the natural frequency of the first order is contained in the horizontal acceleration record, the ratio approaches 20%, as obtained by the previous frequency response analysis.

6. CONCLUSION

This paper analyzed the response of concrete gravity dams to horizontal seismic motion and vertical seismic motion, and the following conclusions were drawn.

First, from the frequency response analysis:

(1) As for the acceleration at the top of the concrete gravity dam, the vibration mode of the second order has the largest effect for horizontal seismic motion, while the vibration mode of the third order has the largest effect for vertical seismic motion.

(2) With regard to the horizontal acceleration at the top of the concrete gravity dam, the maximum response value of the vibration mode of the third order to vertical seismic motion is about 40% of the maximum response of the vibration mode of the second order to horizontal seismic motion. As for the vertical acceleration at the top of the dam, the maximum response value of the vibration mode of the third order to vertical seismic motion is about the same as the maximum response value of the vibration mode of the

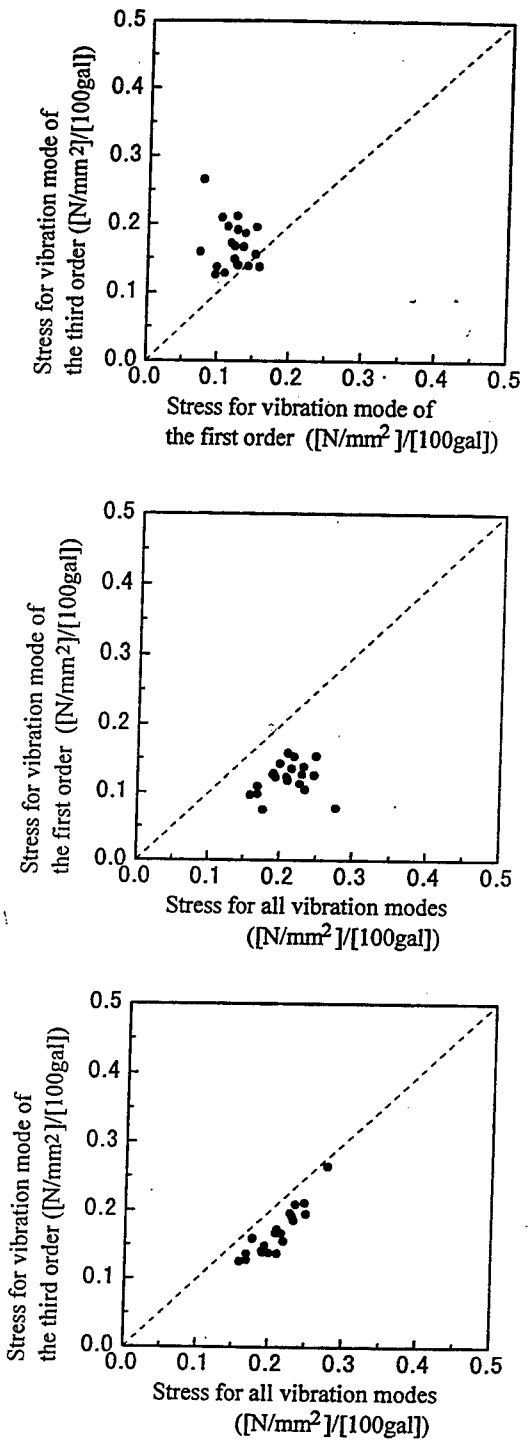

Figure 10 Comparison between response for vibration mode of the first order and response for vibration mode of the third order to vertical seismic motion

second order to horizontal seismic motion.

(3) Regarding the vertical stress at the heel of the concrete gravity dam, the vibration mode of the first order has the largest effect for horizontal seismic motion, while the vibration mode of the third order has the largest effect for vertical seismic motion.

(4) As for the vertical stress at the heel of the dam, the maximum response value of the vibration mode of the third order to vertical seismic motion is about 20% of the maximum response value of the vibration mode of the first order to horizontal seismic motion.

Second, from the dynamic analysis using measured seismic acceleration records:

(5) When horizontal seismic motion and vertical seismic motion have the same magnitude of acceleration, the maximum response of vertical stress generated at the heel of the dam by vertical seismic motion is about 20%-40% of that generated by horizontal seismic motion, and the ratio gets smaller as the stress caused by the horizontal seismic motion increases.

From the above results, it is concluded that vertical seismic motion has a significantly smaller effect on the stress of the concrete gravity dam than horizontal seismic motion, and in particular, for an earthquake that produces a large stress in the dam body, the vertical seismic motion has a smaller effect. Since the maximum vertical acceleration during a large earthquake is about one half to one-third of the maximum horizontal acceleration, the effects of the vertical seismic motion are assumed to be about 10% of the effects of horizontal seismic motion. Therefore, for practical purposes, the results of the analysis are not greatly affected even if the effects of vertical seismic motion are disregarded.

References

Committee on Evaluation of Earthquake Resistance of Dams: Report of Committee on Evaluation of Earthquake Resistance of Dams, November, 1995 (in Japanese)

Nagayama, I: Simplified Seismic Design Method for Concrete Gravity Dams, Engineering for Dams, Japan Dam Engineering Center, No. 25, pp. 15-23, 1988 (in Japanese)

Nagayama, I. and S. Jikan: Study on Dynamic Behavior of Concrete Dam during Earthquake with Hydrodynamic Interaction, International Symposium on Earthquake and Dams, ICOLD, 1987

Subbottom Absorption Coefficients for Seismic Analysis of Concrete Dams

by

Luis Armando de Béjar*

ABSTRACT

This paper succinctly describes research in progress on the mathematical representation of the vertical radiation of energy towards infinity from the bottom of the impounded reservoir in a dam system upon earthquake-induced water-foundation rock interaction. The random variation of the three-dimensional acoustic-impedance field is modeled on the basis of field experimental data obtained at the site of a selected prototype dam (Folsom Dam). The Boundary Element Method (B.E.M.) for dynamic potential problems effectively renders both deterministic and stochastic estimates of the hydrodynamic pressure on the upstream face of the dam due to stationary harmonic excitation. Theoretically derived response functions will be experimentally verified with a small-scale physical model on a centrifuge.

KEYWORDS: Acoustic Impedance, Boundary Elements, Coefficient of Reflection, Concrete Gravity Dams, Harmonic Ground Motion, Random Fields, Subbottom Absorption.

1 INTRODUCTION

When modeling the earthquake response of concrete dams, including water-structure-foundation rock interaction, analysts frequently assume the reservoir to be resting on a horizontal rigid bottom. Such representation consistently leads to overestimations of the effective hydrodynamic pressure on the upstream face of the dam, because no attempt is made to model the escaping energy of the pressure waves refracted at the bottom surface in the real situation. When a water pressure wave traveling downwards strikes the bottom surface, part of the propagating energy is reflected back into the reservoir and another part is transmitted to the foundation medium on account of its finite stiffness. This refracted energy may be assumed to continue propagating vertically towards infinity, actually constituting an equivalent energy-dissipating mechanism introducing radiation damping that effectively reduces the response of the system.

Consequently, realistic assessment of the response of dam systems to earthquake excitation requires experimentally-based appropriate modeling of the subbottom absorption of energy. In particular, the characterization of the acoustic impedance field (or, equivalently, the coefficient of reflection field) is found to adequately map into the corresponding equivalent damping in the boundary conditions of the governing equations of motion (Hall and Chopra 1982). This investigation attempts to complement the current state of knowledge of seismic dam engineering by developing a technique based on field information to reliably represent the effect of subbottom absorption during the earthquake response of concrete dams.

---

*Structural Mechanics Division,
Research Analysis Group,
Structures Laboratory,
USAE Waterways Experiment Station,
Vicksburg, MS 39180-6199

2 PRIOR EXPERIMENTAL RESEARCH

As a first research effort, field tests were conducted at key locations at the site of seven selected concrete dams within the U.S. (Ghanaat and Redpath 1995). The exercise attempted to identify the average coefficient of reflection by detonating engineered explosives and analyzing the recorded reflected waves at Monticello Dam, Pine Flat Dam, Hoover Dam, Glen Canyon Dam, Morrow Point Dam, Crystal Dam, and Folsom Dam.

Analysis of the results showed excessive scattering (The average coefficient of reflection spanned the whole range from slightly negative values to values near 0.8) and raised two major concerns: (1) the identification of the coefficient of reflection for the foundation rock was obstructed by the influence in the records of the acoustic impedance for the sediments deposited over time on the reservoir bottom, and (2) due to the irregularity of the local bottom topography, the real field of the coefficient of reflection is expected to be sensitive to the frequency content of the incident excitation impulse. These concerns motivated the present stage of the investigation where deeper soil-rock strata will also be surveyed at, at least, two different dominant input frequencies at each location, from which an average will be computed.

3 B.E.M. FOR POTENTIAL PROBLEMS UNDER HARMONIC EXCITATION

As a starting simplification that lends itself to direct experimental verification using a centrifuge, a smooth analytical model of the reservoir geometry at the site of a prototype dam site (Folsom Dam) will be subjected to stationary harmonic excitation sweeping the whole domain of input frequencies. The B.E.M. in elastodynamics is a most effective tool for the analysis of the associated potential problem to construct the frequency response function of the reservoir for the Fourier Transform of the hydrodynamic pressure field (Brebbia and Domínguez 1992; Domínguez 1993).

The B.E.M. effectively reduces the dimension of the three-dimensional problem to two and solves the resulting system of algebraic simultaneous equations for the values of the field and its directional derivative only where it is needed: at the boundary, part of which is precisely the upstream face of the dam.

After discretizing the boundary into a series of N quadratic elements, assuming initial conditions at rest, Betti's Reciprocal Theorem yields the following Somigliana's Identity for the hydrodynamic pressure field evaluated at the i-th boundary node:

$$c^i p^i + \sum_{j=1}^{N} \int_{\Gamma_j} p \cdot \frac{\partial p^*}{\partial n} \, d\Gamma = \sum_{j=1}^{N} \int_{\Gamma_j} p^* \cdot \frac{\partial p}{\partial n} \, d\Gamma, \qquad (1)$$

where p represents the hydrodynamic pressure field, $\partial p/\partial n$ is the corresponding traction field, $c^i = 1/2$ for a smooth boundary, and the asterisk is attached to quantities associated with the fundamental solution.

Equations (1) may be formulated for each node of the boundary elements and the resulting system of equations put in the form:

$$[A]\{X\} = \{B\}, \qquad (2)$$

such that {X} contains all unknowns.

4 ELLIPSOIDAL IDEALIZATION FOR PROTOTYPE DAM SITE

Folsom Dam is selected as the prototype dam site to start the investigation, and its reservoir is taken as half-ellipsoidal for the purpose of analysis. Figure 1 shows a schematic of the reservoir configuration with the dam at the intersection of the rim of the ellipsoidal surface with its principal horizontal minor axis. All dimensions are in meters. Figure 2 shows the plan view of an example of a full mesh of conforming quadratic elements for B.E.M. harmonic analysis.

Taking advantage of the quadrant-symmetric geometry of the idealization, only 1/8-th of the ellipsoid needs to be actually resolved (see Figure 3); however, the corresponding basic fundamental solution must be compounded with that for mirror-image points, with respect to the free surface of the reservoir (Chandrashaker and Humar 1993). The harmonic excitation is applied in the direction normal to the upstream face of the dam.

5 MIXED BOUNDARY CONDITION

On the curved portion of the surface to be analyzed, the boundary condition is mixed (of the Robbin's type, Brebbia and Domínguez 1992) and is given by (Hall and Chopra 1982):

$$\partial p/\partial n = -\rho \cdot a_n + i\omega q p, \qquad (3)$$

in which $\partial p/\partial n$ is the projection of the gradient of the pressure field at the point in question onto the normal to the ellipsoidal surface, ρ is the water mass density, a_n is the component of fluid acceleration in the direction normal to the ellipsoidal surface, ω is the frequency of the excitation, qC is the relative impedance of the subbottom rock material with respect to that of water (C being the velocity of propagation of P-waves in water), and $i = \sqrt{-1}$.

6 GEOPHYSICAL SURVEY FOR α

The coefficient of reflection for the subbottom rock material may be obtained directly from its relative impedance by means of the expression (Hall and Chopra 1982):

$$\alpha = \frac{1 - q \cdot C}{1 + q \cdot C} \qquad (4)$$

The field of the relative acoustic impedance at the specific site (Folsom Dam, in this particular case) will be characterized on the basis of experiments applying comprehensive geophysical surveys using water-borne techniques (Mc Gee, Ballard, and Caulfield 1995). Figure 4 illustrates a typical chart correlating the recorded acoustic reflection from different depths below the bottom surface to the corresponding acoustic impedance.

7 ANALYTICAL MODEL AND COMPUTER IMPLEMENTATION OF MATHEMATICAL MODELS

The main idea behind the analytical model is the generalization of the one-dimensional energy-dissipating mechanism described above into the three-dimensional space, which is subsequently reduced to two dimensions by

the boundary element technique. To focus the idea, Figure 5 illustrates the continuous variation of the α-parameter over the surface of the 1/8-th ellipsoid at hand, corresponding to locally one-dimensional, but globally three-dimensional energy absorbers.

The macro-algorithm to solve the harmonic dynamic potential problem under the multifacet set of mixed boundary conditions is exhibited in Figure 6. Program WESH3QBE-WS (Waterways Experiment Station Harmonic Three-dimensional Quadratic Boundary Element Capability: Water-Soil/Rock Interaction) applies the B.E.M. recursively on the basis of eq. (3). Initially, only the real component of the gradient is entered as a boundary condition to the potential problem (~ Neumann-type boundary condition), which is solved for the field and its gradient everywhere on the boundary. Subsequently, the boundary condition on the ellipsoidal surface is modified to include the appropriate imaginary component, and the potential problem is now solved successively, until convergence is attained. The solution for the hydrodynamic pressure field (Complex, for being a general Fourier Transform in the frequency domain) is finally computed wherever it is needed within the domain. Of course, the main interest is the hydrodynamic pressure on the upstream face of the dam, which is directly located on the boundary.

As a simple example of application, the idealization for the reservoir at Folsom Dam is resolved under stationary harmonic excitation with α=1 (rigid bottom surface). Figure 7 shows schematically the location of Node 241 at the center of the upstream face of the dam, and Figure 8 shows the corresponding frequency response function for the hydrodynamic pressure at this node. The spikes in the function correspond to the natural frequencies of vibration of the reservoir.

8 DIRECT STOCHASTIC B.E.M.

The uncertainty in the continuous random field of the acoustic impedance of the elastic subbottom medium may be approximately described using its second-moment characterization: the mean and the correlation functions in the spatial-parameter space. Given this characterization, and taking other variables entering the formulation of the potential problem as deterministic, the stochastic B.E.M. with constant elements effectively yields the second moment characterization of the random hydrodynamic pressure field on the boundary of the domain, in particular, on the upstream face of the dam.

The vector of mean values of the response at nodal points, $\{m_p\}$, and the corresponding correlation matrix, $[K_p]$, are obtained by solving the following system of linear equations (Burczyński 1985):

$$\begin{aligned} [A]\{m_p\} &= [B]\{m_\sigma\} \\ [A]\{H_i\} &= c^i\{C_i\} \\ [A]\{K_{p_i}\} &= c^i\{H_i\} \\ i &= 1,2,\ldots,N \end{aligned} \qquad (5)$$

where [A] and [B] are known stochastic matrices in terms of the known moments of the acoustic impedance random field, $\{m_\sigma\}$ is a vector of mean values of specified random boundary conditions (σ), and $\{C_i\}$ is a stochastic vector constructed from the elements of [B] and the correlation matrix associated with σ.

9 MULTIDIMENSIONAL THEORY OF RANDOM FIELDS IN SPACE. LOCAL AVERAGING

The experimental data collected from the geophysical survey provide the information needed to propose a sound variance function for the two-dimensional random field of the acoustic impedance at the subbottom of the reservoir, and to estimate the scale of fluctuation through local averaging (Vanmarcke 1983). These are the ingredients needed to formulate the correlation structure of the random field which in turn gives the second moment discrete characterization needed as input for the stochastic B.E.M. solution.

10 EXPERIMENTAL VERIFICATION

Deterministic predictions of the frequency response function for the hydrodynamic pressure field on the upstream face of the dam will be experimentally verified using a small-scale physical model of Folsom Dam subjected to harmonic excitation on a centrifuge at WES. The experiments are difficult to devise because it is not possible to prevent the spurious influence of hydrodynamic pressure waves reflected at the boundaries of a physical model and coming into the subbottom surface from below. These physical boundaries are necessarily located at finite distances from the structure and prevent the propagation of energy towards infinity, which is precisely the main aspect of the dam system response under this investigation.

11 CONCLUSIONS

The B.E.M. in elastodynamics provides an effective platform for the earthquake analysis of dams including reservoir-subbottom interaction. The analysis may be carried out in either a deterministic or a stochastic environment. The required description of the acoustic impedance field for the subbottom elastic material hinges in this investigation on data collected from water-borne geophysical surveys at the dam site. For the sake of simplicity in the development of analytical models and their experimental verification, the input excitation is initially taken as stationary harmonic; however, general input ground motions will be considered at later stages of the research program.

12 ACKNOWLEDGMENT

This investigation is a work unit of the Earthquake Engineering Research Program on Civil Works of the U.S. Army Engineer Waterways Experiment Station in Vicksburg, MS. Permission was granted by the Chief of Engineers to publish this paper.

13 REFERENCES

1 Hall, J.F., and Chopra, A.K. (1982). "Two-Dimensional Dynamic Analysis of Concrete Gravity and Embankment Dams Including Hydrodynamic Effects." *Earthquake Engineering and Structural Dynamics*, Vol 10, pp 305-332.

2 Ghanaat, Y., and Redpath, B.B. (1995) "Measurements of Reservoir-Bottom Reflection Coefficient at Seven Concrete Dam Sites." *Technical Report QS95-01*. Report to U.S. Army Engineer Waterways Experiment Station and Bureau of Reclamation. Quest Structures, Emeryville, CA.

3 Brebbia, C.A., and Domínguez, J. (1992) *Boundary Elements: An Introductory Course.* 2nd Edition. McGraw-Hill, New York, N.Y.

4 Domínguez, J. (1993) *Boundary Elements in Dynamics.* Computational Mechanics Publications, Southampton, U.K.

5 Chandrashaker, R., and Humar, J.L. (1993) "Fluid-Foundation Interaction in the Seismic Response of Gravity Dams." *Earthquake Engineering and Structural Dynamics*, Vol 22, pp 1067-1084.

6 Mc Gee, R.G., Ballard, R.F., and Caulfield, D.D (1995). "A Technique to Assess the Characteristics of Bottom and Subbottom Marine Sediments." *Technical Report DRP-95-3.* U.S. Army Corps of Engineers: Dredging Research Program, Washington, D.C.

7 Burczyński, T. (1985). "The Boundary Element Method for Stochastic Potential Problems." *Applied Mathematical Modelling.* Vol 9, pp 189-194.

8 Vanmarcke, E. (1983). *Random Fields: Analysis and Synthesis.* M.I.T. Press, Cambridge, MA.

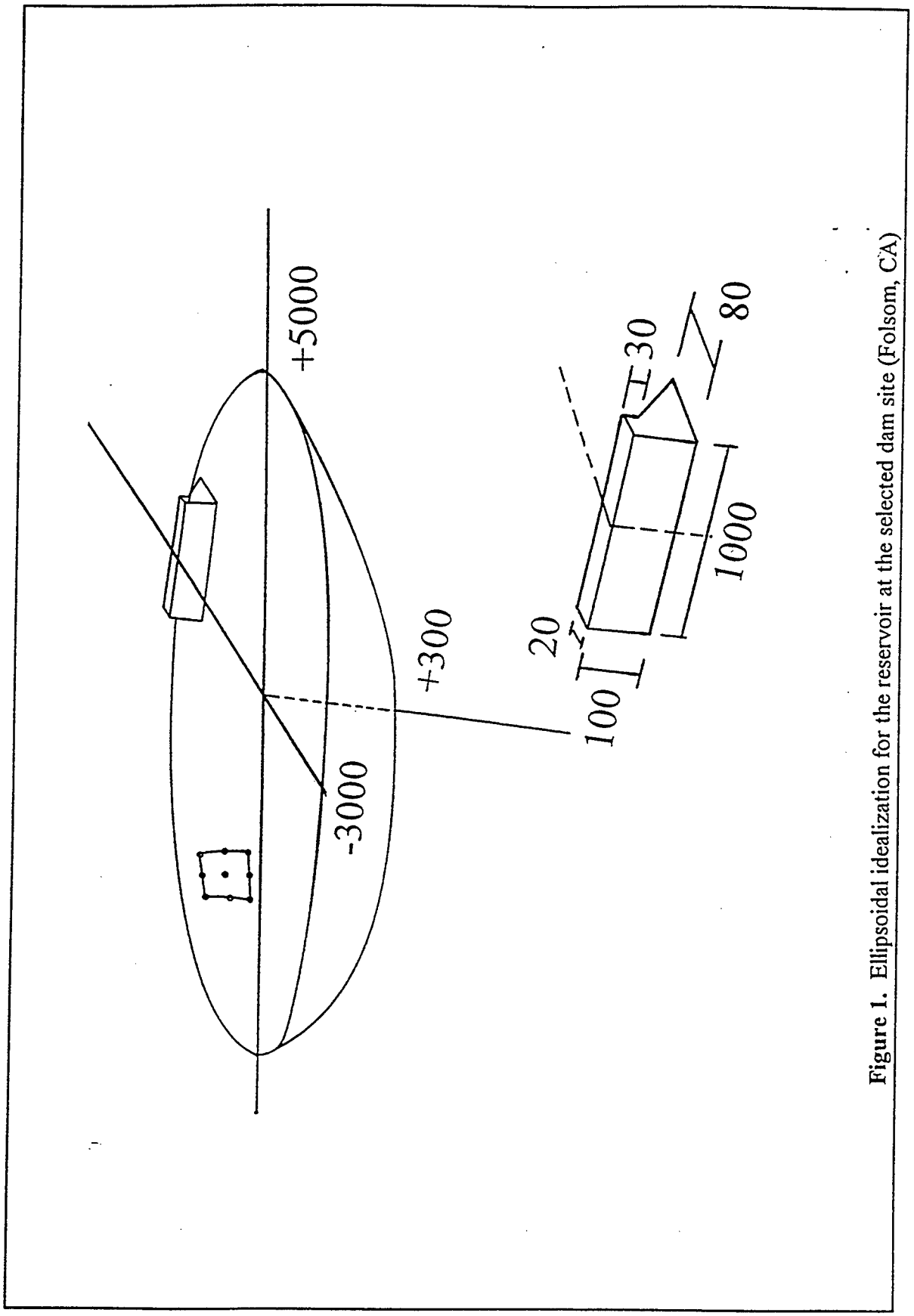

Figure 1. Ellipsoidal idealization for the reservoir at the selected dam site (Folsom, CA)

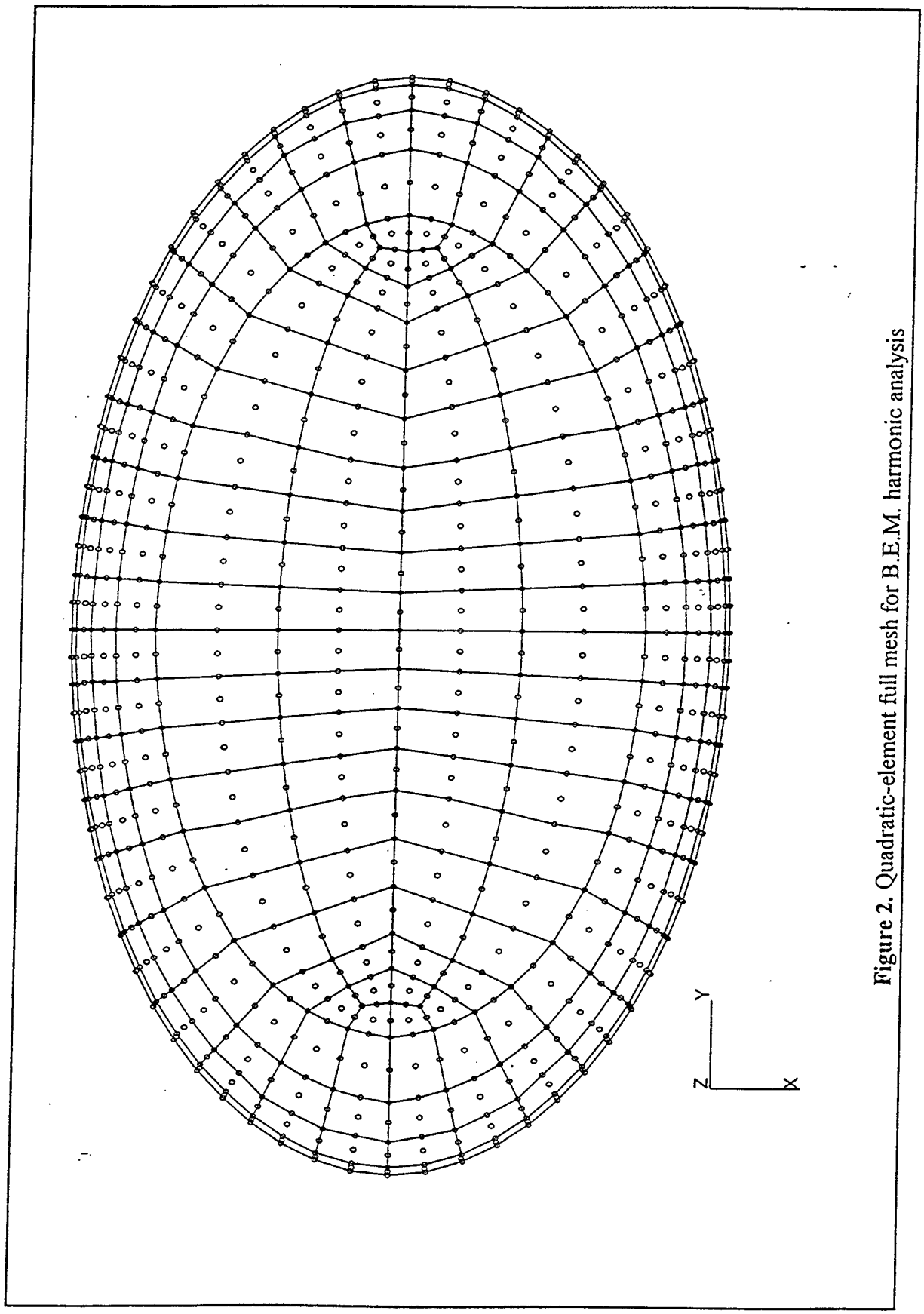

Figure 2. Quadratic-element full mesh for B.E.M. harmonic analysis

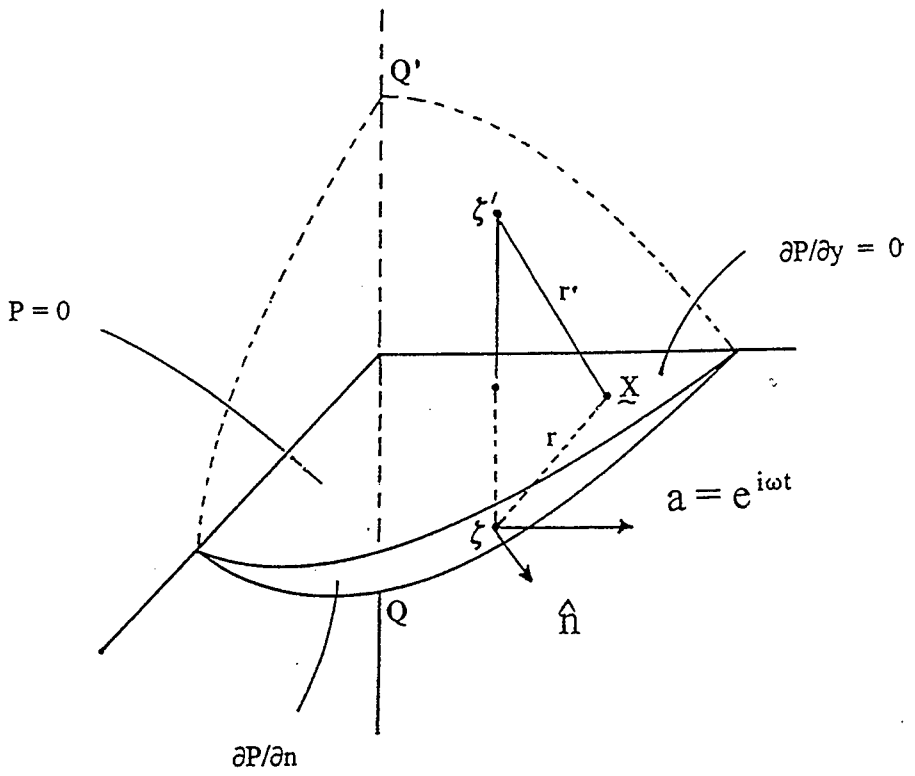

Figure 3. Taking advantage of quadrant-symmetric reservoir configuration

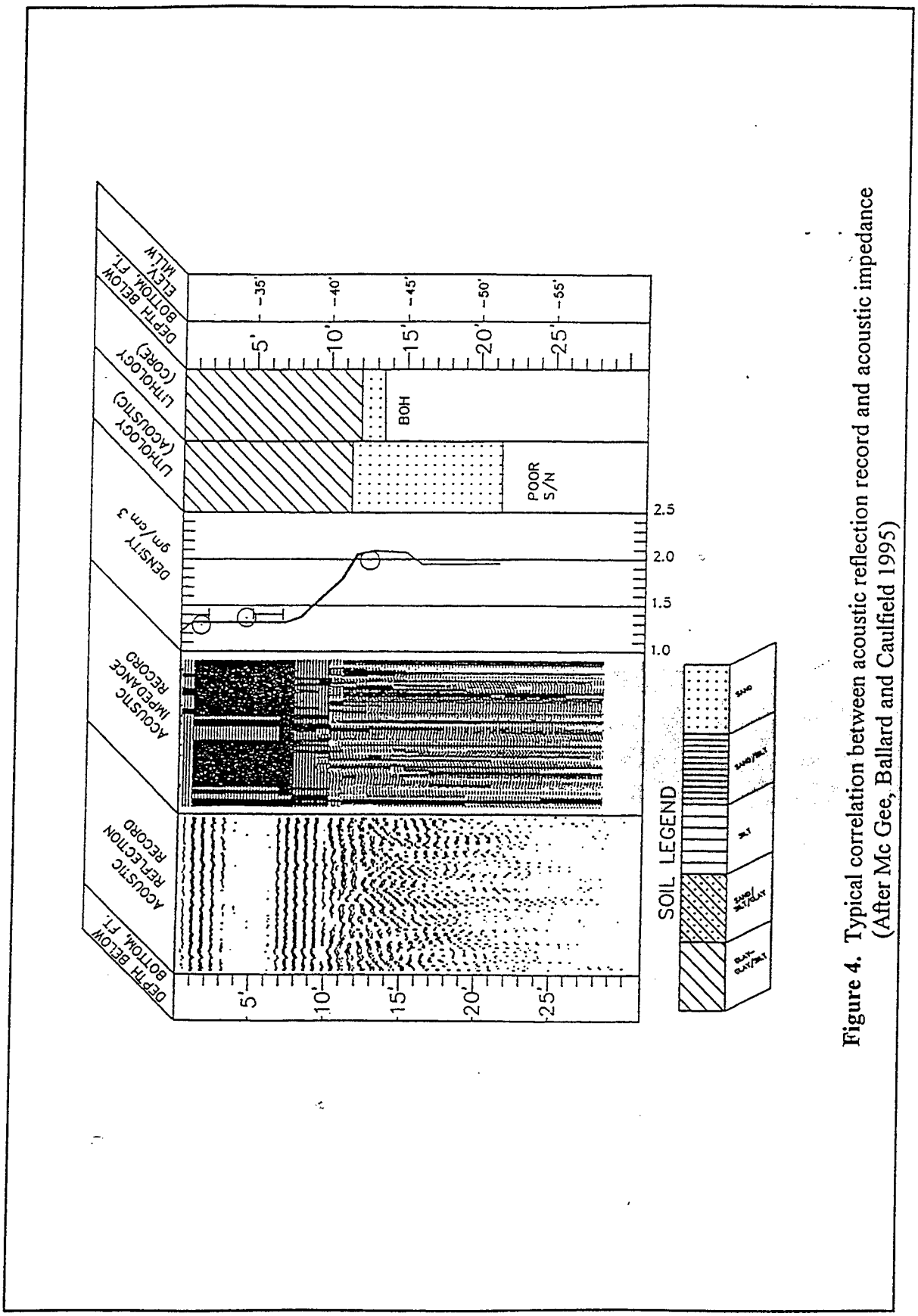

Figure 4. Typical correlation between acoustic reflection record and acoustic impedance (After Mc Gee, Ballard and Caulfield 1995)

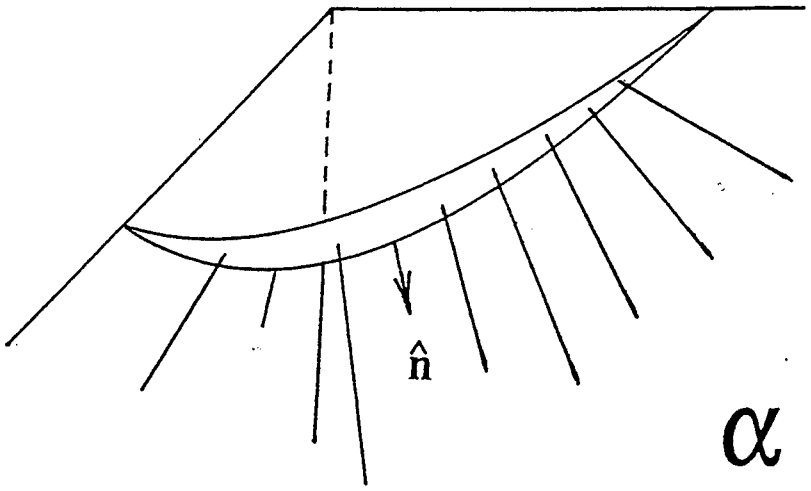

Figure 5. One-dimensional physical idealization of energy absorbers in space

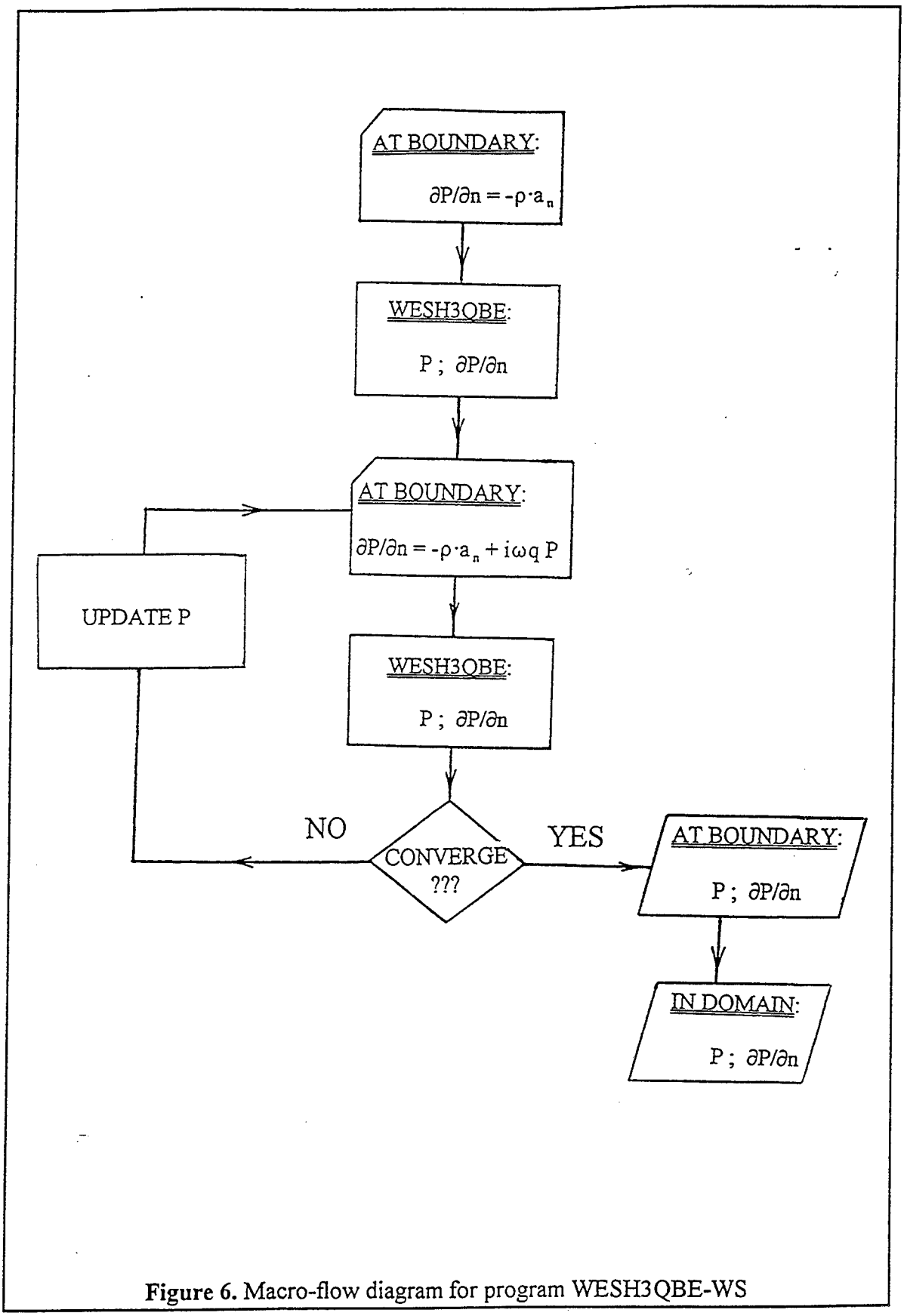

Figure 6. Macro-flow diagram for program WESH3QBE-WS

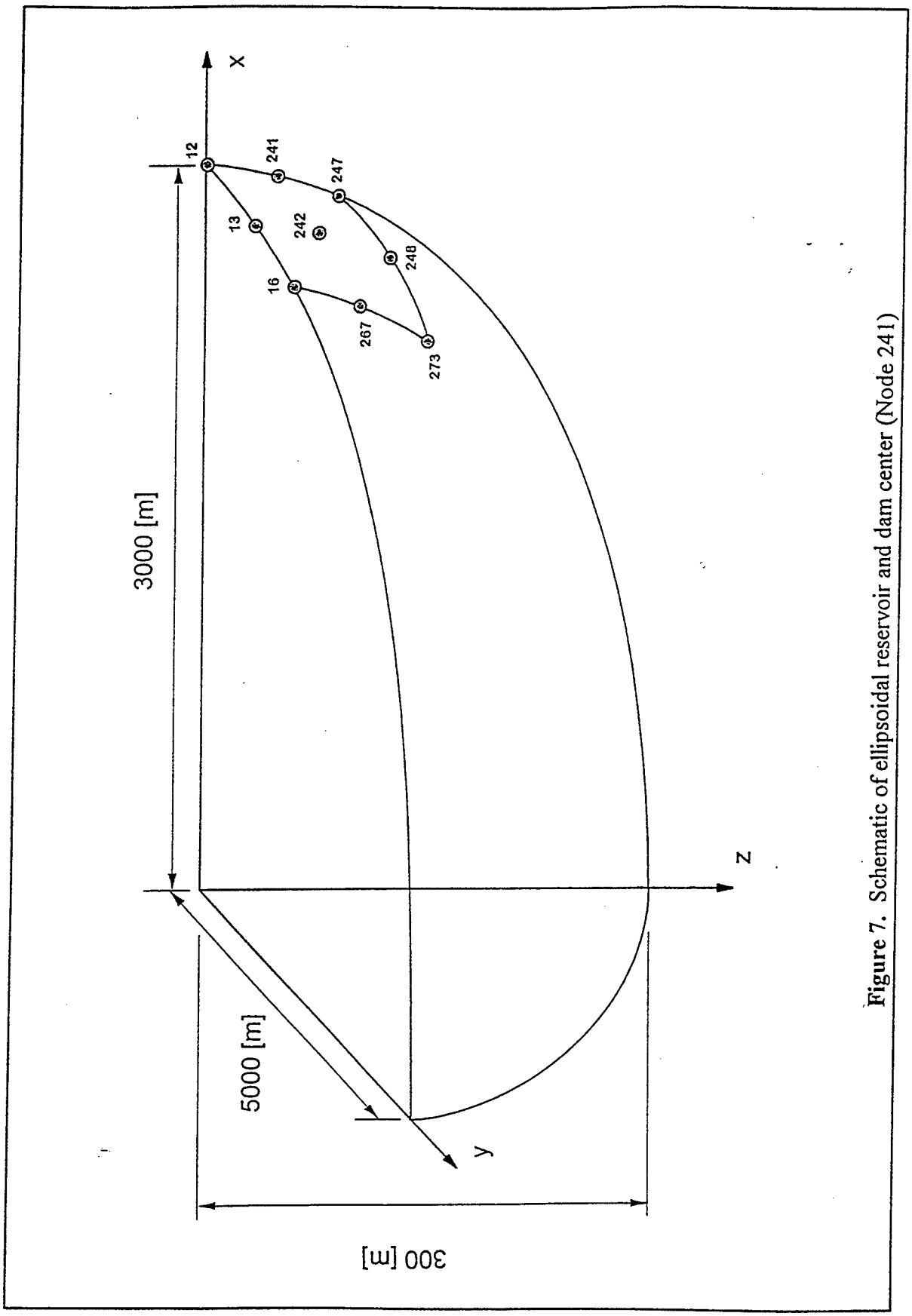

Figure 7. Schematic of ellipsoidal reservoir and dam center (Node 241)

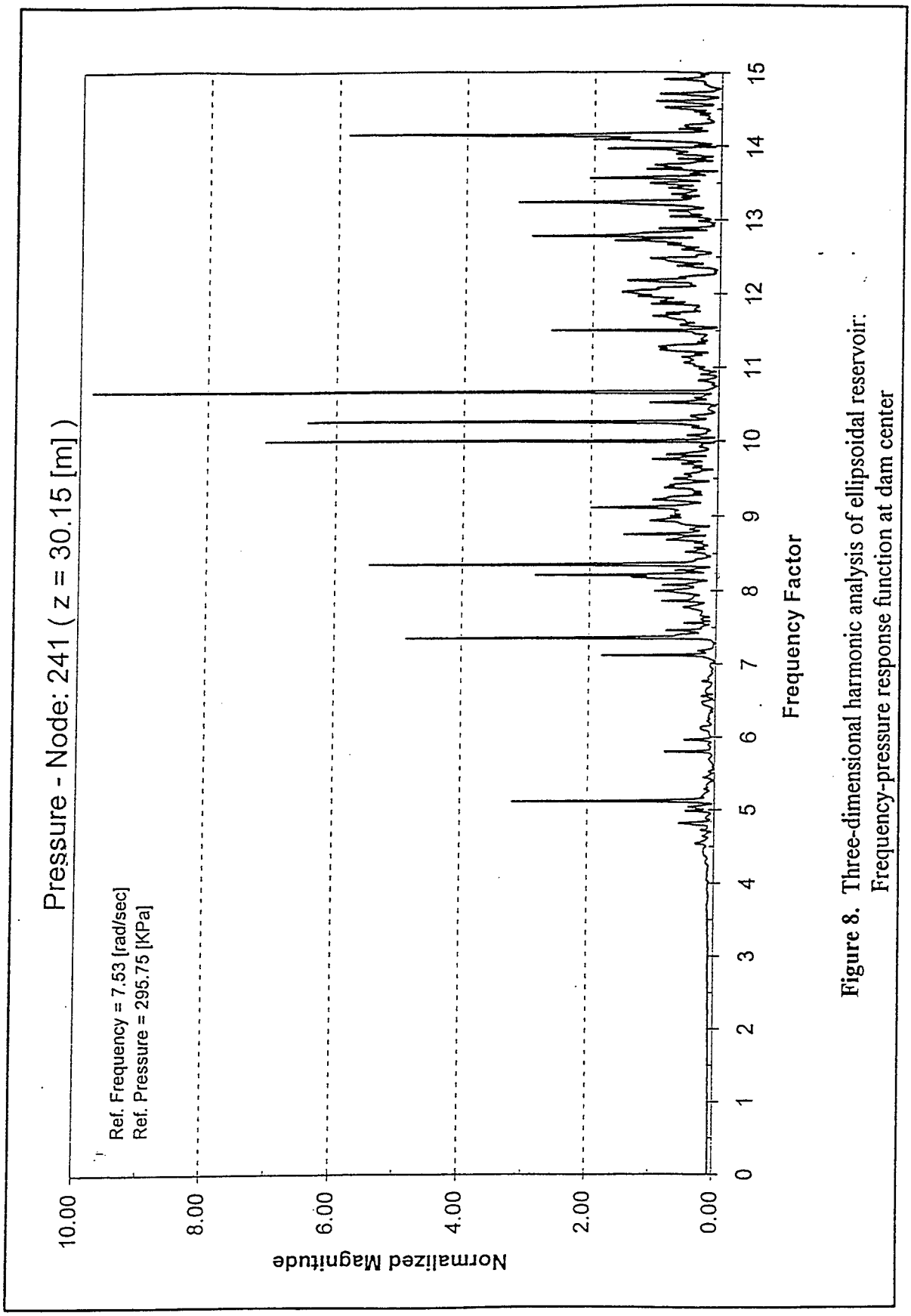

Figure 8. Three-dimensional harmonic analysis of ellipsoidal reservoir: Frequency-pressure response function at dam center

Numerical Model Development for Seismic Analysis of Concrete Dams

by

Luis Armando de Béjar*

ABSTRACT

This investigation develops experimentally-based finite-boundary element capabilities for the evaluation of the comprehensive nonlinear response of mass and roller-compacted concrete dams under earthquake excitations in three-dimensional (3-D) space. Brief descriptions of the outstanding characteristics of the models and the current state of their development are given.

KEYWORDS: Concrete Dams, Concrete Plasticity Models, Mass Concrete, Roller-Compacted Concrete Dams.

1 CONVENTIONAL CONCRETE DAMS

1a INTRODUCTION

Public safety involving life and property of affected populations calls for the evaluation of the ultimate capacity of concrete dams in the event of a strong ground motion excitation. The assessment of dam-system behavior in the vicinity of failure requires experimentally-based spatial modeling of material and geometric nonlinearities.

The objective of this investigation is to develop an experimentally-verified finite-boundary element computer capability for the evaluation of the comprehensive nonlinear response of conventionally-placed concrete gravity and arch dams under earthquake excitations. The analytical approach considers the material nonlinear behavior of mass concrete first, and the geometric nonlinearities introduced by the cyclic opening and closing of joints during dynamic response will be considered at later stages of the research program. Models for the plastic behavior of concrete in 3-D space are being incorporated into a general finite-element capability (NIKE). The surrounding media, impounded water and foundation rock, are assumed to remain elastic during earthquake response and will be modeled using boundary-element techniques. Theoretical predictions of ultimate behavior will be experimentally verified with small-scale physical models on a centrifuge at the U.S. Army Engineer Waterways Experiment Station.

1b PLASTICITY MODEL FOR MASS CONCRETE

Concrete is assumed to be a continuous, isotropic, and linearly elastic-plastic strain hardening-ultimate strength-plastic strain softening-residual strength-fracture material. The model hinges on the notion of surface evolution in the principal-stress space. The initial discontinuous surface, the ultimate strength surface, and the residual strength surface are postulated to be dependent on three invariants: the first invariant of the stress tensor, and the second and third invariants of the deviatoric component of the stress tensor. The elastic-plastic stress-strain

---

*Structural Mechanics Division,
Research Analysis Group,
Structures Laboratory,
USAE Waterways Experiment Station,
Vicksburg, MS 39180-6199

incremental relationships of concrete are formulated using a slightly modified flow rule with respect to that of the classical theory of plasticity.

Figure 1 illustrates the initial discontinuous surface and the ultimate strength surface, idealized as concentric surfaces of revolution about the hydrostatic axis in the principal-stress space. Initially, the state of stress is within the linear-elastic region. Upon increasing the intensity of the excitation, as the state-of-stress point touches the initial discontinuous surface, plastic flow takes place in the hardening regime. The initial discontinuous surface expands until it gets in contact with the ultimate-strength surface. At any instant during the history of surface evolution, if unloading occurs, it will take place elastically, and the system retains the last position of the initial discontinuous surface as the current one for subsequent reloading. After the ultimate-strength surface is reached, the softening regime starts, and the ultimate-strength surface evolves until touching the residual-strength surface, at which time fracture is imminent.

1c EFFECT OF LATERAL CONFINEMENT

The notion of plastic flow in mass concrete is supported by experimental evidence, whenever adequate confinement is provided by lateral stresses (Pramono and Willam 1989). Figure 2 illustrates the point. In the figure, σ_z is the vertical normal stress acting on cylindrical specimens in a standard triaxial test, and σ_r is the radial confinement stress acting laterally on the specimen. Beyond the transition points (TP), specimens exhibit clear ductile behavior; however, some softening ductility is also observed in specimens with even only a moderate amount of lateral confinement.

1d COMMON IDEALIZATIONS FOR THREE-DIMENSIONAL ANALYSIS

To avoid numerical difficulties in local regions of failure surfaces, these are commonly postulated as smooth surfaces, in the sense that at least the first-order partial derivatives exist everywhere. Similar idealizations are also proposed in this model. Figure 3 illustrates this point for a set of deviatoric traces (i.e., intersections of the failure surface with various planes normal to the hydrostatic axis, at a distance from the origin given by σ, the mean normal stress). In the figure, θ is the polar angle of similarity ($\theta=0$ represents the tensile plane, while $\theta=\pi/3$ represents the compression plane). Figures 4 and 5 show, in addition to the deviatoric traces, the meridians (i.e., the intersections of the failure surface with planes containing the hydrostatic axis) for typical failure surfaces in the hardening and the softening regimes, respectively. In the figures, ρ is the deviatoric stress; in Figure 4 (hardening region), k is the normalized strength parameter; and in Figure 5 (softening region), c is the decohesion parameter (Etse and Willams 1994).

1e THREE-INVARIANT FAILURE SURFACE FORMULATION

Commonly used failure surfaces for finite-element numerical analysis of material nonlinearities in mathematical models are functions of the pressure (DYNA3D, Model 16; see Malvar et al. 1994) and the second invariant of the deviatoric stress tensor, J_2. To introduce a third invariant, a dependence on the Lode's similarity angle θ is sought. If r_c is the distance from the hydrostatic axis to the failure surface at the compressive meridian, and r_t is the distance at the tensile meridian, then at any intermediate position the distance $r\epsilon(r_t, r_c)$ is given by

$$r' = \frac{2(1-\psi^2)\cos\theta + (2\psi-1)\sqrt{4(1-\psi^2)\cos^2\theta + \sin^2\theta - 4\psi}}{4(1-\psi^2)\cos^2\theta + (1-2\psi)^2}, \quad (1)$$

where $r' = r/r_c$ and $\psi = r_t/r_c$. Note that r' depends only on ψ and θ, and that ψ depends on the pressure (For $\theta=0$, one obtains $r' = \psi$, corresponding to pure tension, whereas for $\theta=\pi/3$, one obtains $r' = 1$, corresponding to pure compression). The value of θ may be computed from

$$\cos 3\theta = \frac{3\sqrt{3}}{2} \frac{J_3}{J_2^{3/2}}, \quad (2)$$

where J_3 is the third invariant of the deviatoric stress tensor.

1f STRAIN-RATE ENHANCEMENTS

Strain-rate effects are included in the model by modifying the effective plastic strain λ according to the expressions:

$$\lambda = \int_0^{\epsilon_p} \frac{d\epsilon_p}{r_f\,(1 + p/r_f f_t)^{b_1}}, \quad for\ p \geq 0, \quad (3a)$$

and

$$\lambda = \int_0^{\epsilon_p} \frac{d\epsilon_p}{r_f\,(1 + p/r_f f_t)^{b_2}}, \quad for\ p < 0. \quad (3b)$$

where p is the pressure, r_f is the enhancement factor, $d\epsilon_p$ is the effective plastic strain increment, and $b_{1,2}$ is the damage evolution parameter.

Volumetric damage is included in the formulation by incrementing the modified effective plastic strain according to .

$$\Delta\lambda = b_3\, f_d\, k_d\, (\epsilon_v - \epsilon_{v,yield}) \quad (4)$$

where b_3 is an input scalar multiplier, f_d is a factor depending on J_2 and the pressure, k_d is an internal scalar multiplier, ϵ_v is the volumetric strain, and $\epsilon_{v,yield}$ is the volumetric strain at yield.

An example of the effects of b_2 and b_3 on the strain-stress response of a single element subjected to uniaxial and triaxial tensile tests is shown in Figures 6 and 7, respectively.

2 ROLLER-COMPACTED CONCRETE GRAVITY DAMS (RCC DAMS)

2a INTRODUCTION

It is clear at this time that RCC dam construction is often the most economical alternative at a given site. The competitive advantage of a rapid and continuous construction process, of having the intake and outlet works incorporated to the body of the dam, and of using the downstream face of the dam as an energy-dissipator spillway, attracts the attention of designers to this low-volume method of construction. Moreover, RCC gravity dams are operationally very efficient because of the watertightness obtained from the combination of high-paste RCC quality

construction of horizontal lifts and a conventional concrete upstream-face membrane.

However, at this time, analysts lack adequate tools for the reliable prediction of the structural response of RCC gravity dams under strong ground motion. No available models represent the specific spatial material behavior of RCC, and in particular, the behavior of horizontal lift lines. This investigation aims at the satisfaction of this need: to develop an experimentally-based finite-element computer capability for the evaluation of the comprehensive nonlinear response of RCC gravity dams under earthquake excitations.
The approach of the research hinges on experimental sampling at a selected RCC dam (Elk Creek Dam; refer to Hopman 1992), immediately followed by laboratory controlled tests. The material characterization obtained from the experiments will be incorporated into a finite-boundary element analytical capability to model the hydrodynamics of the dam system under earthquake. Finally, theoretical predictions will be experimentally verified on a small-scale physical model of the RCC dam on a centrifuge at WES.

2b FIELD SAMPLING

At this time, the construction of the dam at Elk Creek has come to a halt at a height of one-third of its design height (249 ft). This circumstance favors the assessment of aging effects on RCC by comparing test results from recent experiments with the results obtained at the time of initial construction and with the results of experiments to be conducted in a second stage of this experimental research program at the time of the conclusion of the dam construction. Sample cores of RCC of 8-in. nominal diameter were recently obtained at Elk Creek Dam from four different holes spaced every 150 ft, each of approximately 20 ft of depth from the exposed upper horizontal surface. Figure 8 shows a schematic of location of the drilled holes, with a small offset from the downstream edge.

2c CONTROLLED LABORATORY EXPERIMENTS

Typical samples vary in length from 3 to 4 ft, and include the traces of at least two lift lines each. Direct shear tests will detect specific planes of weakness in the samples (if any, because surface preparation before placing consecutive lifts proceeded with diligent quality control during the initial construction process, including the placement of a 2-in. layer of mortar). Figures 9a-b show the cross section and an elevation, respectively, of typical sample cores received at the laboratory at WES. The maximum size of the aggregate was specified and carefully controlled to be 3 in.

Laboratory tests at WES consist of two phases. In the first phase, ultrasonic velocity logging is applied to the cores to non-destructively identify any degree of anisotropy in the specimens. The second phase targets the identification of mechanical properties (elastic parameters: moduli of elasticity and Poisson's ratios corresponding to the 3-D characterization of the material; strengths and failure envelopes). Specific tests to be conducted in the laboratory include direct-pull tension tests, and Brazilian cylinder-split tests, for correlation (Raphael 1984); unconfined compression tests and triaxial compression tests; and direct shear tests. Laboratory testing and analysis of the results are currently taking place.

2d MATHEMATICAL MODELS AND EXPERIMENTAL VERIFICATION

At this stage of the investigation, the description of the mathematical models is only qualitative. The parameters obtained through the laboratory tests will define constitutive relations for the RCC material in matrix form, which will be incorporated into a hybrid finite-boundary element capability currently being developed for the hydrodynamic analysis of the dam-reservoir system upon earthquake excitation. Eventually, the model will also include an analytical representation of the subbottom absorption of energy during the dynamic interaction (see companion paper in this workshop). Finally, theoretical predictions will be experimentally verified on a small-scale physical model of the RCC Elk Creek Dam on a centrifuge at WES.

3 CONCLUSIONS

Plasticity models are being incorporated into a general finite-boundary element capability for the representation of material nonlinear behavior of mass concrete in gravity dams subjected to multidimensional earthquake excitations. Further advances will include the implementation of viscoplastic models (Bićanić and Zienkiewicz 1983) and the representation of crack propagation within conventional concrete. In a parallel research effort, a similar capability is being developed for RCC gravity dams, on the basis of the results of controlled laboratory tests on field specimens at Elk Creek Dam.

4 ACKNOWLEDGMENT

This investigation is a work unit of the Earthquake Engineering Research Program on Civil Works of the U.S. Army Engineer Waterways Experiment Station in Vicksburg, MS. Permission was granted by the Chief of Engineers to publish this paper.

5 REFERENCES

1 Chen, A.C.T., and Chen, W-F. (1975). "Constitutive Relations for Concrete." *Journal of Engineering Mechanics Division*, ASCE, Vol 101, pp 465-481.

2 Pramono, E., and Willam, K. (1989). "Fracture Energy-Based Plasticity Formulation of Plain Concrete." *Journal of Engineering Mechanics Division*, ASCE, Vol 115, pp 1183-1204.

3 Etse,G., and Willam, K. (1994). "Fracture Energy Formulation for Inelastic Behavior of Plain Concrete." *Journal of Engineering Mechanics Division*, ASCE, Vol 120, pp 1983-2011.

4 Malvar, L.J., Crawford, J.E., Wesevich, J.W., and Karagozian & Case (1994). "A New Concrete Material Model for DYNA3D." Technical Report TR-94-14-3 prepared for Defense Nuclear Energy. Defense Nuclear Energy, Alexandria, VA.

5 Raphael, J.M. (1984). "Tensile Strength of Concrete." *ACI Journal*, Title No. 81-17, pp 158-165.

6 Hopman, D.R. (1992). "Lessons Learned from Elk Creek Dam." *Roller-Compacted Concrete III.* Edited by Hansen, K.D., and Mc Lean, F.G. *Proceedings of the ASCE Conference on RCC Construction, pp 162-180.* San Diego, CA

7 Bićanić, N., and Zienkiewicz, O.C. (1983). "Constitutive Model for Concrete under Dynamic Loading." *Earthquake Engineering and Structural Dynamics*, Vol 11, pp 689-710.

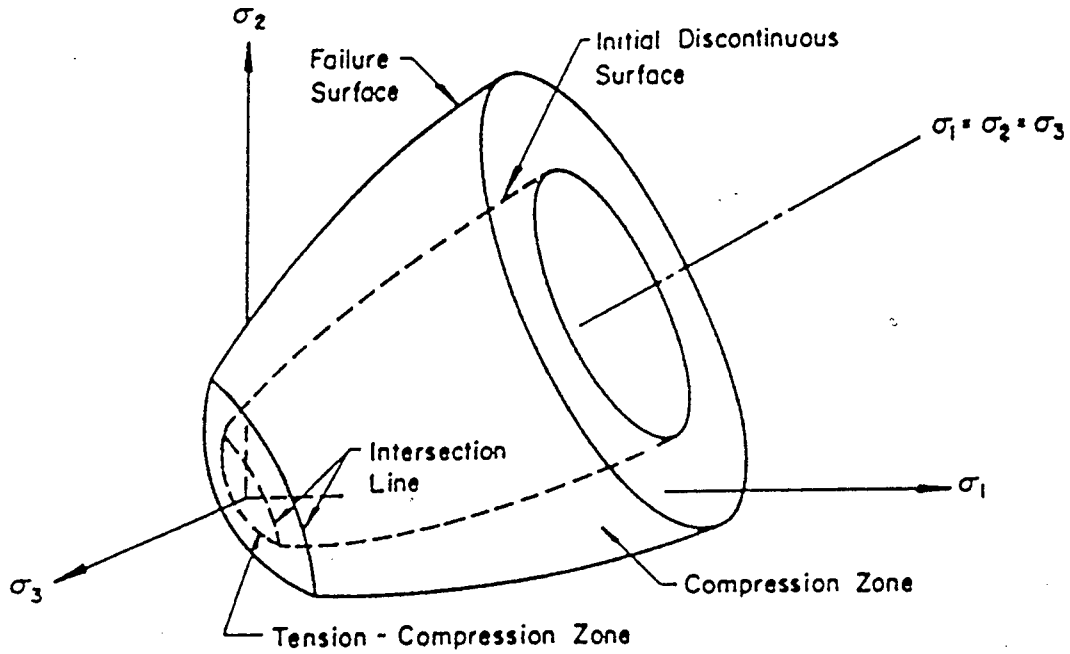

Figure 1. Triaxial State of Stress: Idealizations (After Chen and Chen 1975)

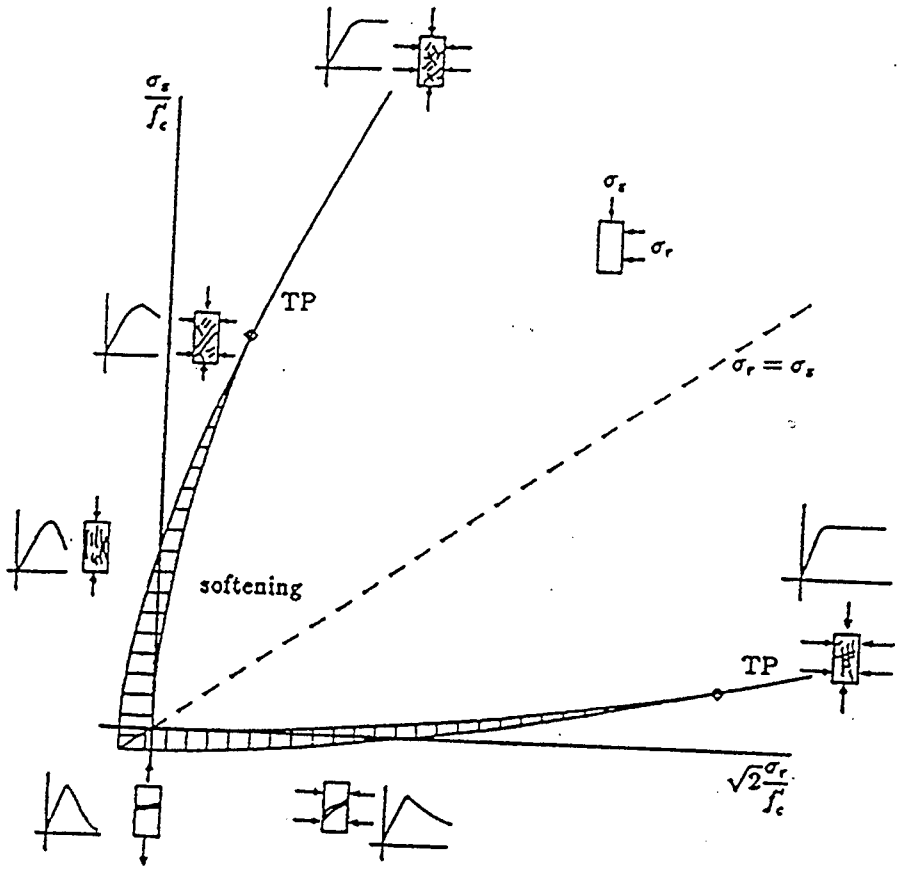

Figure 2. Experimental effect of multiaxial state of stress (After Pramono and Willam 1989)

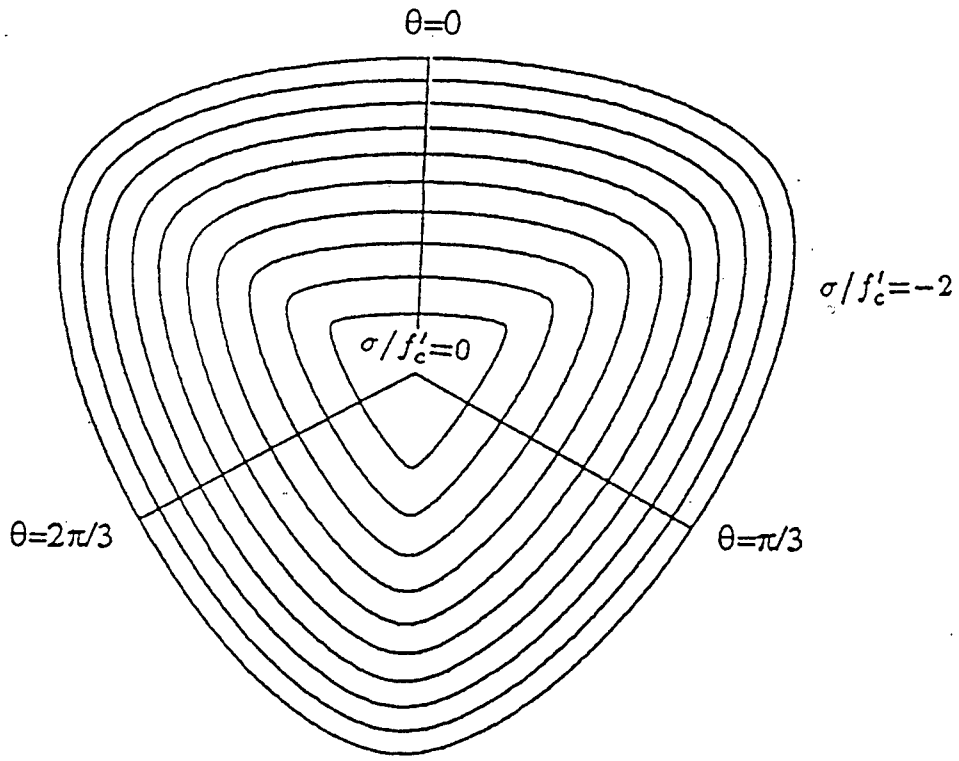

Figure 3. "Smooth" idealization of deviatoric traces
(After Etse and Willam 1994)

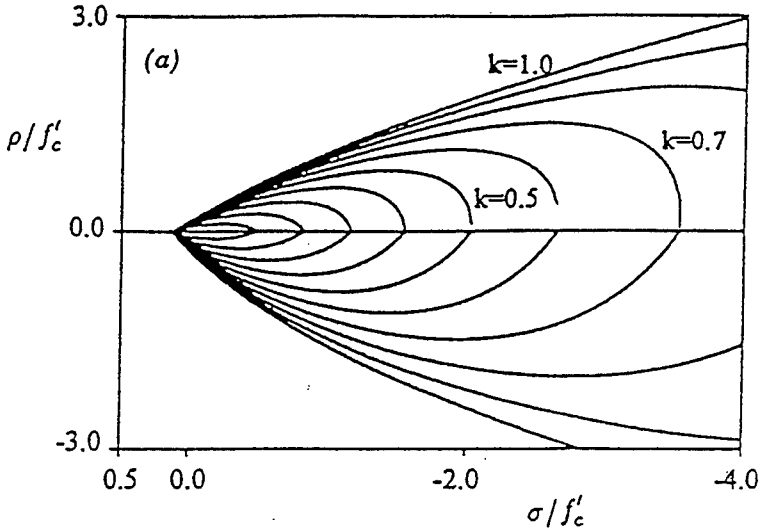

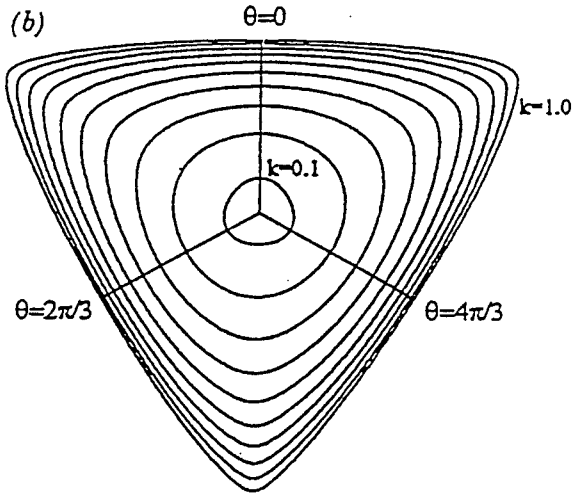

Figure 4. Hardening regime: Meridians and deviatoric traces (After Etse and Willam 1994)

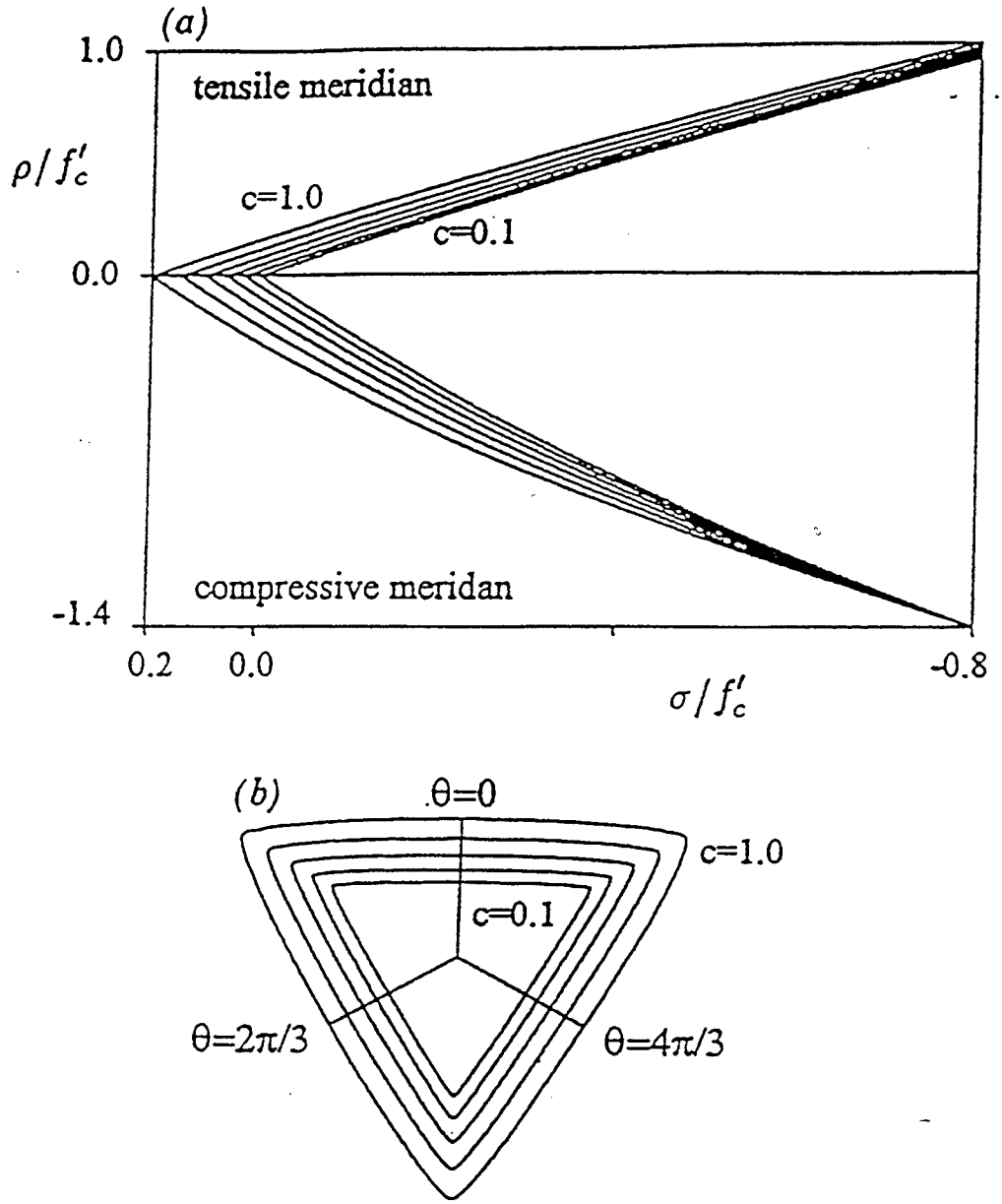

Figure 5. Softening regime: Meridians and deviatoric traces (After Etse and Willam 1994)

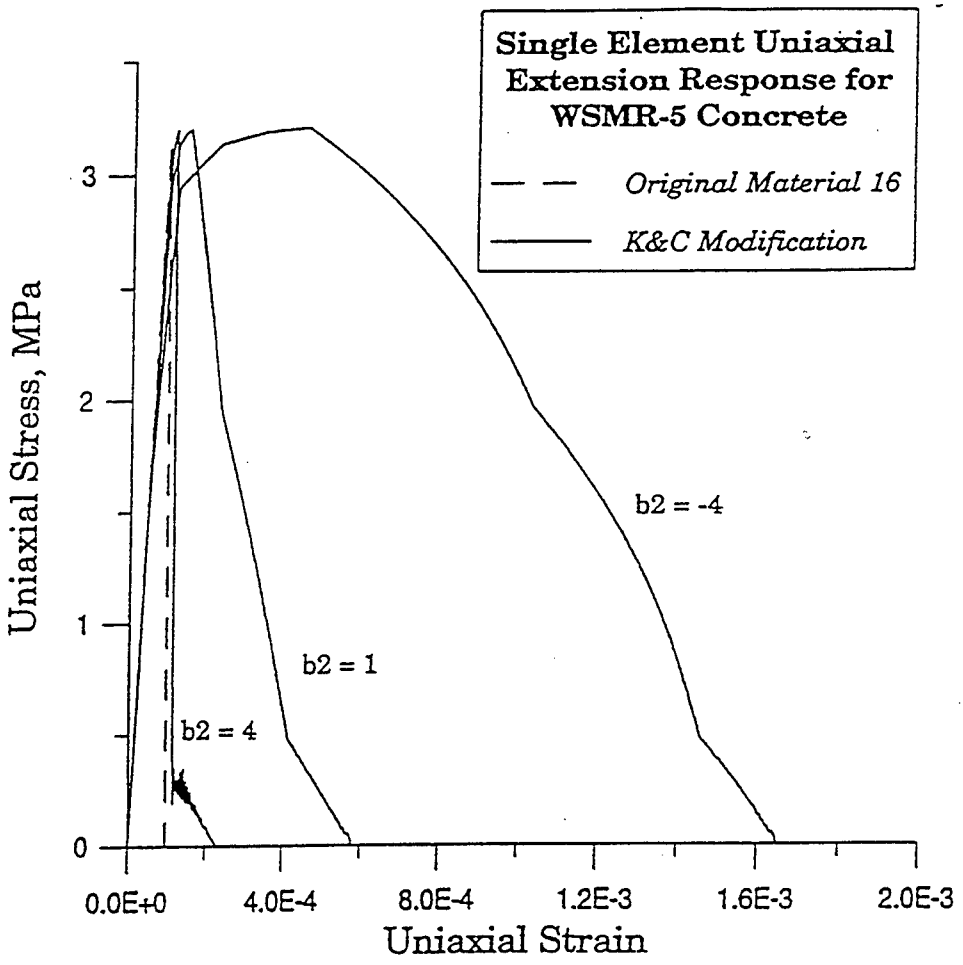

Figure 6. One-dimensional strain-rate enhancements (After Malvar, Crawford, Wesevich, Karagozian and Case 1994)

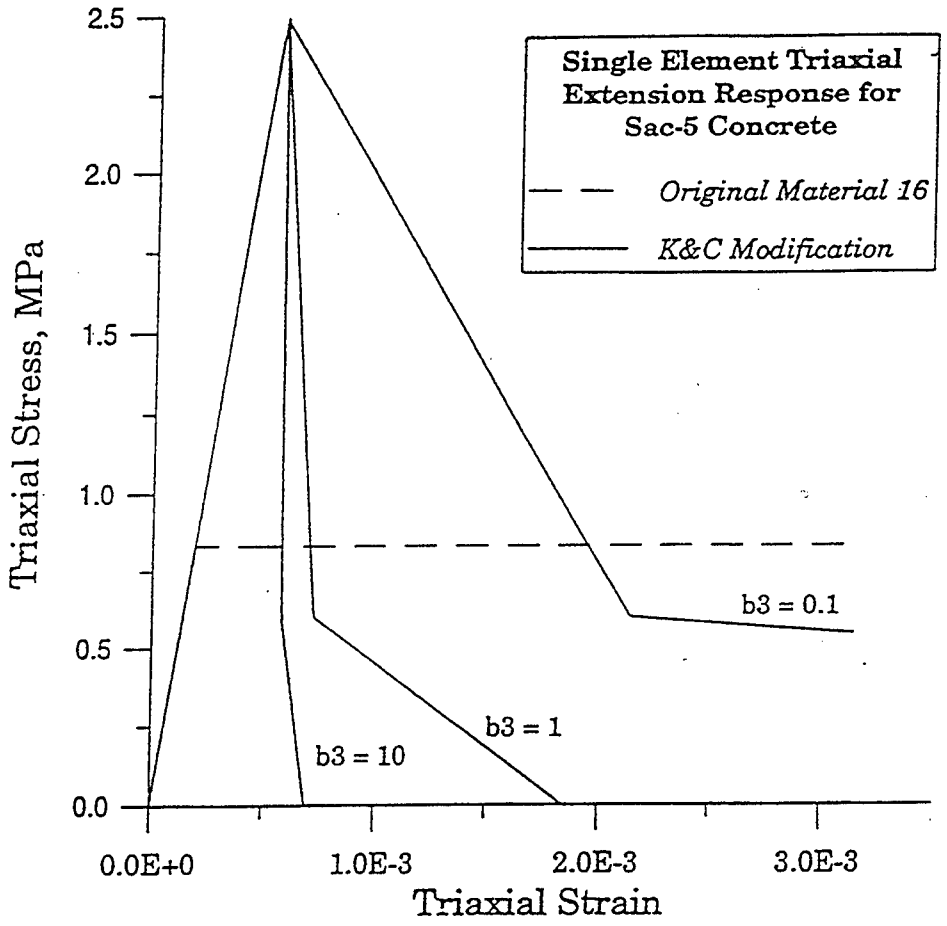

Figure 7. Three-dimensional strain-rate enhancements (After Malvar, Crawford, Wesevich, Karagozian and Case 1994)

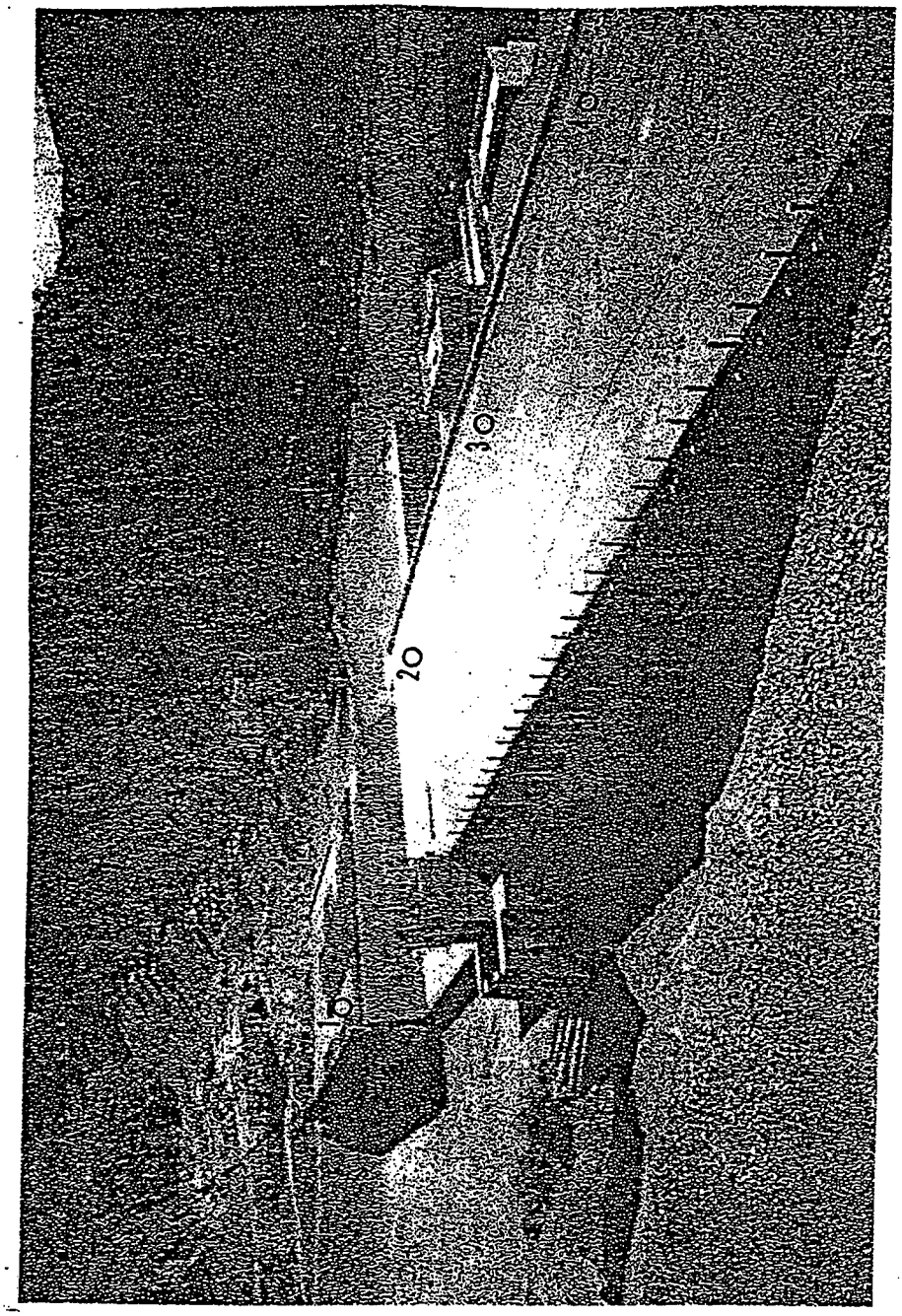

Figure 8. Schematic of location of four sampling holes at Elk Creek Dam

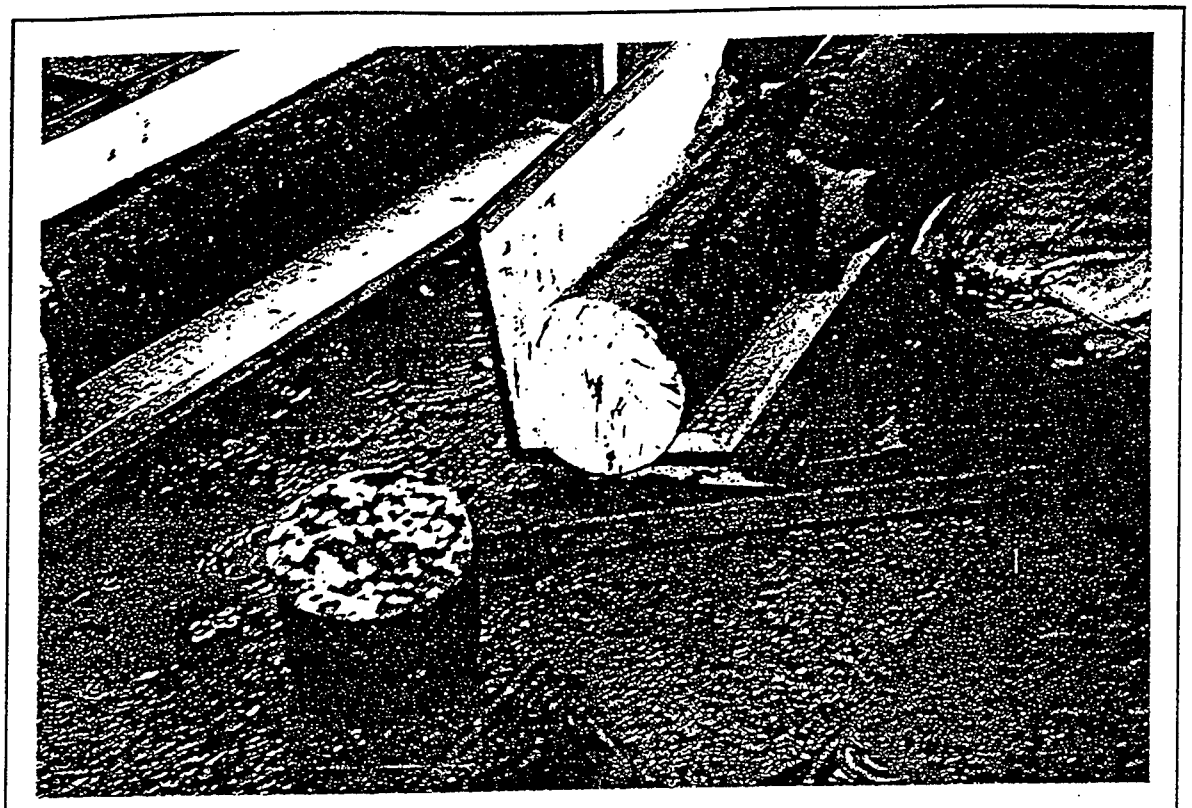

Figure 9a. Typical 8"-diameter RCC cores sampled at Elk Creek Dam: Cross-Section

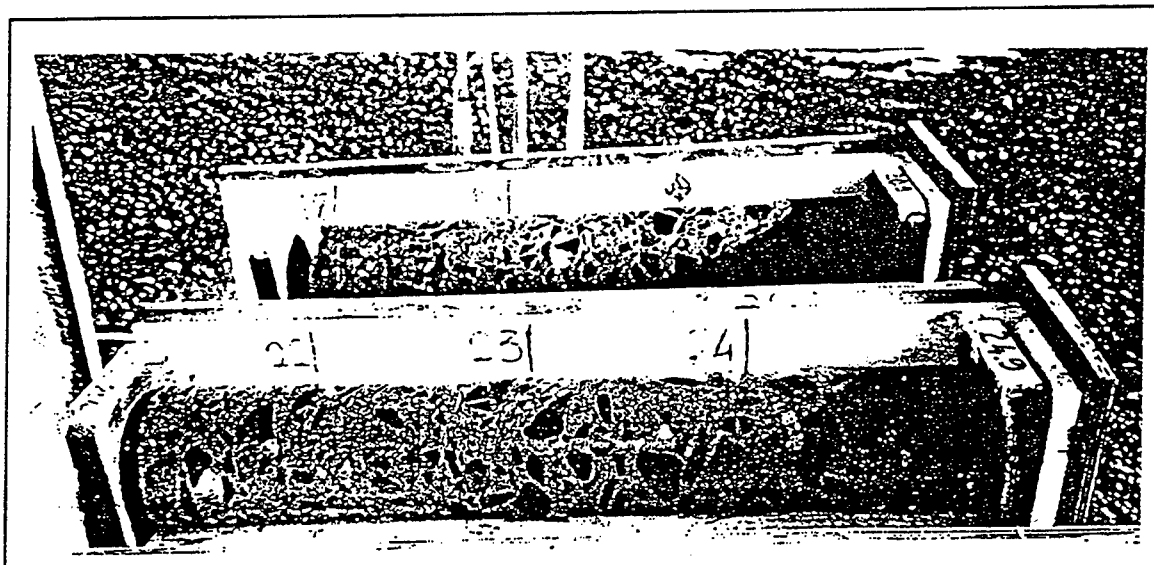

Figure 9b. Typical 8"-diameter RCC cores sampled at Elk Creek Dam: Lateral View

Time-Domain, Nonlinear Dynamic Analysis of Concrete Dams

by

Tommy Bevins* and Robert Ebeling*

ABSTRACT

Ongoing research into the analysis of concrete dams during earthquake shaking at the U.S. Army Engineer Waterways Experiment Station (WES) and within the earthquake engineering community has advanced to the stage in which nonlinear performance of mass concrete can be included in the dynamic analysis. This paper describes the current state (Nov 96) of computer code development of EQTime2D, a new computer code which will account for foundation-structure-reservoir interactions and include the nonlinear performance of mass concrete.

KEYWORDS: Concrete Dams, Earthquake Engineering, Dynamic Analysis, and Nonlinear Performance.

1 INTRODUCTION

This paper will describe the current state of development of the computer code, EQTime2D, at WES under the Corps' Earthquake Engineering Research Program. The authors are responsible for the development of EQTime2D and are implementing the nonlinear constitutive stress-strain model and crack model being developed for mass concrete by a companion structural engineering work unit. The numerical solution of the equation of motion of the finite-element model of the dam section is being formulated in the time domain because of the nonlinear aspects of the problem being solved. When completed, EQTime2D will be used to solve for the dynamic response to earthquake shaking of a two-dimensional (2-D) concrete gravity dam section. Following the completion of EQTime2D, development of a second nonlinear computer code (EQTime3D) will commence for analyzing a three-dimensional (3-D), representation of concrete gravity or arch dam.

2 BACKGROUND: STATE OF PRACTICE

The states of practice for the dynamic analysis of concrete dams subjected to earthquake shaking are the finite-element computer codes, EGAD (Fenves and Chopra 1984) and GDAP (Ghanaat 1993). EGAD is used to solve for the dynamic response of a 2-D concrete dam section and accounts for the structure-foundation and structure-reservoir interactions which occur during earthquake shaking. Two important features of this computer code are its ability to model the compressibility of the reservoir and to account for the absorptive reservoir bottom (Figure 1). Because EGAD uses frequency-domain equations, its applications are restricted to linear problems (i.e., linear stress-strain model and no cracking). GDAP solves for the dynamic response using time-history modal

---

*Research Civil Engineers
USAE Waterways Experiment Station
Vicksburg, MS 39180-6199

superposition of a 3-D representation of a concrete dam as idealized in Figure 2. Like EGAD, structure-foundation interaction is considered in the analysis by including a portion of the foundation in the model. Structure-reservoir interaction is accounted for by using the added mass procedure to model the hydrodynamic effects. . Because the water is assumed incompressible in an added mass formulation, no absorptive reservoir bottom can be included in the model.

In summary, neither GDAP nor EGAD accounts for nonlinear performance due to nonlinear stress-strain response or cracking within the mass concrete during earthquake shaking. Both computer codes are formulated using procedures which are strongly affiliated with the solution of linear problems.

3 OBJECTIVE

The objective is to develop an EGAD-type (2-D) computer program and a GDAP-type (3-D) computer program to account for the effects of nonlinear stress-strain response of mass concrete and for the effects of cracking. The structure-foundation interaction and structure-reservoir interaction will be accounted for in both computer codes. A compressible reservoir model will be used, which will allow for the modeling of a reservoir and reservoir-bottom interaction.

4 EQTime2D

EQTime2D will be a 2-D, nonlinear, time-domain, reservoir-interaction code for the analysis of concrete dams subject to earthquakes. EQTime2D uses NIKE2D (Hallquist 1979) as a base code. EQTime2D builds on the existing nonlinear, time-domain, implicit solution in NIKE2D and adds the reservoir, foundation, nonlinear concrete model.

5 ACCOMPLISHMENTS TO DATE (NOV 96)

The work to date has focused on restructuring and reducing the size of the code. This work will facilitate the additions and modifications required to incorporate the reservoir-foundation modeling and the nonlinear mass concrete material model. The code size has been reduced by 60 percent. This reduction was accomplished by removing sections not directly applicable to solving the earthquake analysis problem.

Verification analyses were made to ensure that EQTime2D continues to yield correct results after the restructuring and modifications. The verification problems are compared to EAGD. The first verification problem is a modal analysis of an elastic monolith on a rigid foundation (Figure 3). The results from this analysis are shown in Table 1.

Table 1. Modal analysis comparison.

Mode	Frequency (rad/sec)	
	EQTime2D	EAGD
1	20.21	20.12
2	42.35	41.85
3	55.75	55.73
4	73.49	72.57
5	109.9	108.4

These results show excellent agreement between EQTime2D and EAGD. The second verification problem is a time-history analysis of a monolith on a rigid foundation with earthquake ground motions. The displacements at the crest (Figure 4) are in excellent agreement between the two codes,

EQTime2D and EAGD. Also, the maximum principle stresses (Figure 5a) are in excellent agreement. A detailed view of the maximum principal stress near the peak response is shown in Figure 5b. The slight differences between the two codes are attributed to the difference in the methodology used for applying damping. EAGD, a frequency-domain analysis code, allows the same damping value for all frequencies. EQTime2D, a time-domain analysis code, uses Rayleigh damping (Bathe 1982). Rayleigh damping is a quadratic function, expressing damping as a combination of the mass and stiffness matrices. The actual percent damping will vary with frequency.

6 FUTURE TASKS

The next major phase (ongoing) in developing EQTime2D is incorporating an experimentally verified nonlinear model for concrete (de Bejar 1996). The model is a three-invariant plasticity model with strain-rate enhancement and damage. The concrete model has been developed and verified in DYNA3D (Malvar et al. 1994). The WES has been extensively involved in the development and verification of this model. This effort will adapt the current model for mass concrete and roller-compacted concrete.

The reservoir, reservoir bottom, and foundation will be modeled using the Boundary Element Method (BEM) in the finished product. The BEM is being developed in a concurrent work unit (de Bejar 1996). The boundary-element model and finite-element model will be explicitly coupled. This coupling allows modeling of the reservoir-structure, reservoir and reservoir-bottom, and reservoir-foundation interactions.

7 CONCLUSION

This research will provide the Corps with technology capable of assessing the stability of concrete gravity and arch dams during earthquake shaking. It has the potential to provide savings by providing the analytical tools which will more accurately model the dynamic response of the dam as compared to those procedures currently being used.

8 ACKNOWLEDGMENT

The authors are grateful for the support provided by all those involved with the Corps' Earthquake Engineering Research Program. Permission was granted by the Chief of Engineers to publish this information.

9 REFERENCES

Fenves, G., and Chopra, A.K. 1984 (Aug). "EGAD-84, A Computer Program for Earthquake Analysis of Concrete Gravity Dams," Report No. UCB/EERC-84/11, Earthquake Engineering Research Center, University of California, Berkeley, CA, 92 pp.

Ghanaat, Y. 1993 (Aug). "User's Manual-GDAP, Graphics-Based Dam Analysis Program Version 3.25," Instruction Report ITL-93-3, U.S. Army Engineer Waterways Experiment Station, Vicksburg, MS.

Hallquist, J.O. 1979 (March). "NIKE2D: An implicit, Finite Deformation, Finite-Element Code for Analyzing the Static and Dynamic Response of Two-Dimensional Solids," University of California, Lawrence Livermore National Laboratory, Rept. UCRL-52678.

Bathe, Klaus-Jurgen (1982). Finite-Element Procedures in Engineering Analysis. Prentice-Hall, Inc., Englewood Cliffs, NJ.

de Bejar, L.A. (1996). "Subbottom Absorption Coefficients for Seismic Analysis of Concrete Dams." U.S.-Japan Workshop on Advanced Research on Earthquake Engineering for Dams. U.S. Army Engineer Waterways Experiment Station, Vicksburg, MS 39180.

de Bejar, L.A. (1996). "Numerical Model Development for Seismic Analysis of Concrete Dams." U.S.-Japan Workshop on Advanced Research on Earthquake Engineering for Dams. U.S. Army Engineer Waterways Experiment Station, Vicksburg, MS 39180.

Malvar, L. J., Crawford, J.E., Wesevich, J.W., and Karagozian & Case (1994). "A New Concrete Material Model for DYNA3D." Technical Report TR-94-14-3 prepared for Defense Nuclear Agency, Alexandria, VA.

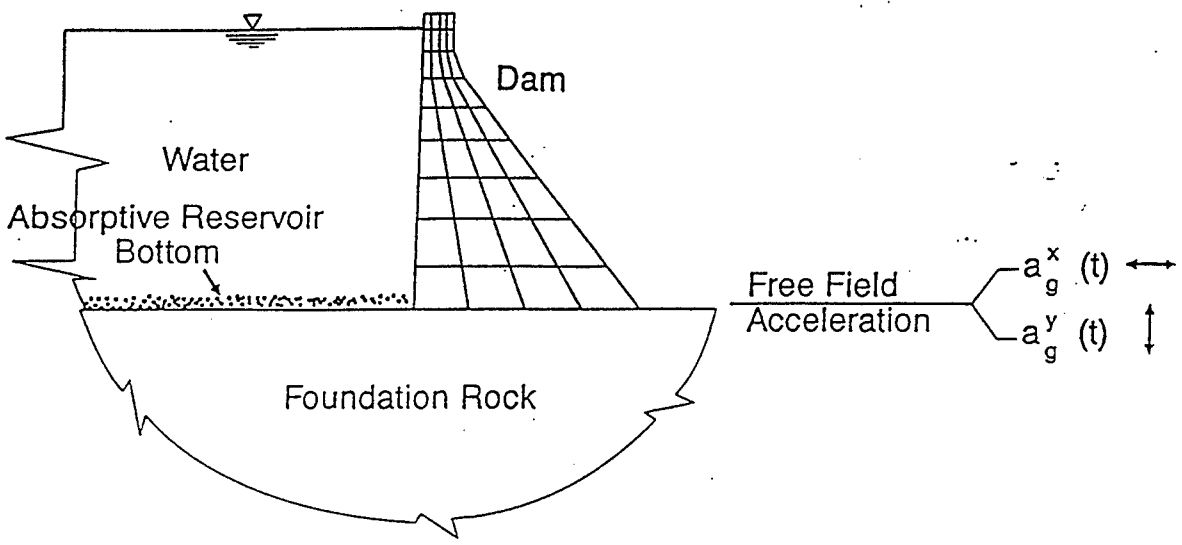

Figure 1 Two-dimensional finite element model of a concrete gravity dam - EGAD

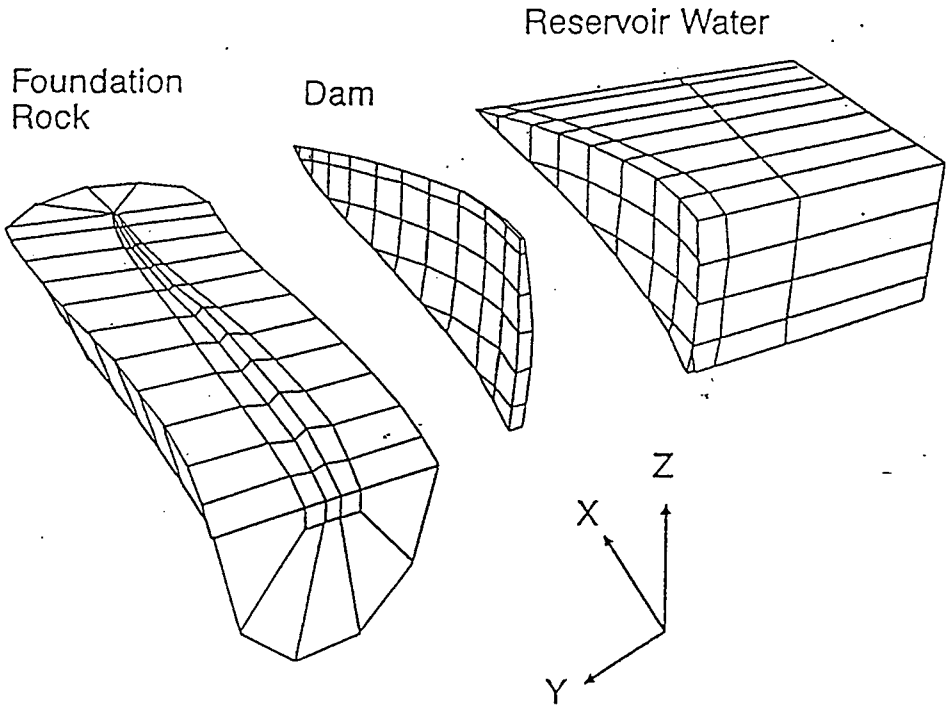

Figure 2 Three-dimensional finite element model of an arch dam - GDAP.

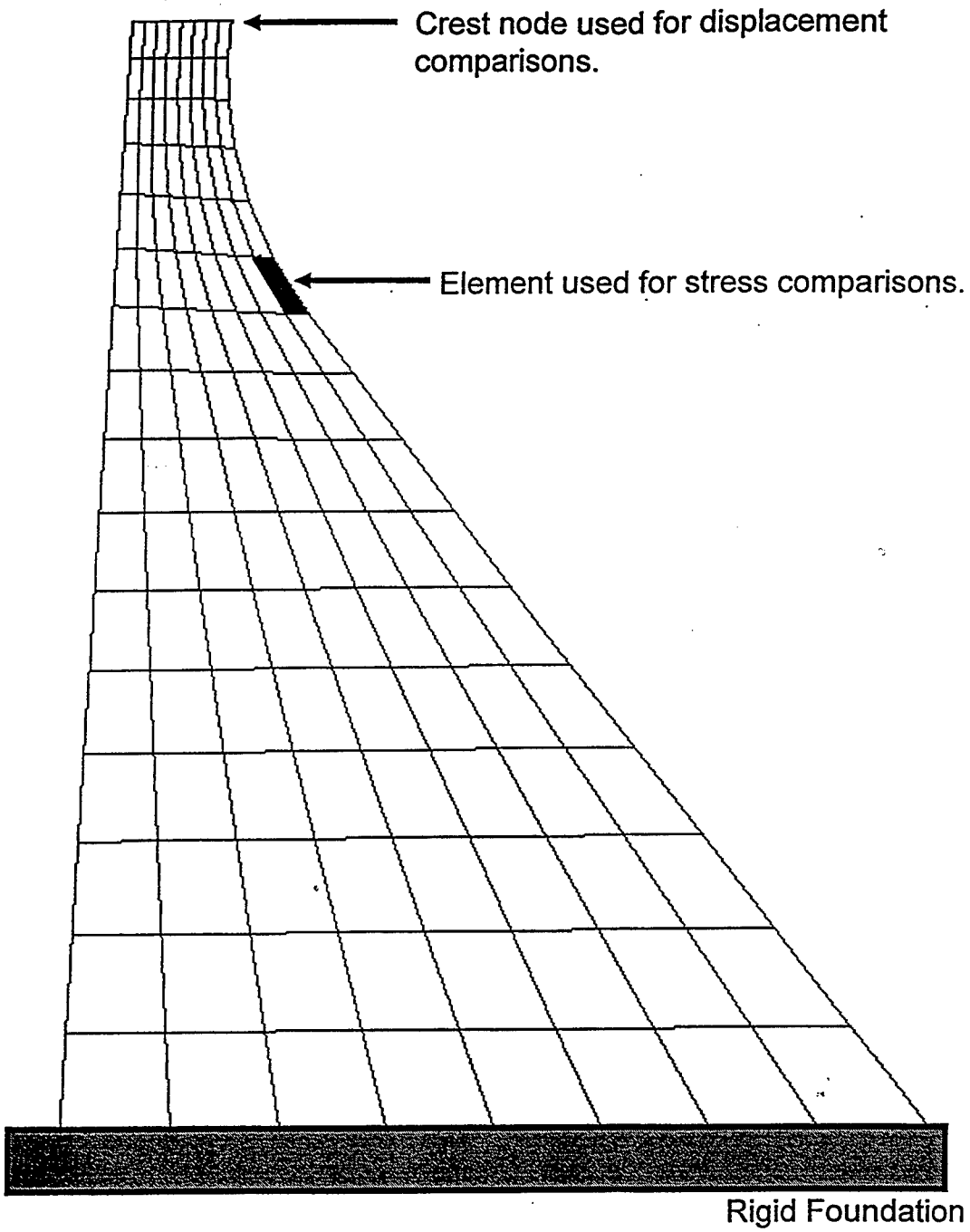

Figure 3 Finite element model for monolith used in validation analysis.

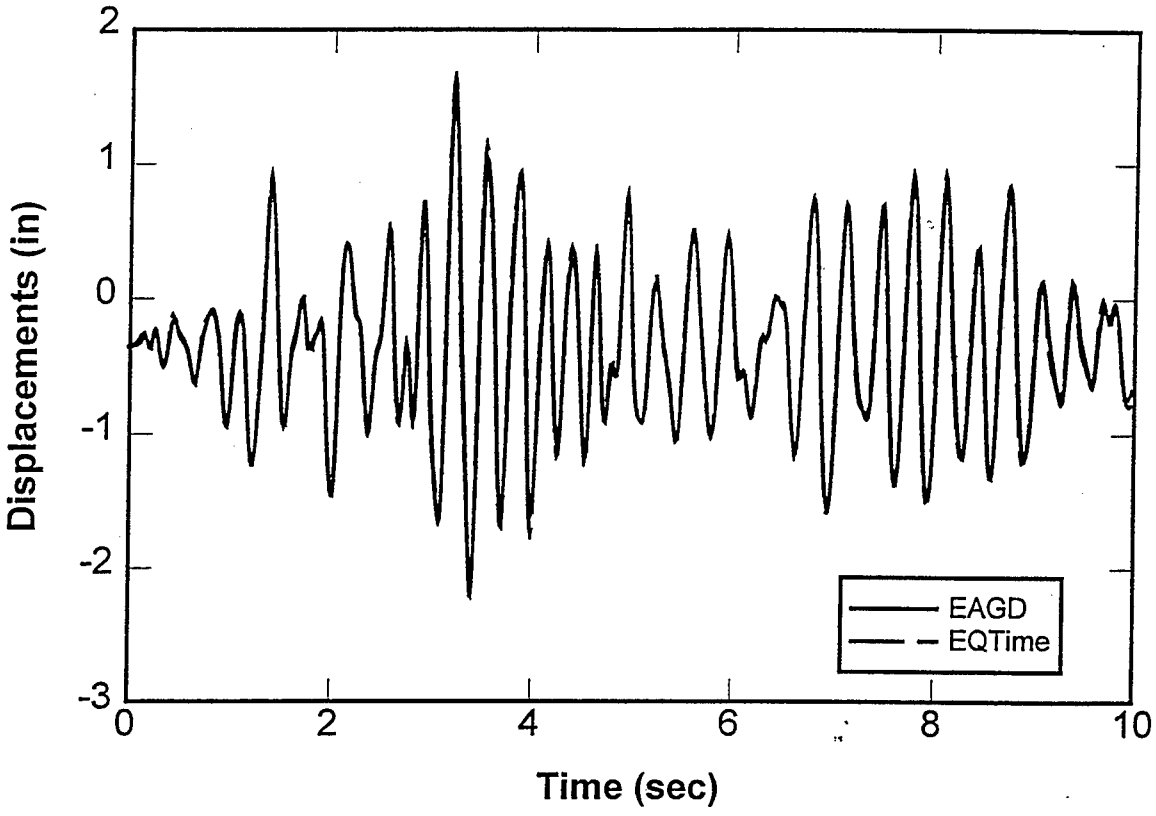

Figure 4 Crest node displacement comparison between EQTime2D and EAGD.

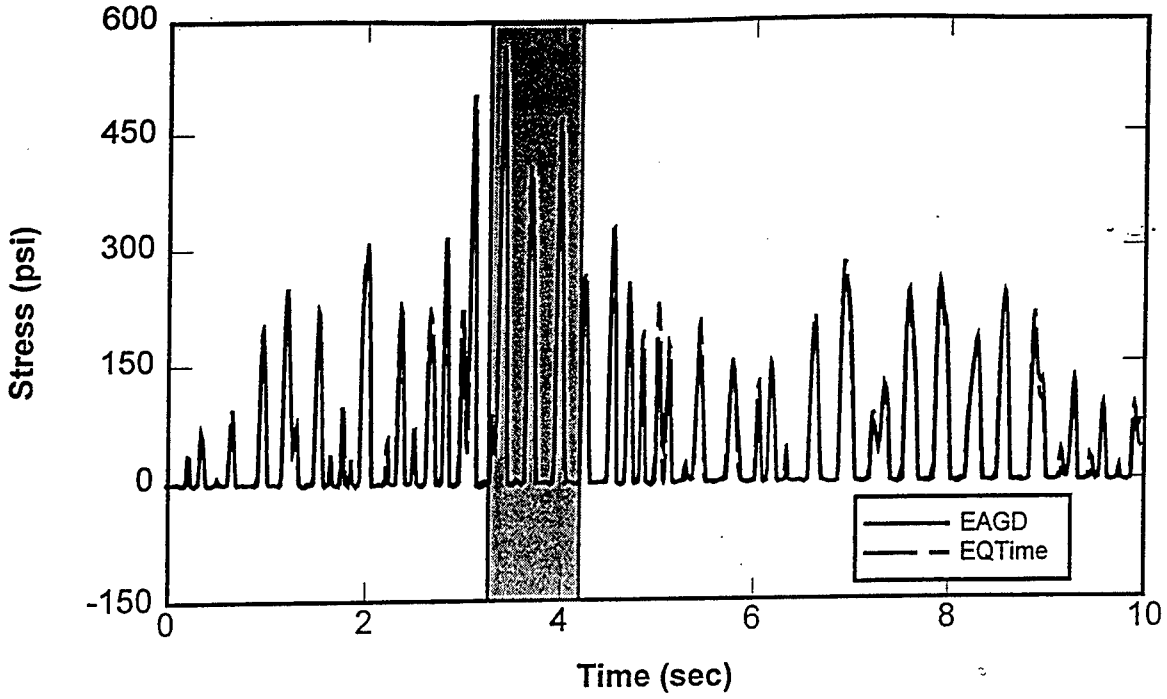

Figure 5a Comparison of maximum principal stress.

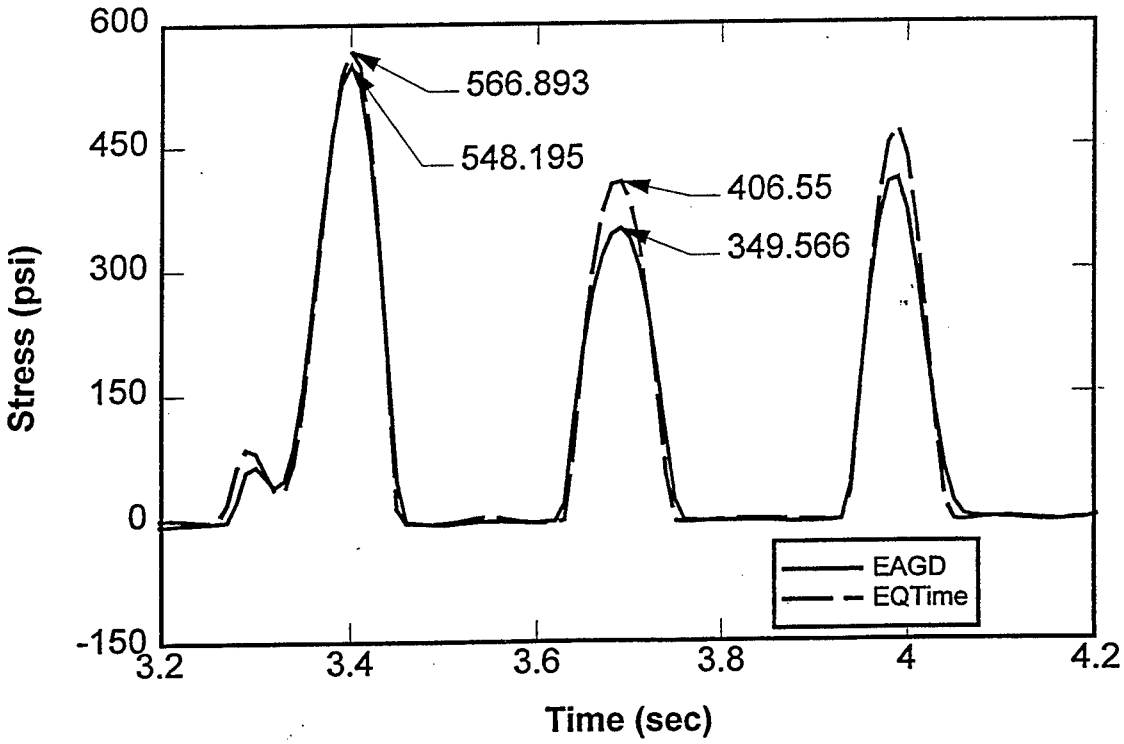

Figure 5b Detail of stress comparison near peak response.

Seismic Behavior of Ground and Main Structure of Nagaragawa Estuary Barrage

by

Katsuya Taguchi[1], Toshiki Kawakami[2], Yokito Sugimura[3], Ken-ichi Fujita[4], Nobuyuki Shirakawa[5]

ABSTRACT

Four strong earthquakes including the 1995 Hyogo-ken Nanbu earthquake (17 January 1995; magnitude 7.2) were recorded at the Nagaragawa Estuary Barrage, where transducers are installed the office, a barrage column, and the ground of the barrage site. Though the maximum amplitude of acceleration observed is not great, seismic records covering a wide range from a depth of approximately 100 m to a barrage column was obtained in an earthquake. Thus, these records are considered to be useful for the investigation of the whole response of the barrage including the ground.

This study analyzes records of strong earthquakes, including the 1995 Hyogo-ken Nanbu earthquake, and discusses the behaviour of the ground and the barrage based on investigations such as a response analysis of data recorded at a ground depth of approximately 100 m.

Key words: *River Estuary Barrage, Seismic Observation, Seismic Behaviour*

1. OUTLINE OF THE BARRAGE

1.1 Barrage facility

The Nagaragawa Estuary Barrage is one of the largest movable barrages in Japan. Specifications and a typical cross section of the barrage are shown in Table 1 and Fig. 1, respectively. The location and a plan view of the barrage are given in Figs. 5 and 6, respectively.

Table 1 Specifications

Length		661.0 m
Movable Section		555.0 m
Fixed Section		106.0 m
Standard Pier	Width	5.0 m
		20.0 m
	Height	10.8 m
	Footing Thickness	3.0 m

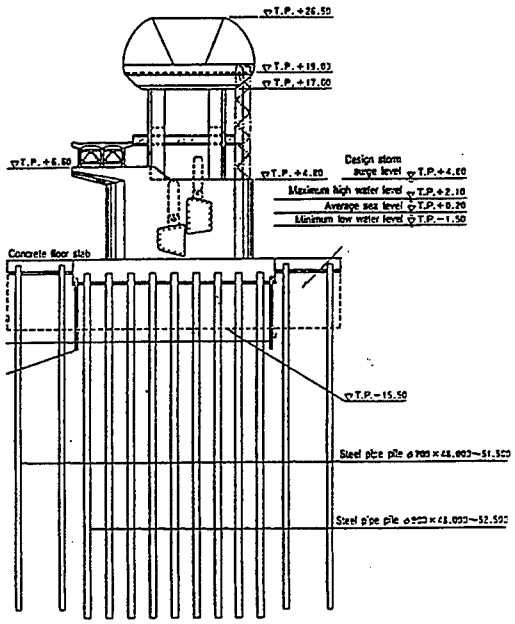

Fig.1 Typical Cross Section

1.2 Geology

The barrage is located in the Nobi Plain. The bedrock of the Nobi Plain and its vicinities consists of Paleozoic and Mesozoic sedimentary rocks (sandstone, mudstone, chert, etc.), which

1) Directer, Recearch Institute, Water Resources Development Public Corporation (WARDEC)
2) Head, Design Division, First Contruction Department, ditto
3) Head, Concrete Dam Devision, Reserch Institutte, ditto
4) Deputy Head, Design Devision, First Construction Department, ditto
5) Senior Research Engineer, Fill Dam Division, Research Institute, ditto, 936 Jinde-Urawa-shi, Saitama-ken, 338 Japan

have been confirmed to exist deep under the plain surface. The bedrock lies with a gentle tilt, shallower to the east and north (approx. 1,200m) and deeper to the west (approx. 2,000 m).

Alluvium and diluvium are thickly distributed around the barrage. Because diluvium and the deeper beds contain well consolidated gravel layer and can be used as the foundation of bearing piles, the Upper Pliocene first gravel layer (N-value of 50 or greater; shear wave velocity of 500 m/s or greater), which generally lies at a depth of 40-60 m, is used as the load bearing layer. Though the first gravel layer can be treated as a bedrock surface (the upper surface of a sufficiently hard bed that lies under the vibrating ground in a seismic design), the Middle Pliocene second gravel layer, which lies at a greater depth of approximately 100 m, is used as a bedrock surface in this study, so that the analytical precision of the seismic design is improved.

The first and the second gravel layers were deposited during regression periods of about 20,000 and 160,000 years ago, respectively. The deposition of the alluvium, on the other hand, started about 10,000 years ago.

The geologic structure of the barrage site has been elucidated down to a depth of approximately 2 km. There is no Quaternary faults right beneath the barrage. All the faults that need to be considered are more than approximately 2 km away from the barrage, and their orientations do not pose a threat to the barrage site area (within 300 m from the barrage structure).

The geology of the barrage site and a typical section of the Nobi Plain[1] are respectively shown in Figs. 2 and 3.

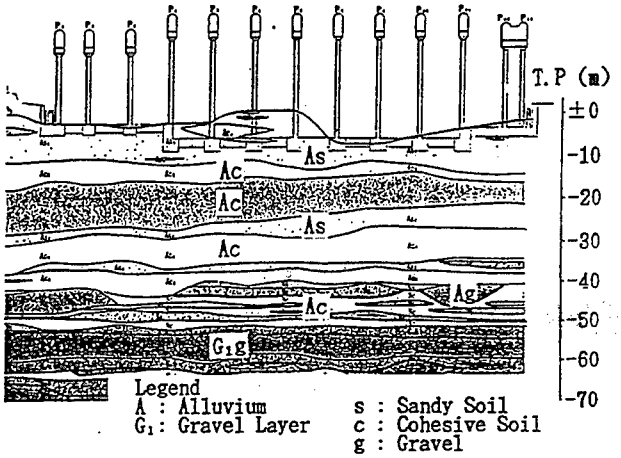

Fig. 2 Geology of The Barrage Site

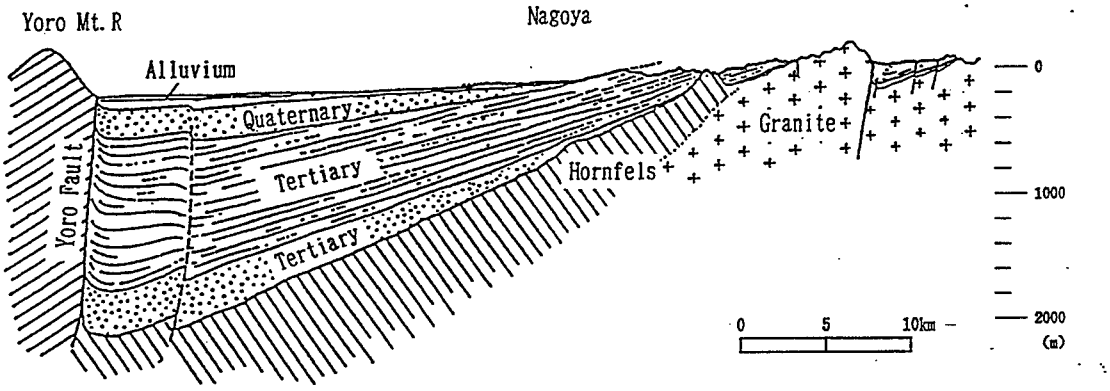

Fig. 3 Typical Section of The Nobi Plain(Revised The Reference Literature[1])

1.3 Earthquake history

The Nobi Plain is in a zone of very strong earthquake motion. The Nobi earthquake (28 October 1891; magnitude 8.0), one of the greatest epicenter-on-the-land-type earthquakes in the Japanese history of seismic observation, had its epicenter at approximately 60 km north of the Nagaragawa Estuary Barrage. The Nobi earthquake, which was the greatest earthquake that affected the barrage site in the past, is estimated to have generated a ground acceleration of approximately 220 gal at the site.

1.4 Design of The Barrage

The Nagaragawa Estuary Barrage was designed by the seismic coefficient method. A design horizontal seismic coefficient of 0.30 was adopted based on the seismic history, the fault distribution, design horizontal seismic coefficients of nearby bridges, and estimated acceleration in the past earthquakes. Because the weight of the superstructure of the barrage was reduced before the start of construction to further improve earthquake resistance, the barrage can withstand a horizontal seismic coefficient of up to 0.42 [2]. This value is greater than a value of 0.30 for the reinforced concrete (RC) piers of the Hanshin Expressway Wangan Line, which suffered little in the 1995 Hyogo-ken Nanbu earthquake. The value of 0.42 is also better than design horizontal seismic coefficients of 0.415 and 0.345 for the RC piers of the Tengu Bridge and the Isuzu Bridge, which suffered only minor damage in the 1974 Izuhanto-Oki earthquake (9 May 1974; magnitude 6.9) even though the bridges were located at only approximately 1 km from the activated fault.

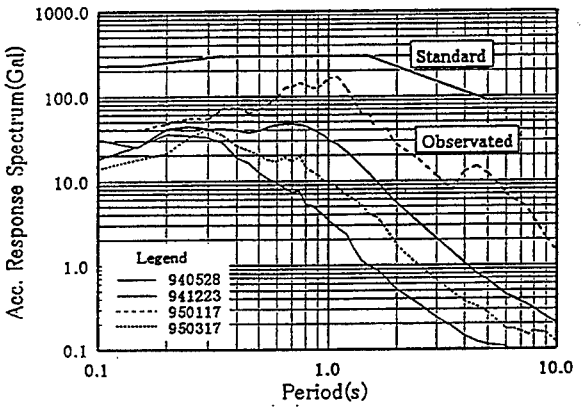

Fig.4 Acceleration Response Spectrum

To investigate earthquake resistance, the barrage underwent a dynamic analysis using the response spectrum method. A standard acceleration response spectrum used for the analysis is presented in Fig. 4. The spectrum is based on a strong-motion accelerogram recorded on the ground, using a damping constant of 0.05 and an acceleration close to that of the design horizontal seismic coefficient. The analytical results, obtained after properly correcting the effect of the ground, indicated that there would be no stress exceeding the seismic stress estimated from the seismic coefficient method.

2. CHARACTERISTICS OF EARTHQUAKES

Characteristics of earthquakes observed at the Nagaragawa Estuary Barrage are summarized in Table 2, and acceleration response spectra of seismograms (parallel to barrage axis; damping coefficient of 0.05) for different earthquakes recorded at the basement of the office are superimposed in Fig. 4.

Though the maximum amplitude of acceleration observed was not great, seismic records covering a wide range from a depth of approximately 100 m to a barrage column was obtained in an earthquake, and some seismograms contain a frequency component close to the natural frequency of the barrage column. Thus, these records are considered to be useful for improving the precision of the seismic design by investigating the whole

Table 2 Chracteristics of Earthquakes

	Date	Magnitude	Depth (km)	Distance (km)	Maximum Accerelation (Gal)	Pedominant Frequency (Hz)	Maximum Accerelation (Gal)	Pedominant Frequency (Hz)
(1)	1994. 5.28	5.2	44	46	17.48	0.95	23.83	1.12
(2)	1994.12.23	4.6	42	42	10.39	3.00	11.94	2.97
(3)	1995. 1.17	7.2	14.3	160	39.60	0.94	40.28	0.87
(4)	1995. 3.17	5.1	11	109	11.37	2.97	11.44	3.00
					Perpendicular to Barrage Axis		Parallel to Barrage Axis	

Notes Date, Magnitude, Depth:The Meteorlogical Agency release
Distance:Calculated Value by Research Institute of WARDEC
Maximam Accerelation, Pedominant Frequency:Observed Value on the Basement of the Office

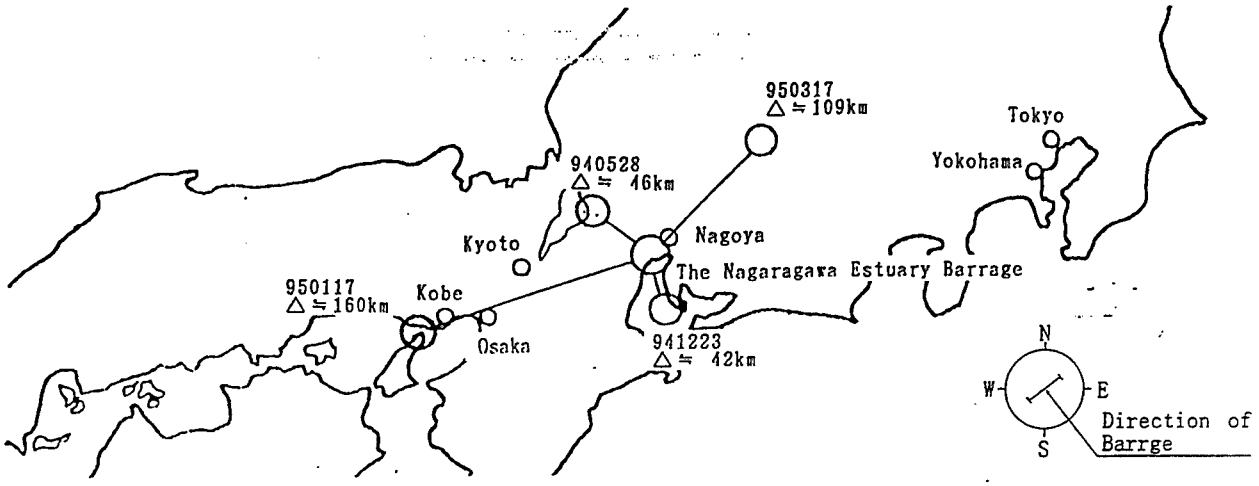

Fig. 5 Location of The Barrage and The Epicenters

response of the barrage.

The location of the barrage and the epicenters of the investigated earthquakes are shown in Fig. 5. The earthquakes (1) to (4) in Table 2 are respectively referred to as earthquakes 940528, 941223, 950117, and 950317.

3. ARRANGEMENT OF SEISMOMETERS

A total of four seismometers (accelerometers) including eight transducers are installed at the Nagaragawa Estuary Barrage: two seismometers including four transducers for each of the P9 barrage column and the office areas.

The barrage main structure can be divided into the footing, the barrage column, the gate columns, and the operating room. Because the structural components greatly differ in their shapes and material characteristics, they are expected to exhibit quite different seismic responses. To verify this point, transducers are installed on each of the different structural components of the P9 typical section barrage column. The transducers on the footing and on the center of crossbeam between gate columns are on the central axis of the direction perpendicular to barrage axis, the transducer on the floor slab of the operating room is on the barrage axis, and the transducer on the crest of barrage is at the intersection of the two axis.

To investigate the response of the ground,transducers are also installed at levels of T.P. (Tokyo Peil) -97.51 m, -52.60 m, and -2.90 m in a bore hole drilled within the office site. The bearing piles of the barrage is supported by the first gravel layer at the level of T.P. -52.60 m. The bedrock surface corresponds to the second gravel layer at the level of T.P. -97.51 m. A level of T.P. -2.90 m corresponds to the ground surface when the embankment is removed. Because seismic records of strong ground motions observed at a particular barrage site is generally limited, strong ground motions observed at sites other than the barrage site are converted to the ground motion on the bedrock surface of the barrage site, and then accelerograms deduced by incorporating the ground characteristics of the barrage site are selected to carry out a dynamic analysis of the barrage. This approach improves the precision of the analysis. The transducer installed on the basement of the office has the same purpose as the transducer installed at T.P. -2.90 m, but is likely to be affected by the building structure. Whether a temporary inspection is needed after an earthquake is decided based on the ground motion observed at the basement.The arrangement of seismometers is described in Fig. 6.

The transducers installed in the office, the P9 barrage column, and the ground are connected to different recorders to cope with different seismic components. While the transducers installed on the footing, the crest of barrage, and

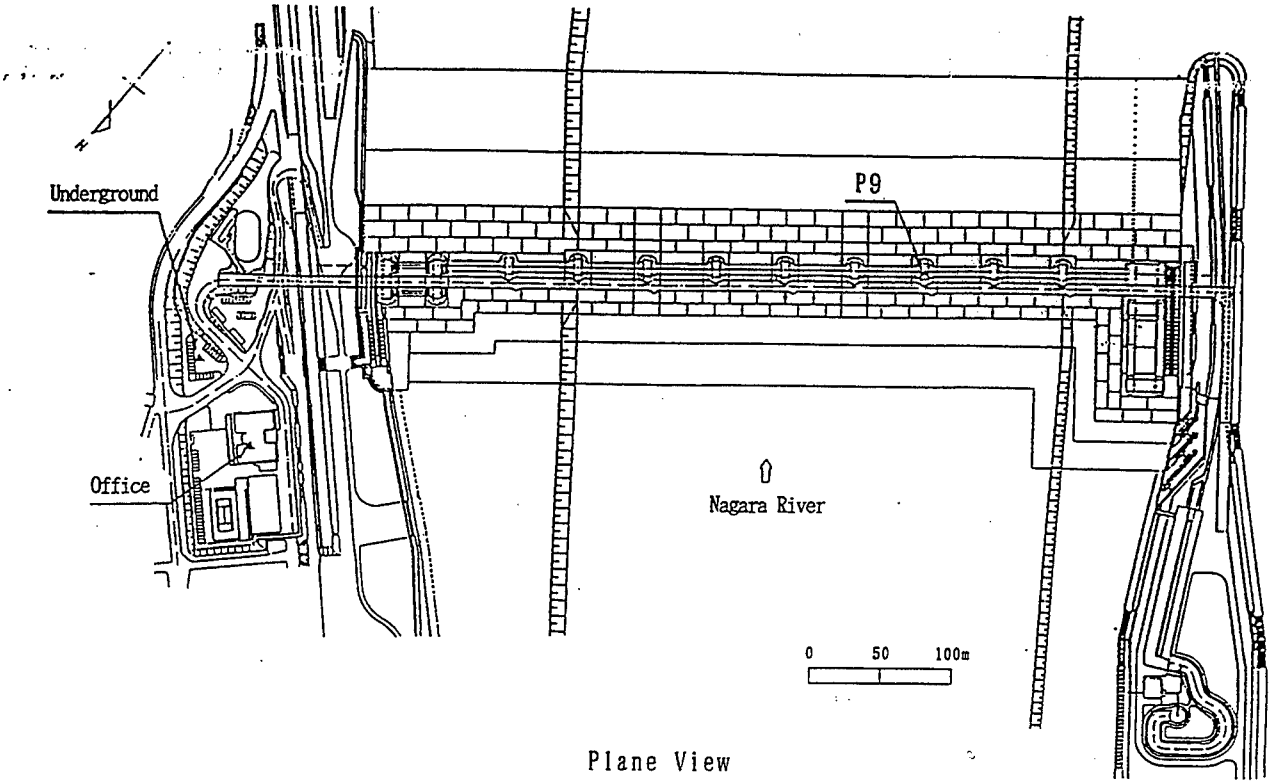

Plane View

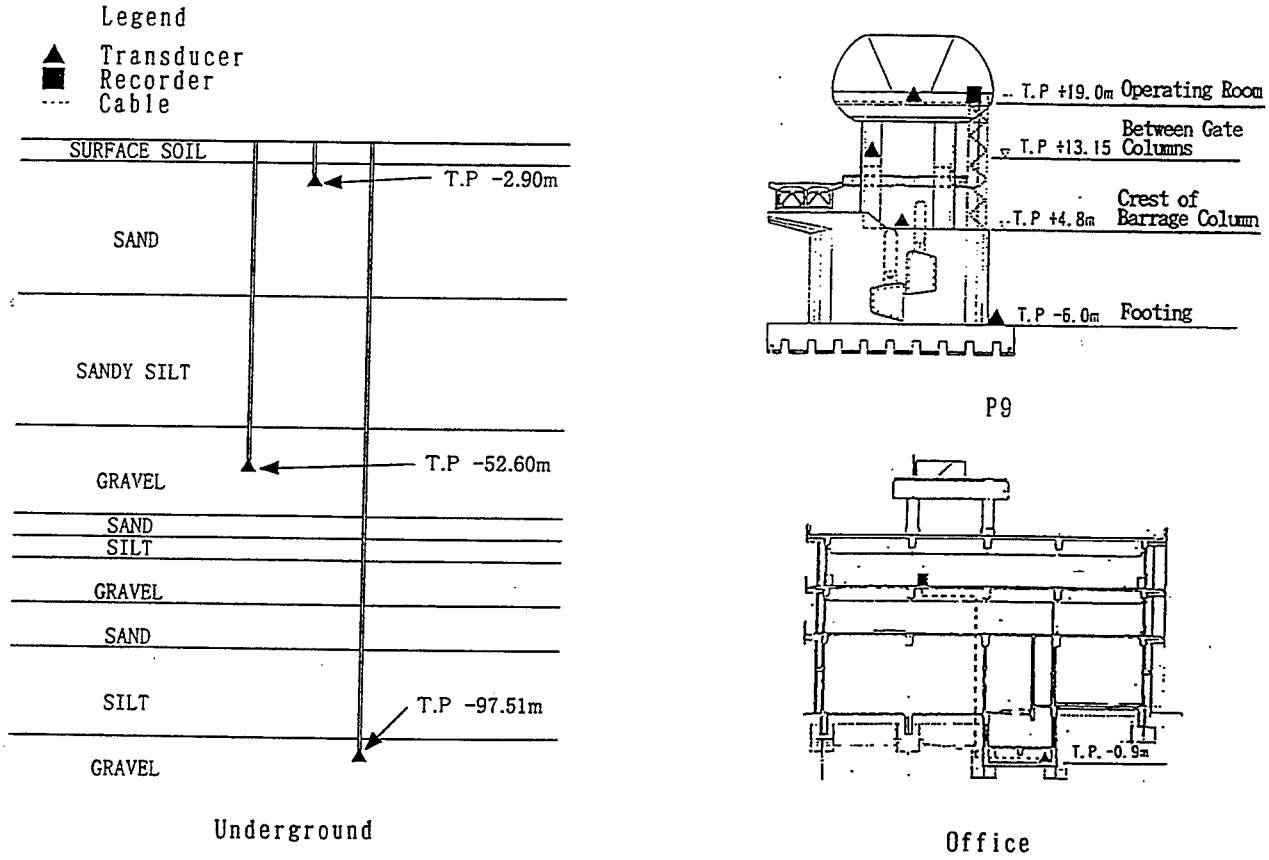

Underground

Office

Detail Drawing

Fig.6 Arrangement of Seismometers

the floor slab of the operating room are connected to the same recorder, the transducer installed on the center of crossbeam between gate columns is connected to another recorder. Here, the transducer and the recorder related to the office is referred to as seismometer 1, the transducers and the recorder related to the footing, the crest of barrage, and the floor slab of the operating room are referred to as seismometer 2, the transducer and the recorder related to the center of the crossbeam between gate columns is referred to as seismometer 3, and the transducers and the recorder related to the ground is referred to as seismometer 4.

Observation started on 1 April 1994 for seismometers 1 and 2, on 13 December 1994 for seismometer 3, and on 11 March 1995 for seismometer 4. Because seismometers 2 and 3 were adjusted in January 1995 after seismometer 3 was installed, they did not record the data of earthquake 950117.

4. SEISMIC BEHAVIOUR

4.1 Observed Seismograms

Time histories of acceleration and displacement for each directional component are shown in Fig. 7 for the main tremor segments of the observed seismograms (3-s segments for earthquakes 940528, 941223, and 950317, and a 20-s segment for earthquake 950117). Furthermore, acceleration Fourier spectra of the direction parallel and perpendicular to barrage axis, acceleration transfer functions, and maximum amplitude distributions of acceleration and displacement are respectively given in Figs. 8, 9, and 10.

The acceleration Fourier spectrum ratio given by the vertical axis of Fig. 8 is a nondimensional value of acceleration Fourier spectrum divided by the value (shown at the upper right of each diagram) that corresponds to the dominant frequency at the floor slab of the operating room (for the P9 barrage column data) or at the office (for the office and the ground data). Transfer functions deduced from a ground response analysis, which will be discussed later, are also provided in Fig. 9.

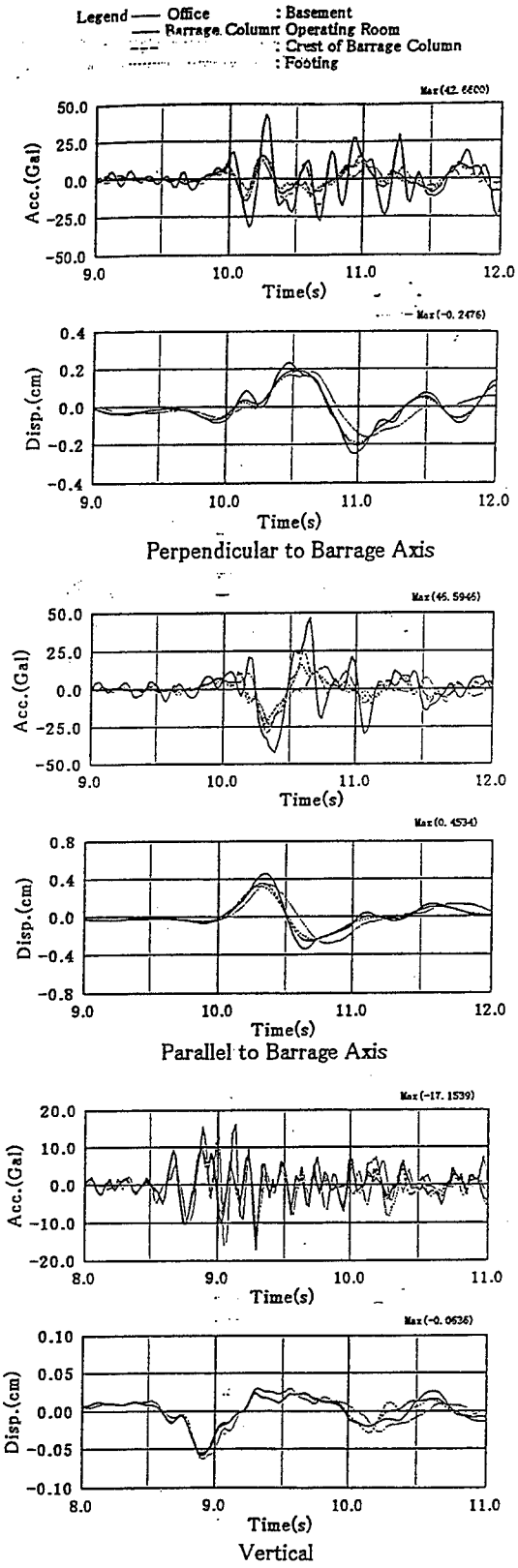

Fig.7(1) Time Histories (940528)

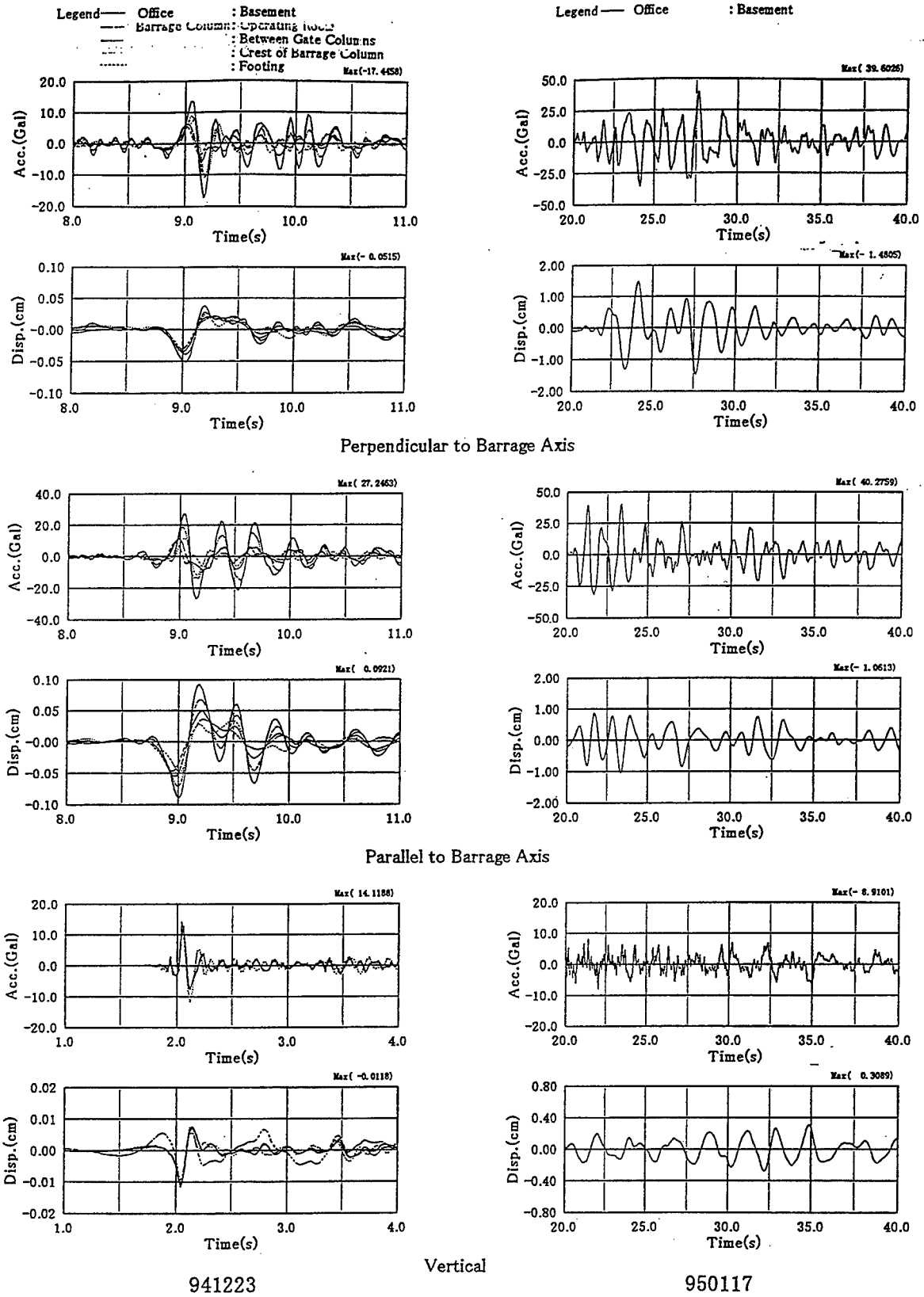

Fig.7(2) Time Histories (941223, 950317)

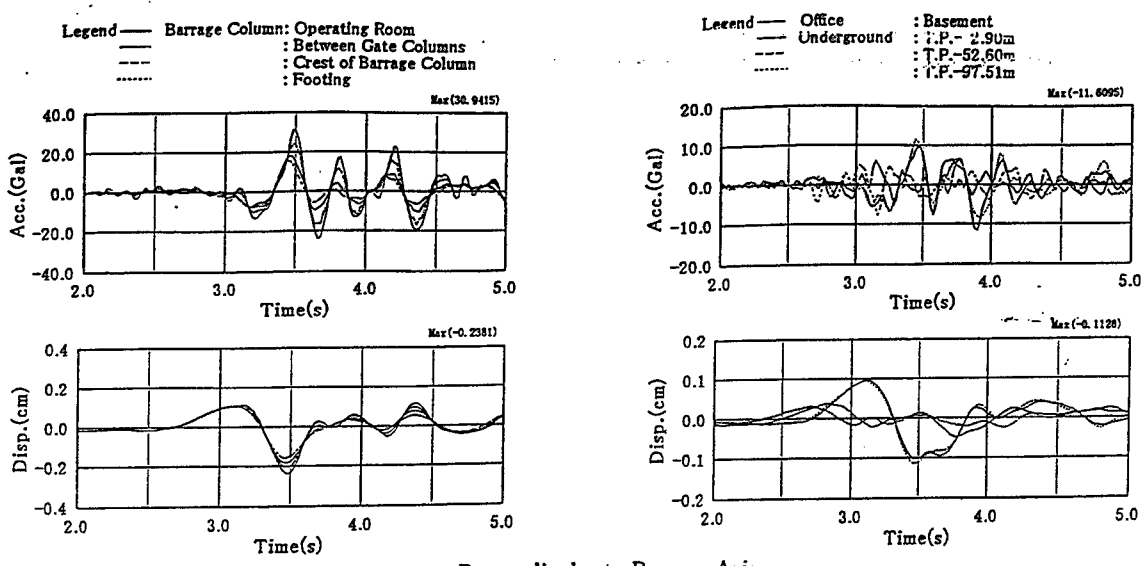

Perpendicular to Barrage Axis

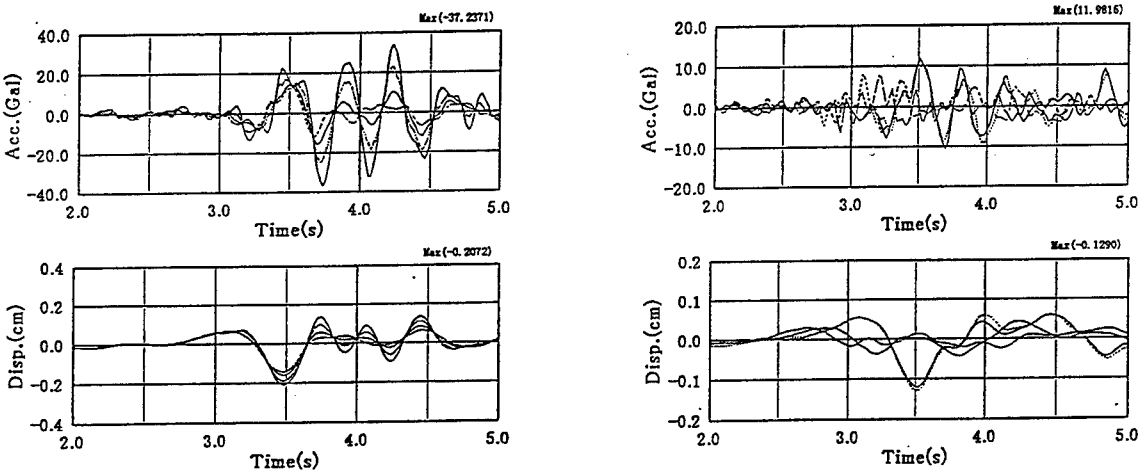

Parallel to Barrage Axis

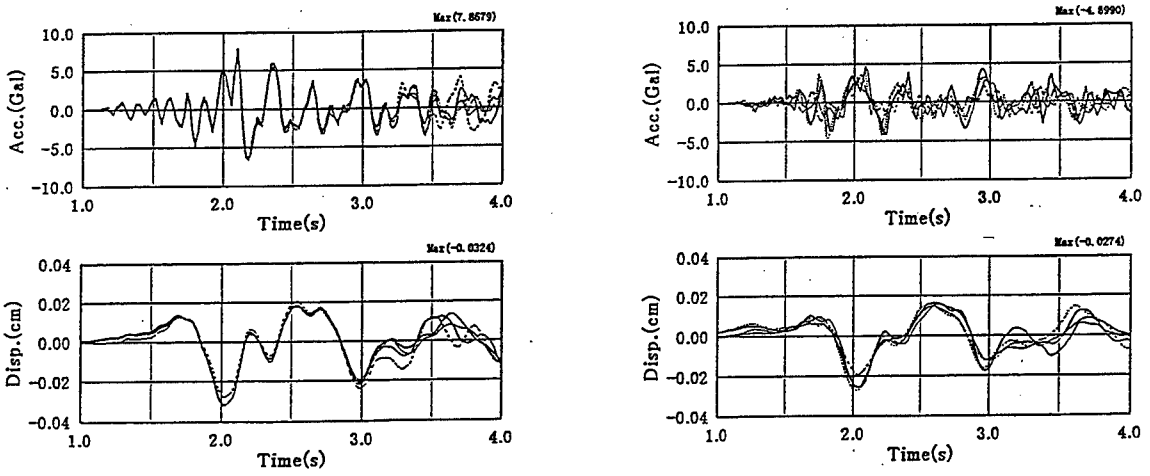

Vertical

Barrage Column P9 Underground

Fig.7(3) Time Histories (950317)

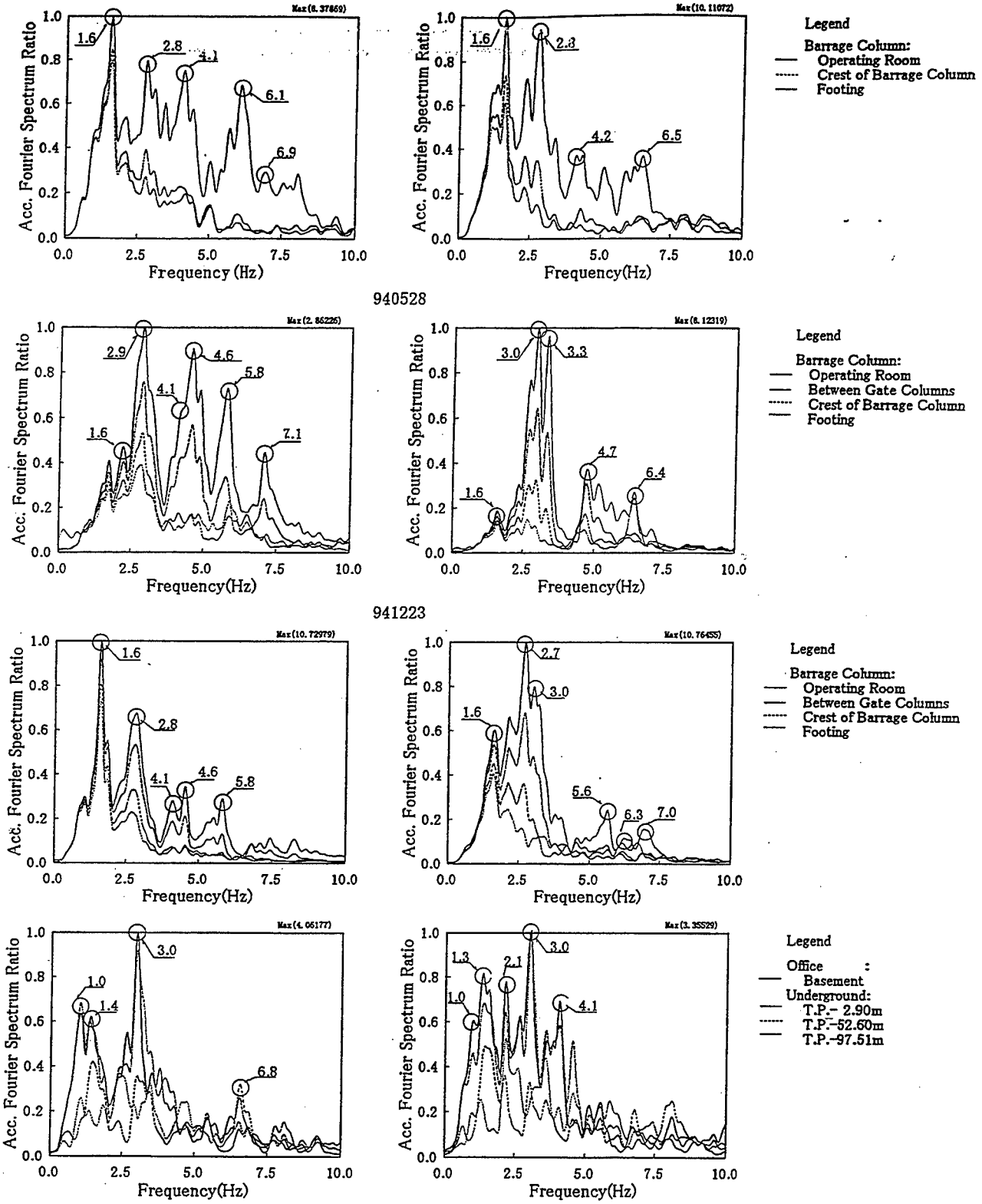

Fig.8 Acceleration Fourier Spectrum

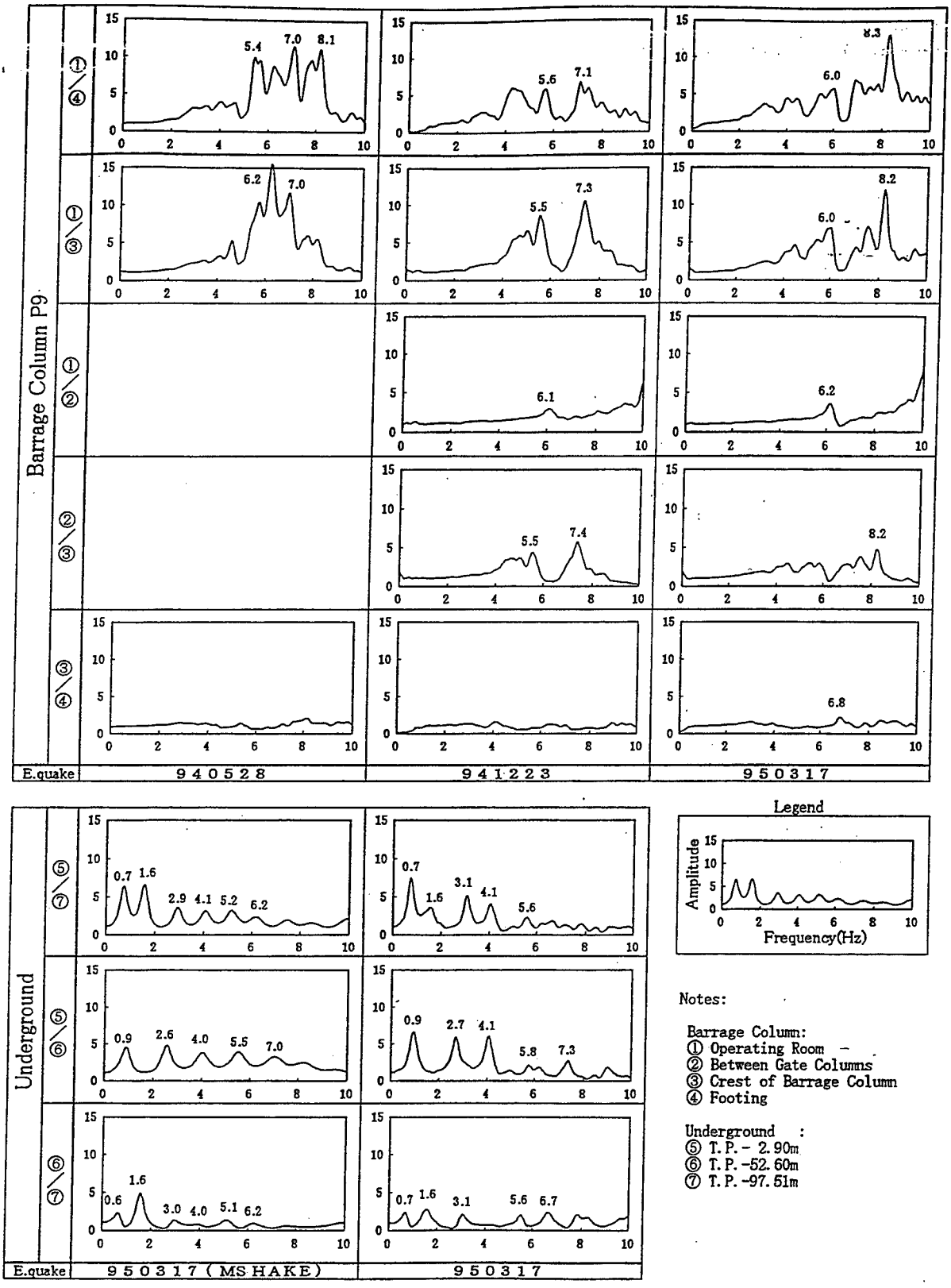

Fig.9(1) Accelaration Transfer Functions(Perpendicular to Barrage Axis)

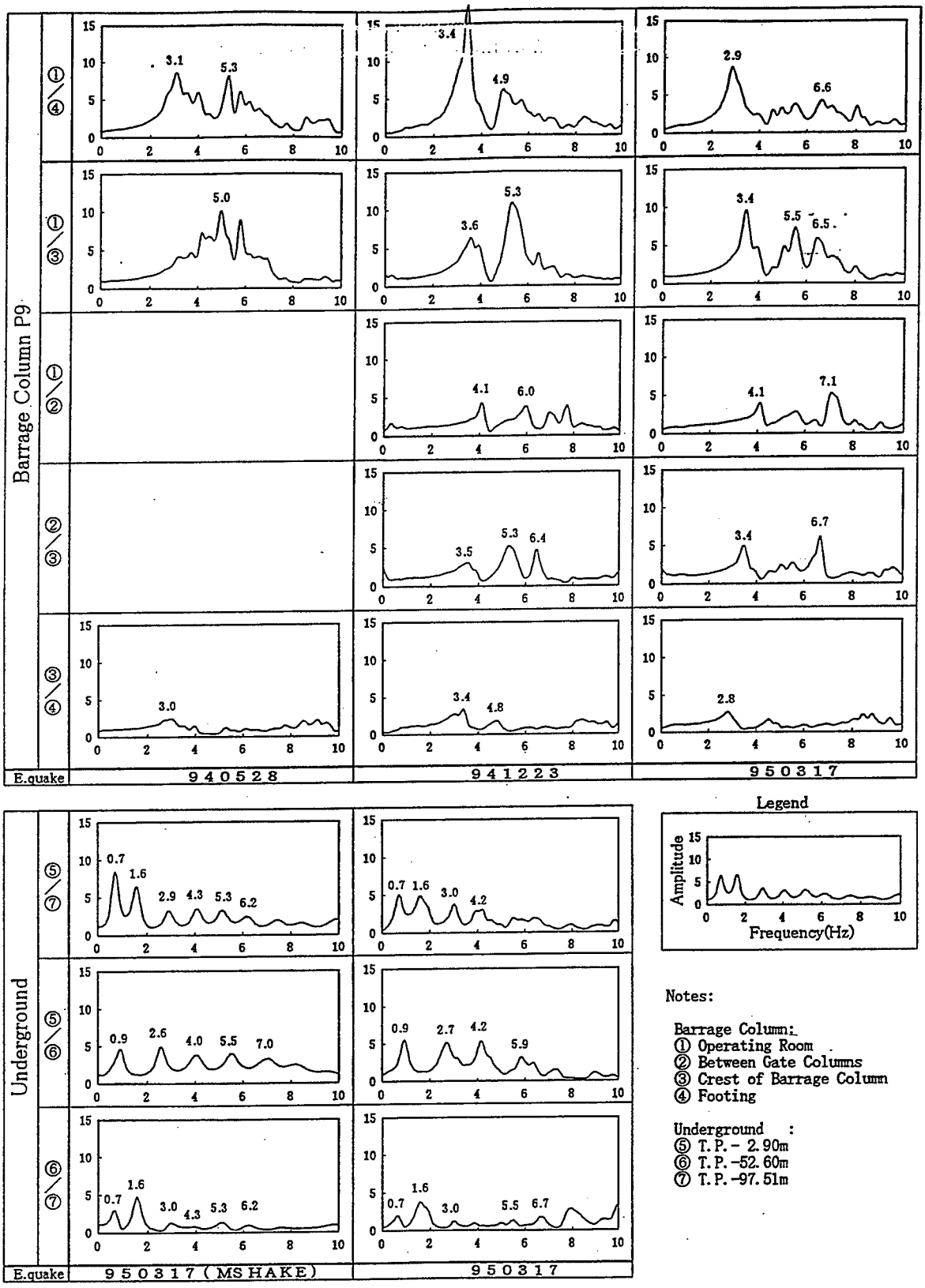

Fig.9(2) Accelaration Transfer Functions(Parallel to Barrage Axis)

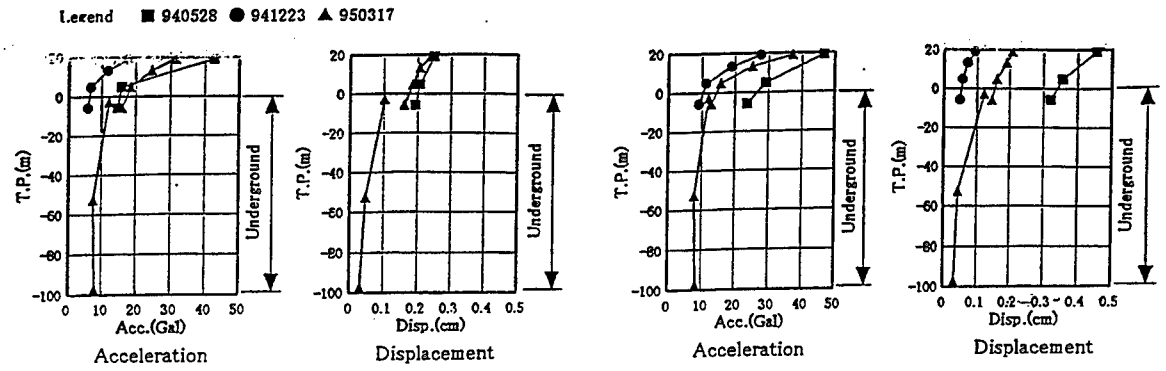

Fig.10 Maximam Amplitude Distribution

4.2 Ground Behaviour

Dominant frequencies (response to upward transmitting waves) obtained from a ground response analysis, in which the seismograms of earthquake 950317 recorded at T.P. -97.51 m and -52.60 m in the ground were used as input motions, are listed in Table 3.

With a premise that the maximum amplitude of acceleration in the input seismogram is not great, the following are suggested from Fig. 8, Fig. 9, and Table 3 regarding frequency characteristics.

(1) A frequency of 0.7 Hz deduced form the ground response analysis prevails at a depth of T.P. -52.60 m or greater in the ground, but a greater frequency of 0.9 Hz (with a shorter period) prevails in the shallower ground. On the other hand, 1.0 Hz prevails in the acceleration Fourier spectra recorded at T.P. -2.90 m in the ground and at the basement of the office.

(2) A frequency of 1.6 Hz deduced from the ground response analysis is prominent at a depth of T.P. -52.60 m or greater in the ground, but is not observed in the shallower ground. However, this frequency is prominent in the acceleration Fourier spectra of the barrage column, regardless of the seismogram or the directional component. This indicates that the vibration at the end of the pile is transmitted up to the barrage column. This trend is more prominent in the direction perpendicular to barrage axis, in which the stiffness of piles, or the number of piles, is greater compared to the direction parallel to barrage axis.

(3) While a frequency of 3.0 Hz deduced from the ground response analysis is prominent at a depth of T.P. -52.60 m or greater in the ground, a smaller frequency of 2.6 Hz (with a longer period) prevails in the shallower ground. Frequencies of 2.7-3.0 Hz are prominent in the acceleration Fourier spectra of the barrage column, regardless of the seismogram or the directional component.

The following is suggested from Fig. 10 regarding the maximum amplitude of acceleration and displacement.

- The absolute values of maximum amplitude do not change significantly at a depth of T.P.

Table 3 Dominant Frequencies

	Mode	Frequency (Hz)	
① / ③	1st	0.7 (1.43)	0.7 (1.43)
	2nd	1.6 (0.63)	1.6 (0.63)
	3rd	2.9 (0.34)	2.9 (0.34)
① / ②	1st	0.9 (1.11)	0.9 (1.11)
	2nd	2.6 (0.38)	2.6 (0.38)
	3rd	4.0 (0.25)	4.0 (0.25)
② / ③	1st	0.6 (1.67)	0.7 (1.43)
	2nd	0.6 (1.67)	1.6 (0.63)
	3rd	3.0 (0.33)	3.0 (0.33)
		Perpendicular to Barrage Axis	Parallel to Barrage Axis

Notes ①: T.P.- 2.90m
②: T.P.-52.60m
③: T.P.-97.51m
In of parentheses: Period(unit:s)

-52.60 m or greater in the ground, but increase rapidly in the shallower ground. This trend is in agreement with the geologic feature that the first gravel layer and the underlying beds are hard.

4.3 Behaviour of The Barrage

Characteristic values, such as frequencies, of the typical section barrage column obtained from a modal analysis are listed in Table 4.

With the premise that the maximum amplitude of observed acceleration is not great, the following are suggested from Figs. 8 and 9 regarding frequency characteristics.

(1) In the direction perpendicular to barrage axis, the frequency components of the ground are directly reflected in the acceleration Fourier spectra of the recorded seismograms, with dominant frequencies of 1.6 Hz and 2.8-2.9 Hz. In addition, 4.1 Hz, which is close to the first order value of 3.8 Hz deduced from the modal analysis, is observed in earthquakes 940528, 941223, and 950317; 6.1 Hz, which is close to the second order value of 5.9 Hz deduced from the analysis is observed in earthquake 940528; and 5.8 Hz is observed in earthquakes 941223 and 950317.

(2) In the direction parallel to barrage axis, frequency components of 1.6 Hz and 2.7-3.0 Hz are dominant in the acceleration Fourier spectra of the recorded seismograms. The component of 2.7-3.0 Hz corresponds to the first order value of 2.9 Hz deduced from the modal analysis. The prevalence of 1.6 Hz and comparison with the responses observed in the direction perpendicular to barrage axis indicate that the frequency components of the ground are also enhanced. In addition, the second order value of 6.3 Hz deduced from the analysis is observed in earthquake 950317; 6.4 Hz, which is close to the second order value, is observed in earthquake 941223; and 6.5 Hz is observed in earthquake 940528.

(3) The first order mode found in the ground is not prominent in the barrage column probably because the maximum amplitude of observed acceleration is not great.

The following are suggested from Fig. 10 regarding the maximum amplitude of acceleration and displacement.

(1) Regardless of the seismogram, the maximum absolute amplitude of acceleration and displacement in the direction parallel and perpendicular to barrage axis becomes greater, in general, in the order of the footing, the crest of barrage, the gate columns, and the floor slab of the operating room. Also regardless of the seismogram, the difference in the maximum amplitude between the footing and the crest of barrage is greater than that between the crest of barrage and the floor slab of the operating room. This agrees with the structural properties of the barrage column and the gate column (the barrage column has a greater stiffness).

(2) With the exception of earthquake 950317, the maximum absolute amplitude of acceleration and displacement is generally greater in the direction parallel to barrage axis than in the direction perpendicular to barrage axis. This is probably due to the anisotropy of stiffness (elongated in the direction perpendicular to barrage axis) in the barrage column and the gate column.

Table 4 Natural Frequencies and Others

Frequency and Others		Mode							
		1st	2nd	3rd	total	1st	2nd	3rd	total
Frequency (Hz)		3.84	5.88	6.67		2.94	6.25	7.14	
Period (S)		0.26	0.17	0.15		0.34	0.16	0.14	
EMR (%)	x	59.83	34.09	0.25	94.17	41.04	47.43	0.00	88.47
	y	0.20	0.00	99.40	99.60	0.00	0.00	99.92	99.92
		Perpendicular to Barrage Axis				Parallel to Barrage Axis			

Notes x :Perpendicalar or Parallel to Barrage Axis y :Vertical

4.4 Verification of The Behaviour of The Ground and The Barrage

The responses of the ground and the barrage were calculated by using the seismograms of earthquakes 940528, 941223, and 950317 recorded at the basement of the office (the ground level), and the analytical results were compared with the observed records.

Fig. 11 shows the analytical model, which is a barrage column pile foundation system of the typical section barrage column with a closed gate condition in the direction parallel to barrage axis. The ground part is modeled by the finite element method, and the structural part is modeled as a frame system. Because the maximum amplitude of acceleration is not great, the model was treated as an elastic body to facilitate the evaluation of analytical results.

As an example, observed and calculated time histories of acceleration are compared in Fig. 12. Though restriction is provided by the premise that the maximum amplitude of input acceleration is not great, the general agreement between the observed and the calculated results confirms the validity of the whole data.

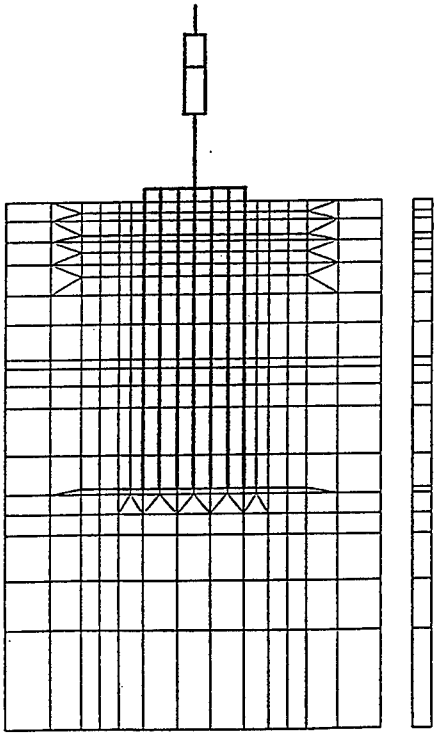

Fig.11 The Analytical Model

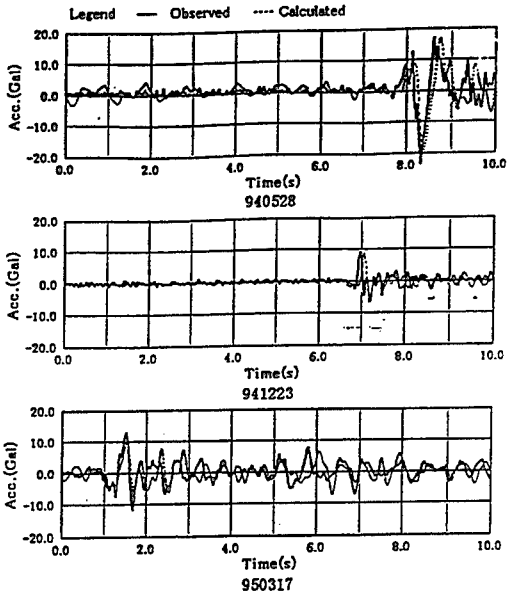

Fig.12 Time Histories Acceleration

5. SUMMARY

On condition that the maximum amplitude of input acceleration is not great, some trends are identified in the surrounding ground and the seismic behaviour of the Nagaragawa Estuary Barrage.

After the 1995 Hyogo-ken Nanbu earthquake, characteristics of seismic ground motions are being studied in various aspects. Further characteristics of the seismic behaviour of the Nagaragawa Estuary Barrage will be revealed if seismograms with a great maximum amplitude of acceleration are obtained at the barrage.

ACKNOWLEDGEMENT

The authors are grateful to Professor Choshiro Tamura of Nihon University for providing valuable advice.

REFERENCES

1)Toru Kuwabara :The Nobi and the tilted block movement,1968

2)River Bureau, Public Works Reserch Institute and Chubu Reginal Construction Bureau of Ministory of Construction,WARDEC:Technical Report of the Nagaragawa Estuary Barrage, (appendix),1995

Preliminary Results of Initial Intake Tower Substructure Experimentation

by

Richard C. Dove, PE[1]

ABSTRACT

This paper contains a brief overview of some aspects of the results of the first Intake Tower Substructure (ITS) experiment. The results of this experiment indicate that ductility can be found in the response of lightly reinforced intake towers. The application of displacement-based analysis techniques to problems of this sort was also examined and found to show promise.

KEYWORDS: Earthquake, reinforced concrete, ductility, intake towers

1 INTRODUCTION

In the event of an earthquake, it is vitally important that the catastrophic failure of a dam and subsequent sudden release of the reservoir be prevented. An important part of the prevention of such a failure is maintaining the ability to control the release of water after the earthquake. If a dam is damaged, the prompt and controlled lowering of the water level will remove hydrostatic pressure and help to prevent the propagation of the damage into a catastrophic failure. For most earthen dams, and some concrete dams, the release of water is controlled through a reinforced concrete intake tower. The functional survival of such towers is therefore very important and is the main concern of this research effort.

The success of the tower in resisting failure is dependent upon the magnitude of the earthquake loads and the structural details controlling the nonlinear dynamic response and failure mechanisms of the specific tower. Currently, available analysis techniques and engineering guidance for intake towers may not properly include these factors. The development and validation of better design and analysis procedures and guidance is the primary goal of this research effort. The research conducted and reported in this paper is the initial step in a planned multi-year effort to accomplish this goal. The paper contains a brief overview of some aspects of the results of the first ITS experiment. Complete coverage of this subject will be contained in a formal technical report, now in preparation.

1.1 Objective

The overall objective of the ITS experimental series is to understand the nonlinear response of a lightly reinforced intake tower. The ultimate objective is the development and/or validation of approximate or simplified analysis procedures for the evaluation of the ductility of existing intake towers.

[1]Research Structural Engineer
USAE Waterways Experiment Station
Vicksburg, MS 39180

1.2 Approach

The first ITS experiment consisted of the static loading to failure of a 1/8th-scale model of a typical intake tower configuration. In addition to modeling a typical Corps tower, the physical properties of the component were selected to be similar to the Lake Burnt Mills tower. This tower will be decommissioned in FY97, and it is possible that the U.S. Army Engineer Waterways Experiment Station (WES) will have the opportunity to conduct dynamic experiments on the structure. Correlation of the results of the ITS experiment with results of these full-scale dynamic experiments will be of great interest. The ITS-1 experiment took place at the Structures Laboratory loading floor using the large-scale load frame constructed to conduct this and subsequent experiments. The frame was designed to withstand a load of 200 kip vertically and 400 kip horizontally at the maximum specimen height of 20 ft. This load capacity is based upon preliminary analysis of 1/8th- to 1/6th-scale models of intake towers spanning the structural characteristics of interest. Figure 1 shows the Large Scale Load Frame.

Three specific structural responses were identified for study. The first is the overall ductility response of the model under a one-way excursion load. Basically, the ductility response can be defined as the load-deflection or moment-curvature relationship of the model as it deflects into the plastic range to failure. The ductility of a structure is often given as the ratio of total deflection or curvature at failure, to the maximum elastic response.

The second area of interest is the response of the base of the model. The base of a cantilever structure is where moment loads are greatest and is obviously a critical section. In actual towers, a construction joint is usually found at this critical section. The conjunction of maximum loads with a construction joint indicates that the response of the joint may have a major influence on the ductility response of the structure. For this reason, modeling this joint and gathering data on its response were expected to be very important. Measurements of the response of this region of the structure are also important to the development of simplified methods of analysis. In order to reduce a three-dimensional analysis of a tower to a two-dimensional problem, the tower can be idealized as a series of parallel walls attached to perpendicular walls forming a series of I-beams. The effective width of the flange of the equivalent I-beam is analogous to the effective width of a T-beam formed by a reinforced beam and a reinforced floor slab. Current guidance as to the effective width is based on elastic theory and, hence, needs to be carefully considered before application to a problem where plastic response is expected. Measurement of the distribution of stresses and strains in the plane of the cold joint, and monitoring of the progression of plastic response were identified as important.

Currently, a displacement-based analysis method that seems very promising for application to problems of this type is being evaluated. This method attempts to explicitly consider earthquake-induced structural displacements. A major component of this analysis is the plastic hinge length. For a tower model, the plastic hinge length can be defined as the height of the zone at the base of the tower, over which plastic rotations must occur so that the total deflection at the top of the tower is equal to the deflection due to elastic and plastic rotations. The plastic hinge length is an empirical and analytical parameter, and the measurement of the distribution of stresses and strains in the plastic hinge zone and monitoring of the progression of the formation of the plastic hinge were expected to be very important.

The third area of interest is the dynamic characteristics of the model. As part of the validation of the analytical model, a pre-experiment modal survey of the experiment model was conducted. The mode shapes and frequencies generated were to be compared to the calculated values. Generation of mode shapes is an elastic process and is useful in the validation of the elastic model. Modal surveys of the experiment model during and after experimentation were also conducted. The surveys were expected to yield information on the changes in the mode shapes and frequencies

due to the damage accumulated during experimentation.

1.3 Experiment Configuration

Figure 2 shows the overall experiment layout for the ITS-1 experiment. The 50-kip hydraulic loader, mounted horizontally, was used to provide a one-way excursion load at the top of the experiment model. This 50-kip loader is servocontrolled and is capable of applying a variety of load/time histories including load reversals, a capability that will be utilized in later experimentation. The loader assembly can incorporate a load cell for measurement and control of the applied load. The 50-kip rams, mounted vertically, provided simulation of the dead load of the full-scale tower. The dead load was held constant throughout the experiment.

The dimensions and configuration of the experimental component are shown in Figure 3. The component consisted of an 18-in. thick 9-ft by 9-ft heavily reinforced concrete base that was bolted to the load floor, a 40-in. by 52-in., 10-ft tall tower section with 5-5/8-in. thick walls, and a steel loading ring. All concrete was to have a 28-day strength (f'_c) of 3,500 psi. A construction joint (cold joint) was located at the base of the tower section for ease of construction and to simulate an almost universal existence of cold joints in critical sections of prototype structures. This cold joint was expected to have a significant impact on the response of the component and was carefully constructed.

The reinforcing layout of the tower section is shown in Figure 4. The vertical reinforcement consisted of two layers of D1 deformed wire at a 2-in. center-to-center spacing. The horizontal reinforcement consisted of two layers of D1 deformed wire at a 1-1/2-in. center-to-center spacing. The area of a D1 wire was 0.01 $in.^2$ and, with the specified spacing, the vertical steel percentage (ρ_v) was 0.18%. The specified horizontal steel percentage (ρ_h) was 0.24%. The total steel percentage is, thus, 0.42% with a ρ_v-to-ρ_h ratio of 0.75. The D1 steel was heat-treated to an actual yield strength of 45 ksi. These values are representative of the lower midrange of those encountered in the population of existing Corps intake towers.

2 EXPERIMENTAL RESULTS

A one-way excursion experiment was completed on ITS-1 on 26 September, 1995. The experiment was conducted using the large scale load frame constructed for this and subsequent experiments. Load was applied to the specimen with hydraulic loaders. A vertical load was applied to the structure and held constant throughout the experiment to simulate dead load. A horizontal load was applied by a deflection-controlled loader at a rate of 0.001 in./sec. The experiment was temporarily stopped six times to allow for the modal survey, measurement, and photography of the structure. The experiment required approximately 4 hr to conduct. Seventy-two channels of active data were recorded, 10 modal surveys were conducted, and passive measurements of structural response were recorded. Video and still photography were included. The following presents the results of the experiment as well as some of the preliminary and post experiment analyses of the structure.

2.2 Structural Response

Two photographs of the response of ITS-1, at an imposed deflection of 2 in., can be seen in Figures 7 and 8. Visual inspection of the model during loading led to several observations. Damage to the model was limited to the bottom of the tower section at the interface with the rigid base. The damage consisted of one tension crack that extended across the east (tension) wall and into both the north and south side walls. The tension crack did not appear to indicate simply a failure of the cold joint located in this area. The crack did not follow the interface of the cold joint, but rather appeared to dip downward below the cold joint into the concrete base material before returning to the surface at the far side of the wall. No evidence of a crushing failure of the concrete in the west (compression) wall was observed. Figure 8

shows a close-up view of the south corner of the east wall at the maximum-imposed deflection of 2 in. On the left of the photograph ruptured reinforcement is clearly visible with the necking and elongation that are typical of a ductile tension failure. The ruptured rebar was observed across the entire east wall as well as for a distance of approximately 21.5 in. along the north wall and 16.5 in. along the south wall as measured from the east wall. The crack sloped downward into the experimental specimen and extended below the interface of the tower section and into the base slab.

2.3 Active Instrumentation Response

Seventy-two channels of active data were recorded during the experiment. Of these channels, 57 were strain measurements, six measured deflections of the model, and two measured deflection and load in the horizontal hydraulic loader. The constant vertical load applied to the top of the structure was monitored but not recorded. Recording took place at 10 samples per second and, thus, during the approximate four hours of the experiment, a total of about 1,000,000 samples were taken for the 72 channels. All plotting and data analyses were conducted with the structural response plotted against the deflection imposed on the model by the horizontal loader as measured by the loader deflection gage.

2.4 Load Response

The most important response measured in this experiment is the relationship of the horizontal load imposed at the top of the structure to the horizontal deflection measured at the same location. The relationship is the most direct measurement of the deflection ductility of the structure and also relates indirectly to the curvature ductility. Figure 9 shows the force imparted by the horizontal loader versus the deflection of the loader. The force was measured by a load cell mounted on the loader, deflection was measured by the loader's internal deflection gage.

Examination of the load-deflection history shows a linear-elastic response up to a deflection of 0.148 in. with a load of 29,292 lb. At this point, the section appears to crack resulting in a 11.5% reduction in the load carried by the structure to 25,928 lb at a deflection of 0.175 in. The decrease in load capacity after cracking was expected, as the cracking moment capacity of the section had been calculated to be less than the yielding moment in this lightly reinforced member. An abrupt downward excursion of the load curve below the general trend of the curve at about 0.17 in. is due to the fact that the experiment was put on hold at this deflection so that a modal survey could be conducted. During the delay, and subsequent holds, the structure relaxed slightly, causing a reduction of the load carried. When the experiment was restarted, the load curve rose back to approximately the pre-hold value and continued. Therefore, the modal survey holds conducted at the deflections of 0.17 in., 0.23 in., 0.38 in., 0.45 in., 0.68 in., 0.98 in., and 1.98 in. apparently had little effect on the overall response of the structure.

After the decrease in load to 25,928 lb at 0.175 in., a gradual increase in load of about 2.3% of the peak value, to 26,600 lb at a deflection of 0.72 in. was experienced. The increase in load may reflect the redistribution of stress in the section as well as strain hardening of the rebar as yielding occurred. At about 0.72 in., a pronounced decrease in load began. A reduction of approximately 30% of the peak value was incurred, resulting in a value of 17,763 lb at a deflection of 1.96 in. The decrease in load reflects the rupturing of steel as deflection continued. The load appears to be asymptotic to a value of 17,763 lb, reflecting the diminishing contribution of the reinforcing steel to the capacity of the section to the point where the simple restoring moment of the actual and imposed dead load contributed the majority of resistance.

The deflection ductility is readily apparent on further examination of the load-deflection curve. Deflection ductility can be defined as the ratio of the deformation that a structure or element can undergo without a significant loss of initial

yielding resistance to the initial yield deformation (Bertero). Using this definition, with the deflection at initial yielding of 0.175 in., a maximum deflection before significant loss of initial yielding resistance of 0.75 in., the deflection ductility is 4.3.

A deflection ductility of 4.3 is a significant finding in that displacement ductilities of conventionally reinforced concrete can be expected to be in a range of between 3 and 5. In conventionally reinforced concrete, a similar ductility allows load-reduction factors in the range of between 1/2 and 1/3. However, load reduction is only allowed if it can be demonstrated that brittle failure mechanisms do not lead to an unacceptable strength reduction with cyclic loads. This was not a cyclic experiment and, therefore, can only be used to demonstrate that the experiment model has the potential for significant ductility. Future cyclic load experiments will show how much of this ductility can be safely utilized.

2.5 Deflection Response

Horizontal deflections were measured at 2-ft intervals up the structure. These measured deflections are shown plotted against the deflection imposed on the structure by the horizontal loader in Figure 10. Two distinct regions can be seen in the plot. The curve changes shape and slope at the imposed deflection of 0.148 in. This is the same deflection that corresponds to the onset of cracking, as seen in the load-deflection curve discussed in the previous section.

Both the pre-cracking and post-cracking deflections were closely examined. The pre-cracking deflections were relatively small for measurement with the gages used; however, some trends were apparent. Curves were fit to the data and used to generate an approximate deflected shape of the structure just prior to cracking, as shown in Figure 11. The deformed shape of the structure does not appear to be that of a cantilever beam. A cantilever beam would be expected to exhibit a shape described by a second-order equation without an inflection point. The observed deflected shape appears to have an inflection point, or reversal in curvature, somewhere in the upper third of the structure. The observed shape implies that a restraining moment may have existed at the top of the structure. The apparent moment may have been the result of an inadvertent restraint of the top of the structure by the roller apparatus used to apply vertical load. The apparent restraining force does not appear to affect the post-cracking response. The pre-cracking deflections measured by these gages were close to the lower limit of accuracy of the gages; thus detailed conclusions as to the deflected shape based on these measurements should be viewed with some degree of skepticism. The vertical load applicator has been redesigned to reduce any inadvertent restraint in future experiments.

The horizontal deflections measured after cracking were very linear in nature, and first-degree curves fit to these data show a very high degree of correlation. The slopes of the curves corresponded to the relative heights at which the measurements were made, implying that a large part of the measured deflections were due to a rigid body rotation of the tower. The deflected shape of the structure generated from these data (Figure 12) was also linear, and the nature of these curves tends to confirm that rigid-body rotation of the tower dominated its post-cracking deflection.

2.6 Strain Response

Fifty-seven strain gage measurements were made during the experiment. Both vertical and horizontal gages were located throughout the model, with most of the gages located in the expected failure zone at the base of the tower. Extensive analysis of these measurements can be found in the technical report. A few selected results are shown in Figures 13 through 16.

Figure 13 shows the strain distribution for the outermost gages in the east (tension) wall up to a horizontal loader deflection of about 0.148 in. It is evident that the strains were maximum at the location of the side walls, as is to be expected due to the redistribution of load to the rigid side walls. The maximum strain at an

imposed deflection of 0.148 in. was approximately 600 in./in. x 10^6. Shortly after the imposition of this deflection, the section apparently cracked. The post-cracking strains are not shown in Figure 13 because the post-cracking tensile strain measured by a gage is determined by whether or not gage happens to fall exactly within the crack path. Hence, the post-cracking strain distribution is not very meaningful.

Figure 14 shows the strain distribution for the outermost gages in the west (compression) wall up to a horizontal loader deflection of about 2.0 in. As for the east (tension) wall, it is evident that the strains were also maximum at the location of the side walls. The maximum compressive strain at an imposed deflection of 0.5 in. appears to have been approximately 700 in./in. x10^6. This relatively large number is based upon one gage and, hence, may be suspect. After an imposed deflection of about 1.6 in., the wall begins to go into tension, implying that the neutral axis is located to the exterior of the outermost layer of steel. The maximum tensile strain was about 400 in./in. x 10^6, a value that is close to the strain to be expected near the tensile capacity of concrete.

The section strain distribution at an imposed deflection of 0.148 in. is shown in Figure 15. This is the deflection just prior to the occurrence of cracking. A well-defined strain distribution is visible. Tensile strains are concentrated at the corners of the east (tension) wall, with a localized peak visible immediately across from the interior corner of the structure. This peak strain is 400 in./in. x 10^6 to 500 in./in. x 10^6 in tension, a range considered close to failure for concrete. The apparent location of the neutral axis remains at about 8 in. from the structure centerline, towards the compression wall.

The post-cracking section strain distribution, recorded at an imposed deflection of 0.18 in., is shown in Figure 16. The post-cracking strain distribution is not as uniform as the pre-cracking distribution because the strains measured are dependent upon whether or not a crack intersects the location of the gage. After cracking, almost all the strain is localized in the immediate vicinity of the crack and, hence, only gages in this vicinity will record these large strains. The large tensile strains that were recorded (25,000 in./in. x 10^6 to 38,000 in./in. x 10^6) are values that exceed the yielding strain, approximately 1,750 in./in. x 10^6, of the steel used in this model. The fact that this occurs immediately after cracking shows that, due to the low reinforcement ratio in the structure, the cracking capacity of the section is greater than the elastic capacity of the reinforcement. This result was expected from the pre-experiment analysis. The apparent location of the neutral axis shifts well into the west (compression) wall.

2.7 Modal Response

A substantial effort was expended to collect modal response before, during, and after the experiment. These data promises to be very useful in the estimation of the changes in the modal response of intake towers due to accumulation of damage during an earthquake. The shifting of the period may have the effect of reducing the load acquired from the earthquake, thus, substantially increasing effective capacity of the structure. The analysis of these data is ongoing, but two examples of the type of data acquired are shown in Figures 17 and 18. The first peak in the pre-experiment plot appears to be the fundamental mode of the structure at about 60 Hz. The first peak of the post-experiment plot appears to begin at a substantially lower frequency (longer period). Such a trend can prove beneficial if it can be substantiated; however, the coherence in the post-experiment survey is quite low for many frequencies. This occurrence reflects the nonlinear nature of the damaged structure and perhaps the elimination of some modes of response. Considerable work remains to be done in the analysis of these data and the quantification of any benefit of the shift of modal response.

3 ANALYSIS

One objective of this research effort is the evaluation of the displacement-based analysis of intake towers. The fundamental premise of this method is the explicit consideration of the earthquake-induced displacements of a structure. The displacement-based analysis method is used as part of a response spectrum analysis of a tower. It attempts, in a simplified manner, to account for the shift of the structure fundamental frequencies with formation of plastic regions in the structure. As cracking and yielding occur, the structure softens and the period of the structure increases. Often this shifts the period out to a region of lower magnitude in the response spectrum, decreasing the loads on the structure.

The displacement-based analysis procedure follows three steps. In the first step, the displacement demand is calculated by response spectrum analysis assuming cracked section properties. These cracked section properties can be approximated by using a fraction of the section moment of inertia (I) or a fraction of the Young's modulus (E) for the material. This assumes that the elastic response approximates inelastic displacement.

In the second step of the displacement-based method, the displacement capacity of the structure is calculated. First, the moment-curvature relationship (M-Phi Diagram) of the section is calculated using stress block factors or a layer-by-layer approach. These procedures have been computerized in the RESPONSE and M-Phi computer codes. The curvatures calculated are used to calculate the displacement capacity of the structure using the following equation:

$$\delta_u = \frac{\phi_y l^2}{3} + (\phi_u - \phi_y) l_p (l - \frac{l_p}{2})$$

where δ_u is the ultimate displacement at the elevation of interest, φ_y is the curvature at the base of the tower when yielding of steel first occurs, φ_u is the ultimate curvature at the base of the tower, l is the structure height to the elevation of interest, and l_p is the plastic hinge length.

The value assumed for the plastic hinge length has a major influence on the results of this calculation. Determination of the plastic hinge length for reinforced concrete sections is a complex, poorly understood problem that depends on section shape, structure aspect ratio, reinforcing diameter and strength, and shear and axial load magnitudes. Two equations found in the literature to estimate plastic hinge length, in the units of inches, are:

$$l_p = 0.08l + 0.15 d_b F_y$$

or

$$l_p = 0.3 d_b F_y$$

where l is the structure height (in.); d_b, the reinforcing bar diameter (in.); and F_y, the reinforcing steel yield strength (ksi). Both equations attempt to include the influence of reinforcement variation (Nicoletti) and are defined as being applicable to ductile and brittle structures, respectively. Numerous other empirical equations for approximation of the plastic hinge length exist in the literature (Moehle 1992), (Park 1975), (U.S. Department of Transportation 1995) and are also being evaluated but are not presented in this paper.

In the final step in the displacement-based method, the demand-to-capacity ratio is calculated:

$$\frac{\delta_{Demand}}{\delta_u} < 1 \rightarrow OK$$

$$\frac{\delta_{Demand}}{\delta_u} > 1 \rightarrow Not - OK$$

where δ_{Demand} is the displacement demand calculated in the first step; and δ_u, the ultimate displacement capacity calculated in step 2.

The displacement-based analysis concept was used to predict the ductility response of ITS-1. The moment-curvature relationship was calculated using the RESPONSE (Felber) computer program. Because 1.2 times the calculated cracking moment was greater than the ultimate moment, the structure was classified as a "brittle" structure, and the single crack assumption should apply. The plastic hinge length of 1.32 in. was calculated based on this single crack assumption. This resulted in a calculated displacement ductility ratio of 1.84. A multi-crack assumption resulted in a hinge length of 10.26 in. and a calculated displacement ductility ratio of 7.25. The multi-crack assumption was considered an upper limit of predicted response.

Figure 19 shows these predicted values plotted against the measured response. Overall the analysis concept shows considerable promise. It is obvious that the cracking moment was over-predicted and the ultimate moment under-predicted by the RESPONSE program. The discrepancies are not due to any shortcoming of the displacement-based analysis concept but rather may be a result of the simplifying assumptions inherent in the formulation of the program, the iterative process of solution, or the definition of the material properties. Further analysis is being conducted to address these issues.

Of greater interest is a comparison of the calculated and measured displacement ductility ratios and the plastic hinge length. The calculated displacement ductility ratios of 1.84 may be reasonable when compared to the measured value of 5.06 if consideration is given to the fact that the measured value is only due to a one-way excursion. As noted above, this was not a cyclic experiment and, therefore, can only be used to demonstrate that the experimental model has the potential for significant ductility. Future cyclic experiments will show how much of this ductility can be safely utilized.

Comparison of the calculated to experimental plastic hinge length is not a straightforward process. The plastic hinge length is not a directly measurable quantity, rather it is a parameter that relates the plastic curvature at the base of the structure to the plastic displacement at the top of the structure. It can be thought of as the distance over which the plastic curvature must act to result in the plastic displacement measured. The total displacement is equal to the sum of the elastic and plastic displacements. Further details are given in the technical report; however, some important observations are given herein. Using the measured yield and ultimate displacements, the measured concrete strains, the estimated ultimate steel strains from rebar tests, the required plastic hinge length can be calculated. The plastic hinge length calculated for this experiment was 1.1 in., which is very close to the single crack estimate.

For under-reinforced structures such as intake towers, ductility is dependent of the ultimate steel strain, as failure occurs when the rebar ruptures, not when concrete crushes. Figure 20 shows the relationship of ultimate steel strain and plastic hinge length on the displacement ductility ratio of the tower model. For the plastic hinge length of 1.1 in. calculated for this model, the ductility ratio does not appear to be very sensitive to variation in ultimate steel strain. However, accurate information is difficult to obtain on the ultimate steel strain capacity of the rebar in existing structures, of varying ages. The strain capacity of the rebar is also influenced by cyclic loading effects as well as construction details. This is clearly an area needing further consideration.

4 CONCLUSIONS

The purpose of this paper is to give an overview of the preliminary results of the ongoing effort in Research Program 387 - Earthquake Engineering - Structures, Work Unit 32911, Nonlinear Dynamic Response and Failure Mechanisms of Intake Towers. Substantial progress has been made in the effort to develop workable engineering procedures for the proper consideration of ductility in the analysis of existing intake towers. Specifically, the application of the displacement-based analysis shows considerable promise. However, this is a

complex and difficult problem, and much work remains to be accomplished.

Several specific areas have been identified as needing further consideration. The first area of concern is the proper estimation of the plastic hinge length. Embedded in this problem is the proper consideration of the influence of cyclic loading, dynamic effects, material properties, shear and axial loads, section geometry, and construction details. A second area that needs to be investigated is the proper estimation of the shift of the tower's natural period with damage. A substantial reduction of loads may be possible if this can be reliably accomplished.

A continuing effort is underway to address these areas of concern. Further experimentation is underway to address the influence of cyclic loading and variation in steel reinforcement. Future work will attempt to address some aspects of dynamic effects, material properties, shear and axial loads, section geometry, and construction details.

5 ACKNOWLEDGMENT

The data presented herein, unless otherwise noted, were obtained from Research Program 387 - Earthquake Engineering - Structures, Work Unit 32911, Nonlinear Dynamic Response and Failure Mechanisms of Intake Towers, conducted at the U.S. Army Engineer Waterways Experiment Station. Permission was granted by the Chief of Engineers to publish this information

6 REFERENCES

Bertero, V.V., "Design Guidelines for Ductility and Drift Limits," UCB/EERC-91/15, July 1991.

Nicoletti, J. P., and Priestly, M.J.N. Review Comments of Draft Appendix B, "Seismic Design and Evaluation of Free-Standing Intake Towers," Letter from URS Consultants to Commander, U.S. Army Engineer Division, Huntsville, AL, 1995.

Moehle, J.P., "Displacement-Based Design of RC Structures Subjected to Earthquakes," Earthquake Spectra, Volume 8, No. 3, 1992.

Park, R., and Paulay, T, *Reinforced Concrete Structures*, John Wiley and Sons, Inc., New York, 1975.

U.S. Department of Transportation, Federal Highway Administration, *Seismic Retrofitting Manual for Highway Bridges*, Publication No. FHWA-RD-94-052, May 1995.

Felber, A. J., "RESPONSE: A Program to Determine the Load-Deformation Response of Reinforced Concrete Sections," M.A.Sc. thesis, Department of Civil Engineering, University of Toronto,1990.

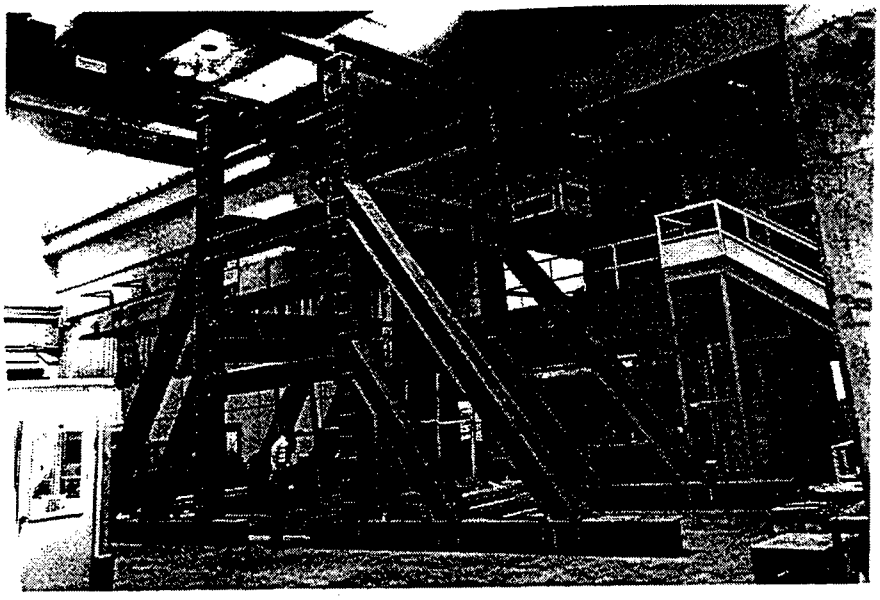

Figure 1. Large Scale Load Frame during construction of ITS-1.

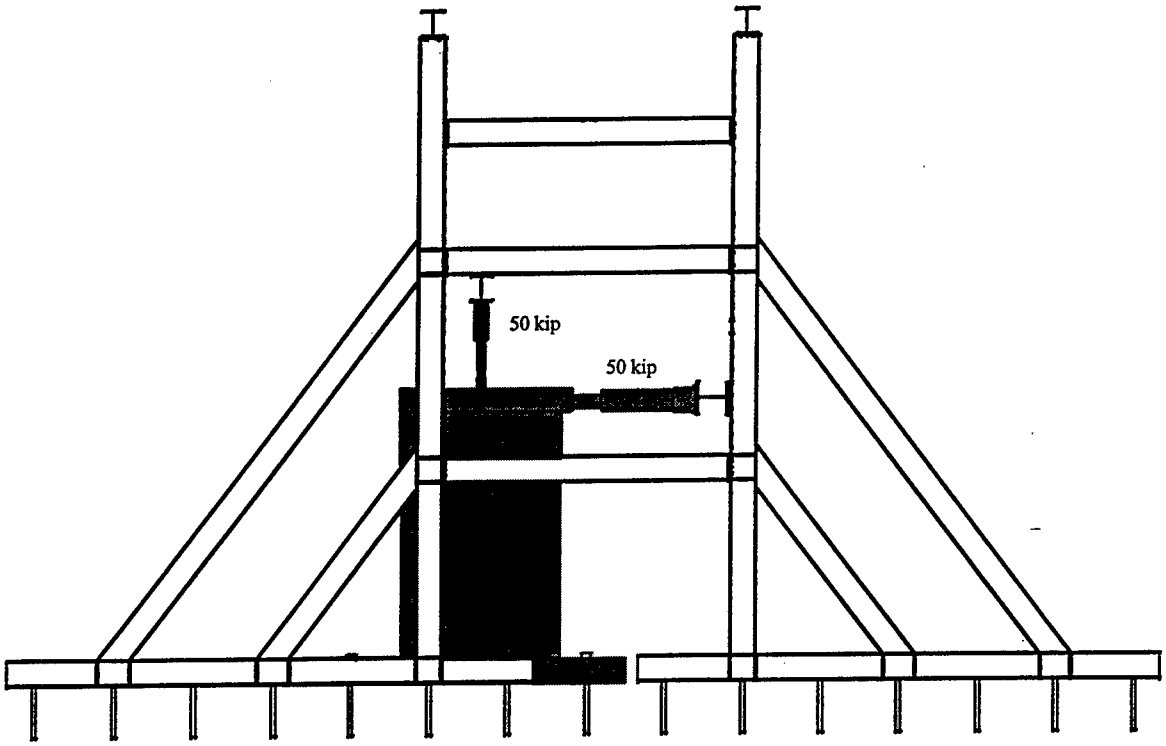

Figure 2. Overall experiment layout, ITS-1.

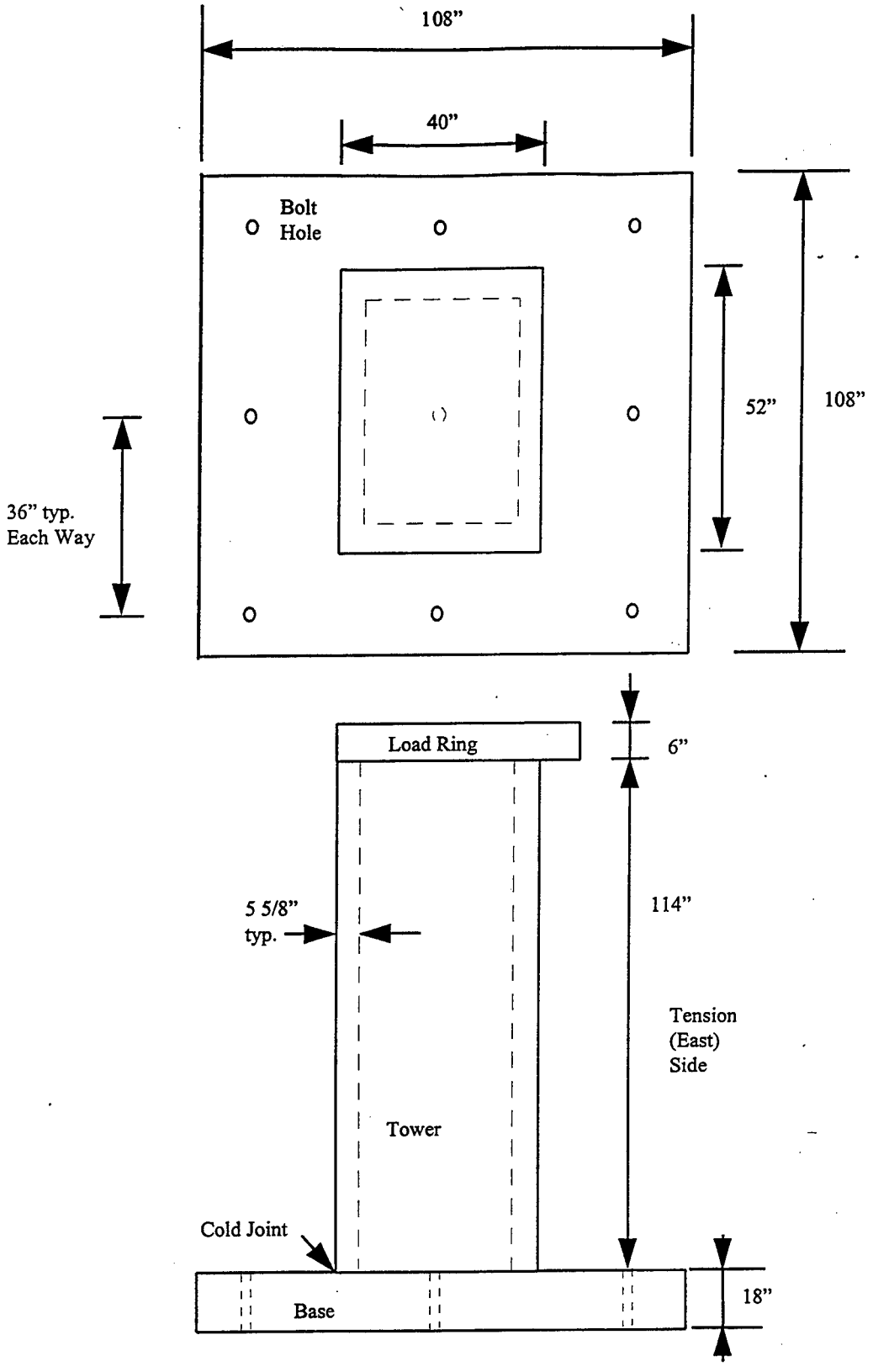

Figure 3. ITS-1 dimensions and configuration.

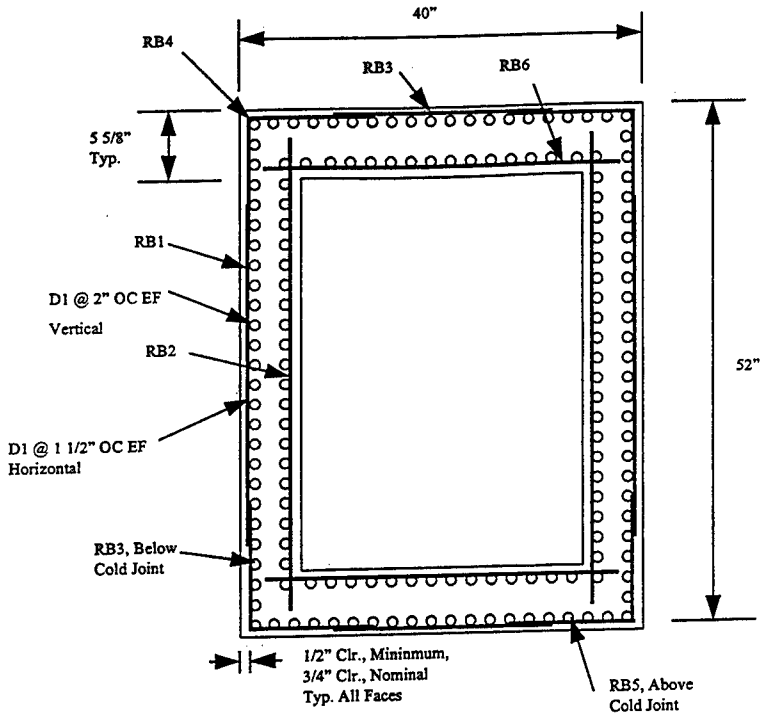

Figure 4. ITS-1, reinforcement layout.

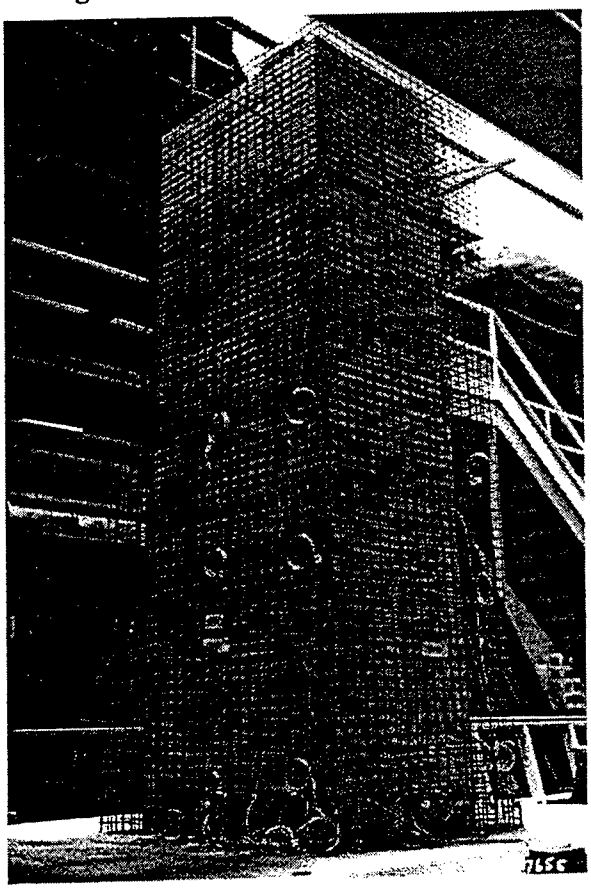

Figure 5. Completed reinforcing cage for ITS-1.

Figure 6. Pre-experiment view of east (tension) wall, ITS-1.

Figure 7. Post-experiment view of east (tension) wall, imposed top deflection of 2 in. , ITS-1.

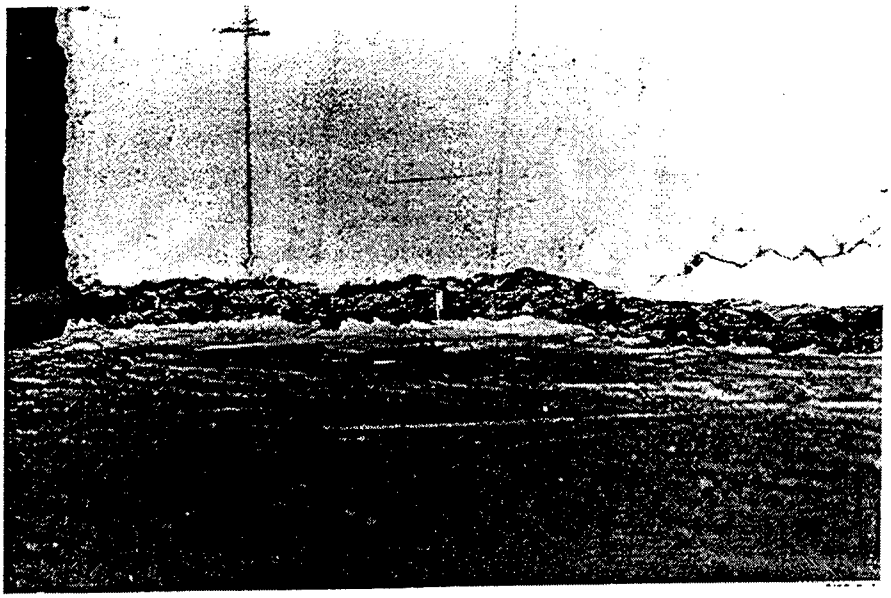

Figure 8. Close-up view of south-east corner, imposed top deflection of 2 in., ITS-1.

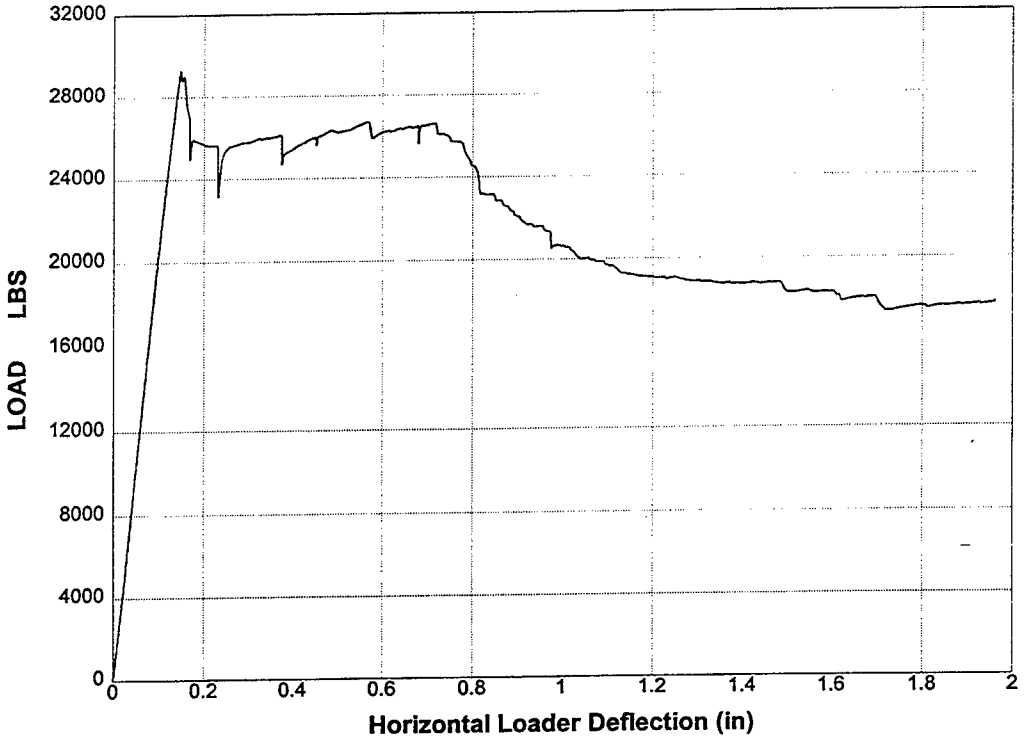

Figure 9. Horizontal load versus horizontal loader deflection.

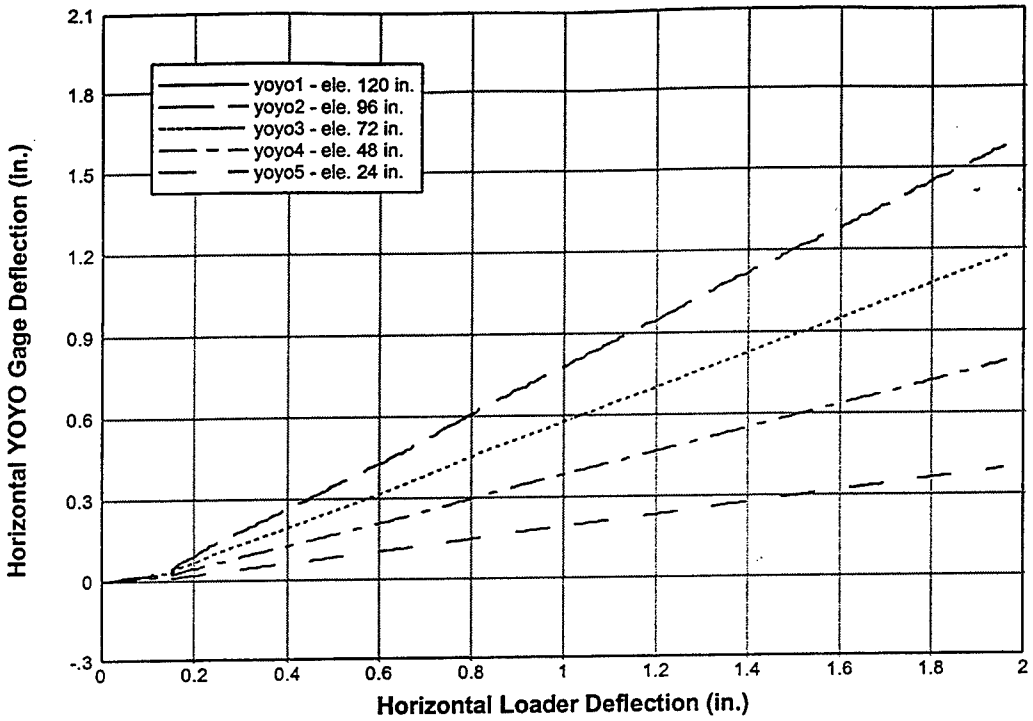

Figure 10. Horizontal deflection at various elevations, plotted against imposed loader deflection.

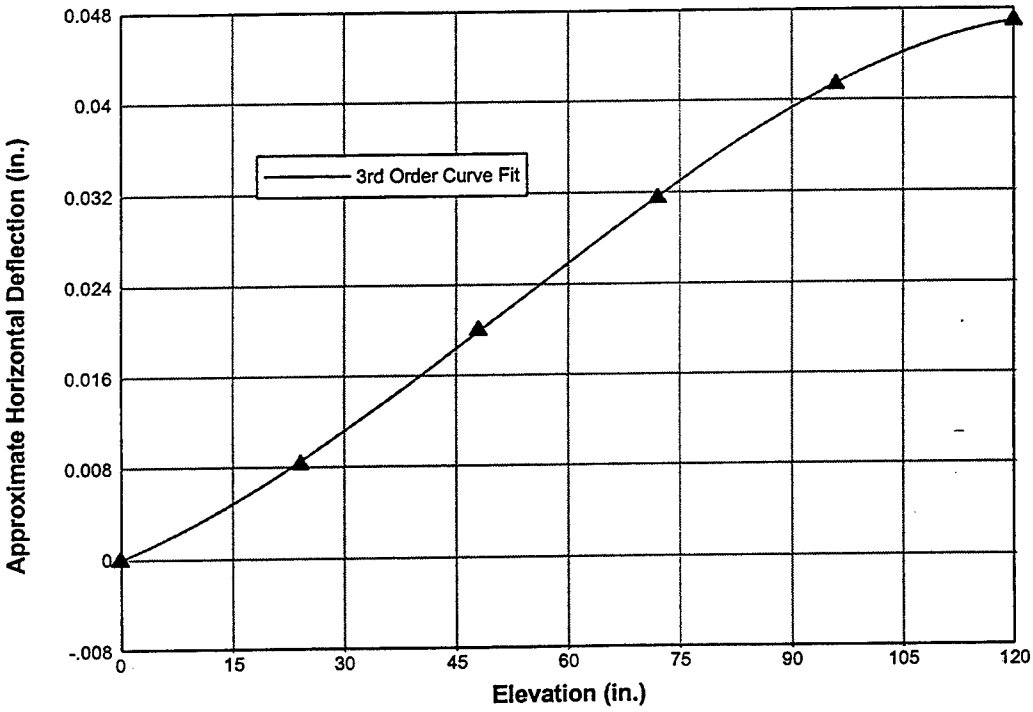

Figure 11. Structure deflected shape just prior to cracking, approximated from linear curve fits of deflection gage data.

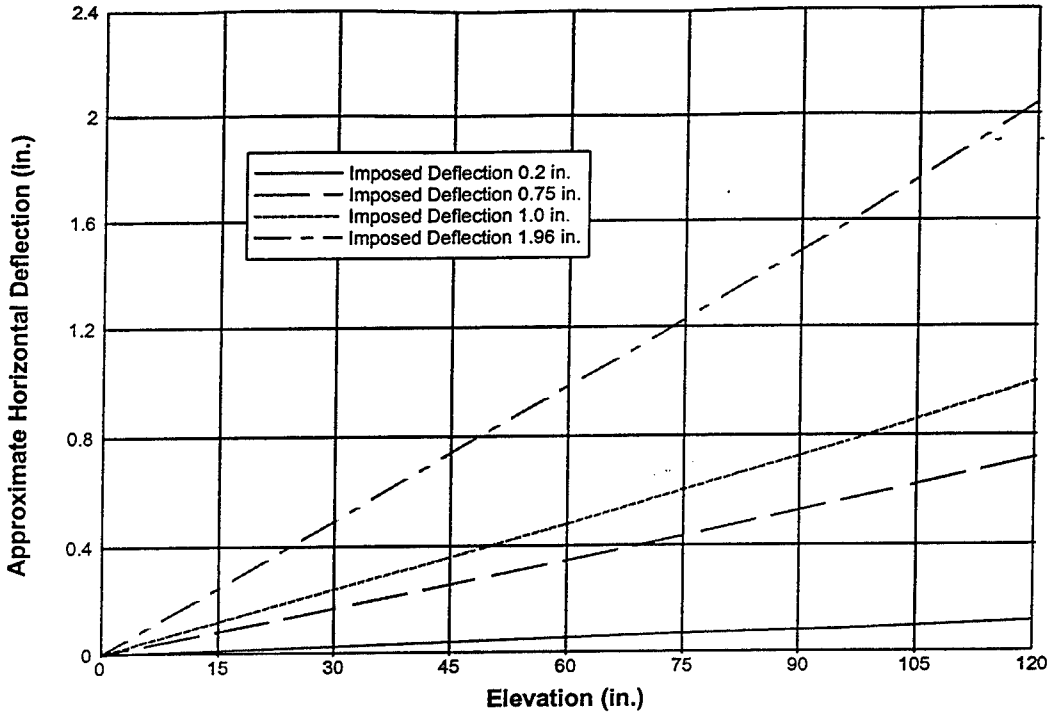

Figure 12. Structure deflected shape after cracking, as measured by horizontal deflection gages.

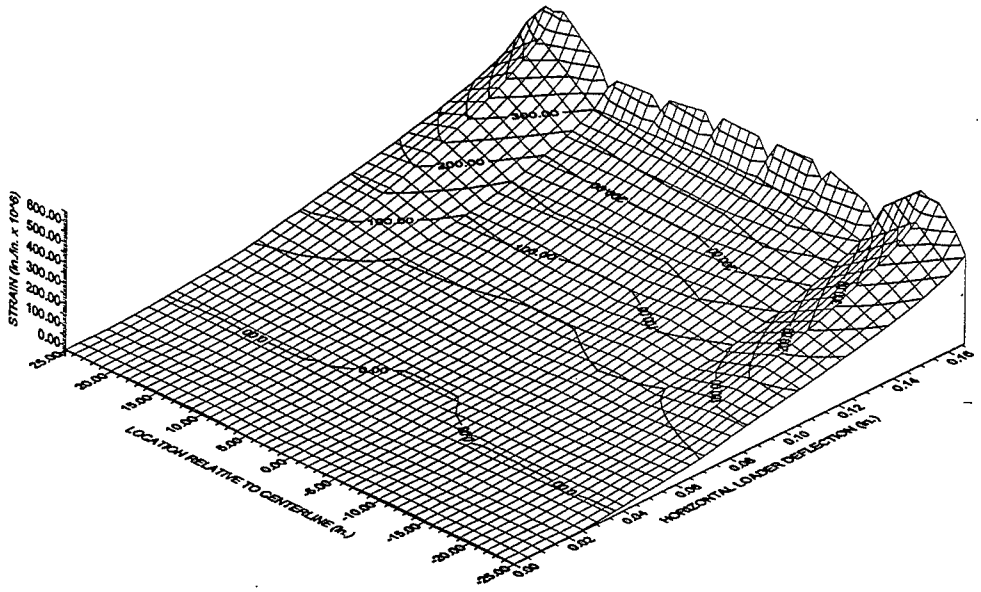

Figure 13. Distribution of vertical strain in outermost rebars in the east (tension) wall up to initial yielding.

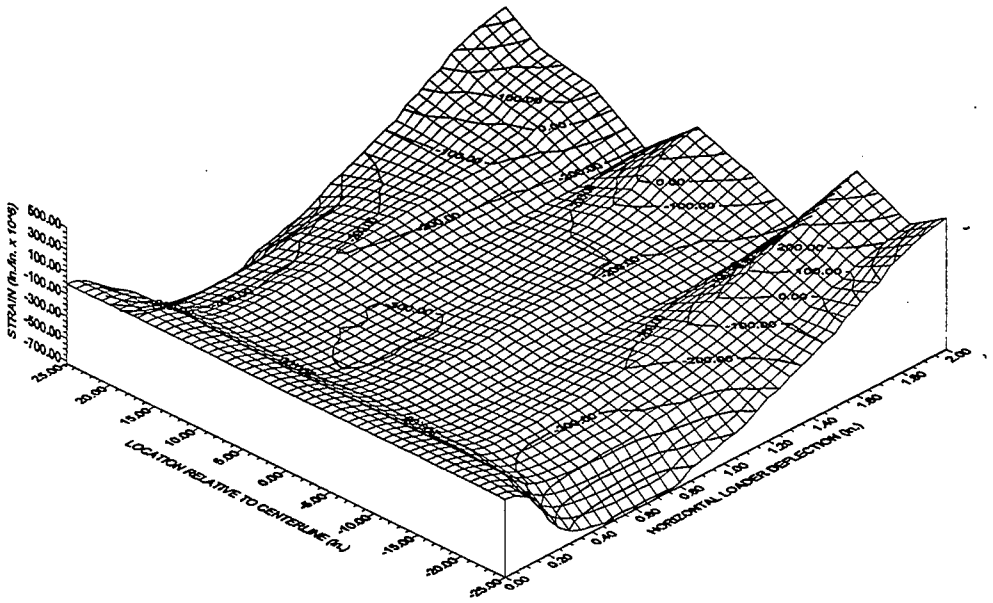

Figure 14. Distribution of vertical strain in outermost rebars in the west (compression) wall, up to final deflection.

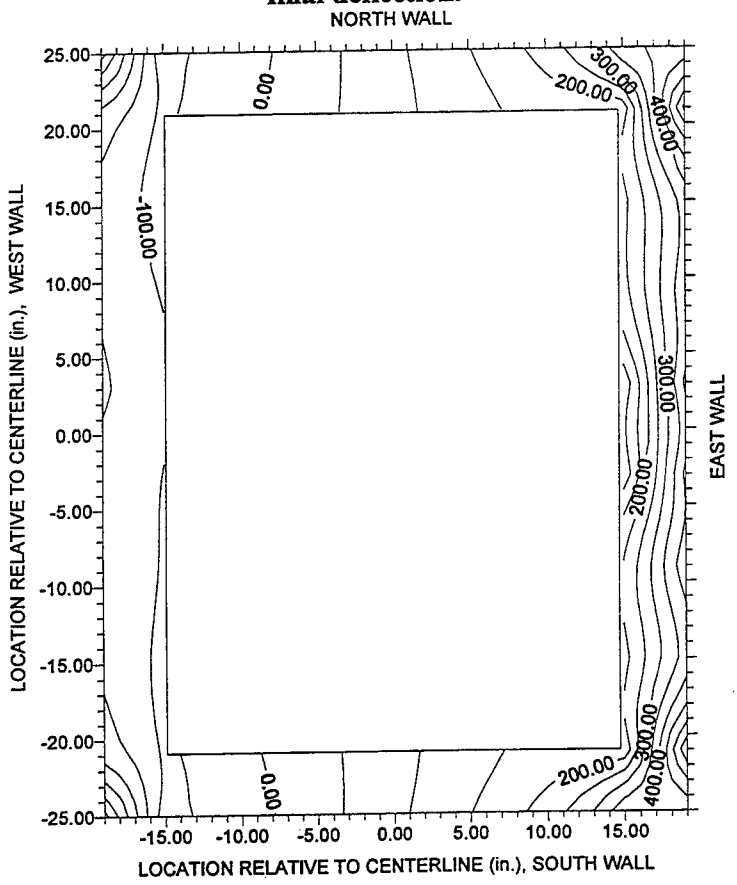

Figure 15. Vertical strain distribution at base of structure for 0.148 in. horizontal loader deflection.

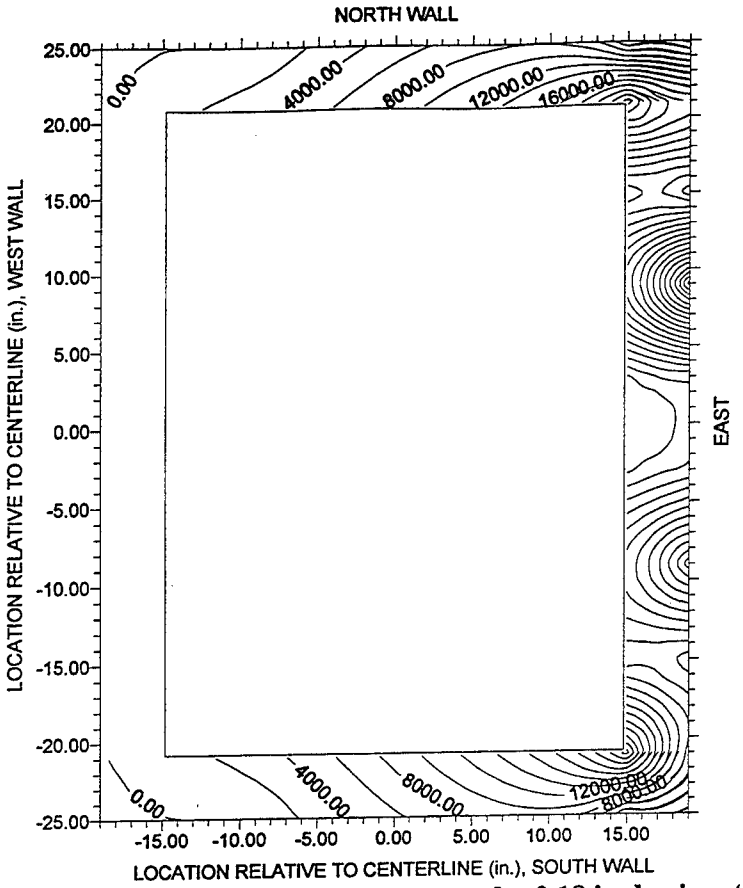

Figure 16. Vertical strain distribution at base of structure for 0.18 in. horizontal loader deflection.

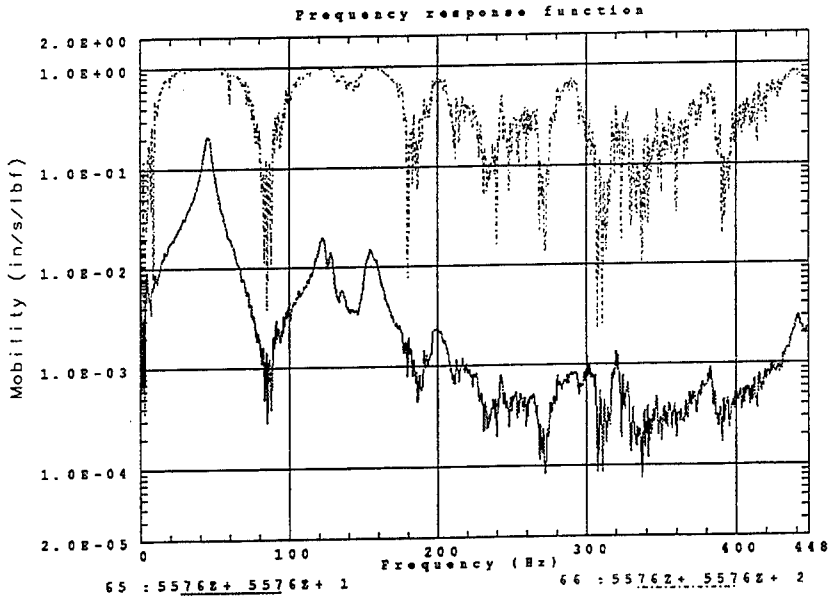

Figure 17. Pre-experiment modal response of tower model.

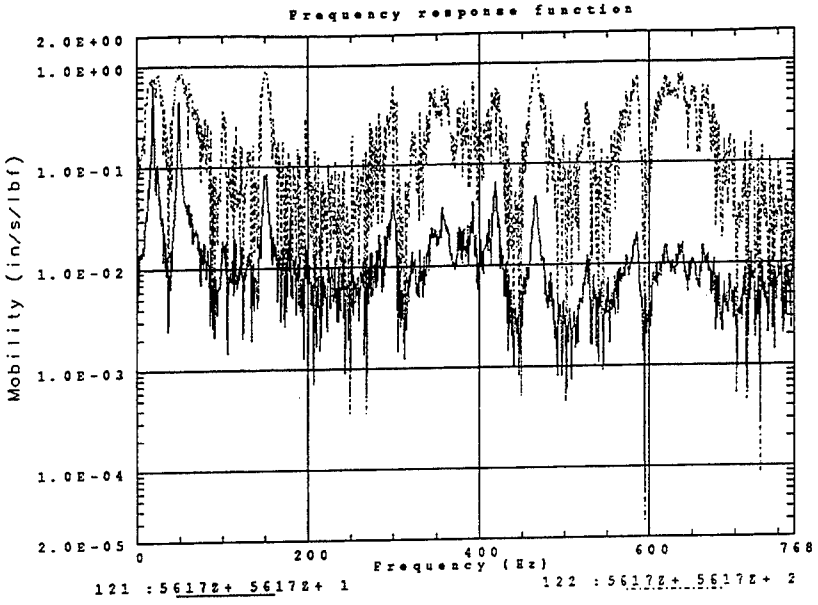

Figure 18. Post-experiment modal response of tower model.

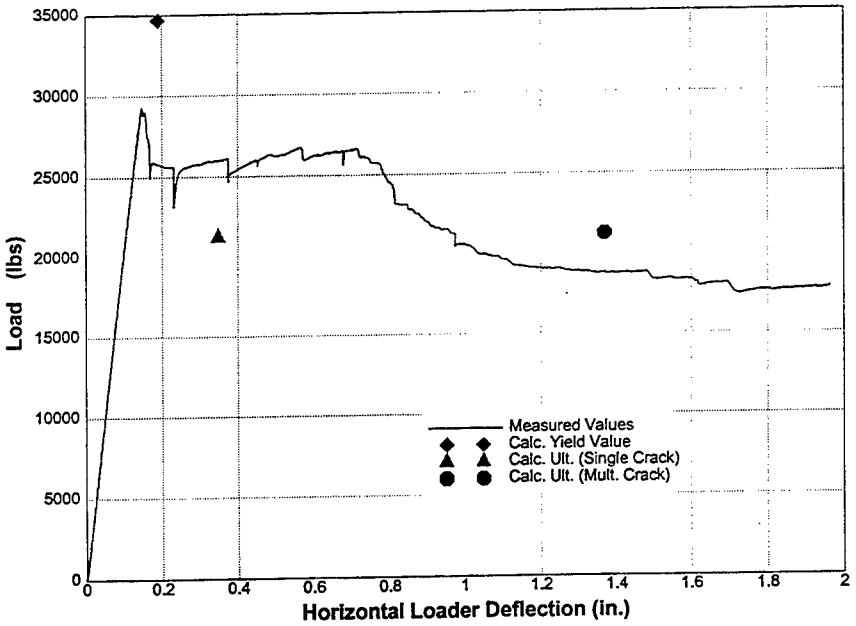

Figure 19. Pre-experiment calculated ductilities compared to measured response.

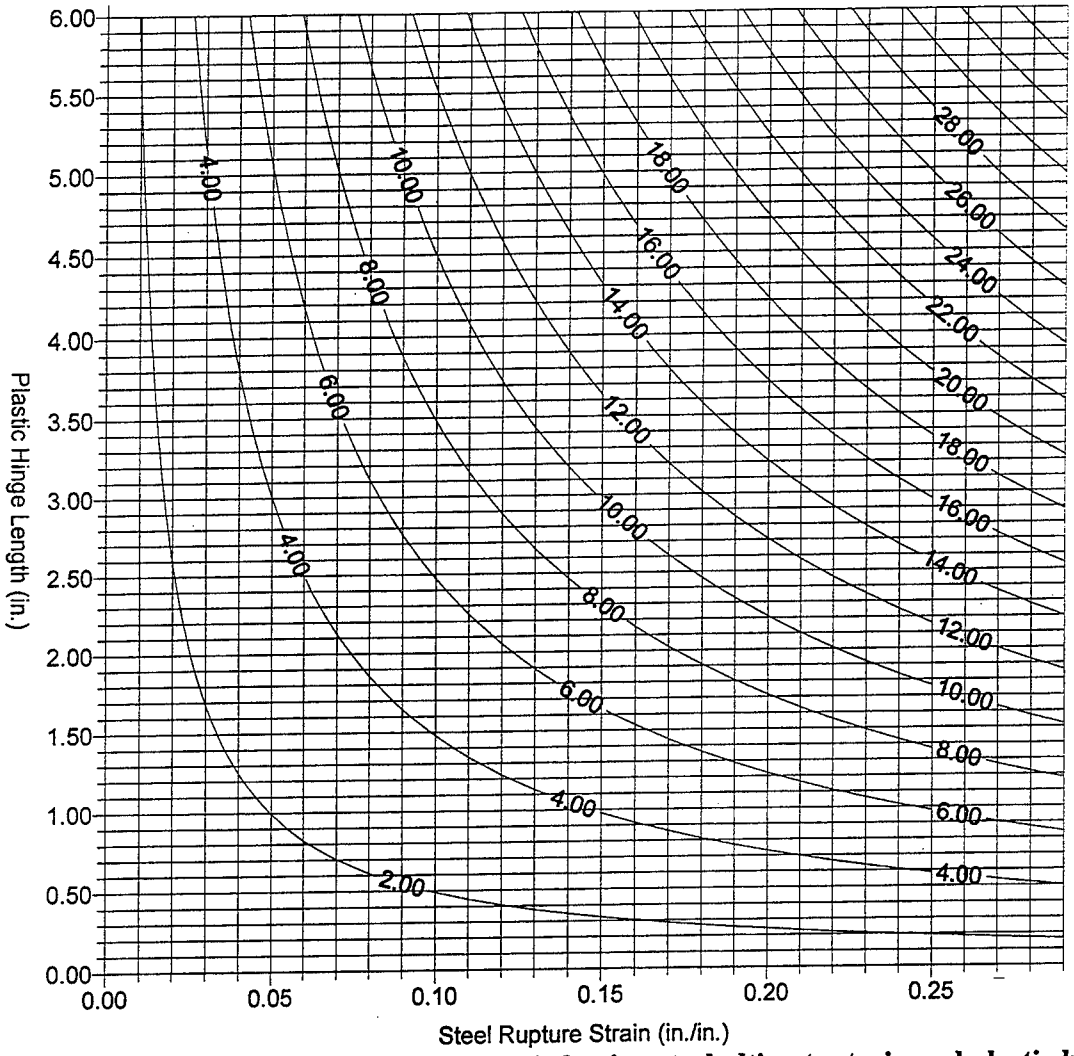

Figure 20. Relationship of ductility ratio to reinforcing steel ultimate strain and plastic hinge length, for tower model with invariant elastic response.

REPORT DOCUMENTATION PAGE

Form Approved
OMB No. 0704-0188

1. AGENCY USE ONLY *(Leave blank)*	2. REPORT DATE	3. REPORT TYPE AND DATES COVERED
	July 1998	Final Report

4. TITLE AND SUBTITLE
First U.S.-Japan Workshop on Advanced Research on Earthquake Engineering for Dams, 12-14 November 1996

5. FUNDING NUMBERS

6. AUTHOR(S)
Mary E. Hynes, Robert Hall, Julia C. Baker, Yoshikazu Yamaguchi

7. PERFORMING ORGANIZATION NAME(S) AND ADDRESS(ES)
U.S. Army Engineer Waterways Experiment Station
3909 Halls Ferry Road
Vicksburg, MS 39180-6199
Public Works Research Institute of Japan
1, Asahi, Tsukuba-shi, Ibaraki-ken 305

8. PERFORMING ORGANIZATION REPORT NUMBER
Miscellaneous Paper GL-98-1

9. SPONSORING/MONITORING AGENCY NAME(S) AND ADDRESS(ES)
United States-Japan Committee on Natural Resources Panel on Wind and Seismic Effects

10. SPONSORING/MONITORING AGENCY REPORT NUMBER

11. SUPPLEMENTARY NOTES
Available from National Technical Information Service, 5285 Port Royal Road, Springfield, VA 22161.

12a. DISTRIBUTION/AVAILABILITY STATEMENT
Approved for public release, distribution is unlimited.

12b. DISTRIBUTION CODE

13. ABSTRACT (Maximum 200 words)

The First U.S.-Japan Workshop on Advanced Research on Earthquake Engineering for Dams was held under the sponsorship of the U.S. Army Engineer Waterways Experiment Station and the Public Works Research Institute of Japan (PWRI) under the auspices of Task Committee D, Earthquake Engineering for Dams, of the UJNR Panel on Wind and Seismic Effects, in Vicksburg, Mississippi, 12-14 November 1996. The workshop provided a valuable forum to exchange technical information on earthquake engineering for dams in both countries. The workshop was attended by 11 Japanese participants, 26 U.S. participants, and 1 visitor from the United Kingdom. Four agencies and two universities were represented in the Japanese delegation. The U.S. participants were drawn from the U.S. Army Corps of Engineers and the U.S. Bureau of Reclamation.

14. SUBJECT TERMS
Concrete dams
Deformation analysis
Dynamic response
Earthquake engineering
Earthquake ground motions
Embankment dams
Liquefaction
Roller-compacted concrete dams

15. NUMBER OF PAGES
388

16. PRICE CODE

17. SECURITY CLASSIFICATION OF REPORT	18. SECURITY CLASSIFICATION OF THIS PAGE	19. SECURITY CLASSIFICATION OF ABSTRACT	20. LIMITATION OF ABSTRACT
Unclassified	Unclassified	Unclassified	